

Morphological study of the effect of the cytoskeletal disrupting agent carbendazim on the oviduct of the Japanese quail (*Coturnix coturnix japonica*)

By

Wahabu Hamisi Kimaro

Submitted in fulfillment of the requirements for the degree *Philosophiae* Doctor in the Faculty of Veterinary Science, University of Pretoria

2012

ACKNOWLEDGEMENTS

This study was supported by DAAD (doctoral scholarship), Sokoine University of Agriculture, University of Pretoria and The South African Veterinary Research Foundation.

My sincere gratitude goes to my supervisor Professor M.-C. Madekurozwa for designing and hands-on supervision of this research. Her guidance, critics and keen scrutiny of my write-up contributed enormously in the production of this thesis.

I also like to thank my co-supervisor Professor H. Groenewald for his guidance, professional advice and support during the entire period of my study.

My heartfelt thanks are due to Mrs W.Olivier for her technical and administrative assistance which has resulted to a smooth completion of my study in South Africa. Schematic drawings of Fig. 1.1 and 1.2 would have been difficult without her artistical touch.

Technical assistance rendered by staff of electron microscopy unit, Anatomy Department and histopathology laboratory is gratefully acknowledged. A personal assistance offered by Mrs Erna van Welpé during SEM breakdown contributed much in the production of this work.

I thank the management of Sokoine University of Agriculture for granting me a study leave which has enabled me to pursue a doctoral study in the University of Pretoria.

Lastly, I would like to extend my sincere appreciation to my family for their moral and financial support during my study. Your persistent encouragement and prayers have contributed much to the completion of my study.

DECLARATION

Kimaro, W.H.

Ihereby confirm that, the work presented here is my original research. It has not been submitted by me for a degree into this University or any other tertiary institution. The University of Pretoria in consultation with the author reserves the right of permission for duplication of the whole thesis or in part thereof.



23/08/2012

.....

.....

Signature

Date

TABLE OF CONTENTS

Acknowledgements.....	2
Declaration.....	3
Acronyms.....	5
List of figures	6
List of tables	13
Summary	14
Chapter One.....	16
General introduction.....	16
Chapter Two.....	25
Effect of carbendazim on the infundibulum.....	25
Chapter Three.....	144
Effect of carbendazim on the magnum.....	144
Chapter Four.....	251
Effect of carbendazim on the shell gland.....	251
Chapter Five.....	351
Effect of carbendazim on sperm storage tubules.....	351
Chapter Six.....	404
General discussion and conclusion.....	404
Appendix 1.....	411

ACRONYMS

- LM: Light microscope
LSAB+: Linked Strepto Avidin Biotin Plus kit
PAS: Periodic Acid Schiff
SST: Sperm Storage Tubules
SEM: Scanning Electron Microscope
TEM: Transmission Electron Microscope
UVJ: Utero-Vaginal Junction

LIST OF FIGURES

Fig. 1.1: Schematic drawing of the avian oviduct	20
Fig. 1.2: Schematic drawing of the oviductal mucosa.....	21
Fig. 2.1: A gross photograph showing Japanese quail reproductive organs <i>in situ</i>	37
Fig. 2.2: Histogram showing mean oviduct weight	37
Fig. 2.3: LM funnel region of the infundibulum: control bird.....	38
Fig. 2.4: LM funnel region of the infundibulum: carbendazim 400 mg/kg.....	39
Fig. 2.5: LM funnel region of the infundibulum: carbendazim MBC 800 mg/kg.....	40
Fig. 2.6: LM funnel region of the infundibulum: 5 days post-exposure.....	41
Fig. 2.7: LM tubular region of the infundibulum: control bird.....	44
Fig. 2.8: LM tubular region of the infundibulum: carbendazim 400 mg/kg.....	46
Fig. 2.9: LM tubular region of the infundibulum: 5 days post-exposure.....	47
Fig. 2.10: LM tubular region of the infundibulum: 12 days post-exposure.....	48
Fig. 2.11: LM tubular region of the infundibulum: 32 days post-exposure.....	49
Fig. 2.12: PAS/Alcian blue, funnel region of the infundibulum: control bird.....	50
Fig. 2.13: PAS/Alcian blue, tubular region of the infundibulum: control bird.....	54
Fig. 2.14: PAS/Alcian blue, tubular region of the infundibulum: carbendazim.....	55
Fig. 2.15: PAS/Alcian blue, tubular region of the infundibulum: 12 days post-exposure.....	56
Fig. 2.16: E-cadherin, infundibulum: control bird.....	61
Fig. 2.17: E-cadherin, infundibulum: 32 days post-exposure.....	62
Fig. 2.18: Laminin, tubular region of the infundibulum: control bird.....	63
Fig. 2.19: Laminin, tubular region of the infundibulum: 12 days post-exposure.....	64
Fig. 2.20: Vimentin, tubular region of the infundibulum: control bird.....	65
Fig. 2.21: Vimentin, infundibulum mucosa: 8 days post-exposure.....	66
Fig. 2.22: Vimentin, infundibulum mucosa: 12 days post-exposure.....	67
Fig. 2.23: SEM funnel region of the infundibulum: control bird.....	69
Fig. 2.24: SEM funnel region of the infundibulum: carbendazim 400 mg/kg.....	70
Fig. 2.25: SEM funnel region of the infundibulum: 5 days post-exposure.....	71
Fig. 2.26: SEM funnel region of the infundibulum: 12 days post-exposure.....	72
Fig. 2.27: TEM funnel region of the infundibulum: control bird.....	79
Fig. 2.28: TEM funnel region of the infundibulum: control bird.....	80
Fig. 2.29: TEM funnel region of the infundibulum: carbendazim 400 mg/kg.....	81
Fig. 2.30: TEM funnel region of the infundibulum: carbendazim 400 mg/kg.....	82
Fig. 2.31: TEM funnel region of the infundibulum: carbendazim 800 mg/kg.....	83
Fig. 2.32: TEM funnel region of the infundibulum: 5 days post-exposure.....	84
Fig. 2.33: TEM funnel region of the infundibulum: 8 days post-exposure.....	86

Fig. 2.34: TEM funnel region of the infundibulum: 8 days post-exposure.....	87
Fig. 2.35: TEM funnel region of the infundibulum: 12 days post-exposure.....	88
Fig. 2.36: TEM funnel region of the infundibulum: 32 days post-exposure.....	89
Fig. 2.37: TEM funnel region of the infundibulum: 32 days post-exposure.....	90
Fig. 2.38: SEM tubular region of the infundibulum: control bird.....	92
Fig.2.39: SEM tubular region of the infundibulum: carbendazim 400 mg/kg.....	93
Fig. 2.40: SEM tubular region of the infundibulum: carbendazim 800 mg/kg.....	93
Fig. 2.41: SEM tubular region of the infundibulum: 8 days post-exposure.....	94
Fig. 2.42: SEM tubular region of the infundibulum: 12 days post-exposure.....	95
Fig. 2.43: TEM tubular region of the infundibulum: control bird.....	98
Fig. 2.44: TEM tubular region of the infundibulum: control bird.....	99
Fig. 2.45: TEM tubular region of the infundibulum: control bird.....	100
Fig. 2.46: TEM <i>lamina propria-submucosa</i> , infundibulum: control bird.....	101
Fig. 2.47: TEM tubular gland in the infundibulum: control bird.....	102
Fig. 2.48: TEM gland cell in the tubular region of the infundibulum: control bird.....	103
Fig. 2.49: TEM tubular region of the infundibulum: carbendazim 400 mg/kg.....	107
Fig. 2.50: TEM tubular region of the infundibulum: carbendazim 400 mg/kg.....	108
Fig. 2.51: TEM tubular region of the infundibulum: carbendazim 400 mg/kg.....	109
Fig. 2.52: TEM tubular region of the infundibulum: carbendazim 400 mg/kg.....	110
Fig. 2.53: TEM tubular region of the infundibulum: carbendazim 800 mg/kg.....	111
Fig. 2.54: TEM tubular region of the infundibulum: carbendazim 800 mg/kg.....	112
Fig. 2.55: TEM tubular region of the infundibulum: carbendazim 800 mg/kg.....	113
Fig. 2.56: TEM tubular region of the infundibulum: carbendazim 800 mg/kg.....	114
Fig. 2.57: TEM tubular gland in the tubular region: carbendazim 800 mg/kg.....	115
Fig. 2.58: TEM tubular region of the infundibulum: 5 hours post-exposure.....	122
Fig. 2.59: TEM tubular region of the infundibulum: 24 hours post-exposure.....	123
Fig. 2.60: TEM tubular region of the infundibulum: 24 hours post-exposure.....	124
Fig. 2.61: TEM tubular region of the infundibulum: 5 days post-exposure.....	125
Fig. 2.62: TEM tubular region of the infundibulum: 8 days post-exposure.....	126
Fig. 2.63: TEM tubular region of the infundibulum: 8 days post-exposure.....	127
Fig. 2.64: TEM tubular region of the infundibulum: 12 days post-exposure.....	128
Fig. 2.65: TEM tubular region of the infundibulum: 32 days post-exposure.....	129
Fig. 2.66: TEM tubular region of the infundibulum: 32 days post-exposure.....	130
Fig. 2.67: TEM basal lamina in the tubular region: 32 days post-exposure.....	131
Fig. 2.68: TEM tubular gland: 32 days post-exposure.....	132
Fig. 2.69: TEM gland cells: 32 days post-exposure.....	133
Fig. 3.1: LM magnum from a control bird.....	154

Fig. 3.2: LM magnum: Carbendazim 400 mg/kg.....	155
Fig. 3.3: LM tubular glands in the magnum: carbendazim 400 mg/kg.....	156
Fig. 3.4: LM magnum: carbendazim 800 mg/kg.....	157
Fig. 3.5: LM magnum: 24 hours post-exposure.....	160
Fig. 3.6: LM magnum: 5 days post-exposure.....	161
Fig. 3.7: LM magnum: 8 days post-exposure.....	162
Fig. 3.8: LM magnum: 12 days post-exposure.....	163
Fig. 3.9: LM magnum: 32 days post-exposure.....	164
Fig. 3.10: PAS/Alcian blue, magnum from a control bird.....	165
Fig. 3.11: PAS/Alcian blue, magnum: carbendazim 100 mg/kg.....	167
Fig. 3.12: PAS/Alcian blue, magnum: carbendazim 400 mg/kg.....	168
Fig. 3.13: PAS/Alcian blue, magnum: 5 days post-exposure.....	170
Fig. 3.14: PAS/Alcian blue, magnum: 8 days post-exposure.....	171
Fig. 3.15: PAS/Alcian blue, magnum: 12 days post-exposure.....	172
Fig. 3.16: PAS/Alcian blue, magnum: 32 days post-exposure.....	173
Fig. 3.17: E-cadherin, magnum from a control bird.....	175
Fig. 3.18: E-cadherin, magnum 8 days post-exposure.....	175
Fig. 3.19: E-cadherin, magnum 32 days post-exposure.....	176
Fig. 3.20: Laminin, magnum from a control bird.....	178
Fig. 3.21: Laminin, magnum 12 days pos-exposure.....	179
Fig. 3.22: Vimentin, magnum from a control bird.....	181
Fig. 3.23: Vimentin, magnum 48 hours post-exposure to 400 mg/kg.....	182
Fig. 3.24: Vimentin, magnum 32 days post-exposure to 400 mg/kg.....	183
Fig. 3.25: SEM mucosal surface in the magnum of a control bird.....	185
Fig. 3.26: SEM magnum: carbendazim 400 mg/kg.....	186
Fig. 3.27: SEM magnum: 5 days post exposure.....	188
Fig. 3.28: SEM magnum: 8 days post-exposure.....	189 - 191
Fig. 3.29: SEM magnum: 12 days post-exposure.....	192
Fig. 3.30: TEM luminal epithelium in the magnum of a control bird.....	195
Fig. 3.31: TEM ciliated cell in the magnum of a control bird.....	196
Fig. 3.32: TEM non-ciliated cell in the magnum of the control bird.....	197
Fig. 3.33: TEM tubular gland in the magnum of a control bird.....	198
Fig. 3.34: TEM apical region of a tubular gland in the magnum of a control bird.....	199
Fig. 3.35: TEM supporting cell in the <i>lamina propria-submucosa</i> of a control bird.....	200
Fig. 3.36: TEM luminal epithelium in the magnum: carbendazim 400 mg/kg.....	204
Fig. 3.37: TEM non-ciliated cell in the magnum: carbendazim 400 mg/kg.....	205
Fig. 3.38: TEM glandular tissue in the magnum: carbendazim 400 mg/kg.....	206

Fig. 3.39: TEM supporting cell in the <i>lamina propria-submucosa</i> : carbendazim 400 mg/kg.....	207
Fig. 3.40: TEM luminal epithelium in the magnum: carbendazim 800 mg/kg.....	208
Fig. 3.41: TEM ciliated cell in the magnum: carbendazim 800 mg/kg.....	209
Fig. 3.42: TEM non-ciliated cell in the magnum: carbendazim 800 mg/kg.....	210
Fig. 3.43: TEM tubular gland in the magnum: carbendazim 800 mg/kg.....	211
Fig. 3.44: TEM tubular gland in the magnum: carbendazim 800 mg/kg.....	212
Fig. 3.45: TEM supporting cell in the <i>lamina propria-submucosa</i> : carbendazim 800 mg/kg.....	213
Fig. 3.46: TEM: luminal epithelium in the magnum, 5 hours post-exposure to 400 mg/kg.....	220
Fig. 3.47: TEM glandular tissue in the magnum: 5 hours post-exposure.....	221
Fig. 3.48: TEM luminal epithelium in the magnum: 5 days post-exposure.....	222
Fig. 3.49: TEM ciliated cell in the magnum: 5 days post-exposure.....	223
Fig. 3.50: TEM luminal epithelium in the magnum: 5 days post-exposure.....	224
Fig. 3.51: TEM desmosomes along plasma membranes: 5 days post-exposure.....	225
Fig. 3.52: TEM tubular gland in the magnum: 5 days post-exposure.....	226
Fig. 3.53: TEM supporting cell in the <i>lamina propria-submucosa</i> : 5 days post-exposure.....	227
Fig. 3.54: TEM luminal epithelial cells in the magnum: 8 days post-exposure.....	228
Fig. 3.55: TEM ciliated cell in the magnum: 8 days post-exposure.....	229
Fig. 3.56: TEM luminal epithelium in the magnum: 8 days post-exposure.....	230
Fig. 3.57: TEM luminal epithelium in the magnum: 12 days post-exposure.....	231
Fig. 3.58: TEM luminal epithelium in the magnum: 32 days post-exposure.....	232
Fig. 3.59: TEM luminal epithelium in the magnum: 32 days post-exposure.....	233
Fig. 3.60: TEM basal lamina underlying the luminal epithelium: 32 days post-exposure.....	234
Fig. 3.61: TEM tubular gland in the magnum: 32 days post-exposure.....	235
Fig. 3.62: TEM supporting cell in the <i>lamina propria-submucosa</i> : 32 days post-exposure.....	236
Fig. 4.1: LM mucosal layer in the shell gland of a control bird.....	259
Fig. 4.2: LM mucosal layer in the shell gland of a control bird.....	260
Fig. 4.3: LM mucosal layer in the shell gland: carbendazim 400 mg/kg.....	261
Fig. 4.4: LM mucosal layer of the shell gland: carbendazim 800 mg/kg.....	262
Fig. 4.5: LM mucosal layer of the shell gland: 5 days post-exposure.....	264
Fig. 4.6: LM mucosal layer in the shell gland: 8 days post-exposure.....	265
Fig. 4.7: LM mucosal layer in the shell gland: 12 days post-exposure.....	266
Fig. 4.8: LM mucosal layer in the shell gland: 32 days post-exposure.....	267

Fig. 4.9: PAS/Alcian blue, mucosal layer in the shell gland of a control bird.....	269
Fig. 4.10: PAS/Alcian blue, mucosal layer in the shell gland: carbendazim 100 mg/kg.....	270
Fig. 4.11: PAS/Alcian blue, mucosal layer in the shell gland: carbendazim 400 & 800 mg/kg.....	271
Fig. 4.12: PAS/Alcian blue, mucosal layer in the shell gland: 5 days post-exposure.....	273
Fig. 4.13: PAS/Alcian blue, mucosal layer in the shell gland: 8 days post-exposure.....	274
Fig. 4.14: E-cadherin, shell gland from a control bird.....	276
Fig. 4.15: E-cadherin, shell gland: carbendazim 800 mg/kg.....	277
Fig. 4.16: E-cadherin, shell gland: 8 days post-exposure.....	277
Fig. 4.17: E-cadherin, shell gland: 32 days post-exposure.....	278
Fig. 4.18: Laminin, mucosal layer in the shell gland of a control bird.....	280
Fig. 4.19: Laminin, mucosal layer in the shell gland: 12 days post-exposure.....	281
Fig. 4.20: Vimentin, shell gland from a control bird.....	283
Fig. 4.21: SEM mucosal surface of the shell gland in a control bird.....	285
Fig. 4.22: SEM mucosal surface of the shell gland: carbendazim 100 mg/kg.....	286
Fig. 4.23: SEM mucosal surface of the shell gland: carbendazim 400 mg/kg.....	287
Fig. 4.24: SEM mucosal surface of the shell gland: carbendazim 800 mg/kg.....	288
Fig. 4.25: SEM mucosal surface of the shell gland: 24 hours post-exposure.....	290
Fig. 4.26: SEM mucosal surface of the shell gland: 5 days post-exposure.....	291
Fig. 4.27: SEM mucosal surface of the shell gland: 8 days post-exposure.....	292
Fig. 4.28: SEM mucosal surface of the shell gland: 32 days post-exposure.....	293
Fig. 4.29: TEM luminal epithelium of the shell gland in a control bird.....	296
Fig. 4.30: TEM non-ciliated cell in the shell gland of a control bird.....	297
Fig. 4.31: TEM tubular gland in the shell gland of a control bird.....	298
Fig. 4.32: TEM luminal epithelium in the shell gland: carbendazim 400 mg/kg.....	302
Fig. 4.33: TEM ciliated cells in the shell gland: carbendazim 400 mg/kg.....	303
Fig. 4.34: TEM ciliated and non-ciliated cells in the shell gland: carbendazim 400 mg/kg.....	304
Fig. 4.35: TEM tubular gland in the shell gland: carbendazim 400 mg/kg.....	305
Fig. 4.36: TEM luminal epithelium of the shell gland: carbendazim 800 mg/kg.....	306
Fig. 4.37 TEM non-ciliated cell in the shell gland: carbendazim 800 mg/kg.....	307
Fig. 4.38: TEM tubular gland in the shell gland: carbendazim 800 mg/kg.....	308
Fig. 4.39: TEM luminal epithelium in the shell gland: 5 hours post-exposure.....	318
Fig. 4.40: TEM epithelial cells in the shell gland: 5 hours post-exposure.....	319
Fig. 4.41: TEM gland cell in the shell gland: 5 hours post-exposure.....	320
Fig. 4.42: TEM apical region of a ciliated cell: 24 hours post-exposure.....	321
Fig. 4.43: TEM luminal epithelium in the shell gland: 5 days post-exposure.....	322

Fig. 4.44: TEM luminal epithelium in the shell gland: 5 days post-exposure.....	323
Fig. 4.45: TEM luminal epithelium in the shell gland: 5 days post-exposure.....	324
Fig. 4.46: TEM tubular gland in the shell gland: 5 days post-exposure.....	325
Fig. 4.47: TEM gland cells in the shell gland: 5 days post-exposure.....	326
Fig. 4.48: TEM luminal epithelium in the shell gland: 8 days post-exposure.....	327
Fig. 4.49: TEM luminal epithelial in the shell gland: 8 days post-exposure.....	328
Fig. 4.50: TEM tubular gland in the shell gland: 8 days post-exposure.....	329
Fig. 4.51: TEM luminal epithelium in the shell gland: 12 days post-exposure.....	330
Fig. 4.52: TEM non-ciliated cell in the shell gland: 12 days post-exposure.....	331
Fig. 4.53: TEM non-ciliated cell in the shell gland: 12 days post-exposure.....	332
Fig. 4.54: TEM tubular gland in the shell gland: 12 days post-exposure.....	333
Fig. 4.55 TEM luminal epithelium in the shell gland: 32 days post-exposure.....	334
Fig. 4.56: TEM epithelial cells in the shell gland: 32 days post-exposure.....	335
Fig. 4.57: TEM epithelial cells in the shell gland: 32 days post-exposure.....	336
Fig. 4.58: TEM luminal epithelium in the shell gland: 32 days post-exposure.....	337
Fig. 4.59: TEM tubular gland in the shell gland: 32 days post-exposure.....	338
Fig. 4.60: TEM tubular gland in the shell gland: 32 days post-exposure.....	339
Fig. 5.1: LM the <i>mucosa</i> in the UVJ region of a control bird.....	358
Fig. 5.2: LM the <i>mucosa</i> in the UVJ region: carbendazim 400 mg/kg.....	359
Fig. 5.3: LM the <i>mucosa</i> in the UVJ region: carbendazim 800 mg/kg.....	360
Fig. 5.4: LM the <i>mucosa</i> in the UVJ region: 5 days post-exposure.....	362
Fig. 5.5: LM the <i>mucosa</i> in the UVJ region: 12 days post-exposure.....	363
Fig. 5.6: LM of the SST in the UVJ region: 32 days post-exposure.....	364
Fig. 5.7: E-cadherin, mucosal layer at UVJ region of the oviduct from a control bird.....	366
Fig. 5.8: E-cadherin, the <i>mucosa</i> at UVJ region: 5 and 32 days post-exposure.....	367
Fig. 5.9: Laminin, the mucosa at UVJ region from a control bird.....	369
Fig. 5.10: Laminin, the SST in the UVJ at days 5, 8 and 12 post-exposure.....	370
Fig. 5.11: Laminin, the mucosa at UVJ region: 32 days post-exposure.....	371
Fig. 5.12: Vimentin, the mucosa at UVJ region from a control bird.....	372
Fig. 5.13: SEM the mucosal surface in the UVJ region from a control bird.....	374
Fig. 5.14: SEM the mucosal surface at UVJ region: carbendazim 400mg/kg.....	375
Fig. 5.15: SEM the mucosal surface at UVJ region: 5 days post-exposure.....	376
Fig. 5.16: TEM the SST from a control bird.....	379
Fig. 5.17: TEM the apical regions of the SST cells from a control bird.....	380
Fig. 5.18: TEM the basal regions of the SST cells from a control bird.....	381
Fig. 5.19: TEM the SST from a bird treated with 400 mg/kg.....	382
Fig. 5.20: TEM apical regions of SST cells from a bird treated with 400 mg/kg.....	383

Fig. 5.21: TEM the SST from a bird treated with 800 mg/kg.....	384
Fig. 5.22: TEM the SST: 5 days post-exposure.....	387
Fig. 5.23: TEM the apical regions of SST cells: 5 days post-exposure.....	388
Fig. 5.24: TEM the SST: 8 days post-exposure.....	389
Fig. 5.25: TEM the apical regions of SST cells: 8 days post-exposure.....	390
Fig. 5.26: TEM the SST: 12 days post-exposure.....	391
Fig. 5.27: TEM the SST: 32 days post-exposure.....	392
Fig. 5.28: TEM the apical regions of the SST cells: 32 days post-exposure.....	393
Fig. 5.29: TEM degenerating SST cells: 32 days post-exposure.....	394
Fig. 5.30: TEM the basal regions of SST cells: 32 days post-exposure.....	395

LIST OF TABLES

Table 1.1: Periods of sample collection.....	19
Table 2.1: Oviduct parameters (mean \pm SE) in control and carbendazim-treated Japanese quails: experiment I.....	28
Table 2.2: Oviduct parameters (mean \pm SE) of Japanese quails following carbendazim treatment: experiment II.....	29
Table 2.3: Morphometric analysis (mean \pm SE) of funnel region of the infundibulum: experiment I.....	30
Table 2.4: Morphometric analysis (mean \pm SE) of funnel region of the infundibulum: experiment II.....	31
Table 2.5: Morphometric analysis (mean \pm SE) of the tubular region of the infundibulum: experiment I.....	32
Table 2.6: Morphometric analysis (mean \pm SE) of the tubular region of the infundibulum: experiment II.....	34
Table 2.7: PAS/Alcian blue staining intensity in the tubular region of the infundibulum: experiment I.....	51
Table 2.8: PAS/Alcian blue staining intensity in the tubular region of the infundibulum: experiment II.....	53
Table 2.9: Immunoreactivities for e-cadherin, laminin and vimentin in the infundibulum of the control and carbendazim-treated Japanese quails.....	60
Table 3.1: Histomorphometrical parameters (mean \pm SE) in the magnum: experiment I....	148
Table 3.2: Morphometric parameters (mean \pm SE) of the magnum: experiment II.....	149
Table 3.3a: PAS/Alcian blue staining intensity in the magnum: experiment I.....	167
Table 3.3b: PAS/Alcian blue staining intensity in the magnum: experiment II.....	170
Table 3.4: Immunohistochemical staining for e-cadherin, laminin and vimentin in the magnum of the control and carbendazim-treated birds.....	146
Table 4.1: Mean \pm SE of histomorphometrical parameters in the shell gland: experiment I..	255
Table 4.2: Mean \pm SE histomorphometrical parameters in the shell gland: experiment II...	257
Table 4.3a: PAS/Alcian blue staining intensity in the shell gland: experiment I.....	269
Table 4.3b: PAS/Alcian blue staining intensity in the shell gland: experiment II.....	272
Table 4.4a: Immunohistochemical parameters in the shell gland: experiment I.....	282
Table 4.4b: Immunohistochemical parameters in the shell gland: experiment II.....	283
Table 5.1: Mean \pm SE histomorphometrical parameters of the SST: experiment I.....	355
Table 5.2: Mean \pm SE morphometric parameters of the SST: experiment II.....	356

SUMMARY

Morphological study of the effect of the cytoskeletal disrupting agent carbendazim on the oviduct of the Japanese quail (*Coturnix coturnix japonica*)

By

WAHABU HAMISI KIMARO (BVM, MSc.)

Supervisor: Professor Mary-Cathrine Madekurozwa (BVSc., BSc (Hons), PhD).
Co-supervisor: Professor Herman Groenewald (BVSc., MSc., PhD).
Department: Anatomy and Physiology
Degree: PhD

Carbendazim (methyl-2-benzimidazole carbamate), a derivative of N-substituted esters of carbamic acid, is widely used as a fungicide on field crops. Carbendazim is of major concern to human and animal health due to the presence of its metabolites and residues in the environment. Several studies have shown the effect of carbendazim on the reproductive systems of male mammals and birds. Relatively little is known of the effect of carbendazim on the female reproductive tract. Therefore, this study was undertaken to establish the effect of carbendazim on the morphological, histochemical and immunohistochemical features of selected regions of the oviduct in the Japanese quail. The functional implication for each region was also considered.

A total of 102 sexually mature Japanese quails were used in this study. The study was divided into two experiments. In Experiment I, different doses of carbendazim, in a sunflower oil base, were administered orally to determine the minimum toxic dose which would cause degenerative lesions in the oviduct. The determined dose was used in the Experiment II to establish the time-course effects of carbendazim on the Japanese quail.

In Experiment I, 400 mg/kg bodyweight of carbendazim was the minimum toxic dose which caused both macroscopic and microscopic changes in the oviduct. The effect of carbendazim was dose dependent. In Experiment II, the effect of carbendazim was more pronounced with time lapse post-exposure. Macroscopically, increases in oviductal weight, luminal epithelial height and glandular diameter were observed in the initial stages post-exposure. Atrophy and a reduction in oviductal weight were observed in later stages.

Microscopically, carbendazim caused hyperaemia and oedema in all sections of the oviduct examined. Leukocytic infiltrations, pyknotic nuclei and cellular swelling were also observed. The histochemical results showed a reduction in PAS positive granules in the luminal and glandular epithelia of all oviductal sections. There were also decreases in the immunostaining intensities of E-cadherin, laminin and vimentin in all oviductal regions.

Scanning electron microscopic results showed a loss of cilia, as well as swollen microvilli. Short ciliary stems and shallow pits were also observed in areas exhibiting a loss of cilia.

At the ultrastructural level, luminal and glandular epithelia contained cells with degenerating nuclei and cytoplasmic organelles. The observed degenerative changes included pyknosis, karyorhexis, swollen mitochondria, dilated cisternae of rough endoplasmic reticulum, vacuolation and an increased number of lysosomes. Lipofuscin granules and filamentous aggregation were also observed. Compound cilia and myelin figures were frequently observed in the later stages of degeneration. Invagination and occasional duplication of the basal lamina, underlying both luminal and glandular epithelia, were also observed.

The observed degenerative changes suggested oviductal regression in carbendazim-treated birds. Degeneration of epithelial and glandular cells may lower the fertility and productivity of exposed birds.

CHAPTER ONE

GENERAL INTRODUCTION

1.1 Background information

The impact of environmental contaminants on the health of both humans and wildlife is of increasing concern. According to McLachlan (2001), environmental contaminants contain chemicals, which are known to have an adverse effect on endocrine function, thus leading to impaired reproductive performance. The report further stated that environmental contaminants have a direct toxic effect on sexual differentiation, growth and development.

Carbendazim (methyl-2-benzimidazole carbamate) and benomyl (methyl-1-butylcarbamoyl) are derivatives of the benzimidazole group of fungicides, which are N-substituted esters of carbamic acid (carbamate). Carbendazim can also be produced from benomyl by dissociation when dissolved in water. According to a report by the International Program on Chemical Safety (IPCS) of 1986, benomyl and carbendazim became commercially available in 1970. Since then, both chemicals (benomyl and carbendazim) have been widely used as fungicides and nematocides on fields of crops, as well as on post-harvest produce (Carter & Laskey 1982).

The mode of action of benomyl and its metabolite carbendazim has been well documented (Davidse 1973; Seiler 1975; Burland & Gull 1984). A report by Burland & Gull (1984) showed that carbendazim inhibits mitosis by binding β -tubulin subunits of microtubules. By binding to the β -tubulin, carbendazim and benomyl interrupt mitotic spindle formation and thus inhibit microtubule assembly. Seiler (1975) suggested that the chemical structure of benomyl could be the underlying factor in its ability to inhibit microtubule assembly. Benomyl has a benzimidazole ring, which is an analogue of purine. It interferes with DNA synthesis by inhibiting metabolic processes involving purine. In addition, benomyl contains a carbamate group, which is typically described as "spindle poison" (Davidse 1973). The adsorption of the carbamate side group interferes with the formation of a micro-fibrillar spindle apparatus, thus affecting microtubule assembly.

Studies on the biodegradation of benomyl and carbendazim have shown the presence of metabolite residues in plants (Still & Mansager 1975), soil (IPCS 1986), surface and ground water (IPCS 1986) and fruits (Pico, la Farre, Soler & Barcelo 2007). Although considered less toxic, the level of benomyl and carbendazim metabolites in food and potable water is increasing (Finnish National Board of Health, 1982). Due to the increasing levels of benomyl and carbendazim metabolites in the environment it is likely that aquatic and terrestrial organisms are being exposed to these chemicals.

Several studies have shown the effect of benomyl and its metabolite carbendazim on the male reproductive system in mammals and birds (Carter & Laskey 1982; Hess, Moore, Linder & Abuel-atta 1991; Lim & Miller 1997; Aire 2005). The reports show that these compounds cause both gross and histological testicular lesions. In the male rat, carbendazim was reported to disrupt spermatogenesis and cause an occlusion of efferent ducts in the testis (Hess *et al.* 1991; Nakai, Hess, Moore, Guttroff, Strader & Linder 1992; Nakai & Hess 1994; Hess & Nakai 2000). In the domestic fowl and the Japanese quail carbendazim caused germ cell degeneration, as well as the obstruction of efferent ducts (Aire 2005). According to Aire (2005), the effect of carbendazim on the testis is due to the disruption of microtubules and intermediate filaments in Sertoli cells.

In female mammals, carbendazim has been shown to stimulate aromatase production and activity (Morinaga Yanase, Nomura, Okabe, Goto, Harada & Nawata 2004). The high levels of aromatase (cytochrome P450 enzyme) increases the concentration of oestrogen in circulation by accelerating the conversion rate of androgen into oestrogen. High concentrations of oestrogen in the female reproductive system cause early depletion of ovarian follicles, formation of multi-ovular follicles and disrupt meiotic spindle organization (Sangvai, Thie & Hofmann 1997; Iguchi, Fukazawa & Uesugi 1990; Can and Semiz 2000). Although carbendazim has been shown to affect oogenesis in the female rat (Food and Agriculture Organization/World Health Organization, 1985), the effect of this chemical on the reproductive system of the female bird is still perplexing. This study therefore, was undertaken to establish the short-term and medium-term effects of the fungicide

carbendazim on the morphology of the female reproductive tract in the sexually mature Japanese quail.

1.2 GENERAL MATERIALS AND METHODS

1.2.1 Experimental animals and management

A total of 102 female Japanese quails were used in this study. The birds were purchased from Irene Animal Improvement Research Station, Pretoria. They were kept under a deep litter housing system in the avian facility of the Department of Anatomy and Physiology. Both males and females were housed together and allowed to breed freely. Food (growers mash) and water were provided *ad libitum*. Light was maintained at a ratio of 14:10 (light/darkness) throughout the experiment. The protocol of this study was approved by the Animal Use and Care Committee (AUCC) of the Faculty of Veterinary Science, University of Pretoria.

1.2.2 Experimental design

The study was divided into two experiments: I & II.

1.2.2.i Experiment I (dose-dependent oviductal degeneration)

A total of 30 sexually mature female Japanese quails were used in this study. The aim of this preliminary study was to determine the minimum effective dose of carbendazim, which causes an identifiable gross and/or histological lesion in the female reproductive tract of the Japanese quail. This dose was used in subsequent studies to determine the pathological effects of carbendazim on the female reproductive tract of the Japanese quail.

In this experiment, a single dose of carbendazim in a sunflower oil base was administered *per os*. The birds were divided into five dosage groups: 0 mg/kg bodyweight (control group); 25 mg/kg bodyweight; 100 mg/kg bodyweight; 400 mg/kg bodyweight and 800 mg/kg bodyweight. The control group received only the oil base. The birds were sacrificed 48 hours post-exposure to carbendazim.

1.2.2.ii Experiment II (time-course oviduct degeneration)

In experiment II, a single dose of the minimum effective dose of carbendazim (determined in experiment I) was administered to 36 birds in order to evaluate the short-term (up to 12 days) and medium-term (up to 32 days) effects of carbendazim on the oviduct of sexually mature Japanese quails. The control group (36 birds) received only the oil base. The effect of carbendazim on the gross morphological, morphometrical, histological, immunohistochemical and ultrastructural features of the oviduct was evaluated in a spatio-temporal period, as indicated in Table 1.1 below.

Table 1.1: Periods of sample collection

Dosage	400 mg/kg (As determined in experiment I)					
Duration	5h	24h	5d	8d	12d	32d
Treated group	6	6	6	6	6	6
Control group	6	6	6	6	6	6

In both experiments (I and II), the birds were sacrificed by inhalation anaesthesia with carbon dioxide after recording the live bodyweight. The thoraco-abdominal cavity was opened and the oviduct was collected immediately. The gross oviductal parameters detailed in Chapter Two were recorded. Thereafter, tissue samples from selected regions of the oviduct (infundibullum, magnum, shell gland and utero-vaginal junction) were fixed in 10% buffered formalin for further histological and immunohistochemical studies (Fig. 1.1). Additional tissues from each region of the oviduct were fixed in 2.5% glutaraldehyde buffered in a 0.1M Millonig's solution (pH 7.3) for transmission and scanning electron microscopic studies.

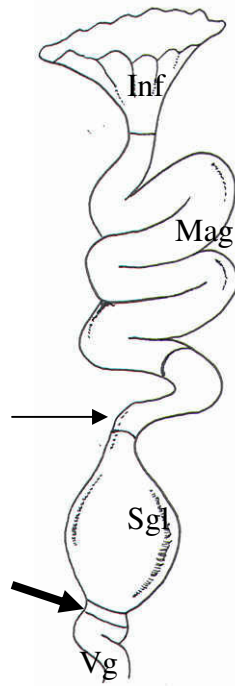


FIG.1.1. Schematic drawing of the avian oviduct showing infundibulum (Inf), magnum (Mag), isthmus (thin arrow) shell gland (Sgl), utero-vaginal junction (thick arrow) and vagina (Vg). (Adapted from Berg et al. 2001).

1.2.3 Experimental procedure

1.2.3.i Light microscopic observations and morphometry

Following fixation in 10% buffered formalin for 48 hours, tissue samples from the infundibulum, magnum, shell gland and utero-vaginal junction (UVJ) were processed using an automated tissue processor (Shandon excelsior, Thermo Electron Corporation, Germany). The processing involved dehydration in a series of alcohol concentrations (50%, 60%, 80% 95% to absolute alcohol), clearing in xylene (two changes), infiltration, as well as embedding using molten wax (Drury & Wallington 1976). Tissue sections (5 μ m thick) were mounted on glass slides and stained with haematoxylin and eosin (H&E) using an automated stainer (Shandon Veristain Germini, Thermo Electron Corporation, Germany). Other stains used included Periodic Acid Schiff (PAS) and Alcian blue.

Tissue sections were examined under a bright field light microscope at magnifications of X40 and/or X100. Epithelial height (simple columnar or cuboidal) was determined by measuring the height of 15 cells in five different primary folds

(Berg, Holm, Brandt & Brunström 2001). The height of pseudostratified epithelium was measured where up to five nuclei were cut at same level. The height of primary folds was measured by drawing a vertical line from the base to the luminal end of the fold (Fig. 1.2). Glandular width was measured by drawing a perpendicular line across the gland (Fig. 1.2). Glandular luminal diameter was determined by measuring the perpendicular distance between two opposing gland cells. All measurements were done using an image analyser (AnalySIS®; Olympus BX 50, Optical Company LTD, Japan). Photomicrographs were taken using a CC-12 digital camera mounted on the image analyser.

Morphometrical data were analysed using analysis of variance (ANOVA); SPSS version 17. A probability of 5% was considered significant.

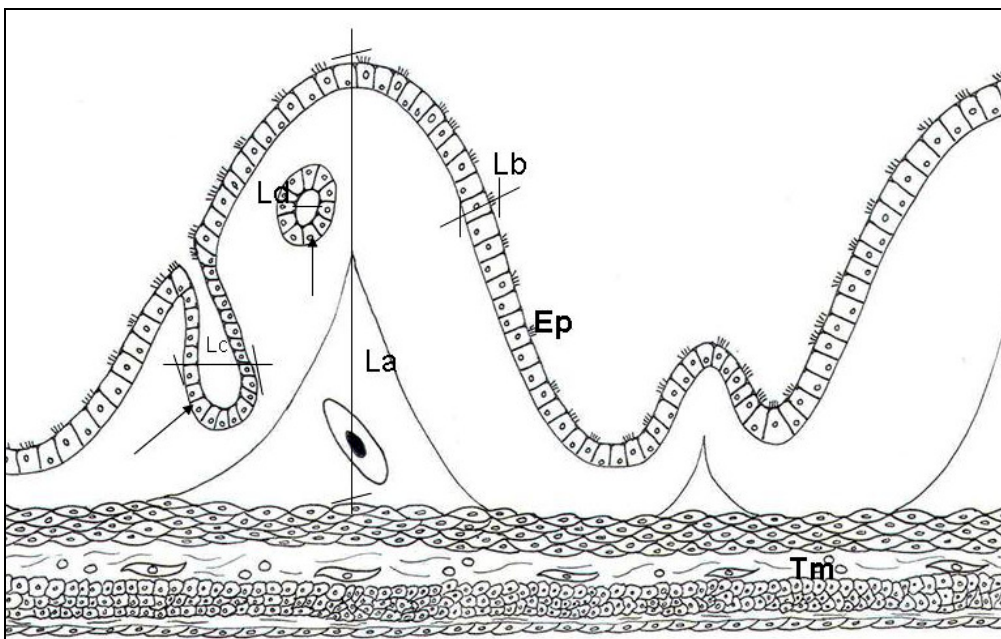


FIG. 1.2: Schematic drawing of the oviductal mucosa of the Japanese quail showing the luminal epithelium (Ep), tubular glands (arrows) and *tunica muscularis* (Tm). Mucosal fold height, luminal epithelium height and glandular width are shown by line La, Lb and Lc respectively. Glandular luminal diameter is indicated by Ld.

1.2.3.ii Immunohistochemistry

Immunohistochemical staining was performed on 5µm thick sections using a LSAB plus kit (Dakocytomation, Denmark). Tissue sections were deparaffinized and endogenous peroxidase activity was blocked with 3% (v/v) hydrogen peroxide in

water in a humidified chamber for 5 minutes. The sections were then rinsed in 0.01M phosphate buffer saline solution (PBS, pH 7.4) for 5 minutes. Thereafter, tissue sections were microwaved at 750 W for three cycles of 5 minutes each. After being allowed to cool for 20 minutes the sections were rinsed with PBS and then incubated for 1 hour at room temperature with the appropriate primary antibodies. The sections were then rinsed in PBS and incubated for 15 minutes with a ready-to-use biotinylated secondary antibody (LSAB-plus kit, Dakocytomation, Denmark). Thereafter, the sections were rinsed in PBS and subsequently incubated for 15 minutes with the streptavidin component of the LSAB-plus kit. After rinsing the sections in PBS, bound antibody was visualized following the addition of a 3,3'-diaminobenzidine tetrachloride solution (LSAB-plus kit, Dakocytomation, Denmark).

Commercially available antibodies against e-cadherin, laminin and vimentin (Dakocytomation, Denmark) were used at dilutions 1:100, 1:50 and 1:50 respectively.

1.2.3.iii Scanning electron microscopy

Tissue samples for scanning electron microscopic study were pinned onto dental wax strips, rinsed in 0.1M Millonig's buffer and fixed in buffered 2.5% glutaraldehyde. Post-fixation was done using 1% osmium tetroxide for 2 hours. After fixation the samples were rinsed in the same buffer, dehydrated in graded series of alcohol and dried with CO₂ in a critical-point chamber. Samples were viewed and photographed in a Philips XL20 scanning electron microscope.

1.2.3.iv Transmission electron microscopy

Tissue samples from the infundibulum, magnum, shell gland and utero-vaginal junction were post-fixed in 1% osmium tetroxide for 2 hours. Thereafter, tissue samples were rinsed in 0.1M Milonig's buffer, dehydrated in a series of alcohol concentrations and embedded in epoxy:resin at a ratio of 1:2 for 1 hour, 1:1 for 2 hours and 100% resin overnight. Semi-thin sections were cut using a glass knife and stained with toluidine blue. Ultra-thin sections were cut using a diamond knife, stained with lead acetate and counter stained by uranyl citrate. The samples were

viewed with a Philips CM10 transmission electron microscope (FEI, The Netherlands).

1.3 REFERENCES

- AIRE, T. A. 2005. Short-term effects of carbendazim on the gross and microscopic features of the testes of Japanese quails (*Coturnix coturnix japonica*). *Anatomy and Embryology*, 210:43-49.
- BERG, C., HOLM, L., BRANDT, I. & BRUNSTROM, B. 2001. Anatomical and histological changes in the oviducts of Japanese quail, *coturnix japonica*, after embryonic exposure to ethynylloestradiol. *Reproduction*, 121:155-165.
- BURLAND, T.G. & GULL, K. 1984. Molecular and cellular aspects of the interaction of benzimidazole fungicides with tubulin and microtubules, in *Mode of action of antifungal agent*, edited by A.P.J. Trinci & J.F. Riley, Cambridge University Press. pp. 299 - 320.
- CAN, A. & SEMIZ, O. 2000. Diethylstilbestrol (DES)- induced cell cycle delay and meiotic spindle disruption in mouse oocytes during in-vitro maturation. *Molecular Human Reproduction*, 6:154-162.
- CARTER, S. D. & LASKEY, J. W. 1982. Effect of benomyl on reproduction in the male rat. *Toxicology Letters*, 11:87-94.
- DAVIDSE, L.C. 1973. Antimitotic activity of methyl benzimidazole-2-yl carbamate (MBC) in *Aspergillus nidulans*. *Pest Biochemistry and Physiology*, 3:317-325.
- DRURY, R.A.B. & WALLINGTON, E.A. 1976. *Carleton's Histological Techniques* (4th ed.). London: Oxford University Press. pp. 21–70.
- FINNISH NATIONAL BOARD OF HEALTH, 1982. The toxicity of the benzimidazole type fungicides: benomyl, carbendazim and thiophanate-methyl. *Second report*, Helsinki.
- FOOD AND AGRICULTURE ORGANIZATION/WORLD HEALTH ORGANIZATION, 1985. Pesticide residues in food: Report of the 1984 joint meeting of the FAO working party of experts on pesticide residues and the WHO expert group on pesticide residues. *FAO Plant Production and Protection*, Paper 62.
- HESS, R. A., MOORE, B. J., LINDER, R. E. & ABUEL-ATTA, A. A. 1991. The fungicide benomyl (methyl-1-(butylcarbamate)-2-benzimidazolecarbamate) causes testicular dysfunction by inducing sloughing of germ cells and occlusion of efferent ductules. *Fundamentals of Applied Toxicology*, 17:733-745.

- HESS, R. A. & NAKAI, M. 2000. Histopathology of the male reproductive system induced by the fungicide benomyl. *Histology and Histopathology*, 15:207-224.
- IGUCHI, T., FUKAZAWA, Y. & UESUGI, Y. 1990. Polyovular follicles in mouse ovaries exposed neonatally to diethylstilbestrol in vivo and in vitro. *Biology of Reproduction*, 43:478-484.
- INTERNATIONAL PROGRAM ON CHEMICAL SAFETY, 1986. Environmental health criteria for carbamate pesticides: A general introduction , 64.(www.inchem.org).
- LIM, J. & MILLER, M. G. 1997. The role of the benomyl metabolite carbendazim in benomyl-induced testicular toxicity. *Toxicology and Applied Pharmacology*, 142:401-410.
- McLACHLAN, J. A. 2001. Environmental signaling: what embryos and evolution teach us about endocrine disrupting chemicals. *Endocrine Reviews*, 22:319-341.
- MORINAGA, H., YANASE, T., NOMURA, M., OKABE, T., GOTO, K., HARADA, N. & NAWATA, H. 2004. A benzimidazole fungicide, benomyl and its metabolite carbendazim induce aromatase activity in human ovarian granulosa-like tumor cell line (KGN). *Endocrinology*, 145:1860-1869.
- NAKAI, M. & HESS, R. A. 1994. Morphological changes in the rat Sertoli cell induced by the microtubule poison carbendazim. *Tissue and Cell*, 26:917-927.
- NAKAI, M., HESS, R. A., MOORE, B. J., GUTTROFF, R. F., STRADER, L. F. & LINDER, R. E. 1992. Acute and long-term effects of a single dose of the fungicide carbendazim (methyl-2-benzimidazole carbamate) on the male reproductive system in the rat. *Journal of Endocrinology*, 13:507-518.
- PICO, Y., LA FARRE, M., SOLER, C. & BARCELO, D. 2007. Identification of unknown pesticides in fruits using ultra-performance liquid chromatography-quadrupole time-of-flight mass spectrometry Imazilil as a case study of quantification. *Journal of chromatography*, 1176:123-134.
- SANGVAI, M., THIE, J. & HOFMANN, G. E. 1997. The effect of intrauterine diethylstilbestrol exposure on ovarian reserve screening. *American Journal of Obstetrics and Gynaecology*, 177:568-572.
- SEILER, J. P. 1975. Toxicology and genetic effects of benzimidazole compounds. *Mutation Research*, 32:151-168.
- STILL, G. G. & MANSAGER, E. R. 1975. Alfalfa metabolism of propham. *Pesticide Biochemical Physiology*, 5:515-522.

CHAPTER TWO

The effect of carbendazim on the structure of the infundibulum in the sexually mature Japanese quail: gross, histological, immunohistochemical and ultrastructural studies

2.1. Introduction

The infundibulum is the most proximal region of the avian oviduct. It is conveniently divided into two parts: a proximal funnel region and a distal tubular region. The wall of the infundibulum is composed of a *tunica mucosa*, *tela submucosa*, *tunica muscularis* and *tunica serosa* (Baumel, King, Breazile, Evans & Vanden Berge 1993). The mucosal and submucosal layers are arranged in longitudinal folds, which are lined by simple columnar epithelium. The epithelium consists of ciliated and non-ciliated cells (Wyburn, Johnston, Draper & Davidson 1970). The presence of a ciliated epithelium lining the infundibulum facilitates the distal movement of the oocyte. Although occasional non-ciliated (granular) cells have been reported in the infundibular lining of domestic fowl (Aitken & Johnson, 1963), ciliated cells are the predominant cell type in this oviductal region (Wyburn *et al.* 1970; Gilbert 1979). The tubular region of the infundibulum appears thick due to the enlargement of the mucosal, submucosal and muscular layers. The tubular region in the Japanese quail contains tubular glands, which extend from the luminal epithelium into the underlying *lamina propria-submucosa* (Fitzgerald 1969). Similar tubular glands have been observed in the domestic fowl (Aitken & Johnson 1963; Wyburn *et al.* 1970).

Studies in the domestic fowl (Aitken & Johnson 1963; Wyburn, *et al.* 1970; Aitken, 1971; Chousalkar & Roberts, 2008) and Japanese quail (Rahman, Iwasawa & Yoshizaki 2007) have shown that the infundibulum plays an important role in the process of egg formation. During egg formation, the ovulated oocyte is received by the dilated funnel region of the infundibulum. As the oocyte descends distally, fertilization occurs in the tubular region of the infundibulum (Okamura & Nishiyama 1978). The tubular region of the infundibulum contains glandular grooves (*Fossae glandulares infundibuli*) which are thought to be sperm storage tubules (Tingari &

lake 1973). In addition, secretory cells in the luminal and glandular epithelia are known to produce the chalazae of the developing egg (Rahman *et al.* 2007).

As mentioned in the introduction, the function of a tissue depends on its cellular composition. The cytoskeleton plays a major role in maintaining cellular structure and function (Helfand, Mendez, Pugh, Delsert & Goldman 2003). Disruption of the cytoskeleton may impact on cellular structure and subsequently tissue or organ function. Carbendazim, a cytoskeletal disrupting agent, has been reported to cause testicular injury in the Japanese quail (Aire 2005). There is currently a paucity of information on the effect of carbendazim on the morphology of the oviduct in the female Japanese quail. Therefore, in this Chapter, the gross anatomical, immunohistochemical and ultrastructural effects of carbendazim on the infundibulum in the Japanese quail are reported.

2.2. Materials and methods

A total of 102 sexually mature female Japanese quails were used in this study. The study was divided into two experiments as described in Chapter One.

2.2.i. Gross observation and morphometry of the entire oviduct

After opening the thoraco-abdominal cavity, an *in situ* visual assessment of the oviduct was made. Gross morphometric parameters, such as, the weight and length of the oviduct were recorded. The group average for the morphometric data was subsequently calculated. Relative oviductal weight (%) was calculated as: (weight of oviduct/bodyweight) x 100. Differences in oviductal parameters were analysed statistically using Analysis of Variance (ANOVA); SPSS version 17.

2.2.ii. Histology

Tissue samples from both the funnel and tubular regions of the infundibulum were fixed in 10% buffered neutral formalin for 48 hours. Thereafter, the tissue samples were processed routinely for light microscopy, following the standard procedures described in Chapter One.

2.2.iii. Immunohistochemistry

Formalin-fixed sections of the tubular region of the infundibulum were used in the current study. The tubular region was selected for Immunohistochemical study because it contains secretory cells which are known to produce chalazae of an egg. The tissue sections were processed and immunostained using a LSAB plus kit (Dakocytomation, Denmark) following the standard technique described in Chapter one. Antibodies against e-cadherin (1:100), laminin (1:50) and vimentin (1:50) were used.

2.2.iv. Transmission and Scanning electron microscopy

Tissue samples from the funnel and tubular regions of the infundibulum were immersion-fixed in 2.5% glutaraldehyde in 0.1M Millonig's buffer (pH 7.3) for 24 hours. Thereafter, the tissue samples were post-fixed in 2% osmium tetroxide. Following post-fixation, the samples were processed for transmission electron microscopy (TEM) and scanning electron microscopy (SEM) using standard techniques.

2.3. Results

2.3.1. Gross observations

2.3.1.i. Control birds

The oviduct in the control Japanese quails was observed lying on the ventral surface of the left kidney. The oviduct occupied the left thoraco-abdominal cavity with little extension to the right (Fig. 2.1). The oviduct was pinkish-brown in colour, with the magnum appearing paler than the rest of the tract. The oviduct was well-vascularized. The weight of the oviduct ranged from 5g to 13g (mean \pm SE; 6.8 ± 0.4 g). The oviduct length was between 20cm and 33cm (mean \pm SE; 27 ± 1.6 cm). These parameters are shown in Table 2.1 below.

2.3.1.ii. Carbendazim-treated birds

2.3.1.ii.a Experiment I (Dose-dependent oviductal degeneration)

The location of the oviduct in carbendazim-treated birds was similar to the control birds. Congestion was a notable feature in the oviduct of carbendazim-treated birds. Table 2.1 summarizes the measured oviductal parameters of control birds, as well as, carbendazim-treated birds fed different doses of the fungicide. The Table shows a slight increase in oviduct weight at doses of 25 mg/kg and 400 mg/kg bodyweight carbendazim when compared to the control group. At 800 mg/kg bodyweight carbendazim, there was a decrease in oviduct weight. However, the observed increase and decrease in oviduct weight were not statistically significant ($p < 0.05$). Similarly, no significant change was observed in oviduct length ($p < 0.05$) 48 hours post-exposure to any dose of carbendazim used. A slight decrease in oviduct length was observed in the 100 mg/kg, 400 mg/kg and 800 mg/kg bodyweight carbendazim-treated groups.

Table 2.1: Oviduct parameters (mean \pm SE) in control and carbendazim-treated Japanese quails

Treatment groups	Absolute oviduct weight (g)	Relative oviduct weight (%)	Oviduct length (cm)
0 mg/kg	6.81 \pm 0.38	4.15	27.63 \pm 1.59
25 mg/kg	9.9 \pm 1.17	5.57	29.17 \pm 2.77
100 mg/kg	6.33 \pm 0.9	3.84	24.88 \pm 3.73
400 mg/kg	7.87 \pm 1.42	4.39	23.63 \pm 1.43
800 mg/kg	6.01 \pm 0.44	3.86	25.13 \pm 0.52

2.3.1.ii.b Experiment II (Time-course oviductal degeneration).

Table 2.2 summarizes oviductal parameters of control and carbendazim-treated birds, recorded at different time intervals post-exposure to 400 mg/kg bodyweight carbendazim. There was a general increase in weight of the oviduct from 5 hours to 8 days post-exposure to carbendazim (Fig. 2.2). The increase in oviduct weight was statistically significant ($p < 0.05$). Beyond 8 days post-exposure to carbendazim,

there was a decrease in oviduct weight. A significant decrease in oviduct weight ($p < 0.05$) was observed at day 32 post-exposure to 400 mg/kg bodyweight carbendazim. Similarly, oviduct length was also affected by carbendazim exposure. The decrease in oviduct length was significant at day 32 when compared to the control group ($p < 0.05$) as well as the day 8 treatment group.

Table 2.2: Oviduct parameters (mean \pm SE) of Japanese quails following oral administration of 400 mg/kg bodyweight carbendazim

Periods post administration	Absolute oviduct weight (g)	Relative oviduct weight (%)	Oviduct length (cm)
Control	6.68 \pm 0.25	3.67	31.66 \pm 1.24
5 hours	6.66 \pm 0.37*	3.95*	25.0 \pm 2.58*
24 hours	6.49 \pm 0.69	3.88	26.7 \pm 1.97
5 days	7.27 \pm 0.2	4.03	29.3 \pm 0.64
8 days	9.78 \pm 1.13* ^a	5.30* ^a	31.1 \pm 1.1*
12 days	7.73 \pm 0.24	4.43	29.2 \pm 0.9
32 days	3.21 \pm 1.47* ^a	2.06* ^a	24.33 \pm 3.06* ^a

^a Mean value differs significantly from the control ($P < 0.05$).

* Indicates significant change of the mean value between observation periods post-exposure to carbendazim ($p < 0.05$).

2.3.2 Tissue morphometry

2.3.2.1 Funnel region

2.3.2.1.i Control birds

Table 2.3 summarizes morphometric parameters measured in control and carbendazim-treated birds. The primary folds measured between 24.33 and 121.14 μm in height. The luminal epithelium ranged from 6.33 to 19.43 μm in height.

2.3.2.1.ii Carbendazim treated birds

2.3.2.1.ii.a Experiment I

This experiment aimed to establish the minimum effective dose that would cause pathological changes within 48 hours of various doses of carbendazim.

There was slight decrease in the luminal epithelial height in carbendazim-treated birds in the funnel region of the infundibulum. However, this decrease of epithelial height was not statistically significant ($P < 0.05$). In addition, no significant morphometric changes were observed in the height of mucosal folds of in the funnel region of the infundibulum.

Table 2.3: Morphometric analysis (mean \pm SE) of the infundibulum (funnel region) in control and carbendazim-treated Japanese quails

Dosage (mg/kg)	1 ^o fold height (μm)	Epithelial height (μm)
0	62.47 \pm 4.2	11.6 \pm 0.15
25	49.95 \pm 4.82	9.18 \pm 0.09
100	52.37 \pm 3.9	10.13 \pm 0.1
400	45.04 \pm 5.88	11.09 \pm 0.66
800	61.21 \pm 8.34	8.08 \pm 0.14

2.3.2.1.ii.b. Experiment II (Time-course oviductal degeneration)

Experiment II investigated the short-term (5 hours to 12 days post-exposure) and medium-term (32 days post-exposure) effects of carbendazim on the oviduct in the Japanese quail. A single dose of the minimum effective dose (400 mg/kg body weight carbendazim), determined in experiment I was used.

The measured morphometric parameters are summarized in Table 2.4. Carbendazim caused a decrease in the height of primary mucosal folds in the funnel region of the infundibulum. The decrease was statistically significant at days 8, 12 and 32 in the funnel region when compared to the control ($P < 0.05$). Within the treatment groups,

carbendazim caused a significant decrease in the height of primary mucosal folds between 5 hours and 8 days; 5 hours and 12 days, as well as 5 hours and 32 days in the funnel infundibular region. Epithelial height in the funnel region of the infundibulum was generally unchanged.

Table 2.4: Morphometric analysis of infundibulum (mean \pm SE) following exposure to 400 mg/kg carbendazim

Periods post-exposure	1 ^o fold height (μm)	Epithelial height (μm)
Control	62.47 \pm 4.2 ^a	11.6 \pm 0.15
5 hours	36.92 \pm 1.94*	9.64 \pm 0.17
24hours	26.48 \pm 1.89	9.79 \pm 0.15
5 days	28.4 \pm 2.13	10.31 \pm 0.14
8days	20.82 \pm 2.17 ^{a*}	10.35 \pm 0.14
12 days	24.67 \pm 1.89 ^{a*}	11.12 \pm 0.69
32 days	26.96 \pm 2.32 ^{a*}	10.01 \pm 0.14

^a Indicates a significant change between control and treatment group.

* Indicate a significant change within periods post exposure to carbendazim.

2.3.2.2 Tubular region

2.3.2.2.i Control birds

Table 2.5 summarizes morphometric parameters measured in control and carbendazim-treated birds. The primary folds measured between 37.14 and 438.46 μm in height. The epithelium measured between 10.19 and 47.02 μm (mean 20.11 \pm 0.79 μm) in height. The tubular glands measured between 2.58 and 23.49 μm in width, with a luminal diameter of between 0.54 and 7.22 μm .

2.3.2.2.ii Carbendazim-treated birds

2.3.2.2.ii.a. Experiment I (Dose-dependent oviductal degeneration)

There was a slight decrease in luminal epithelial height in the tubular region of the infundibulum in carbendazim-treated quails. This decrease was not statistically significant ($p < 0.05$). When compared to the control group, a significant increase in the height of mucosal folds was observed at doses of 400 mg/kg and 800 mg/kg bodyweight carbendazim. Furthermore, a significant increase in the height of mucosal folds in this region was observed within the treatment groups, for example: between 100mg/kg and 400mg/kg bodyweight; 100 mg/kg and 800mg/kg bodyweight, as well as between 400 mg/kg and 800 mg/kg bodyweight of carbendazim.

Administration of carbendazim caused a dose-dependent decrease in glandular width. However, the observed decrease in glandular width was not statistically significant ($p < 0.05$). Consistent with a decrease in glandular width, the glandular luminal diameters also decreased. The decrease in luminal diameter was statistically significant between control and carbendazim treatments, as well as within treatments ($p < 0.05$).

Table 2.5: Morphometric analysis (mean \pm SE) of the tubular region of the infundibulum in control and carbendazim-treated Japanese quails

Dosage (mg/kg)	1 ^o fold height (μ m)	Epithelial height (μ m)	Gland width (μ m)	Luminal diameter (μ m)
0	135.76 \pm 15.57	20.11 \pm 0.79	9.4 \pm 0.63	2.77 \pm 0.22
25	123.08 \pm 37	17.93 \pm 0.31	9.01 \pm 1.3	2.73 \pm 0.32*
100	97.88 \pm 19.98*	16.61 \pm 0.31	9.76 \pm 0.63	2.91 \pm 0.39 ^{a*}
400	193.72 \pm 39.28 ^{a*}	29.16 \pm 2.24	6.31 \pm 0.29	1.17 \pm 0.12 ^{a*}
800	177.33 \pm 28.69 ^{a*}	16.91 \pm 0.24	5.75 \pm 0.24	0.87 \pm 0.06 ^{a*}

^a Indicates a significant change between control and treatment groups.

* Indicate a significant change within treatment doses of carbendazim.

2.3.2.2.iib. *Experiment II (Time-course oviductal degeneration)*

The measured morphometric parameters are summarized in Table 2.6. There was a general increase in epithelial height, in the tubular region of the infundibulum from 5 hours to 32 days post-exposure. The increase in epithelial height was statistically significant at 24 hours, 5 days, 12 days, as well as 32 days post-exposure to carbendazim, when compared to the control group. In addition, the increase in epithelial height was statistically significant ($p < 0.05$) within the periods post-exposure to carbendazim, that is: between 5 hours and 5 days; 5 hours and 12 days, as well as 5 hours and 32 days.

There was a statistically significant decrease in the height of primary mucosal folds in the tubular region at 24 hours, 5 days, 8 days and 32 days when compared to the control. Within the treatment groups, there was a significant decrease in the height of primary folds between 5 hours and 24 hours, 5 hours and 5 days, and between 5 hours and 32 days.

A decrease in the width of the tubular glands was observed in the tubular region of the infundibulum. However, the observed decrease in glandular width was not statistically significant. In contrast, there was a statistically significant decrease in glandular luminal diameter at day 8 and day 12 post-exposure ($p < 0.05$). At day 32 post-exposure to carbendazim there was an increase in luminal diameter. However, the observed increase in the luminal diameter was not statistically significant ($p < 0.05$).

Table 2.6: Morphometric analysis of the tubular region of the infundibulum (mean \pm SE) following exposure to 400 mg/kg bodyweight carbendazim

Periods post-exposure	1 ^o fold height (μ m)	Epithelial height (μ m)	Gland width (μ m)	Luminal diameter (μ m)
Control	135.76 \pm 15.57	20.11 \pm 0.79	9.39 \pm 0.63	2.77 \pm 0.22
5 hours	99.07 \pm 5.66*	22.64 \pm 0.44*	6.14 \pm 0.22	1.2 \pm 0.07*
24hours	41.03 \pm 7.67 ^{a*}	28.32 \pm 1.77 ^a	6.6 \pm 0.31	1.45 \pm 0.16
5 days	35.31 \pm 3.64 ^{a*}	48.71 \pm 1.37 ^{a*}	4.49 \pm 0.19	1.04 \pm 0.09
8days	71.53 \pm 13.18 ^a	21.23 \pm 0.42	3.06 \pm 0.16	0.95 \pm 0.09 ^{a*}
12 days	98.17 \pm 11.15	25.63 \pm 0.65 ^{a*}	3.13 \pm 0.11	0.71 \pm 0.06 ^{a*}
32 days	64.25 \pm 7.58 ^{a*}	34.27 \pm 1.34 ^{a*}	5.84 \pm 0.26	3.69 \pm 0.39

^a Indicates a significant change between control and treatment group.

* Indicate a significant change within periods post exposure to carbendazim.

2.3.3 Histological observations

2.3.3.1 Funnel region

2.3.3.1.i Control birds

In the funnel region, primary and occasional secondary folds were identified (Fig. 2.3a). The folds were lined by a ciliated simple columnar epithelium (Fig. 2.3a). A round to oval nucleus was located either centrally or apically in the cell. In the crypts of the mucosal folds, simple cuboidal cells were observed (Fig. 2.3b).

The *lamina propria-submucosa* was composed of loose connective tissue, a few blood vessels and scattered lymphocytes. The *tunica muscularis* was thin, with ill-defined inner circular and outer longitudinal layers. The *tunica serosa* enclosed the infundibulum. The layer contained loose connective tissue fibres and a few fibrocytes. A simple squamous epithelium (mesothelium) lined the serosa.

2.3.3.1.ii Carbendazim-treated birds

2.3.3.1.ii.a. *Experiment I (Dose-dependent oviductal degeneration)*

This experiment aimed to establish the minimum effective dose that would cause pathological changes within 48 hours of various doses of carbendazim.

No histological degenerative change was observed in the infundibulum 48 hours post-exposure to 25 mg/kg and 100 mg/kg bodyweight carbendazim. At a dose of 400mg/kg body weight carbendazim, the surface epithelium contained cells with pyknotic nuclei, cytoplasmic pallor and vacuoles (Fig. 2.4 a & b). Hyperaemia and leukocytic infiltrations were observed in the *lamina propria-submucosa*.

At a dose of 800 mg/kg body weight carbendazim, hyperaemia and leukocytic infiltrations were still the predominant degenerative changes observed (Fig. 2.5). At this dose, aggregates of inflammatory cells were evident in the *lamina propria-submucosa* and around blood vessels in the vascular zone between the two layers of the *tunica muscularis* (Fig. 2.5).

2.3.3.1.ii.b. *Experiment II (Time-course oviductal degeneration)*

Experiment II investigated the short-term (5 hours to 12 days post-exposure) and medium-term (32 days post-exposure) effects of carbendazim on the oviduct in the Japanese quail. A single dose of the minimum effective dose (400 mg/kg body weight carbendazim), determined in experiment I was used.

5 and 24 hours post-exposure

No degenerative changes were observed in the mucosal layer of the funnel region of the infundibulum, 5 and 24 hours post-exposure to 400 mg/kg bodyweight carbendazim.

5, 8 and 12 days post-exposure

At 5 and 8 days post-exposure, a few degenerating luminal epithelial cells contained pyknotic nuclei and exhibited pallor cytoplasm (Fig. 2.6 a & b). Leukocytic infiltrations and hyperaemia were evident in the *lamina propria-submucosa*.

32 days post-exposure

At day 32 post-exposure to carbendazim, no light morphological changes were seen in the mucosal layer of the funnel region of the infundibulum.

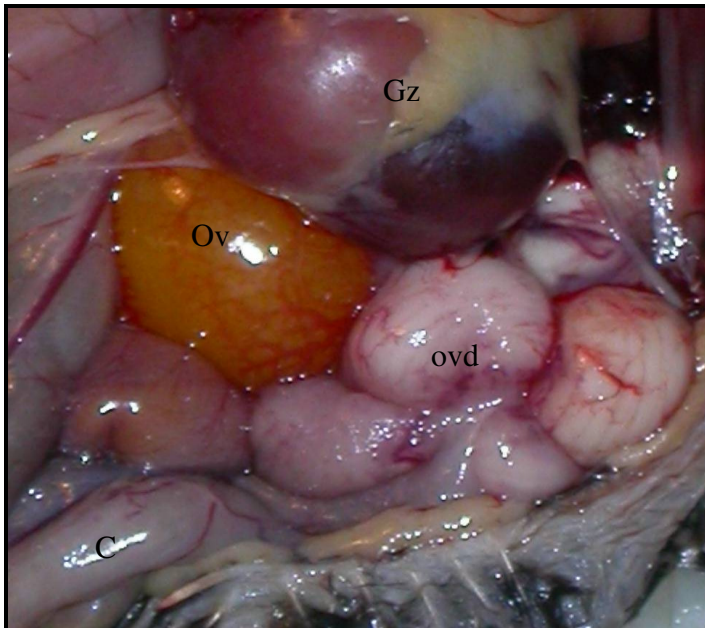


Fig 2.1: A photograph from a control bird showing Japanese quail reproductive organs *in situ*. The oviduct (ovd) occupies a large part of the thoraco-abdominal cavity. Ov: ovarian follicle; Gz: gizzard; C: colon.

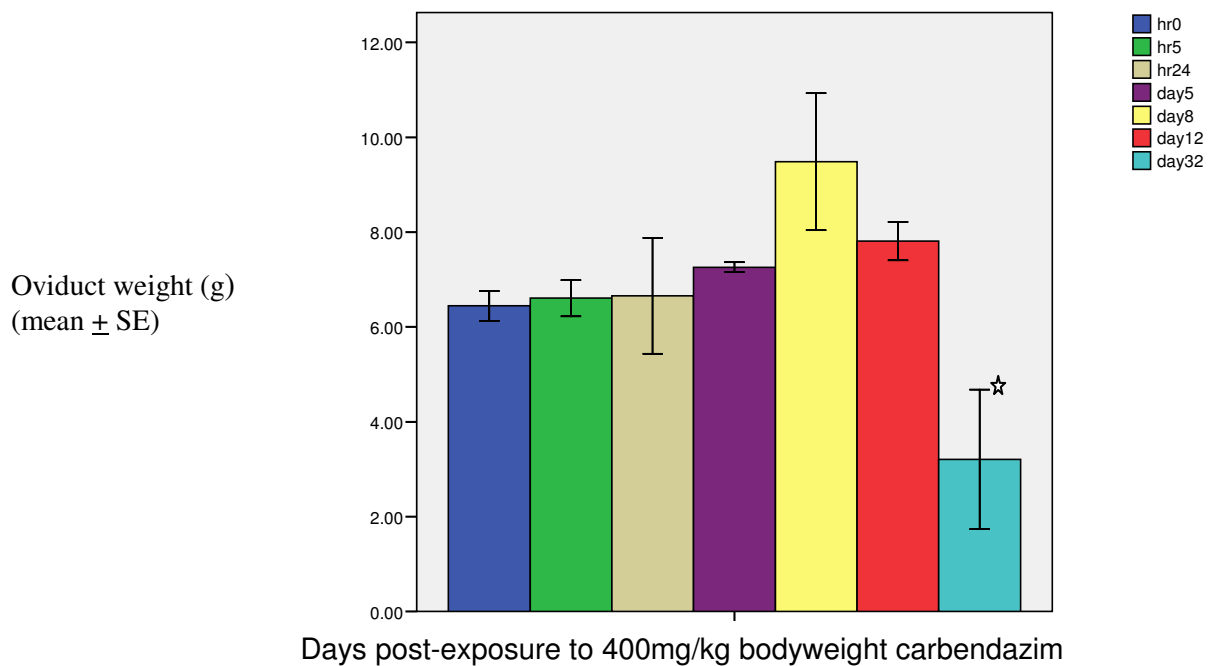


Fig. 2.2: Histogram showing mean oviduct weight recorded at different time periods post-exposure to 400 mg/kg bodyweight carbendazim. Note an increase in weight from 5 hours to 8 days. A significant decrease is seen on day 32 (asterisk).



Fig. 2.3: Light microscopic photomicrographs of the infundibulum (funnel region) from a control bird. **a.** The *tunica mucosa* is thrown into primary (Pr) and occasional secondary (Sc) folds. A few blood vessels (thin arrows) are seen in the *lamina propria-submucosa*. The *tunica muscularis* (asterisk) contains ill-defined inner circular and outer longitudinal layers. A *tunica serosa* (thick arrow) encloses the infundibulum. L: lumen. **b.** A higher magnification photomicrograph of the infundibular funnel region. The epithelium contains simple ciliated columnar cells (arrow). Cuboidal cells (arrowhead) line the base of the fold.

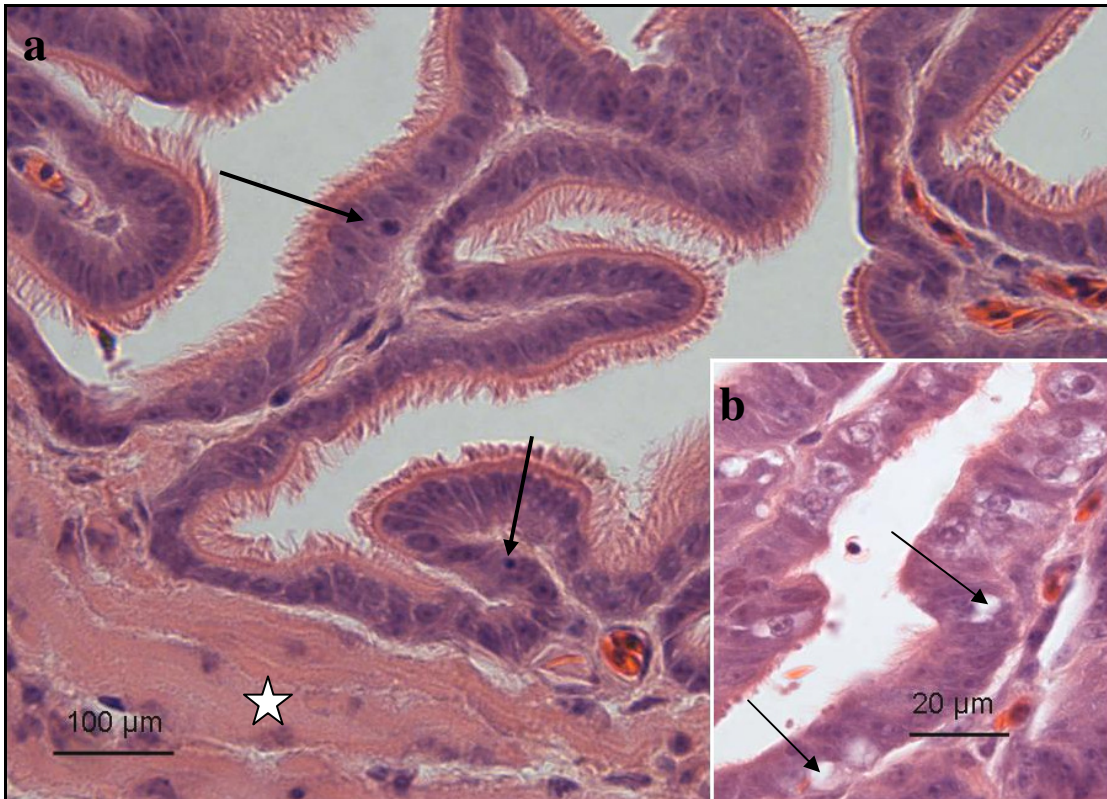


Fig. 2.4: Light microscopic photomicrograph of the funnel region of the infundibulum from a bird treated with 400 mg/kg bodyweight carbendazim. **a.** Cells with pyknotic nuclei (arrows) are observed in the luminal epithelium. Asterisk: *tunica muscularis*. **b.** A higher magnification photomicrograph of the luminal epithelium in the funnel region. Note the presence of vacuolated degenerating cells (arrows) in the luminal epithelium.

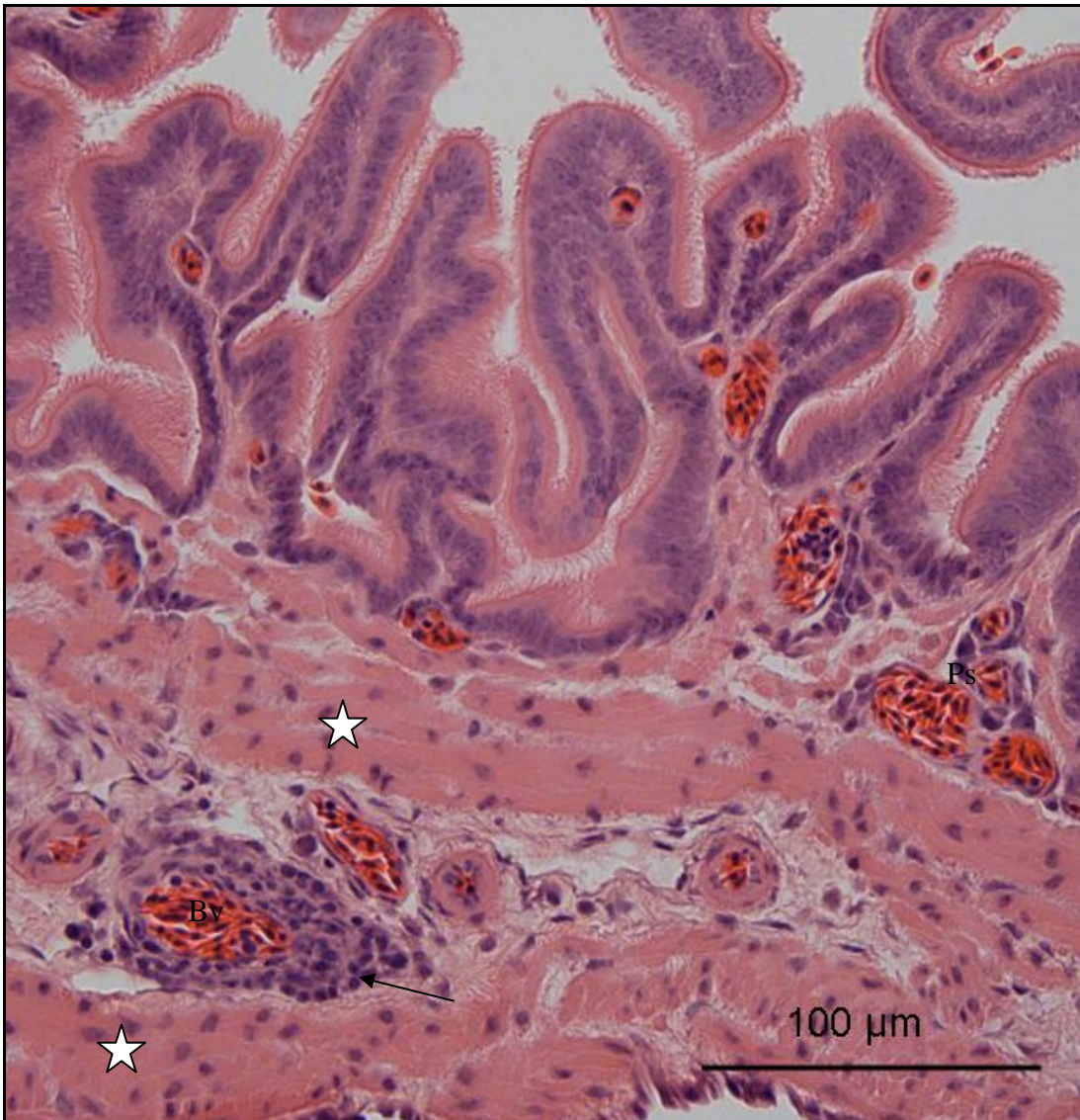


Fig. 2.5: Light microscopic photomicrograph of the funnel region of the infundibulum from a bird exposed to 800 mg/kg bodyweight carbendazim. Hyperaemia is evident in the *lamina propria-submucosa* (Ps). Note the aggregation of inflammatory cells (arrow) around a blood vessel (Bv) in the vascular zone between two layers of *tunica muscularis* (asterisks).

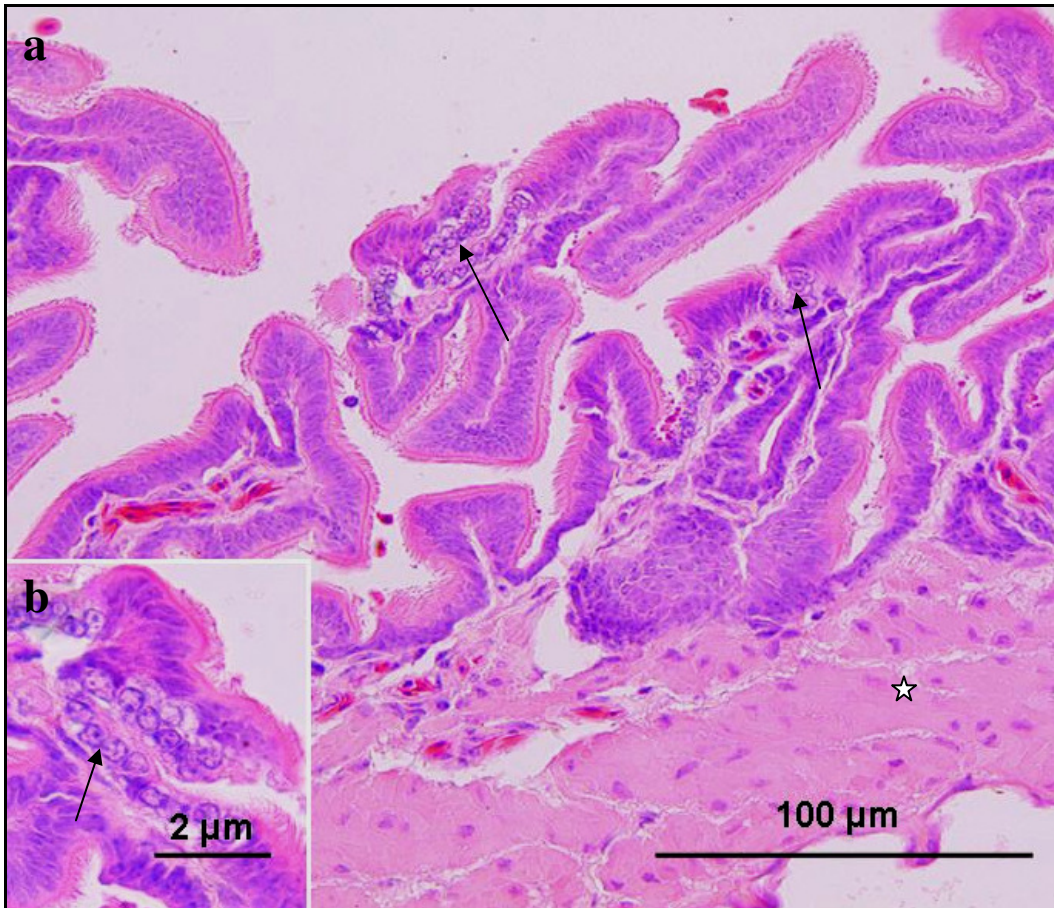


Fig. 2.6: Light microscopic photomicrographs of the funnel region of the infundibulum, 5 days post-exposure to 400 mg/kg bodyweight carbendazim. **a.** Cells with pale cytoplasm (arrows) are observed in the epithelium. Asterisk: *tunica muscularis*. **b.** A higher magnification photomicrograph of degenerating epithelial cells displaying cytoplasmic pallor (arrow).

2.3.3.2 Tubular region

2.3.3.2.i Control birds

In the tubular region of the infundibulum, both primary and secondary mucosal folds were observed (Fig. 2.7a). The luminal epithelium was ciliated simple columnar (Fig. 2.7a). A few non-ciliated (granular) cells were also observed in the epithelium. Ciliated columnar cells were observed in the crypts of the mucosal folds.

Underlying the epithelium was the *lamina propria-submucosa*. In addition to the presence of loose connective tissue, blood vessels and scattered lymphocytes, numerous tubular glands (*glandulae tubi infundibularis*) were observed in this region

(Fig. 2.7b). The tubular glands were lined by a simple cuboidal epithelium (Fig. 2.7b inset).

The muscular layer (*tunica muscularis*) was composed of inner circular and outer longitudinal layers of smooth muscle cells (Fig. 2.7 a & b). A few blood vessels were observed in the vascular zone between the muscle layers. A *tunica serosa* formed by loose connective tissue fibres enclosed the infundibulum. A simple squamous epithelium (mesothelium) lined the serosa.

2.3.3.2.ii Carbendazim-treated birds

2.3.3.2.ii.a. *Experiment I (Dose-dependent oviductal degeneration)*

No histological degenerative change was observed in the tubular region of the infundibulum 48 hours post-exposure to 25 mg/kg and 100 mg/kg bodyweight carbendazim. At a dose of 400mg/kg bodyweight carbendazim, the surface epithelium contained cells with pyknotic nuclei, cytoplasmic pallor and vacuoles (Fig. 2.8a). No histological changes were observed in the glandular epithelium. Hyperaemia and leukocytic infiltrations were observed in the *lamina propria-submucosa* (Fig. 2.8b). The aggregates of inflammatory cells were observed around blood vessels in the *lamina propria-submucosa* (Fig. 2.8c) as well as in the vascular zone between the *tunica muscularis*.

At a dose of 800 mg/kg bodyweight carbendazim, hyperaemia and leukocytic infiltrations were still the predominant degenerative changes observed. At this dose, aggregates of inflammatory cells were evident in the *lamina propria-submucosa* and around blood vessels in the vascular zone between the two layers of the *tunica muscularis*.

2.3.3.2.ii.b. *Experiment II (Time-course oviductal degeneration)*

No histological degenerative changes were observed in the tubular region of the infundibulum 5 and 24 hours post-exposure to 400 mg/kg bodyweight carbendazim.

5 days post-exposure

Histological degenerative changes in the tubular region of the infundibulum were observed at 5 days post-exposure to carbendazim. Hyperaemia was observed in the *lamina propria-submucosa*, as well as in the vascular zone associated with the *tunica muscularis*. Leukocytic infiltrations were also evident in the *lamina propria-submucosa* (Fig. 2.9a). In this region, cells with pyknotic nuclei were observed in the luminal epithelium (Fig. 2.9b). In addition, a few swollen cells in the luminal epithelium contained pale cytoplasm and fragmented nuclei (Fig. 2.9c).

8 days post-exposure

Eight days post-exposure to carbendazim, cellular swelling and pyknosis were observed in the luminal epithelium of the tubular region of the infundibulum. In addition, hyperaemia and leukocytic infiltrations were still the predominant pathological changes observed in the *lamina propria-submucosa* as well as in the vascular zone between the *tunica muscularis*.

12 days post-exposure

Twelve days post-exposure to carbendazim, accumulations of fluid in the interstitium and hyperaemia were observed in the *lamina propria-submucosa* (Fig. 2.10). At this stage, tubular glands were separated by empty clear spaces.

32 days post-exposure

At day 32 post-exposure to carbendazim, aggregates of inflammatory cells were the predominant degenerative change observed in the *lamina propria-submucosa* (Fig. 2.11). At this stage, very few luminal epithelium cells were ciliated. The glandular lumina were dilated. In a few instances, the dilated lumina were filled with exudate (Fig. 2.11 inset).

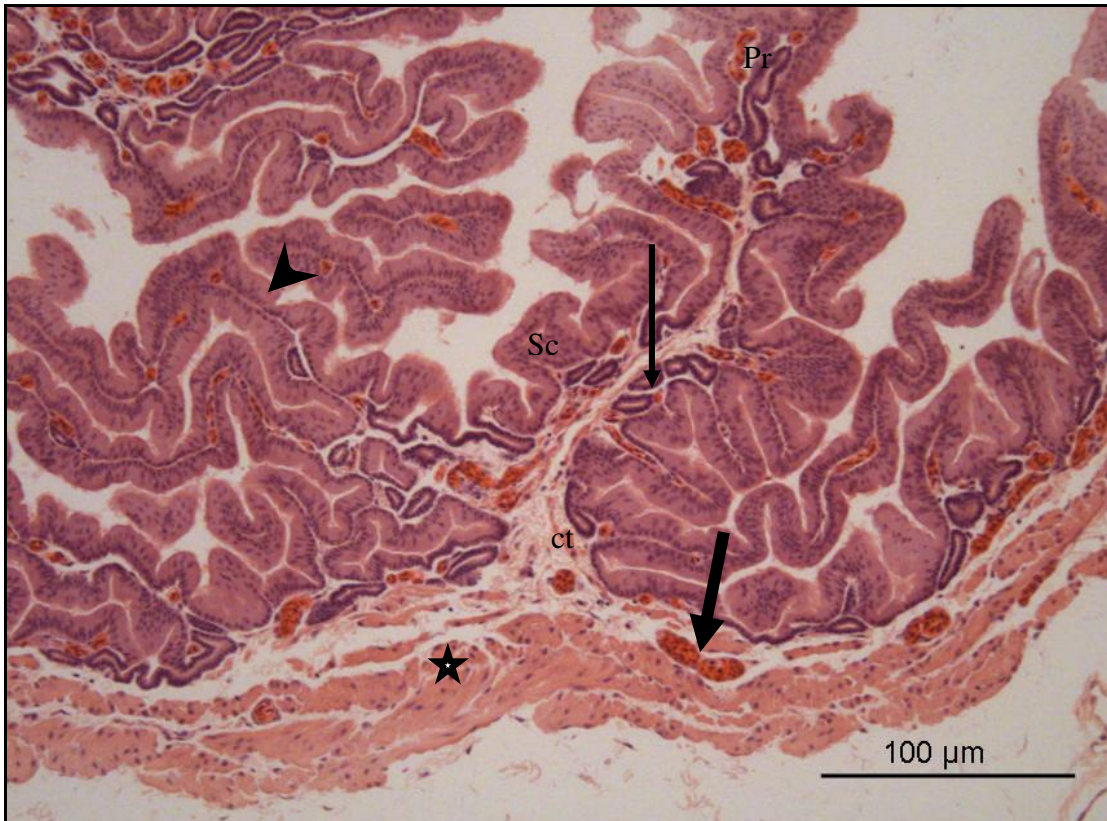


Fig. 2.7a: Survey photomicrograph of the tubular region of the infundibulum from a control bird. Note the presence of primary (Pr) and secondary (Sc) mucosal folds. The mucosal folds are lined by a ciliated simple columnar epithelium (arrowhead). Blood vessels (thick arrow), tubular glands (thin arrow) and loose connective tissue (ct) are observed in the *lamina propria-submucosa*. Asterisks: *tunica muscularis*.

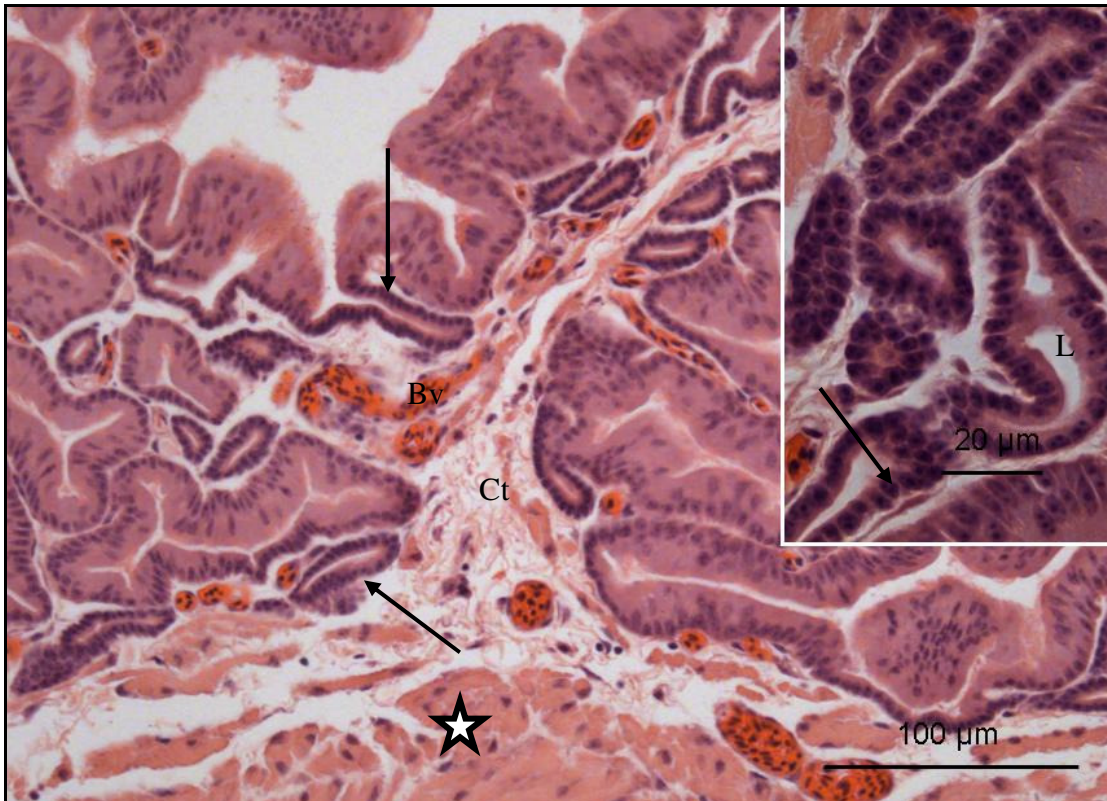


Fig. 2.7b: Photomicrograph of the tubular region of the infundibulum from a control bird. The tubular glands (arrows) are formed by epithelial invaginations. Ct: connective tissue; Bv: blood vessels; asterisk: *tunica muscularis*. Inset: A simple cuboidal epithelium (arrow) lines the tubular glands. L: glandular lumen.

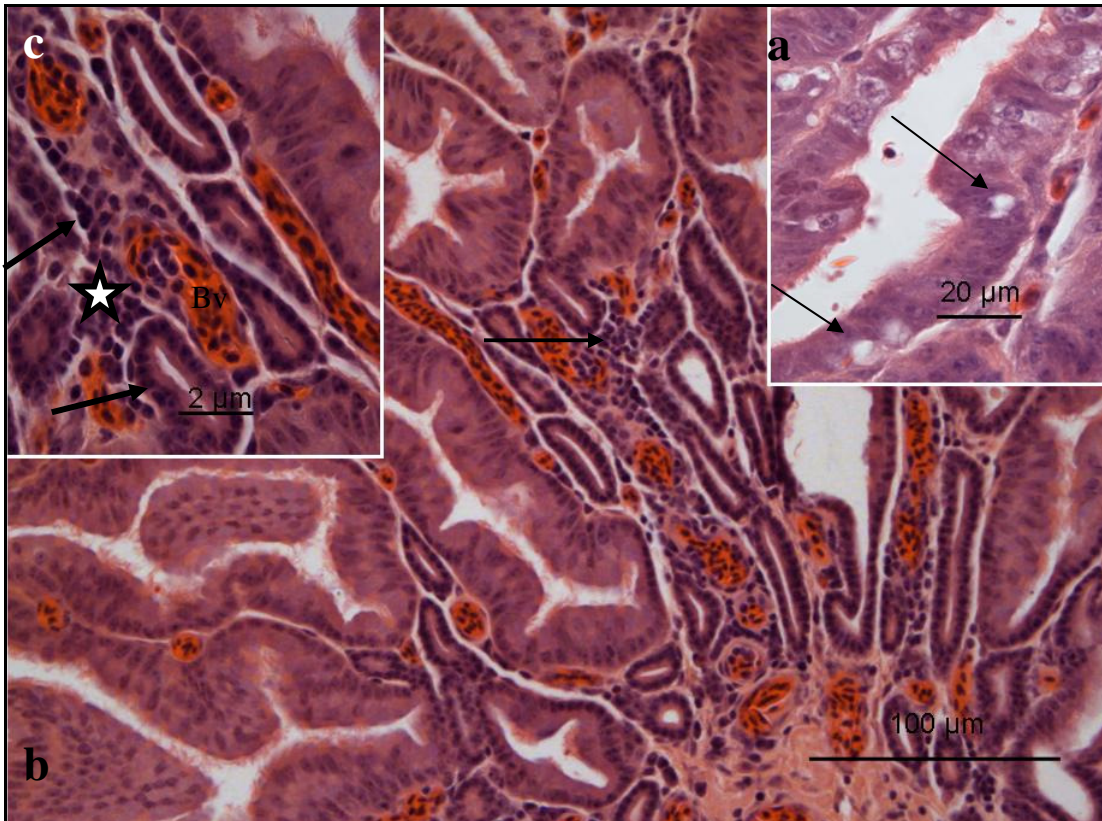


Fig. 2.8: Photomicrographs of the tubular region of the infundibulum from a bird exposed to 400 mg/kg bodyweight carbendazim. **a.** A photomicrograph of the luminal epithelium. Note the presence of vacuolated degenerating cells (arrows) in the luminal epithelium. **b.** Aggregates of leukocytes (arrow) are observed in the *lamina propria-submucosa*. **c.** High magnification photomicrograph showing leukocytic infiltrations (asterisk) adjacent to blood vessels (Bv) and tubular glands (arrows).

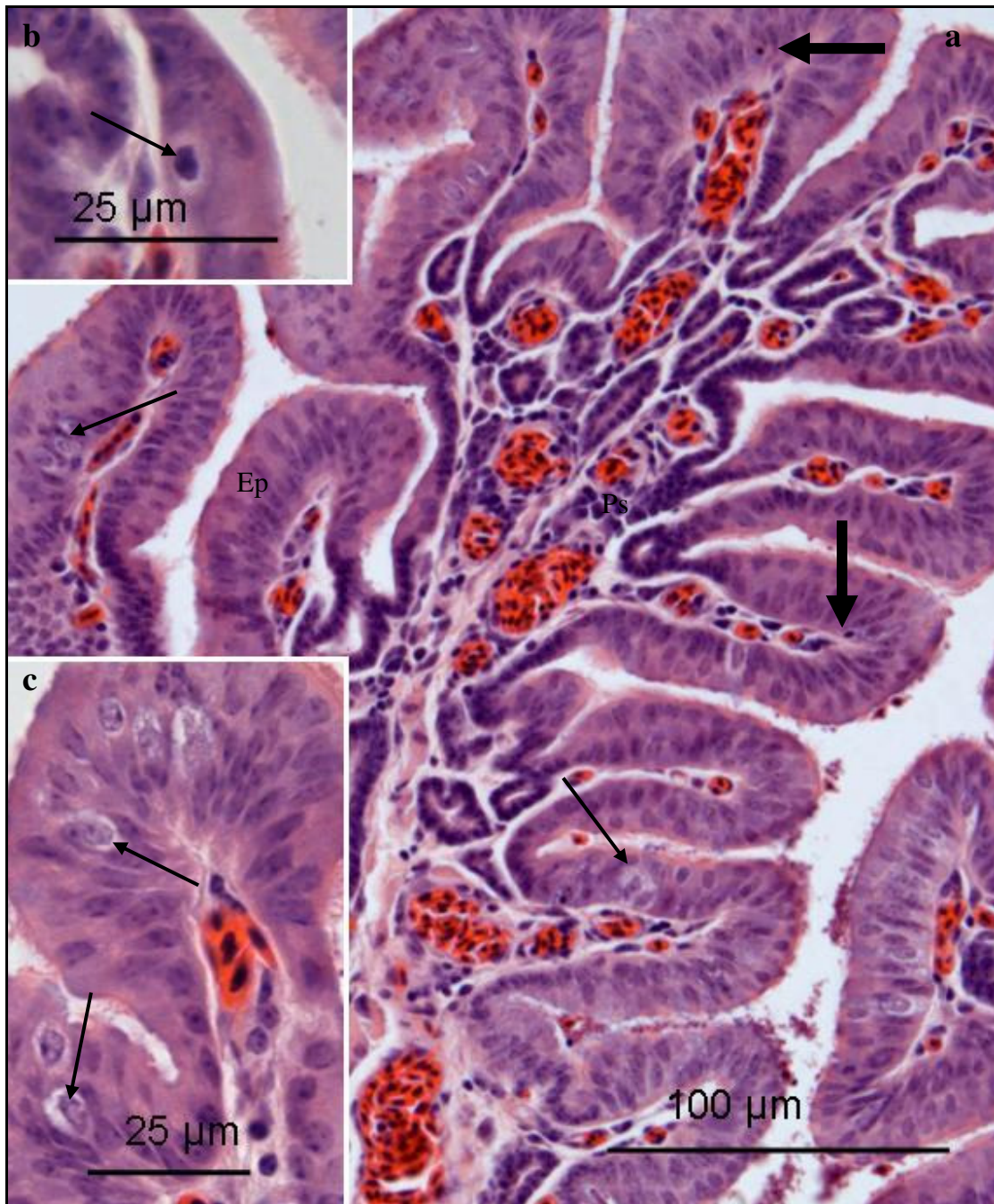


Fig. 2.9: Photomicrographs of the tubular region of the infundibulum 5 days post-exposure to 400 mg/kg body weight carbendazim. **a.** Hyperaemia is observed in the *lamina propria* (Ps). A diffuse leukocytic infiltration is also evident. A few swollen cells (thin arrows) and cells with pyknotic nuclei (thick arrows) are observed in the luminal epithelium (Ep). **b.** A higher magnification photomicrograph of the luminal epithelium showing a cell with a pyknotic nucleus (arrow). **c.** Swollen cells (arrows), displaying cytoplasmic pallor, are observed in the luminal epithelium.

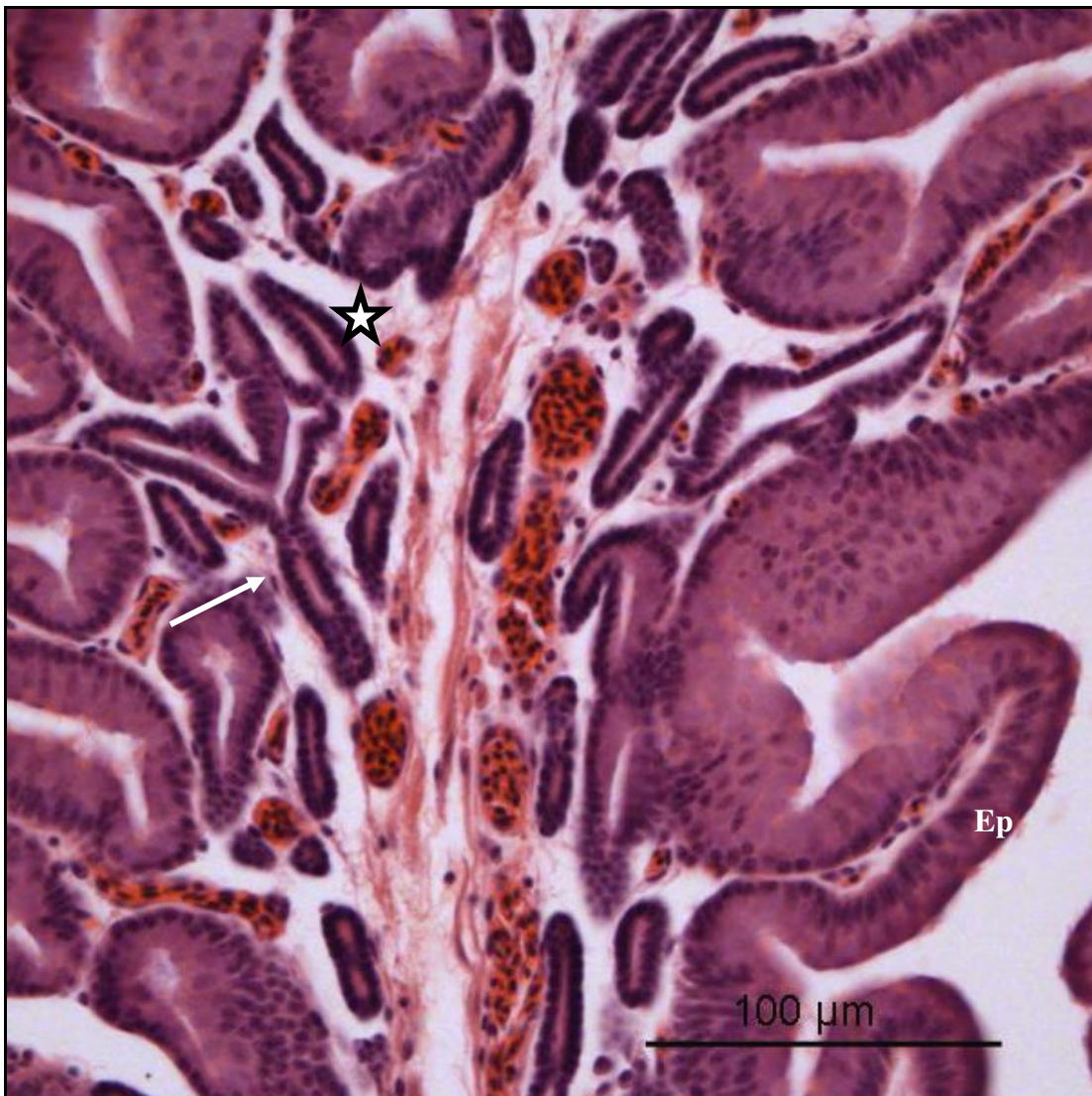


Fig. 2.10: Photomicrograph of the tubular region of the infundibulum 12 days post-exposure to 400 mg/kg body weight carbendazim. Oedema and hyperaemia are observed in the *lamina propria-submucosa* (asterisks). The epithelium (Ep) and tubular glands (arrow) in this section appear normal.

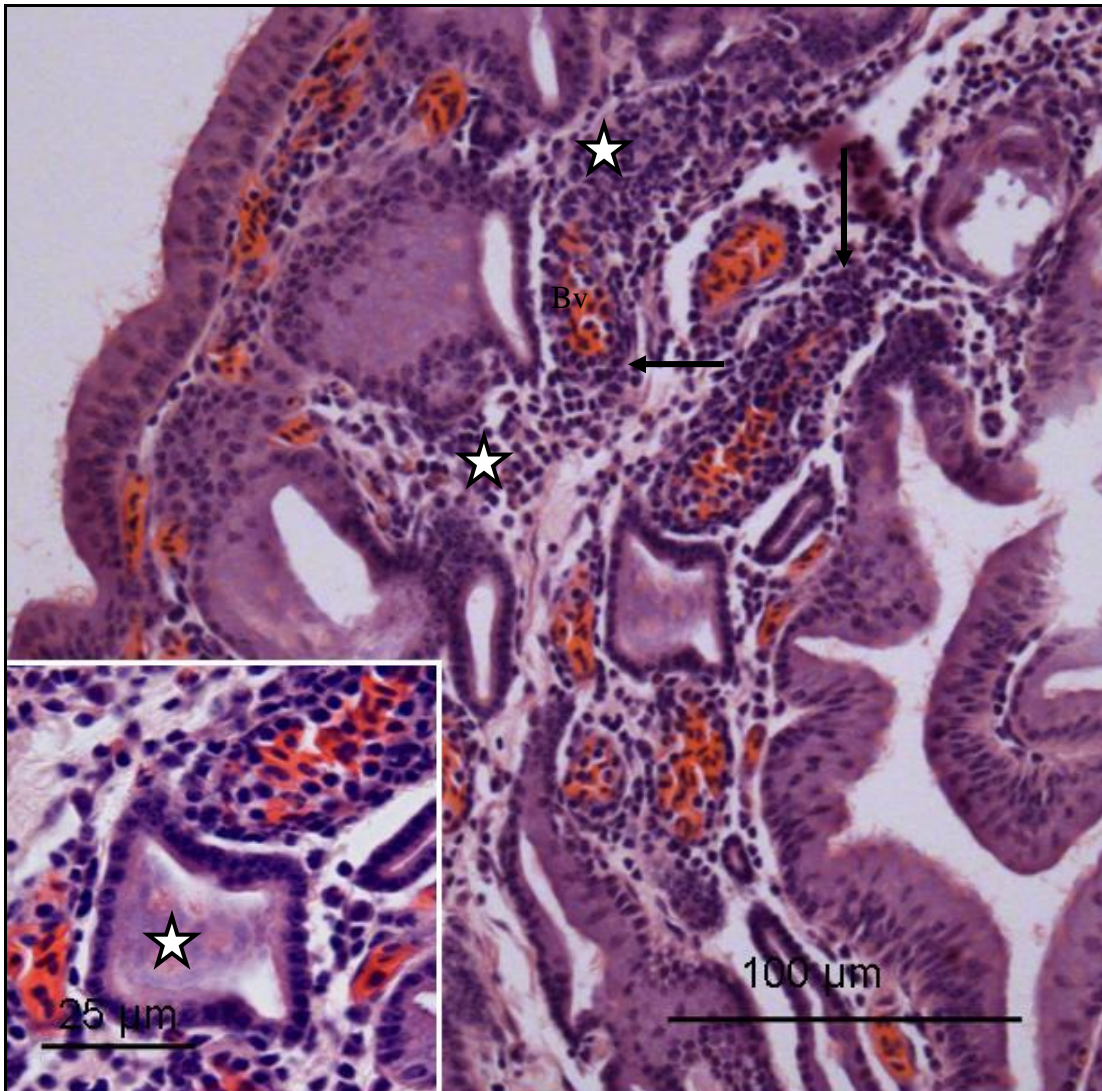


Fig. 2.11: Photomicrograph of the tubular region of the infundibulum 32 days post-exposure to 400 mg/kg bodyweight carbendazim. A diffuse leukocytic infiltration (asterisks) is observed in the *lamina propria-submucosa*. Aggregates of inflammatory cells (arrows) are also observed adjacent to the blood vessels (Bv). Inset: Dilated glandular lumen filled with exudate (asterisk).

2.3.4 Histochemistry

2.3.4.1 Funnel region

Luminal epithelial cells in the funnel region of the infundibulum showed a weak to absent reaction for periodic acid Schiff (Fig. 2.12). No alcian blue reaction was observed in these cells. Following carbendazim exposure, no changes in PAS staining intensity or pattern was observed.

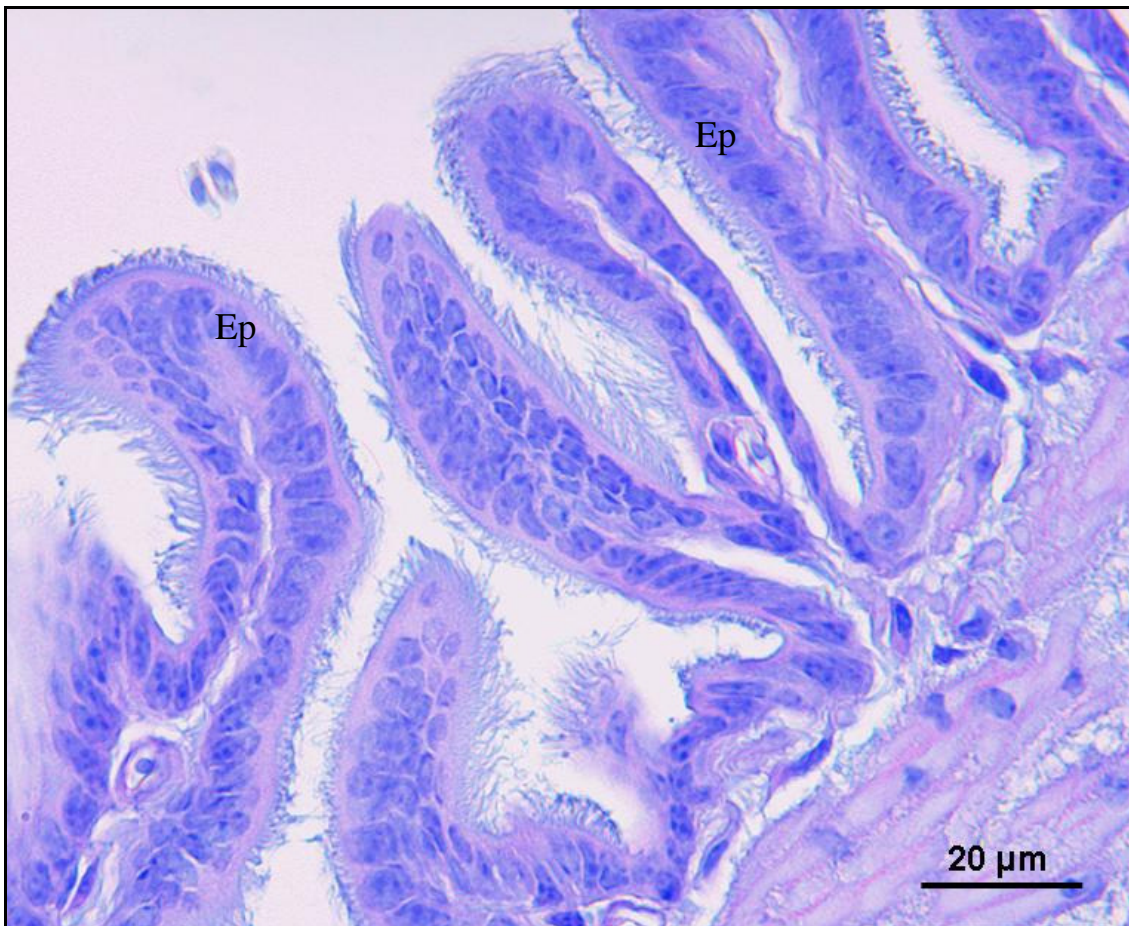


Fig. 2.12: Light microscopic photomicrograph of the funnel region of the infundibulum from a control bird. Weak PAS staining is observed in the cytoplasm of epithelial cells (Ep).

2.3.4.2 Tubular region

The use of Periodic acid Schiff (PAS)/Alcian blue stain showed positive reaction for PAS stain in non-ciliated cells of the luminal epithelium as well as in the gland cells. However, both cells were negative for Alcian blue stain. Tables 2.7 a & b summarize the PAS/Alcian blue staining intensity observed in the control and carbendazim-treated birds in experiment I (dose dependent effects of carbendazim) and II (time-course effects of carbendazim).

2.3.4.2.i Control birds

A strong reactivity for PAS was observed in the non-ciliated cells of the luminal epithelium (Fig. 2.13a). The positive PAS granules were observed in both the basal and supranuclear regions of the cells. No PAS staining reaction was observed in the

cytoplasm of the ciliated cells (Fig. 2.13b). In the glandular epithelium, staining for PAS was observed in the supranuclear regions of the gland cells (Fig. 2.13c). Cells in the luminal epithelium and glandular epithelium were negative for Alcian blue stain.

2.3.4.2.ii Carbendazim-treated birds

2.3.4.2.ii.a *Experiment I*

No PAS/Alcian blue histochemical changes were observed at doses of 25mg/kg and 100mg/kg bodyweight carbendazim. When compared to the control, a moderate reactivity for PAS was observed at a dose of 400mg/kg bodyweight carbendazim (Table 2.7). However, at this dose, positive staining for PAS was concentrated in the supranuclear regions of non-ciliated cells of the luminal epithelium (Fig. 2.14a). No change in staining intensity or distribution was detected in the glandular epithelium compared to the control group. At a dose of 800mg/kg bodyweight carbendazim, a weak reactivity for PAS was evident in the supranuclear regions of non-ciliated cells of the luminal epithelium (Fig. 2.14b). At this dose the gland cells also showed weak PAS staining (Fig. 2.14b). No Alcian blue stain reaction was observed in the luminal epithelial cells or glandular cells following carbendazim treatment.

Table 2.7: PAS/Alcian blue staining intensity in the tubular region of the infundibulum in control and carbendazim-treated Japanese quails

Carbendazim dose (mg/kg)	Non-ciliated cells (epithelium)		Gland cells	
	PAS	Alcian blue	PAS	Alcian blue
0	+++	-ve	+++	-ve
25	+++	-ve	+++	-ve
100	+++	-ve	+++	-ve
400	+	-ve	+++	-ve
800	+/-	-ve	+	-ve

+++ indicates strong; ++ moderate; + weak; +/- weak or negative, -ve negative staining.

2.3.4.2.iib Experiment II

5 and 24 hours post-exposure

Five and twenty-four hours post-exposure to 400 mg/kg bodyweight carbendazim, strong staining for PAS was observed in both the non-ciliated cells of the luminal epithelium and gland cells (Table 2.8). The cells showed negative reaction for Alcian blue stain.

5 and 8 days post-exposure

Five and eight days post-exposure to carbendazim, non-ciliated cells in the luminal epithelium stained moderate for PAS and negative for Alcian blue. At this stage, the gland cells stained weakly for PAS. No reactivity for Alcian blue was observed in the gland cells.

12 days post-exposure

Twelve days post-exposure to 400mg/kg bodyweight carbendazim, weak staining for PAS was observed in both the non-ciliated cells of the luminal epithelium and gland cells (Fig. 2.15). The PAS positive stained granules were concentrated in the apical cytoplasmic regions of these cells. At this stage, non-ciliated cells of the luminal epithelium as well as the gland cells were still showing negative reaction for Alcian blue stain.

32 days post-exposure

Thirty-two days post-exposure to carbendazim, a few non-ciliated cells of the luminal epithelium as well as gland cells stained moderate for PAS. The cells were negative for Alcian blue.

Table 2.8: PAS/Alcian blue staining intensity in the tubular region of the infundibulum at different periods post-exposure to 400 mg/kg bodyweight carbendazim

Time periods	Non-ciliated cells (epithelium)		Gland cells	
	PAS	Alcian blue	PAS	Alcian blue
Control	+++	-ve	+++	-ve
5 hours	+++	-ve	+++	-ve
24 hours	+++	-ve	+++	-ve
5 days	++	-ve	++	-ve
8 days	++	-ve	++	-ve
12 days	+	-ve	+	-ve
32 days	++	-ve	++	-ve

+++ indicates strong; ++ moderate; + weak; +/- weak or negative, -ve negative staining.

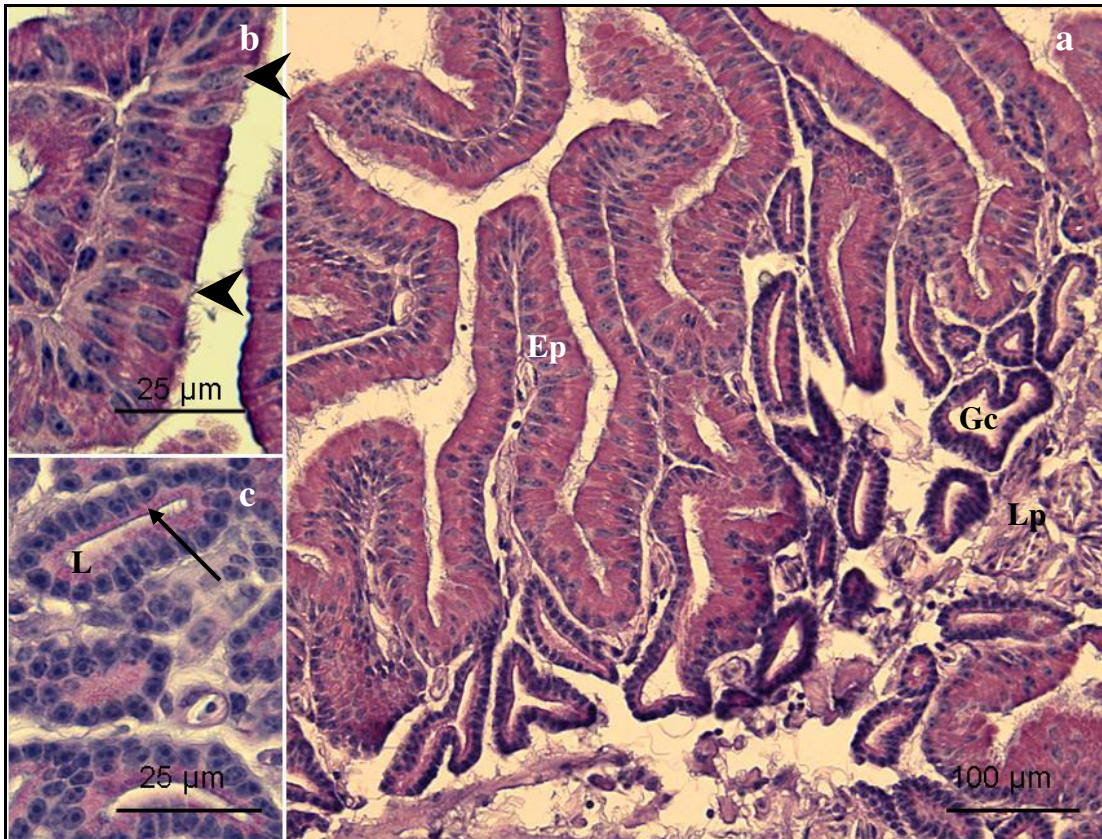


Fig. 2.13: **a.** A survey photomicrograph of the tubular region of the infundibulum from a control bird. Strong reactivity for PAS is observed in the luminal epithelial cells (Ep) as well as in the gland cells (Gc). Lp: lamina propria-submucosa. **b.** Higher magnification photomicrograph of the luminal epithelium. Ciliated cells (arrowheads) show a negative reaction for PAS. **c.** Higher magnification photomicrograph of the glands in the tubular region of the infundibulum. PAS positive granules are concentrated in the supranuclear regions of the gland cells (arrow). L: glandular lumen.

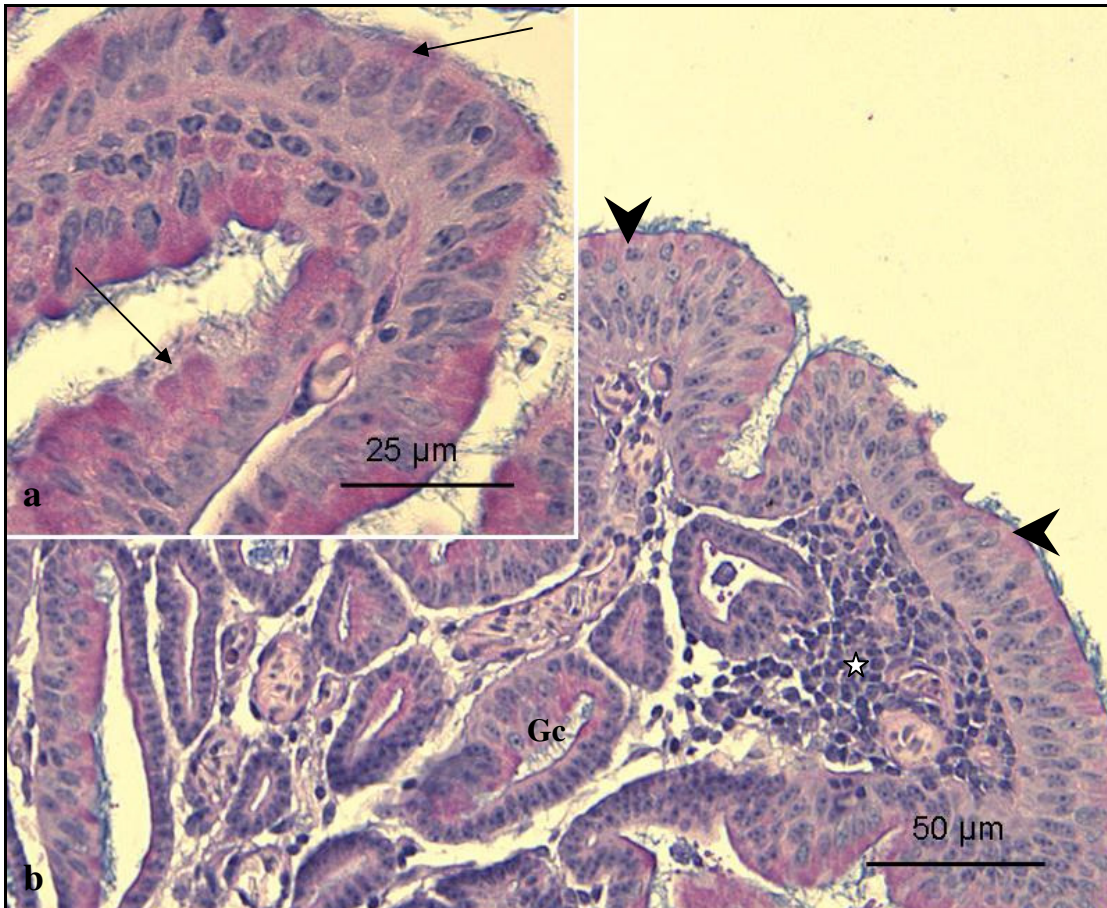


Fig. 2.14: Photomicrographs of the luminal epithelium in the tubular region of the infundibulum from a bird treated with (a) 400 mg/kg and (b) 800 mg/kg bodyweight carbendazim. a. A moderate reaction for PAS is observed in the supranuclear regions of non-ciliated cells of the luminal epithelium (arrows). b. A few non-ciliated cells (arrowheads) in the luminal epithelium show weak PAS reaction. Note that the PAS positive granules are also concentrated in the supranuclear regions. Gc: tubular glands; Asterisk: leukocytic infiltration.



Fig. 2.15: Photomicrograph of the luminal epithelium in the tubular region of the infundibulum 12 days post-exposure to 400mg/kg bodyweight carbendazim. Non-ciliated cells (arrows) show staining for PAS in the apical cytoplasmic regions.

2.3.5 Immunohistochemistry

Immunoreactivity for e-cadherin, laminin and vimentin was assessed in the mucosal layer of the tubular part of the infundibulum of both the control and carbendazim-treated birds. A qualitative assessment of the staining intensity was visually graded as strong (+++), moderate (++), weak (+) or negative (-). The observed changes of staining intensity are summarized in Table 2.9.

2.3.5.1 E-cadherin

2.3.5.1.i Control group

Strong immunoreaction for e-cadherin was observed in the plasma membranes of both ciliated and non-ciliated luminal epithelial cells (Fig. 2.16a). The staining

granules were observed in the lateral and basal cytoplasmic regions (Fig. 2.16b). Strong immunoreactivity for e-cadherin was also observed in the plasma membrane of glandular epithelial cells, endothelium, as well as, mesothelium (Fig. 2.16a).

2.3.5.1.ii Carbendazim-treated birds

2.3.5.1.ii.a Experiment I

No staining reactions were observed in the mucosal layer of the infundibulum 48 hours post-exposure to carbendazim. Both luminal and glandular epithelial cells were negative for e-cadherin.

2.3.5.1.ii.b Experiment II

No immunohistochemical changes were observed in the infundibular mucosa within 5 and 24 hours post-exposure to carbendazim at a dose of 400 mg/kg bodyweight. During these periods, strong e-cadherin immunoreactivity was observed in both the luminal and glandular epithelium.

At days 5, 8, and 12 post-exposure to carbendazim, both luminal and glandular epithelial cells stained negative for e-cadherin. However, at 32 days post-exposure to carbendazim, weak e-cadherin immunoreactivity was observed in a few epithelial cells (Fig. 2.17). At this stage, the plasma membranes of the glandular cells remained negative.

2.3.5.2. Laminin

2.3.5.2.i Control group

Strong immunoreactivity for laminin was observed in the basement membrane underlying the luminal and glandular epithelia (Fig. 2.18a). In addition, laminin immunoreactivity was also observed in the basement membranes of the endothelium, as well as, smooth muscle cells in the *tunica muscularis*.

2.3.5.2.ii Carbendazim-treated birds

2.3.5.2.ii.a *Experiment I*

No immunohistochemical changes were observed in the infundibulum 48 hours post-exposure to carbendazim.

2.3.5.2.ii.b *Experiment II*

At 5 and 24 hours post-exposure to carbendazim, strong immunoreactivity for laminin was observed in the basement membrane underlying luminal and glandular epithelia, endothelium, as well as, smooth muscle cells in the *tunica muscularis*.

At days 5, 8, 12 and 32 post-exposure to carbendazim, the basement membrane underlying luminal and glandular epithelia, as well as endothelium and smooth muscle cells stained moderate to strong for laminin. At these stages, the basement membrane was conspicuous thick and discontinuous in some areas (Fig. 2.19 a,b&c)

2.3.5.3. Vimentin

2.3.5.3.i Control group

Strong vimentin immunoreactivity was observed in both ciliated and non-ciliated epithelial cells (Fig. 2. 20a). The immunoreaction was observed in the apical and basal cytoplasmic regions (Fig. 2. 20b). No vimentin immunoreaction was observed in the gland cells. Endothelial cells lining the blood vessels and capillaries below the epithelium and between the glands stained positive for vimentin (Fig. 2.20c). Fibroblasts and fibrocytes in the *lamina propria-submucosa* and *tunica muscularis*, as well as mesothelial cells of the *tunica serosa* showed strong immunoreactivity for vimentin.

2.3.5.3.ii Carbendazim-treated birds

2.3.5.3.iii *Experiment I*

400 and 800 mg/kg carbendazim treated groups

At dosages of 400 mg/kg and 800 mg/kg bodyweight carbendazim, weak to negative vimentin immunoreactions were observed in both ciliated and non-ciliated epithelial cells. The staining reaction was seen around the nucleus. Endothelial cells stained moderate for vimentin. Glandular cells remained negative for vimentin.

2.3.5.3.iii *Experiment II*

At 5 and 24 hours post-exposure to 400 mg/kg bodyweight carbendazim, no changes in staining characteristics were observed in the luminal epithelial cells. At days 5 and 8 days post-exposure to 400 mg/kg bodyweight carbendazim, a weak to negative immunoreaction for vimentin was observed in both ciliated and non-ciliated epithelial cells. At these stages, the endothelium and fibrocytes in the lamina propria-submucosa stained moderately for vimentin (Fig. 2.21). Gland cells stained negative.

At day 12 post-exposure to carbendazim, both ciliated and non-ciliated epithelial cells stained moderate to strong for vimentin (Fig. 2.22a). The staining reaction was concentrated in the basal cytoplasmic regions (Fig. 2.22b). At this stage, fibrocytes and endothelial cells in the *lamina propria-submucosa and tunica muscularis* stained moderate for vimentin. No vimentin immunoreaction was observed in the glandular cells.

Strong to moderate vimentin immunoreaction was also observed in the epithelial cells 32 days post-exposure to carbendazim. At this stage, the staining reactions were observed around the nucleus and in the apical cytoplasmic regions. Fibrocytes and endothelial cells in the *lamina propria-submucosa* also stained strongly for vimentin.

Table 2.9: Immunoreactivities for e-cadherin, laminin and vimentin in the luminal epithelial cells of the infundibulum of control and carbendazim-treated Japanese quails

Time periods	e-cadherin	Laminin	Vimentin
Control	+++	+++	+++
5 hours	+++	+++	+++
24 hours	+++	+++	+++
5 days	-	++/+++	+/-
8 days	-	++/+++	+/-
12 days	-	++/+++	++/+++
32 days	+	++/+++	+++

+++ : strong, ++ : moderate, + : weak, - : negative

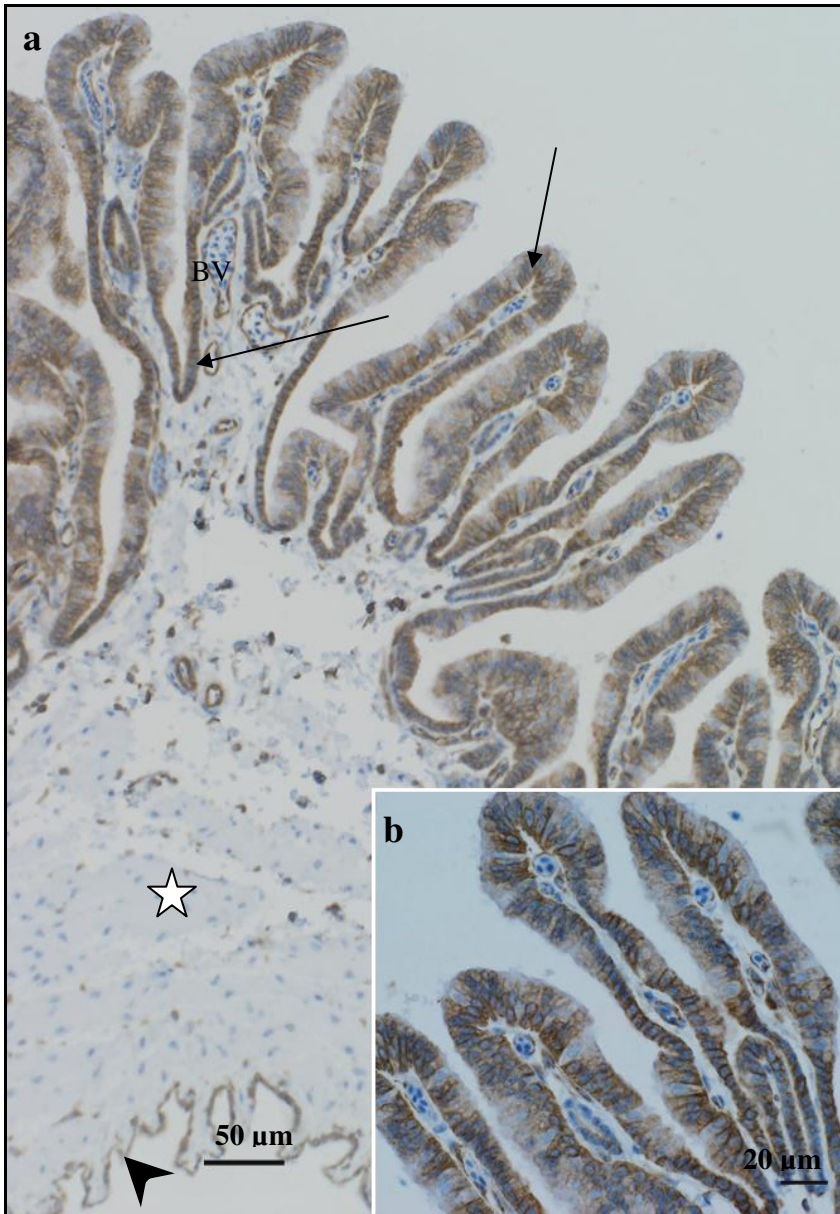


Fig. 2.16: Photomicrographs of the infundibulum from a control bird. **a.** Strong immunoreactivity for e-cadherin is observed in luminal and glandular epithelial cells (arrows), endothelium (BV), as well as, mesothelial cells (arrowhead). Asterisk: *tunica muscularis*. **b.** A higher magnification photomicrograph of the luminal and glandular epithelium. Note the distribution of e-cadherin immunoreactive granules in the lateral and basal plasma membranes.

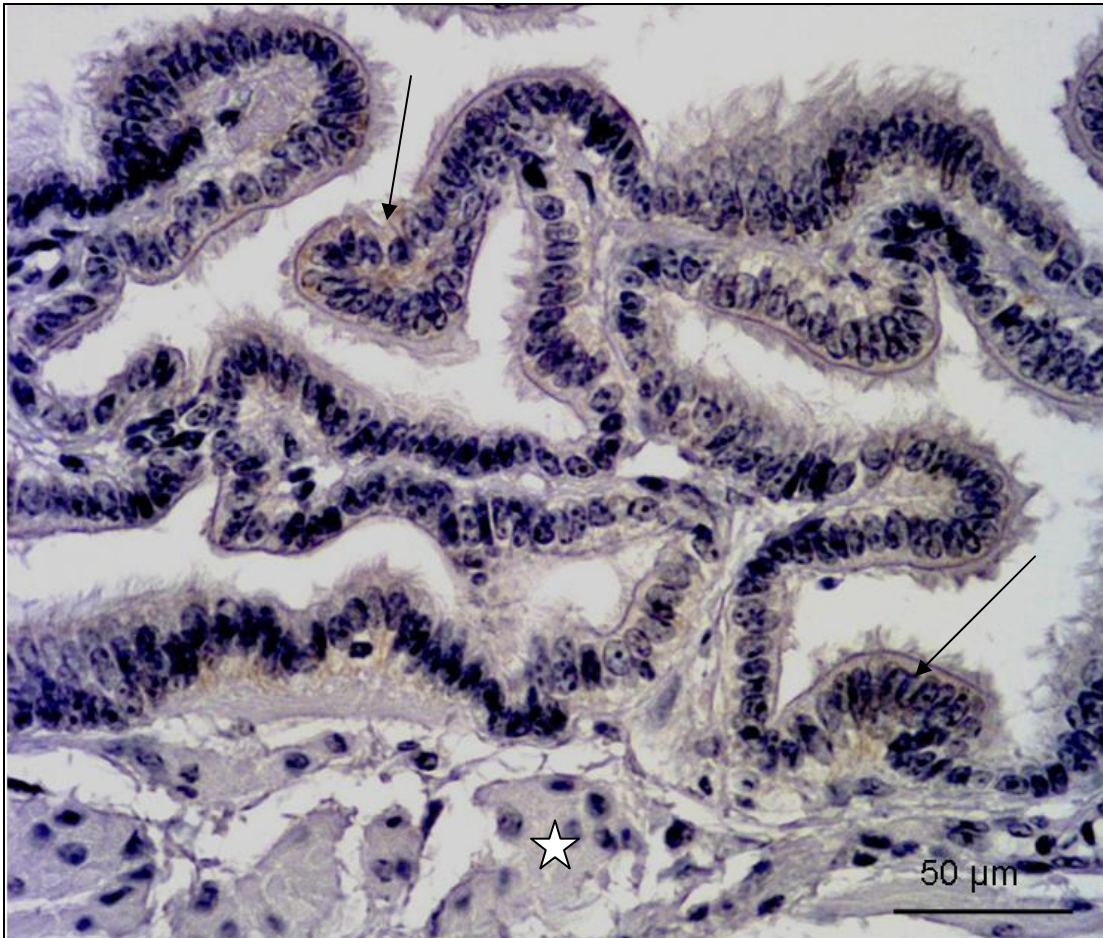


Fig. 2.17: Photomicrograph of the infundibulum 32 days post-exposure to 400 mg/kg bodyweight carbendazim. A weak e-cadherin immunoreaction is observed in the luminal epithelial cells (arrows). Asterisk: *Tunica muscularis*.

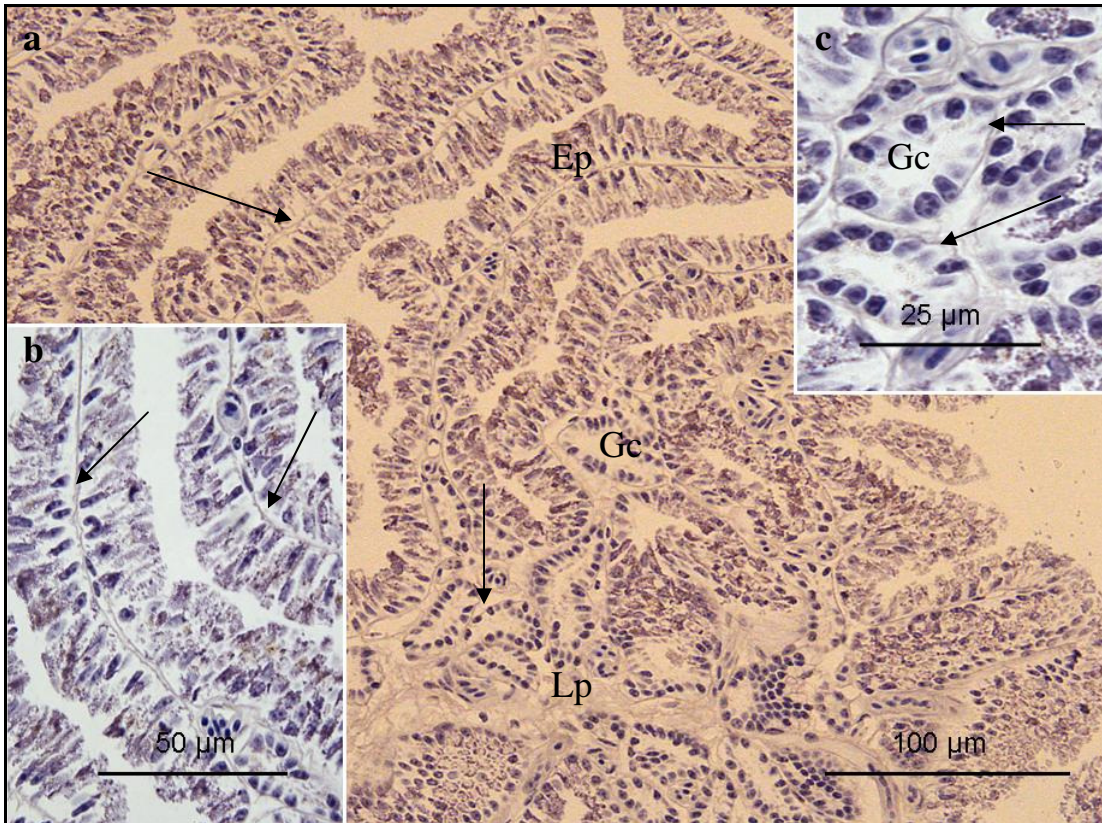


Fig. 2.18: **a.** A survey photomicrograph of the tubular region of the infundibulum from a control bird. Laminin immunoreactivity is observed in the basement membranes (arrows) underlying the luminal epithelium (Ep), tubular glands (Gc) and endothelium in the *lamina propria-submucosa* (Lp). **b.** A higher magnification photomicrograph of the luminal epithelium. Note the strong immunoreactivity for laminin in the basement membrane (arrows). **c.** A high photomicrograph of the tubular glands (Gc) in the tubular region of the infundibulum. A continuous basement membrane (arrows) is immunopositive for anti-laminin antibody.

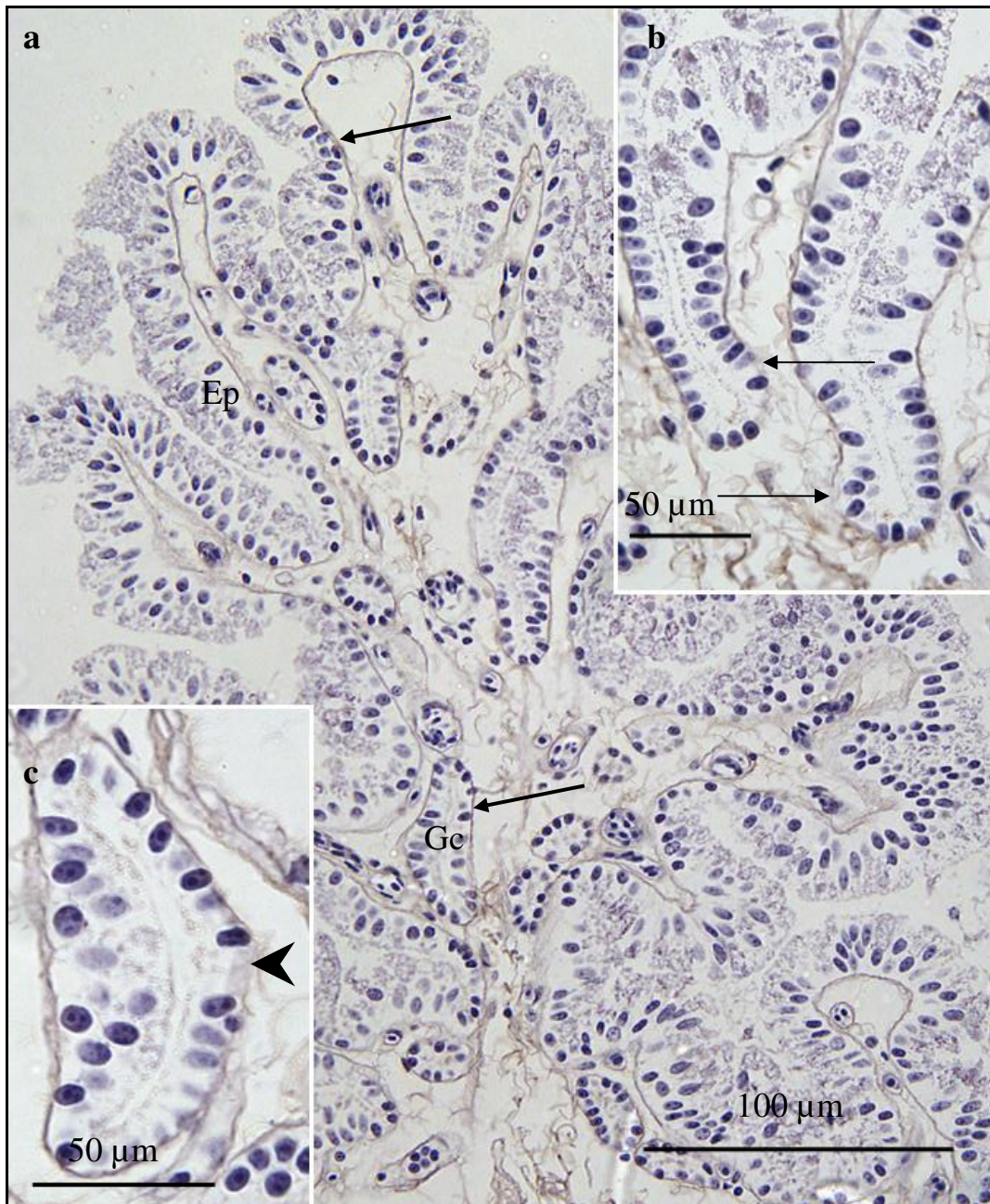


Fig. 2.19: **a.** A low magnification photomicrograph of the tubular region of the infundibulum, 12 days post-exposure to carbendazim. Immunoreactivity for laminin is observed in the basement membranes (arrows) underlying the luminal epithelium (Ep) and tubular glands (Gc). **b.** A high magnification photomicrograph of the luminal epithelium showing the discontinuation of the basement membrane (arrowhead). **c.** A discontinuous basement membrane (arrow) is observed underlying an atubular gland.

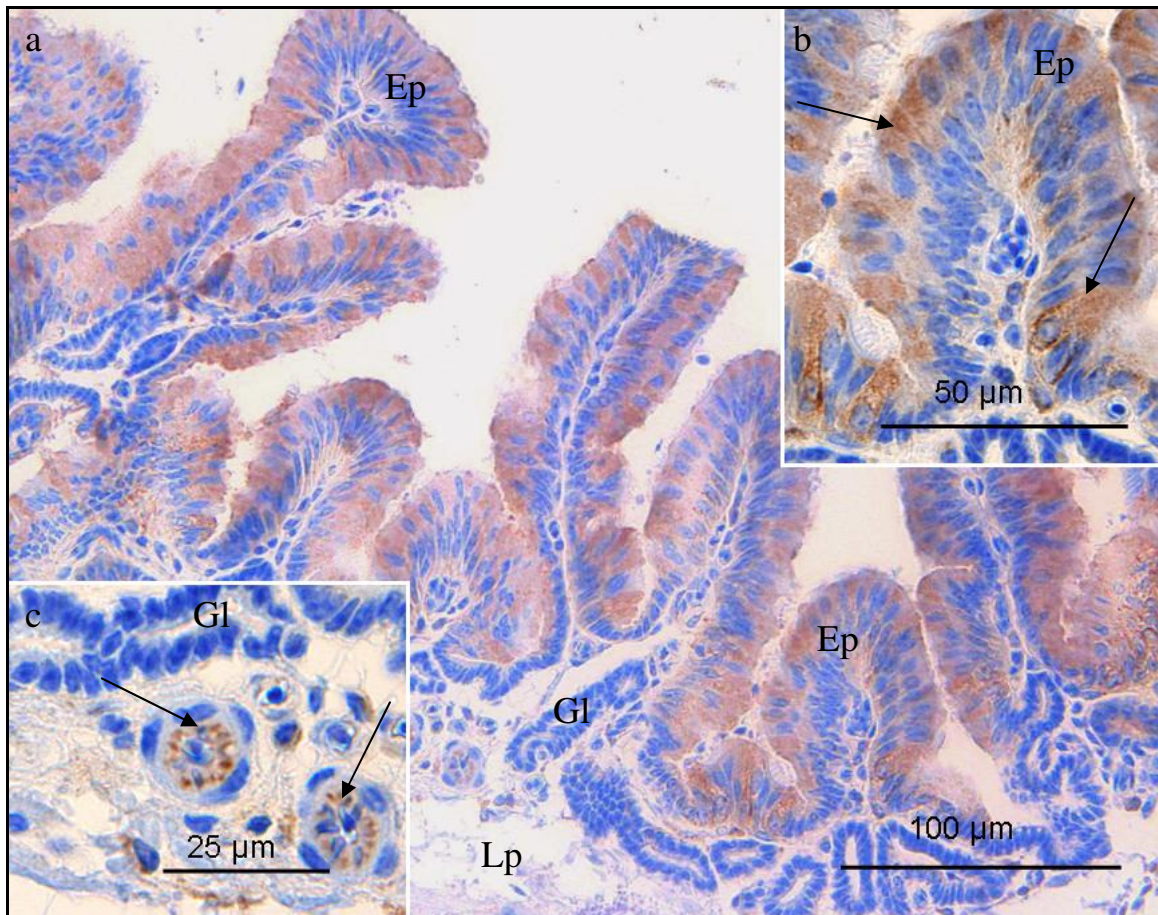


Fig. 2.20: Photomicrographs of the mucosal layer in the tubular region of the infundibulum of a control bird. **a.** Strong vimentin immunoreaction is observed in the luminal epithelium (Ep). GI: tubular glands; Lp: *lamina propria-submucosa*. **b.** The staining reaction is observed in the basal and apical cytoplasmic regions (arrows) of the luminal epithelial cells (Ep). **c.** Strong vimentin immunoreaction is seen in the endothelial cells (arrows). Note the absence of vimentin immunoreactivity in the glandular epithelium (GI).

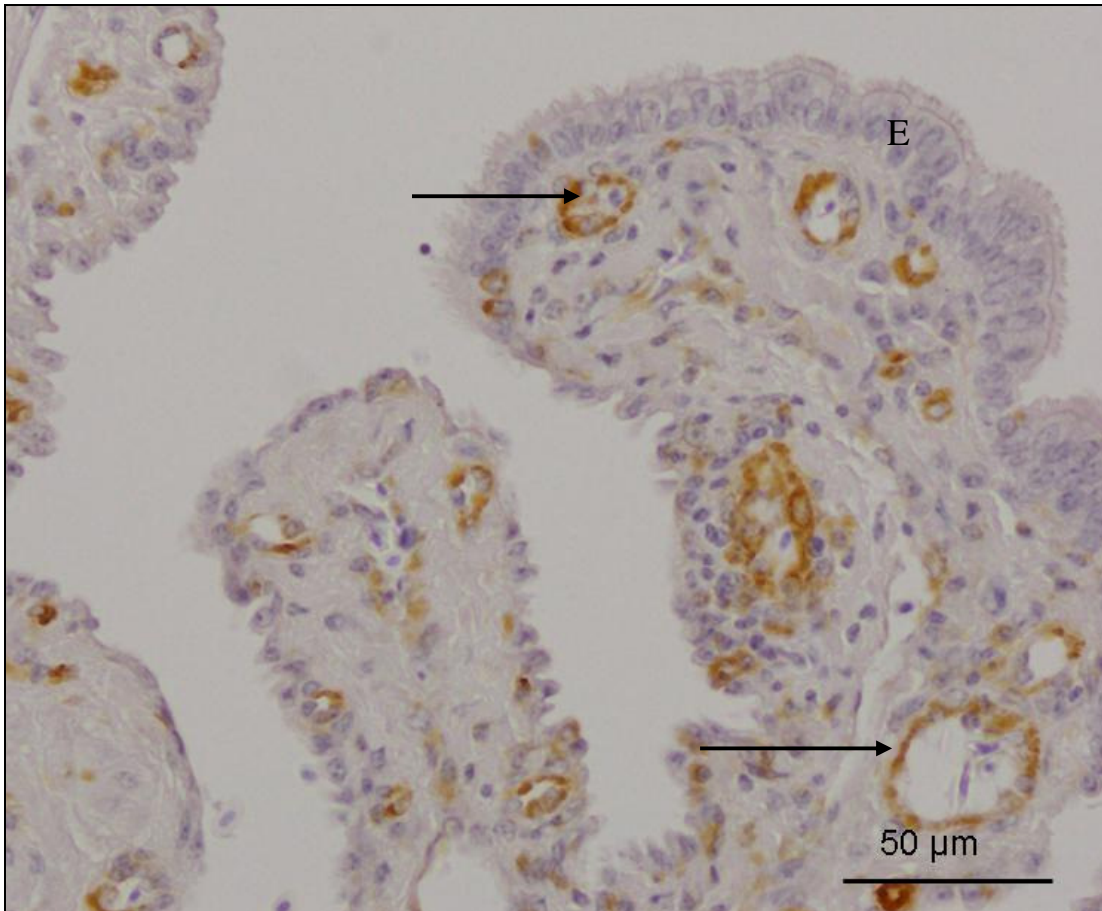


Fig. 2.21: Photomicrograph of infundibular mucosa 8 days post-exposure to 400 mg/kg bodyweight carbendazim. Immunoreaction for vimentin is observed in endothelial cells (arrows). Note the absence of vimentin immunoreaction in the epithelial cells (E).

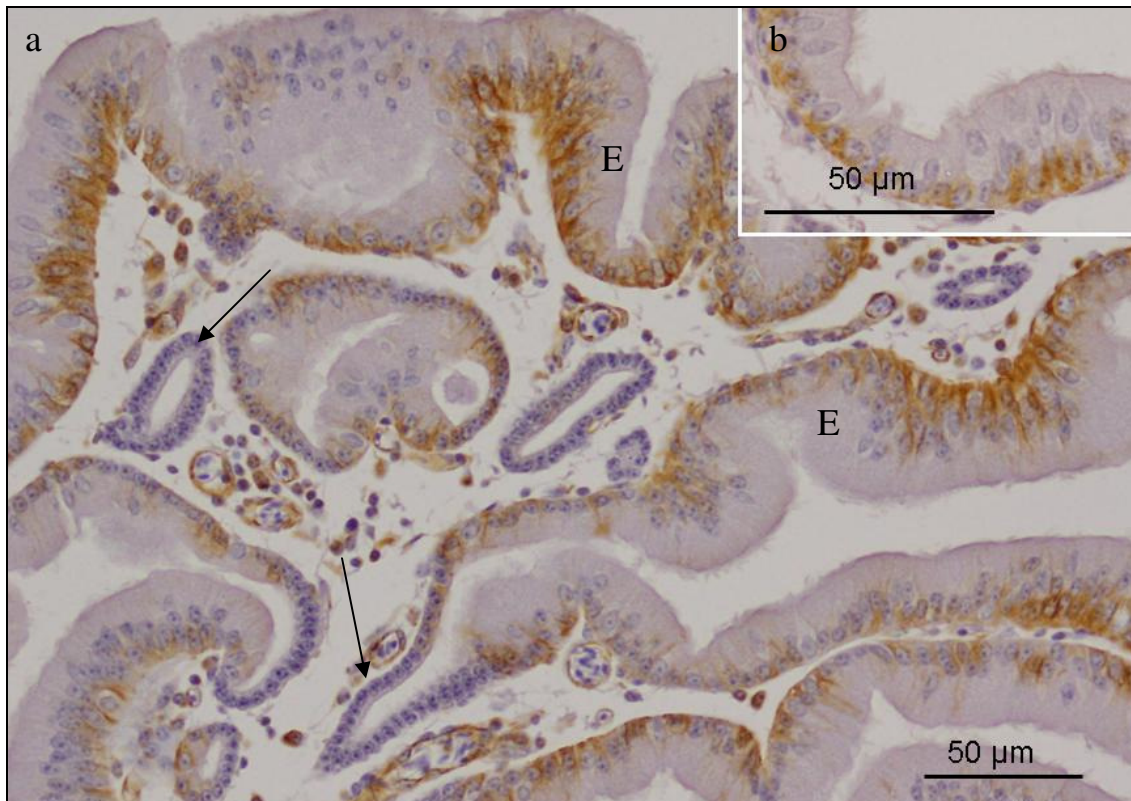


Fig. 2.22: Photomicrographs of the infundibulum 12 days post-exposure to 400 mg/kg bodyweight carbendazim. **a.** Moderate to strong vimentin immunoreactivity is evident in the luminal epithelial cells (E). Tubular glands (arrows) are negative for vimentin. **b.** A higher magnification photomicrograph of the luminal epithelium. Note the perinuclear and basal immunoreaction.

2.3.6 Ultrastructural observations

2.3.6.1 Funnel region

2.3.6.1.1. Scanning electron microscopy

2.3.6.1.1.i Control birds

The mucosal surface of the funnel region of the infundibulum was thrown into primary and secondary folds (Fig. 2.23a). The surface epithelium lining the mucosa consisted of ciliated and non-ciliated cells (Fig. 2.23b). The ciliated cells, which were the predominant cellular type, exhibited long cilia. The non-ciliated cells displayed dome-shaped apical regions, which were covered by microvilli (Fig. 2.23c).

2.3.6.1.1.ii Carbendazim-treated birds

2.3.6.1.1.ii.a *Experiment I*

25 and 100 mg/kg bodyweight carbendazim

There were no morphological changes observed on the mucosal surface following administration of 25 mg/kg and 100 mg/kg bodyweight carbendazim.

400 and 800 mg/kg bodyweight carbendazim

At doses of 400 and 800 mg/kg bodyweight carbendazim, a few areas of cilia loss were observed (Fig. 2.24a). In these areas, remnants of lost cilia were seen as short stems (Fig. 2.24b). In areas where a complete loss of cilia had taken place, shallow pits were evident.

2.3.6.1.1.ii.b *Experiment II*

No degenerative changes were observed on the mucosal surface 5 and 24 hours post-exposure to 400 mg/kg bodyweight carbendazim.

5 and 8 days post-exposure

At 5 and 8 days post-exposure to carbendazim, areas of cilia loss were observed (Fig. 2.25). Swollen cilia were identified arising from some cells. At this stage, non-ciliated cells were lined by a few microvilli.

12 and 32 days post-exposure

At 12 and 32 days post-exposure to carbendazim, areas of cilia loss were still identified on the mucosal surface (Fig. 2.26). However, at these stages no swollen cilia were evident.

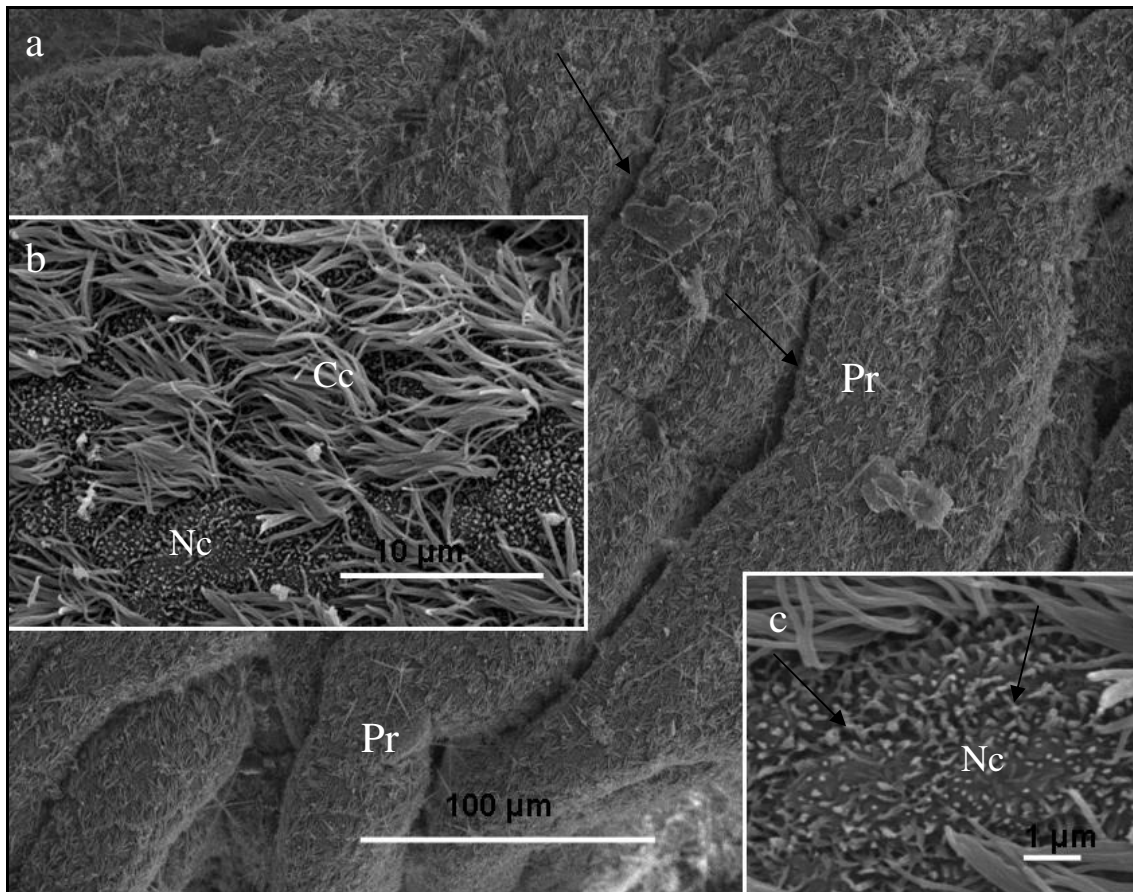


Fig. 2.23: **a.** A survey scanning electron photomicrograph of the funnel region of the infundibulum of a control bird. Primary folds (Pr) are observed, separated by clefts (arrows). **b.** Mucosal surface containing ciliated (Cc) and non-ciliated (Nc) cells. **c.** A higher magnification electron photomicrograph of non-ciliated cells (Nc). Long microvilli (arrows) are seen on the surface of these cells.

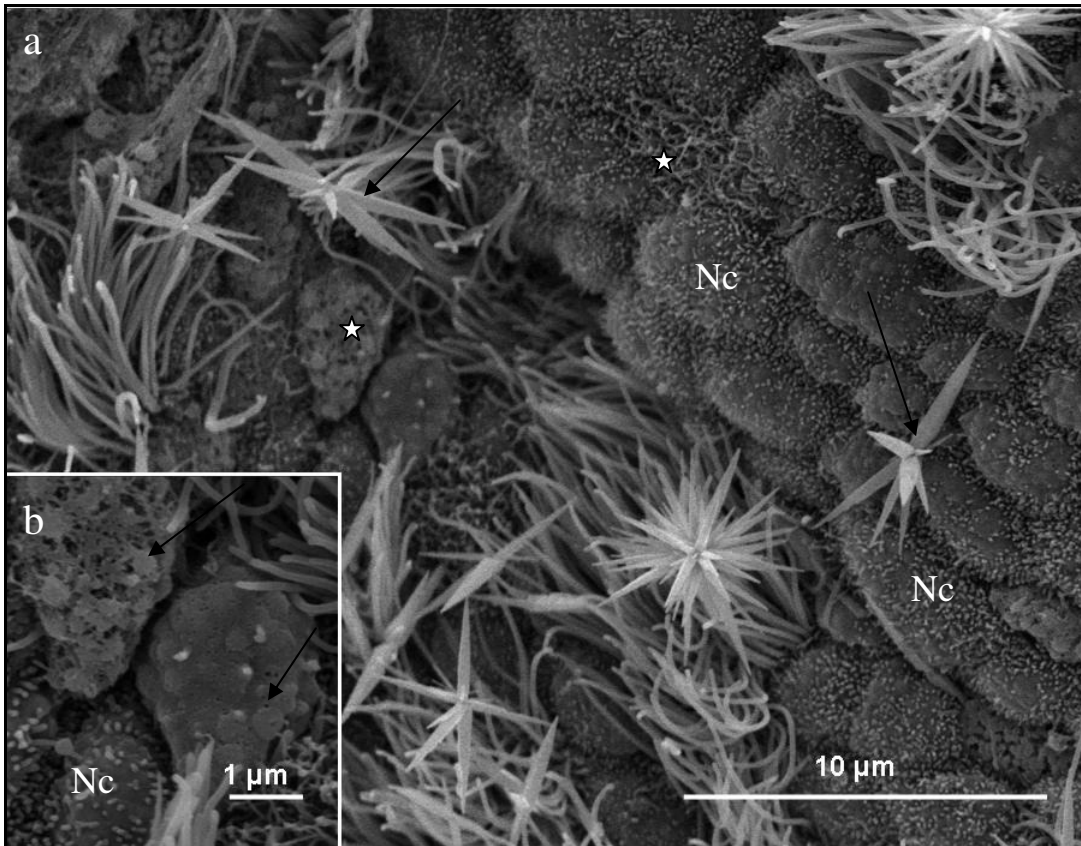


Fig. 2.24: **a.** A survey scanning electron photomicrograph of the funnel region of the infundibulum from a bird treated with 400 mg/kg bodyweight carbendazim. Areas of deciliation (asterisks) are observed. Note the presence of a few swollen cilia (arrows). Nc: non-ciliated cells. **b.** A higher magnification photomicrograph of cells displaying cilia loss. Cilia stems (arrows) indicate remnants of lost cilia.

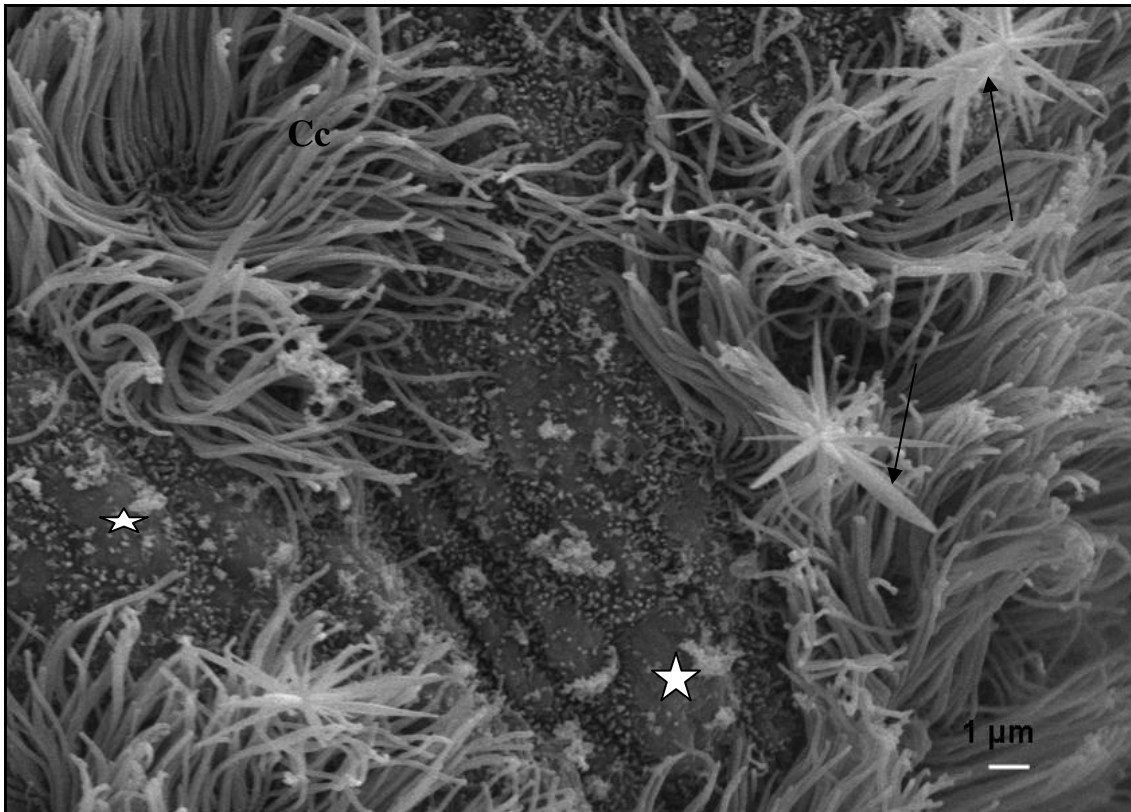


Fig. 2.25: Scanning electron photomicrograph of the funnel region of the infundibulum, 5 days post-exposure to 400 mg/kg bodyweight carbendazim. Areas of deciliation (asterisks) are observed. Swollen cilia (arrows) are also observed. Cc: ciliated cell with normal cilia.

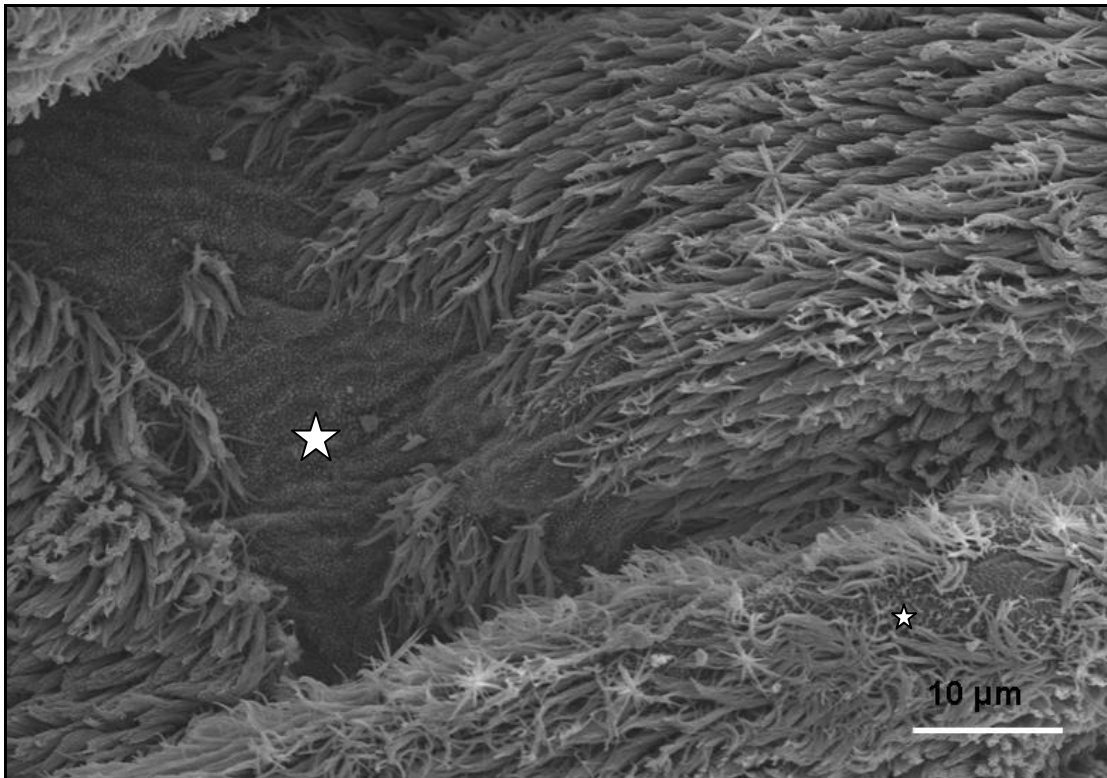


Fig. 2.26: Scanning electron photomicrograph of the funnel region of the infundibulum, 12 days post-exposure to 400 mg/kg bodyweight carbendazim. Areas of deciliation (asterisks) are observed.

2.3.6.1.2. *Transmission electron microscopy*

2.3.6.1.2.i Control birds

The mucosal layer of the funnel region of the infundibulum was lined by simple to pseudostratified ciliated columnar epithelium consisting of ciliated and a few non-ciliated cells (Fig. 2.27a).

Ciliated cells

Ciliated cells were the predominant cell type observed. The ciliated cells contained centrally located round or oval nuclei. The cells were lined by long cilia and a few microvilli (Fig. 2.27b). Apically, the ciliated cells contained basal bodies which anchored the cilia. Striated rootlets and basal feet supported the basal bodies. Mitochondria, rough endoplasmic reticulum cisternae (RER), Golgi complexes and a

few lysosomes were seen in the apical cytoplasmic region. Only a few mitochondria and cisternae of RER were observed in the basal cytoplasmic region.

Non-ciliated cells

The dome-shaped apical regions of the non-ciliated cells were elevated above the luminal surface (Fig. 2.28a). The cells contained basally located round or oval nuclei. The apical plasma membrane of these cells was lined by long microvilli (Fig. 2.28a). A few cytoplasmic organelles, including mitochondria, RER and Golgi complexes were observed in the apical cytoplasmic regions. The cytoplasm of these cells contained electron dense granules.

Plasma membrane and basal lamina

Desmosomes and interdigitations of the lateral plasma membrane linked adjacent cells (Fig. 2.28b). A homogenous basal lamina which measured approximately 70 nm in thickness supported the epithelium. Both the lamina densa and lamina lucida layers of the basal lamina were clearly differentiated (Fig. 2.28c).

2.3.6.1.2.ii Carbendazim-treated birds

2.3.6.1.2.ii.a Experiment I

There were no degenerative changes observed in the mucosal layer at doses of 25 mg/kg and 100 mg/kg bodyweight carbendazim.

400 mg/kg bodyweight carbendazim

Ciliated cells

Degenerating ciliated cells contained pyknotic nuclei surrounded by electron lucent cytoplasm (Fig. 2.29a). Numerous lysosomes were observed in the apical cytoplasmic regions. Swollen mitochondria and dilated cisternae of RER were evident throughout the cytoplasm (Fig. 2.29a). In a few degenerating cells,

compound cilia were observed (Fig. 2.29b). In these cells, basal bodies and striated rootlets were structurally normal.

Non-ciliated cells

Degenerating non-ciliated cells protruded above the luminal surface (Fig. 2.30a). Numerous lysosomes were observed in the elevated regions of the degenerating non-ciliated cells (Fig. 2.30b). At this dose, a few, short microvilli lined the apical plasma membrane of these cells.

Plasma membrane and basal lamina

Desmosomes linking adjacent luminal epithelial cells were intact (Fig. 2.29c). No degenerative changes were observed in the basal lamina. The basal lamina measured approximately 120 nm in thickness. Both lamina lucida and lamina densa were visible.

800 mg/kg bodyweight carbendazim

Ciliated cells

At a dose of 800 mg/kg bodyweight carbendazim, degenerating ciliated cells with pyknotic nuclei were observed (Fig. 2.31a). A few degenerating cells, contained crenated nuclei, which exhibited chromatin condensation and marginalized nucleoli. Swollen mitochondria were seen in both the apical and basal cytoplasmic regions. A few dilated cisternae of RER and myelin figures were identified in the basal cytoplasmic regions of the degenerating cells (Fig. 2.31b).

Non-ciliated cells

Degenerating non-ciliated cells contained pyknotic nuclei, swollen mitochondria and a few dilated cisternae of RER.

Plasma membrane and basal lamina

Desmosomes linking adjacent epithelial cells were structurally normal. The basal lamina underlying the epithelium measured approximately 80 nm in thickness. No degenerative changes were observed in the basal lamina.

2.3.6.1.2.iib Experiment II

There were no morphological changes observed in the mucosal layer of the funnel region of the infundibulum 5 and 24 hours post-exposure to 400 mg/kg bodyweight carbendazim.

5 days post-exposure

Ciliated cells

Five days post-exposure to carbendazim, degenerating ciliated cells contained an electron lucent cytoplasm, which contained swollen mitochondria and dilated cisternae of RER. Numerous lysosomes were observed in the apical cytoplasmic regions (Fig. 2.32a). Pyknotic nuclei were also observed in the degenerating ciliated cells. In a few cells, a fragmented apical plasma membrane and deciliation were observed (Fig. 2.32a).

Non-ciliated cells

Degenerating non-ciliated cells were lined by a few short microvilli (Fig. 2.32a). The cells contained pyknotic nuclei and swollen mitochondria (Fig 2.32b).

Plasma membrane and basal lamina

Desmosomes along the lateral plasma membranes were structurally normal. At this stage, invaginations of the basal lamina underlying the luminal epithelium were occasionally encountered (Fig. 2.32c). The basal lamina measured approximately

125 nm in thickness. In some areas of the basal lamina, the lamina lucida was indistinct.

8 days post-exposure

Ciliated cells

Degeneration of the ciliated cells was also evident 8 days post-exposure to carbendazim. The degenerating ciliated cells contained pyknotic nuclei. Nuclei exhibiting chromatin condensations and marginalized nucleoli were also observed in degenerating cells (Fig. 2.33a). The cytoplasm of these cells contained material of intermediate electron density. In both the apical and basal cytoplasmic regions, dilated RER cisternae, swollen mitochondria and numerous lysosomes were observed (Fig. 2.33b). Glycogen granules were identified in the apical cytoplasmic region. In a few degenerating ciliated cells, loss of cilia was evident. Although basal bodies were intact in these cells, striated rootlets anchoring the basal bodies were indistinct.

Non-ciliated cells

Degenerating non-ciliated cells were observed protruding above the mucosal surface (Fig. 2.34a). These cells contained pyknotic nuclei and numerous primary lysosomes throughout the cytoplasm. A few secondary lysosomes and myelin figures were observed in the apical cytoplasmic regions. At this stage, degenerating cells were lined by a few microvilli.

Plasma membrane and basal lamina

Desmosomes along the lateral plasma membrane were morphologically normal. A basal lamina measuring approximately 94 nm in thickness underlined the luminal epithelium. Invaginations of the basal lamina were still observed (2.34b).

12 days post-exposure

Twelve days post-exposure to carbendazim, degeneration of epithelial cells was still observed.

Ciliated cells

Degenerating ciliated cells contained electron lucent cytoplasm with numerous vacuoles and pyknotic nuclei (Fig. 2.35a). In a few degenerating ciliated cells, blebbing of the nuclear membrane was observed (Fig. 2.35b).

Non-ciliated cells

At this stage, non-ciliated cells were lined by relatively few microvilli. Swollen mitochondria and dilated cisternae of the RER were commonly observed. A few degenerating cells contained pyknotic nuclei.

Plasma membrane and basal lamina

Desmosomes linking adjacent epithelial cells were structurally normal. A basal lamina of approximately 120 nm in thickness underlined the epithelium. No morphological changes were observed in the basal lamina.

32 days post-exposure

Ciliated cells

Thirty-two days post-exposure to carbendazim, degenerating ciliated cells contained crenated nuclei (Fig. 2.36a). A few pyknotic nuclei were also observed. Numerous vacuoles and dilated cisternae of RER were identified throughout the cytoplasm of the degenerating cells (Fig. 2.36a). Myelin figures were observed in the basal cytoplasmic regions (Fig. 2.36b). In these cells, basal bodies and striated rootlets were structurally normal.

Non-ciliated cells

Dilated cisternae of RER and swollen mitochondria were the predominant degenerative changes observed in the apical and basal regions of the non-ciliated cells (Fig. 2.37). At this stage, a few degenerating non-ciliated cells were devoid of microvilli along the apical plasma membranes. Numerous lysosomes were observed in the apical cytoplasmic regions.

Plasma membrane and basal lamina

No degenerative changes were observed in either the plasma membrane or underlying basal lamina.

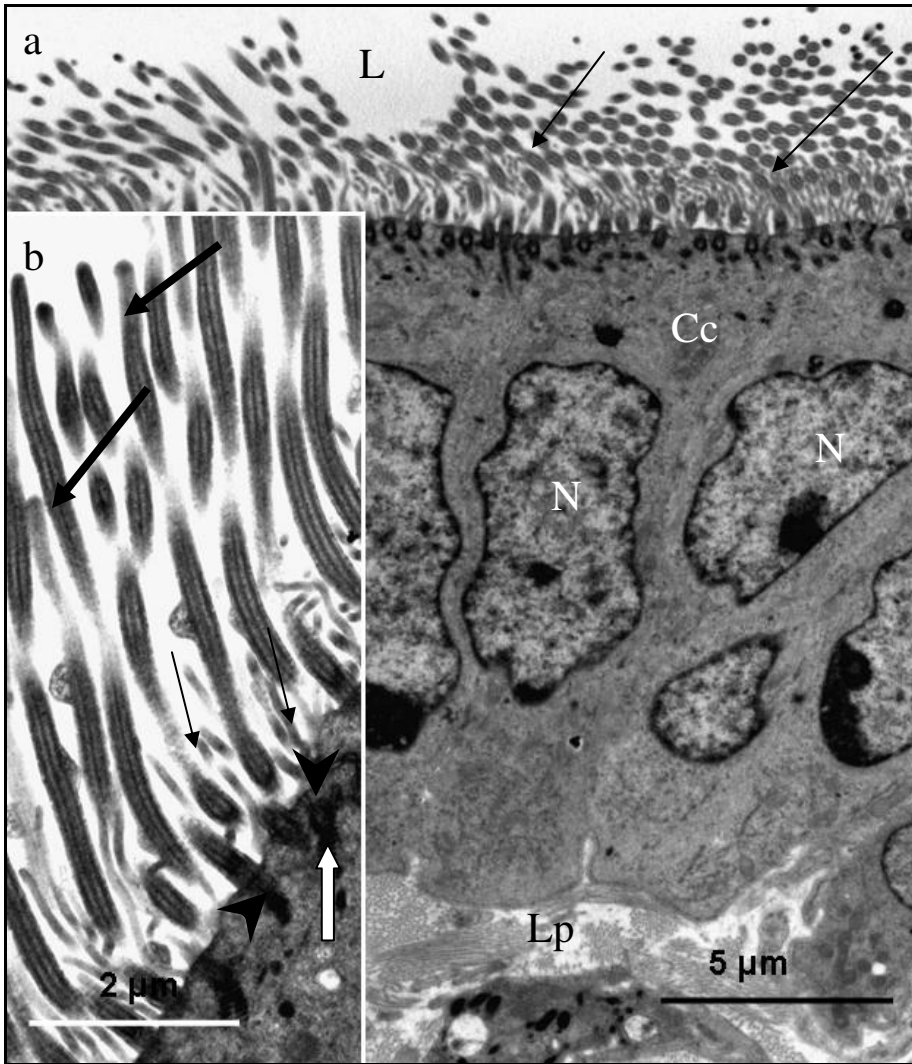


Fig. 2.27: Transmission electron photomicrographs of the funnel region of the infundibulum from a control bird. **a.** Simple ciliated columnar epithelium lines the mucosa. Centrally-located oval nuclei (N) are observed in the ciliated cells (Cc). The ciliated cells are lined by cilia (arrows). L: lumen, Lp: *lamina propria-submucosa*. **b.** Apical region of a ciliated cell. Long cilia (thick arrows) and microvilli (thin arrows) are observed. Arrowheads: basal bodies supporting the cilia; White arrow: striated rootlets anchoring the basal body.

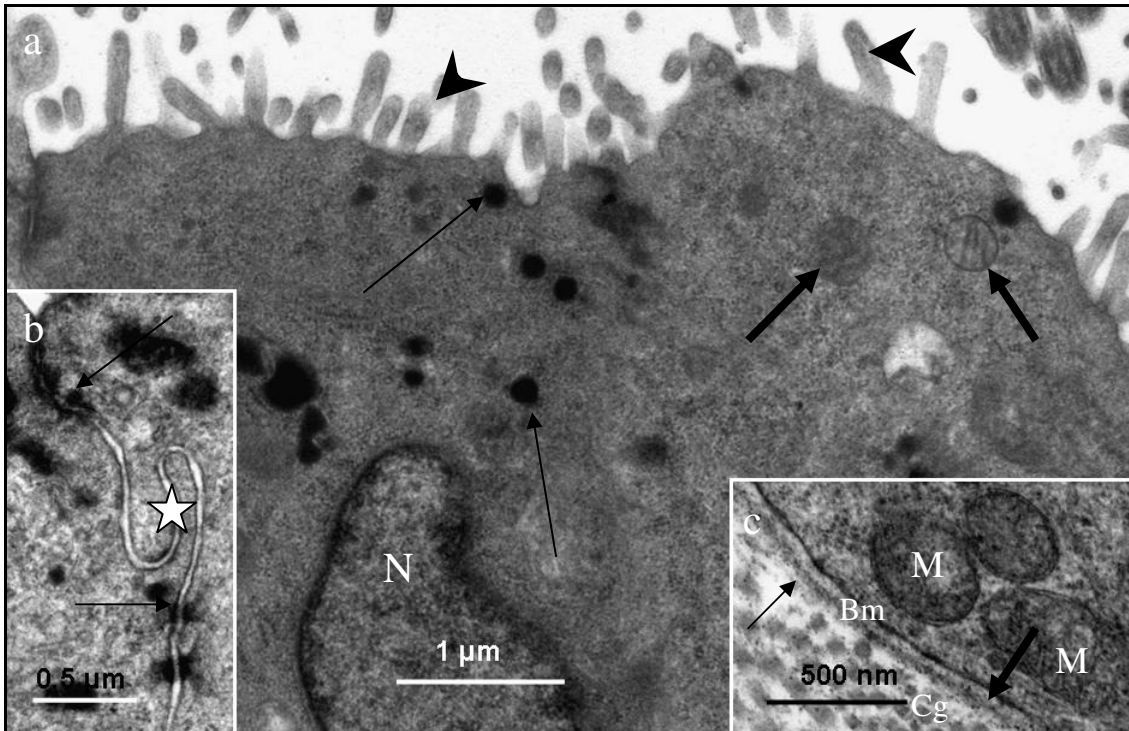


Fig. 2:28: **a.** Transmission electron photomicrograph of the apical region of non-ciliated cells in the funnel region of the infundibulum from a control bird. Long microvilli (arrowheads) are observed lining the apical plasma membrane. A few mitochondria (thick arrows) and lysosomes (thin arrows) are seen in the apical cytoplasmic region. N: nucleus. **b.** Desmosomes (arrows) and interdigitations (asterisk) are observed along the lateral plasma membrane. **c.** Electron photomicrograph of the basal region of a non-ciliated cell. The basal lamina (Bm) underlying an epithelial cell is observed. Both lamina densa (thin arrow) and lamina lucida (thick arrow) are clearly identified. Note the presence of numerous mitochondria (M) in this region. Cg: collagen fibres.

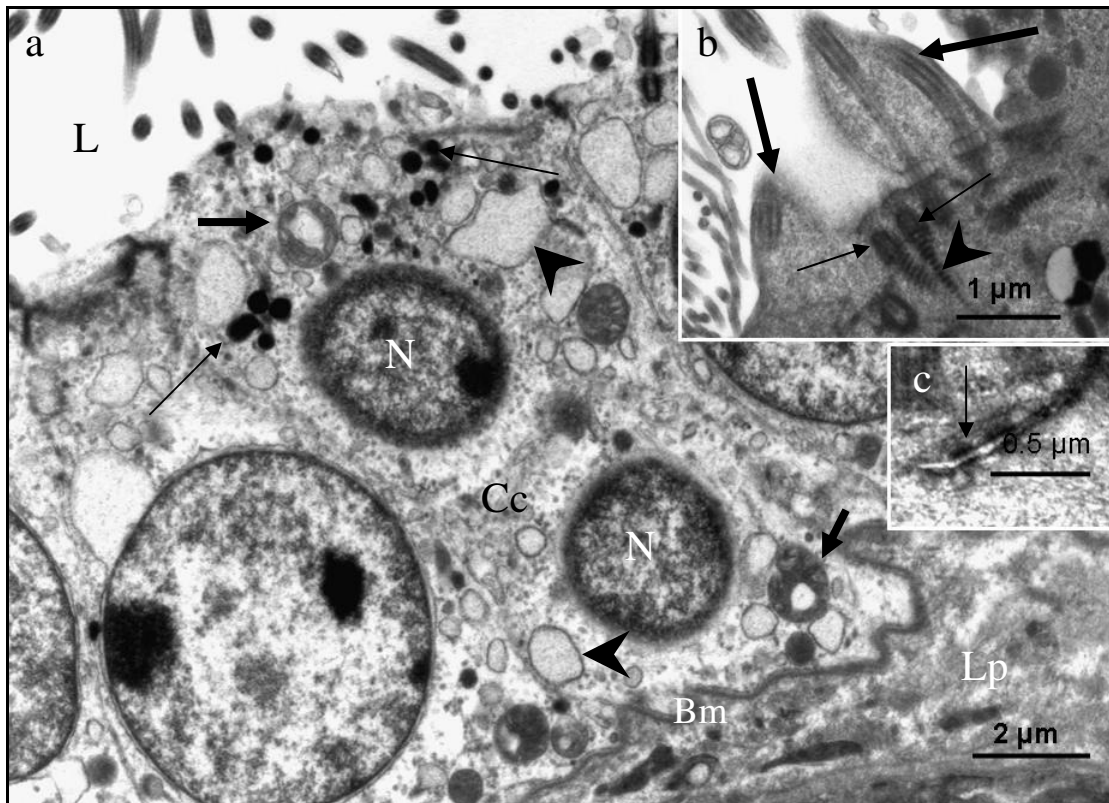


Fig. 2.29: Transmission electron photomicrographs of the funnel region of the infundibulum from a bird treated with 400 mg/kg bodyweight carbendazim. **a.** Degenerating ciliated cells (Cc) contain pyknotic nuclei (N), swollen mitochondria (thick arrows) and dilated cisternae of RER (arrowheads). Numerous lysosomes (thin arrows) are observed in the apical cytoplasmic regions. Note the ciliary loss. Bm; basal lamina; L: lumen; Lp: *lamina propria-submucosa*. **b.** Apical region of degenerating ciliated cells. Compound cilia (thick arrows) are observed. Thin arrow: Basal bodies. Arrowheads: Striated rootlets. **c.** An intact desmosome (arrow) linking adjacent cells.

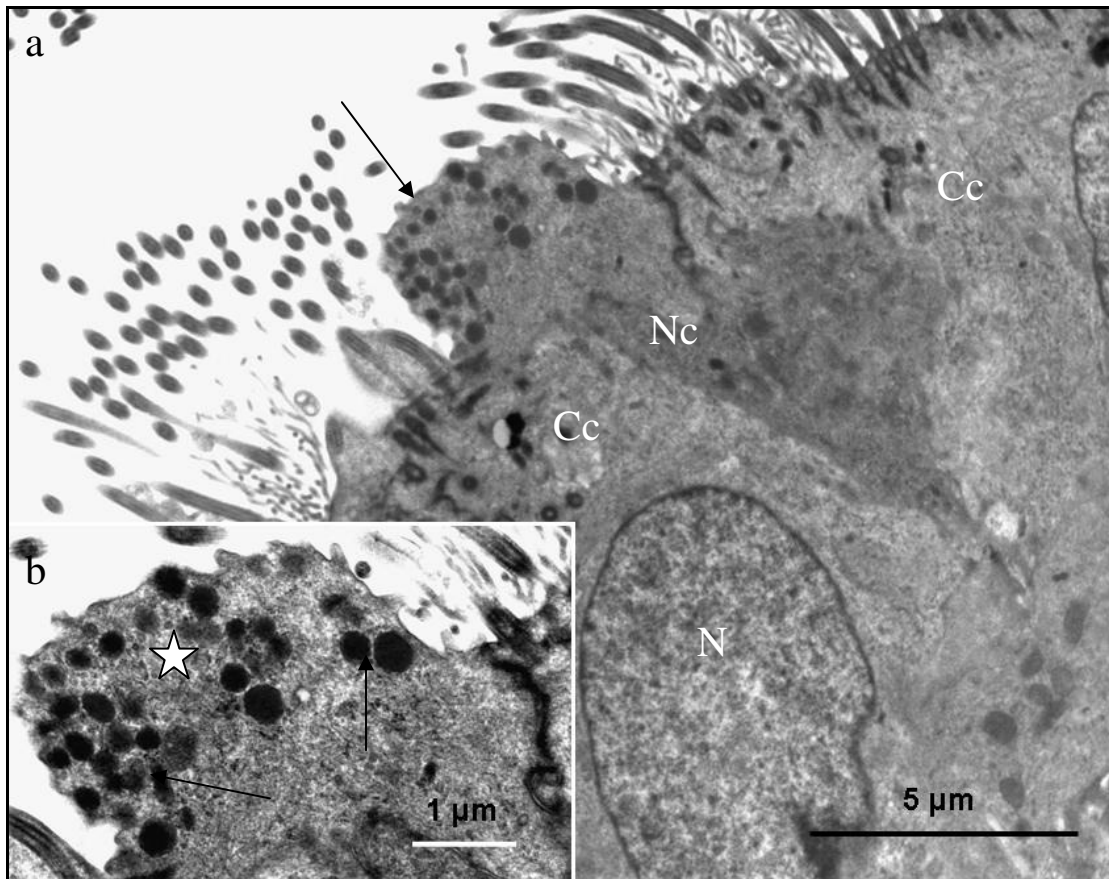


Fig. 2.30: Transmission electron photomicrographs of the funnel region of the infundibulum from a bird treated with 400 mg/kg bodyweight carbendazim. **a.** Raised apical region (arrow) of a degenerating non-ciliated cell (Nc). Cc: ciliated cells; N: nucleus. **b.** A higher magnification electron photomicrograph of the apical enlargement (asterisk) of a non-ciliated cell. Arrows: Lysosomes.

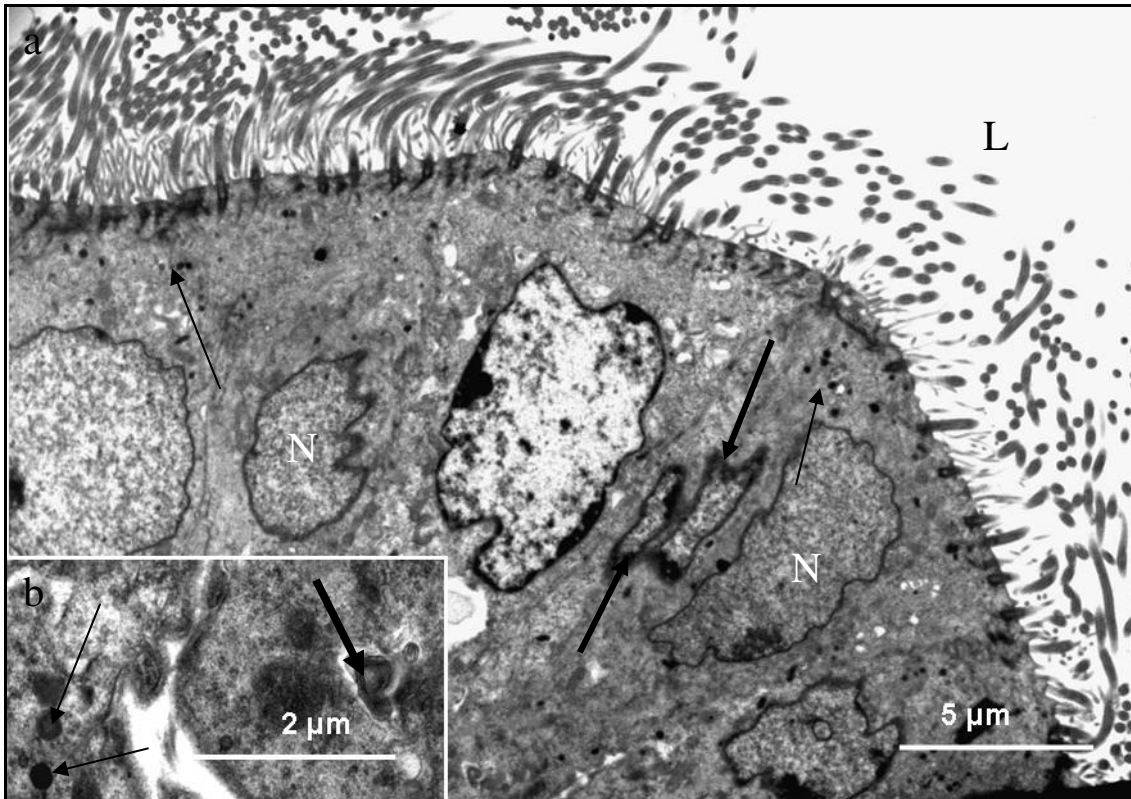


Fig. 2.31: **a.** A survey transmission electron photomicrograph of the funnel region of the infundibulum from a bird treated with 800 mg/kg bodyweight carbendazim. Degenerating nuclei (thick arrows) are observed. Numerous lysosomes (thin arrows) are observed in the apical cytoplasmic regions. N: cretated nucleus. **b.** Basal region of degenerating cells. A myelin figure (thick arrow) and lysosomes (thin arrows) are observed in this region.

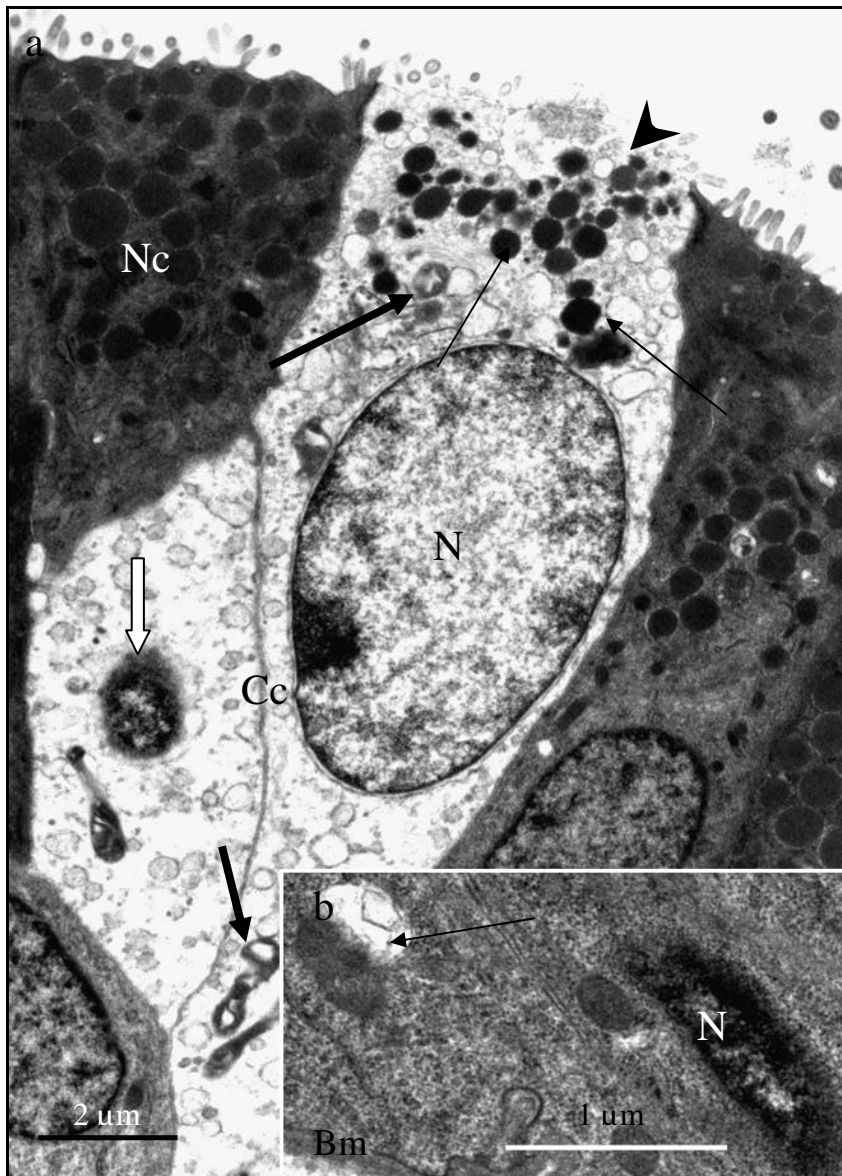


Fig. 2.32: Transmission electron photomicrographs of the funnel region of the infundibulum, 5 days post-exposure to 400 mg/kg bodyweight carbendazim. **a.** Degenerating ciliated cells (Cc). Thin arrows: Lysosomes. Arrowhead: deciliated and discontinuous apical plasma membrane. Thick arrow: swollen mitochondria. White arrow: pyknotic nucleus. Nc: non-ciliated cell lined by relatively few microvilli. **b.** Basal region of degenerating non-ciliated cell indicating pyknotic nucleus (N) and swollen mitochondrion (arrow). Bm: basal lamina.

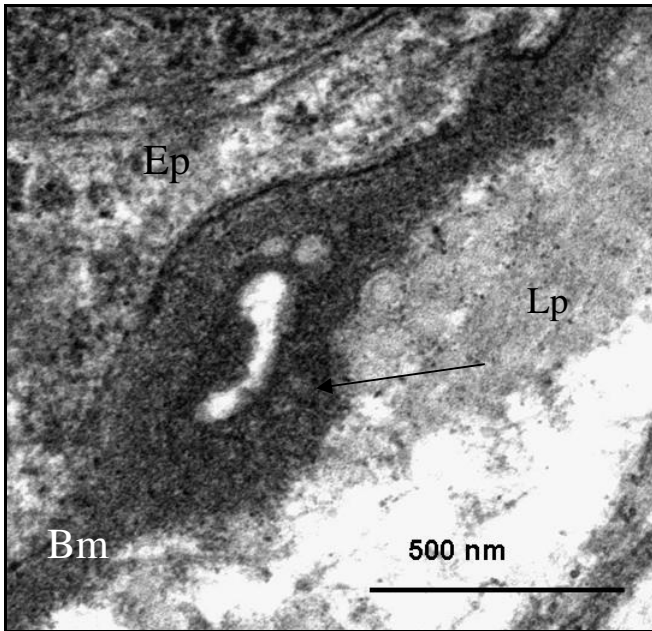


Fig. 2.32c: Transmission electron photomicrograph of the basal lamina (Bm) underlying the epithelium in the funnel region of the infundibulum, 5 days post-exposure to 400 mg/kg bodyweight carbendazim. Folding of the basal lamina (arrow) is observed. At this stage, lamina lucida is indistinct. Ep: epithelium; Lp: *lamina propria-submucosa*.

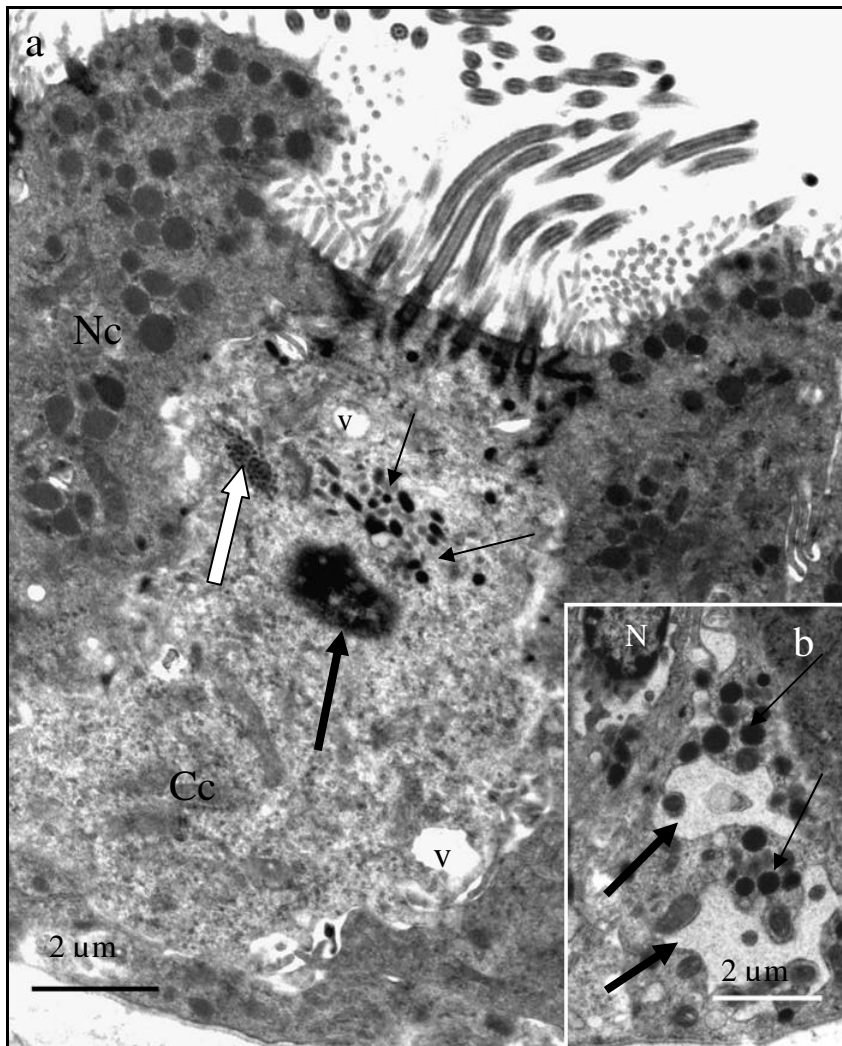


Fig. 2.33: Transmission electron photomicrographs of the funnel region of the infundibulum, 8 days post-exposure to 400 mg/kg bodyweight carbendazim. **a.** A pyknotic nucleus (thick arrow) and numerous lysosomes (thin arrows) in a degenerating ciliated cell (Cc). V: Vacuoles. White arrow: Glycogen granules. Nc: degenerating non-ciliated cell. **b.** Basal cytoplasmic region of a degenerating ciliated cell. Thick arrows: dilated cisternae of RER. Thin arrows: lysosomes. N: degenerating nucleus.

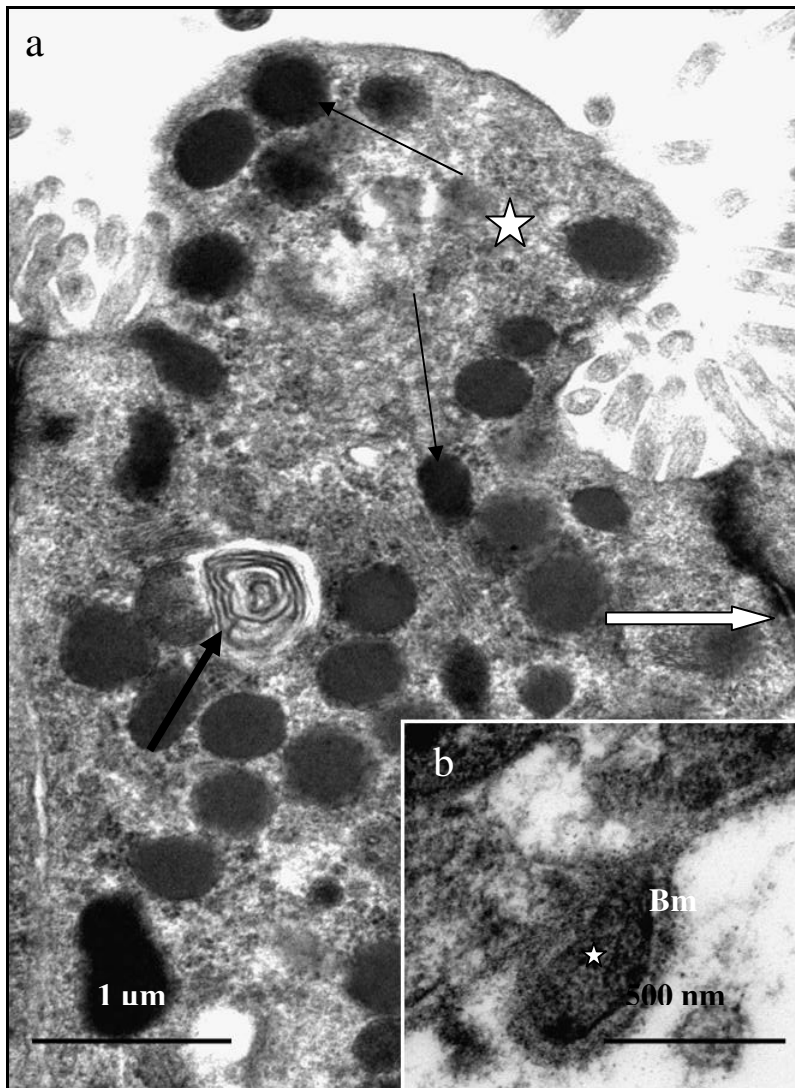


Fig. 2.34: **a.** Transmission electron photomicrograph of a degenerating non-ciliated cell in the funnel region of the infundibulum, 8 days post-exposure to 400 mg/kg bodyweight carbendazim. Asterisk: Apical protrusion. Thick arrow: Myelin figure. Thin arrows: Lysosomes Open arrow: an intact desmosome linking the adjacent cell. **b.** Asterisk: bulging of the basal plasma membrane. Bm: folded basal lamina.

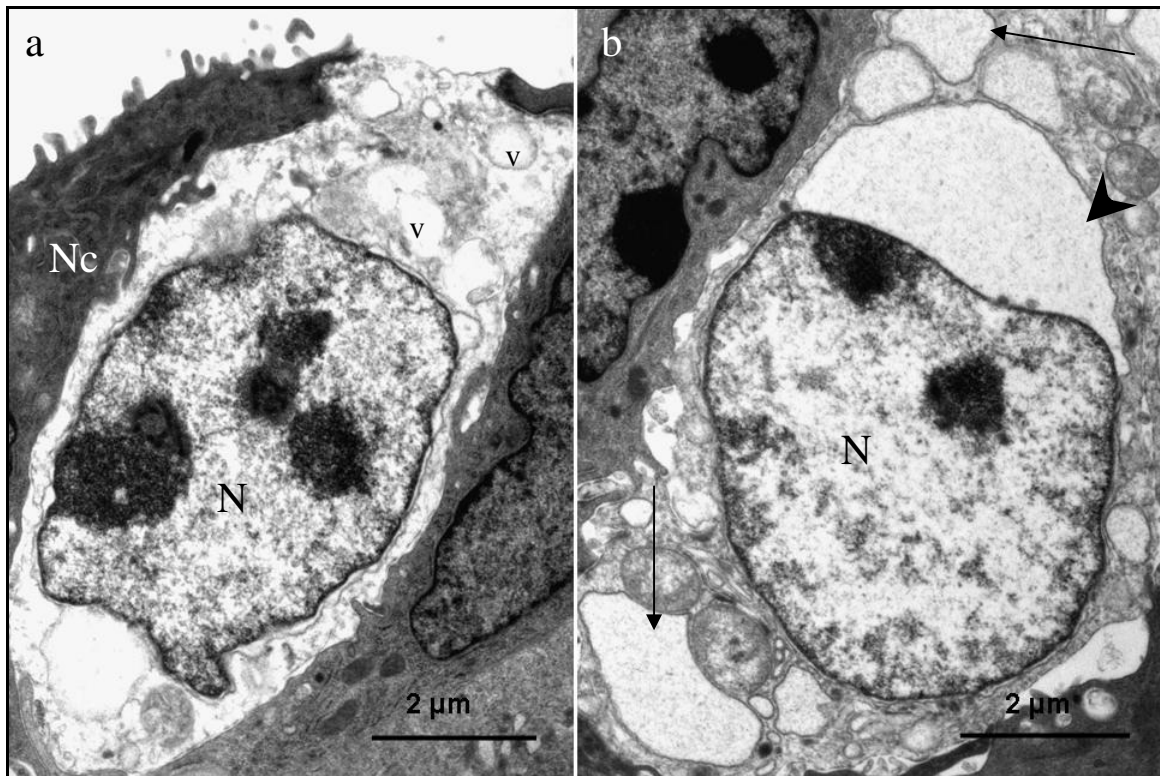


Fig. 2.35: Transmission electron photomicrographs of degenerating ciliated cells in the funnel region of the infundibulum, 12 days post-exposure to 400 mg/kg bodyweight carbendazim. **a.** Degenerating ciliated cell (Cc) displaying electron lucent cytoplasm. V: Vacuoles (v). N: nucleus. Nc: non-ciliated cell. **b.** Nuclear membrane blebbing (arrowhead) and dilated cisternae of RER (arrows) are observed in a degenerating ciliated cell. N: nucleus.

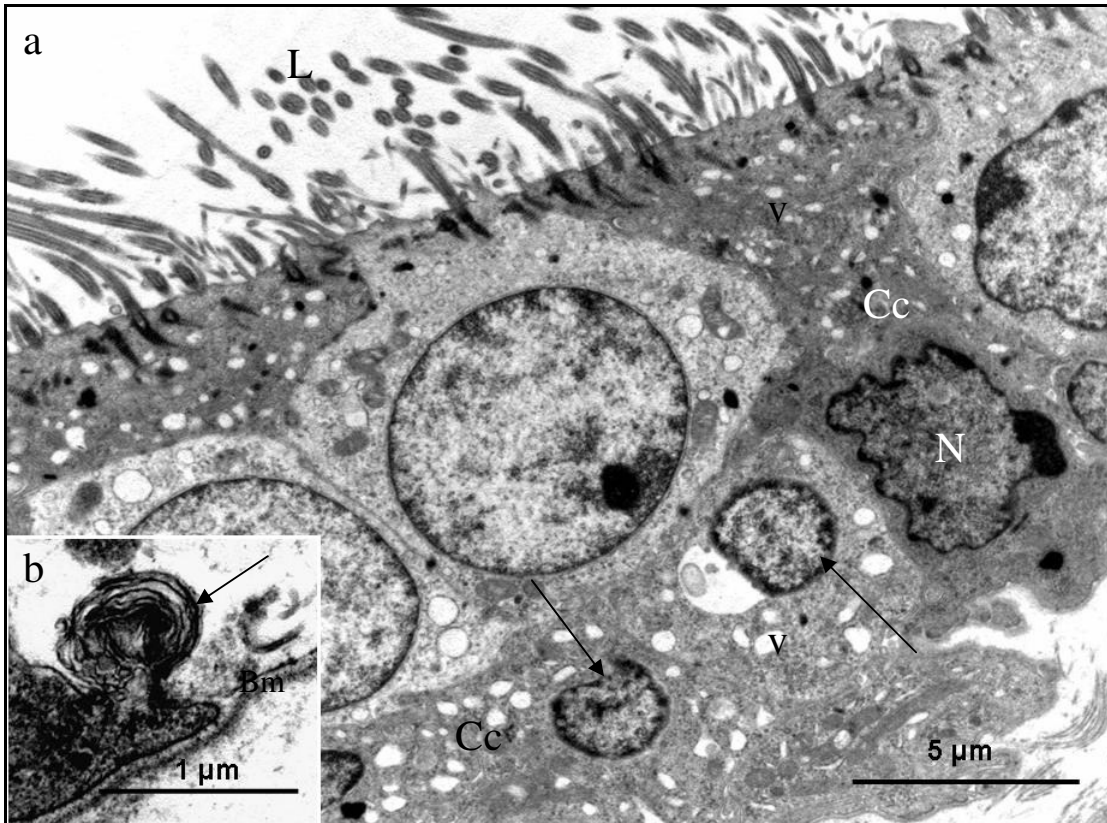


Fig. 2.36: Transmission electron photomicrographs of the funnel region of the infundibulum, 32 days post-exposure to 400 mg/kg bodyweight carbendazim. **a.** A Crenated nucleus (N) and pyknotic nuclei (arrows) are observed in degenerating ciliated cells (Cc). V: Vacuoles. L: lumen. **b.** Basal cytoplasmic region of a degenerating ciliated cell. Arrow: myelin figure Bm: basal lamina.

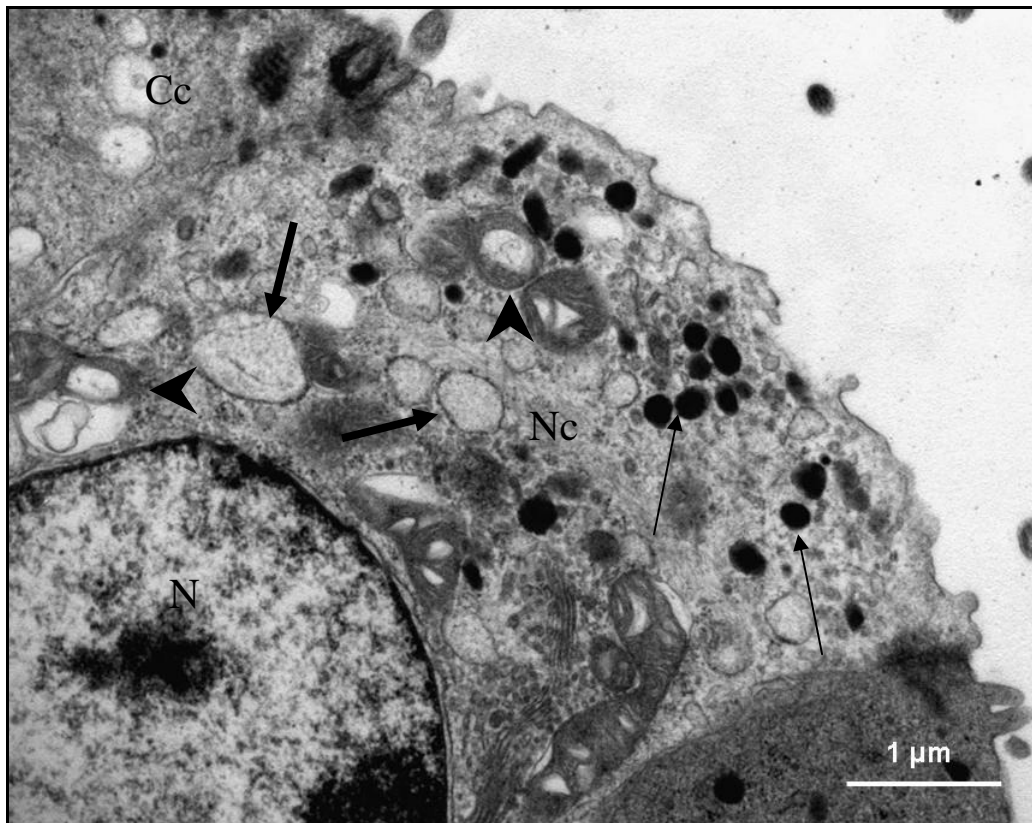


Fig. 2.37: Transmission electron photomicrograph of a degenerating non-ciliated cell (NC) in the funnel region of the infundibulum, 32 days post-exposure to 400 mg/kg bodyweight carbendazim. Note the loss of microvilli in this cell. Thick arrows: Dilated cisternae of RER. Arrowheads: swollen mitochondria. Thin arrows: Lysosomes. Cc: ciliated cell

2.3.6.2 Tubular region

2.3.6.2.1 Scanning electron microscopy

2.3.6.2.1.i Control birds

The mucosal surface of the infundibulum was arranged in longitudinally-oriented folds (Fig. 2.38a). Both primary and secondary folds were identified. The surface epithelium consisted of evenly distributed ciliated and non-ciliated cells (Fig. 2.38b). Ciliated cells exhibited long cilia, which partially obscured adjacent non-ciliated cells (Fig. 2.38b). The non-ciliated cells exhibited dome-shaped apical regions, which were covered by short microvilli (Fig. 2.38c). Round to oval-shaped glandular openings were observed between the epithelial cells (Fig. 2.38b).

2.3.6.2.1.ii Carbendazim treated birds

2.3.6.2.1.ii.a Experiment I (dose-dependent oviductal degeneration)

Doses of 25 mg/kg and 100 mg/kg bodyweight carbendazim did not cause degenerative changes of the infundibular mucosal surface.

400 mg/kg bodyweight carbendazim

At a dose of 400 mg/kg bodyweight carbendazim areas of deciliation were observed (Fig. 2.39a). The areas of deciliation displayed numerous short stalks which were remnants of degenerating cilia (Fig. 2.39b). The microvilli on the non-ciliated cells appeared normal.

800 mg/kg bodyweight carbendazim

Deciliation was also a notable feature in quails fed 800 mg/kg bodyweight carbendazim (Fig. 2.40a). In this group a few inflammatory cells were observed on the luminal surface of the infundibulum. The luminal surfaces of the non-ciliated cells did not exhibit any degenerative changes (Fig. 2.40b).

2.3.6.2.1.ii.b Experiment II (time-course oviductal degeneration)

No degenerative changes were observed on the mucosal surfaces at 5 and 24 hours post-exposure to 400 mg/kg bodyweight carbendazim.

5 and 8 days post-exposure

At days 5 and 8 post-exposure, discrete areas of deciliation were observed (Fig. 2.41a). In these areas of deciliation, short ciliary stems and swollen microvilli were encountered (Fig. 2.41b). Some degenerating ciliated cells contained ciliary tufts with only a few intact cilia (Fig. 2.41a). A few inflammatory cells and erythrocytes were also observed on the luminal surface.

12 and 32 days post-exposure

At days 12 and 32 post-exposure to carbendazim, deciliation continued to be the dominant degenerative change observed (Fig. 2.42a). Cilia with swollen tips and nodular shaft were observed (Fig. 2.42a). The apical part of the degenerating non-ciliated cells was raised above the surface and lined by short, swollen microvilli (Fig. 2.42b).

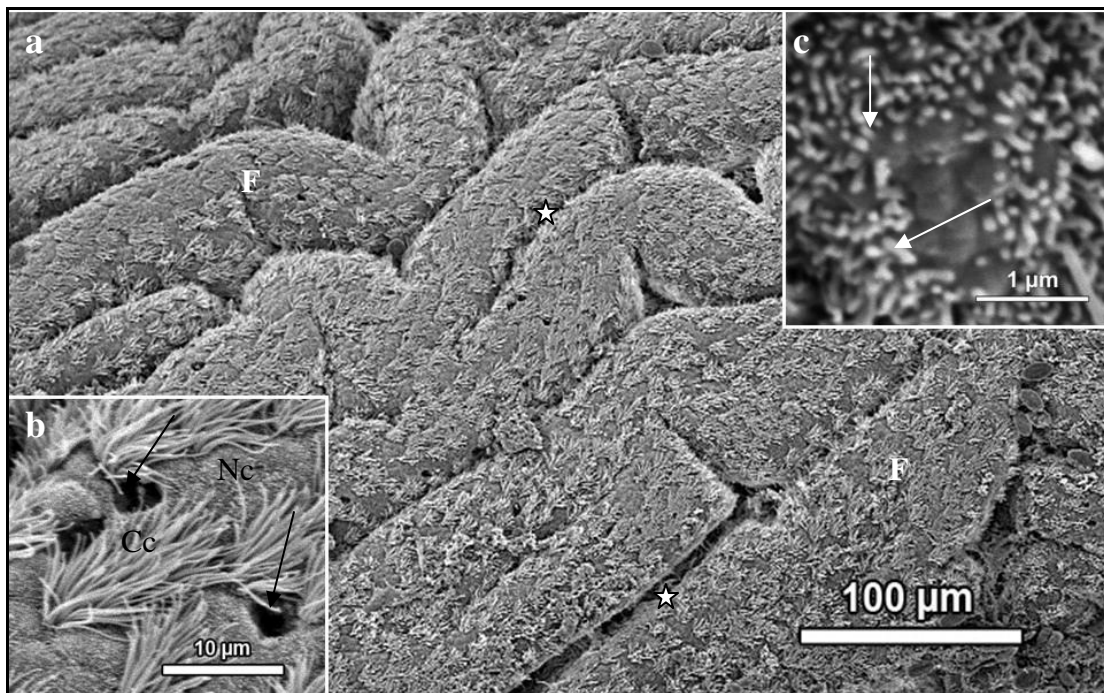


Fig. 2.38: **a.** A scanning electron photomicrograph of the tubular region of the infundibulum from a control bird. The mucosa is thrown into folds (F) separated by clefts (asterisks). **b.** A higher magnification photomicrograph Ciliated (Cc) and non-ciliated (Nc) cells are observed. Glandular openings (arrows) are observed between the epithelial cells. **c.** Apical surfaces of non-ciliated cells. Arrows: microvilli.

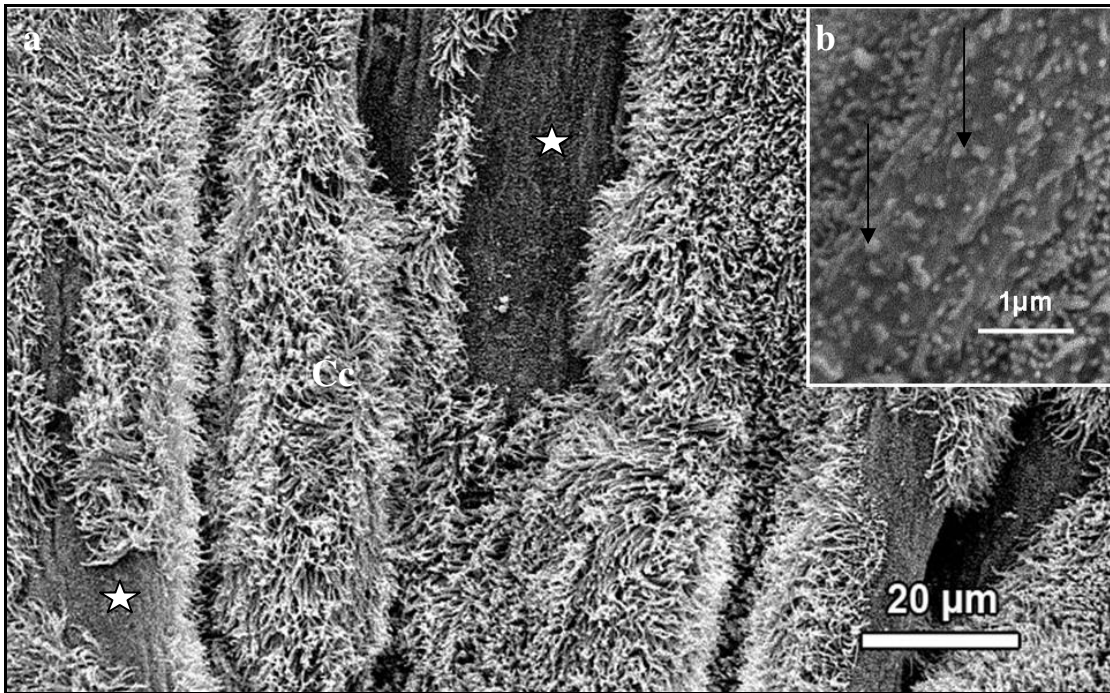


Fig. 2.39: **a.** A survey scanning electron photomicrograph of the tubular region of the infundibulum from a 400 mg/kg bodyweight carbendazim-treated bird. Patchy areas of deciliation (asterisks) are observed. Cc: normal ciliated cells. **b.** A higher magnification photomicrograph of areas of deciliation. . Note the presence of cilia stems (arrows), which are remnants of the lost cilia.

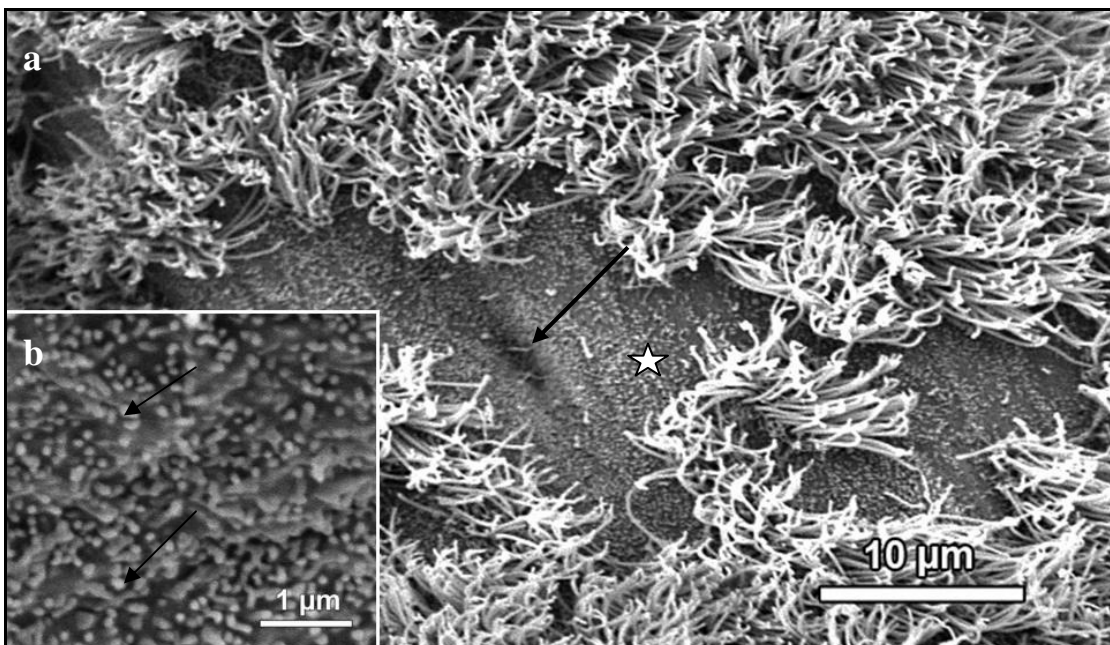


Fig. 2.40: **a.** Scanning electron photomicrograph of the luminal epithelium in the tubular region of the infundibulum of a bird treated with 800 mg/kg bodyweight carbendazim. Asterisk: area of deciliation. Arrow: Glandular opening. **b.** Apical surfaces of non-ciliated cells. Lining microvilli (arrows) appear normal.

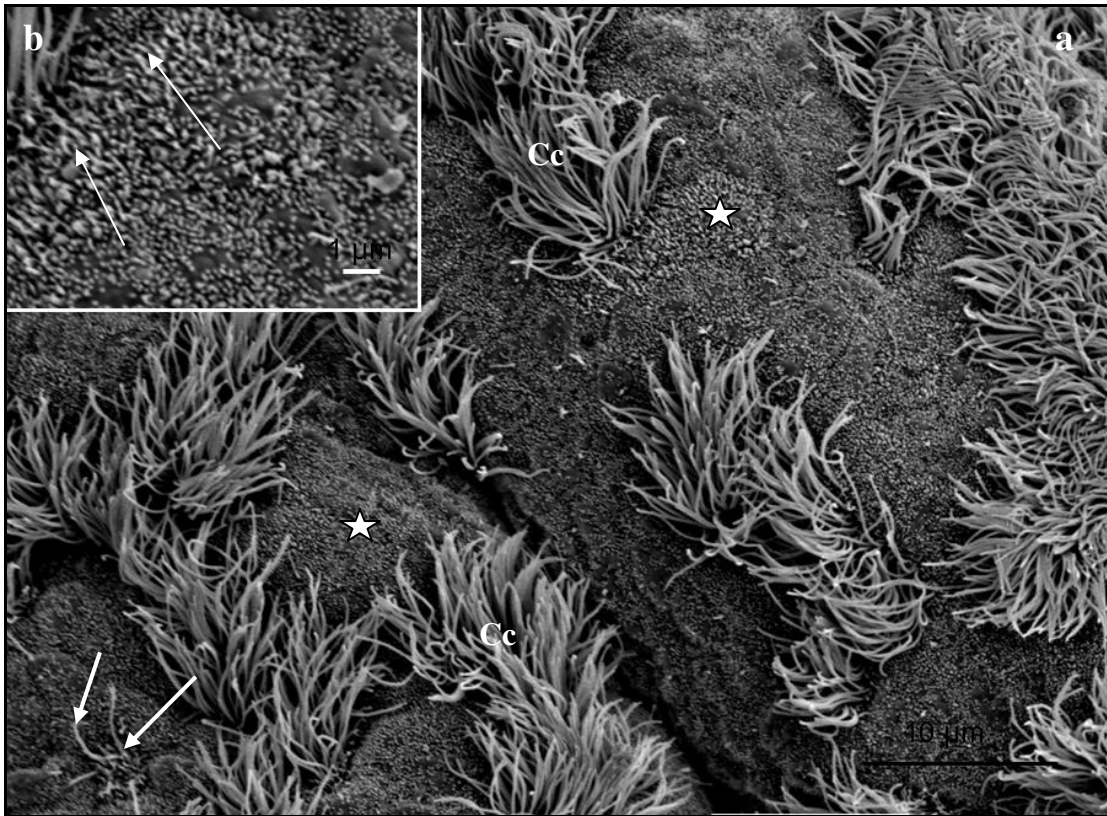


Fig. 2.41: **a.** A scanning electron photomicrograph of the infundibulum, 8 days post-exposure to 400 mg/kg bodyweight carbendazim. Asterisks: areas of deciliation. Arrows: Ciliary tuft with only a few cilia. Cc: Normal ciliated cells with intact cilia. **b.** A higher magnification scanning electron photomicrograph of degenerating ciliated cells. Note the presence of short stems (arrows) on the surface of these cells.

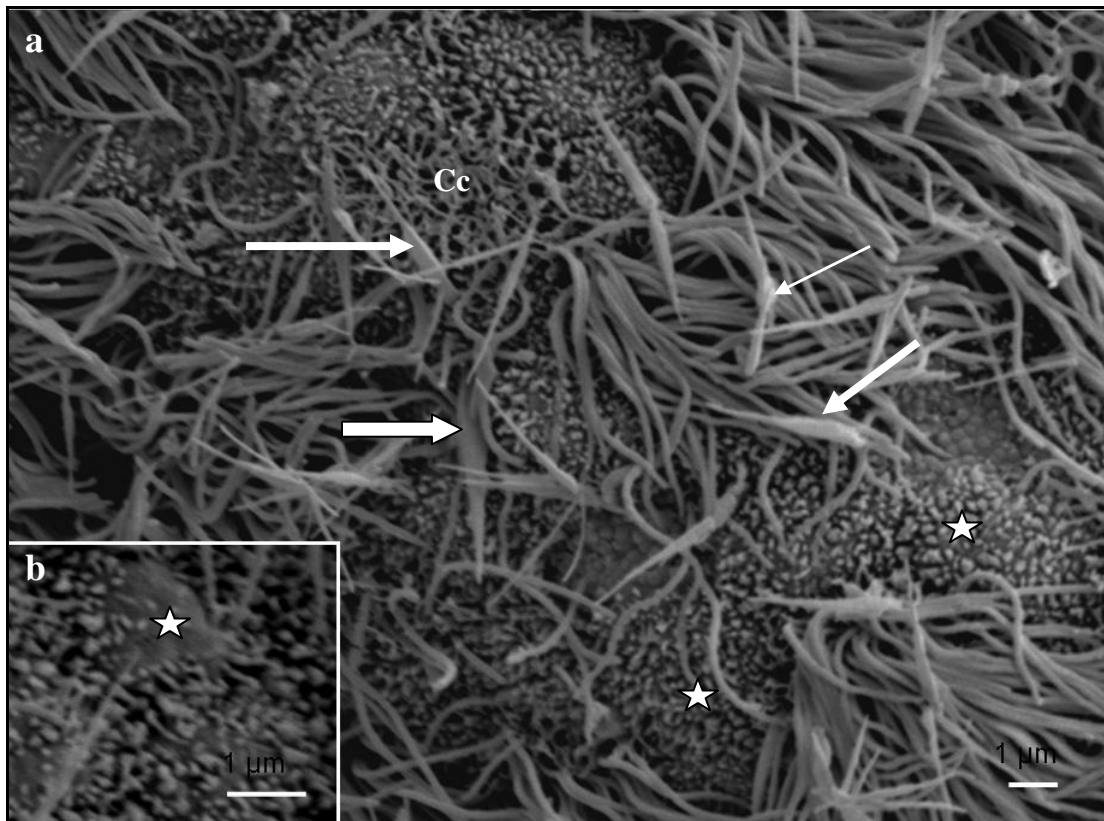


Fig. 2.42: **a.** Scanning electron photomicrographs of the tubular region of the infundibulum, 12 days post-exposure to 400 mg/kg bodyweight carbendazim. Cells exhibiting cilia loss (asterisks) are seen. Thick arrows: Swollen cilia. Thin arrow: Nodular cilium. **b.** Apical surface of a degenerating non-ciliated cell with short, swollen microvilli (asterisk).

2.3.6.2.2 Transmission electron microscopy

2.3.6.2.2.i Control birds

A simple columnar epithelium consisting of ciliated and non-ciliated cells lined the tubular region of the infundibulum (Fig. 2.43). The epithelial cells appeared to be predominantly ciliated.

Ciliated cells

The ciliated cells contained centrally-located, euchromatic, oval nuclei, surrounded by an electron lucent cytoplasm (Fig. 2.43). The cytoplasm of the ciliated cells contained mitochondria, smooth (SER) and rough (RER) endoplasmic reticulum, Golgi complexes, as well as, a few lysosomes (Fig. 2.44a). The apical plasma

membrane of the ciliated cells was lined by cilia and microvilli. Supporting the cilia were basal bodies, anchored by rootlets and basal feet (Fig. 2.44b). The basal bodies were hollow structures consisting of circularly-arranged, nine-triplet microtubules. Anchoring the basal bodies were rootlets, which are striated structures, attached to the lateral aspects of the basal bodies. Associated with basal bodies and rootlets were basal feet, which were composed of filaments or microtubules. Basal bodies, basal feet and rootlets were identified in the apical cytoplasmic regions of the ciliated cells (Fig. 2.44b). On cross section, each cilium was composed of a complex of nine pairs of microtubules surrounding a central pair of microtubules. A plasma membrane lined the cilia. Proximally, the plasma membrane was modified to form a “cilia necklace” (Fig. 2.45a). The apical ends of the cilia were tapered and formed structures termed “cupping plates”.

Non-ciliated cells

Non-ciliated cells in the tubular region of the infundibulum contained round, basally-located nuclei. Membrane-bound secretory granules or bodies, occupied most of the cytoplasm (Fig. 2.43). The secretory granules, which were round to ovoid in shape, contained a homogeneous material of an intermediate electron density. Round to elongated mitochondria were distributed throughout the cytoplasm. A few arrays of SER and RER were also observed. The apical plasma membrane was modified to form numerous, uniform microvilli (Fig. 2.43).

Plasma membrane and basal lamina

Desmosomes and intermediate junctions linked adjacent cells (Fig. 2.45b). A granular basal lamina separated the surface epithelium from the underlying *lamina propria-submucosa* (Fig. 2.45c). The basal lamina, which was approximately 80 nm thick, was composed of a distinct lamina densa and lamina lucida. Underlying the basal lamina were collagen fibres.

Tubular glands

Blood capillaries, loose connective tissue fibres and tubular glands were observed in the *lamina propria-submucosa*. The tubular glands were lined by a simple cuboidal epithelium (Fig. 2.46a). A typical gland cell contained a basally-located, euchromatic nucleus with prominent nucleoli (Fig. 2.46a). The apical region of the cytoplasm in these cells contained numerous membrane-bound secretory granules and occasional bundles of microfilaments (Fig. 2.47a). The secretory granules, which were round in shape, typically contained a homogeneous, electron dense material. The apical cell membrane was lined by short, slender microvilli (Fig. 2.47a). Mitochondria, Golgi complexes and a few lysosomes were observed perinuclearly (Fig. 2.47 b & c). In addition, arrays of SER and RER were occasionally present in the perinuclear area of the gland cells, as well as in the apical cytoplasmic regions (Fig. 2.48a). Desmosomes and occasional tight junctions were observed along the lateral and apical plasma membranes of the gland cells (Fig. 2.48 a & b). In addition, interdigitating folds were observed along the lateral plasma membrane.

A homogeneous basal lamina of approximately 80 nm surrounded the glands (Fig. 2.46b). Blood capillaries and a few supporting cells were occasionally encountered in the *lamina propria-submucosa* between the tubular glands. The supporting cells contained oval to elongated nuclei. A few lysosomes, mitochondria, Golgi complexes, vesicles and RER cisternae were observed in the cytoplasm of the supporting cells (Fig. 2.46c).

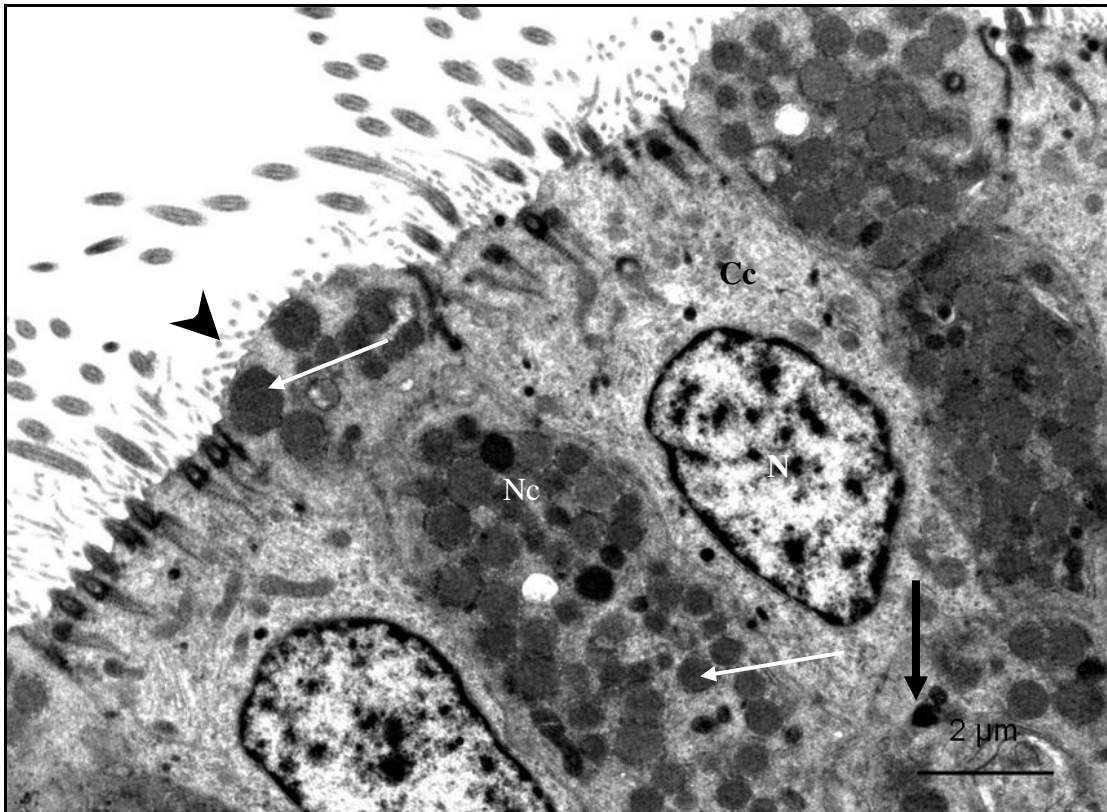


Fig. 2.43: A survey electron photomicrograph of the luminal epithelium in the tubular region of the infundibulum from a control bird. Cc: ciliated cells with electron lucent cytoplasm. Nc: Non-ciliated cell with a dome-shaped apical region lined by short microvilli (arrowhead). N: nucleus. Thick arrow: Lysosome. Thin arrows: Secretory granules.

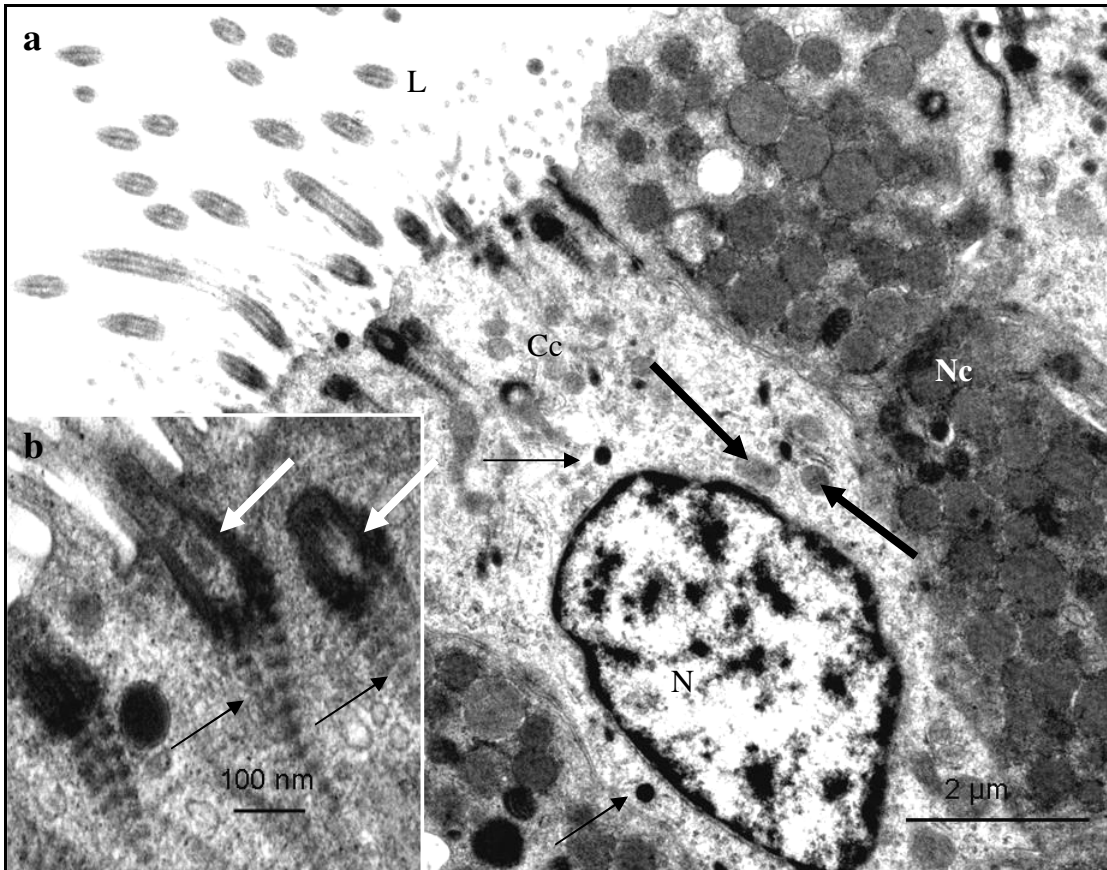


Fig. 2.44: Transmission electron photomicrographs of luminal epithelial cells in the tubular region of the infundibulum of a control bird. **a.** In the ciliated cell (Cc) lysosomes (thin arrows) and mitochondria (thick arrows) are observed perinuclearly. N: nucleus. Nc: non-ciliated cell; L: lumen. **b.** A higher magnification photomicrograph. Thick arrows: Basal bodies. Thin arrows: Striated rootlets.

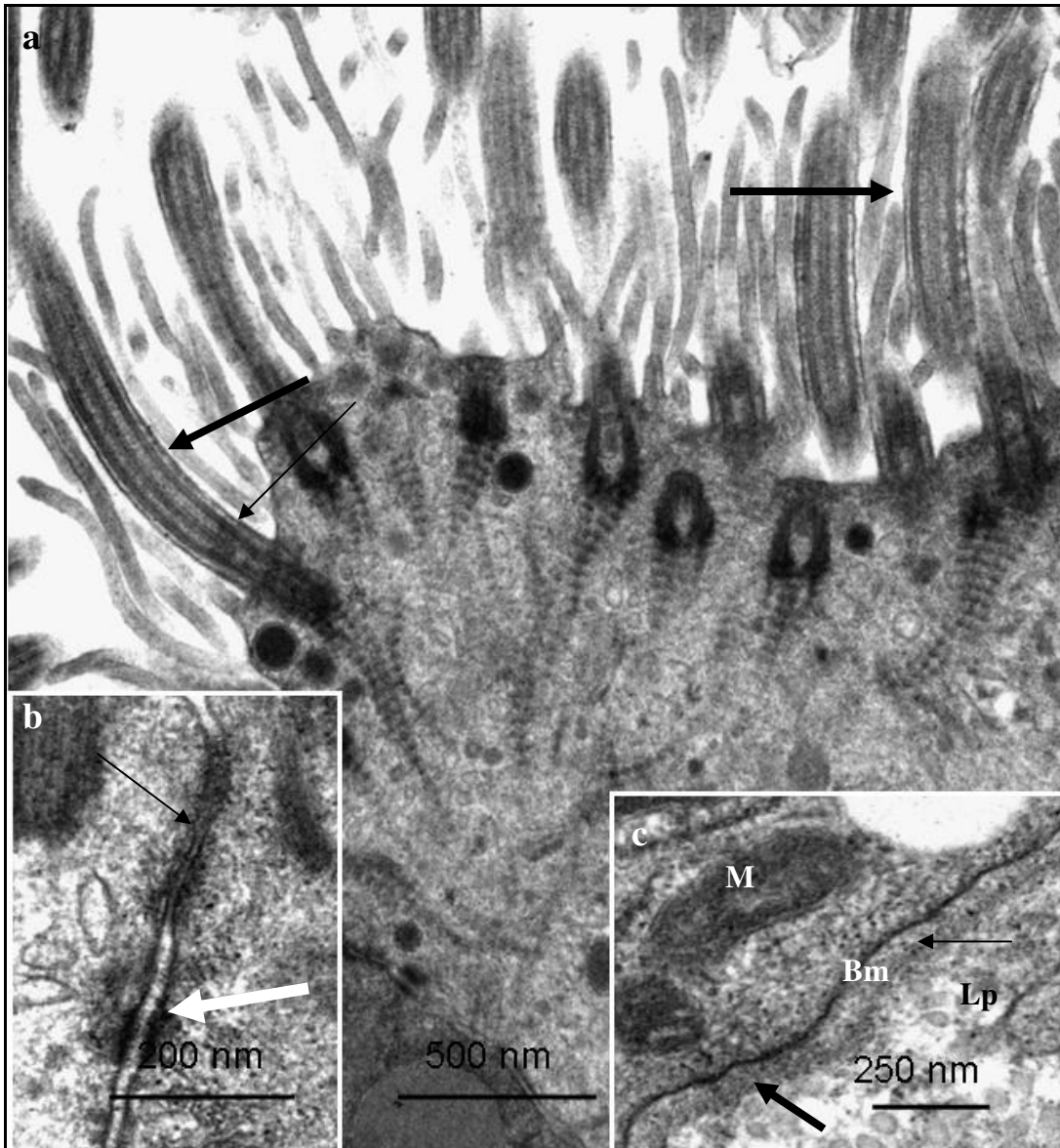


Fig. 2.45: Electron photomicrographs of the apical (a) and basal (c) regions of a ciliated cell in the tubular region of the infundibulum of a control bird. **a.** Thick arrows: Plasma membrane. Thin arrow: Cilia necklace. **b.** A desmosome (thick arrow) and an intermediate junction (thin arrow) along the lateral plasma membranes of adjacent epithelial cells. **c.** Basal lamina (Bm) with a lamina lucida (thin arrow) and densa (thick arrow). Lp: *lamina propria-submucosa*. M: Mitochondrion.

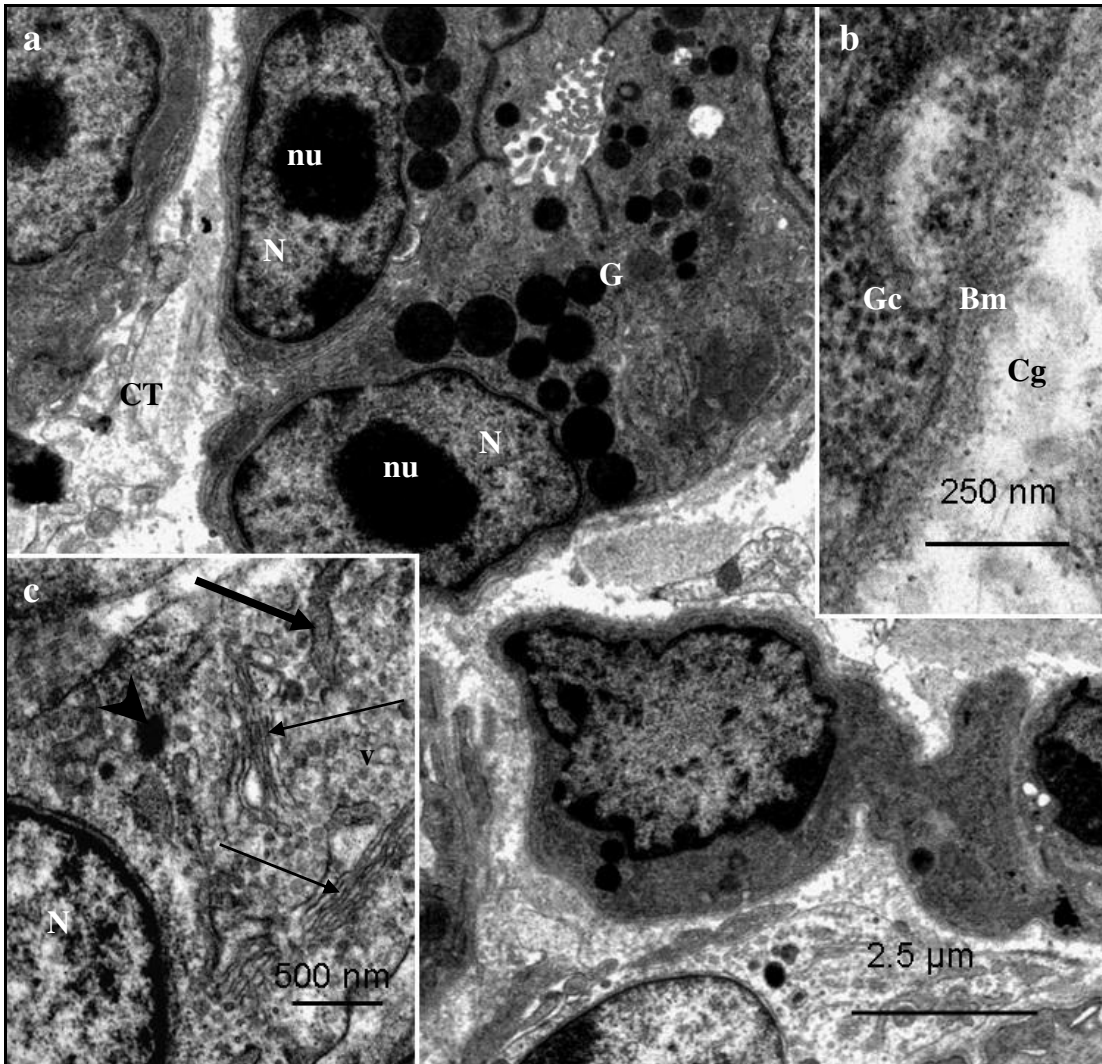


Fig. 2.46: **a.** Survey electron photomicrograph of a tubular gland (G) lined by simple cuboidal epithelium. N: nucleus. Nu: Nucleoli. CT: Connective tissue fibres. **b.** A higher magnification electron photomicrograph of the basal region of a gland cell (Gc). Bm: Basal lamina. Cg: Collagen fibres. **c.** A photomicrograph of a supporting cell. Vesicles (v), Golgi complexes (thin arrows), RER cisternae (thick arrow) and a lysosome (arrowhead) are observed perinuclearly. N: Nucleus.

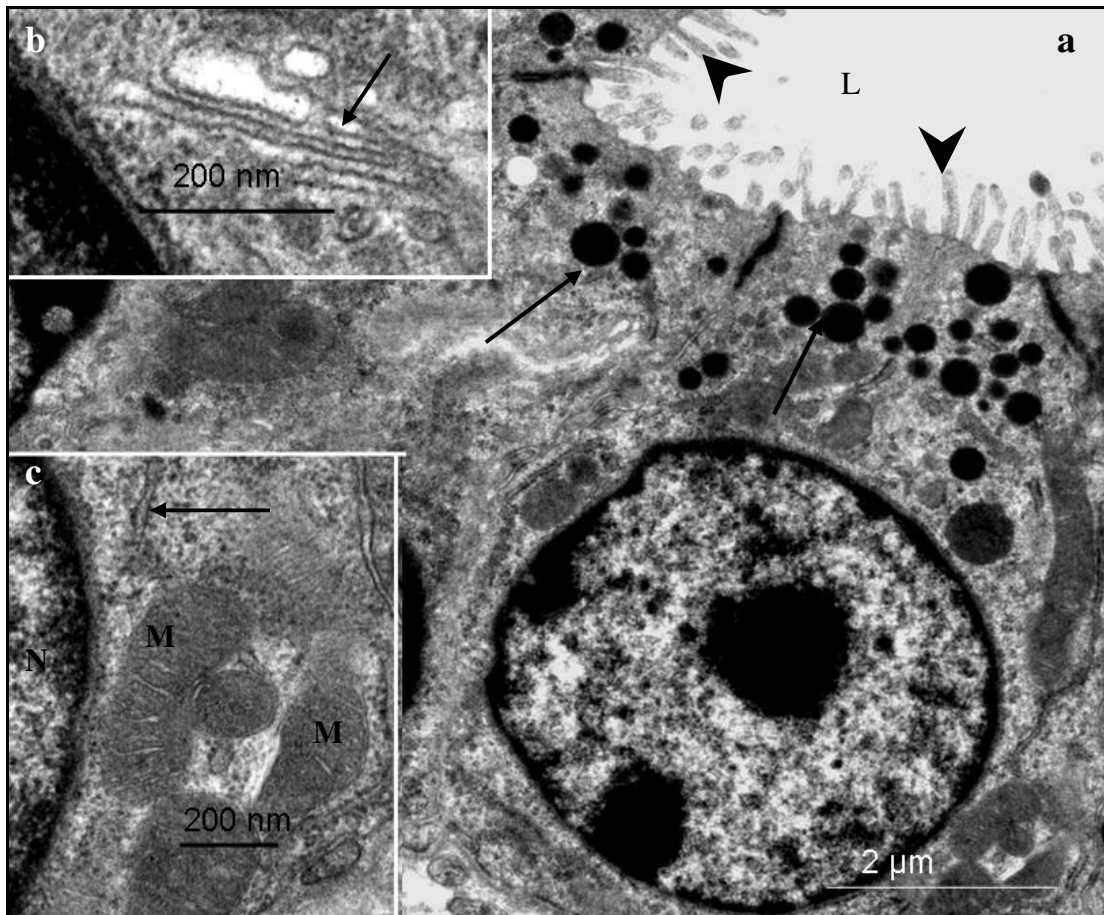


Fig. 2.47: Electron photomicrographs of a tubular gland in the infundibulum of a control bird. **a.** Arrows: Secretory granules. Arrowheads: Microvilli. L: lumen. **b.** A Golgi complex with associated vesicles. **c.** Mitochondria (M) and cisterns of RER (arrow) are seen perinuclearly. N: nucleus.

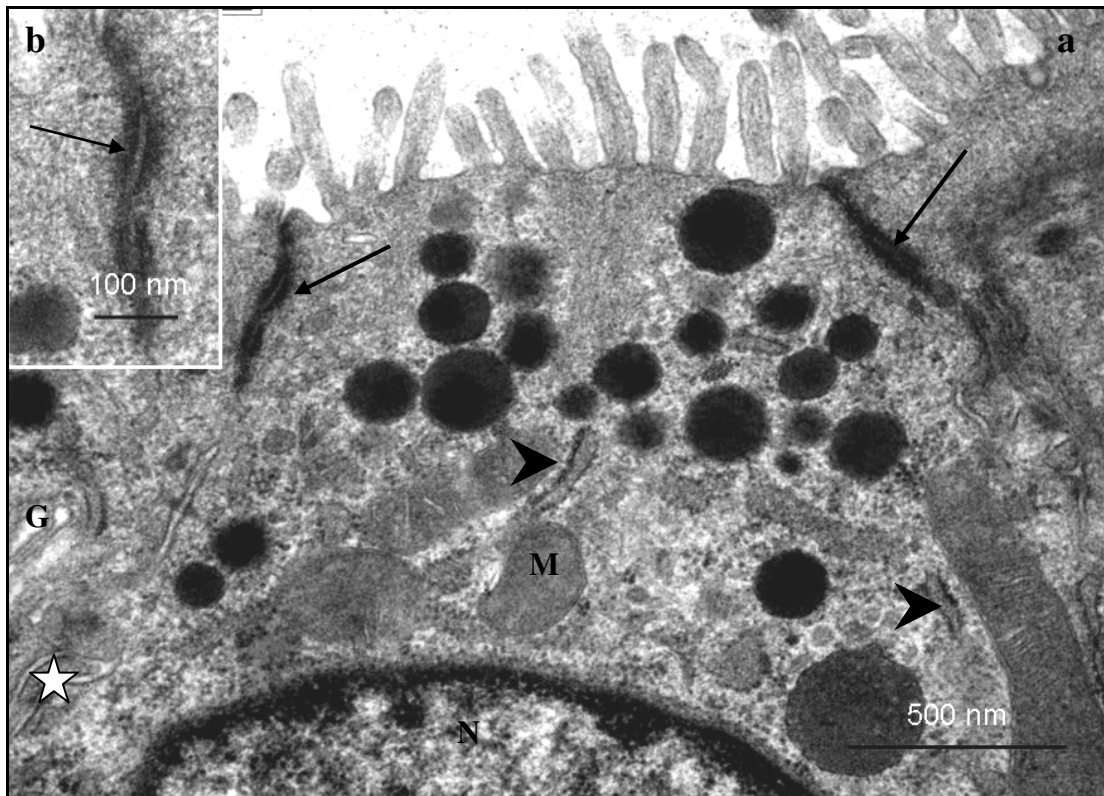


Fig. 2.48: Electron photomicrographs of the apical region of a gland cell in the tubular region of the infundibulum from a control bird. **a.** Arrowheads: RER cisternae. Arrows: Desmosomes. Asterisk: Interdigitating folds. N: nucleus. M: mitochondrion. G: Golgi complex. **b.** Higher magnification photomicrograph showing an apically located desmosome (arrow) linking adjacent gland cells.

2.3.6.2.2.ii Carbendazim treated birds

2.3.6.2.2.ii.a *Experiment I (Dose-dependent oviductal degeneration)*

No ultrastructural changes were observed at doses of 25 mg/kg and 100 mg/kg bodyweight carbendazim.

400 mg/kg bodyweight carbendazim

At a dose of 400 mg/kg bodyweight carbendazim, degenerative changes were observed in both the epithelial and glandular cells.

Ciliated cells

In the epithelial cell layer, deciliation and a loss of microvilli were evident (Fig. 2.49a). The degenerating ciliated cells contained dilated RER cisternae, several lysosomes and vacuolated mitochondria (Fig. 2.49 a & b). In addition, pyknotic nuclei were occasionally observed (Fig. 2.50a). A few vacuoles containing electron dense material were also observed. In a few instances intact basal bodies supported by distinct rootlets were present. Membrane-bound aggregations of detached cilia (“cilia packets”) were observed in the lumen.

Non-ciliated cells

Pyknotic nuclei and vacuoles were the predominant degenerative change observed in the non-ciliated cells (Fig. 2.50a). In addition, dilated nuclear pores were observed in the degenerating nuclei of these cells (Fig. 2.50b). Both normal and degenerating mitochondria were observed adjacent to degenerating nuclei (Fig. 2.50c). The microvilli lining the non-ciliated cells appeared normal.

Plasma membrane and basal lamina

Desmosomes linking adjacent epithelial cells were intact. No degenerative changes were observed in the basal lamina of the luminal epithelial cells.

Tubular glands

Cells with pyknotic nuclei were observed in the glandular epithelium (Fig. 2.51a). The cytoplasm of the degenerating gland cells contained a few degenerating secretory granules (Fig. 2.51a). The secretory granules contained a central electron lucent area surrounded by an electron dense band (Fig. 2.51b). Numerous vacuoles and myelin figures were observed in the basal cytoplasmic regions of the gland cells (Fig. 2.52 a & b). Lysosomes were observed in the apical cytoplasmic regions of the gland cells (Fig. 2.52c). Lysosomes were differentiated from secretory granules based on size and the presence of heterogeneous electron dense material. The secretory

granules were larger than the lysosomes and contained homogeneous material of medium electron density.

Cellular junctions and luminal microvilli in the tubular glands were structurally intact. Cellular debris was seen in the glandular lumina. The basal lamina surrounding the glandular cells appeared normal. A few swollen mitochondria were observed in the enclosing degenerating supporting cells (Fig. 2.51a).

800 mg/kg bodyweight carbendazim

At a dose of 800 mg/kg bodyweight carbendazim, degenerative changes were observed in the epithelial lining, as well as in the glandular tissue. The observed changes in this treatment group were more severe than those observed in the 400 mg/kg bodyweight carbendazim group.

Ciliated cells

Pyknotic nuclei, swollen mitochondria and vacuoles were frequently observed in degenerating ciliated cells (Fig. 2.53a). In a few degenerating ciliated cells, the cytoplasm contained particles of an intermediate electron density. Aggregations of intermediate filaments were observed in the apical cytoplasmic regions of the ciliated cells. Deciliation, as well as, dilated RER cisternae were evident in these cells (Fig. 2.53b). Nuclear membrane blebbing, margination of nuclear chromatin and cells with pleomorphic nuclei were also observed (Fig. 2.53 a & b). In a few cells the rootlets, anchoring ciliary basal bodies to the cytoplasm, were indistinct. Compound (multi-tubular) cilia were frequently observed in degenerating ciliated cells (Fig. 2.54a). The compound cilia contained up to six axonemes surrounded by a common plasma membrane (Fig. 2.54b). Blebbing of the plasma membrane surrounding the compound cilia was an occasional occurrence.

Non-ciliated cells

At a dose of 800 mg/kg bodyweight carbendazim, clusters of degenerating secretory granules were present in the apical and basal cytoplasmic regions of the non-ciliated

cells. The degenerating secretory granules, which had crenated enclosing membranes, contained a central area of intermediate electron density surrounded by an electron lucent material (Fig. 2.55a). In a few instances, coalesced secretory granules were observed. At this dose, degenerating non-ciliated cells contained pyknotic nuclei, swollen mitochondria and dilated RER. The degenerating nuclei exhibited nucleolar margination and blebbing of the nuclear membrane (Fig. 2.55b). In addition, dilated nuclear pores were evident in the pyknotic nuclei (Fig. 2.55c). Phagocytosed compound cilia were an occasional occurrence in the non-ciliated cells (Fig. 2.56). At this dose the microvilli lining the non-ciliated cells appeared normal.

Plasma membrane and basal lamina

Intact apical desmosomes were observed between adjacent epithelial cells. However, along the lateral plasma membranes a disruption of the cellular junctions resulted in the presence of wide intercellular spaces (Fig. 2.53a). No structural changes were observed in the basal lamina.

Tubular glands

Degenerating cells, some with pyknotic nuclei, were observed in the tubular glands (Fig. 2.57a). The degenerating gland cells were devoid of secretory granules. Cellular debris and macrophages were identified in the lumina of the tubular glands (Fig. 2.57b). The lining microvilli and cellular junctions of the gland cells were intact.

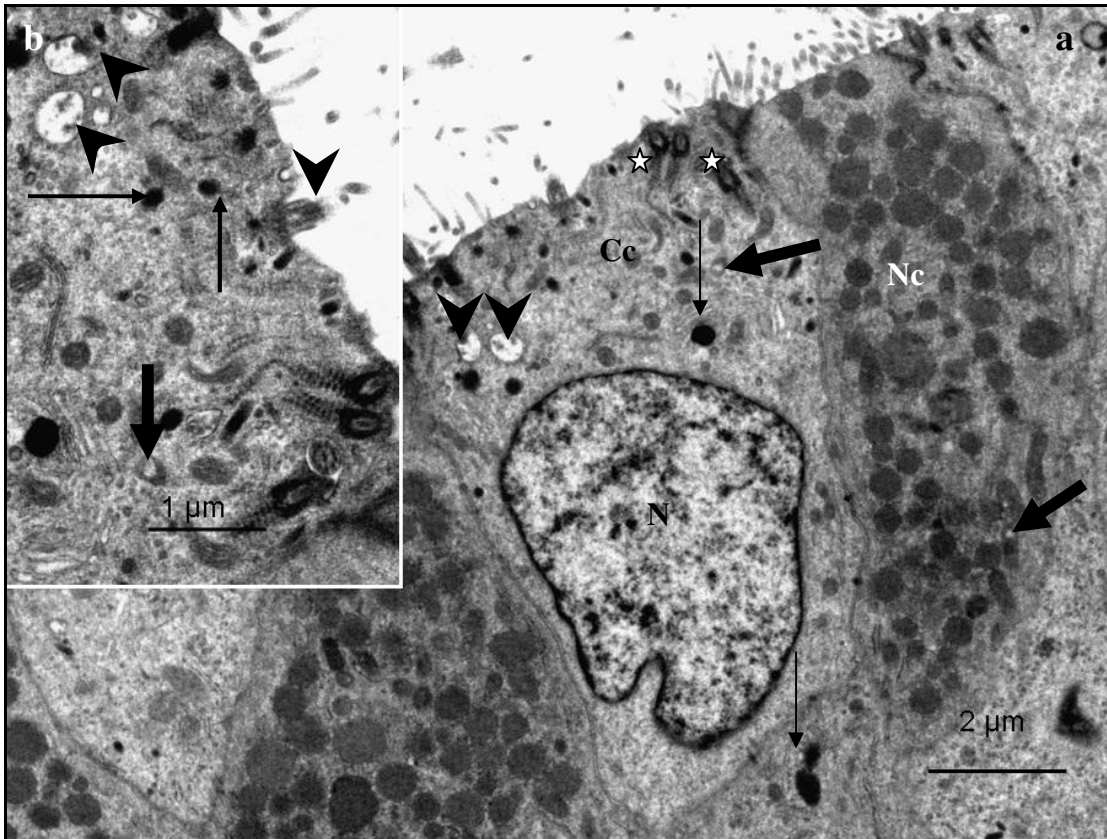


Fig. 2.49: Electron photomicrographs of luminal epithelial cells in the tubular region of the infundibulum of a bird treated with 400 mg/kg bodyweight carbendazim. **a.** Note the sparse covering of microvilli on the apical aspect of the ciliated cells (Cc). Deciliation has occurred resulting in the presence of only a few basal bodies (asterisks). Thin arrows: Lysosomes. Arrowheads: Vacuoles. Thick arrows: Vacuolated mitochondria. Nc: Non-ciliated cell. N: nucleus. **b.** A photomicrograph of the apical region of a degenerating ciliated cell. Vacuoles (arrowheads), a vacuolated mitochondrion (thick arrow) and several lysosomes (thin arrows) are identified. Arrowhead: Cilium.

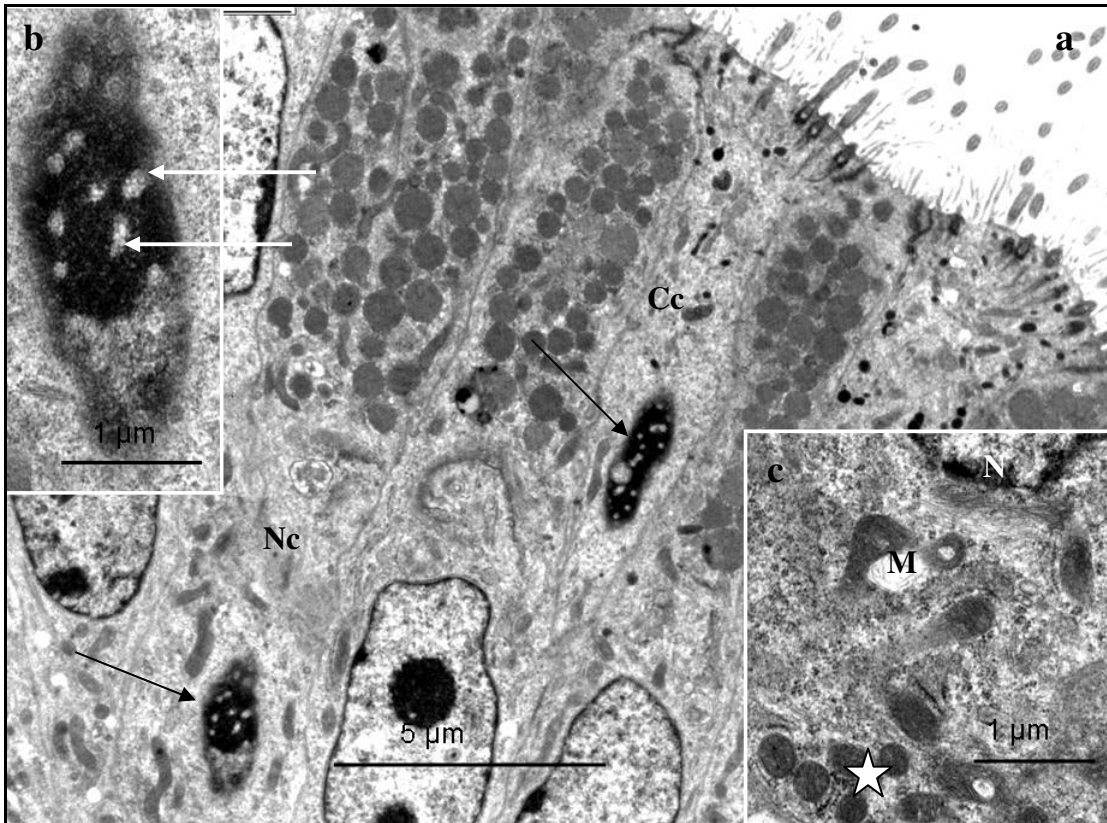


Fig. 2.50: **a.** A survey electron photomicrograph of the luminal epithelium in the tubular region of the infundibulum of a bird treated with 400 mg/kg bodyweight carbendazim. Pyknotic nuclei (arrows) in ciliated (Cc) and non-ciliated (Nc) cells. **b:** A higher magnification photomicrograph of a pyknotic nucleus in a non-ciliated cell. Arrows: Dilated nuclear pores. **c:** A photomicrograph of the cytoplasm in a non-ciliated cell. A vacuolated mitochondrion (M) and normal mitochondria (asterisk) are observed adjacent to the nucleus (N).

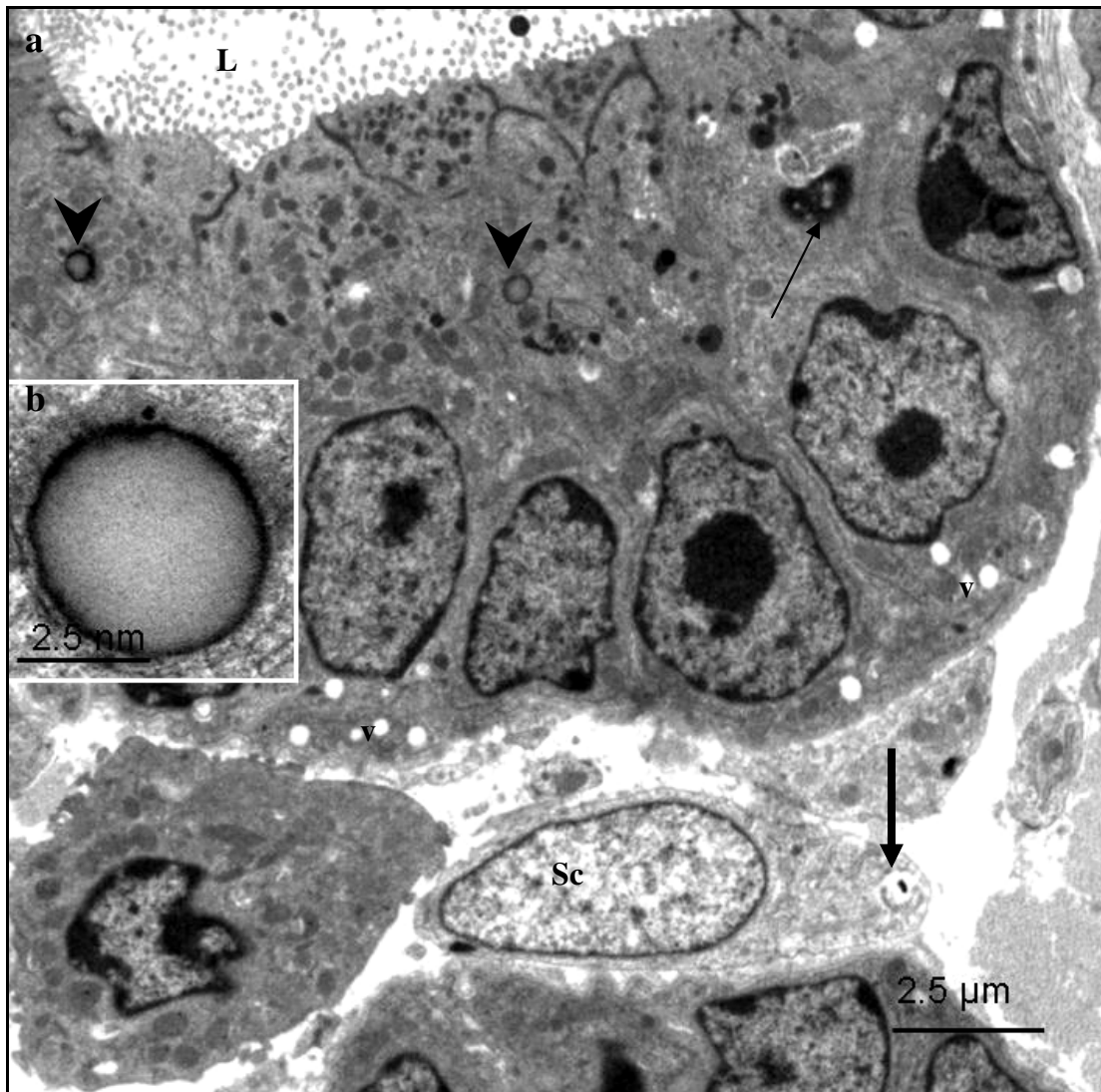


Fig. 2.51: **a.** A survey electron photomicrograph of a tubular gland and surrounding cells in the tubular region of the infundibulum from a bird treated with 400 mg/kg bodyweight carbendazim. Thin arrow: Pyknotic nucleus. V: Vacuoles. Arrowheads: Secretory granules. A swollen mitochondrion (thick arrow) is seen in an adjacent supporting cell (Sc). L: glandular lumen. **b.** A higher magnification photomicrograph of a degenerating secretory granule.

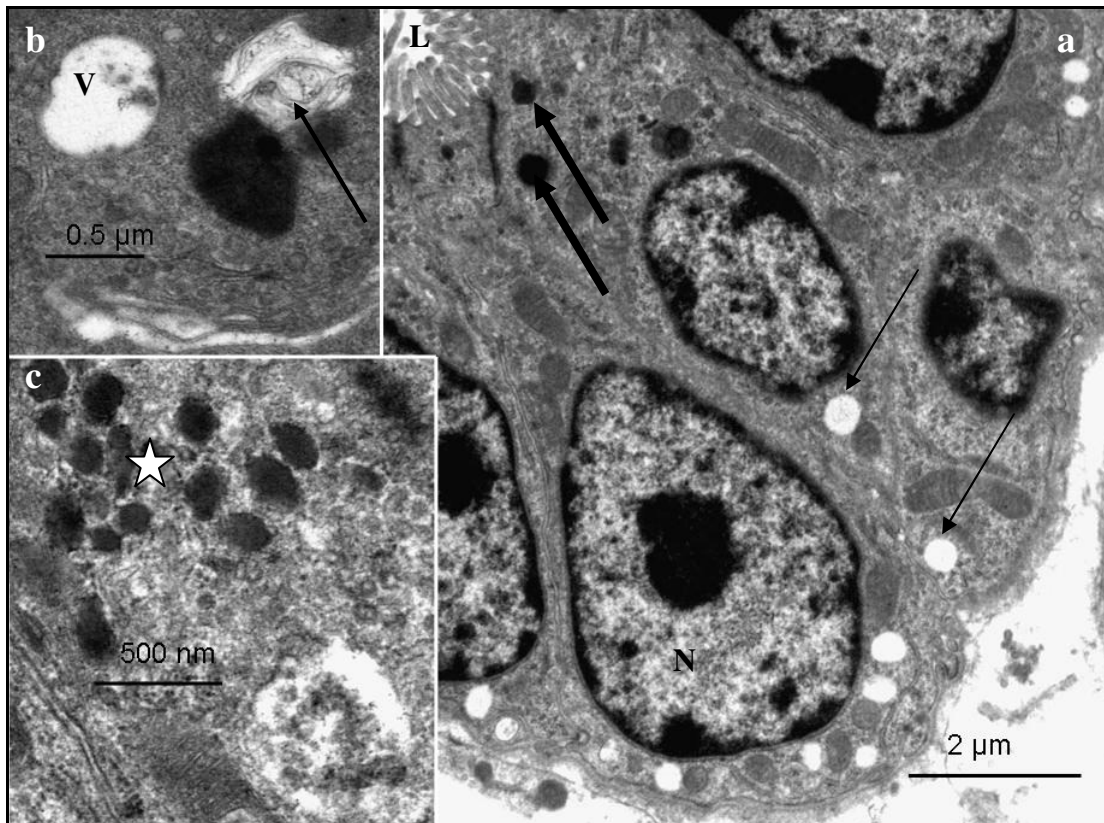


Fig. 2.52: Electron photomicrographs of a gland in the tubular region of the infundibulum from a bird treated with 400 mg/kg bodyweight carbendazim. **a**: Thin arrows: Vacuoles. Thick arrows: Lysosomes. N: nucleus, L: lumen. **b**: A higher magnification electron photomicrograph of the basal cytoplasmic region of a gland cell. Arrow: Myelin figure. V: vacuole. **c**: Photomicrograph of the apical cytoplasm of a gland cell with numerous lysosomes (asterisk).

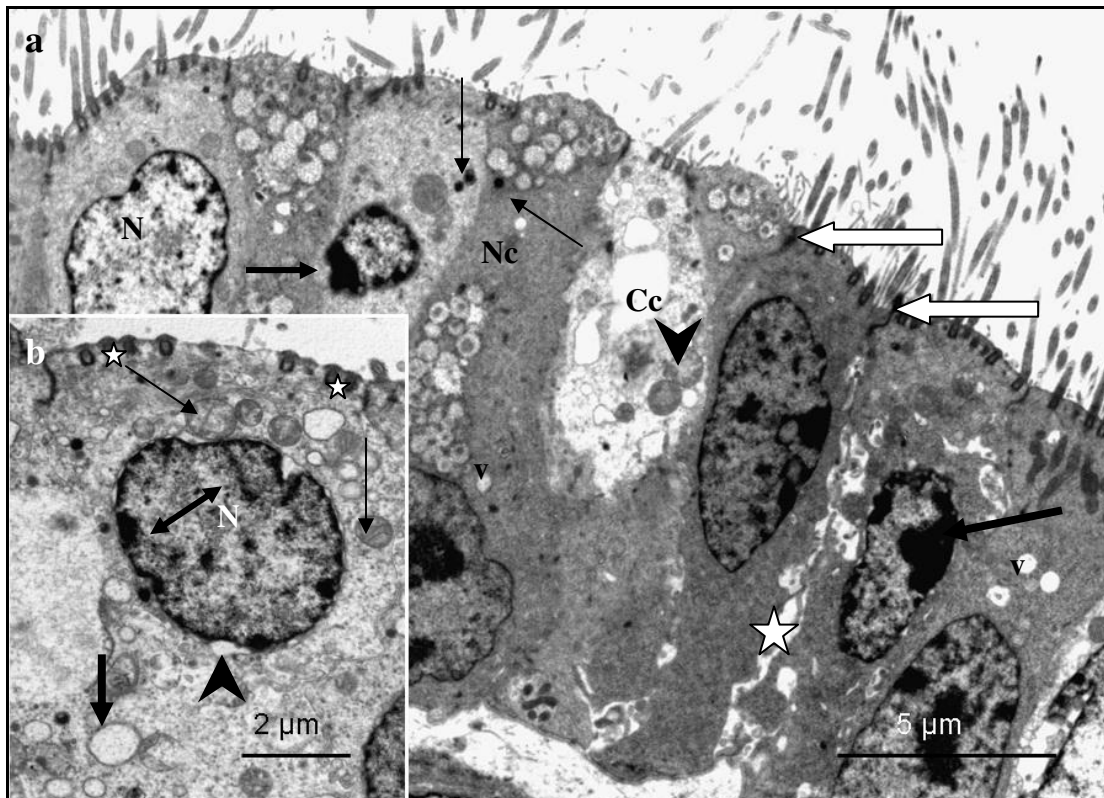


Fig. 2.53: **a.** A survey electron photomicrograph of the luminal epithelium in the tubular region of the infundibulum of a bird treated with 800 mg/kg bodyweight carbendazim. Cc: Ciliated cell. Nc: Non-ciliated cell. Arrowhead: Swollen mitochondrion. V: Vacuoles. Thin arrows: Lysosomes. Thick arrows: Chromatin margination. Asterisk: Wide intercellular spaces **b.** Degenerating nucleus (N) in a ciliated cell. Double arrow: Condensation and margination of nuclear chromatin. Arrowhead: Blebbing of the nuclear membrane. Thick arrow: Dilated RER cistern. Thin arrows: Aggregates of swollen mitochondria. Asterisks: Basal bodies.

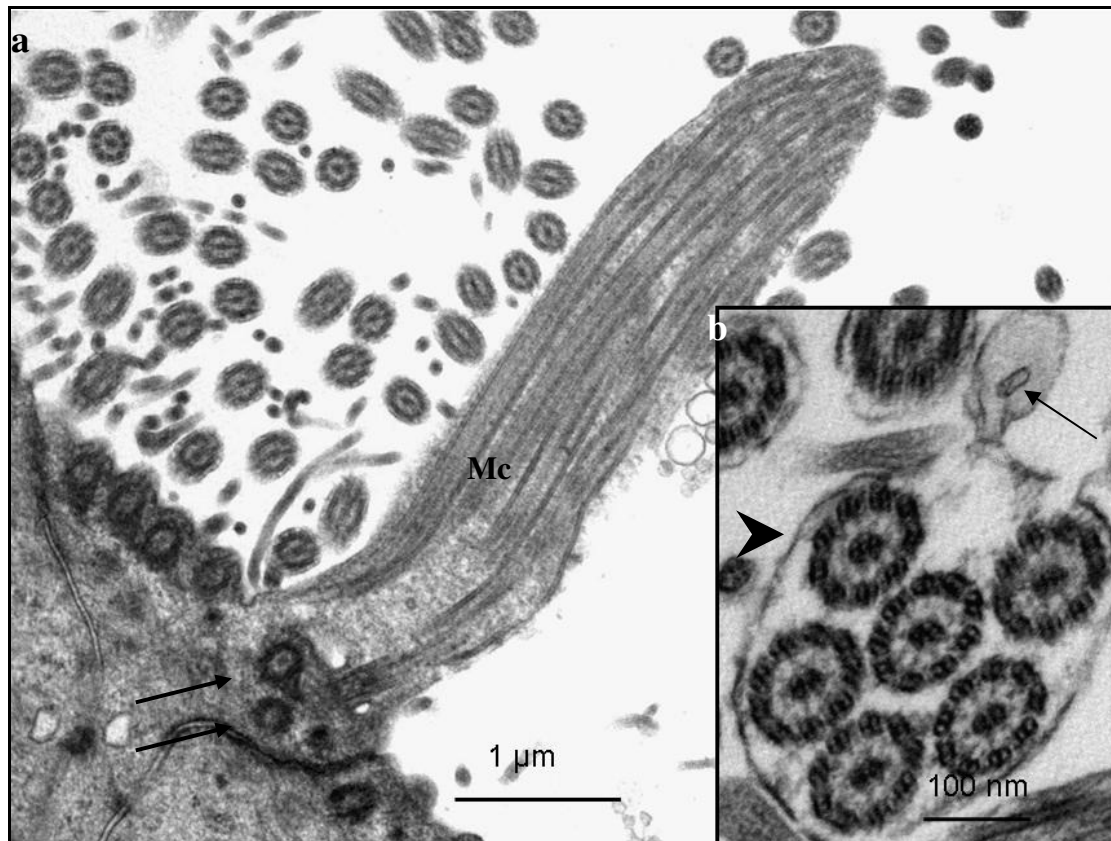


Fig. 2.54: Electron photomicrographs of the apical region of a ciliated cell in the tubular region of the infundibulum from a bird treated with 800 mg/kg bodyweight carbendazim. **a.** Compound cilia (Mc) supported by multiple basal bodies (arrows). Note the absence of rootlets. **b.** Arrowhead:Compound cilia. Arrow: Blebbing of plasma membrane.

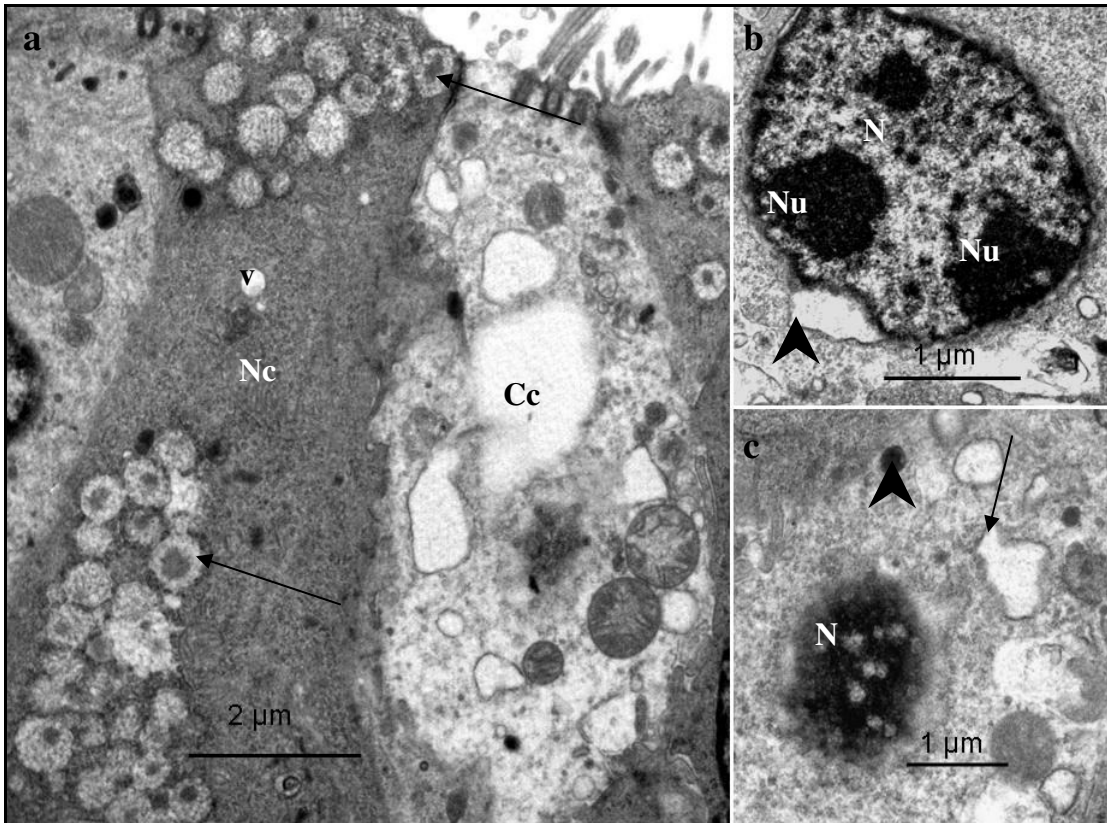


Fig. 2.55: Electron photomicrographs of luminal epithelial cells in the tubular region of the infundibulum from a bird treated with 800 mg/kg bodyweight carbendazim. **a.** Arrows: Groups of secretory granules. Cc: degenerating ciliated cell; V: vacuole. Degenerating nucleus (N) in a non-ciliated cell. **b.** Marginalized nucleoli (Nu), and a blebbed nuclear membrane (arrowhead) are evident. **c.** A higher magnification electron photomicrograph of a non-ciliated cell. N: Pyknotic nucleus with dilated pores. Arrow: Dilated RER. Arrowhead: lysosome.

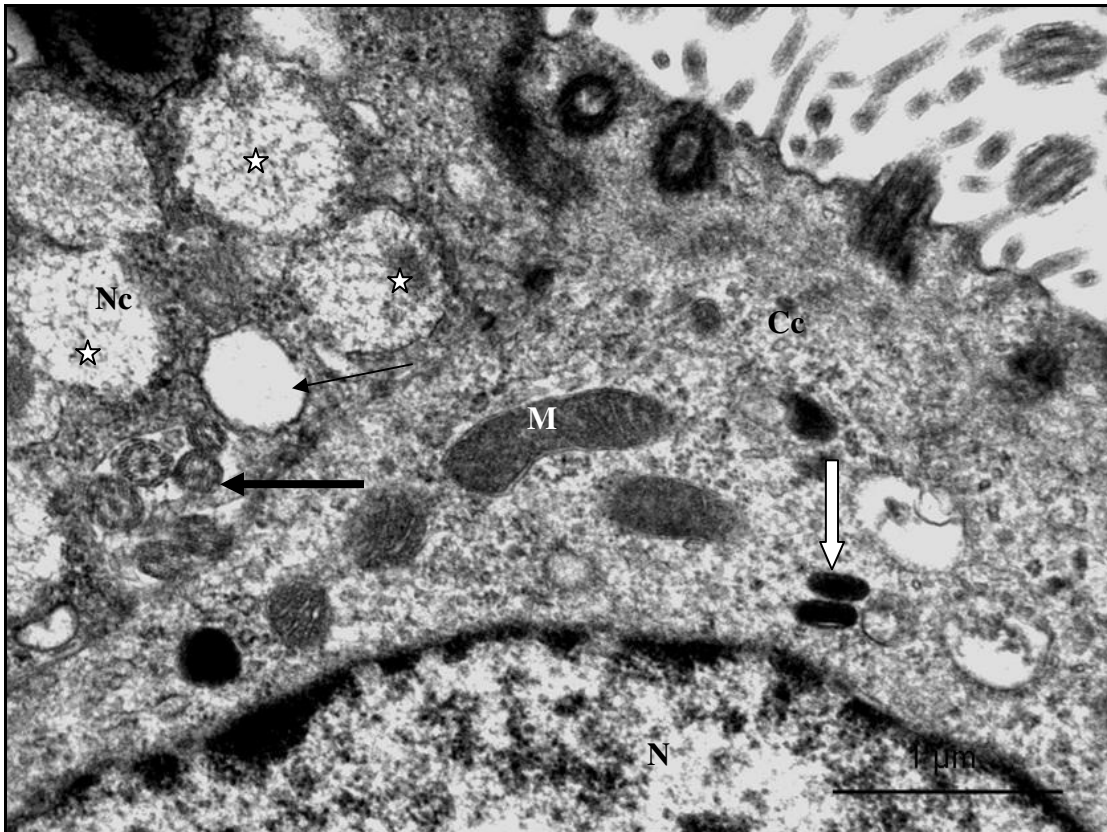


Fig. 2.56: Electron photomicrograph of the apical regions of ciliated (Cc) and non-ciliated (Nc) epithelial cells in the tubular region of the infundibulum from a bird treated with 800 mg/kg bodyweight carbendazim. Thick arrow: Intracellular compound cilia. Asterisks: Degenerating secretory granules. Thin arrow: Dilated SER cistern. White arrow: Lysosomes. N: nucleus. M: mitochondrion.

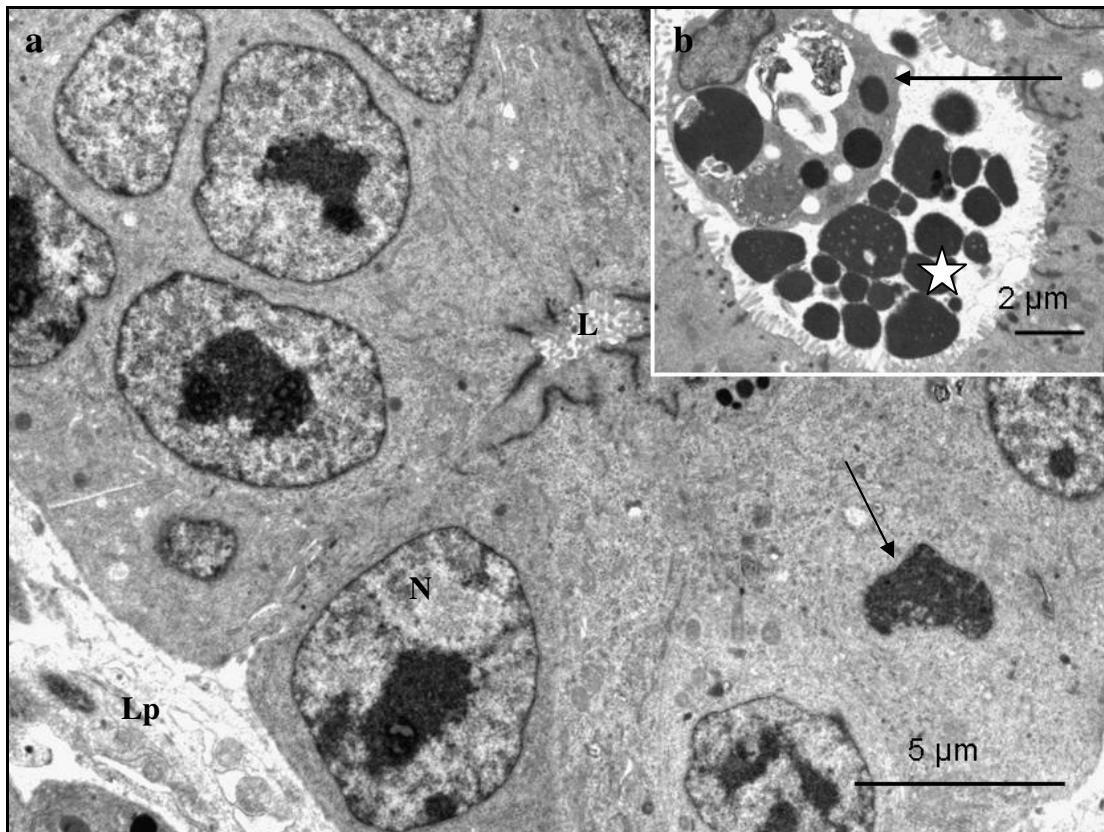


Fig. 2.57: Electron photomicrograph of a tubular gland in the tubular region of the infundibulum from a 800 mg/kg bodyweight carbendazim-treated bird. **a.** Arrow: Pyknotic nucleus. Lp: lamina propria; N: normal nucleus. **b.** Cellular debris (asterisk) and a macrophage (arrow) are observed in the glandular lumen.

2.3.6.2.2.iib Experiment II (time-course oviductal degeneration)

5 hours post-exposure

Ciliated cells

Degenerative changes were present in the tubular region of the infundibulum 5 hours post-exposure to 400 mg/kg bodyweight carbendazim. The observed changes included: nuclear invagination; condensation and margination of nuclear chromatin; blebbing of the nuclear membrane; cytoplasmic vacuolation and mitochondrial swelling (Fig. 2.58 a & b). In addition, cytoplasmic condensation was observed in some cells (Fig. 2.58a). The basal bodies and rootlets of these cells appeared normal.

Non-ciliated cells

No degenerative changes were observed in the non-ciliated cells.

Plasma membrane and basal lamina

Desmosomes linking adjacent epithelial cells were intact. The basal lamina underlying the luminal epithelium was structurally normal.

Tubular glands

Cytoplasmic vacuolation and myelin figures were identified in the tubular gland cells.

24 hours post-exposure

Ciliated cells

Twenty-four hours post-exposure to carbendazim, numerous lysosomes and vacuoles were observed in the cytoplasm of ciliated cells (Fig. 2.59 a & b). The vacuoles were concentrated perinuclearly, as well as in the basal cytoplasmic regions. Swollen mitochondria, as well as, mitochondria with disintegrating, enclosing membranes were observed in the ciliated cells. Cellular junctions and cilia appeared intact.

Non-ciliated cells

Degenerating non-ciliated cells contained a few swollen mitochondria (Fig. 2.59a). Relatively few microvilli lined the luminal surface of the degenerating non-ciliated cell. No structural changes were observed in the secretory granules of the non-ciliated cells.

Plasma membrane and basal lamina

No morphological changes were observed in either the plasma membrane or basal lamina.

Tubular glands

The lining microvilli and cellular junctions of the gland cells were intact. A few myelin figures and cytoplasmic vacuolation were evident. Cells with a few swollen mitochondria were observed in the tubular glands (Fig. 2.60 a & b). In addition, nuclei of the degenerating gland cells exhibited condensed and marginalized nuclear chromatin (Fig. 2.60a). These gland cells contained a few secretory granules, which were concentrated apically (Fig. 2.60b). Degenerating secretory granules displayed centrally located electron lucent particles enclosed by an outer electron dense band (Fig. 2.60a).

5 days post-exposure

Ciliated cells

Ultrastructural observations 5 days post-exposure to carbendazim revealed the presence of pyknotic nuclei (Fig. 2.61a), myelin figures (Fig. 2.61b) and numerous lysosomes in the apical cytoplasmic regions of degenerating ciliated cells. Swollen mitochondria and dilated cisternae of RER were also observed in the cytoplasm of degenerating cells.

Non-ciliated cells

Pyknotic nuclei were also observed in degenerating non-ciliated cells. The cytoplasm also contained swollen mitochondria and dilated cisternae of RER.

Plasma membrane and basal lamina

At this stage, cellular junctions between the epithelial cells were still intact (Fig. 2.61c). A homogenous basal lamina supported the epithelium.

Tubular gland

Pyknotic nuclei and cytoplasmic vacuoles were observed in degenerating tubular gland cells. No morphological changes were observed in the basal lamina.

8 days post-exposure

Ciliated cells

Eight (8) days post-exposure to carbendazim, a few ciliated cells contained nuclei which exhibited blebbing of the nuclear membrane, nucleolar margination, as well as, condensation and margination of the nuclear chromatin (Fig. 2.62 a & b). Majority of degenerating ciliated cells at this stage contained pyknotic nuclei, swollen mitochondria and vacuoles (Fig. 2.62b). The cytoplasm in these cells was electron lucent.

Non-ciliated cells

Very few morphologically normal non-ciliated cells were encountered in the luminal epithelium at this stage. The degenerating non-ciliated cells exhibited relatively few microvilli (Fig. 2.62b). Swollen mitochondria and dilated cisternae of RER were commonly observed. Secretory granules in these cells were structurally normal.

Plasma membrane and basal lamina

The basal lamina underlying the epithelial cells was approximately 125 nm thick. At this stage, invagination and occasional duplication of the basal lamina were observed (Fig. 2.62c). In addition, the basal lamina lacked a distinct lamina lucida. The lamina

densa of the basal lamina contained electron dense particles, which obliterated the lamina lucida.

Tubular gland

Occasional degenerating tubular gland cells contained pyknotic nuclei (Fig. 2.63a). Numerous lysosomes were identified in the supranuclear regions of the degenerating gland cells (Fig. 2.63a). Swollen mitochondria, vacuoles and degenerating secretory granules were also observed (Fig. 2.63a).

In the initial stages of degeneration, the degenerating secretory granules displayed three zones. A small central zone, which contained an electron lucent material. An intermediate zone, composed of a thick electron dense band, and an outer or peripheral zone. The outer zone, which was larger than the intermediate zone contained particles of an intermediate electron density (Fig. 2.63b). In the advanced stages of degeneration, the entire secretory granule contained an electron lucent material circumscribed by a narrow electron dense band (Fig. 2.63c). At this stage, cellular junctions along the lateral plasma membranes of the gland cells were intact. However, the basal lamina was discontinuous and contained electron dense deposits (Fig. 2.63d). Duplication of the basal lamina underlying the glandular epithelium was also observed (Fig. 2.63d).

12 days post-exposure

Ciliated cells

Twelve days post-exposure to carbendazim, the presence of myelin figures in the ciliated epithelial cells was a common feature. Swollen mitochondria and pyknotic nuclei were also observed (Fig. 2.64 a & b). Degenerating nuclei displayed nucleolar and chromatin margination. In these nuclei chromatin condensation was also evident (Fig. 2.64a). Degenerating ciliated cells also exhibited numerous cytoplasmic vacuoles (Fig. 2.64c).

Non-ciliated cells

Degenerating non-ciliated cells contained swollen mitochondria and pyknotic nuclei. Coalesced secretory granules were observed in degenerating cells. The degenerating secretory granules contained a homogeneous electron lucent material (Fig. 2.64a).

Plasma membrane and basal lamina

Desmosomes along the lateral plasma membranes were intact. The basal lamina underlying the luminal epithelium displayed changes similar to the 8 days post-exposure group.

Tubular glands

Cells with swollen mitochondria and pyknotic nuclei were observed in the tubular glands. Margination of nuclear chromatin was also observed in a few of the degenerating glandular cells. Duplication of the basal lamina was still evident.

32 days post-exposure

Ciliated cells

Thirty-two days post-exposure to 400 mg/kg bodyweight carbendazim, the formation of compound (multi-tubular) cilia was a frequent occurrence (Fig. 2.65a). Most compound cilia contained at least ten axonemes. At this stage, pyknotic nuclei, swollen mitochondria and vacuoles were observed in degenerating ciliated cells (Fig. 2.65b). Myelin figures and nuclear membrane blebbing were also observed in these cells (Fig. 2.65c). In addition, nucleolar and chromatin margination were evident (Fig. 2.65a). Aggregations of granular material (Fig. 2.66a) and filamentous bundles (Fig. 2.66b) were evident in the apical cytoplasmic regions of degenerating ciliated cells.

Non-ciliated cells

In non-ciliated cells, pyknotic nuclei and apical cytoplasmic protrusions were frequently encountered (Fig. 2.66c). Swollen mitochondria, myelin figures and dilated RER cisternae were also observed in degeneration non-ciliated cells.

Plasma membrane and basal lamina

Desmosomes linking adjacent cells were intact. Underlying the epithelial cells was a thick basal lamina (approximately 200 nm), which was duplicated in some areas (Fig. 2.67).

Tubular glands

At this stage the degenerating tubular gland cells contained irregular-shaped nuclei, which displayed nucleolar and chromatin margination, as well as, nuclear membrane blebbing (Fig. 2.68 a & b). Occasional pyknotic nuclei and aggregation of lysosomes were also observed in degenerating gland cells (Fig. 2.68a & 2.69a). Numerous vacuoles were observed in the apical and basal cytoplasmic regions of the cells (Fig. 2.69a). A few electron lucent secretory granules were identified in the perinuclear regions of the degenerating gland cells (Fig. 2.69b). Although apical cellular junctions were occasionally intact (Fig. 2.68a), no cellular junctions were observed along the lateral plasma membranes. The glandular lumen contained cellular debris and secretory material (Fig. 2.68a). The gland cells were lined by a few short microvilli. The basal lamina underlying the glandular epithelium was similar to that observed in the 8 and 12 day carbendazim post-exposure groups.

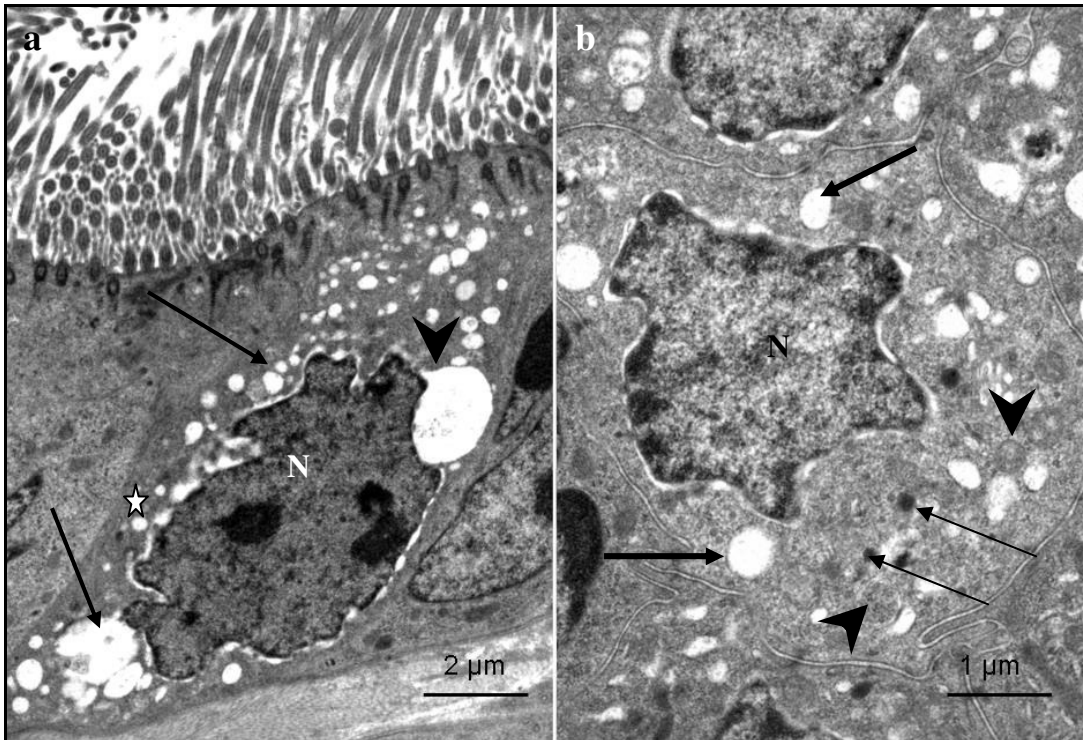


Fig. 2.58: Electron photomicrographs of luminal epithelial cells in the tubular region of the infundibulum 5 hours post-exposure to 400 mg/kg bodyweight carbendazim. **a.** Cytoplasmic vacuolation (arrows) and blebbing of the nuclear membrane (arrowhead) are observed. Asterisk: Cytoplasmic condensation. N: nucleus. **b.** A higher magnification photomicrograph of degenerating epithelial cells. A crenated nucleus (N) exhibiting chromatin margination is observed. Thick arrows: Vacuoles. Arrowheads: Swollen mitochondria. Thin arrows: Lysosomes.

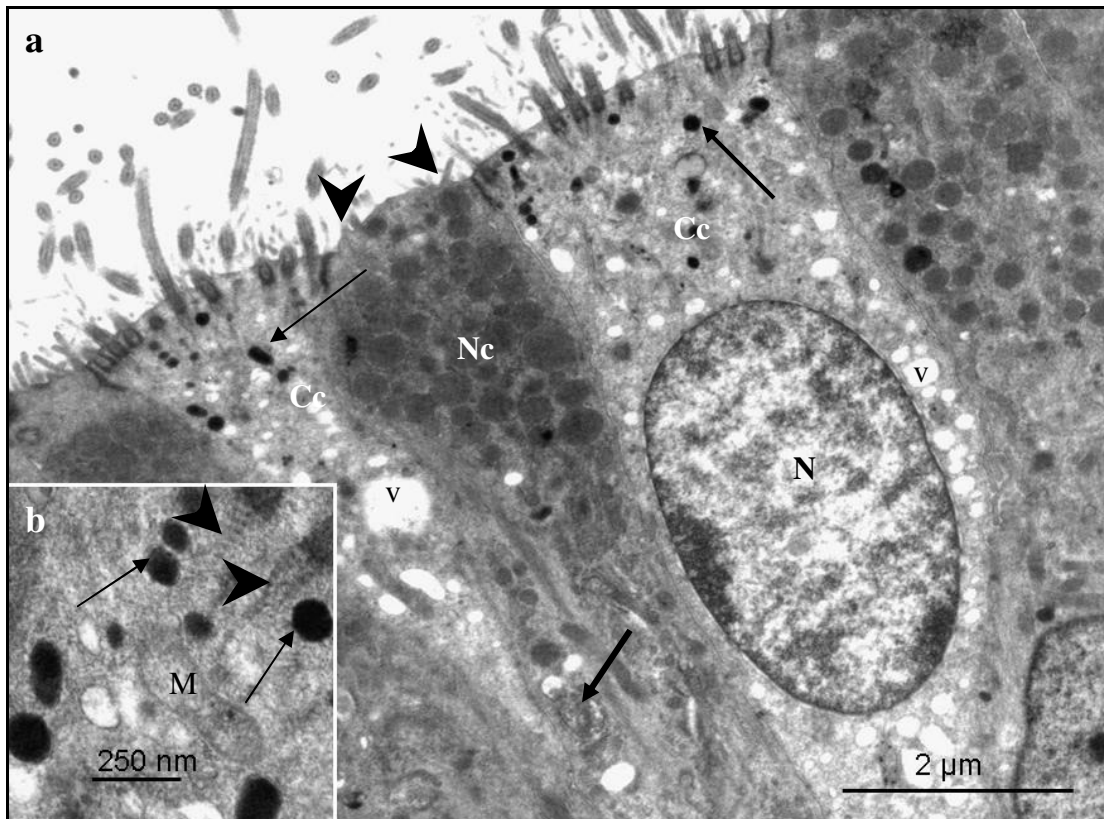


Fig. 2.59: Electron photomicrographs of the luminal epithelium in the tubular region of the infundibulum, 24 hours post-exposure to 400 mg/kg bodyweight carbendazim. **a.** Cc: Ciliated cells. Nc: Non-ciliated cell. Thin arrows: Lysosomes. V: Vacuoles. Thick arrow: Swollen mitochondrion. Arrowheads: Microvilli. N: nucleus. **b.** A higher magnification photomicrograph of the apical cytoplasmic region of a ciliated cell. Note that at this stage the basal striated rootlets (arrowheads) anchoring the cilia are distinct. Arrows: lysosomes; M: mitochondrion.

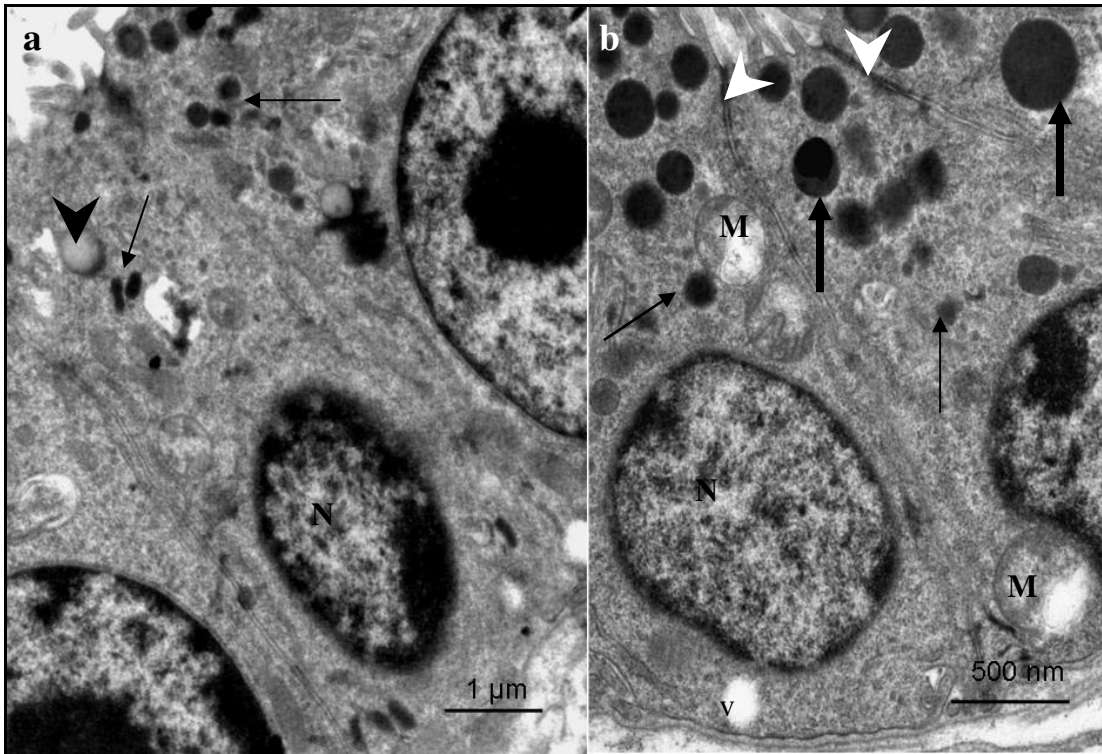


Fig. 2.60: Electron photomicrographs of tubular gland cells in the tubular region of the infundibulum 24 hours post-exposure to 400 mg/kg bodyweight carbendazim. **a.** Degenerating nucleus (N) exhibits chromatin margination. Arrows: Lysosomes. Arrowhead: Degenerating secretory granule **b.** A higher magnification photomicrograph of gland cells. Thick arrows: Secretory granules. Thin arrows: Lysosomes. M: Swollen mitochondrion. Arrowheads: Cellular junctions. N: nucleus; v: vacuole.

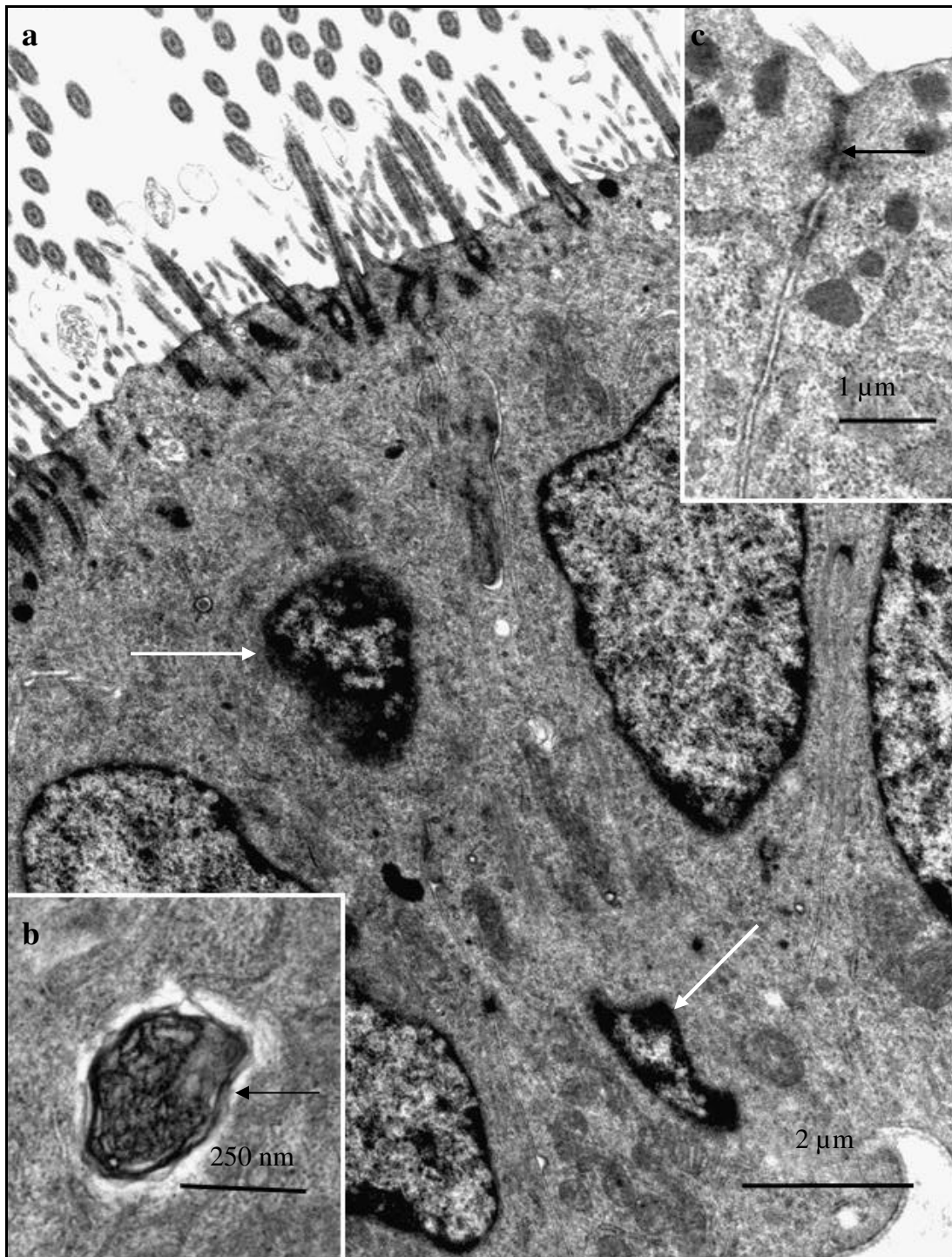


Fig. 2.61: **a.** A survey electron photomicrograph of the luminal epithelium lining the tubular region of the infundibulum, 5 days post-exposure to 400 mg/kg bodyweight carbendazim. Arrows: Pyknotic nuclei. **b.** Arrow: Myelin figure. **c.** Arrow: intact desmosome.

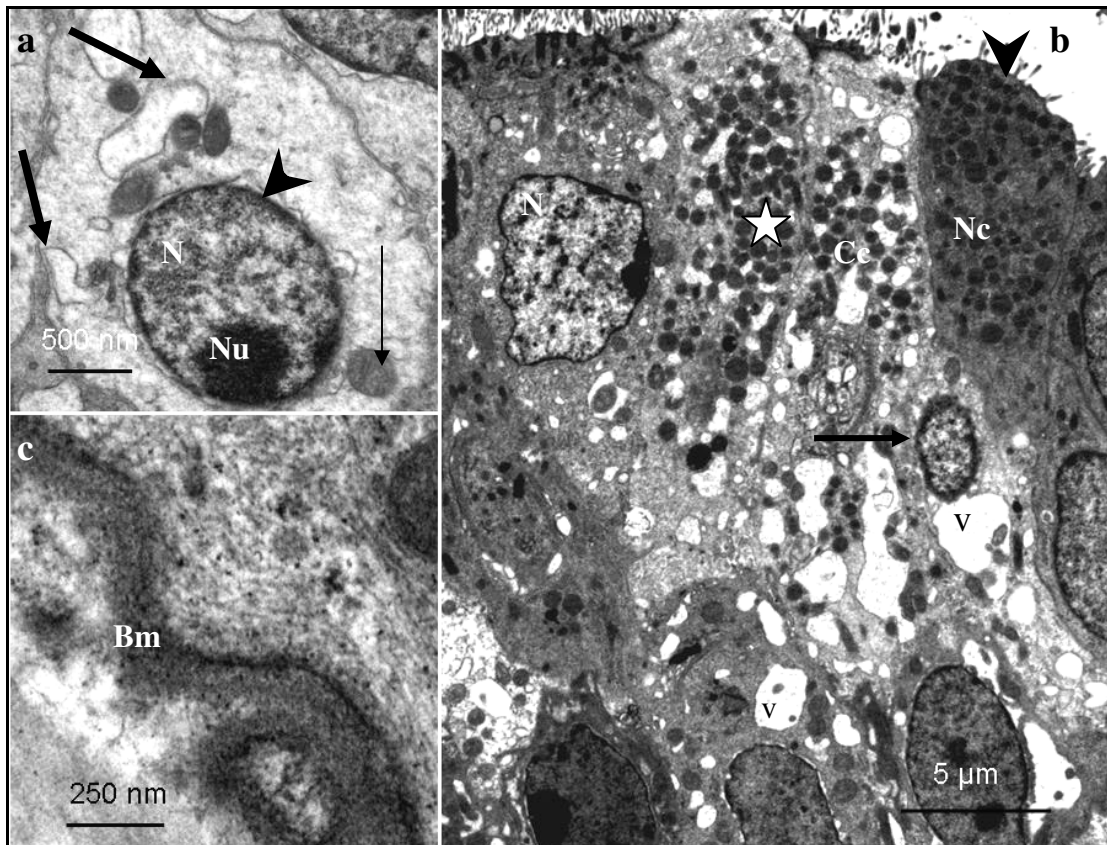


Fig. 2.62: **a.** A higher magnification electron photomicrograph of a degenerating ciliated cell. Nu: nucleolar margination. Arrowhead: Nuclear membrane blebbing. Thin arrow: Swollen mitochondrion. Thick arrow: Dilated RER cisternae. **b.** A survey electron photomicrograph of the luminal epithelium in the tubular region of the infundibulum, 8 days post-exposure to 400 mg/kg bodyweight carbendazim. Degenerating ciliated (Cc) and non-ciliated (Nc) cells. V: Vacuoles. Asterisk: Lysosomes. Arrow: Nucleus with condensed and marginalized chromatin. N: A nucleus with nucleolar margination. Arrowhead: Microvilli. **c.** Photomicrograph of the basal lamina (Bm).

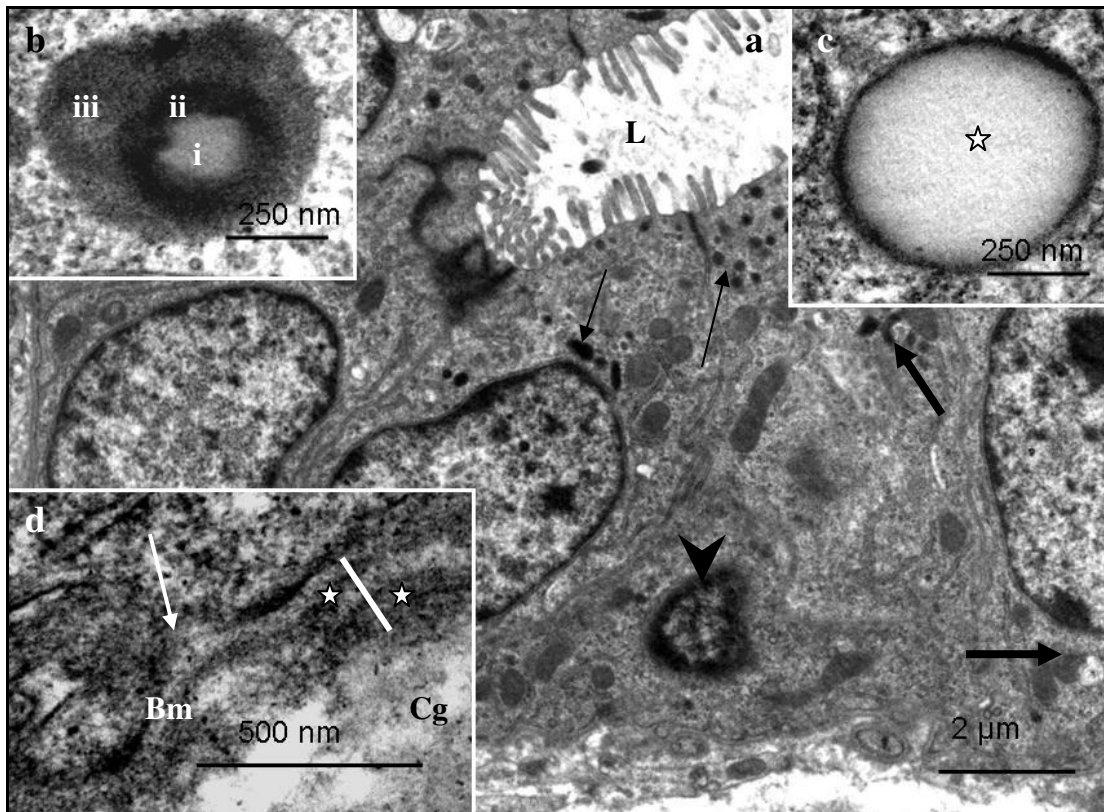


Fig. 2.63: **a.** An electron photomicrograph of a tubular gland in the tubular region of the infundibulum, 8 days post-exposure to 400 mg/kg bodyweight carbendazim. Thin arrows: Lysosomes. Thick arrows: Swollen mitochondria. Arrowhead: Pyknotic nucleus. L: glandular lumen. **b.** A secretory granule in the initial stages of degeneration displays central (i), intermediate (ii) and outer (iii) zones. **c.** A secretory granule (asterisk) in the advanced stages of degeneration. **d.** Photomicrograph of a basal lamina (Bm), which is discontinuous (arrow) and duplicated (asterisks). The line indicates the entire thickness of the basal lamina. Cg: collagen fibres.

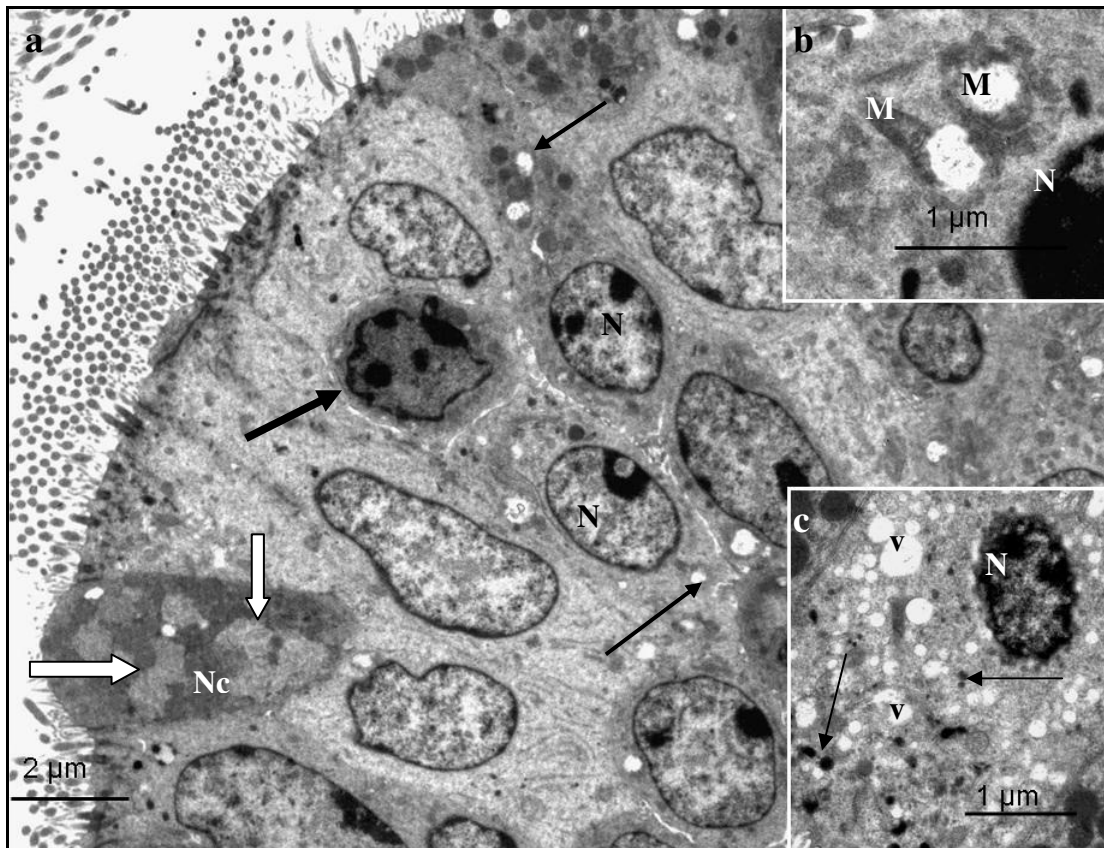


Fig. 2.64: **a.** A survey electron photomicrograph of the luminal epithelium in the tubular region of the infundibulum 12 days post-exposure to 400 mg/kg bodyweight carbendazim. Thin arrows: Swollen mitochondria. Thick arrow: Pyknotic nucleus. Nucleolar and chromatin marginations are observed in the nuclei of several epithelial cells (N). Coalesced degenerating secretory granules (open arrows) are observed in a non-ciliated cell (Nc). **b.** Swollen mitochondria (M) are observed adjacent to a nucleus (N). **c.** Photomicrograph of a degenerating ciliated cell. V: Vacuoles. N: Pyknotic nucleus. Arrows: Lysosomes.

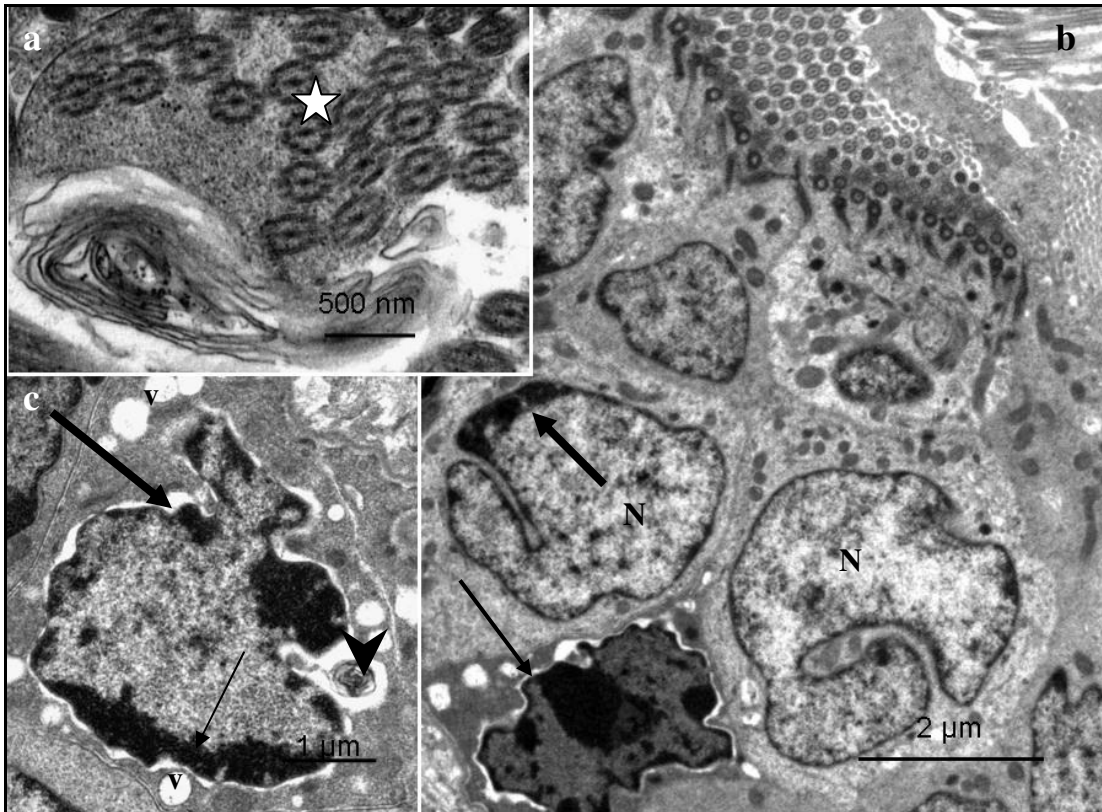


Fig. 2.65: Electron photomicrographs of luminal epithelial cells in the tubular region of the infundibulum, 32 days post-exposure to 400 mg/kg bodyweight carbendazim. **a.** Note the presence of a myelin figure next to compound cilia (asterisk). **b.** Irregular-shaped nuclei (N) and a pyknotic nucleus (thin arrow). Thick arrow: Nuclear chromatin margination. **c.** An irregular-shaped nucleus (N) in a degenerating ciliated cell exhibits chromatin margination (thin arrow), nuclear membrane blebbing (thick arrow) and a myelin figure (arrowhead). v: vacuoles.

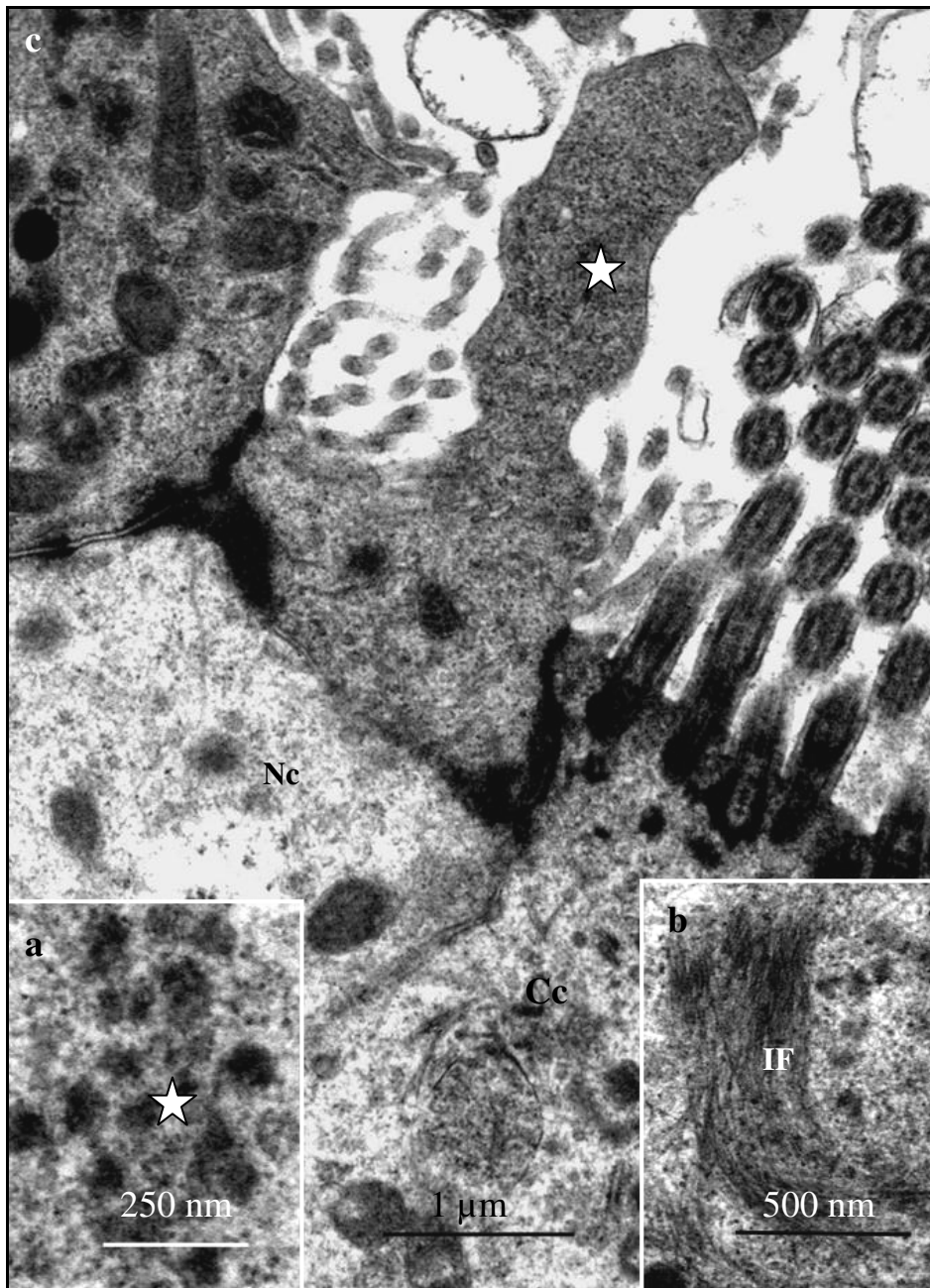


Fig. 2.66: Electron photomicrographs of the apical region of the luminal epithelium in the tubular region of the infundibulum, 32 days post-exposure to 400 mg/kg bodyweight carbendazim. **a.** Granular aggregations (asterisk) in a degenerating ciliated cell. **b.** A bundle of filaments (IF) in the apical cytoplasmic region of a degenerating ciliated cell. **c.** A cytoplasmic protrusion (asterisk) from the apical region of a non-ciliated cell (Nc).



Fig. 2.67: An electron photomicrograph of the basal lamina (Bm) underlying the luminal epithelium in the tubular region of the infundibulum 32 days post-exposure to 400 mg/kg bodyweight carbendazim. Note the duplication of the basal lamina, resulting in the presence of two basal laminae (asterisks 1&2). From the basal plasma membrane of the epithelial cells (Ep), the layers of the basal lamina are: inner lamina lucida (a); inner lamina densa (b); outer lamina lucida (c) and outer lamina densa (d). Collagen fibres (Cg) attach to the outer lamina densa. The line shows the thickness of the entire basal lamina (Bm).

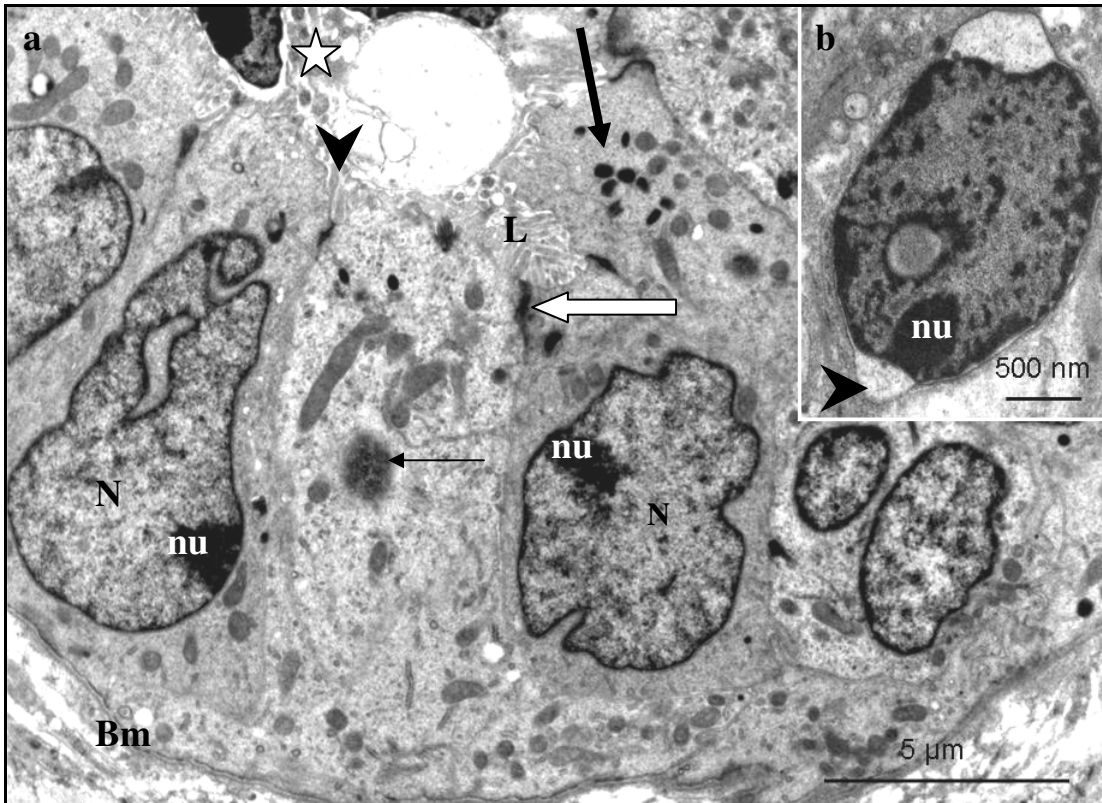


Fig. 2.68: **a.** A survey electron photomicrograph of a tubular gland, 32 days post-exposure to 400 mg/kg bodyweight carbendazim. Irregular-shaped nuclei (N) display nucleoli (nu) margination. Thin arrow: Pyknotic nucleus. Thick arrow: Lysosomes. Block arrow: intact desmosome. Asterisk: Secretory material and cellular debris. L: Lumen. Bm: basal lamina. Arrowhead: Microvilli. **b.** A higher magnification electron photomicrograph of a degenerating nucleus in a gland cell. Nu: Nucleolar margination. Arrowhead: Blebbing of the nuclear membrane.

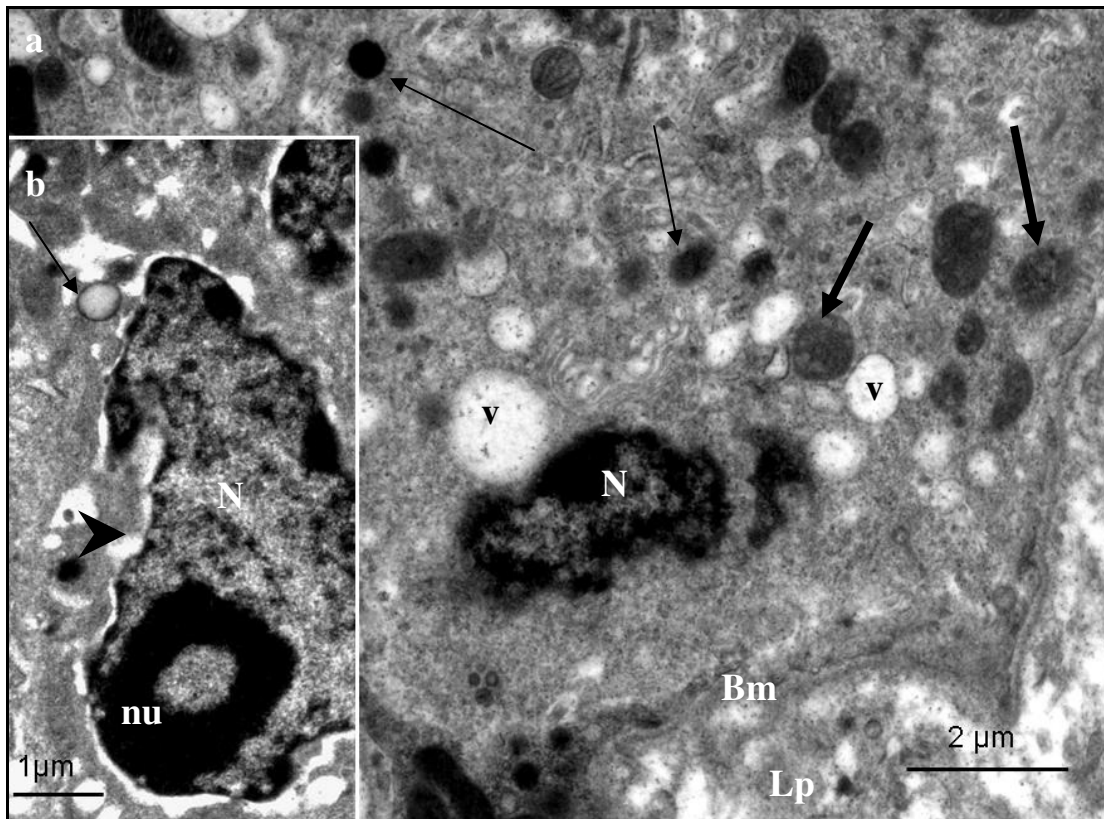


Fig. 2.69: Electron photomicrographs of gland cells in the tubular region of the infundibulum, 32 days post-exposure to 400 mg/kg bodyweight carbendazim. **a.** Degenerating gland cell containing a pyknotic nucleus (N), numerous vacuoles (v) and lysosomes (thin arrows). Bm: a discontinuous basal lamina underlying the tubular gland. . Lp: *lamina propria-submucosa*. Thick arrows: Degenerating mitochondria. **b.** Degenerating gland cell. Thin arrow: Secretory granule. N: Nucleus. Nu: nucleolar margination. Arrowhead: Nuclear membrane blebbing.

2.4 Discussion

The observations reported in the present study have provided information on macroscopic and microscopic features of the oviduct in the sexually mature Japanese quail. The observations of normal oviductal morphology aided the interpretation of the morphological changes post-exposure to methyl-2-benzimidazole carbamate (carbendazim).

Gross morphology and statistical analysis

Based on the results of the current study, macroscopic findings of the control birds are consistent with the results of Fitzgerald (1969). Exposure to low doses of carbendazim (25mg/kg and 100mg/kg bodyweight) did not affect the weight or the

length of the oviduct within 48 hours. In addition, no gross lesions were observed at these doses. The effect of carbendazim was observed at doses of 400mg/kg and 800mg/kg bodyweight. Several reports have shown a correlation between the dose of carbendazim and severity of observed effects. In dogs pathological changes due to carbendazim exposure were observed in the liver, kidneys and haemopoietic system when administered at high doses (FAO/WHO, 1985; Janardhan, Rao & Sisoda, 1988). Similar observations have also been reported in the rat, rabbit and hamster (Mantovani, Maranghi, Ricciardi, Macri, Stazi, Attias & Zappini, 1998) and in the male Japanese quail (Aire, 2005). In this study, a dose of 400 mg/kg bodyweight carbendazim was found to be the lowest toxic dose which caused macroscopic changes in the quail oviduct. However, doubling the dose to 800 mg/kg did not cause a significant macroscopic degenerative change when compared to the observed lesions in the 400 mg/kg bodyweight carbendazim-treated group.

The results of Experiment II (time-course oviductal degeneration) showed a significant oviductal weight decrease post-exposure to 400 mg/kg bodyweight carbendazim. The weight decrease was preceded by a transient weight increase from 24 hours to 8 days post-exposure to carbendazim. Similar observations have been made in rats fed repeated doses of carbendazim (Jacobsen, Østergaard, Lam, Poulsen, Frandsen, Ladeforged & Meyer, 2004). The transient increase in weight of the oviduct observed in this study could be due to oedema and inflammatory process as a result of carbendazim poisoning. It is also assumed that the increase in oviductal weight might be due to an increased plasma level of cytochrome P₄₅₀ enzyme due to carbendazim treatment. Carbendazim has been shown to stimulate the synthesis and activity of cytochrome P₄₅₀ enzyme (Morinaga, Yanase, Nomura, Okabe, Goto, Harada & Nawata, 2004). The cytochrom P₄₅₀ enzyme causes cellular hypertrophy and increased organ weight (Amacher, Schomaker & Burkhardt, 1988). In the rat, high plasma levels of this enzyme correlated with an increase in liver weight (Amacher et al., 1998). The current study did not establish the plasma level of cytochrome P₄₅₀. Therefore, further investigations are needed to ascertain the effect of carbendazim on the activity of this enzyme in birds.

A decrease in oviductal weight was observed at days 12 and 32 post-exposure to carbendazim. The observed weight decrease suggests a regression of the

reproductive tract in the exposed birds. This idea is supported by a report by Williams & Ames (2004) which shows a weight decrease in regressing oviducts of passerine birds. In addition, a report by YU & Marquardt (1973) shows a reduction in oviductal weight during the regression period in the domestic fowl.

Histology and histochemistry

The histological morphology of the infundibulum in the control birds conform to the observations made by Makita & Kiwaki (1968), Fitzgerald (1969) and Wyburn, Johnston, Draper & Davidson (1970). The histological findings showed that carbendazim caused degeneration of the infundibulum at high doses. In addition, the extent of degeneration tends to increase with time post-exposure to carbendazim. This was indicated by atrophy of the tubular glands coupled with a reduction in the PAS positive granules in both the luminal and glandular epithelium. Atrophy of tubular glands indicates oviductal involution and regression. In the domestic fowl, oviduct regression was marked by glandular atrophy (Yu & Marquardt, 1973). Reduction of PAS positive granules indicates morphological and functional changes as a result of carbendazim toxicity. This was evident at day 12 post-exposure to carbendazim whereby weak PAS positive granules was observed on the apical cytoplasmic region. However, at day 32 post-exposure, a moderate PAS staining was seen in these areas. The presence of moderately stained PAS granules at day 32 post-exposure could be an indication of functional recovery of the epithelium.

Immunohistochemistry

In the present study, a decrease in e-cadherin immunoreaction was observed in both luminal and glandular epithelia of carbendazim exposed birds. The decrease in e-cadherin immunostaining in epithelial cells of treated birds could be due to a weak interaction between α & β -catenin, as well as α -catenin and the cytoskeleton along the lateral plasma membranes. This assertion has been shown in several toxicological studies involving cytoskeletal disruption and the reduction in immunoreaction for cadherins (Cabello, Galaz, Botella, Calaf, Pacheko, Stockert, Villanueva, Caneë & Juarranz, 2003; Starcevic, Bortolin, Woodcroft & Novak, 2001). A study by Starcevic et al. (2001) showed the effect of kepone on the adherens

junctions in human epithelial cells. According to the Starcevic *et al.* (2001) report, kepone significantly reduced e-cadherin and β -catenin levels and disrupted the cellular skeleton. In a study by Cabello *et al.* (2003) showed a relationship between cellular degeneration and a decrease in the immunoeexpression of both e-cadherin and β -catenin and the distribution of actin filaments in a human carcinoma cell line treated with the pesticide malathion. In both studies, the disruption of the cellular skeleton correlated with the down expression of e-cadherin and β -catenin.

Laminin immunostaining indicated morphological changes in the basement membrane underlying both luminal and glandular epithelia. The changes were more pronounced at days 12 and 32 post-exposure to carbendazim. At this stage laminin immunolocalization indicated an increased thickness and discontinuation of the basement membrane. Discontinuation of the basement membrane suggests epithelial degeneration due to carbendazim toxicity.

In the current investigation, a decrease in staining intensity for vimentin was observed at days 5 and 8 post-exposure to carbendazim. The decrease in vimentin immunoreaction at these stages of carbendazim treatment suggests disruption of cytoskeletal elements as observed at ultrastructure level. Interestingly, from day 12 to 32 post-exposure, vimentin immunoreactions in the luminal epithelial cells became moderate to strong as compared to the control group. The resumption of vimentin immunoreaction at day 12 and 32 suggests epithelial recovery.

Scanning and transmission electron microscopy

At the scanning electron microscopic level, deciliation and cilia swelling were the predominant degenerative change observed on the mucosal surface of the infundibulum. The deciliation could have been due to a weakening of axonemal microtubules as a result of carbendazim toxicity. As mentioned in Chapter one, carbendazim binds to the β -tubulin subunit of microtubules and thus affects its assembly. Two types of β -tubulin genes (TUB1 and TUB2) have been identified (Cruz & Edlind, 1997). The report showed that the TUB1 gene serves as a principal target during the interaction with benzimidazole fungicides. Cilia swelling could have been caused by increased membrane permeability due to carbendazim toxicity.

In addition to deciliation, TEM results showed the formation of compound cilia. Formation of compound cilia was consistent with the appearance of abnormal basal body attachment in degenerating cilia. The attachment and orientation of basal bodies in the luminal epithelium of the quail oviduct have been studied (Chailley, Boisvieux-Ulrich & Sandoz 1982; Boisvieux-Ulrich *et al.*, 1985; Lemullois, Klotz & Sandoz, 1987; Boisvieux-Ulrich & Sandoz, 1991). The reports have shown that while the basal foot anchors the basal body on the direction of active stroke, the striated rootlets are directed on the opposite direction. This orientation of basal bodies correlates with coordinated cilia movement. In the process of egg laying ciliary movements facilitate the distal movement of the forming egg. It is therefore clear that a strong basal body attachment is required to aid the distal movement of the forming egg. The presence of abnormal cilia and basal body attachment in this study suggested a possible reproductive failure in exposed birds. Further investigation worth to be carried out to confirm this assertion.

In the present study, carbendazim caused an aggregation of intermediate filaments as well as an increase in the number of lysosomes in the apical cytoplasmic regions of degenerating cells. Sandoz, Gounon, Karsenti, Boisvieux-Ulrich, Laine & Paulin (1983) reported the presence of an association between the intermediate filament, keratin, and striated rootlets in the quail oviduct. The filaments and striated rootlets form a network which connects the cytoplasm to the lateral plasma membrane. The observed filamentous aggregation in this study suggests degeneration of microtubules into filament. Similar findings have been reported in mammalian cells exposed to microtubule disrupting agents (Bensch & Malawisa, 1969). According to Bensch & Malawisa (1969) the exposure of human fibroblasts and leukocytes to vinblastine and colchicine results in the dismantling of microtubules into filaments.

In the current investigation, protrusions of the non-ciliated cells were recorded in carbendazim-treated birds. In addition, cellular debris was observed in the glandular lumen at advanced stages. Similar observation was also made in mammalian oviduct (Steinhauer, Boos & Gunzel-apel, 2004). The study (Steinhauer *et al.*, 2004) showed that protrusions of non-ciliated cells, as well as, the presence of cellular debris in the oviduct lumen are signs of a regressing oviduct. This could also be the case in the present study. In fact, oviduct regression occurs by apoptosis (Steffl, Schweiger,

Siguyama & Amselgruber, 2008). The appearance of swollen mitochondria and pyknotic nuclei in carbendazim-treated birds is suggestive of the early stages of apoptosis induced by carbendazim toxicity.

The results of the present study showed the degeneration of tubular gland cells post-exposure to carbendazim. Degeneration of tubular gland cells have also been reported in the domestic fowl fed mercury contaminated seeds (Solomon, 1978). In the Japanese quail, tubular gland cells are known to secrete chalazae and chalaziferous layers (Rahman, *et al.*, 2007). Chalazae controls the axis of rotation during egg laying by maintaining the blastoderm at an oblique position and thus the embryo develops perpendicular to the long axis of the egg (Kochav & Eyal-Giladi, 1971). In addition, tubular gland cells produce sperm-associated bodies (Sultana, Mao & Yoshizaki, 2004) which facilitate binding of spermatozoa to the vitelline membrane during fertilization (Rabbani, Sasanami, Mori & Yoshizaki, 2006). Due to the importance of these cells, any structural or functional alteration will adversely impact on the fertility of the bird. Thus degenerative changes observed in the glandular cells following exposure to carbendazim might pose a potential threat to the fertility of exposed birds.

In this study, cellular junctions (desmosomes) were intact in low doses of carbendazim treatment. However, incidences of desmosomes decreased with time lapse post-exposure to carbendazim and the increase of dosages. The degeneration of desmosomes could have been due to the toxic effect of carbendazim on the cytoskeleton which links the desmosomal proteins, α & β -catenin. The presence of fewer intact desmosomes in treated birds could be explained by the structure of membrane proteins of desmosomes. According to Harmeeet and Alpin (2009), desmosomal cadherins contain plakoglobin (gamma catenin), desmoplakin and plakophilin. Desmosomal cadherins form heterotypic links with intermediate. This type of interaction makes it possible for desmosomal cadherin to initiate and maintain cell to cell adhesions in the absence of classical cadherins. In addition, toxicological studies have shown that while classic cadherins are affected by the pesticide kepone, desmosomal adherins (desmoglein) and gamma catenin levels were not significantly altered (Starcevic *et al.*, 2001). It is possible that low doses of carbendazim did not significantly affect the structure of desmosomal cadherins.

TEM observations showed degenerative changes in the basal lamina underlying both luminal and glandular epithelia. For example, in the funnel region, there was a decreased thickness of the basal lamina at a dose of 800 mg/kg bodyweight. In addition, duplication, breakage and invaginations of the basal lamina underlying luminal and glandular epithelia were observed at day 8 post-exposure to carbendazim. The decrease in thickness of the basal lamina observed suggests atrophy of the epithelium due to carbendazim toxicity. Thickening of the basal lamina can be associated with epithelial recovery as reported in human glomeruli (Beisswenger & Spiro, 1970), skeletal muscles (Gulati, Redi & Zalewski, 1983) and blood vessels of diabetic patients (Giannini & Dyck 1995). This assertion is supported by a report by Vracko (1974) which, states that epithelial regeneration is normally accompanied by formation of a new basal lamina. In the current study, recovery of the basal lamina was observed at day 12 and 32 post-exposure to carbendazim.

Conclusion

This study has highlighted the degenerative and regenerative morphological changes occurring in the infundibular region of the oviduct post-exposure to carbendazim. It is proposed that carbendazim cause oviductal regression by inducing epithelial and glandular cell degeneration; apoptosis through mitochondrial damage and disruption of cytoskeletal component.

2.5 References

- AIRE, T. A. 2005. Short-term effects of carbendazim on the gross and microscopic features of the testes of Japanese quails (*Coturnix coturnix japonoca*). *Anatomy and Embryology*, 210:43-49.
- AITKEN, R.N.C. & JOHNSTON, H.S. 1963. Observations on the fine structure of the infundibulum of the avian oviduct. *Journal of Anatomy*, 97:87.
- AITKEN, R.N.C. 1971. The oviduct, in *Physiology and biochemistry of the domestic fowl*, edited by D.J. Bell & B.M. Freeman. New York: Academic Press, pp. 1237-1289.

- AMACHER, D.E., SCHOMAKER, S.J. & BURKHARDT, J.E. 1998. The relationship among microsomal enzyme induction, liver weight and histological change in rat toxicology studies. *Food and Chemical Toxicology*, 36:831-839.
- BAUMEL, J.J., KING, A.S., BREAZILE, J.E., EVANS, H.E. & VANDEN BERGE, J.C. (Eds) 1993. Handbook of avian anatomy: *nomina anatomica avium*, Cambridge: Nuttall ornithological club, 2:370-384.
- BEISSWENGER, P.J. & SPIRO, R.G. 1970. Human glomerular basement membrane: chemical alteration in diabetes mellitus. *Science*, 168:596-598.
- BENSCH, K.G. & MALAWISA, S.E. 1969. Microtubular crystals in mammalian cells. *The Journal of Cell Biology*, 40:95-107.
- BOISVIEUX-ULRICH, E., LAINE, M.-C. & SANDOZ, D. 1985. The orientation of ciliary basal bodies in quail oviduct is related to the ciliary beating cycle commencement. *Biology of the Cell*, 55:147-150.
- BOISVIEUX-ULRICH, E., LAINE, M.-C. & SANDOZ, D. 1989a. *In vitro* effects of colchicine and nocodazole on ciliogenesis in quail oviduct. *Biology of the Cell*, 67:67-79.
- BOISVIEUX-ULRICH, E., LAINE, M.-C. & SANDOZ, D. 1989b. *In vitro* effects of taxol on ciliogenesis in quail oviduct. *Journal of Cell Science*, 92:9-20.
- BOISVIEUX-ULRICH, E., SANDOZ, D. & ALLART, J.-P. 1991. Determination of ciliary polarity precedes differentiation in the epithelial cells of quail oviduct. *Biology of the Cell*, 72:3-14.
- CHAILLEY, B., BOISVIEUX-ULRICH, E. & SANDOZ, D. 1982. Ciliary membrane events during ciliogenesis of the quail oviduct. *Biology of the Cell*, 46:51-64.
- CHAUSALKAR, K.K. & ROBERTS, J.R. 2007: Ultrastructural study of infectious bronchitis virus infection in infundibulum and magnum of commercial laying hens. *Veterinary Microbiology*, 122:223-236.
- CRUZ, M.-C. & EDLIND, T. 1997. B-tubulin genes and basis for benzimidazole sensitivity of the opportunistic fungus *Cryptococcus neoformans*. *Microbiology*, 143:2003-2008.
- ESCALIER, D., JOUANNET, P. & DAVID, G. 1982. Abnormalities of the ciliary axonemal complex in children: An ultrastructural and kinetic study in a series of 34 cases. *Biology of the Cell*, 44:271-282.
- FITZGERALD, T.C. (Ed) 1969. The coturnix quail: *Anatomy and histology*. Ames: Iowa State University Press.

- FOOD AND AGRICULTURE ORGANIZATION/WORLD HEALTH ORGANIZATION, 1985. Pesticide residues in food: Report of the 1984 joint meeting of the FAO working party of experts on pesticide residues and the WHO expert group on pesticide residues. *FAO Plant Production and Protection*, Paper 62.
- GIANNINI, C. & DYCK, P.J. 1995. Basement membrane reduplication and pericyte degeneration precede development of diabetic polyneuropathy and are associated with its severity. *Annals of Neurology*, 37:498-504.
- GILBERT, A.B. 1979. Female genital organs, in *Form and function in birds*, edited by A.S. King & J. McLelland. London: Academic Press, 1:237-338.
- GULATI, A.K., REDDI, A.H. & ZALEWSKI, A.A. 1983. Changes in the basement membrane zone components during skeletal muscle fibre degeneration and regeneration. *The Journal of Cell Biology*, 97:957-962.
- HELFAND, B.T., MENDEZ, M.G., PUGH, J., DELSERT, C. & GOLDMAN, R.D. 2003. A role for intermediate filaments in determining and maintaining the shape of nerve cells. *Molecular Biology of the Cell*, 14:5069-5081.
- JACOBSEN, H., OSTERGAARD, G., LAM, H.R., POULSEN, M.E., FRANDBSEN, H., LADEFORGED, O. & MEYER, O. 2004. Repeated dose 28-day oral toxicity study in Wistar rats with a mixture of five pesticides often found as residues in food: aldicarb, bromopropylate, carbendazim, chlorpyrifos and mancozeb. *Food and Chemical Toxicology*, 42:1269-1277.
- JANARDHAN, A., RAO, B. & SISODIA, P. 1988. Short-term toxicity of methyl benzimidazole carbamate in dogs. *Bulletin of Environmental Contamination and Toxicology*, 41:704-711.
- KOCHAV, S. & EYAL-GILADI, H. 1971. Bilateral symmetry in chick embryo determination by gravity. *Science*, 171:1027-1029.
- LEMULLOIS, M., KLOTZ, C. & SANDOZ, D. 1987. Immunocytochemical localization of myosin during ciliogenesis of quail oviduct. *European Journal of Cell biology*, 43:429-437.
- LEWIS, L.G. & GIBBINS, J.R. 1968. Differential effects of antimicrotubule agents on the stability and behaviour of cytoplasmic and ciliary microtubules. *Protoplasm*, 65:167-179.
- MAKITA, T. & KIWAKI, S. 1968. The fine structure of infundibulum of the quail oviduct. *Japanese Journal of Zootechnological Science*, 39:246-254.

- MANTOVANI, A., MARANGHI, F., RICCIARDI, C., MACRI, C., STAZI, A.V., ATTIAS, L. & ZAPPINI, G.A. Developmental toxicity of carbendazim : comparison of No-observed-adverse-effect level and benchmark dose approach. *Food and Chemical Toxicology*, 36:37-45.
- MORINAGA, H., YANASE, T., NOMURA, M., OKABE, T., GOTO, K., HARADA, N., & NAWATA, H. 2004. A benzimidazole fungicide, benomyl and its metabolite carbendazim induce aromatase activity in human ovarian granulosa-like tumor cell line (KGN). *Endocrinology*, 145:1860-1869.
- OKAMURA, F. & NISHIYAMA, H. 1978. The passage of spermatozoa through the vitelline membrane in the domestic fowl *Gallus gallus*. *Cell and Tissue Research*, 188:497-508.
- RABBANI, M.G. SASANAMI, T. MORI, M. & YOSHIZAKI, N. 2006. Sperm-egg interaction is mediated by a sperm-associated body in quail. *Development Growth and Differentiation*, 48:33-40.
- PEDERSEN, H. & MYGIND, N. 1976. Absence of axonemal arms in the nasal mucosa cilia in Kartagener's syndrome. *Nature*, 262:494-495.
- RAHMAN, M.A., IWASAWA, A. & YOSHIZAKI, N. 2007. Mechanism of chalaza formation in quail eggs. *Cell and Tissue Research*, 330:535-543.
- SANDOZ, D., GOUNON, P., KARSENTI, E., BOISVIEUX-ULRICH, E., LAINE, M.-C. & PAULIN, D. 1983. Organization of intermediate filament in ciliated cells from quail oviduct. *Journal of Submicroscopic Cytology*, 15:323-326.
- STEFFL, M., SCHWEIGER, M., SIGUYAMA, T. & AMSELGRUBER, W.M. 2008. Review of apoptotic and non-apoptotic events in non-ciliated cells of the mammalian oviduct. *Annals of Anatomy*, 190:46-52.
- STEINHAEUER, N., BOOS, A. & GUNZEL-APEL, A.R. 2004. Morphological changes and proliferative activity in the oviductal epithelium during hormonally defined stages of the oestrous cycle in the bitch. *Reproduction in Domestic Animals*, 39:110-119.
- SULTANA, F., MAO, K.M. & YOSHIZAKI, N. 2004. Possible involvement of sperm-associated body in the process of fertilization in quail. *Zoological Science*, 21:851-858.
- TINGARI, M.D. & LAKE, P.E. 1973. Ultrastructural studies on the uterovaginal sperm-host glands of the domestic hen (*Gallus domesticus*). *Journal of Reproduction and Fertility*, 34:423-431.

- VRACKO, R. 1974. Basal lamina scaffold-anatomy and significance for maintenance of orderly tissue structure. *American Journal of Pathology*, 77:313-346.
- WILLIAMS, T.D. & AMES, C.E. 2004. Top-down regression of the avian oviduct during late oviposition in small passerine birds. *The Journal of Experimental Biology*, 207:263-268.
- WYBURN, G.M., JOHNSTON, H.S., DRAPER, M.H. & DAVIDSON, M.F. 1970. The fine structure of the infundibulum and magnum of the oviduct of *Gallus domesticus*. *Quarterly Journal of Experimental Physiology*, 55:213-232.
- YU, J.Y.-L. & MARQUARDT, R.R. 1973: Development, cellular growth and function of the avian oviduct: studies on the magnum during a reproductive cycle of the domestic fowl (*Gallus domesticus*). *Biology of Reproduction*, 8:283-298.

CHAPTER THREE

The effect of carbendazim on the structure of the magnum in the sexually mature Japanese quail: histological, immunohistochemical and ultrastructural study

3.1 Introduction

Studies on the morphology of magnum have been carried out in several avian species (Yu & Marquardt 1973; Eroschenko & Wilson, 1974; Gilbert, 1979; Davidson 1986; Mao, Sultana, Howlider, Iwasawa & Yoshizaki 2006; Chousalkar & Roberts 2007; 2008; Mohammadpour & Keshtmandi, 2008). According to these studies, the magnum is the longest region of the avian oviduct, making up 50% of the total oviductal length in the domestic fowl (Wyburn, Johnston, Draper, & Davidson, 1970). The wall of the magnum is thicker than that of the infundibulum due to the presence of well developed tubular glands (*glandulae magni*). The mucosal and lamina propria-submucosal layers are thrown into primary and secondary folds, with occasional tertiary folds being present (Wyburn *et al.*, 1970).

Histological studies have shown that the magnum *mucosa* is lined by simple columnar epithelium, consisting of ciliated and non-ciliated (granular) cells (Wyburn *et al.*, 1970; Chousalkar & Roberts, 2008). In the *lamina propria-submucosa*, loose connective tissue fibres are seen interposed between well-developed tubular glands. According to a report by Wyburn *et al.* (1970), the tubular glands in the domestic fowl consist of three types of cells: type A cells, which contain electron dense granules; the intermediate type B cells, with homogeneous low electron density material and type C cells, with a few electron dense granules. A simple cuboidal epithelium lines the tubular glands. The *tunica muscularis* consists of inner circular and outer longitudinal smooth muscle layers. The magnum is enclosed by a loose connective tissue *tunica serosa* lined by simple squamous epithelium.

During the process of egg formation both epithelial and tubular gland cells participate in the synthesis and release of egg-white proteins or albumen. The egg-white proteins synthesized in the magnum include ovalbumen, conalbumen, ovomucoid,

lysozyme and avidin (Palmiter & Gutman, 1972). Reports by Kohler, Grimley & O'malley (1968), O'Malley (1967) and Tuohimaa (1975), have shown that the synthesis of avidin takes place in the epithelial cells. Tubular gland cells are known to produce ovalbumin, lysozyme, ovomucoid and conalbumen (Oka & Schimke, 1969; Palmiter & Gutman, 1972). The peri-albumin layer is secreted by secretory cells at the magnum-isthmus junction (Mao *et al.*, 2006).

The magnum is regarded as a functional unit since the greater part of the albumen or egg-white proteins are produced in this region. Based on this fact it is clear that the production of a viable egg relies on the morphology and function of the luminal epithelium and gland cells. Morphological changes in this region could impact negatively on the formation of normal eggs. As reported in the domestic fowl, morphological changes in the luminal and glandular epithelia of the magnum results in the production of watery eggs (Davidson, 1986).

Morphological changes in the magnum could be as a result of disease or toxins. Balachandran, Bhatnagar & Gcissinger (1985) reported morphological changes in the magnum of domestic fowl fed a diet containing high levels of the toxin methyl mercury. Although carbendazim has been reported to cause structural changes by affecting the organization of cellular skeleton, no published reports appear to be available on the effect of carbendazim on the morphology of the magnum in the Japanese quail. Therefore, in this Chapter, the effects of carbendazim on the morphology of the magnum in the sexually mature Japanese quail are described.

3.2. Materials and methods

A total of 102 sexually mature female Japanese quail were used in this study. The study was divided into two experiments as described in Chapter One.

3.2.i. Histology

Tissue samples from the magnum were fixed in 10% buffered formalin for 48 hours. Thereafter, the tissue samples were processed routinely for light microscopy following standard procedures described in Chapter One.

3.2.ii. Immunohistochemistry

Paraffin embedded sections of the magnum (5 µm thick) were used in the current study. The tissue sections were processed and immunostained using a LSAB plus kit (Dakocytomation, Denmark) following the standard technique described in Chapter One. Antibodies against e-cadherin, laminin and vimentin were used at dilutions of 1:100, 1:50 and 1:50 respectively.

3.2.iii. Transmission and Scanning electron microscopy

Tissue samples from the magnum were immersion-fixed in 2.5% glutaraldehyde in 0.1M Millonig's buffer (pH 7.3) for 24 hours. Thereafter, the tissue samples were post-fixed in 2% osmium tetroxide. Following post-fixation, samples were processed for transmission electron microscopy (TEM) and scanning electron microscopy (SEM) using standard techniques.

3.3. Results

3.3.1 Tissue morphometry

3.3.1.i. Control birds

The mucosal and submucosal layers of the magnum were thrown into primary and secondary folds (Fig. 3.1a). Occasional tertiary folds were also observed. The primary folds measured between 234.84 and 515.88 µm (mean 378.23 ± 21.3) in height. The height of the luminal epithelium ranged from 15.72 µm to 31.51 µm (mean 22.98 ± 0.25).

The *lamina propria-submucosa* contained simple and branched tubular glands (*glandulae magni*). The glands measured between 22.99 and 49.12 µm (mean 33.96 ± 0.84) in width. The glandular lumina diameters varied from 2.04 to 23.12 µm (mean 11.47 ± 0.81).

3.3.1.ii Carbendazim-treated birds

3.3.1.ii.a. Experiment I (Dose-dependent oviductal degeneration)

Table 3.1 summarizes the measured morphometric parameters in the control and carbendazim-treated groups. There was a general decrease in the height of primary mucosal folds in carbendazim-treated groups as compared to the control group (Graph 3.1a). The decrease was significant at doses of 400 mg/kg and 800 mg/kg bodyweight carbendazim when compared to the control group. A significant decrease in the height of the mucosal folds was also observed between the following carbendazim treatment groups: 25 mg/kg and 400 mg/kg; 25 mg/kg and 800mg/kg; 100 mg/kg and 400 mg/kg, as well as, 100 mg/kg and 800 mg/kg bodyweight carbendazim (Table 3.1; Graph 3.1a).

Administration of carbendazim also decreased the height of the luminal epithelium (Graph 3.1b). A significant decrease in the height of the luminal epithelium was seen at doses of 100 mg/kg, 400 mg/kg and 800 mg/kg bodyweight carbendazim when compared to the control group. In addition, a decrease in the luminal epithelial height was also observed between the following carbendazim treatment groups: 25 mg/kg and 400 mg/kg; 25 mg/kg and 800 mg/kg; 100 mg/kg and 400 mg/kg; and between 100 mg/kg and 800 mg/kg bodyweight carbendazim (Table 3.1; Graph 3.1b).

There was a general decrease in the width of the magal glands after exposure to carbendazim. A significant decrease in glandular width was observed at doses of 100 mg/kg, 400 mg/kg and 800 mg/kg bodyweight carbendazim when compared to the control (Table 3.1). In addition, glandular width was significantly decreased between 25 mg/kg and 100 mg/kg; 25 mg/kg and 400 mg/kg; as well as between 100 mg/kg and 800 mg/kg bodyweight carbendazim (Table 3.1).

Luminal diameters were also decreased by carbendazim administration. Significant decreases in luminal diameters were detected at doses of 25 mg/kg, 100 mg/kg, 400 mg/kg and 800 mg/kg bodyweight carbendazim when compared to the control group. In addition, a significant decrease in luminal diameter was observed between 100 mg/kg and 800 mg/kg bodyweight carbendazim treatment groups (Table 3.1).

Table 3.1. Histomorphometrical parameters (mean \pm SE) of the magnum in control and carbendazim-treated Japanese quails.

Dose (mg/kg)	Mucosal fold (μm)	Epithelial height (μm)	Gland width (μm)	Luminal diameter (μm)
0	378.23 \pm 21.34	22.98 \pm 0.25	33.96 \pm 0.84	11.47 \pm 0.81
25	306.97 \pm 19.21 ^b	22.22 \pm 0.31 ^b	32.71 \pm 0.93 ^b	6.34 \pm 0.39 ^a
100	315.77 \pm 23.29 ^c	19.66 \pm 0.29 ^{ac}	26.35 \pm 0.99 ^{abc}	5.27 \pm 0.26 ^{ab}
400	184.16 \pm 84 ^{abc}	15.19 \pm 0.63 ^{abc}	27.3 \pm 0.77 ^{ab}	6.51 \pm 0.3 ^a
800	142.08 \pm 9.83 ^{abc}	8.53 \pm 0.19 ^{abc}	30.09 \pm 0.86 ^{ac}	7.59 \pm 0.35 ^{ab}

^a Differ significantly from control

^{bc} A significant change between carbendazim treatment groups

3.3.1.iib. Experiment II (time course oviductal degeneration)

Table 3.2 summarizes morphometric parameters of the magnum in the Japanese quail at different sampling periods post-exposure to 400 mg/kg bodyweight carbendazim. When compared to the control group, there was a significant decrease in the height of primary mucosal folds at all sampling periods post-exposure to carbendazim (Table 3.2; Graph 3.2a). The decrease in mucosal folds was also statistically significant between sampling periods post-exposure to carbendazim (Table 3.2; Graph 3.2a).

A significant decrease in the height of the luminal epithelium was observed at 24 hours and at days 5, 8, 12 and 32 post-exposure to carbendazim (Table 3.2; Graph 3.2b) when compared to the control. In addition, a significant decrease in luminal epithelium height was observed between sampling periods post-exposure to carbendazim (Table 3.2; Graph 3.2b).

There was a general decrease in the width of the tubular glands at different sampling periods post-exposure to carbendazim (Graph 3.2c). A significant decrease in the glandular width was observed at days 5, 8 and 32 post-exposure to carbendazim, when compared to the control. A significant decrease in glandular width was also observed between the sampling periods post-exposure to carbendazim (Table 3.2;

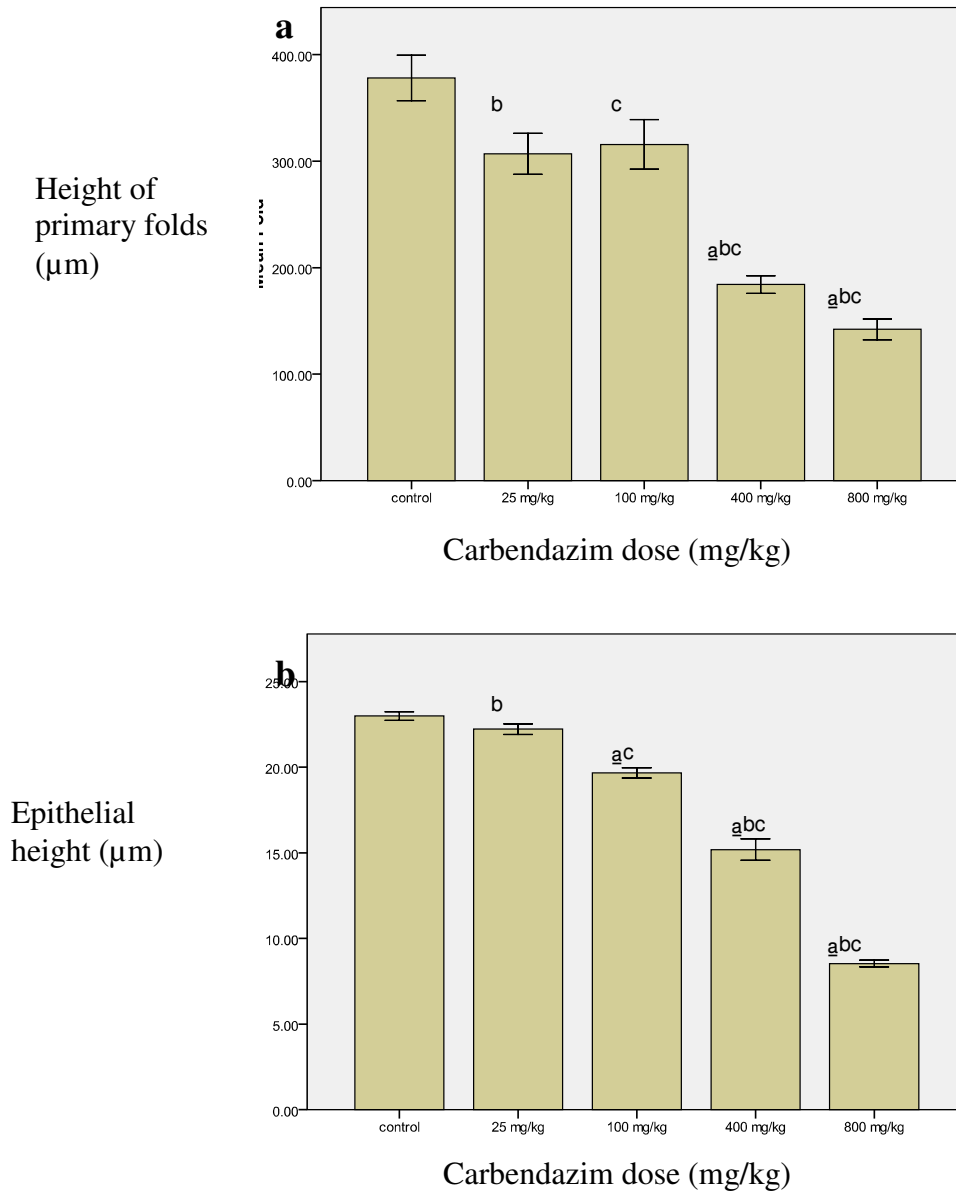
Graph 3.2c). Carbendazim administration significantly decreased the glandular lumina diameters at all time periods post-exposure to carbendazim (Graph 3.2d). The decrease in luminal diameters was also significant between the following sampling periods: 5 hours and days 5, 8, 12 and 32; 24 hours and days 8 and 32; 5 and 32 days; 8 and 32 days; as well as, between 12 and 32 days (Table 3.2; Graph 3.2d).

Table 3.2: Histomorphometrical parameters of the magnum in the control and carbendazim-treated birds.

Periods post-exposure	Primary fold (µm)	Epithelial height (µm)	Gland width (µm)	Luminal diameter (µm)
Control	378.23±21.34	22.98±0.25	33.96±0.84	11.47±0.81
5 hours	193.53±8.49 ^{ab}	22.07±0.22 ^b	34.26±0.97 ^b	9.06±0.37 ^{ab}
24 hours	193.18±12.38 ^{ac}	11.39±0.21 ^{abc}	31.24±0.91 ^c	7.87±0.32 ^{ac}
5 days	152.29±8.93 ^{ad}	12.49±0.29 ^{ab}	22.61±0.66 ^{acd}	6.12±0.3 ^{abd}
8 days	160.43±8.21 ^{ae}	9.26±0.16 ^{abcd}	21.95±1.03 ^{abce}	5.45±0.29 ^{abce}
12 days	90.52±8.26 ^{abcde}	14.92±0.62 ^{abce}	31.49±0.73	7.27±0.28 ^{abf}
32 days	132.41±14.72 ^{abc}	14.07±0.25 ^{abcde}	12.93±0.25 ^{abcde}	1.37±0.11 ^{abcdef}

^a Differ significantly from control

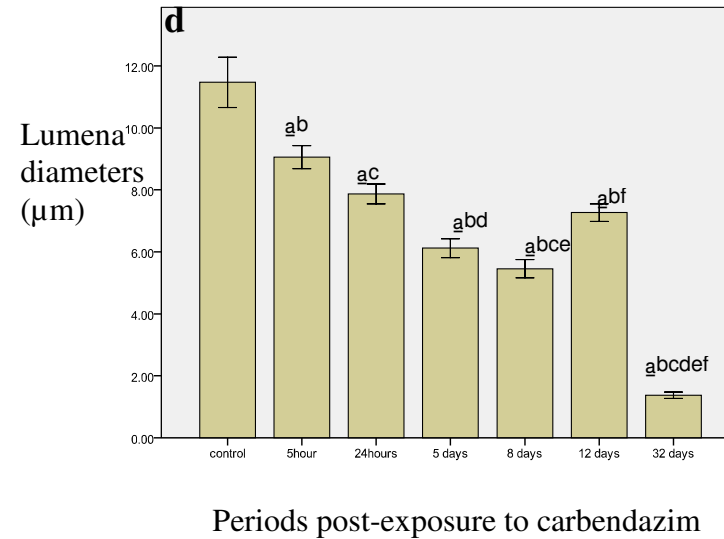
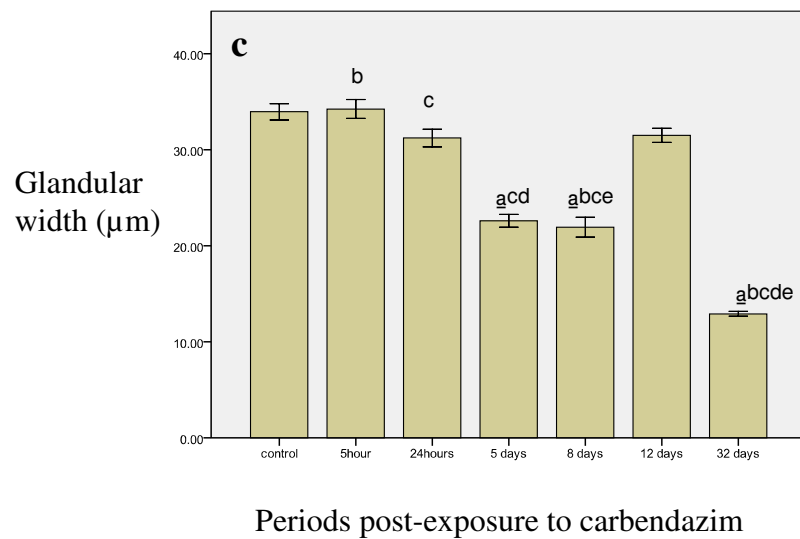
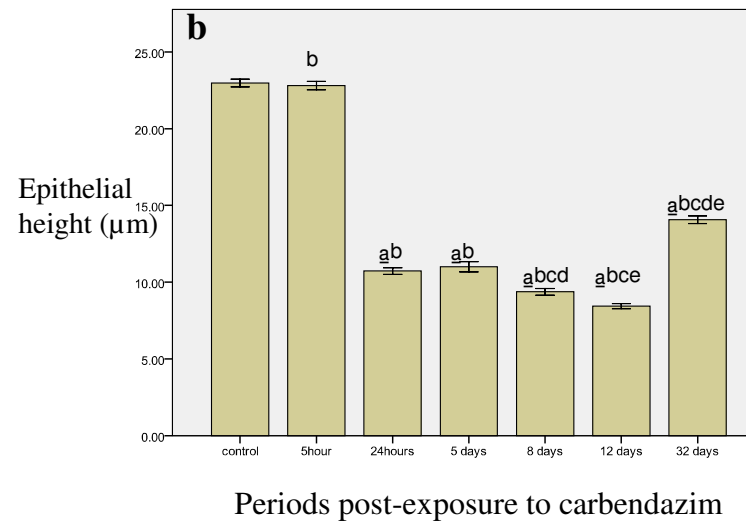
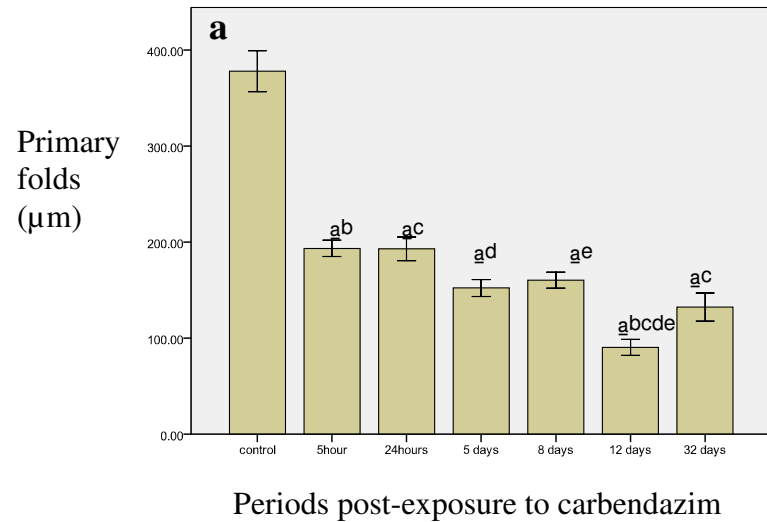
^{bcdef} A significant change between sampling periods post-exposure to 400 mg/kg bodyweight carbendazim.



Graph 3.1: Histograms showing (a) mean \pm SE heights of primary mucosal folds, (b) mean \pm SE heights of luminal epithelium in control and carbendazim-treated Japanese quails. Note a general decrease in the height of primary folds after carbendazim exposure. A progressive decrease in the height of epithelium is also evident.

^a Indicates significant decrease in heights when compared to the control group.

^{bc} Indicates significant change between treatment groups.



Graph 3.2: Histograms showing mean \pm SE of:

- a. Mucosal fold
- b. Luminal epithelium
- c. Glandular width
- d. Glandular lumena diameters

Note the morphometric changes in all parameters due to carbendazim treatment.

^a Indicates significant change from the control

^{bcdef} Indicates significant changes between sampling periods post-exposure to carbendazim.

3.3.2 Histological observations

3.3.1.i Control birds

The simple columnar luminal epithelium lining the mucosal folds was composed of ciliated and non-ciliated (granular) cells (Fig. 3.1b).

The *lamina propria-submucosa* contained simple and branched tubular glands (*glandulae magni*). Loose connective tissue and a few blood vessels were interspaced between the glands (Fig. 3.1a). The gland cells contained round nuclei and eosinophilic granular cytoplasm. The lumina of these glands contained an eosinophilic material.

A thin *tunica muscularis* containing inner circular and outer longitudinal layers was present. A tunica serosa composed of loose connective tissue and a lining of simple squamous epithelium enclosed the magnum (Fig. 3.1a).

3.3.2.ii. Carbendazim-treated birds

3.3.2.ii.a. Experiment I

25 and 100 mg/kg bodyweight carbendazim

No morphological changes were observed in the magnum *mucosa* post-exposure to doses of 25 mg/kg and 100 mg/kg bodyweight carbendazim. In addition, no pathological changes were detected in the *lamina propria-submucosa* post-exposure to these doses.

400 mg/kg bodyweight carbendazim

At a dose of 400 mg/kg bodyweight carbendazim, there was a reduction in the height of the luminal epithelium (Fig. 3.2a). A few degenerating luminal epithelial cells containing pyknotic nuclei were observed (Fig. 3.2b). In the *lamina propria-submucosa*, isolated areas of glandular atrophy were evident (Fig. 3.3a). The

atrophic glands were characterized by cells with shrunken cytoplasm, as well as, fragmented (karyorrhetic) and pyknotic nuclei (3.3b). In a few areas, degenerating gland cells contained numerous vacuoles and cytoplasmic pallor (Fig. 3.3c).

800 mg/kg bodyweight carbendazim

At a dose of 800 mg/kg bodyweight carbendazim, a decrease in luminal epithelium height was still the predominant degenerative change observed (Fig. 3.4a). Vacuolation and cell swelling were observed in degenerating epithelial cells (Fig. 3.4b). Hyperaemia and leukocytic infiltrations were occasionally observed in the *lamina propria-submucosa* underlying the epithelium. In the glandular tissue, numerous vacuoles were observed in degenerating gland cells. No degenerative changes were identified in the *tunica muscularis*.

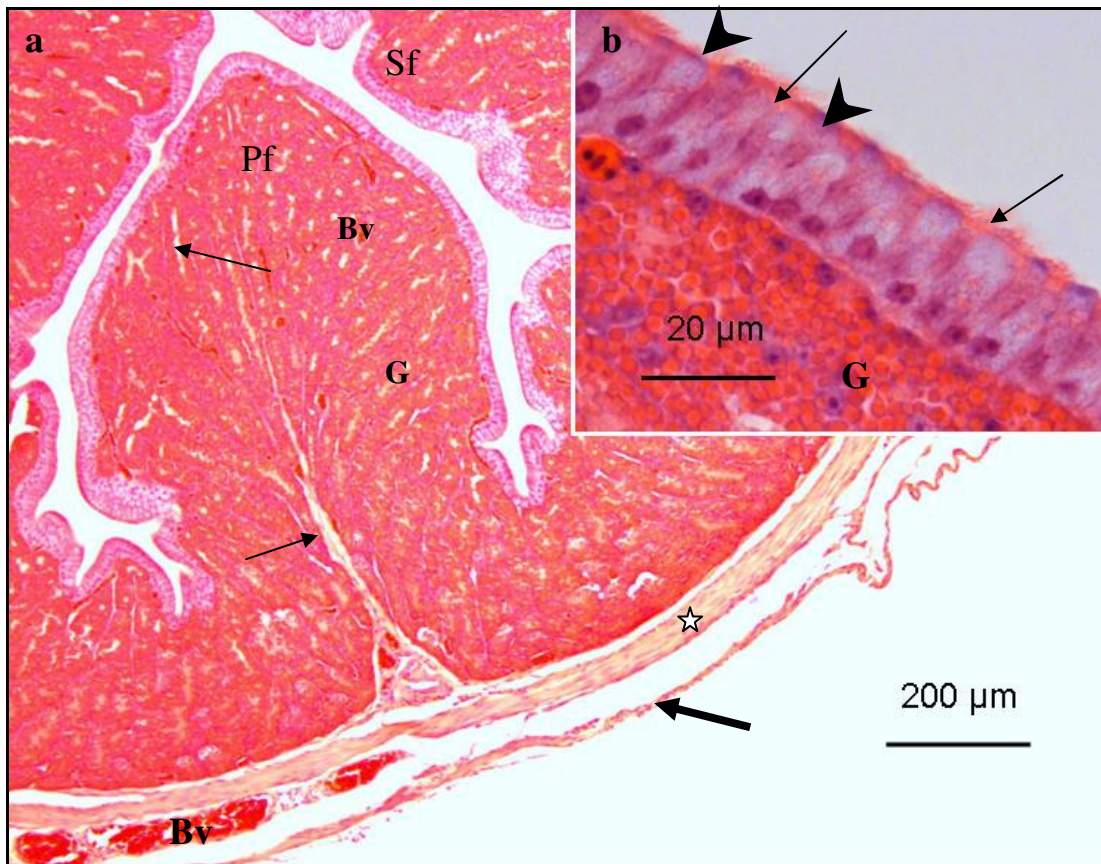


FIG. 3.1: Photomicrographs of the magnum from a control bird. **a.** Pf: Primary fold. Sf: Secondary fold. G: Tubular glands. Bv: Blood vessel. Asterisk: tunica muscularis. Thin arrows: Connective tissue fibres. Thick arrow: tunica serosa. **b.** A higher magnification photomicrograph of the luminal epithelium with ciliated (arrows) and non-ciliated (arrowheads) cells. G: tubular glands. Haematoxylin and eosin (H&E) stain.

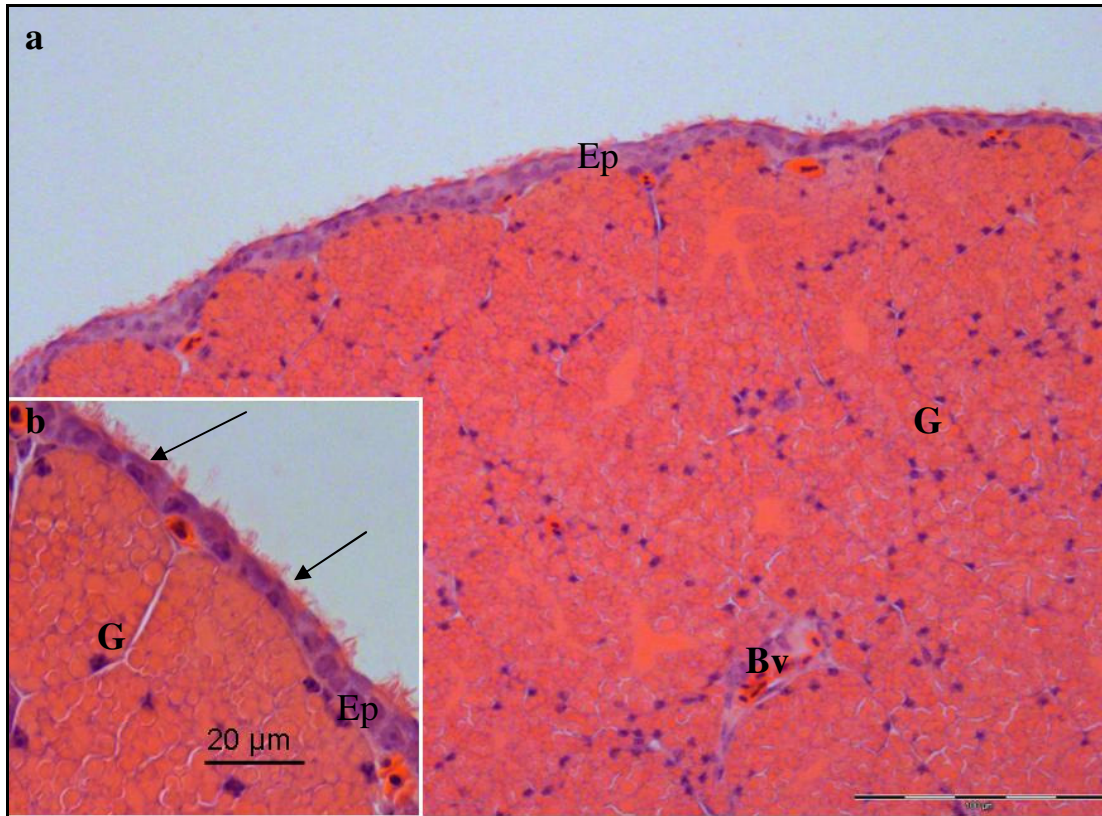


FIG. 3.2: Photomicrographs of the magnum from a bird treated with 400 mg/kg bodyweight carbendazim. **a.** A simple cuboidal epithelium (Ep) lines the mucosal surface. G: Tubular glands. Bv: blood vessel. **b.** A higher magnification photomicrograph of the luminal epithelium (Ep) and tubular glands (G). Arrows: Cells with pyknotic nuclei. H&E stain.

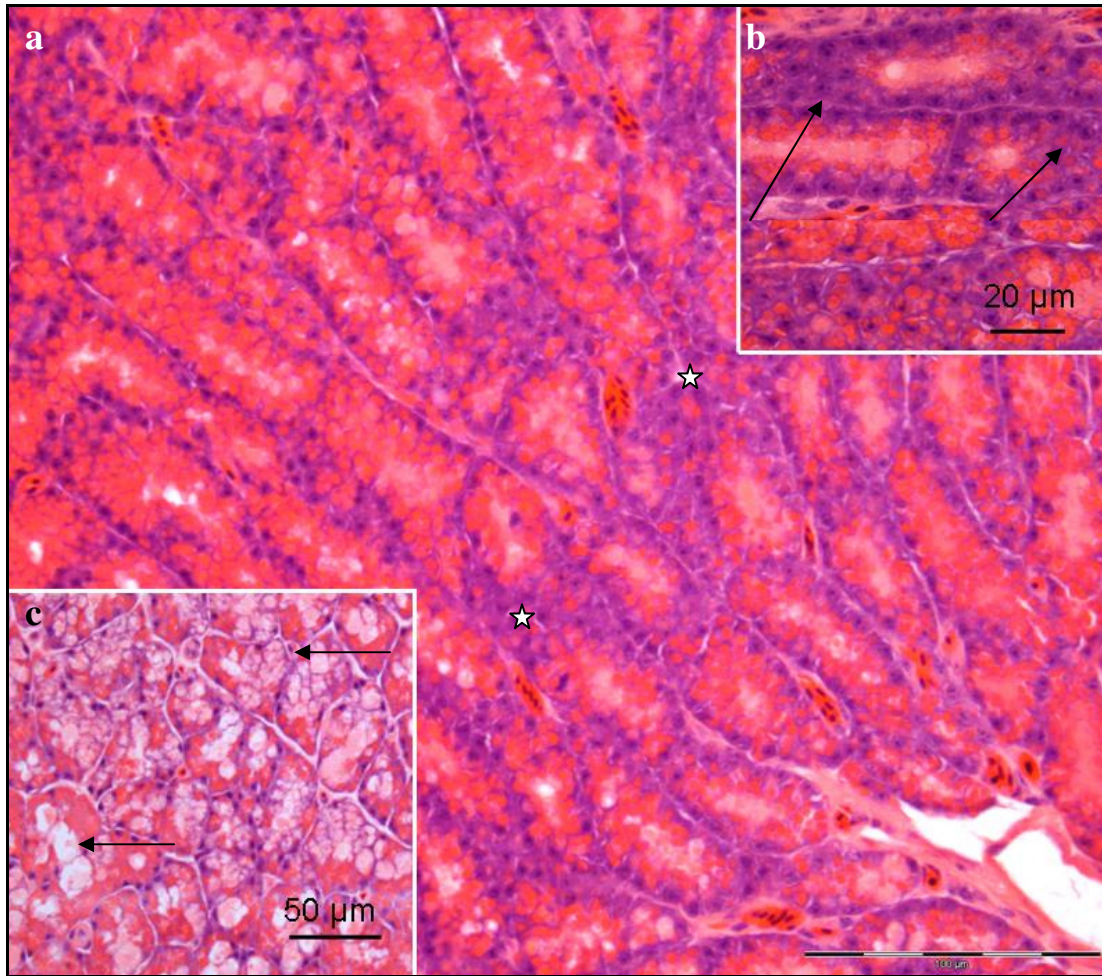


FIG. 3.3: Photomicrographs of the tubular glands in the magnum of a Japanese quail treated with 400 mg/kg bodyweight carbendazim. **a.** Asterisks: Areas of glandular atrophy. **b.** A higher magnification photomicrograph of atrophic gland cells. The degenerating gland cells contain shrunken cytoplasm and pyknotic nuclei (arrows). **c.** Photomicrograph of degenerating magal gland cells with numerous vacuoles (arrows). H&E stain

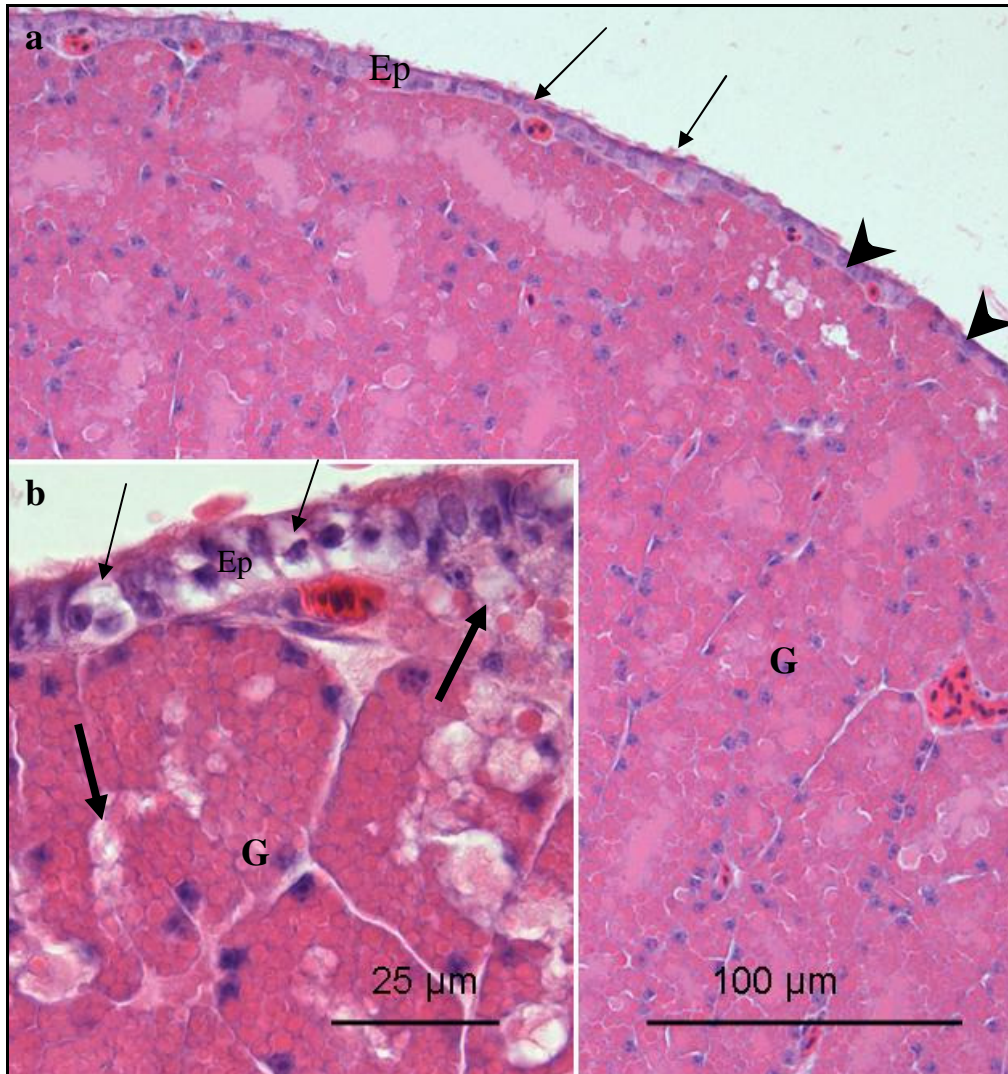


FIG. 3.4: Photomicrographs of the magnum from a bird treated with 800 mg/kg bodyweight carbendazim. **a.** A reduction in the height of the luminal epithelium (Ep) is evident. Arrows: Ciliated cells. Arrowheads: Non-ciliated cells. G: tubular glands. **b.** A higher magnification of the magnum luminal epithelium (Ep) and tubular glands (G). Thin arrows: Swollen epithelial cells. Thick arrows: Vacuoles. H&E stain.

3.3.2.iib. Experiment II (Time-course oviductal degeneration)

Experiment II investigated the short-term (5 hours to 12 days post-exposure) and medium-term (32 days post-exposure) effects of carbendazim on the magnum region of the oviduct in the Japanese quail. A single dose of the minimum effective dose (400 mg/kg bodyweight carbendazim) determined in experiment I, was used.

5 hours post-exposure

No histological degenerative changes were seen in the mucosal and *lamina propria-submucosal* layers of the magnum 5 hours post-administration of 400 mg/kg bodyweight carbendazim.

24 hours post-exposure

Twenty-four hours post-exposure to 400 mg/kg bodyweight carbendazim, a decrease in the height of the luminal epithelial cells was a notable feature of the degenerating magnum (Fig. 3.5a). In the *lamina propria-submucosa*, discrete areas of glandular degeneration were observed. The degenerating gland cells contained numerous vacuoles (Fig. 3.5b). The increased interstitial spaces due to glandular atrophy were also evident.

5 days post-exposure

Five days post-exposure to carbendazim, a decrease in luminal epithelial height was still a notable degenerative change (Fig. 3.6a). In addition, a few epithelial cells contained pyknotic nuclei and cytoplasmic pallor. Hyperaemia and aggregates of inflammatory cells were observed in the *lamina propria-submucosa* (Fig. 3.6b). At this stage, isolated areas of glandular tissue atrophy were evident. The degenerating gland cells contained pyknotic nuclei and numerous cytoplasmic vacuoles. Hyperaemia and perivascular cuffing were observed in the vascular zone between the two layers of the *tunica muscularis*.

8 days post-exposure

Observations at 8 days post-exposure to carbendazim revealed degenerative changes in both the luminal epithelium and *lamina propria-submucosa*. At this stage, relatively few ciliated cells with intact cilia were observed lining the magnum *mucosa*. The degenerating ciliated and non-ciliated epithelial cells were characterized by the presence of pyknotic nuclei and cytoplasmic pallor. In the *lamina propria-submucosa*, atrophy of the tubular glands was observed (Fig. 3.7). Leukocytic

infiltrations were observed between the glands, as well as, around blood vessels (Fig. 3.7). The degenerating gland cells presented pyknotic and karyorrhetic nuclei. Numerous vacuoles were also observed in the degenerating gland cells.

12 days post-exposure

Twelve days post-exposure to carbendazim, degenerative changes were observed in the luminal epithelium and *lamina propria-submucosa*. At this stage, pyknotic nuclei were observed in the luminal epithelial cells. Degenerating gland cells contained numerous vacuoles (Fig. 3.8a). Aggregates of leukocytic infiltration were observed interposed between the glands (Fig. 3.8 b).

32 days post-exposure

Thirty-two days post-exposure to carbendazim, degenerating luminal epithelial cells contained numerous vacuoles (Fig. 3.9a). At this stage, atrophy of the glandular tissue was clearly evident (Fig. 3.9a). The degenerating gland cells contained pyknotic and karyorrhetic nuclei (Fig. 3.9b). Numerous vacuoles were also observed in the degenerating gland cells (Fig. 3.9b). A few inflammatory cells (lymphocytes) were observed in the interstitium.

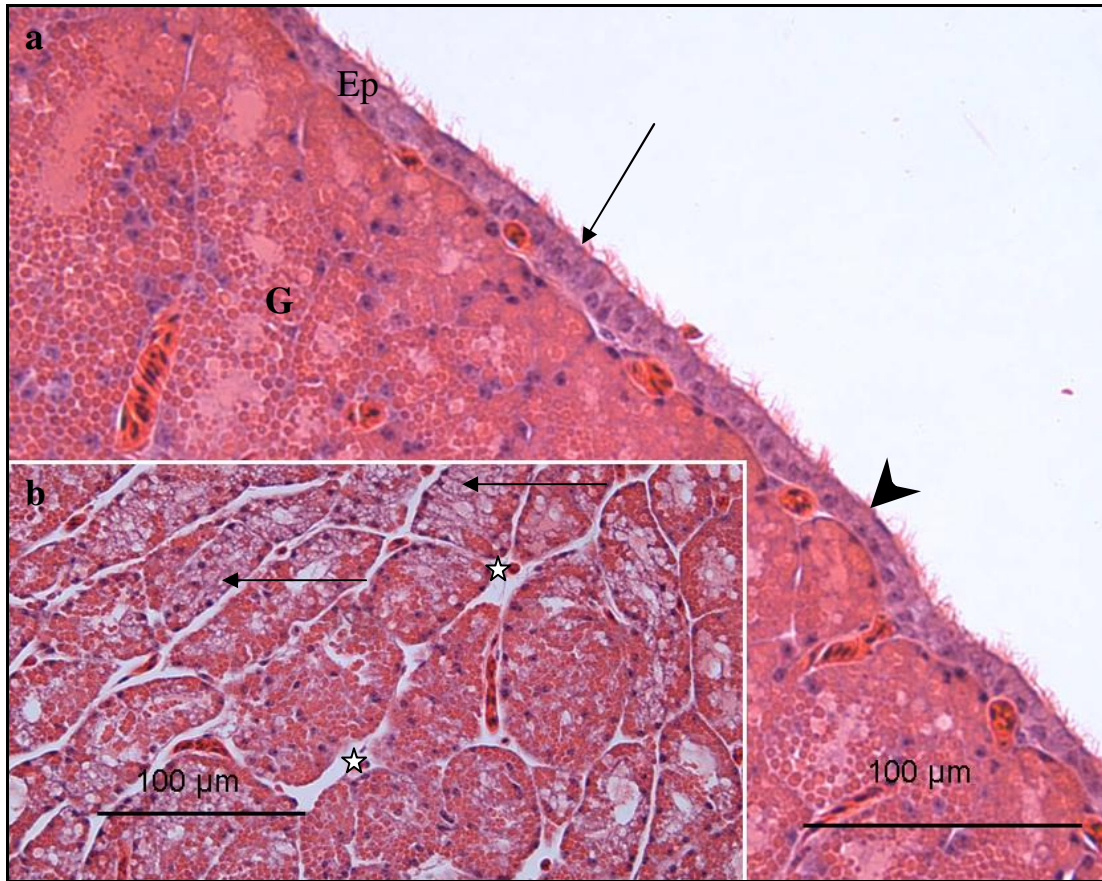


FIG. 3.5: Photomicrographs of the magnum 24 hours post-exposure to 400 mg/kg bodyweight carbendazim. **a.** The epithelium (Ep) is either simple columnar (arrow) or simple cuboidal (arrowhead). G: tubular glands. **b.** Degenerating tubular glands in the magnum. Arrows: Vacuoles. Asterisks: Wide interstitial spaces. Numerous vacuoles (arrows) are observed in the degenerating gland cells. H&E stain.

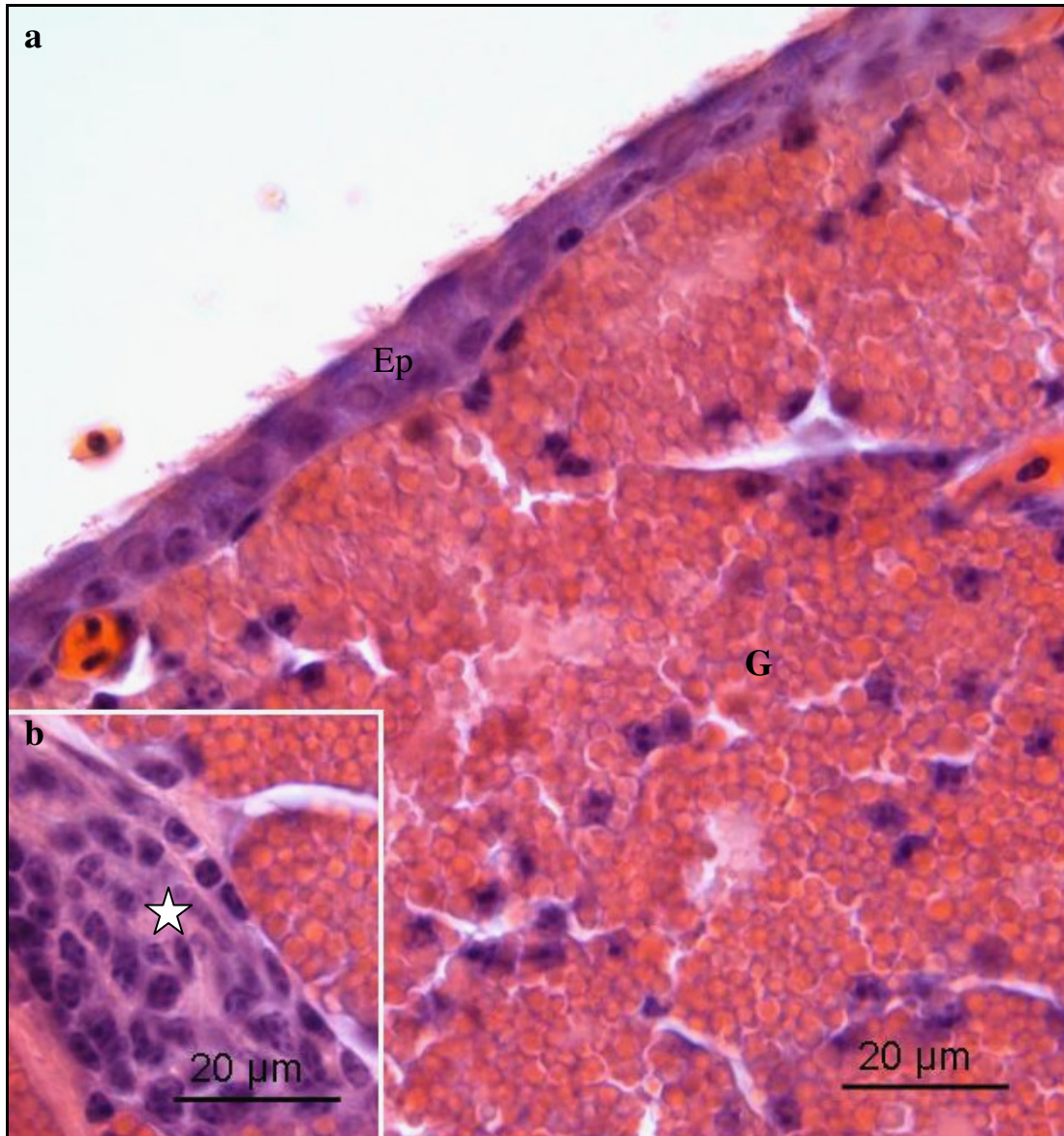


FIG. 3.6: **a.** Photomicrograph of the magnum 5 days post-exposure to 400 mg/kg bodyweight carbendazim. At this stage the *mucosa* is lined by a simple cuboidal epithelium (Ep). G: tubular glands. **b.** A higher magnification photomicrograph showing leukocytic infiltration (asterisk) in the *lamina propria-submucosa* of the magnum. H&E stain.

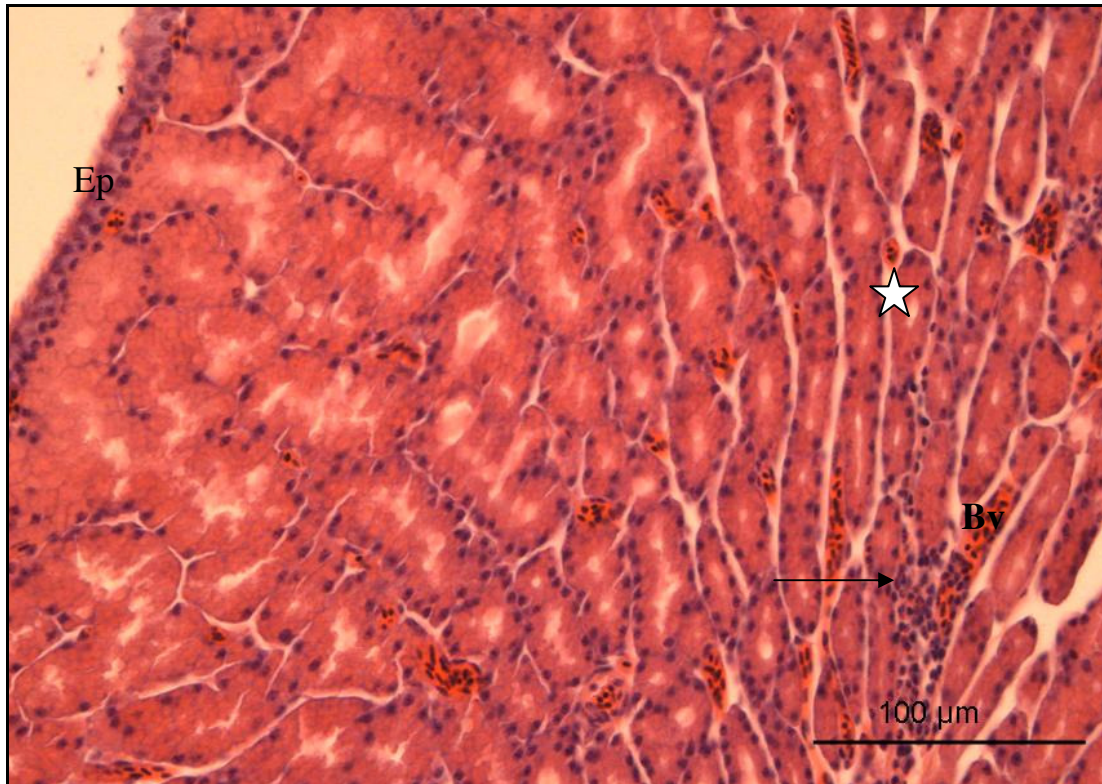


FIG. 3.7: Photomicrograph of the magnum 8 days post-exposure to 400 mg/kg bodyweight carbendazim. Asterisk: Area of glandular atrophy. Arrow: Aggregation of inflammatory cells. Bv: Blood vessels. Ep: luminal epithelium. H&E stain.

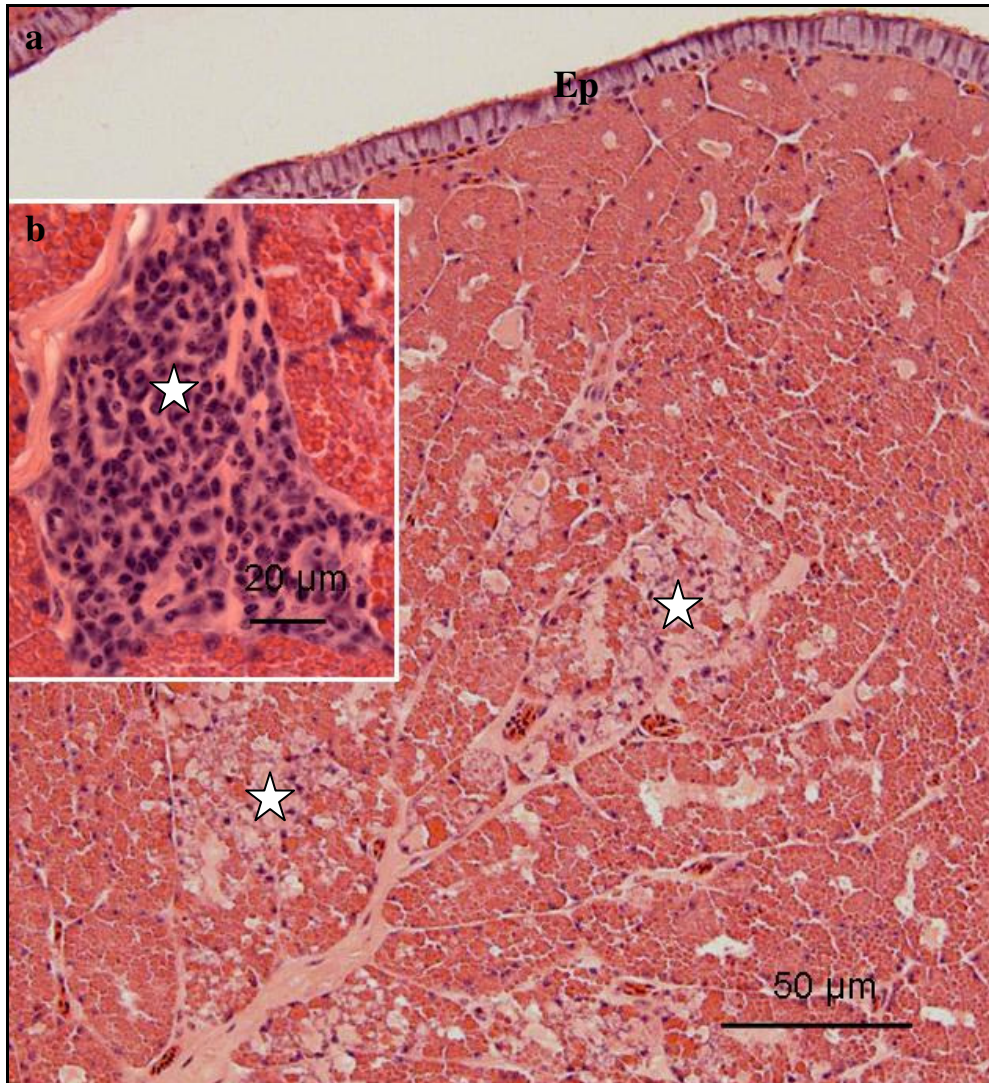


FIG. 3.8: **a.** Photomicrograph of the magnum, 12 days post-exposure to 400 mg/kg bodyweight carbendazim. At this stage a simple columnar epithelium (Ep) lines the magnum. Asterisks: Areas of glandular degeneration. **b.** A high magnification photomicrograph showing aggregations of inflammatory cells (asterisk) in the *lamina propria-submucosa*. H&E stain.

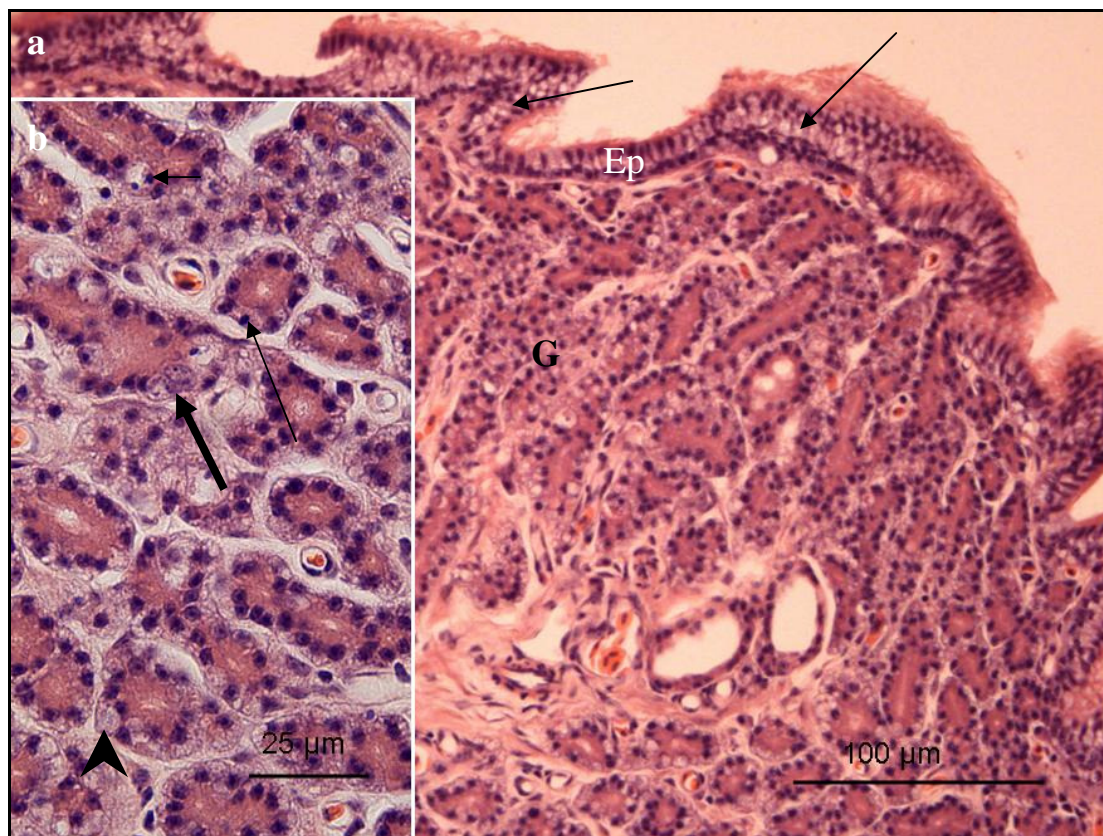


FIG. 3.9: Photomicrographs of the magnum 32 days post-exposure to 400 mg/kg bodyweight carbendazim. **a.** G: Glandular atrophy. Ep: Luminal epithelium with a few vacuoles (arrows). **b.** A higher magnification photomicrograph of atrophic glandular tissue. Thin arrow: Pyknotic nucleus. Thick arrow: Karyorrhetic nucleus. Short arrow: Cytoplasmic pallor. Arrowhead: Vacuolation. H&E stain.

3.3.3. Histochemistry

A subjective assessment of the staining intensity for Periodic Acid Schiff (PAS) and Alcian blue in the luminal and glandular epithelium was conducted. Tables 3.3 a & b summarizes the PAS/Alcian blue staining intensity observed in the control and carbendazim-treated birds in experiment I (dose dependent effects of carbendazim) and II (time-course effects of carbendazim).

3.3.3.i Control birds

A strong reactivity for PAS was observed in the non-ciliated cells of the luminal epithelium (Fig. 3.10a). In these cells, the positive PAS granules were observed in both the basal and supranuclear regions of the cell. In ciliated cells, a moderate PAS staining reaction was observed in the apical cytoplasmic regions (Fig. 3.10b). In the glandular epithelium, staining for PAS was observed in the apical and basal cytoplasmic regions of the gland cells. Cells in the luminal epithelium and glandular epithelium were negative for the Alcian blue stain.

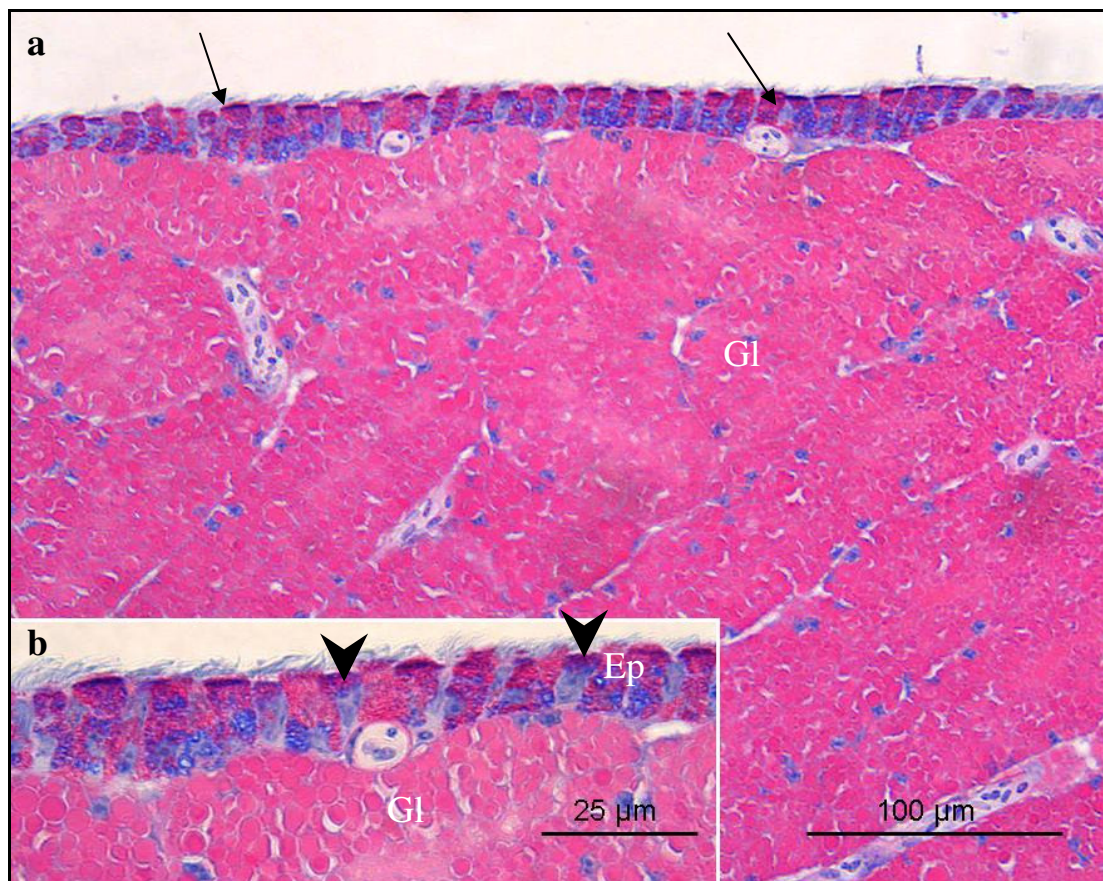


FIG. 3.10: Photomicrographs of the magnum from a control bird. **a.** Arrows: Non-ciliated cells. Gl: Gland cells. **b.** A higher magnification photomicrograph of the luminal epithelium (Ep) and tubular glands (Gl). In the ciliated cells PAS positive granules are present in the apical cytoplasmic regions (arrowheads). Periodic Acid Schiff and Alcian blue stains.

3.3.3.ii Carbendazim-treated birds

3.3.3.iii *Experiment I*

25 mg/kg bodyweight carbendazim

At a dose of 25 mg/kg bodyweight carbendazim, no changes of PAS or Alcian blue staining characteristics observed

100 mg/kg bodyweight carbendazim

At a dose of 100 mg/kg bodyweight carbendazim, a moderate reactivity for PAS was observed in the non-ciliated cells of the luminal epithelium, as well as in the gland cells (Table 3.3a; Fig. 3.11). The PAS positive staining was concentrated in the supranuclear regions of these cells (Fig. 3.11 a&b). No PAS staining granules were observed in ciliated cells (Fig. 3.11b). Both epithelial and glandular cells were negative for Alcian blue stain.

400 mg/kg bodyweight

At a dose of 400 mg/kg bodyweight carbendazim, a moderate reactivity for PAS was observed in the apical cytoplasmic regions of non-ciliated cells in the luminal epithelium (Fig. 3.12a). Ciliated cells were negative for PAS staining (Fig. 3.12a). PAS staining in the gland cells was moderate. The distribution of PAS staining was similar to that of the control group.

800 mg/kg bodyweight carbendazim

At a dose of 800 mg/kg bodyweight carbendazim, relatively few luminal epithelial cells contained PAS positive granules. In this group, a weak reactivity for PAS was evident in the supranuclear regions of non-ciliated cells in the luminal epithelium (Fig. 3.12b). No histochemical changes were observed in either the ciliated cells or the gland cells at this dose. No Alcian blue stain reaction was observed in the luminal epithelial cells or glandular cells following carbendazim treatment.

Table 3.3a: PAS/Alcian blue staining intensity in the magnum of control and carbendazim-treated Japanese quails.

Carbendazim dose (mg/kg)	Non-ciliated cells		Ciliated cells		Gland cells	
	PAS	Alcian blue	PAS	Alcian blue	PAS	Alcian blue
0	+++	-ve	++	-ve	+++	-ve
25	+++	-ve	++	-ve	+++	-ve
100	++	-ve	-ve	-ve	++	-ve
400	++	-ve	-ve	-ve	++	-ve
800	+/-	-ve	-ve	-ve	+++	-ve

+++ indicates strong; ++ moderate; + weak; +/- weak or negative, -ve negative staining.

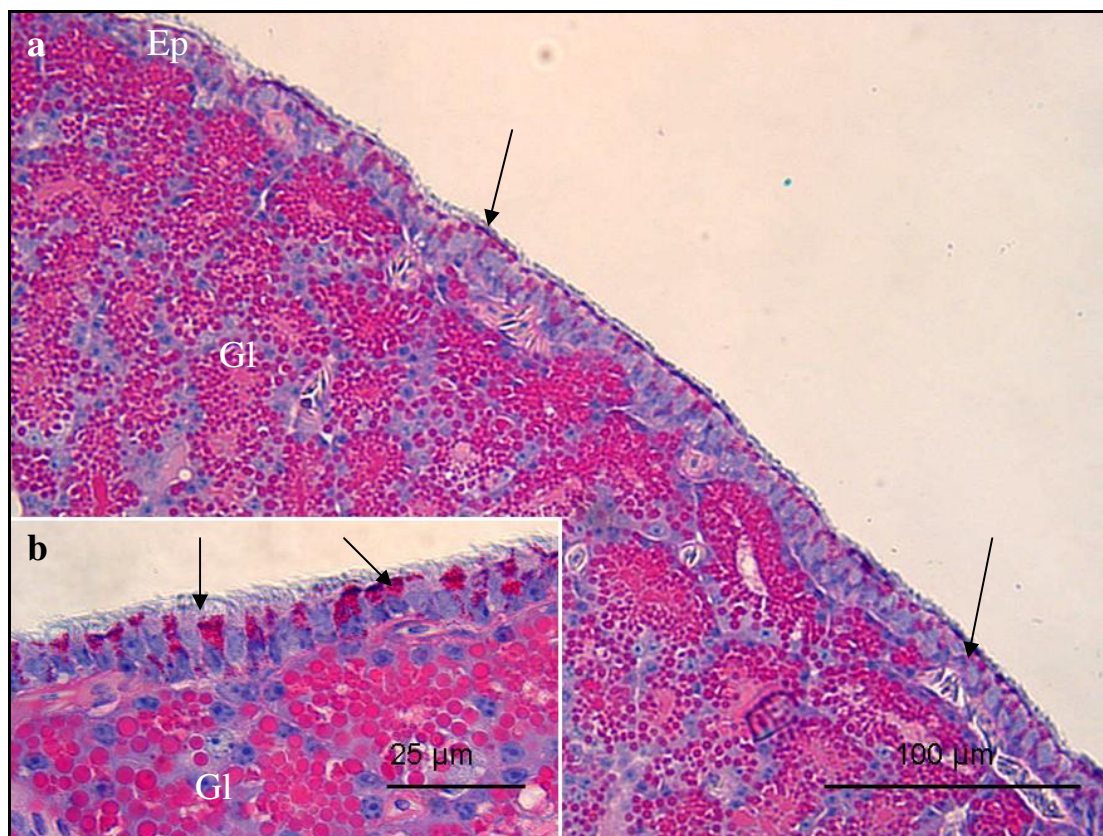


FIG. 3.11: Photomicrographs of the magnum from a bird treated with 100 mg/kg bodyweight carbendazim. **a.** Arrows: Non-ciliated cells. Gl: Gland cells. Ep: luminal epithelium. **b.** A higher magnification photomicrograph of (a). The PAS staining reactivity is observed in the apical cytoplasmic regions (arrows). Gl: tubular glands. PAS/Ab stains.

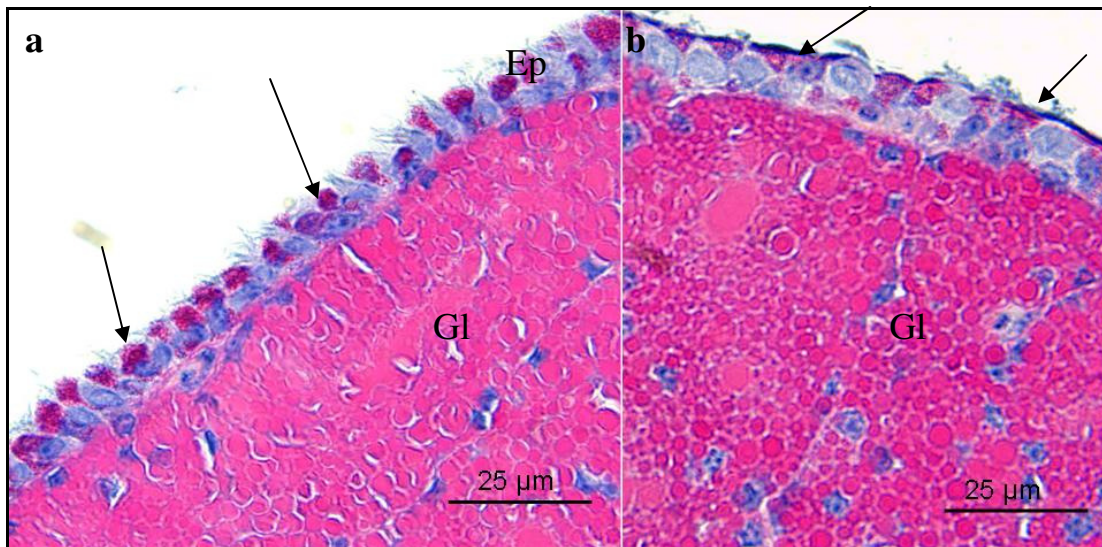


FIG. 3.12: **a.** Photomicrograph of the magnum from a bird treated with 400 mg/kg bodyweight carbendazim. Arrows: Non-ciliated cells. Gl: Gland cells. Ep: luminal epithelium. **b.** Photomicrograph of the magnum from a bird treated with 800 mg/kg bodyweight carbendazim. Note that at this dose relatively few non-ciliated cells (arrows) contain PAS positive granules. Gl: glandular cells. PAS/Ab stains.

3.3.3.iib Experiment II

5 hours post-exposure

Five hours post-exposure to 400 mg/kg bodyweight carbendazim, strong staining for PAS was observed in the non-ciliated cells of the luminal epithelium as well as in gland cells (Table 3.3b). Ciliated cells were negative for PAS staining. Both non-ciliated and gland cells did not stain with Alcian blue.

24 hours and 5 days post-exposure

Twenty-four hours and five days post-exposure to carbendazim, non-ciliated cells in the luminal epithelium exhibited a moderate PAS reaction. The cells did not stain with alcian blue (Fig. 3. 13). The staining reaction was observed in the apical cytoplasmic regions. At this stage, PAS reactivity in the gland cells was comparable to the control group. No reactivity for Alcian blue was observed in the epithelia.

8 days post-exposure

Eight days post-exposure to carbendazim, strong alcian blue reactivity was observed in non-ciliated cells of the luminal epithelium (Fig. 3.14a). At this stage, the non-ciliated cells stained weakly for PAS. In some instances, the non-ciliated cells were negative for PAS. A moderate PAS reactivity was observed in the gland cells (Fig. 3:14b). No reactivity for alcian blue was encountered in the gland cells.

12 days post-exposure

Twelve days post-exposure to 400 mg/kg bodyweight carbendazim, weak staining for PAS was observed in the non-ciliated cells of the luminal epithelium (Fig. 3.15a). The PAS positive granules were concentrated in the apical cytoplasmic regions of these cells (Fig. 3.15b). The gland cells stained moderate for PAS. At this stage, the non-ciliated cells in the luminal epithelium showed weak reactivity for alcian blue (Fig. 3.15b). The gland cells were negative for alcian blue stain.

32 days post-exposure

Thirty-two days post-exposure to carbendazim, non-ciliated cells in the luminal epithelium stained strongly for alcian blue (Fig. 3.16a). In addition, a few non-ciliated cells also showed a weak reaction for PAS (Fig. 3.16b). At this stage, gland cells displayed moderate PAS staining. The gland cells did not stain with Alcian blue (Fig. 3.16a&b).

Table 3.3b: PAS/Alcian blue staining intensity in the magnum at different periods post-exposure to 400 mg/kg bodyweight carbendazim.

Time periods	Non-ciliated cells (epithelium)		Gland cells	
	PAS	Alcian blue	PAS	Alcian blue
5 hours	+++	-ve	+++	-ve
24 hours	++	-ve	+++	-ve
5 days	++	-ve	++	-ve
8 days	+/-	+++	++	-ve
12 days	+	+	++	-ve
32 days	+	+++	+	-ve

+++ indicates strong; ++ moderate; + weak; +/- weak or negative, -ve negative staining.

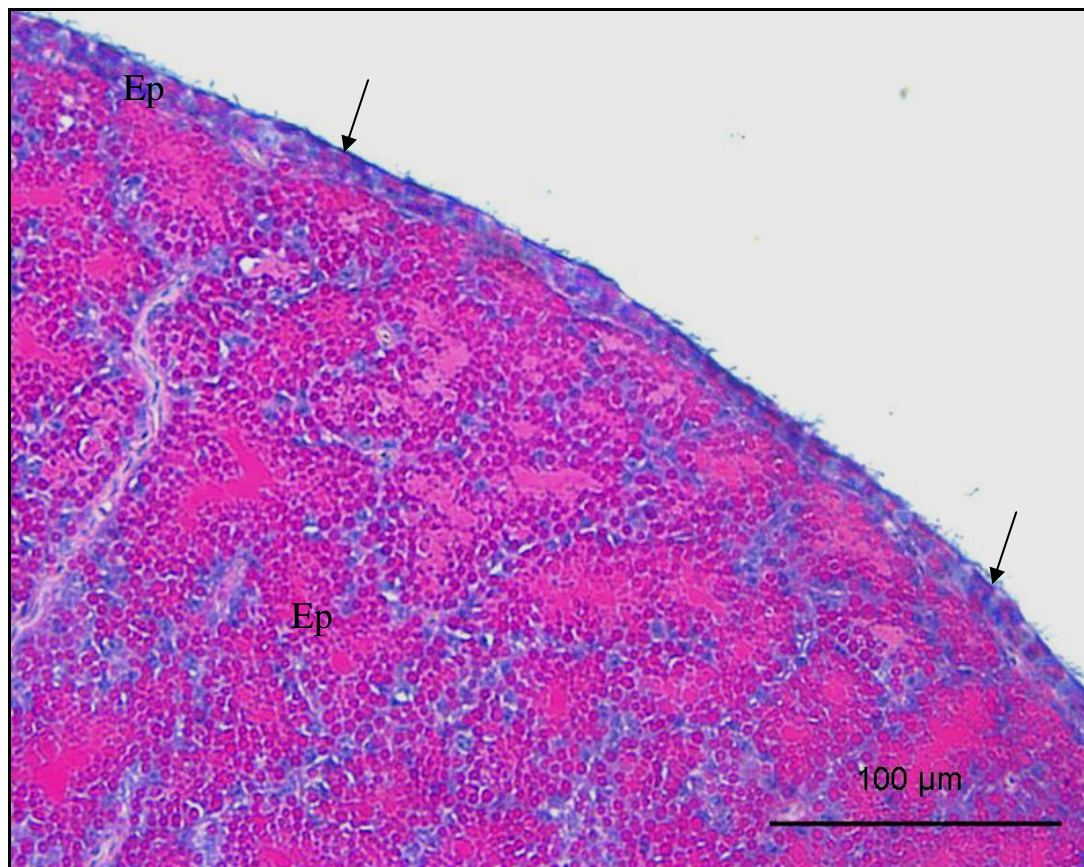


FIG. 3.13: Photomicrograph of the magnum 5 days post-exposure to 400 mg/kg bodyweight carbendazim. PAS granules are observed in the apical cytoplasmic regions of the non-ciliated cells (arrows). EP: Luminal epithelium. Gl. Gland cells. PAS/Ab stains.

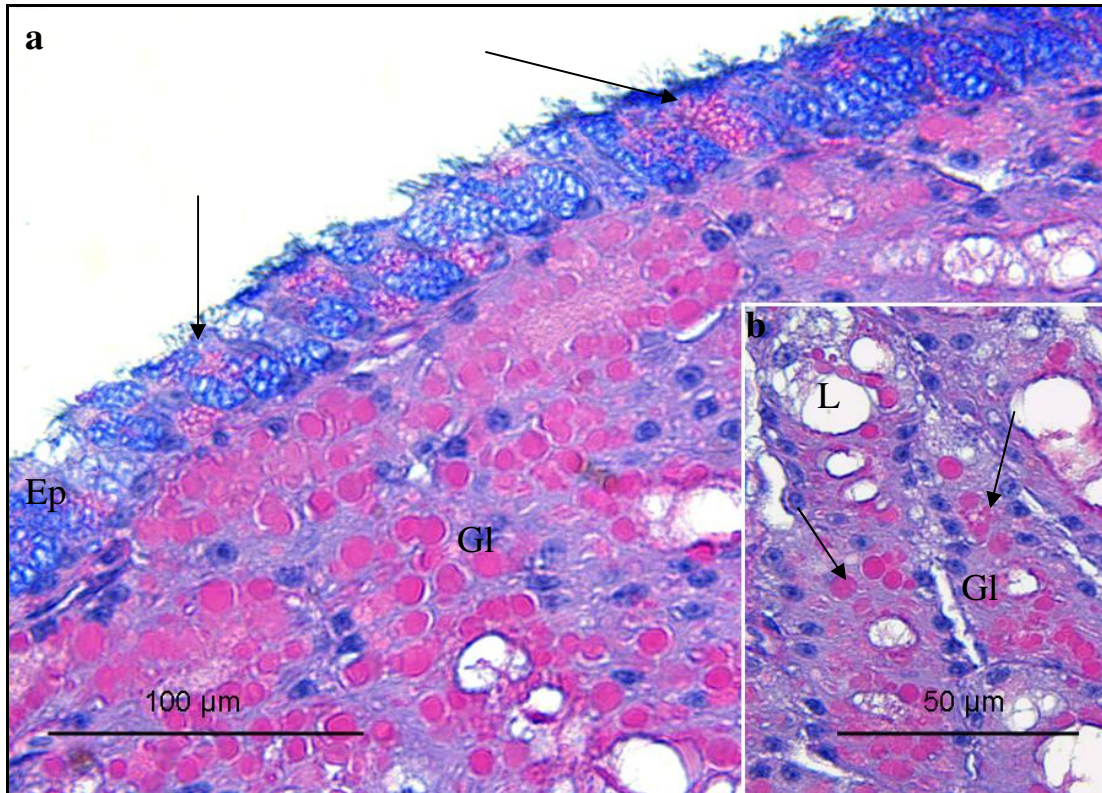


FIG. 3.14: **a.** Photomicrograph of the magnum 8 days post-exposure to 400 mg/kg bodyweight carbendazim. The epithelial cells (Ep) show a strong reactivity for Alcian blue. A few cells in addition to alcian blue, show weak reaction for PAS stain (arrows). Gl: Gland cells. **b.** A higher magnification photomicrograph of the tubular glands (Gl) in the magnum. The gland cells contain a few granules (arrows). L: glandular lumen. PAS/Ab stains.

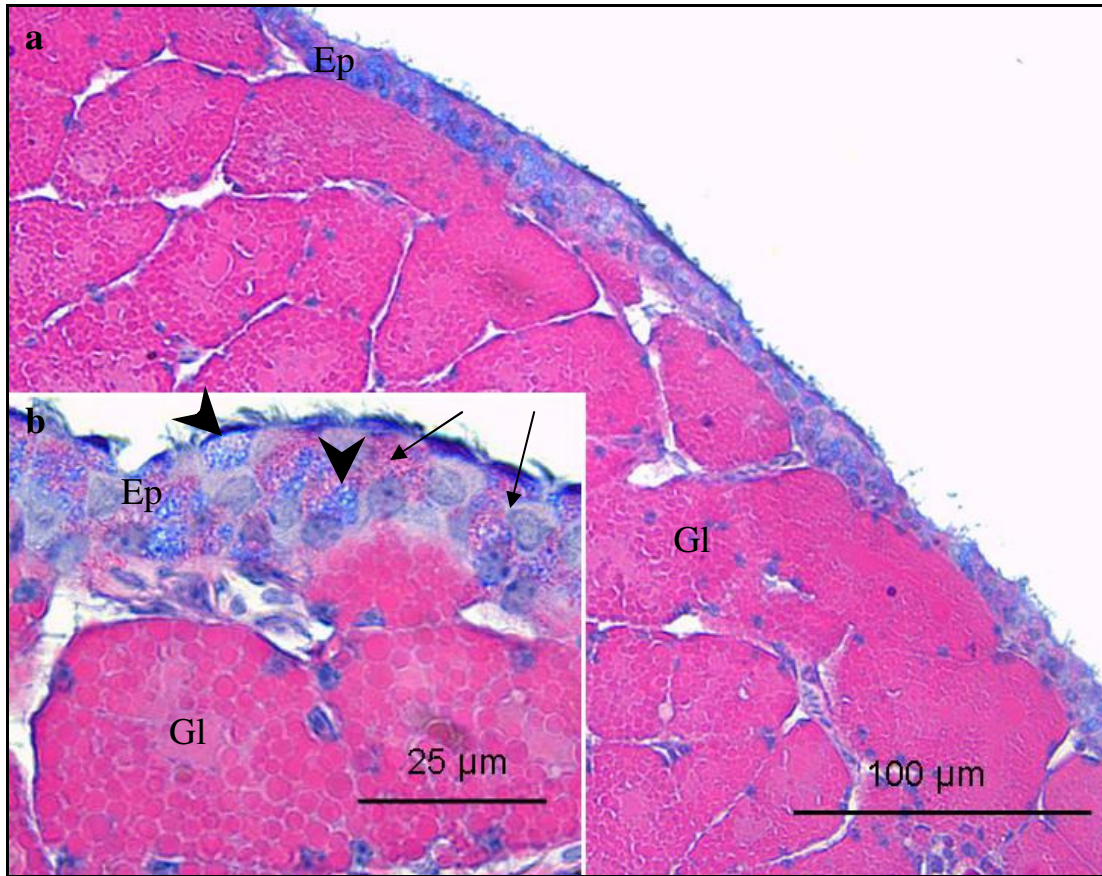


FIG. 3.15: Photomicrographs of the magnum 12 days post-exposure to 400 mg/kg carbendazim. **a.** Ep: Luminal epithelium. Gl: Gland cells. **b.** A higher magnification photomicrograph of the luminal (Ep) and glandular (Gl) maganal epithelia. PAS (arrows) and alcian blue (arrowheads) positive non-ciliated cells. PAS/Ab stains.

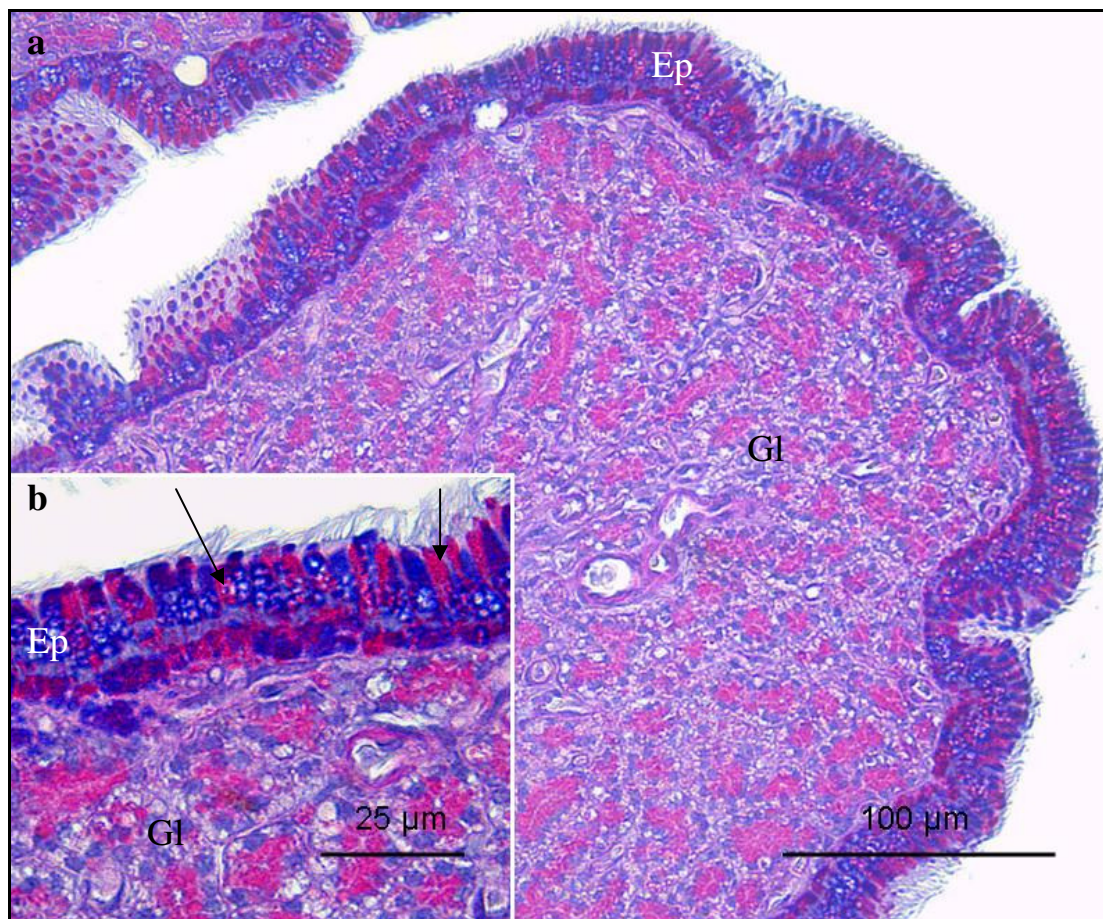


FIG. 3.16: Photomicrographs of the magnum 32 days post-exposure to 400 mg/kg bodyweight carbendazim. **a.** Ep: Alcian blue positive luminal epithelium. GI: PAS positive gland cells. **b.** A higher magnification photomicrograph of the magnum luminal (Ep) and glandular (GI) epithelia. Arrows: PAS positive non-ciliated cells. PAS/Ab stains.

3.3.4 Immunohistochemistry

Immunoreactivity for e-cadherin, laminin and vimentin was assessed in the magnum mucosa of both control and carbendazim-treated Japanese quails. A qualitative assessment of the staining intensity was visually graded as strong, moderate, weak or negative.

3.3.4.1 E-cadherin

3.3.4.1.i Control group

A strong immunoreaction for e-cadherin was observed in the cytoplasm of both ciliated and non-ciliated luminal epithelial cells (Fig. 3.17). The staining granules were observed in both apical and basal cytoplasmic regions. Glandular epithelial cells in the magnum showed moderate immunoreactivity for e-cadherin (Fig. 3.17). No e-cadherin immunoreaction was observed in the *tunica muscularis*.

3.3.4.1.ii Carbendazim-treated birds

3.3.4.1.ii.a *Experiment I*

At dosages of 25 mg/kg and 100 mg/kg bodyweight, e-cadherin immunoreactivity comparable to that observed in the control group was seen 48 hours post-exposure to carbendazim. However, at dosages of 400 mg/kg and 800 mg/kg bodyweight, no staining reactions were observed in the mucosal layer of the magnum. Both luminal and glandular epithelial cells were negative for e-cadherin.

3.3.4.1.ii.b *Experiment II*

No immunohistochemical changes were observed in the mucosal layer of the magnum at 5 and 24 hours post-exposure to carbendazim.

Luminal and glandular epithelia were e-cadherin immunonegative at days 5, 8, and 12 post-exposure to carbendazim (Fig. 3.18). At day 32 post-exposure to carbendazim, strong to moderate e-cadherin immunoreactivity was observed in luminal epithelial cells (Fig. 3.19). The glandular epithelial cells showed weak immunoreactivity for e-cadherin (Fig. 3.19).

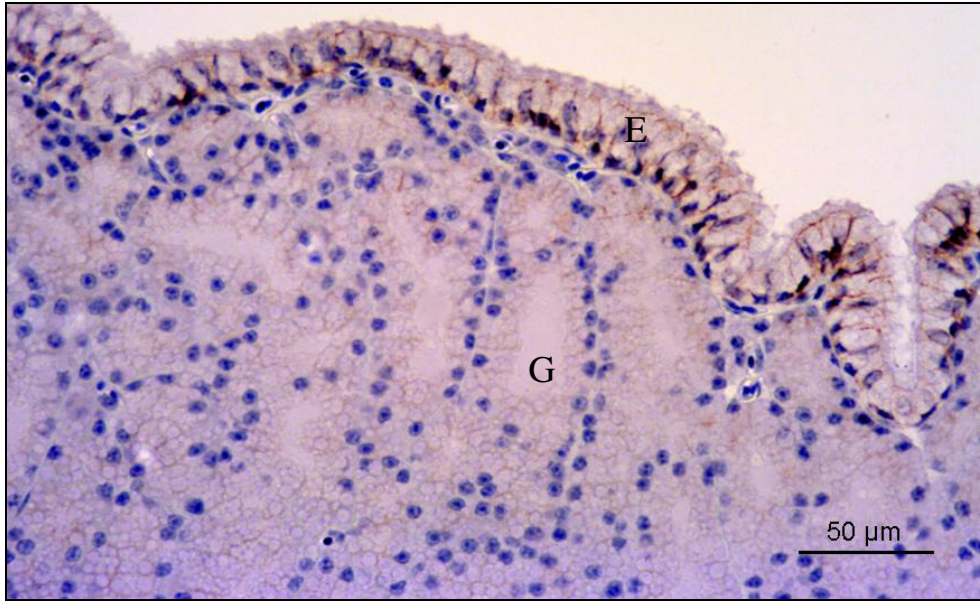


Fig. 3.17: Photomicrograph of E-cadherin immunostaining in the magnum of a control bird. E-cadherin immunoreaction in the luminal epithelium (E) and tubular glands (G).

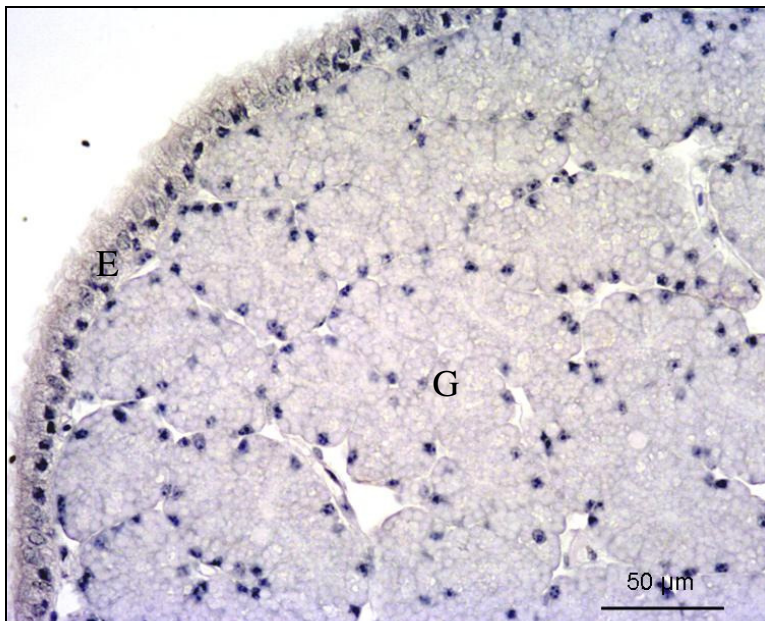


Fig. 3.18: Photomicrograph of E-cadherin immunostaining in the magnum 8 days post-exposure to carbendazim. Both luminal (E) and glandular (G) epithelial cells are e-cadherin immunonegative.

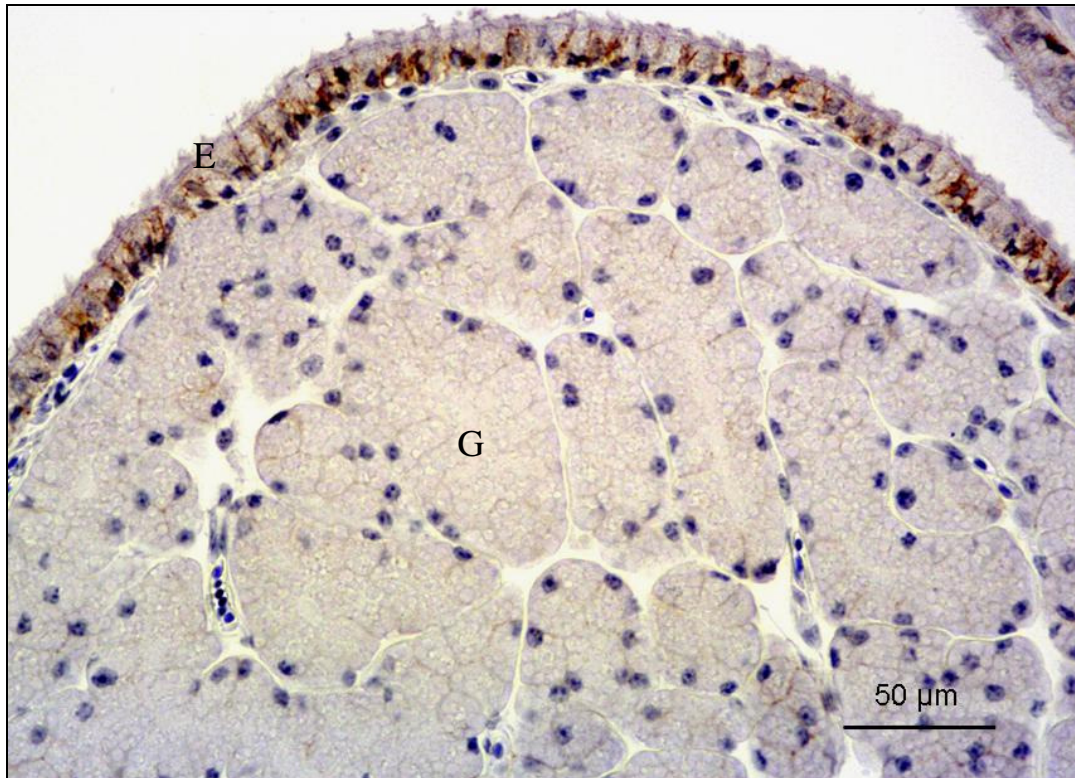


Fig. 3.19: Photomicrograph of E-cadherin immunostaining in the magnum 32 days post-exposure to 400 mg/kg bodyweight carbendazim. E: immunopositive epithelium. G: Gland cells.

3.3.4.2 Laminin

3.3.4.2.i. Control birds

Strong immunoreactivity for laminin was observed in the basement membranes underlying luminal and glandular cells. In addition, the basement membranes associated with smooth muscle cells in the *tunica muscularis* and vascular tunica media were laminin immunopositive (Fig. 3.20 a&b).

3.3.4.2.ii Carbendazim-treated birds

3.3.4.2.ii.a *Experiment I*

400 mg/kg bodyweight carbendazim-treated group

Forty-eight hours post-exposure to a dose of 400 mg/kg bodyweight carbendazim no immunohistochemical changes were observed in the mucosal layer of the magnum.

800 mg/kg bodyweight carbendazim-treated group

Laminin immunoreaction in the basement membrane underlying luminal and glandular epithelia was weak to absent. At this dose, the basement membranes of smooth muscle cells in the tunica media and muscularis showed a moderate to weak immunoreaction for laminin.

3.3.4.2.ii.b *Experiment II*

No immunohistochemical changes were observed at 5 and 24 hours post carbendazim treatment.

At days 5 and 8 post-exposure to carbendazim, moderate to weak immunoreactivity for laminin was observed in the basement membrane underlying both luminal and glandular epithelia, as well as, smooth muscle cells.

At days 12 and 32 post-exposure to carbendazim, strong to moderate laminin immunoreaction was observed in the basement membrane underlying luminal epithelia. During these stages, the basement membrane underlying the glandular epithelium was relatively thick and showed moderate to weak laminin immunoreaction (Fig. 3.21).

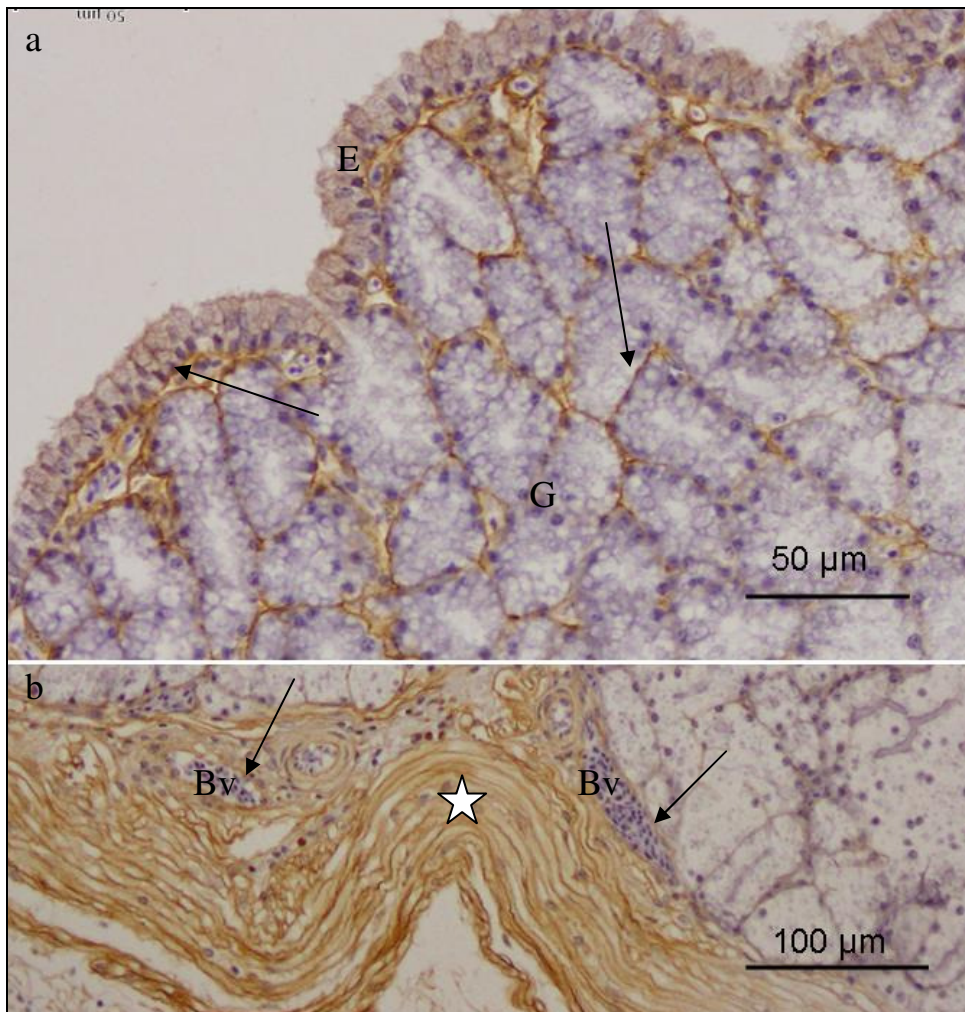


Fig. 3.20: Photomicrographs of laminin immunostaining in the magnum of a control bird. **a.** Arrows: Immunopositive basement membranes of luminal (E) and glandular (G) epithelia. **b.** Laminin immunopositive the tunica muscularis (asterisk) and tunica media (arrows). Bv: Blood vessels.

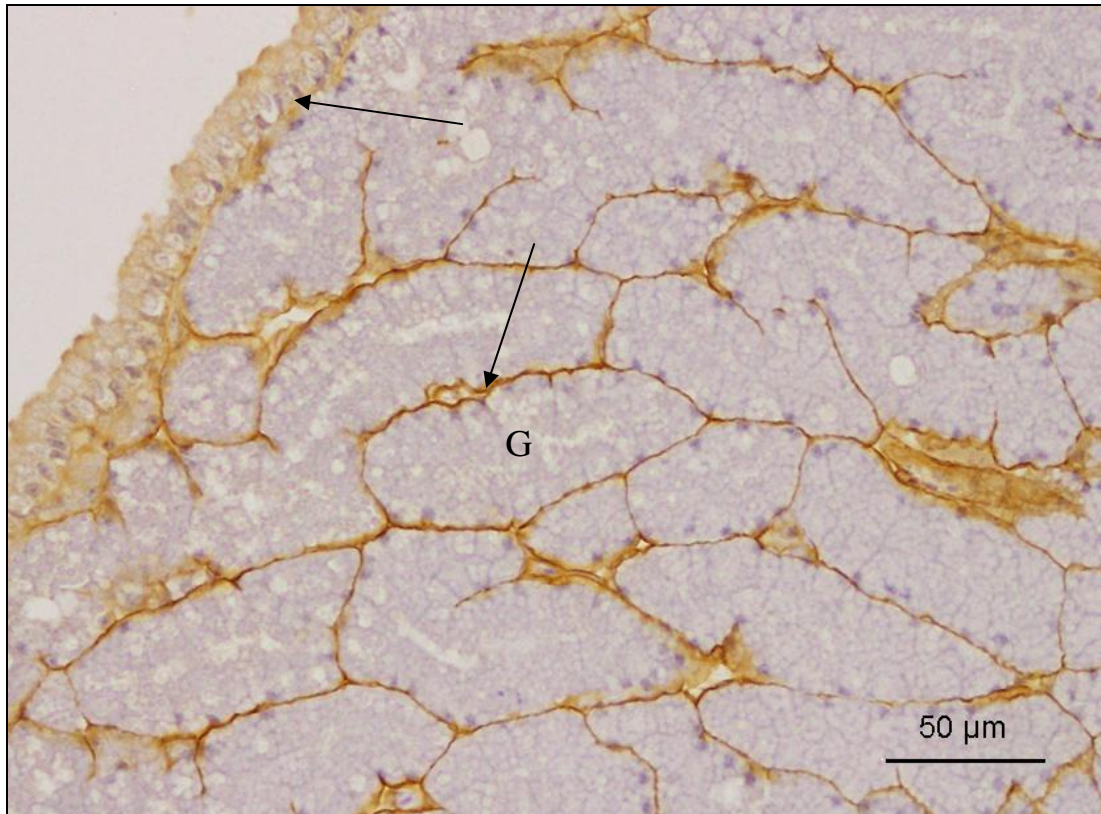


Fig. 3.21: Photomicrograph of laminin immunostaining in the magnum 12 days post-exposure to 400 mg/kg bodyweight carbendazim. Strong immunostaining is observed in the basement membrane (arrows). Note the increased thickness of the basement membrane lining the tubular glands (G).

3.3.4.3. Vimentin

3.3.4.3.i Control group

Strong immunoreaction for vimentin was observed in both ciliated and non-ciliated luminal epithelial cells (Fig. 3.22a). Positive immunoreactivity for vimentin was also present in the endothelium, serosal mesothelium, as well as in a few fibrocytes in the *lamina propria-submucosa* (Fig. 3.22b). The glandular epithelial cells were negative for vimentin (Fig. 3.22a)

3.3.4.3.ii Carbendazim-treated birds

3.3.4.3.iii *Experiment I*

Carbendazim doses of 400 mg/kg and 800 mg/kg bodyweight

Vimentin immunostaining in luminal epithelial cells and endothelial cells was moderate in non-ciliated cells and weak in ciliated cells (Fig. 3.23). Glandular epithelial cells were vimentin immunonegative.

3.3.4.3.iii *Experiment II*

No immunohistochemical changes were observed in the magnal mucosa at 5 and 24 hours post-exposure to carbendazim.

At days 5 and 8 moderate to weak vimentin immunoreactivity was observed in the cytoplasm of non-ciliated cells. Only a few ciliated cells showed weak vimentin immunoreaction. Fibrocytes and endothelial cells also showed moderate to weak vimentin immunoreaction. No immunohistochemical changes were observed in the glandular epithelial cells.

At day 12 post-exposure to carbendazim, luminal epithelial cells, endothelial cells and fibrocytes showed moderate immunoreaction for vimentin. Moderate to strong vimentin immunoreaction was observed in these cells at day 32 post-exposure to carbendazim (Fig. 3.24).

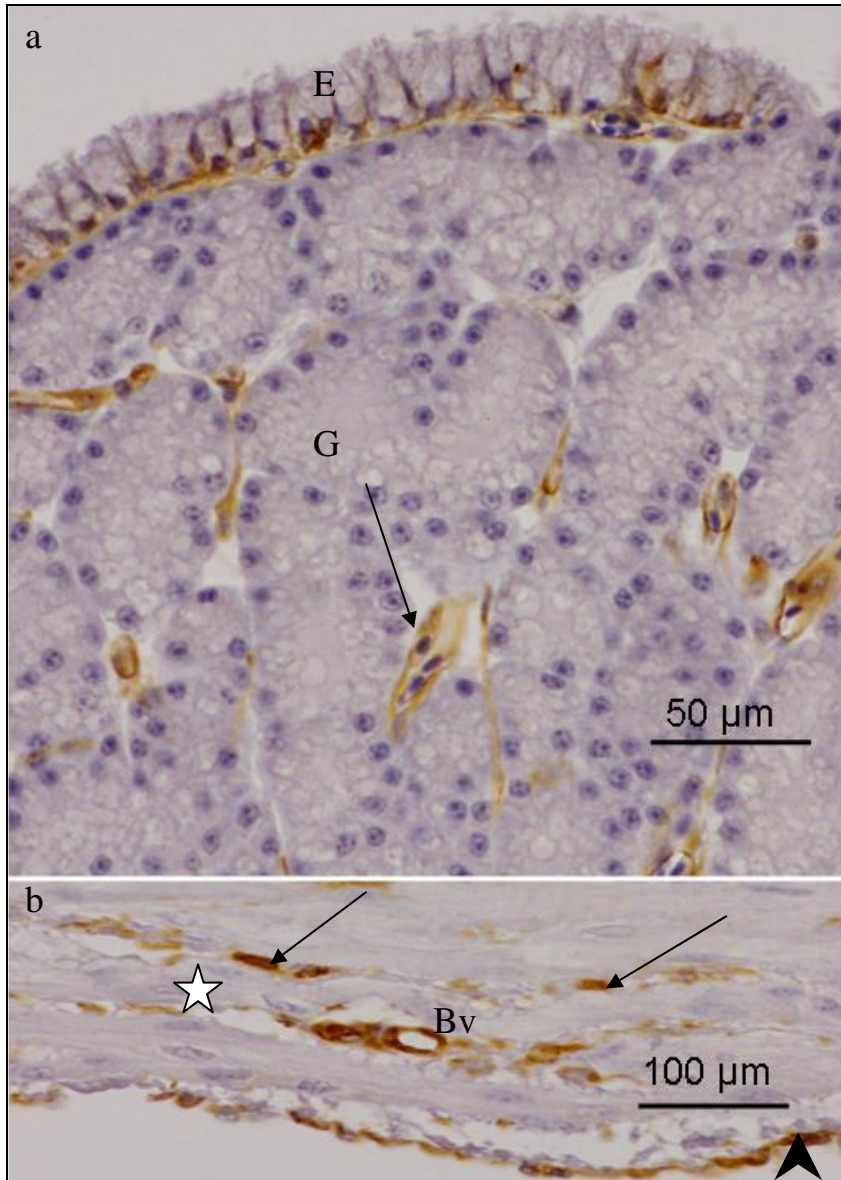


Fig. 3.22: Photomicrographs of vimentin immunostaining in the magnum of a control bird. a. Immunopositive luminal (E) and endothelial (arrow) cells. G: Immunonegative gland cells. B. Immunopositive mesothelial cells (arrowhead), fibrocytes (arrows) and vascular endothelial cells (Bv). Asterisk: Tunica muscularis.

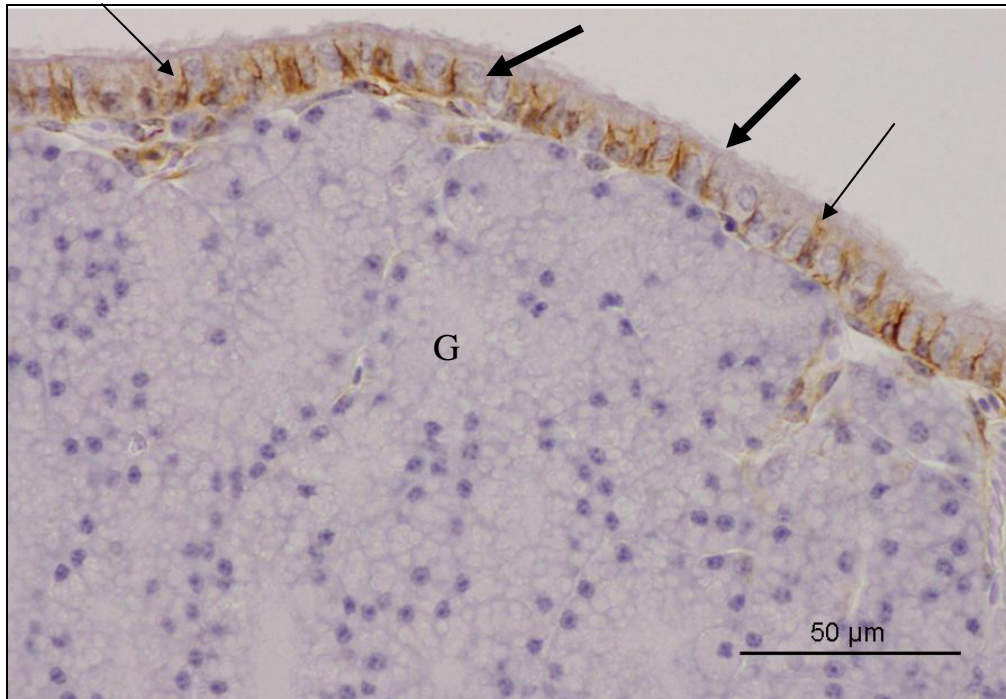


Fig. 3.23: Photomicrograph of vimentin immunostaining in the magnum 48 hours post-exposure to 400 mg/kg bodyweight carbendazim. Thin arrows: Immunopositive non-ciliated cells. Thick arrows: Weak immunostaining in ciliated cells. G: Immunonegative gland cells.

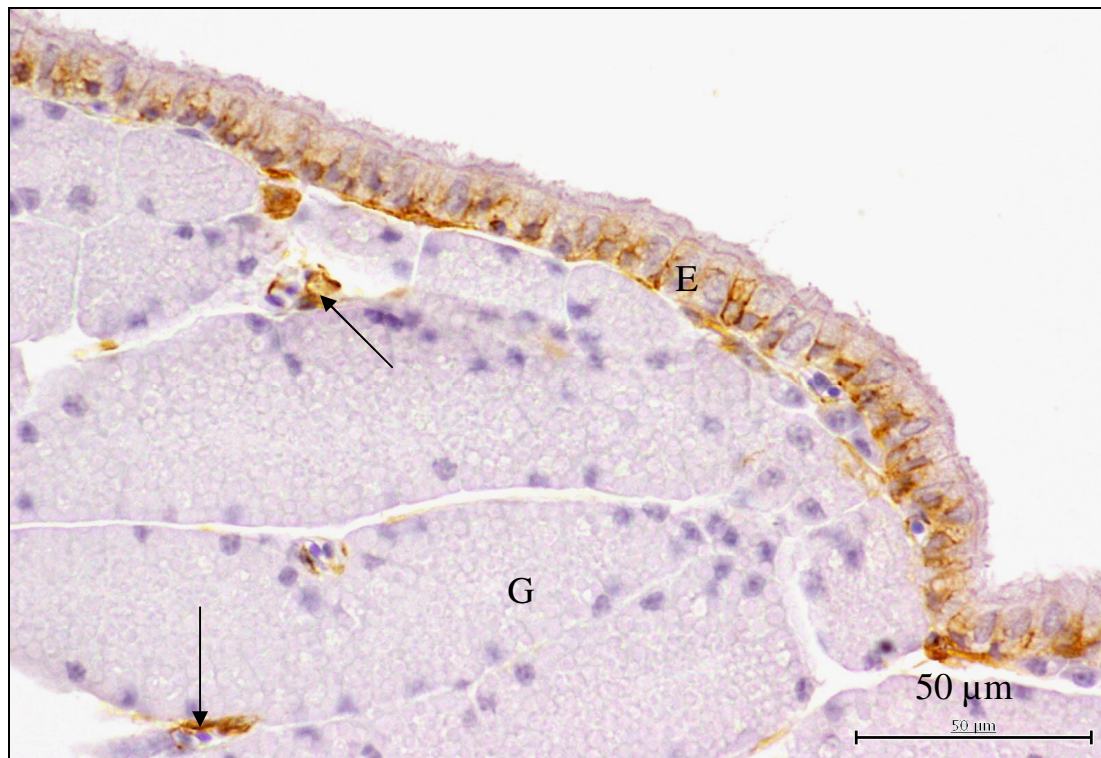


Fig. 3.24: Photomicrograph of vimentin immunostaining in the magnum 32 days post-exposure to 400 mg/kg bodyweight carbendazim. Immunopositive epithelial (E) and endothelial cells (arrows). G: tubular glands.

3.3.5 Ultrastructural observations

3.3.5.1 Scanning electron microscopy

3.3.5.1.i Control birds

The mucosal layer of the magnum formed longitudinally oriented luminal folds (Fig. 3.25a). Both primary and secondary folds were identified. The luminal epithelium consisted of ciliated and non-ciliated cells (Fig.3.25b). The non-ciliated cells exhibited a dome-shaped apical surface, which was covered by microvilli (Fig. 3.25c). . The ciliated cells which appeared to be predominant were lined by long cilia (Fig. 3.25 b). In some instances, the cilia tended to obscure the non-ciliated cells (Fig. 3.25b). Round to oval-shaped glandular openings were identified between the epithelial cells.

3.3.5.1.ii Carbendazim treated birds

3.3.5.1.iii *Experiment I*

25 and 100 mg/kg bodyweight carbendazim

At doses of 25 mg/kg and 100 mg/kg bodyweight carbendazim, no degenerative changes were observed on the magnal mucosal surface. Degenerative changes were observed at doses of 400 mg/kg and 800 mg/kg bodyweight carbendazim.

400 mg/kg bodyweight carbendazim

At a dose of 400 mg/kg bodyweight carbendazim, isolated areas of deciliation were observed (Fig. 3.26a). In these areas, short ciliary stems, which indicated cilia degeneration, were observed. On the apical surface of degenerating non-ciliated cells, microvillous loss was observed (Fig. 3.26b). In a few instances, inflammatory cells were observed on the luminal surface.

800 mg/kg bodyweight carbendazim

At a dose of 800 mg/kg bodyweight carbendazim, deciliation was still the predominant degenerative change observed. In addition, a few inflammatory cells were also observed.

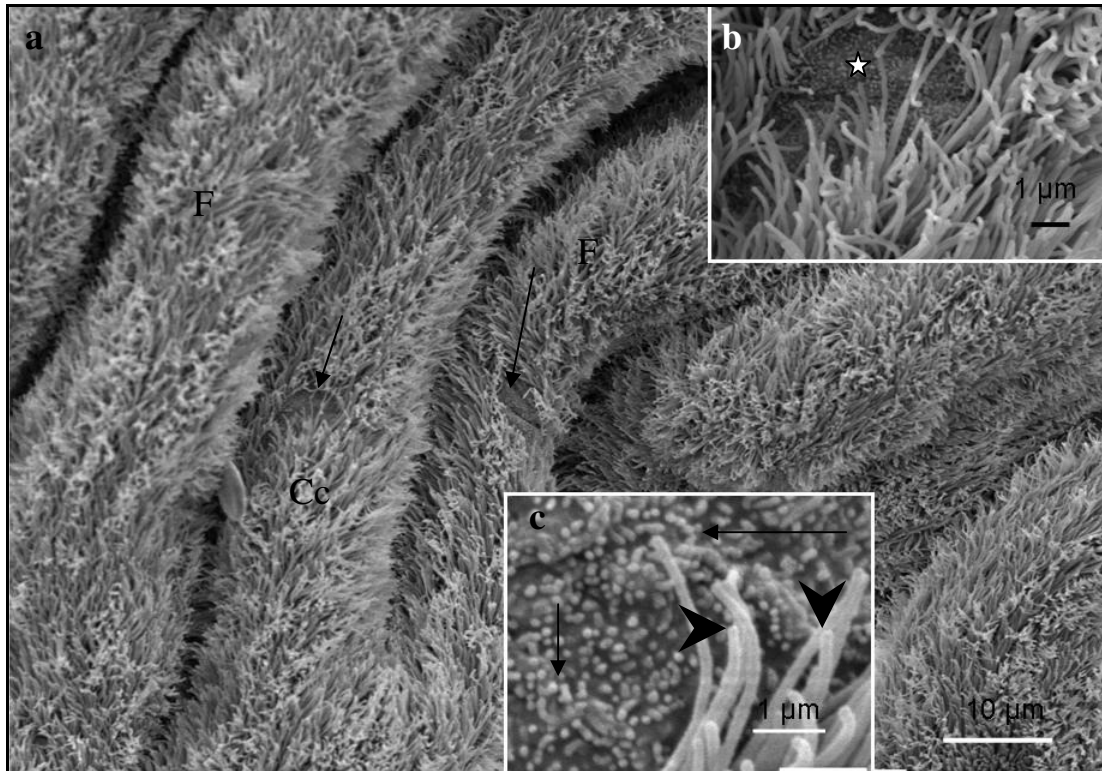


FIG. 3.25: Scanning electron photomicrographs of the mucosal surface in the magnum of a control bird. **a.** F: Mucosal folds. Cc: Ciliated cells. Arrows: Non-ciliated cells. **b.** A higher magnification photomicrograph showing a non-ciliated cell (asterisk) partially obscured by tufts of cilia. **c.** Apical surface of a non-ciliated cells with microvilli (arrows). Arrowheads: cilia.

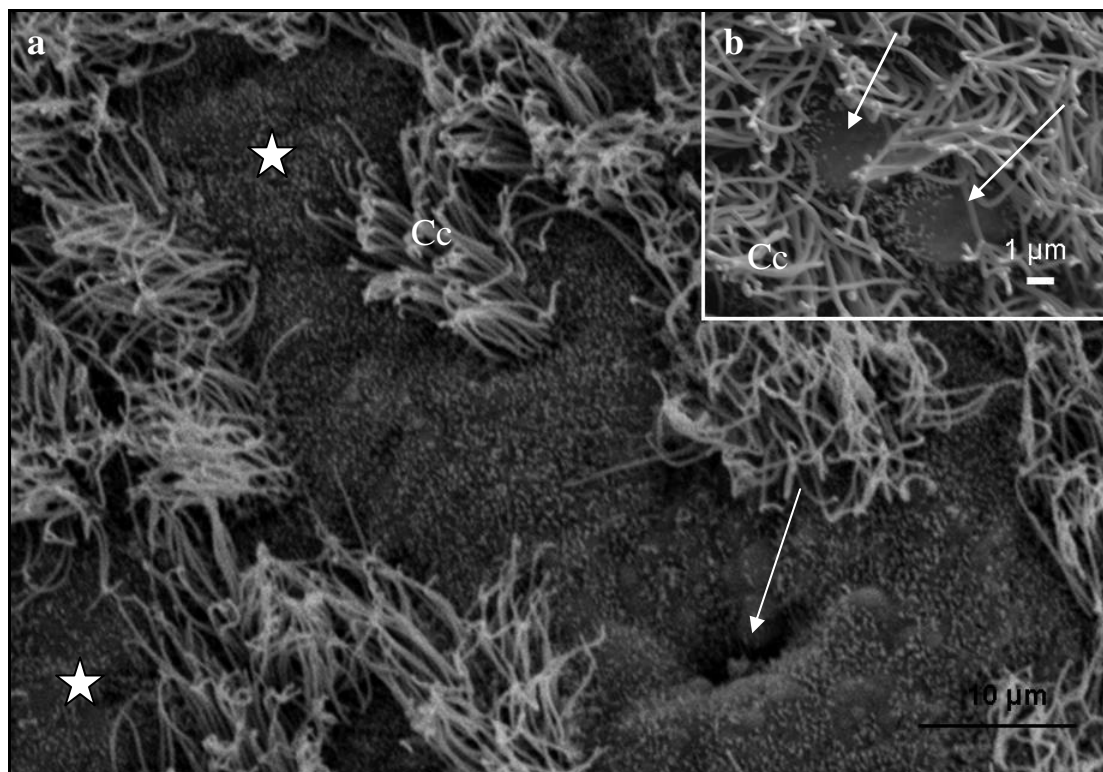


FIG. 3.26: **a.** A survey scanning electron photomicrograph of the mucosal surface of the magnum in a bird treated with 400 mg/kg bodyweight carbendazim. Asterisks: Areas of deciliation. Ciliated cells with intact cilia (Cc) are also observed. Arrow: glandular opening. **b.** A higher magnification photomicrograph showing degenerating non-ciliated cells (arrows). At this dose, the degenerating cells are lined by a few microvilli. Cc: ciliated cells.

3.3.5.1.iib Experiment II

5 and 24 hours post-exposure

No degenerative changes were observed on the mucosal surface of the magnum 5 and 24 hours post-exposure to carbendazim.

5 days post-exposure

Five days post-exposure to carbendazim, degenerating non-ciliated cells were lined by relatively few microvilli (Fig. 3.27a). In some instances degenerating non-ciliated cells were devoid of the microvilli (Fig. 3.27 a&b). Degenerating ciliated cells were

characterized by a loss of cilia. Short cilia stems were seen on the surface of the degenerating ciliated cells. In addition to deciliation, the presence of inflammatory cells was also identified.

8 days post-exposure

Eight days post-exposure to carbendazim, large areas of deciliation were observed (Fig. 3.28a). In these areas, short cilia, as well as, ciliary stems were observed (Fig. 3.28 b&c). In addition, shallow pits were observed in cases where a complete loss of cilia had occurred (Fig. 3.28d). Degenerating non-ciliated cells displayed relatively few microvilli (Fig. 3.28a). Swollen microvilli were occasionally seen on the surface of the degenerating non-ciliated cells (Fig. 3.28c).

12 days post-exposure

Twelve days post-exposure to carbendazim, deciliation was still a notable degenerative feature.. At this stage, numerous inflammatory cells were observed on the mucosal surface (Fig. 3.29). Degenerating non-ciliated cells were lined by a few microvilli.

32 days post-exposure

At day 32 post-exposure to carbendazim, discrete areas of cilia loss were distributed on the mucosal surface. At this stage inflammatory cells were not frequently encountered.

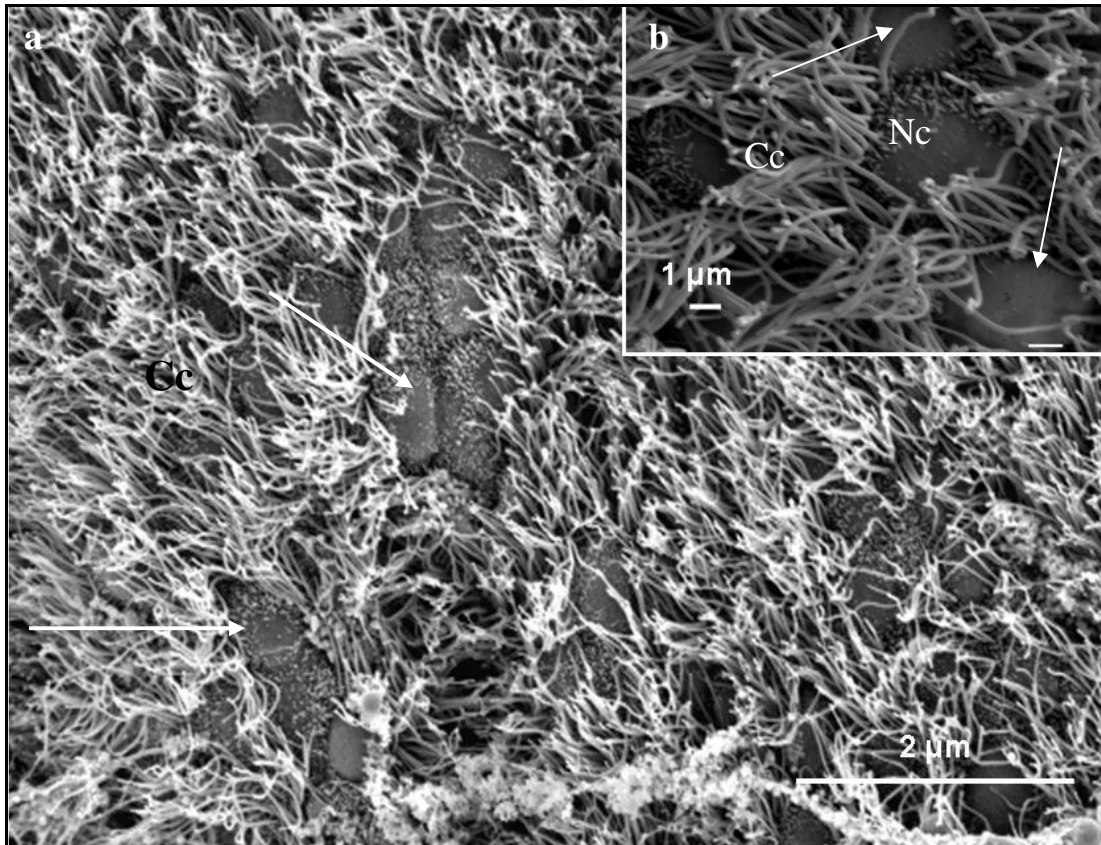


Fig. 3.27: **a.** A survey scanning electron photomicrograph of mucosal surface in the magnum, 5 days post exposure to 400 mg/kg bodyweight carbendazim. Arrows: Degenerating non-ciliated cells lined by relatively few microvilli. Cc: ciliated cells with intact cilia. **b.** A higher magnification photomicrograph of degenerating non-ciliated cells (Nc) and normal ciliated cells (Cc). Note a complete loss of microvilli in some cells (arrows).

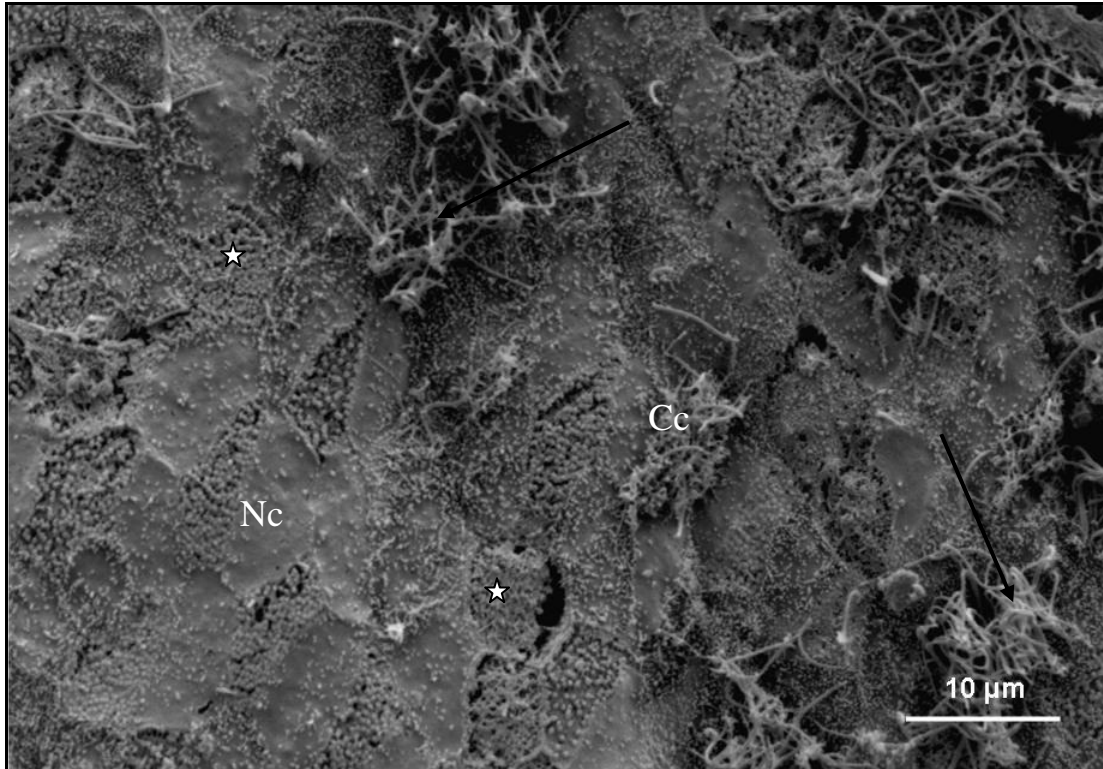


FIG. 3.28a: A survey scanning electron photomicrograph of the mucosal surface in the magnum, 8 days post-exposure to 400 mg/kg bodyweight carbendazim. Asterisks: Areas of deciliation. A few ciliated cells (Cc) are lined by short cilia. Ciliated cells with intact cilia (arrows) are also observed. Non-ciliated cells (Nc) exhibit relatively few microvilli.

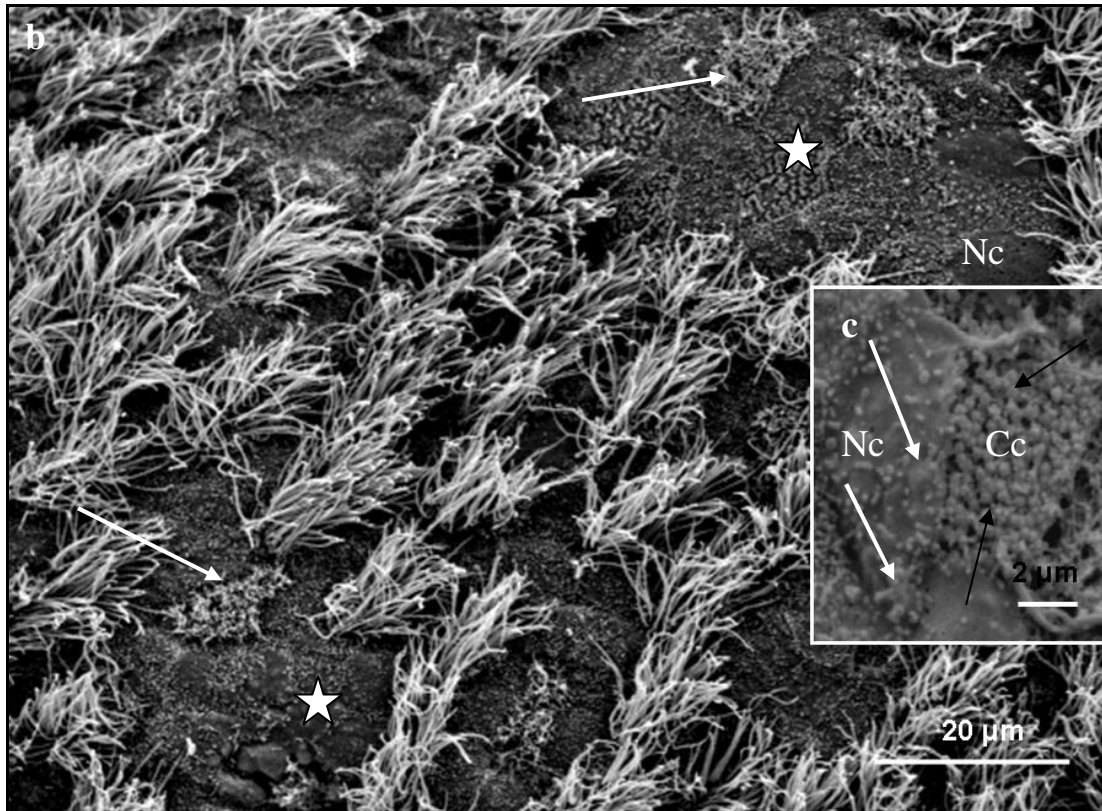


FIG. 3.28b: Scanning electron photomicrograph of the mucosal surface of the magnum, 8 days post-exposure to 400 mg/kg bodyweight carbendazim. Arrows: Short cilia. Asterisks: Areas of deciliation. Note that at this stage, the majority of degenerating non-ciliated cells (Nc) are devoid of microvilli. **c.** Apical surface of degenerating ciliated (Cc) and non-ciliated (Nc) cells. Black arrows: Ciliary stems. White arrows: Swollen microvilli.

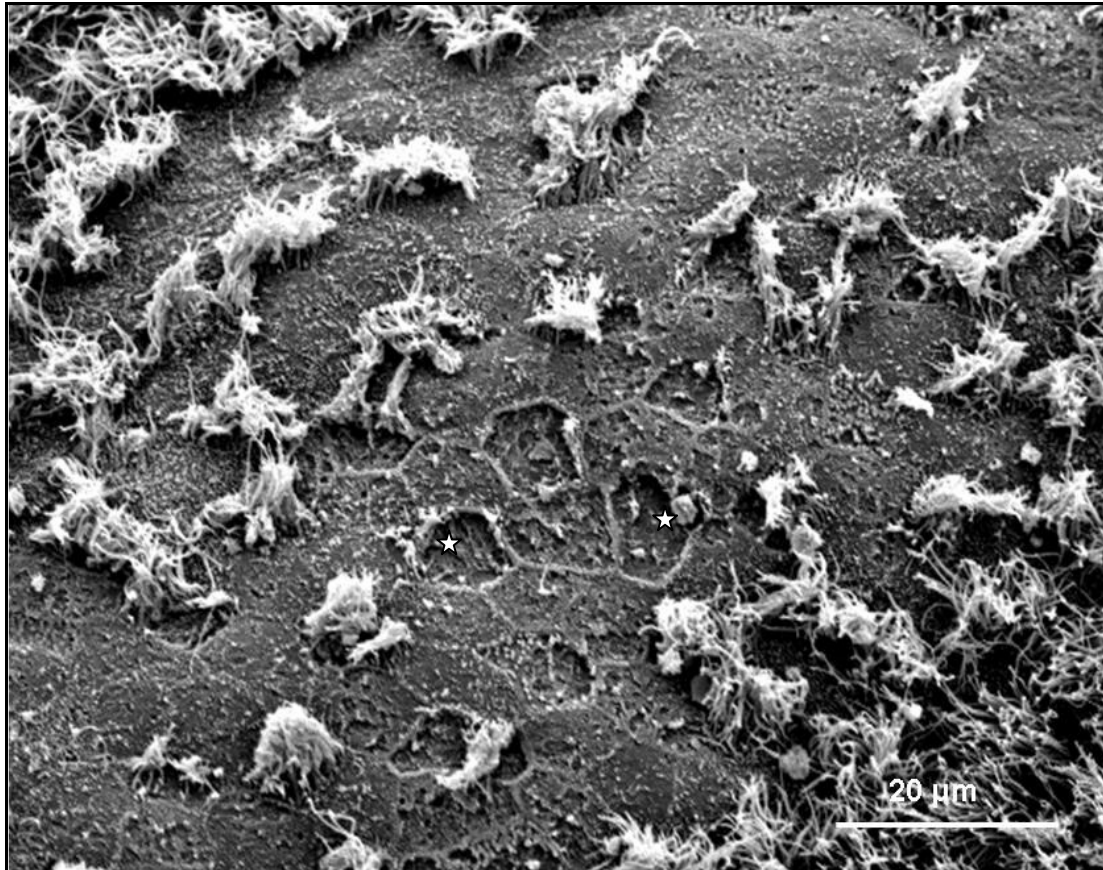


FIG. 3.28d: Scanning electron photomicrograph of the mucosal surface in the magnum, 8 days post-exposure to 400 mg/kg bodyweight carbendazim. Asterisks: Shallow pits due to a loss of cilia.

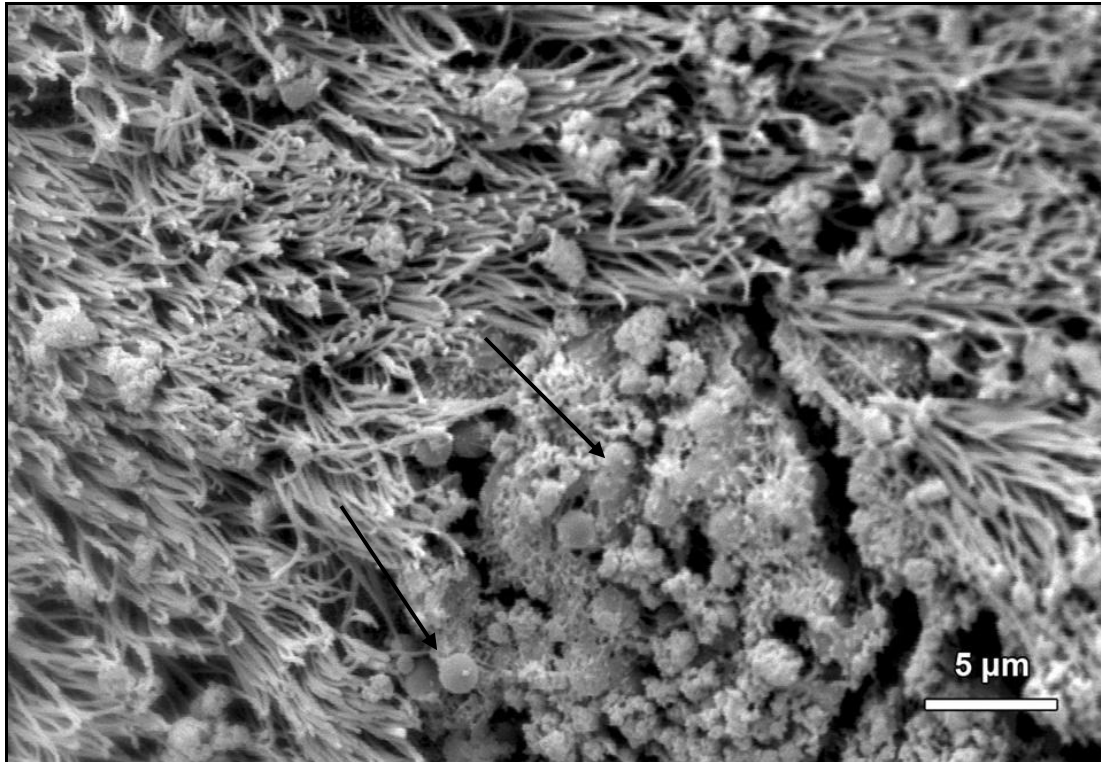


FIG. 3.29: Scanning electron photomicrograph of the mucosal surface of the magnum, 12 days post-exposure to 400 mg/kg bodyweight carbendazim. Arrows: Aggregates of inflammatory cells.

3.3.5.2 Transmission electron microscopy

3.3.5.2.i Control birds

A simple columnar epithelium, composed of ciliated and non-ciliated cells, lined the magnum (Fig. 3.30a).

Ciliated cells

The ciliated cells contained electron lucent cytoplasm. A round to oval nucleus was located in the central cytoplasmic region of the cell. Several cytoplasmic organelles, which included cisternae of RER and mitochondria were observed adjacent to the nucleus (Fig. 3.30b). Golgi complexes and lysosomes were identified in the supranuclear region (Fig. 3.30c). A few filaments were observed perinuclearly (Fig.

3.30d). The apical plasma membranes of ciliated cells exhibited long cilia (Fig. 3.31a). A few microvilli were observed between the cilia (Fig. 3.31a). The cilia were rooted in the cytoplasm and anchored by basal bodies. Supporting the basal bodies were basal feet and striated rootlets (Fig. 3.31a).

Non-ciliated cells

The non-ciliated cells contained basally located round to irregular-shaped nuclei (Fig. 3.30a). In these cells, the cytoplasm was electron dense due to presence of numerous particles. Numerous membrane-bound secretory granules were observed in the central and apical cytoplasmic regions (Fig. 3.32a). The secretory granules contained particles of intermediate electron density. Cisternae of RER and mitochondria were observed infranuclearly (Fig. 3.32b). The apical plasma membrane was lined by microvilli (Fig. 3.32a).

Plasma membrane and basal lamina

Cellular junctions linked the lateral plasma membranes of adjacent epithelial cells (Fig. 3.32c). The luminal epithelial cells rested on a granular basal lamina of approximately 78 nm in thickness. The basal lamina contained laminae lucida and densa (Fig. 3.31b).

Tubular glands

Simple and branched tubular glands were observed in the *lamina propria-submucosa*. The gland cells contained basally located round, euchromatic nuclei (Fig. 3.33a). The cytoplasm contained numerous cisternae of RER and free ribosomes (Fig. 3.33b). In addition, small to medium-sized secretory granules were observed in the apical cytoplasmic regions. Two types of secretory granules were identified: type A and type B. Type A secretory granules contained electron dense particles. Type B granules were larger than type A and contained particles of an intermediate electron density. The gland cells contained a few mitochondria which were located perinuclearly.

Long, slender microvilli lined the apical plasma membranes (Fig. 3.34a). Cellular junctions (desmosomes and occasional tight junctions) were observed along the lateral plasma membranes (Fig. 3.34b). Underlying the magal glands was a basal lamina of approximately 34 nm in thickness, which blended with the loose connective tissue of the *lamina propria-submucosa* (Fig. 3.34c). The basal lamina contained homogeneous particles of intermediate electron density.

Associated with the tubular glands were supporting cells, which contained elongated euchromatic nuclei surrounded by scanty cytoplasm of intermediate electron density (Fig. 3.35a). Several cisternae of RER and a few mitochondria were observed in the cytoplasm (Fig. 3.35b).

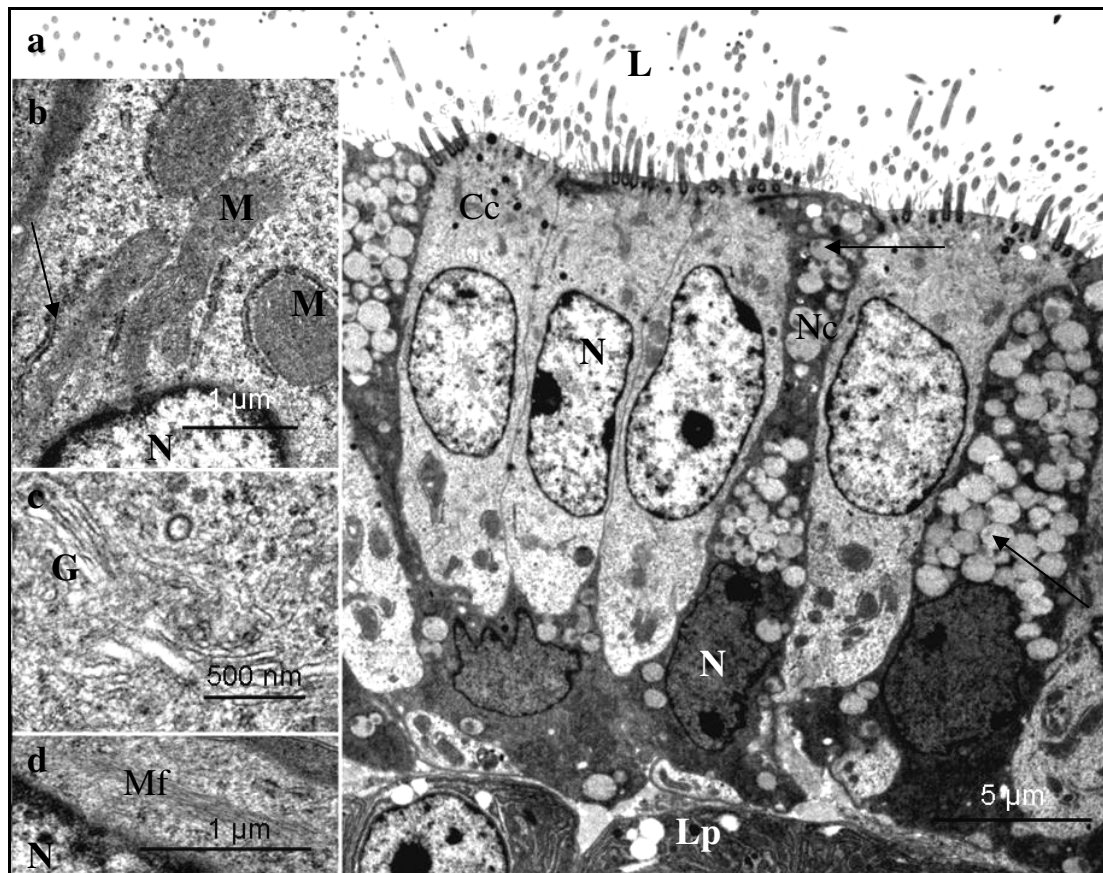


FIG. 3.30: **a.** A survey electron photomicrograph of the luminal epithelium in the magnum of a control bird. Cc: Ciliated cells. Nc: Non-ciliated cells. N: Nucleus. Numerous membrane-bound secretory granules (arrows) are seen in the cytoplasm of non-ciliated cells. Note the presence of electron lucent cytoplasm in the ciliated cells as compared to electron dense of the non-ciliated cells. L: lumen; Lp: *lamina propria-submucosa*. **b.** A higher magnification electron photomicrograph of the cytoplasm in a ciliated cell. M: Mitochondria. Arrow: RER. N: Nucleus. **c.** Supranuclear region of a ciliated cell with a Golgi complex (G). **d.** Microfilaments (Mf) in the perinuclear area of a ciliated cell. N: nucleus.

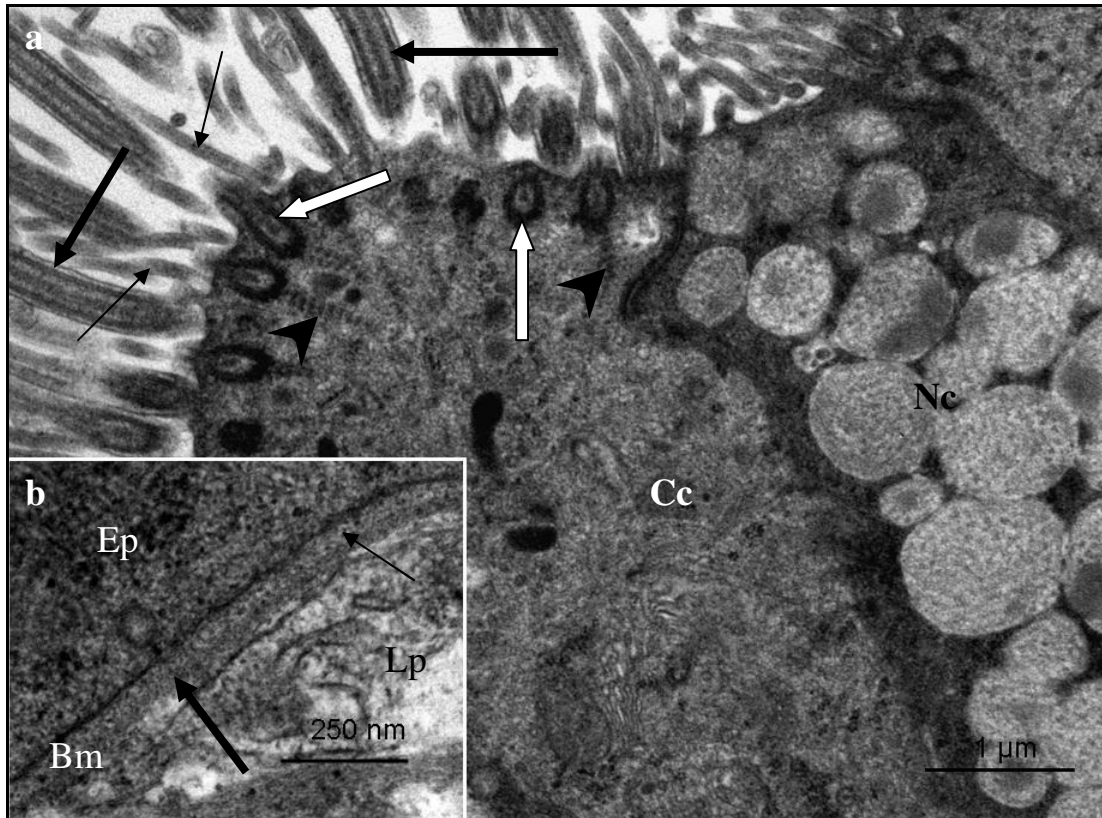


FIG. 3.31: **a.** Electron photomicrograph of the apical region of a ciliated cell (Cc) in the magnum of a control bird. Thick arrows: Cilia. Thin arrows: Microvilli. White arrows: Basal bodies. Arrowheads: Striated rootlets. Nc: non-ciliated cell. **b.** Electron photomicrograph of the basal lamina (Bm) from a control bird. Thin arrow: Lamina lucida. Thick arrow: Lamina densa. Lp: *lamina propria-submucosa*; Ep: epithelial cell.

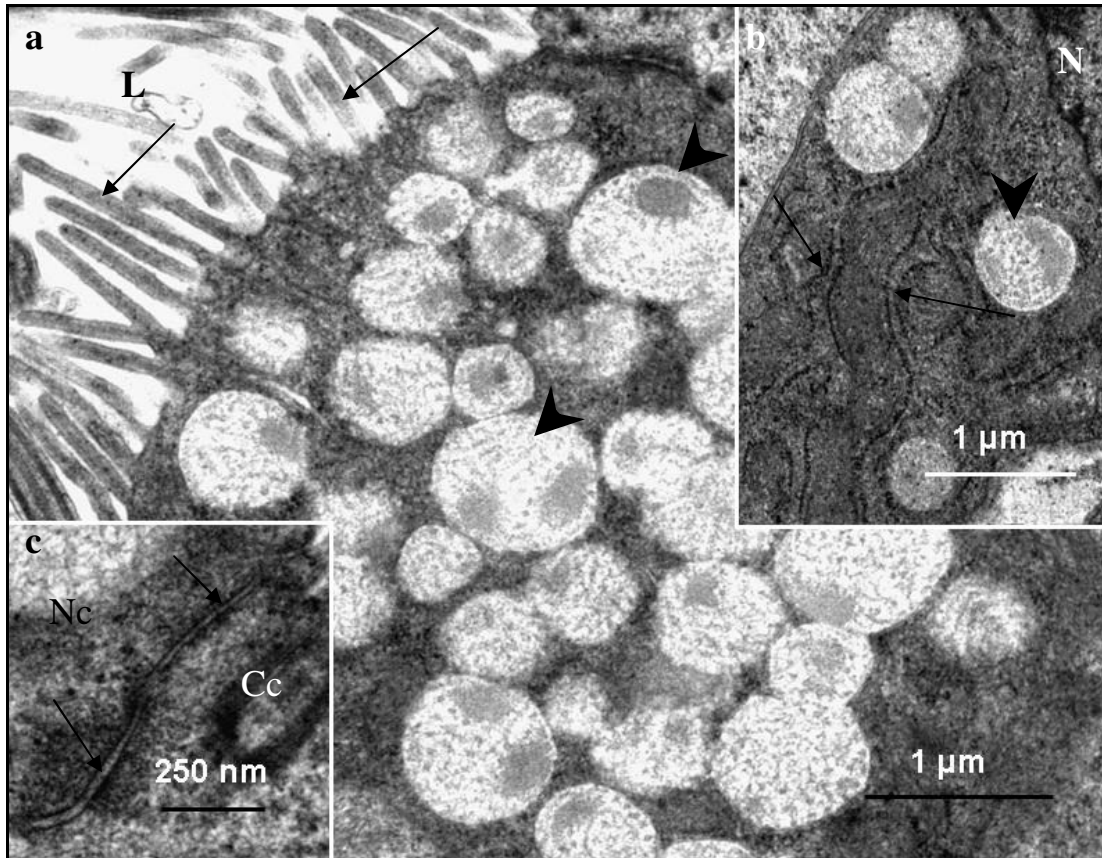


FIG. 3.32: **a.** Electron photomicrograph of the apical region of a non-ciliated cell in the magnum of the control bird. Arrowheads: Secretory granules. Arrows: Microvilli. L: lumen. **b.** Electron photomicrograph of the basal region of a non-ciliated cell. Arrows: RER. N: Nucleus. Arrowhead: secretory granule. **c.** Electron photomicrograph showing desmosomes (arrows) linking adjacent ciliated (Cc) and non-ciliated (Nc) cells.

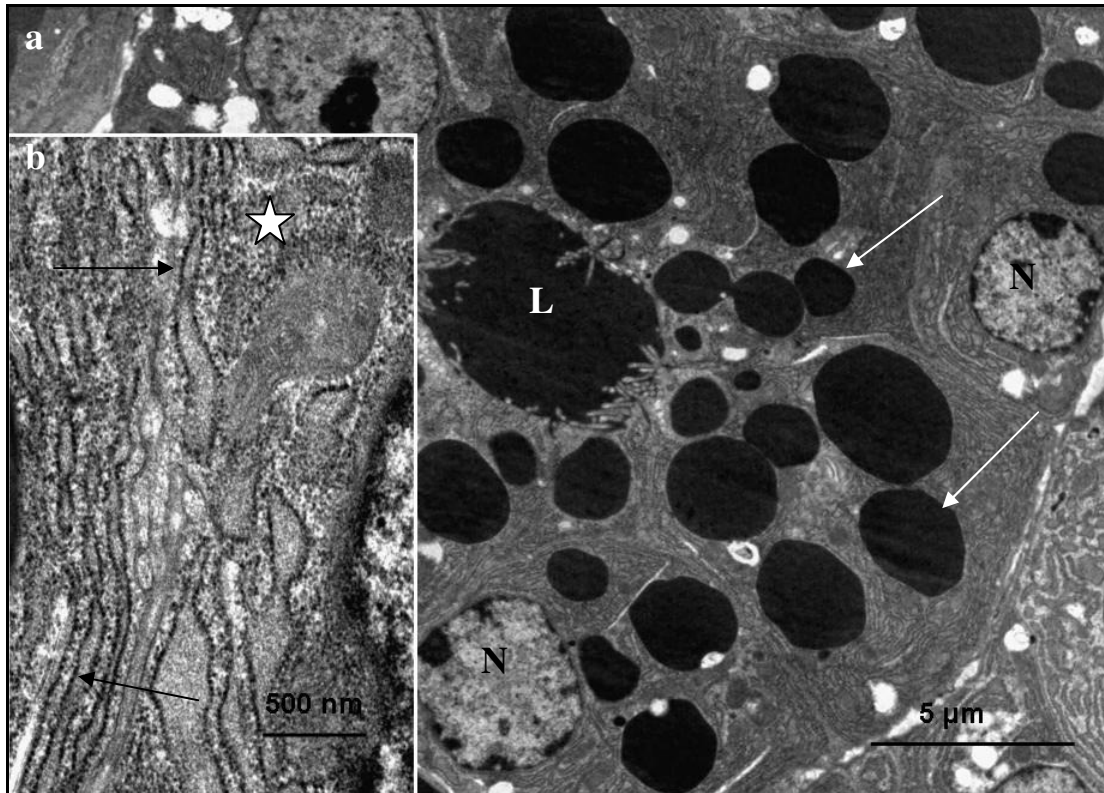


FIG. 3.33: **a.** A survey electron photomicrograph of a tubular gland in the magnum of a control bird. N: Nucleus. Numerous type A secretory granules (arrows) are observed in the cytoplasm. L: glandular lumen. **b.** Electron photomicrograph of RER cisternae (arrows) and free ribosomes (asterisk).

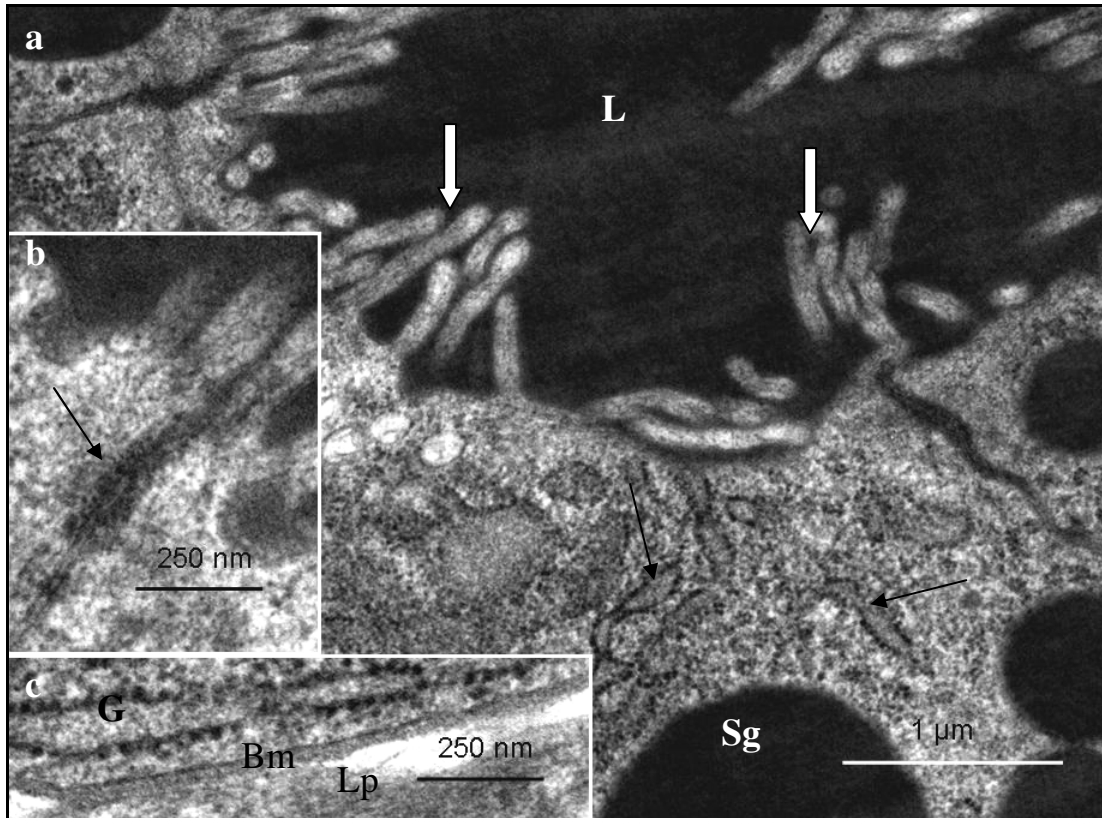


FIG. 3.34: **a.** Electron photomicrograph of the apical region of a tubular gland in the magnum of a control bird. Open arrows: Microvilli. Note the presence of numerous RER cisternae (arrows) in the cytoplasm. Sg: secretory granule. L: glandular lumen. **b.** Electron photomicrograph of a tight junction (arrow). **c.** Basal region of a gland cell (G). Bm: Basal lamina. Lp: *lamina propria-submucosa*.

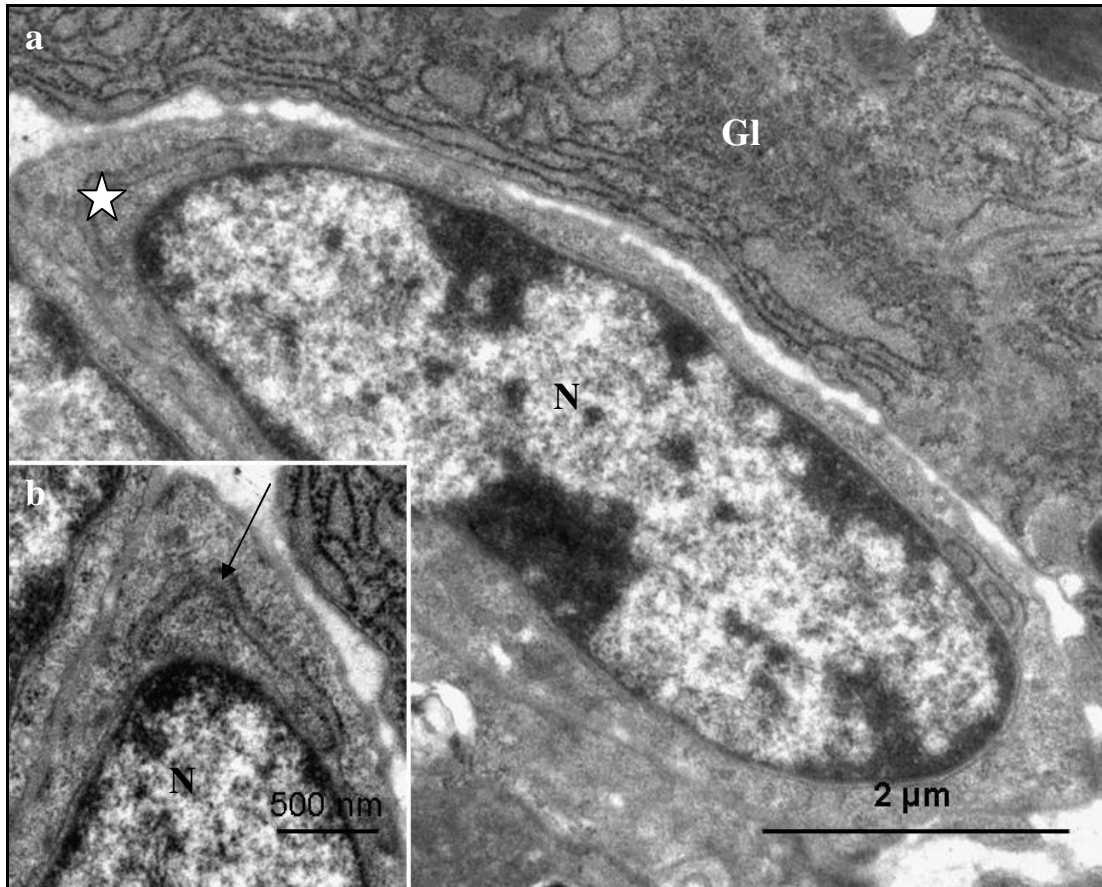


FIG. 3.35: **a.** Electron photomicrograph of a supporting cell in the *lamina propria-submucosa* of a control bird. N: Nucleus. Asterisk: Cytoplasm. GI: Gland cell. **b.** A higher magnification electron photomicrograph of a supporting cell. Arrow: RER. N: Nucleus.

3.3.5.2.ii Carbendazim treated birds

3.3.5.2.ii.a. *Experiment I*

25 and 100 mg/kg bodyweight carbendazim

At the electron microscopic level, carbendazim did not cause morphological changes at doses of 25 mg/kg and 100 mg/kg bodyweight carbendazim. Degenerative changes were observed at doses of 400 mg/kg and 800 mg/kg bodyweight carbendazim. When compared to the 400 mg/kg bodyweight carbendazim group, degenerative changes observed at 800 mg/kg group appeared more severe. The

observed ultrastructural changes in both the luminal and glandular epithelia are detailed below.

400 mg/kg bodyweight carbendazim

Ciliated cells

At a dose of 400 mg/kg bodyweight carbendazim, degenerating ciliated cells contained pyknotic nuclei. Blebbing of the nuclear membrane was also a notable feature. In a few ciliated cells, nuclei exhibiting marginalized chromatin and crenated margins were observed (Fig. 3.36a). At this dose, the ciliated cells were lined by relatively few cilia. Several lysosomes and vacuolated mitochondria were observed in the apical cytoplasmic regions (Fig. 3.36b). Although basal bodies were intact, the rootlets supporting them were indistinct (Fig. 3.36b).

Non-ciliated cells

Degenerating non-ciliated cells were lined by a few microvilli (Fig. 3.37a). In addition, vacuoles and myelin figures were occasionally observed. In these cells swollen mitochondria were also identified.

Plasma membrane and basal lamina

Cellular junctions linking adjacent cells were intact (Fig. 3.37b). No degenerative changes were seen in the basal lamina. The basal lamina was approximately 83 nm in thickness.

Tubular glands

Degenerating glands were characterized by the presence of several vacuoles and swollen mitochondria (Fig. 3.38 a&b). Cellular junctions along the lateral plasma membranes were intact. The basal lamina, which measured approximately 36 nm in thickness appeared normal. At this dose, supporting cells contained electron dense cytoplasm (Fig. 3.39a). A few vacuoles and degenerating mitochondria were also

identified. Degenerating mitochondria were electron dense with dilated cristae (Fig. 3.39b).

800 mg/kg bodyweight carbendazim

Ciliated cells

At a dose of 800 mg/kg bodyweight carbendazim, deciliation and nuclear degeneration were observed in ciliated cells (Fig. 3.40a). The observed nuclear degeneration included: pyknosis, margination of nuclear chromatin and blebbing of the nuclear membrane. Although basal bodies appeared intact, rootlets striations were indistinct (Fig. 3.40b). Swollen mitochondria, vacuoles and dilated RER cisternae were observed in the apical cytoplasmic region (Fig. 3.41). A few lysosomes were also identified in this region.

Non-ciliated cells

Degenerating non-ciliated cells contained pyknotic nuclei and numerous vacuoles. At this dose (800 mg/kg), the non-ciliated cells contained a few secretory granules, which were concentrated in the apical regions of the cell. The degenerating secretory granules contained fragmented particles of an intermediate electron density (Fig. 3.42a).

Plasma membrane and basal lamina

Cellular junctions which were observed along the lateral plasma membrane, appeared intact (Fig. 3.42b). The epithelial cells rested on a basal lamina, which was approximately 70 nm thick. The structure of the basal lamina was similar to that observed in 400 mg/kg bodyweight carbendazim-treated group.

Tubular glands

Vacuolation and pyknosis were observed in degenerating gland cells (Fig. 3.43a). In addition, swollen mitochondria were also observed in these cells (Fig. 3.43b). Dilated

RER cisternae and myelin figures were observed in the perinuclear region of degenerating gland cells (Fig. 3.43c). In some instances, degenerating secretory granules were observed. The degenerating secretory granules displayed condensed, peripherally located electron dense particles (Fig. 3.43d). In addition, degeneration of the limiting membrane was observed. Relatively few microvilli lined the apical plasma membranes of the gland cells. These microvilli appeared thick when compared to the control group (Fig. 3.44a). Cellular junctions along the lateral plasma membranes were structurally normal (Fig. 3.44a). Invaginations of the basal lamina lining the glandular cells were occasionally observed (Fig. 3.44b). At this dose the basal lamina measured approximately 43 nm in thickness. Supporting cells contained crenated nuclei (Fig. 3.45a). In a few cells, blebbing of the nuclear membrane was observed (Fig. 3.45c). Swollen mitochondria and dilated RER cisternae were observed throughout the cytoplasm (Fig. 3.45b). A few lysosomes and vacuoles were occasionally identified.

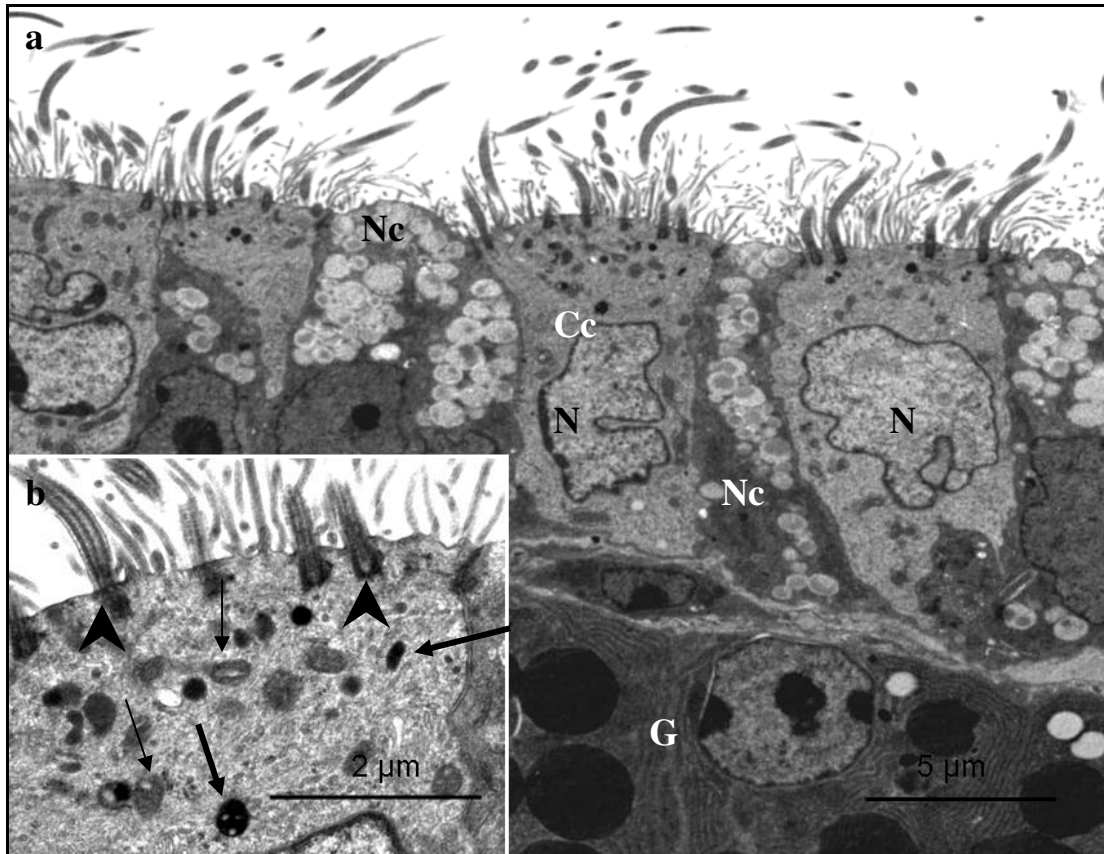


FIG. 3.36: **a.** A survey electron photomicrograph of the luminal epithelium in the magnum of a bird treated with 400 mg/kg bodyweight carbendazim. N: Crenated nuclei with condensation and margination of nuclear chromatin. Cc: Ciliated cells. Nc: non-ciliated cells. G: tubular glands. **b.** Electron photomicrograph of the apical region. Thick arrows: Lysosomes. Thin arrows: Vacuolated mitochondria. Arrowheads: Basal bodies.

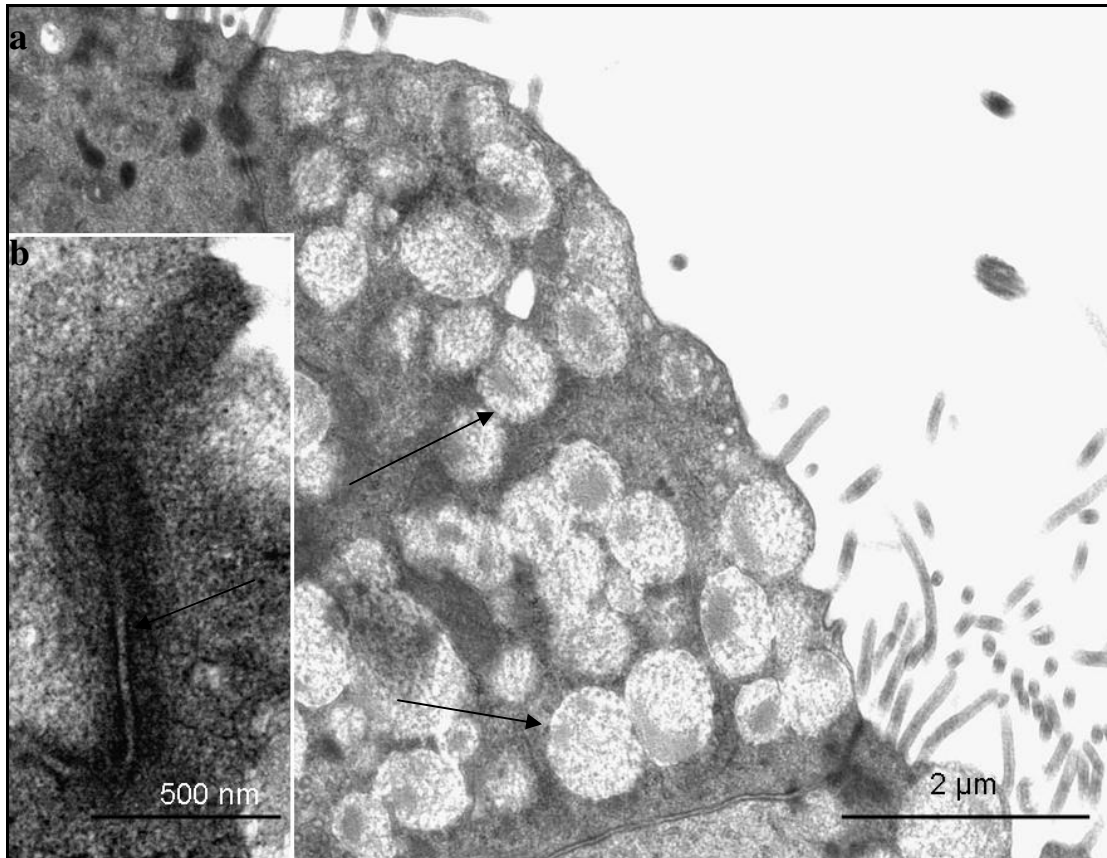


FIG. 3.37: **a.** Electron photomicrograph of the apical region of a non-ciliated cell in the magnum of a bird treated with 400 mg/kg bodyweight carbendazim. Note the scarcity of microvilli lining the apical plasma membrane. Arrows: Secretory granules. **b.** An electron photomicrograph of a desmosome (arrow).

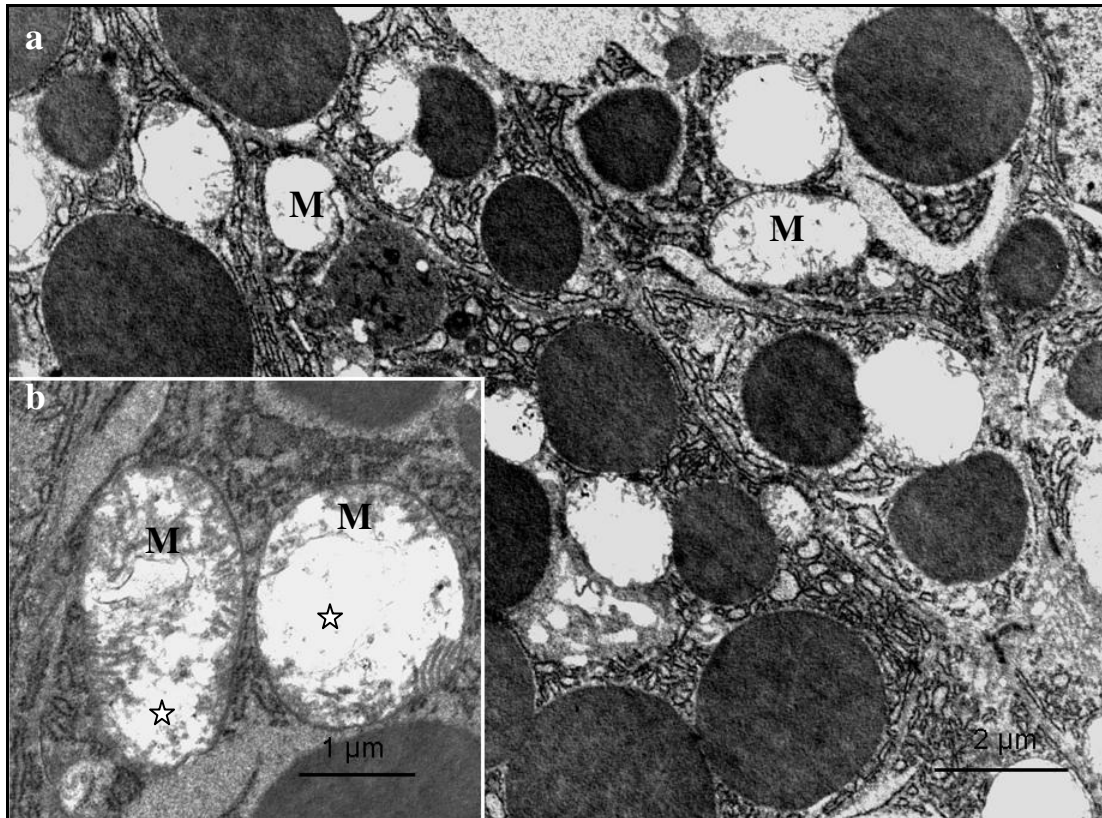


FIG. 3.38: **a.** A survey electron photomicrograph of the glandular tissue in the magnum of a bird treated with 400 mg/kg bodyweight carbendazim. M: Swollen mitochondria. **b.** A higher magnification electron photomicrograph of degenerating mitochondria (M). Note the loss of cristae (asterisks) in these mitochondria.



FIG. 3.39: **a.** Electron photomicrograph of a supporting cell in the *lamina propria-submucosa* of a bird treated with 400 mg/kg bodyweight carbendazim. Electron dense cytoplasm surrounds the nucleus (N). V: Vacuoles. M: Degenerating mitochondria. Thin arrow: lysosome; Thick arrow: cisterns of RER. Gl: tubular glands. **b.** An electron photomicrograph of degenerating mitochondria with dilated cristae (thin arrows). Asterisk: Electron dense granules. N: nucleus. Thick arrow: Lysosome.

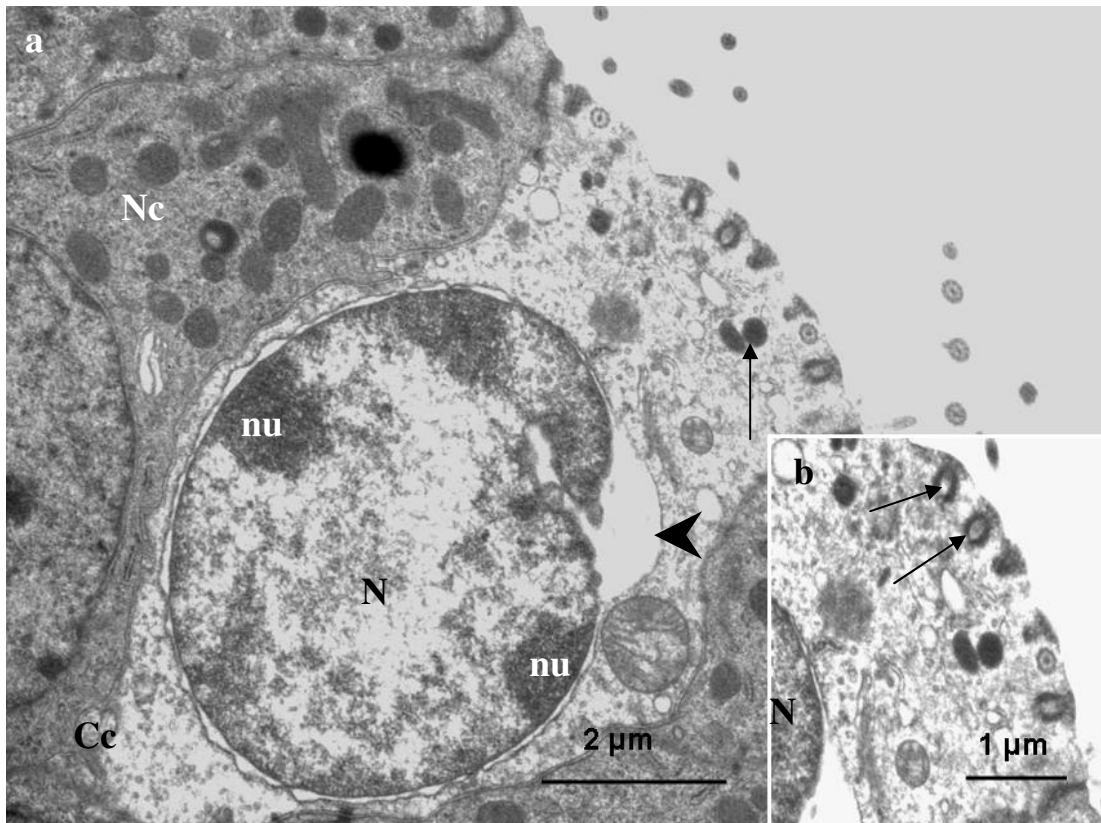


FIG. 3.40: **a.** Electron photomicrograph of the apical region of luminal epithelial cells in the magnum of a bird treated with 800 mg/kg bodyweight carbendazim. Loss of cilia is evident along the apical plasma membrane of the ciliated cell (Cc) shown. Arrowhead: Nuclear membrane blebbing. Nu: Nucleolar margination. N: Nucleus. Arrow: lysosomes; Nc: non-ciliated cell. **b.** A higher magnification electron photomicrograph of the apical region of a degenerating ciliated cell. Basal bodies (arrows) are intact. Note that the basal feet, as well as rootlets supporting the basal bodies are indistinct. N: nucleus.

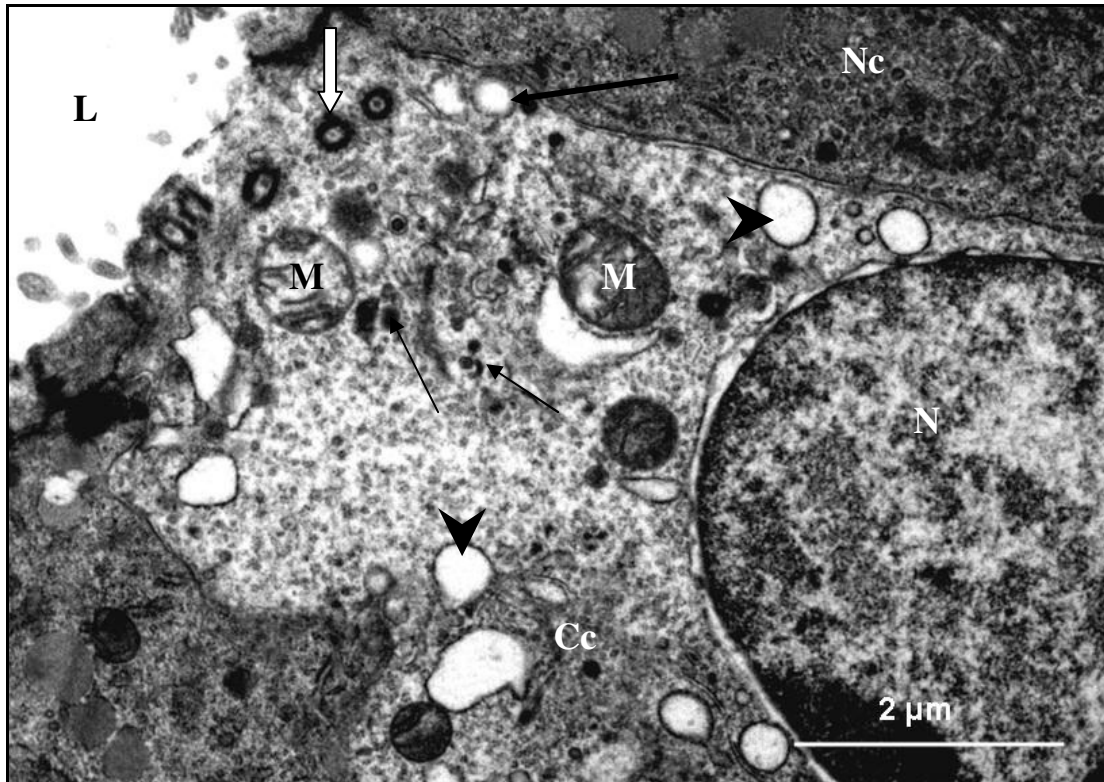


FIG. 3.41: Electron photomicrograph of the apical cytoplasmic region of degenerating ciliated cell (Cc) in the magnum of a bird treated with 800 mg/kg bodyweight carbendazim. M: Swollen mitochondria (M). Arrowheads: Dilated RER cisternae. Thin arrows: Lysosomes. Open arrow: basal body; N: nucleus; Nc: non-ciliated cell; L: lumen.

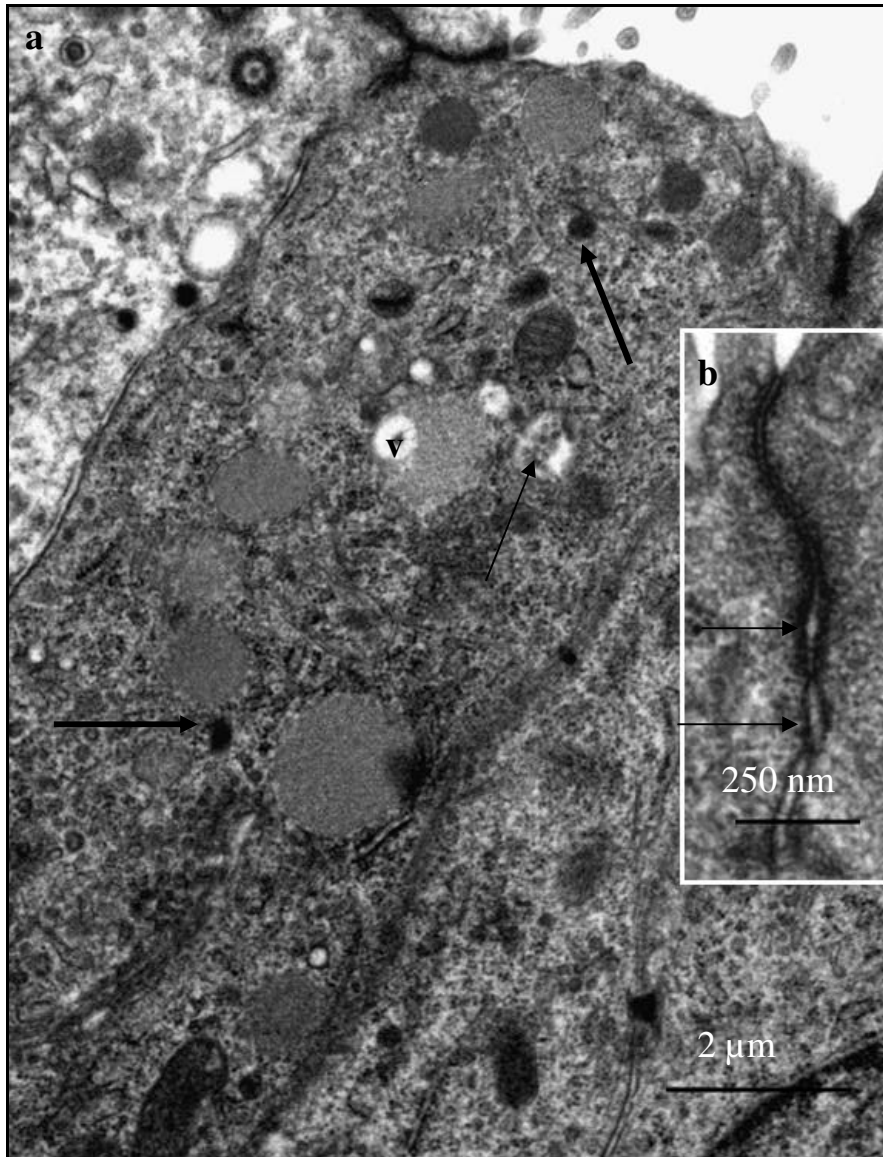


FIG. 3.42: **a.** Electron photomicrograph of a degenerating non-ciliated cell in the magnum of a bird treated with 800 mg/kg bodyweight carbendazim. Thin arrow: Degenerating secretory granule. V: vacuole. Thick arrows: lysosomes. **b.** An electron photomicrograph of desmosomes (arrows).

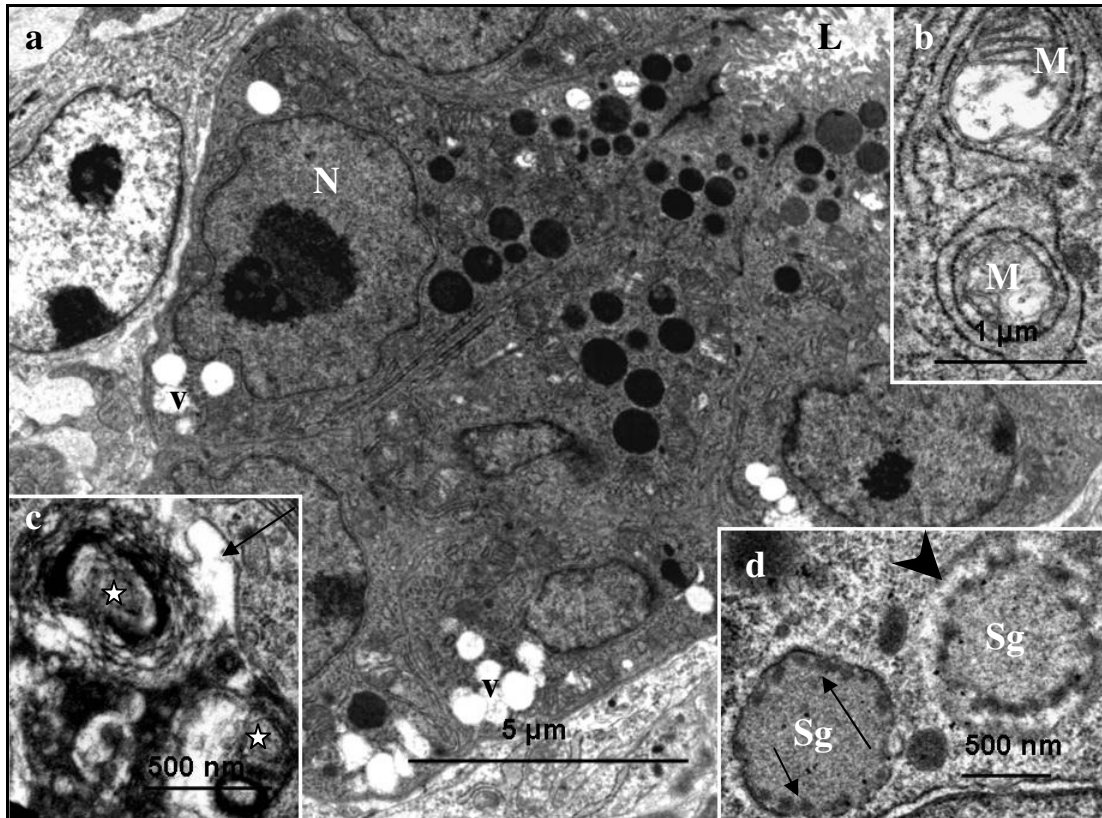


FIG. 3.43: **a.** A survey electron photomicrograph of a tubular gland in the magnum of a bird treated with 800 mg/kg bodyweight carbendazim. V: Vacuoles. L: glandular lumen. N: nucleus. **b.** Electron photomicrograph showing swollen mitochondria (M) in degenerating gland cells. **c.** A photomicrograph of myelin figures (asterisks) and dilated cisternae of RER (arrow). **d.** Electron photomicrograph of degenerating secretory granules (Sg). Note the deposition of electron dense granules (arrows) in the peripheral zone. Discontinuation of the limiting membrane (arrowhead) is also seen.

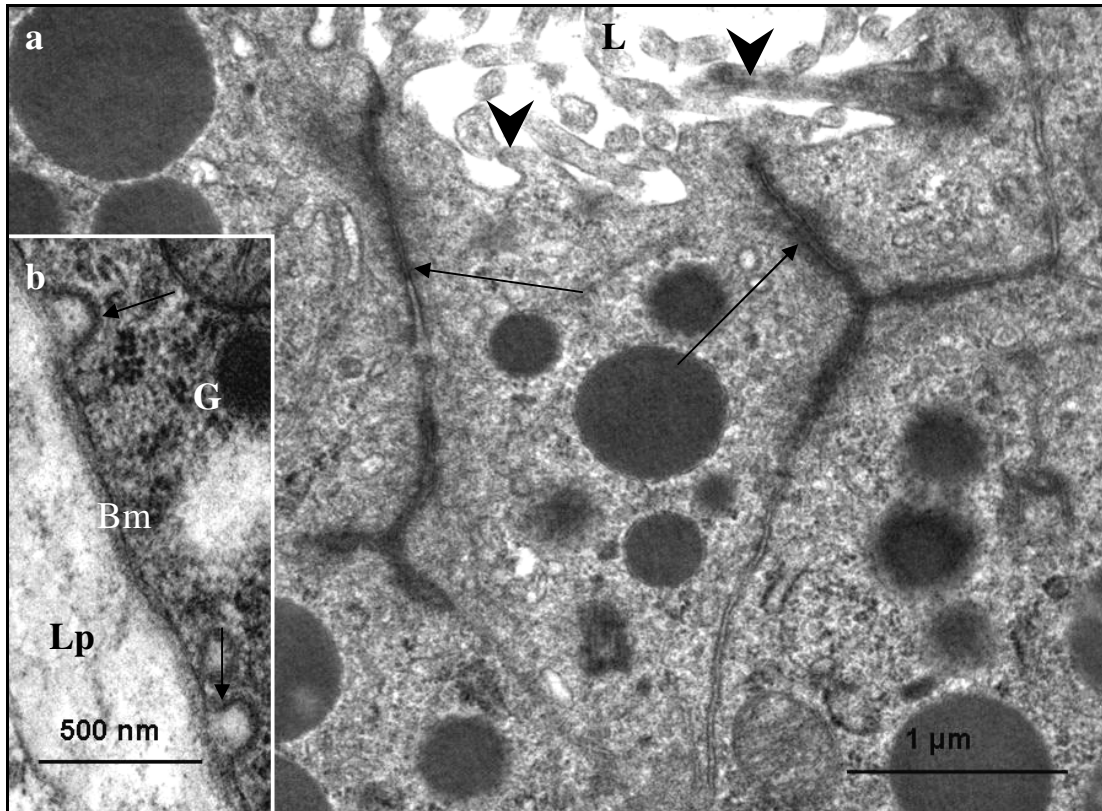


FIG. 3.44: **a.** Electron photomicrograph of the apical region of a gland cell in the magnum of a bird treated with 800 mg/kg bodyweight carbendazim. Arrowheads: Microvilli. Arrows: Intact cellular junctions. L: glandular lumen. **b.** Electron photomicrograph of the basal region of a gland cell. Infolding (arrows) of the basal lamina (Bm) is observed. Lp: *lamina propria-submucosa*. G: gland cell.

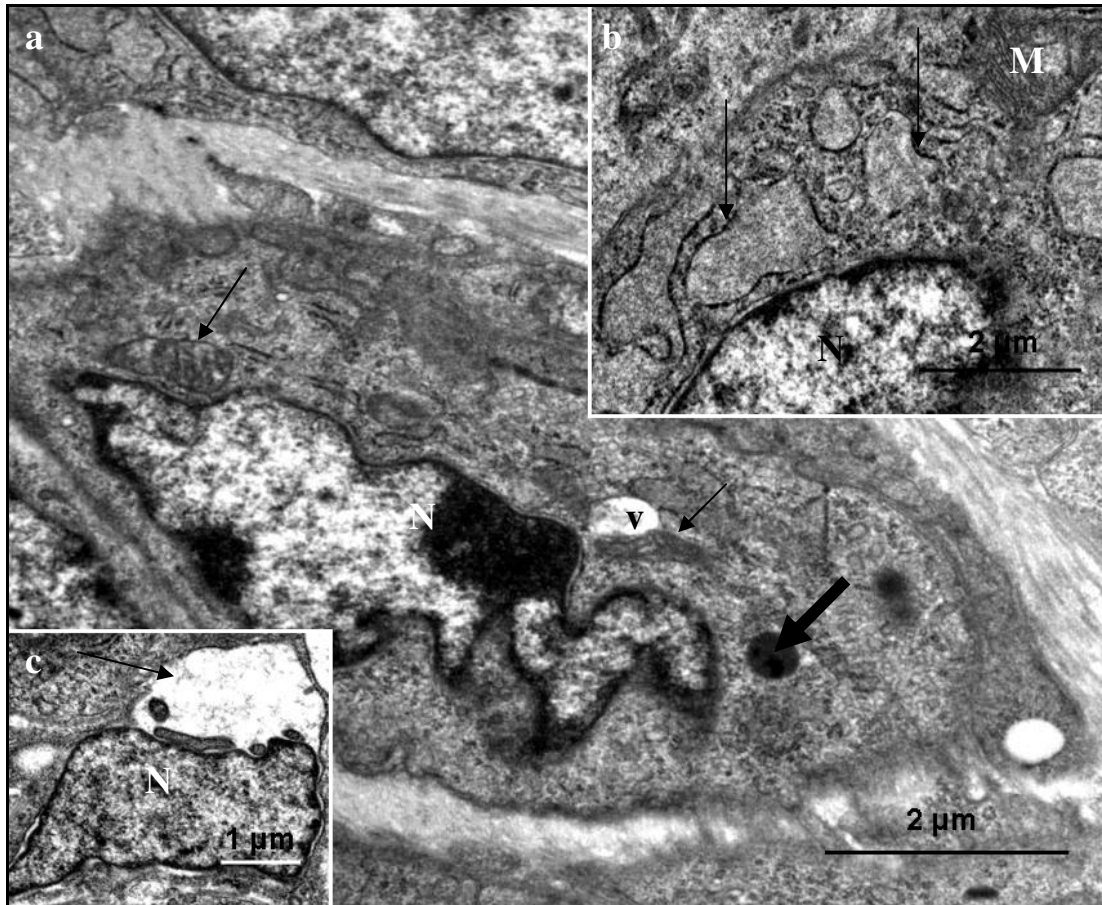


FIG. 3.45: **a.** Electron photomicrograph of a supporting cell in the *lamina propria-submucosa* of a bird treated with 800 mg/kg bodyweight carbendazim. N: Crenated nucleus. Thin arrows: Degenerating mitochondria. v: vacuole; Thick arrow: lysosome. **b.** Photomicrograph of a degenerating supporting cell. Arrows: Dilated RER cisternae. N: nucleus; M: mitochondrion. **c.** An electron photomicrograph of a degenerating nucleus (N) in a supporting cell. Arrow: Nuclear membrane blebbing.

3.3.5.2.iib Experiment II

5 hours post-exposure

Similar to the observation made in the infundibulum (Chapter Two), ultrastructural changes in the magnum appeared 5 hours post-exposure to 400 mg/kg bodyweight carbendazim. At this stage, a few pyknotic nuclei were observed in both the ciliated and non-ciliated cells (Fig. 3.46a).

Ciliated cells

In the ciliated cells, numerous lysosomes were observed in the apical and central cytoplasmic regions (Fig. 3.46a&b).

Non-ciliated cells

The degenerating non-ciliated cells were slender and contained an electron dense cytoplasm (Fig. 3.46a). A few lysosomes were also present in the degenerating non-ciliated cells. The apical plasma membrane did not exhibit ultrastructural changes.

Plasma membrane and basal lamina

Cellular junctions along the lateral plasma membranes were intact. The basal lamina underlying the epithelial cells was structurally normal. The lamina measured approximately 72 nm in thickness. Both lamina lucida and lamina densa were visible (Fig. 3.46c).

Tubular glands

In the *lamina propria*, a few glands contained vacuolated cells and swollen mitochondria (Fig. 3.47a). The cristae of the swollen mitochondria occasionally formed coiled structures (Fig. 3.47b). Dilated cisternae of RER were observed in the degenerating gland cells (Fig. 3.47c). Secretory granules and cellular junctions were intact. The basal lamina (approximately 49 nm thick) lining the magnum glands appeared structurally normal. No degenerative changes were observed in supporting cells.

24 hours post-exposure

Ciliated and non-ciliated cells

Twenty-four hours post-exposure to carbendazim, pyknotic nuclei and swollen mitochondria were the predominant ultrastructural changes observed in the epithelial cells. No structural changes were observed in the basal lamina.

Tubular glands

A few swollen mitochondria and dilated cisternae of RER were observed in the gland cells. Supporting cells were structurally normal.

5 days post-exposure

Ciliated cells

Five days post-exposure to carbendazim degenerating ciliated cells displayed relatively few cilia (Fig. 3.48). The cilia were supported by intact basal bodies. However, striated rootlets anchoring the basal bodies were indistinct. In degenerating ciliated cells, aggregations of lysosomes were observed supranuclearly, as well as in the apical cytoplasmic regions (Fig. 3.48). In a few cells, the cytoplasm appeared electron dense. In the apical cytoplasmic regions of these cells, multi-vesicular bodies, vacuoles and vacuolated mitochondria were observed (Fig. 3.49a&b).

Non-ciliated cells

Degenerating non-ciliated cells contained pyknotic nuclei, surrounded by either electron dense or electron lucent cytoplasm (Fig. 3.50a). Aggregates of degenerating secretory granules were observed supranuclearly. At this stage, the degenerating secretory granules were small laden with electron dense particles (Fig. 3.50b). In a few instances, the apical regions of the degenerating non-ciliated cells protruded into the lumen.

Plasma membrane and basal lamina

Cellular junctions appeared intact. In a few cells, separations of the lateral plasma membranes were occasionally observed (Fig. 3.51a&b). The basal lamina underlying the luminal epithelium measured approximately 81 nm in thickness.

Tubular glands

Pyknotic nuclei, dilated cisternae of RER and swollen mitochondria characterized degenerating magal gland cells (Fig. 3.52a). The degenerating nuclei displayed dilated nuclear pores and condensation of nuclear chromatin (Fig. 3.52b). Degenerating type A secretory granules contained heterogeneous particles. Degenerating type B secretory granules, displayed a large electron dense granule, which was located either centrally or peripherally (Fig. 3.52c). At this stage, the basal lamina was remarkably thick, measuring approximately 328 nm in thickness. The basal lamina presented a thick lamina densa. The lamina lucida was replaced by a narrow lamina containing particles of an intermediate electron density (Fig. 3.52d). At this stage, supporting cells contained crenated nuclei with chromatin margination (Fig. 3.53a). Swollen mitochondria, dilated RER cisternae and numerous lysosomes were features observed in these cells (Fig. 3.53b).

8 days post-exposure

Ciliated cells

Eight days post-exposure to carbendazim, deciliation was detected in degenerating ciliated cells (Fig. 3.54a). The cilia had normal basal bodies supported by indistinct rootlets. In some instances degenerating cilia and compound cilia were observed (Fig. 3.54b&c). On cross-section, the degenerating cilia lacked the typical 9+2 pattern of microtubular arrangement. In these degenerating cilia, the axial microtubule complex (axoneme) contained 1 to 3 doublets and 6 to 8 singlets (Fig. 3.54b).

Pyknosis, chromatin condensation and margination of nucleoli were observed in degenerating ciliated cells (Fig. 3.55a). Swollen mitochondria and several lysosomes were seen in the apical regions of the cytoplasm. In a few degenerating mitochondria, a loss of cristae was observed (Fig. 3.55b). A few secondary lysosomes and vacuoles were also observed in this region (Fig. 3.55b).

Non-ciliated cells

Degenerating non-ciliated cells contained relatively few secretory granules (Fig. 3.56a). The degenerating non-ciliated cells also contained pyknotic nuclei, swollen mitochondria and multi-granular bodies (Fig. 3.56b&c).

Plasma membrane and basal lamina

Intact cellular junctions linked adjacent epithelial cells (Fig. 3.55c). At this stage, the basal lamina underlying luminal epithelium was similar to that observed 5 days post-exposure to carbendazim.

Tubular glands

Degeneration of the magal gland cells was marked by the presence of vacuoles, dilated RER cisternae and coiled mitochondrial cristae. Crystal deposits and a few lysosomes were occasionally observed. Degeneration of supporting cells was similar to that observed 5 days post-exposure to carbendazim.

12 days post-exposure

Ciliated and non-ciliated cells

Pyknotic and irregular-shaped nuclei were the predominant degenerative change observed in the luminal epithelial cells 12 days post-exposure to carbendazim (Fig. 3.57a). Electron lucent cytoplasm was evident in degenerating ciliated cells. Several lysosomes were observed in the apical cytoplasmic regions of both ciliated and non-ciliated cells (Fig. 3.57a).

Plasma membrane and basal lamina

Intact cellular junctions were observed along the lateral plasma membranes of epithelial cells (Fig. 3.57b). At this stage, the basal lamina, which measured approximately 82 nm, contained homogeneous particles of an intermediate electron density. The lamina densa and lamina lucida were indistinct (Fig. 3.57c).

Tubular glands

A few swollen mitochondria were occasionally observed in degenerating gland cells. At this stage the basal lamina lining the glandular cells was approximately 148 nm in thickness. Condensation and margination of the nuclear chromatin were still the main degenerative features observed in degenerating supporting cells. In addition, aggregations of electron dense granules were occasionally observed.

32 days post-exposure

Ciliated cells

Thirty-two days post-exposure to carbendazim, deciliation was still present (Fig. 3.58a). A few cells displayed solitary cilia. In addition, compound cilia were frequently observed (Fig. 3.58a). Intact basal bodies and striated rootlets were observed in the apical cytoplasmic regions. However, in some instances, striated rootlets were absent. Pyknosis and nuclear membrane blebbing were also observed in degenerating ciliated cells (Fig. 3.58b). Swollen mitochondria, numerous lysosomes, as well as, dilated RER cisternae were present in the apical regions of the cytoplasm (Fig. 3.58b). Filamentous aggregations were also observed in this region.

Non-ciliated cells

Degenerating non-ciliated cells contained relatively few secretory granules which were in the process of degeneration (Fig. 3.59a). The degenerating secretory granules displayed fragmented particles of an intermediate electron density in the

central region. The cytoplasm of degenerating non-ciliated cells appeared electron dense and contained numerous dilated RER cisternae (Fig. 3.59b). Myelin figure formations and lysosomes were evident perinuclearly (Fig. 3.59c). At this stage, only a few microvilli lined the apical plasma membranes of the non-ciliated cells. Electron dense deposits and a discontinuous basal plasma membrane were evident in degenerating epithelial cells (Fig. 3.60).

Plasma membrane and basal lamina

Cellular junctions along the lateral plasma membranes were intact. Underlying the epithelial cells was a discontinuous basal lamina, which was approximately 101 nm thick.

Tubular glands

Numerous vacuoles and degenerating secretory granules were observed in the glandular tissue (Fig. 3.61a). In the advanced stages of degeneration, vacuoles filled the cells (Fig. 3.61b). Degeneration of type A granules was marked by the appearance of an electron lucent material which, was located in the central or peripheral regions (Fig. 3.61 c&d). In the advanced stages of degeneration, the electron lucent material occupied the entire secretory granule. At this stage, the secretory granules were enclosed by an electron dense band (Fig. 3.61a). Degeneration of type B secretory granules was marked by fragmentation of centrally located particles and a reduction of electron density. Consequently the granule contained sparsely distributed electron lucent particles (Fig. 3.61a).

Cellular junctions were still intact along the lateral plasma membrane. The basal lamina underlying the glandular epithelium appeared similar to that of the 12 days post-exposure to carbendazim group.

The degeneration of supporting cells was marked by the presence of pyknotic nuclei, lipid droplets and numerous autolysosomes (Fig. 3.62a&b). A few vacuoles with granular electron dense contents were also observed in degenerating cells (Fig. 3.62c).

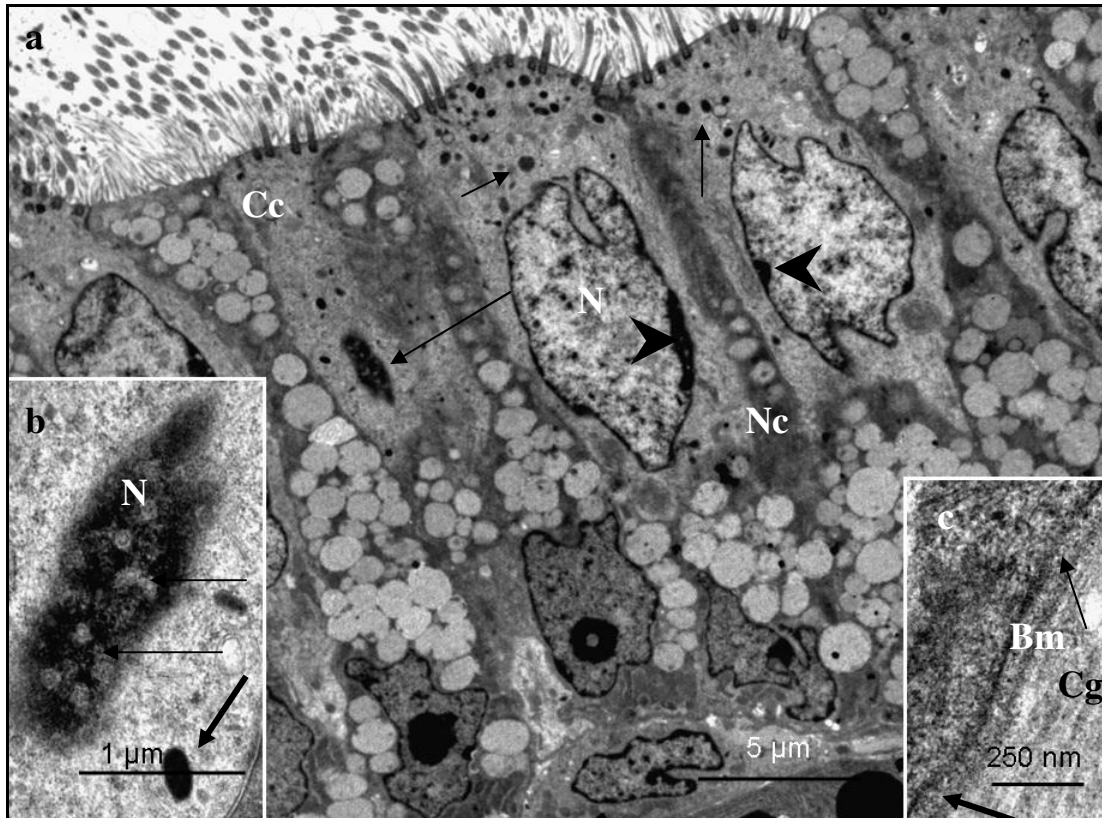


FIG. 3.46: **a.** A survey electron photomicrograph of the luminal epithelium in the magnum, 5 hours post-exposure to 400 mg/kg bodyweight carbendazim. Thin arrow: Pyknotic nucleus. Cc: Ciliated cell. Nc: Non-ciliated cell. N: Nucleus with condensed chromatin and marginalized nucleoli (arrowheads). Short arrows: Lysosomes. **b.** An electron photomicrograph of a degenerating nucleus (N) with dilated nuclear pores (thin arrows). Thick arrow: Lysosome. **c.** Electron photomicrograph of a basal lamina (Bm) with lamina lucida (thin arrow) and lamina densa (thick arrow). Cg: collagen fibres in the *lamina propria-submucosa*.

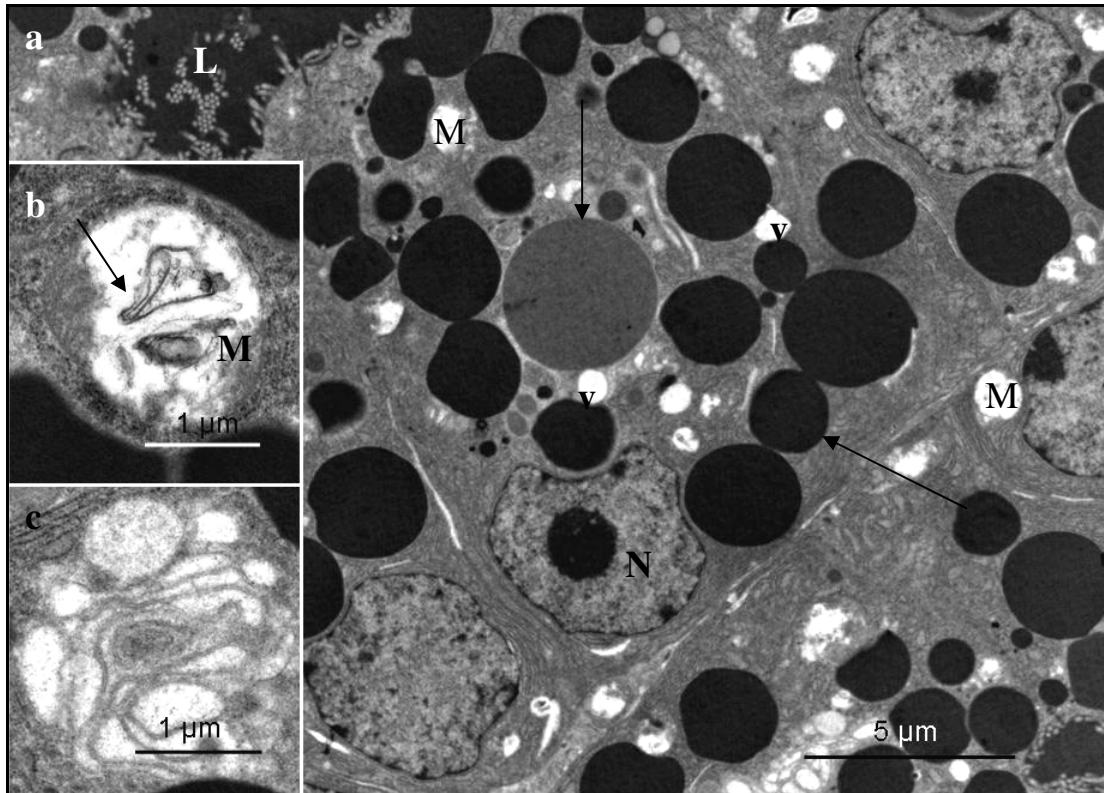


FIG. 3.47: **a.** A survey electron photomicrograph of the glandular tissue in the magnum, 5 hours post-exposure to 400 mg/kg bodyweight carbendazim. V: Vacuoles (v). M: Swollen mitochondria. Secretory granules (arrows) appear normal. N: nucleus; L: glandular lumen. **b.** A photomicrograph of a degenerating mitochondrion (M) with coiled cristae (arrow). **c.** A photomicrograph of dilated RER cisternae in a degenerating gland cell.

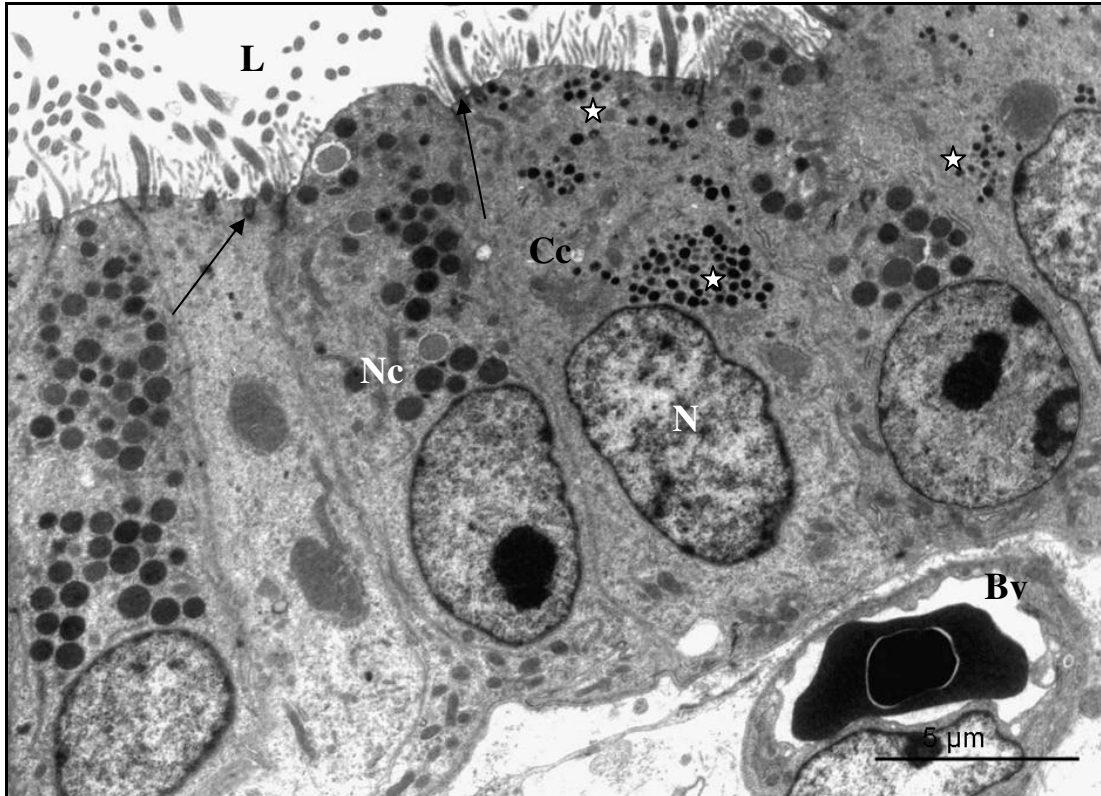


FIG. 3.48: A survey electron photomicrograph of the luminal epithelium in the magnum, 5 days post-exposure to 400 mg/kg bodyweight carbendazim. Cc: Ciliated cells with few cilia. Asterisks: Aggregations of lysosomes. A few cilia are observed along the apical plasma membrane of the degenerating ciliated cells. Note that the striated rootlets supporting the basal bodies (arrows) are indistinct. N: nucleus; Nc: non-ciliated cell; L: lumen; Bv: blood capillary in the *lamina propria-submucosa*.

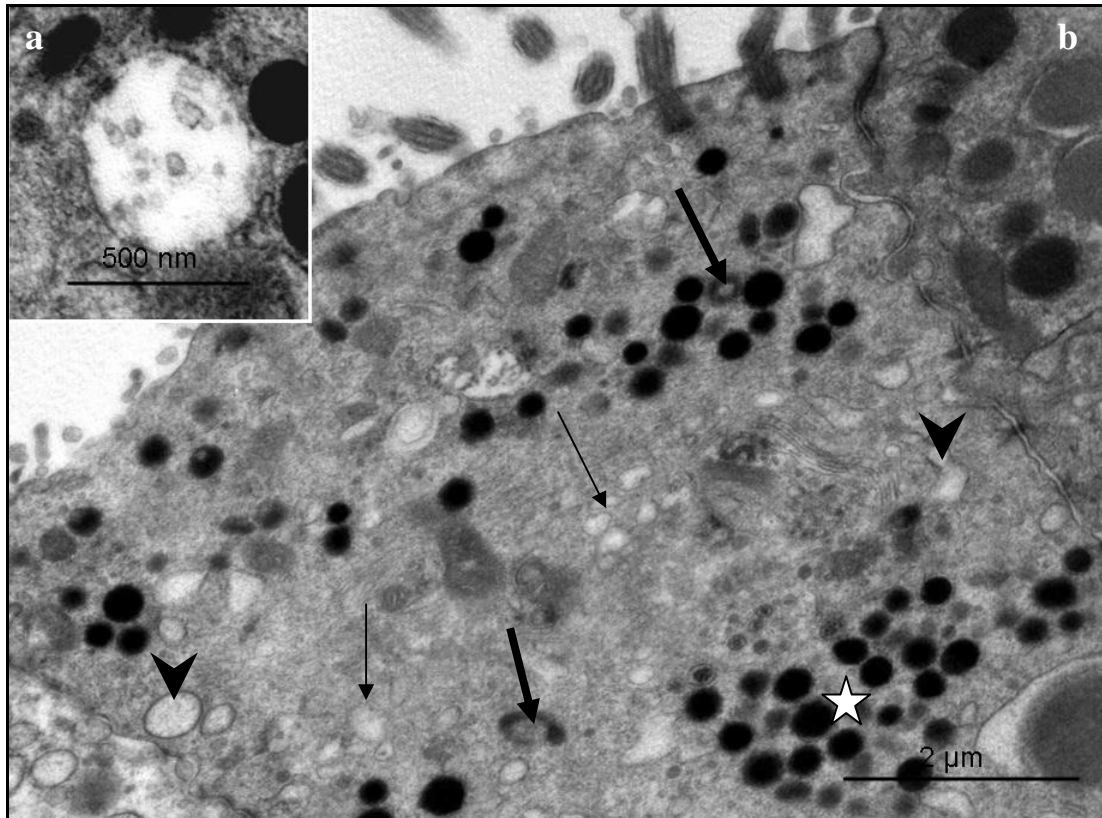


FIG. 3.49: Electron photomicrograph of (a) a multi-vesicular body observed in a degenerating ciliated cell and (b) the apical cytoplasmic region of a degenerating ciliated cell, 5 days post-exposure to 400 mg/kg bodyweight carbendazim. Asterisk: Lysosomes. Thick arrows: Vacuolated mitochondria. Thin arrows: Vacuoles. Arrowheads: Dilated RER cisternae. Note the deciliation along the apical plasma membrane.

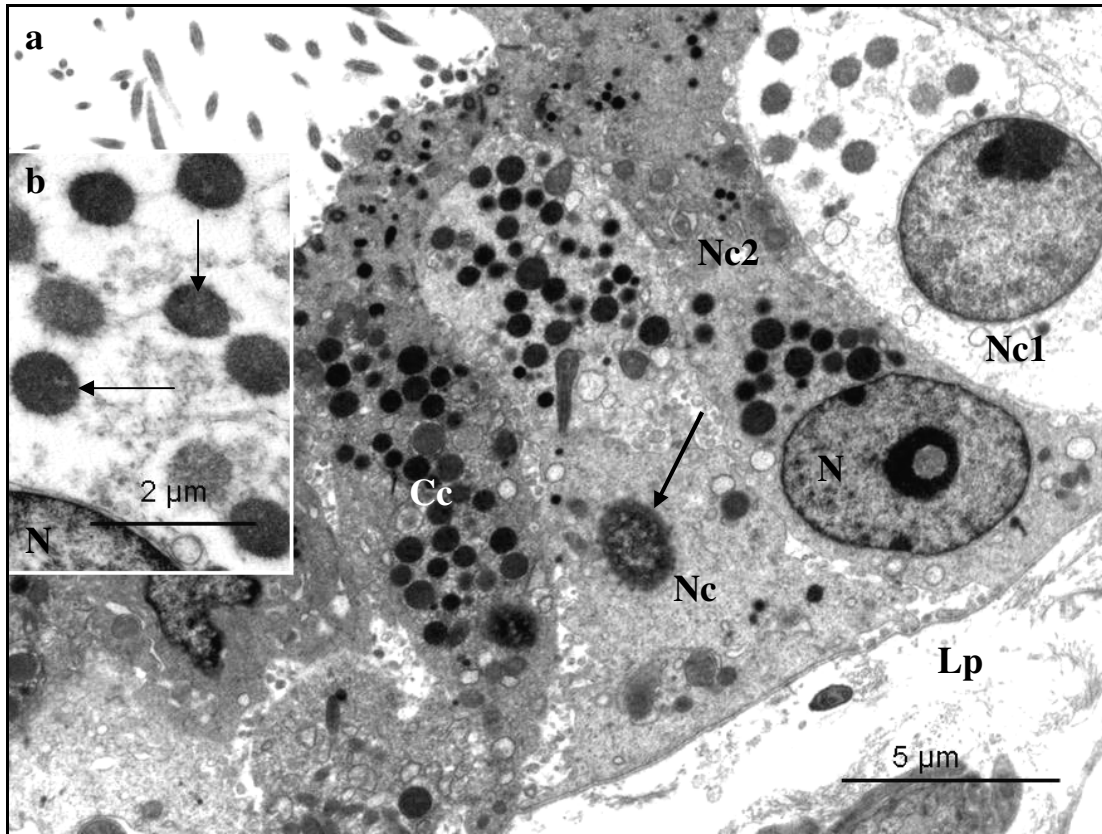


FIG. 3.50: **a.** A survey electron photomicrograph of the luminal epithelium in the magnum, 5 days post-exposure to 400 mg/kg bodyweight carbendazim. Arrow: Pyknotic nucleus. Nc: Non-ciliated cell. Nc1: Cell with electron lucent cytoplasm. Nc2: Cell with electron dense cytoplasm. N: normal nucleus, Cc: ciliated cell. Lp: *lamina propria-submucosa*. **b.** An electron photomicrograph of small secretory granules containing electron dense particles. N: nucleus.

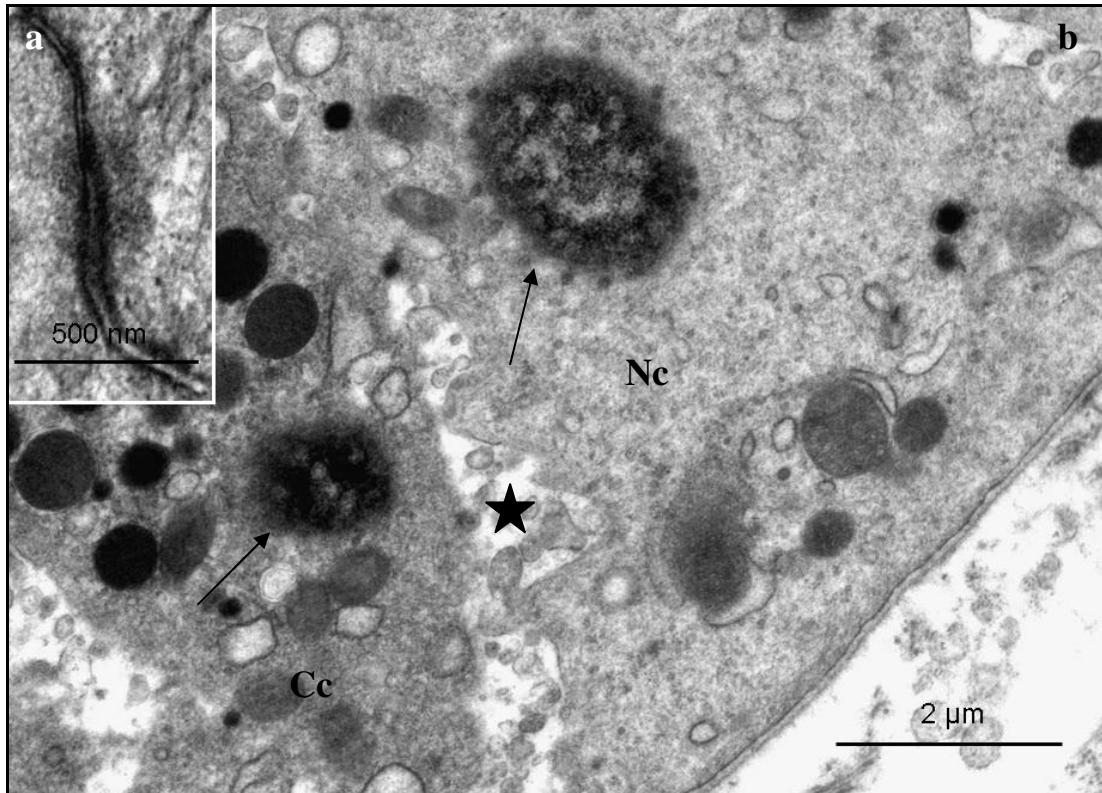


FIG. 3.51: Electron photomicrograph of (a) desmosomes and (b) the basal region of the luminal epithelium of the magnum, 5 days post-exposure to 400 mg/kg bodyweight carbendazim. Note the separation of the lateral plasma membranes (asterisk) in this region. Arrows: pyknotic nuclei in ciliated cell (Cc) and non-ciliated cell (Nc).

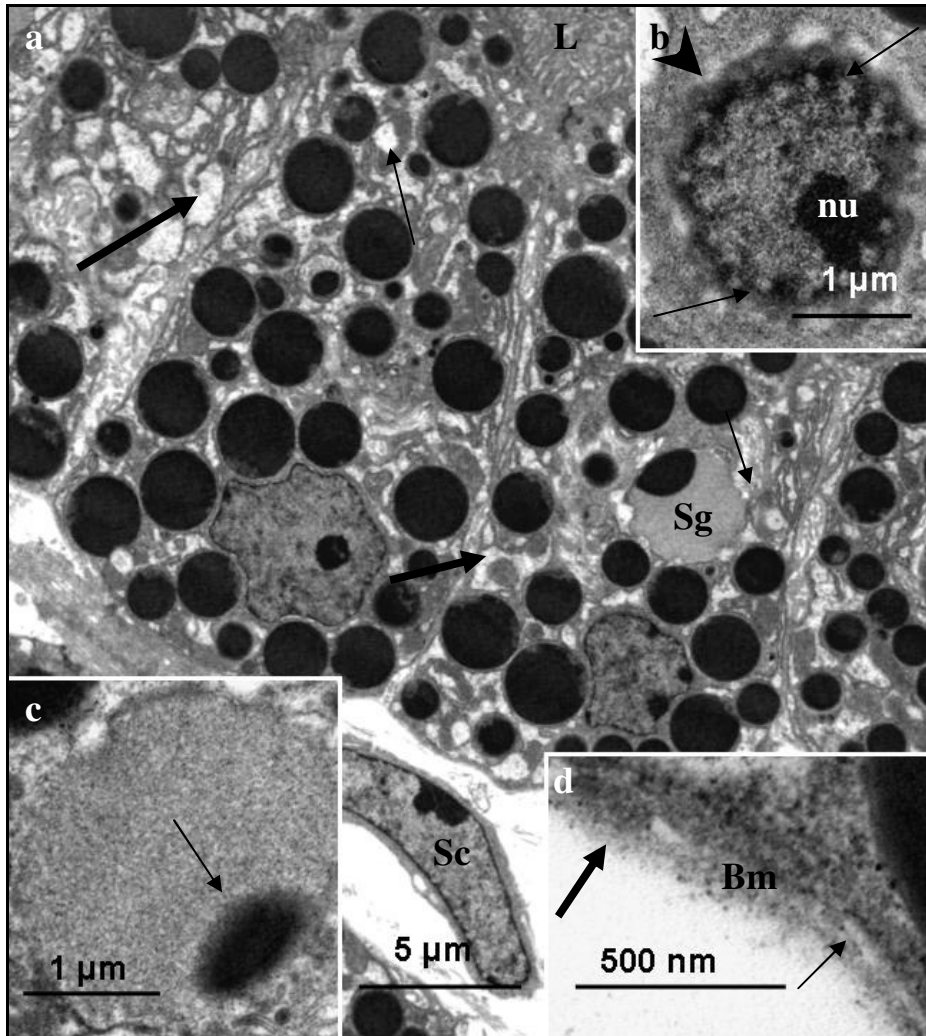


FIG. 3.52: **a.** A survey electron photomicrograph of a tubular gland in the magnum, 5 days post-exposure to 400 mg/kg bodyweight carbendazim. Thick arrows: Dilated RER cisternae. Thin arrows: Swollen mitochondria. Sg: Degenerating Type B secretory granule. L: glandular lumen; Sc: supportive cell. **b.** An electron photomicrograph of a degenerating nucleus with dilated pores (arrows) and a marginalized nucleolus (nu). Note the degeneration of the nuclear membrane (arrowhead). **c.** Degenerating type B secretory granule. An electron dense particle (arrow) is observed in the peripheral zone. **d.** Electron photomicrograph of the basal lamina (Bm) lining a gland cell. The lamina contains a thick lamina densa (thick arrow) and a thin lamina of an intermediate electron density (thin arrow).

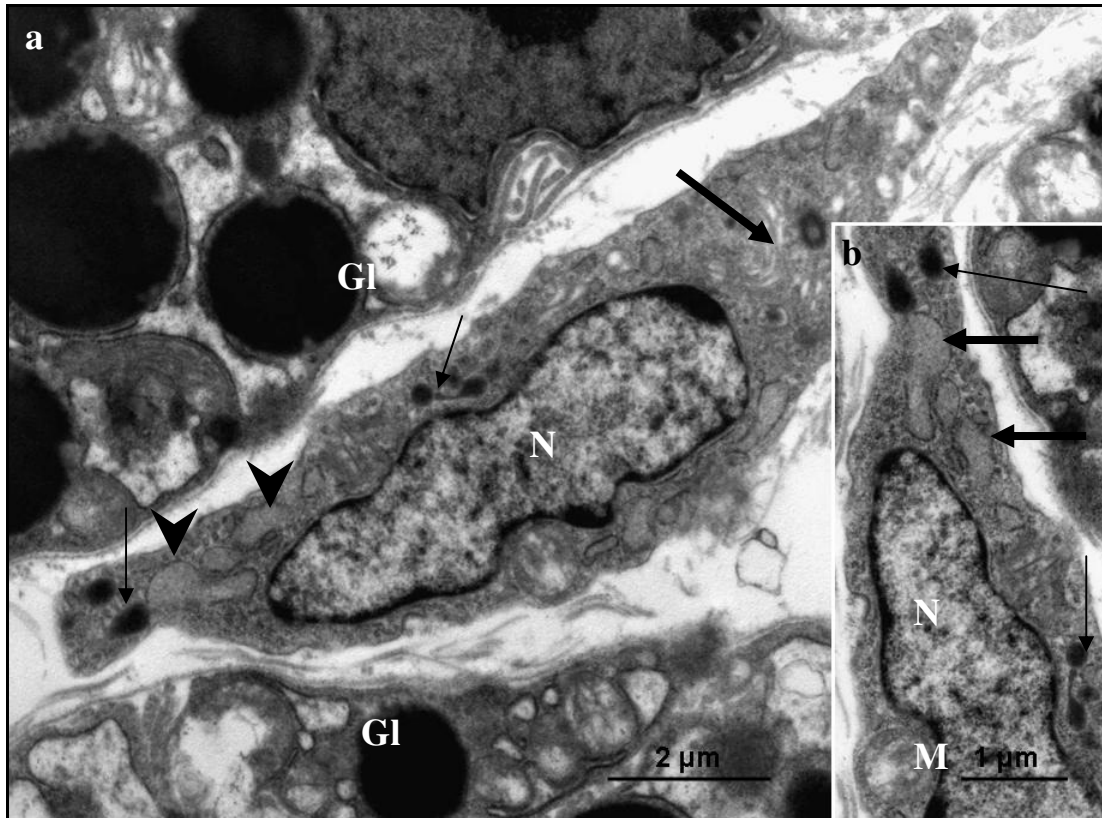


FIG. 3.53: **a.** Electron photomicrograph of a supporting cell in the *lamina propria-submucosa* 5 days post-exposure to 400 mg/kg bodyweight carbendazim. N: Crenated nucleus. Thin arrow: Lysosomes. Arrowheads: Dilated RER cisternae. Thick arrow: Golgi complex. Gl: tubular gland cells. **b.** An electron photomicrograph of dilated RER cisternae (thick arrows), lysosomes (thin arrow) and degenerating mitochondria (M). N: Nucleus.

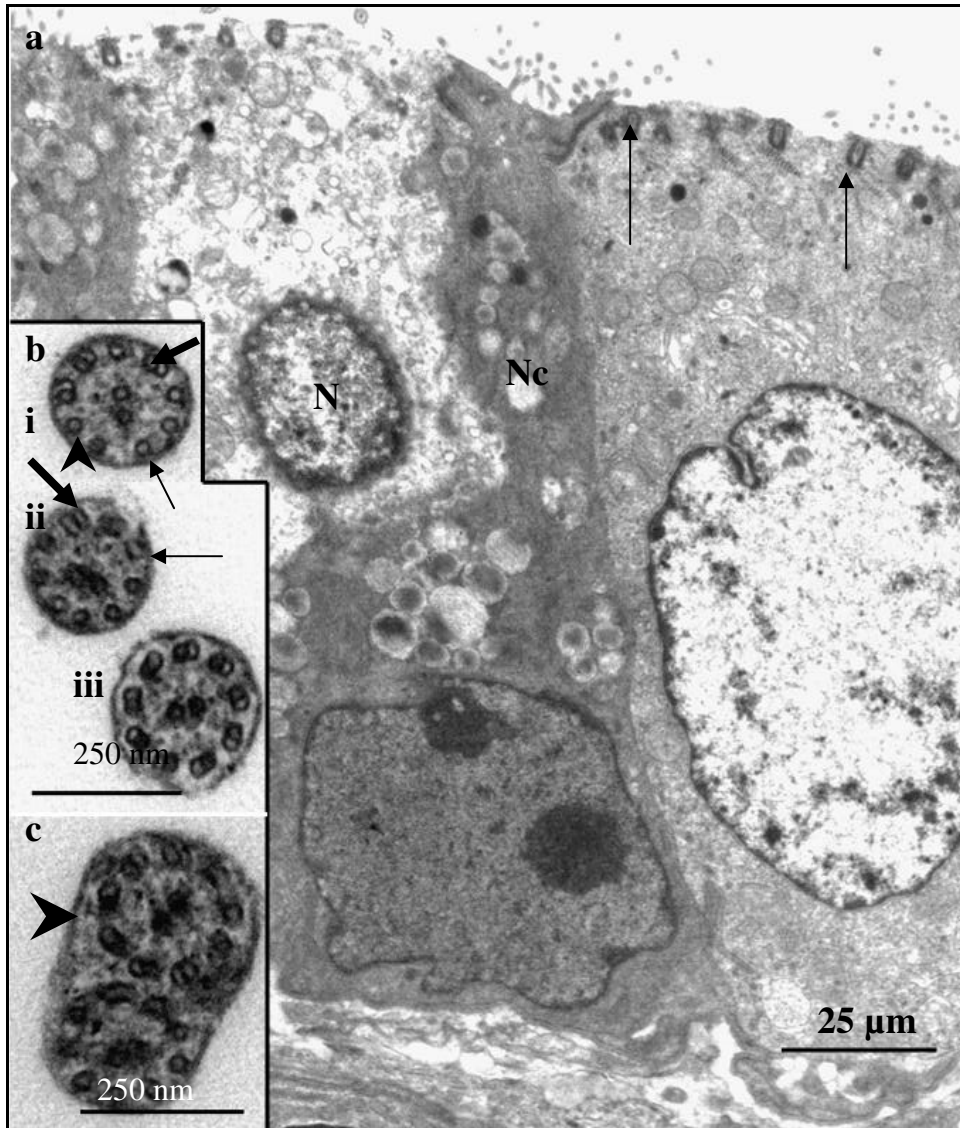


FIG. 3.54: **a**. A survey electron photomicrograph of the luminal epithelial cells in the magnum, 8 days post-exposure to 400 mg/kg bodyweight carbendazim. Loss of cilia is clearly observed at this stage. Arrows: Intact basal bodies. N: Pyknotic nucleus. Nc: non ciliated cell. **b**. A cross-section electron photomicrograph of cilia. Degenerating cilia (“i” & “ii”) contain 1 to 3 doublets (thick arrows) and 6 to 8 singlets (thin arrows). Note loss of dynein arms (arrowhead) in degenerating cilia. “iii” A cross-section of a normal cilium at high magnification. The cilium displays a normal 9+2 microtubular arrangement. **c**. Electron photomicrograph of compound cilia. The cilia are lined by a common plasma membrane (arrowhead). Note the presence of an abnormal axial microtubule complex.

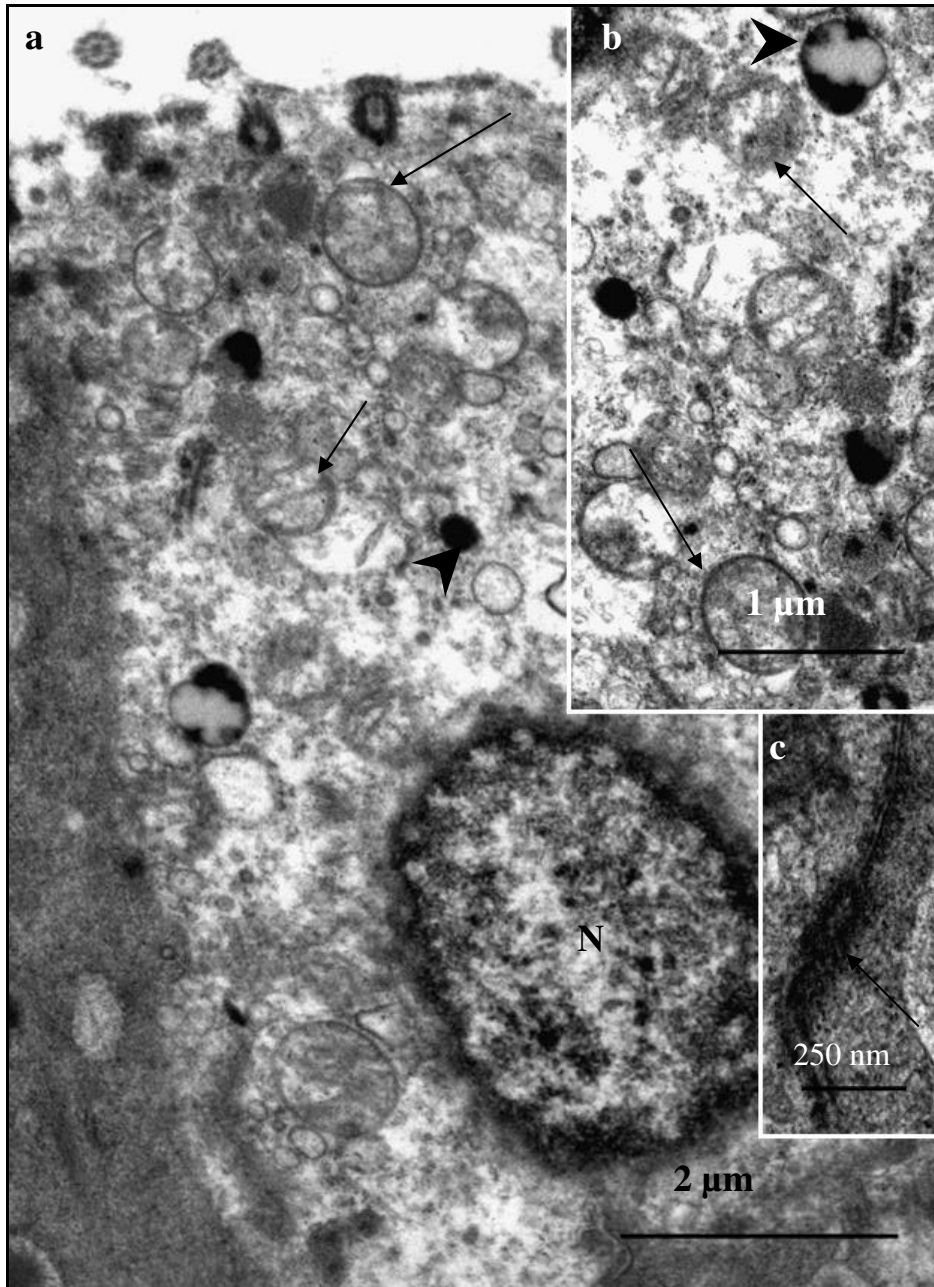


FIG. 3.55: **a.** Electron photomicrograph of a degenerating ciliated cell in the magnum, 8 days post-exposure to 400 mg/kg carbendazim. A pyknotic nucleus (N) displays condensation and margination of nuclear chromatin. Arrows: Swollen mitochondria. Arrowhead: lysosome. **b.** Electron photomicrograph showing mitochondria with degenerating cristae (arrows). Arrowhead: secondary lysosome. **c.** An electron photomicrograph of lateral plasma membranes between adjacent epithelial cells. Arrow: Intact cellular junction.

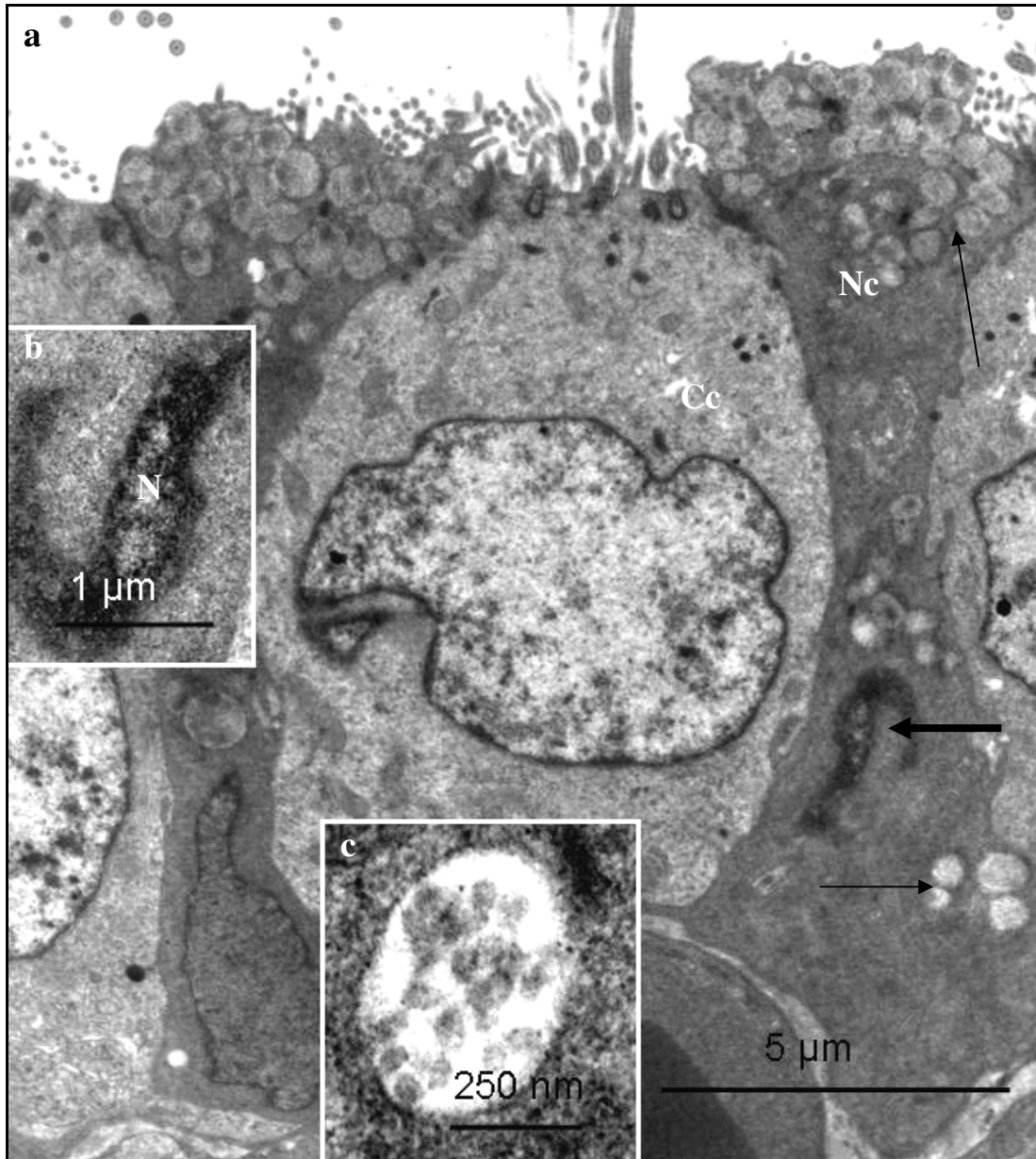


FIG. 3.56: **a.** Electron photomicrograph of the luminal epithelium in the magnum, 8 days post-exposure to 400 mg/kg bodyweight carbendazim. Nc: Non-ciliated cells. Thin arrows: Secretory granules. Thick arrow: Pyknotic nucleus. Cc: ciliated cell. **b.** An electron photomicrograph of a pyknotic nucleus (N). Note the absence of a nuclear membrane. **c.** Electron photomicrograph of a multi-granular body observed in the cytoplasm of a degenerating non-ciliated cell.

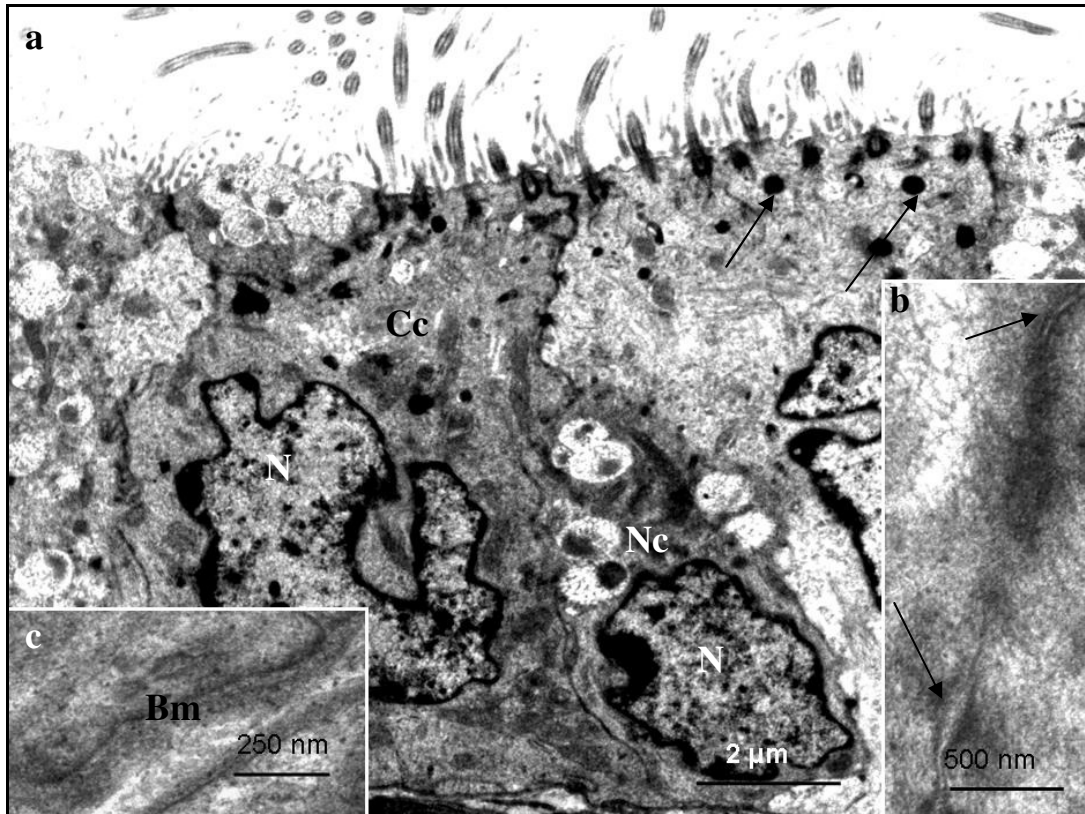


FIG. 3.57: **a.** A survey electron photomicrograph of the luminal epithelium in the magnum, 12 days post-exposure to 400 mg/kg bodyweight carbendazim. N: Irregular-shaped nuclei (N). Degenerating ciliated (Cc) and non-ciliated (Nc) cells. Arrows: Lysosomes. **b.** Arrows: Intact desmosomes (arrows). **c.** An electron photomicrograph of the basal region of a luminal epithelial cell. Bm: Basal lamina with indistinct lamina densa and lucida.

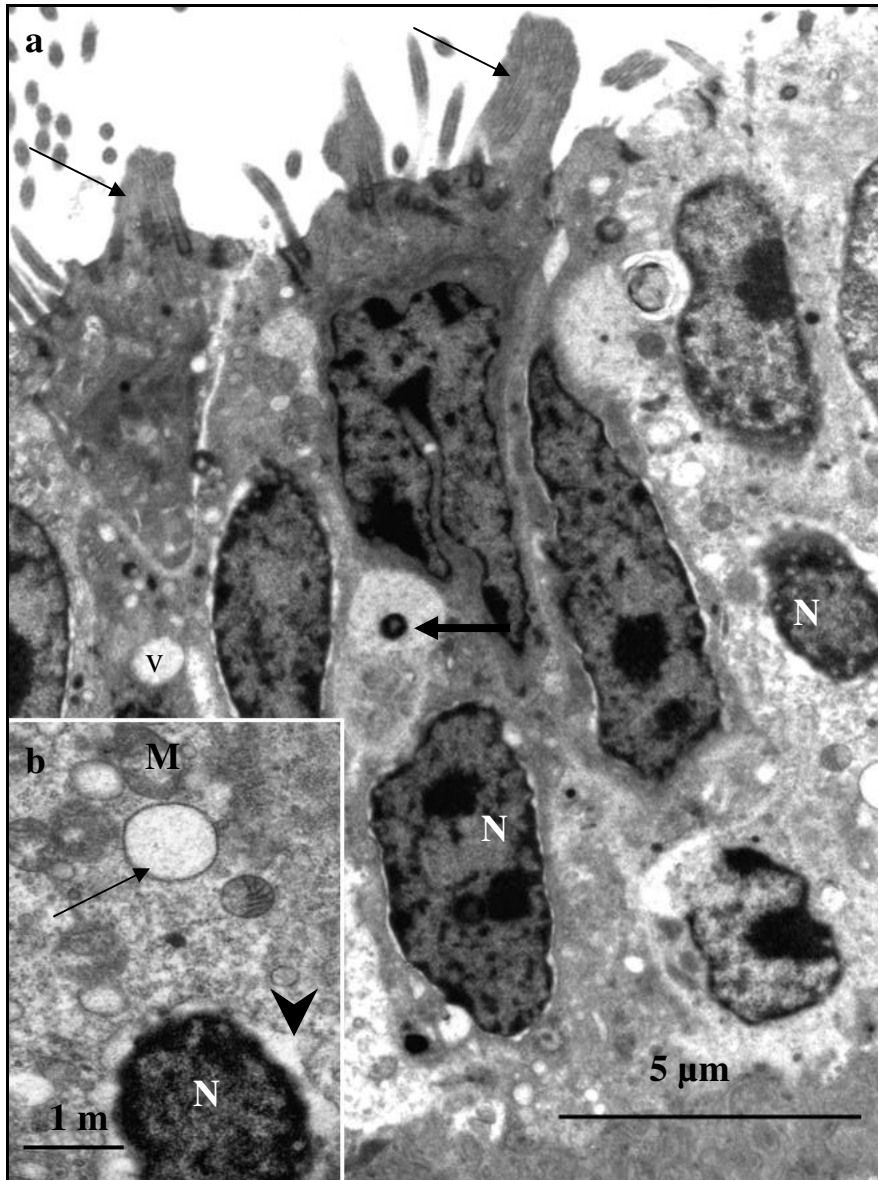


FIG. 3.58: **a.** A survey electron photomicrograph of the luminal epithelium in the magnum, 32 days post-exposure to 400 mg/kg bodyweight carbendazim. Arrows: Compound cilia. N: Degenerating nucleus. V: vacuoles; Thick arrow: lysosome. **b.** An electron photomicrograph of a degenerating ciliated cell. Arrow: Dilated RER cistern. N: Pyknotic nucleus with nuclear chromatin condensation and margination. Arrowhead: Nuclear membrane degeneration. M: swollen mitochondrion.

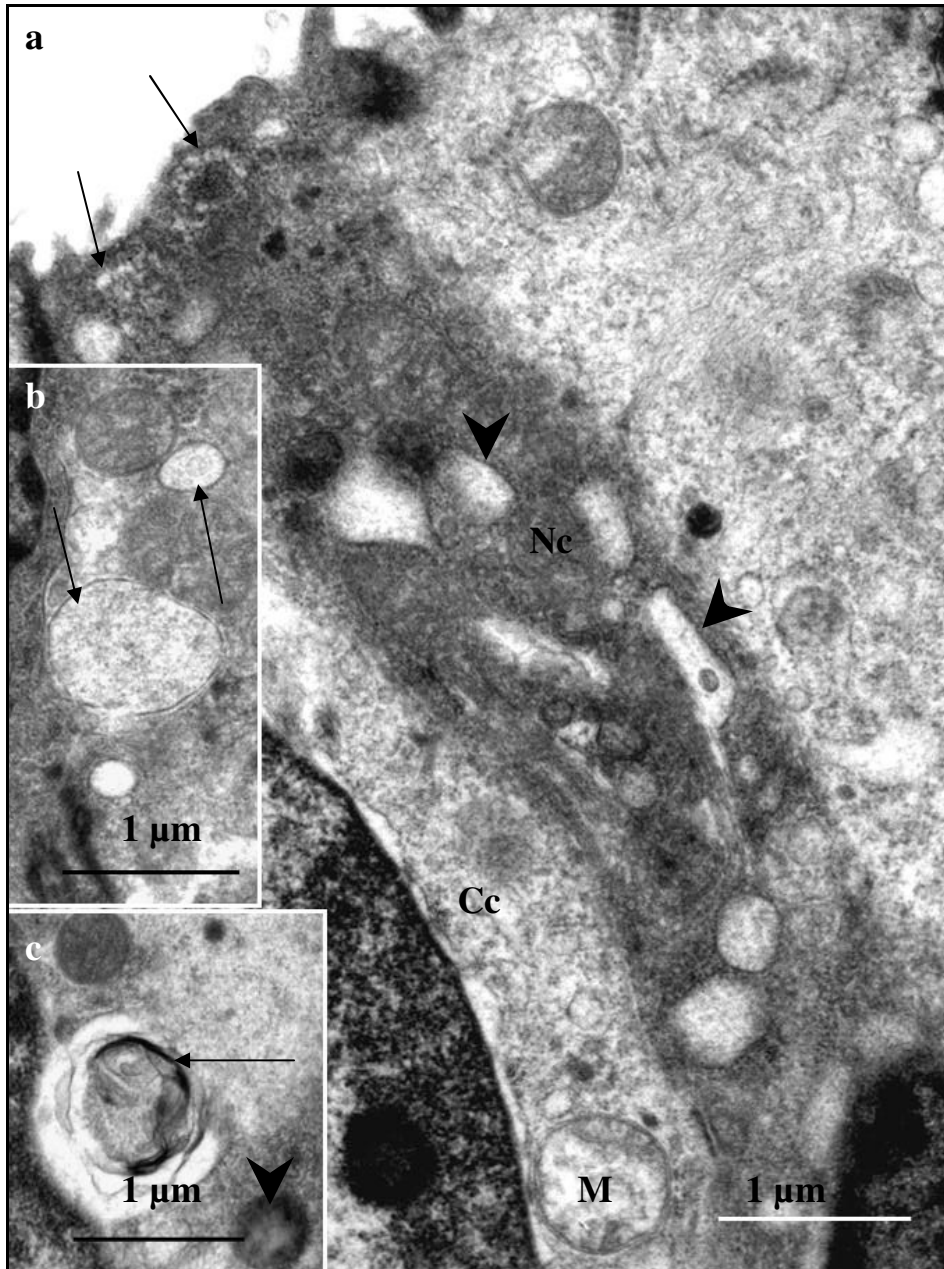


FIG. 3.59: **a.** Electron photomicrograph of the apical region of luminal epithelial cells in the magnum, 32 days post-exposure to 400 mg/kg bodyweight carbendazim. Arrows: Degenerating secretory granules. Nc: Non-ciliated cell. Cc: Ciliated cell. Arrowheads: Dilated RER cisternae. M: Swollen mitochondrion. **b.** An electron photomicrograph of dilated RER cisternae (arrows). **c.** A myelin figure (arrow) and lysosome (arrowhead) in a degenerating non-ciliated cell.

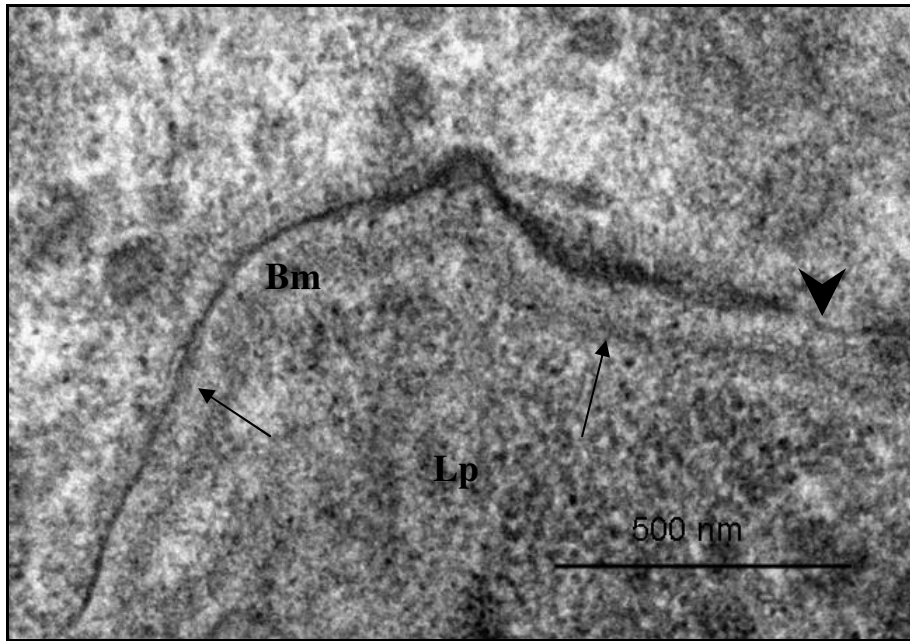


FIG. 3.60: Electron photomicrograph of the basal lamina (Bm) underlying the luminal epithelial cells, 32 days post-exposure to 400 mg/kg bodyweight carbendazim. The lamina lucida (thin arrow) and lamina densa (thick arrow) are distinct. Note a discontinuation of the basal plasma membrane (arrowhead). Lp: *lamina propria-submucosa*.

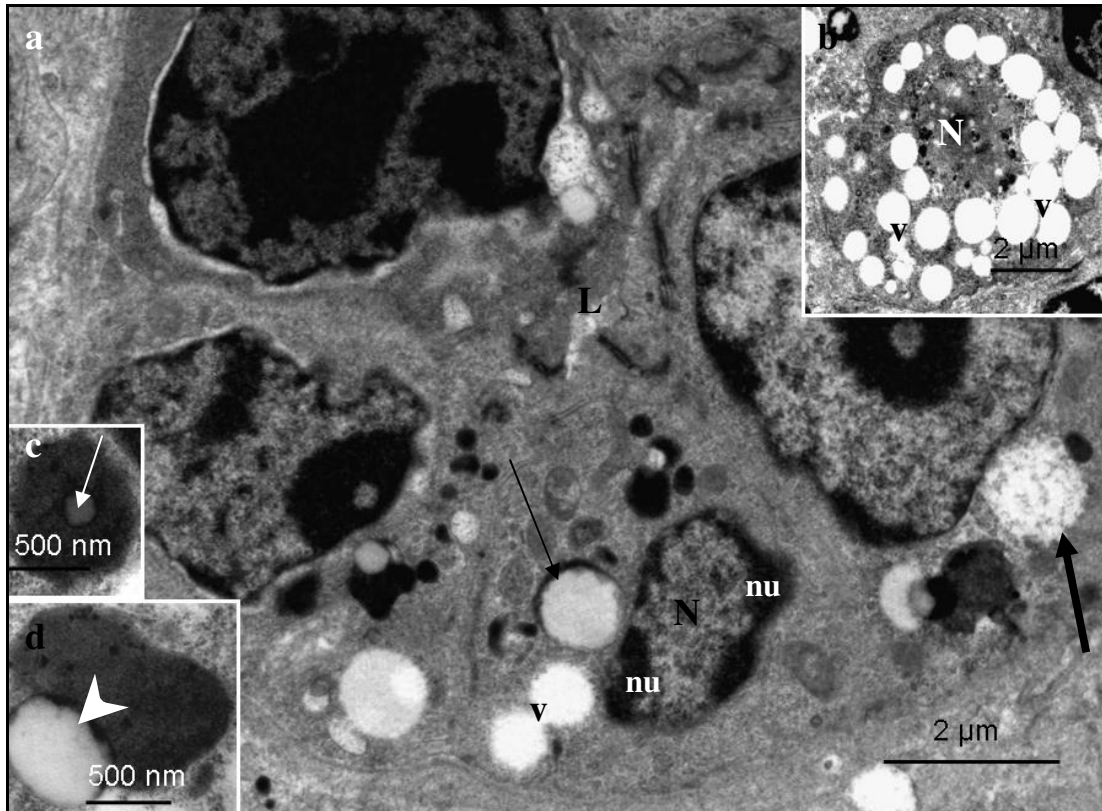


FIG. 3.61: **a.** A survey electron photomicrograph of a tubular gland in the magnum, 32 days post-exposure to 400 mg/kg bodyweight carbendazim. V: Vacuole. Degenerating secretory granules type A (thin arrow) and type B (thick arrow). N: degenerating nucleus displaying nucleoli margination (nu). **b.** Degenerating gland cell containing numerous vacuoles (v). N: nucleus. **c & d.** Type A secretory granules in the initial stages of degeneration. Electron lucent material is observed occupying either central (arrow) or peripheral (arrowhead) region of the granule.

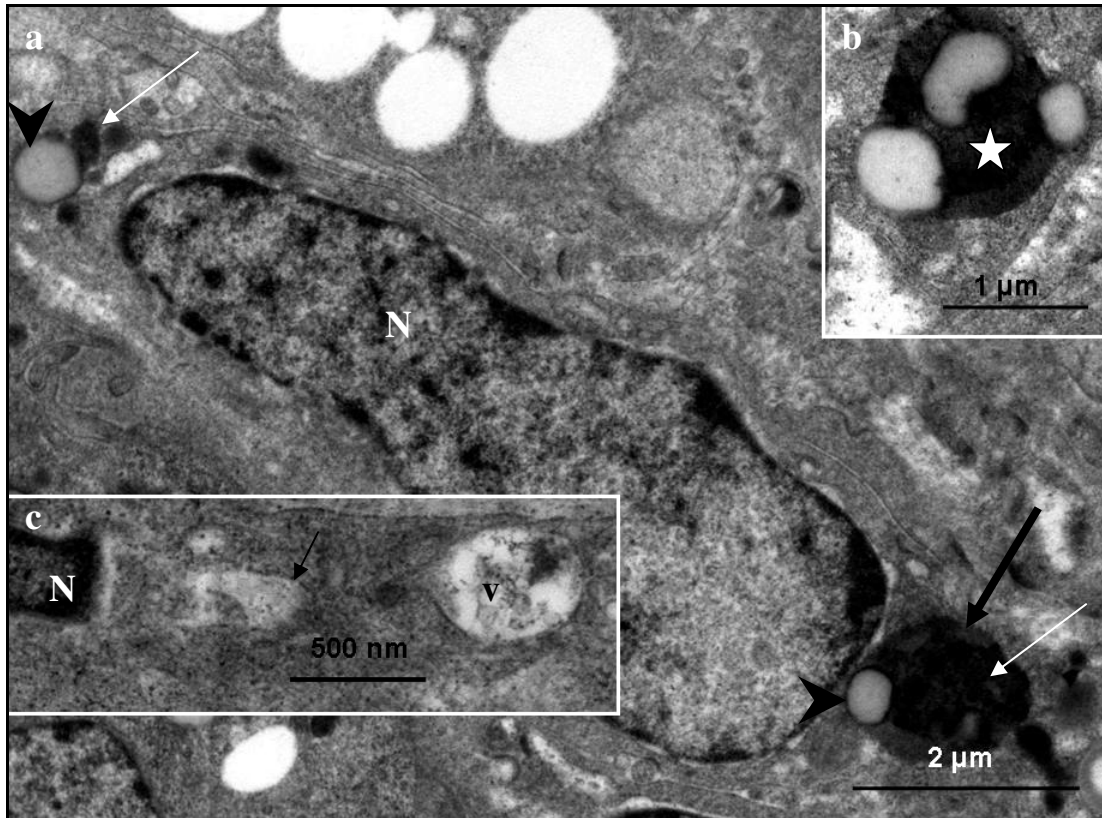


FIG. 3.62: **a.** Electron photomicrograph of a supporting cell in the *lamina propria-submucosa* 32 days post-exposure to 400 mg/kg carbendazim. Secondary lysosome (thick arrow) with electron dense granules (thin white arrows) and lipid droplets (arrow heads). N: Nucleus with chromatin condensation. **b.** A higher magnification photomicrograph of autolysosome (asterisk) observed in (a). **c.** Electron photomicrograph of the cytoplasm of a degenerating supporting cell. A vacuole (v) containing electron dense granules is observed. Arrow: dilated RER cistern. N: pyknotic nucleus.

3.4 Discussion

Histology, histochemistry and statistical analysis

In the control birds, the mucosal layer of the magnum displayed luminal folds, lined by a simple columnar epithelium. Tubular glands extended into the *lamina propria-submucosa*. These findings are in agreement with earlier investigations in the Japanese quail by Fitzgerald (1969), as well as Ereschenko & Wilson (1974). In addition, similar findings have also been observed in the domestic fowl (Wyburn *et*

al. (1970), rhea (Parizzi, Santos, Oliveira, Maia, Sousa, Miglino, & Santos, T. 2008) and brood parasitic birds (Rueda-Cediel, Kattan & Ramirez-pinilla 2008).

A significant decrease in mucosal fold and luminal epithelium height, were observed when high doses (400 mg/kg and 800 mg/kg) of carbendazim were administered. In addition, glandular atrophy was observed at these doses. Low doses (25 mg/kg and 100 mg/kg) of carbendazim did not cause morphological changes in either the mucosal or lamina propria-submucosal layers. This could be due to a rapid elimination of carbendazim from body tissues. When administered at low doses, elimination of carbendazim from animal tissues is rapid through urine, bile and feces after hydrolysis and conjugation in the liver (Gardiner, Kirkland, Klopping & Sherman 1974). According to a report by Ahdaya, Monroe & Guthrie (1981) no metabolite residues were found in the animal's tissues or their products when low doses of carbendazim were administered. In contrast, residues were observed in the eggs, liver and pectoral muscles of Japanese quails fed high doses of carbendazim (Reisinger, Szigeti & Varnagy, 2006). Carbendazim residues were also reported in dogs, rats and dairy cows fed diets containing high levels of the carbendazim parent compound, benomyl. In these animal species carbendazim residues were found in the milk (Ahdaya *et al.* 1981) and liver (Gardiner *et al.* 1974).

In the current investigation, a dose of 400 mg/kg bodyweight carbendazim proved to be the minimum toxic dose level which caused identifiable morphological changes in the magnum. The results of the morphometrical study in experiment Two showed that the administration of a single dose of 400 mg/kg bodyweight carbendazim progressively decreased the heights of primary folds, luminal epithelia and glandular widths from 24 hours post-exposure. The decrease in these parameters suggests the occurrence of oviductal regression. This assertion is supported by a report by Sawyer, Olson & Gorell (1984) which showed a reduction of luminal epithelial height in the regressing oviducts of beagles. Furthermore, a study by Ereschenko & Wilson (1974) showed that oviductal regression in the Japanese quail is characterized by a decrease in the height of epithelial cells, as well as atrophy of glandular tissue.

Histologically, degeneration of luminal epithelial and glandular cells was observed following exposure to 400 mg/kg and 800 mg/kg bodyweight doses of carbendazim.

In addition, following the administration of a single dose of 400 mg/kg bodyweight carbendazim, degenerative changes were more marked. The observed degenerative changes suggested functional impairment, which was supported by a reduction in PAS positive granules at day 8 post-exposure. As mentioned earlier, epithelial and glandular cells are known to produce egg white proteins or albumen (O'Malley 1967; Kohler *et al.* 1968; Oka & Schimke 1969; and Tuohimaa 1975). Degeneration of these epithelial cells could result in a reduction in the quality and quantity of eggs produced. A research report by Davidson (1986) in the domestic fowl demonstrated that morphological changes in epithelial and glandular cells resulted in the production of watery eggs. The formation of watery eggs was also a consequence of abnormal ovalbumen production (Davidson 1986) and the inadequate release of ovomucin (Robinson 1972). Ovomucin and ovalbumen are glycoprotein constituents of albumen (Palmiter & Gutman 1972).

Immunohistochemistry

The current investigation showed the distribution of e-cadherin protein in the plasma membranes of magnal cells. Following carbendazim treatment, no e-cadherin immunoreaction was observed in the plasma membranes at days 5, 8 and 12. The absence of e-cadherin immunoreaction suggests dismantling of e-cadherin proteins due to carbendazim toxicity. Dismantling of e-cadherin has been reported in cultured cells treated with pesticide malathion (Cabello, Galaz, Botella, Calaf, Pacheco, Stockert, Villanueva, Canete & Juarranz, 2003). The report showed that a reduced e-cadherin immunoreaction correlated with morphological changes due to damage of cytoskeletal elements. Morphological changes and a loss of e-cadherin expression was also observed in the current study. An interesting finding was the re-emergence of e-cadherin immunoreaction observed at day 32 post-exposure. At this stage, e-cadherin immunoreactivity was strong to moderate in the luminal plasma membranes. The re-emergence of e-cadherin 32 days post-exposure to carbendazim was indicative of epithelial regeneration.

In the control birds, strong laminin immunostaining was seen in the basement membranes underlying both luminal and glandular epithelia. This observation correlated with a study by Perche & Sandoz (1988), which demonstrated laminin in

the basement membranes underlying oviductal epithelia in the Japanese quail. Following carbendazim administration at a dose of 800g/kg bodyweight, laminin immunostaining was weak to absent in the basement membranes underlying luminal and glandular epithelia. The reduction in laminin immunoreaction in this dosage group was consistent with structural damage observed at the ultrastructural level. In contrast to the observation made in the 800 mg/kg dosage group, no changes were seen at low doses. However, laminin immunoreaction was moderate to weak at days 5 and 8 post-exposure to carbendazim at a dose of 400mg/kg bodyweight. An interesting finding was the thickening of the basement membrane underlying the glandular epithelium. Thickening of the basement membrane has been interpreted as an indication of epithelial regeneration (Vracko, 1974).

In the current study, strong vimentin immunoreactivity was observed in the luminal epithelium, endothelium, mesothelium and fibrocytes in the magnum of control birds. Following carbendazim exposure, vimentin immunoreaction in these cells was weak to absent. The reduction in vimentin immunoreaction could be due to the disruption of cytoskeletal elements by carbendazim. As mentioned in the Introduction, carbendazim disrupts the cytoskeleton by binding to α -tubulin and thus affects microtubule assembly. Several toxicological studies have shown a reduction in vimentin immunoreaction following the administration of chemicals, such as methyl mercury, estramustine and tamoxifen (Sager, 1988; Westeneys, Cadrin, Reuhl and Brown, 1988; Rutberg & Wallin, 1993; Mahasseb, Bell & Habiba, 2009). Reports by Sager (1988) and Westeneys *et al.* (1988) showed a reduction of vimentin immunoreactivity and the disassembly of tubulin and vimentin in cells treated with methyl mercury. Rutberg & Wallin (1993) reported partial disassembly of microtubules and the perinuclear accumulation of vimentin in fibroblasts treated with estramustine. Mahasseb *et al.* (2009) observed a reduction of vimentin immunoreaction and the disruption of cellular structure after an oral exposure to tamoxifen in the rats. Based on the observation made at day 32 post-exposure to carbendazim, the presence of moderate to strong vimentin immunoreaction suggests the reorganization of cytoskeletal elements and cellular recovery.

Scanning and transmission electron microscopy

The results of scanning electron microscopic study in the control birds were consistent with observations made in the domestic fowl (Bakst & Howarth, 1975; Bakst, 1978). Loss of cilia was observed on the mucosal surface at 400 mg/kg and 800 mg/kg bodyweight doses of carbendazim. Deciliation could have been caused by weakening of the cilia shaft due to the disorganization of the axial microtubular complex (axoneme). Carbendazim binds the β -tubulin sub-unit of the microtubule (Burland & Gull (1984) and consequently inhibits the binding of guanosine triphosphate (GTP) to tubulin (Winder, Strandgaard & Miller, 2001). The interaction between carbendazim and axonemal tubulin results in the disruption of microtubules and gives rise to defective cilia. According to Blum (1971) ciliary breakage occurs at a transitional point between the apical plasma membrane and the basal bodies.

Several studies have shown deciliation in regressing reproductive tracts of mammals (Verhage, Mavrogianis, Boice, Li & Fazleabas, 1990; Sawyer *et al.*, 1984) and avian species (Boisvieux-Ulrich, Sandoz & Chailley, 1980; Balachandran, Bhatnagar & Gcissinger, 1985; Madekurozwa, 2005). Loss of cilia can be caused by chemical or physiological responses. Balachandran *et al.* (1985) reported deciliation of the magnum epithelial cells in peking ducks fed high doses of mercury. In the domestic fowl (Boisvieux-Ulrich *et al.*, 1980), deciliation of the oviductal epithelium was observed following ovariectomy. In immature ostriches, loss of cilia was observed during the regressing period (Madekurozwa, 2005). Administration of progesterone was reported to cause deciliation of the oviductal epithelium in the domestic fowl (Boisvieux-Ulrich *et al.* 1980); baboon (Verhage *et al.* 1990), mice (Lauschova, 1999) and in pre-pubertal beagles (Sawyer *et al.*, 1984). Based on the fact that carbendazim elevates plasma levels of luteinizing hormone in male rats (Goldman, Rehinberg, Cooper, Gray, Hein & Mcerloy, 1989) it is possible that the deciliation of the oviductal epithelium observed in the current study, was partly caused by high levels of progesterone. Further hormonal study need to be carried out to confirm this assertion.

In addition to deciliation, TEM results showed degenerating cilia with disrupted (9+2) microtubular arrangements, as well as, the cilia containing multiple axial microtubular

complexes (compound cilia) in the magnum of carbendazim-treated birds. Similar findings were observed in pekin ducks fed diets containing high doses of methyl mercury (Balachandran *et al.*, 1985). Compound cilia have also been reported in the respiratory epithelial cells of domestic fowl affected by infectious laryngotracheitis virus (Purcell, 1971), as well as in human with bronchial carcinoma (Ailsby, 1973) and chronic obstructive pulmonary disease (Escalier, Jouannet & David, 1982). According to a report by Boisvieux-Ulrich *et al.* (1980), the presence of compound cilia in the oviduct is a form of deciliation such that degenerating cilia are shed in groups. This could be the case in the present study. The disorganization of axial microtubular complexes, as well as the formation of compound cilia is indicative of a loss of ciliary movement. As mention in Chapter two, ciliary movement is crucial in the process of egg laying. Loss of cilia motility in the magnum would probably negatively affect the process of egg formation and laying in carbendazim-exposed birds.

The presence of degenerating nuclei in the epithelial and glandular cells was an indicator of necrosis post-exposure to carbendazim. During necrosis, nuclear chromatin disintegrates (karyorrhexis) due to the disorganization of the DNA double strand. Carbendazim has a benzimidazole ring, which is the analogue of purine. It interferes with DNA synthesis by inhibiting metabolic processes involving purine (Seiler, 1975). It can thus be proposed that, the necrosis observed in these cells was attributed to the ability of carbendazim to disrupt DNA synthesis. In support of this idea, a histological study of fungal cells treated with carbendazim demonstrated abnormal chromatin configuration (Davidse, 1973). In addition, chromosomal aberration was observed in rats fed carbendazim daily at a dose of 200 mg/kg (Ruzicska, Peter & Czeizel, 1975). Carbendazim has also been reported to induce cytoplasmic accumulation of Rad26-GFP which controls DNA synthesis (Baschal Chen, Elliott, Herring, Verde & Wolkow, 2006).

Swelling and aggregation of mitochondria, as well as dilatation of RER cisternae and increased number of lysosomes were observed in the degenerating epithelial cells. Similar findings have been observed in birds treated with high levels of methyl mercury (Balachandran *et al.*, 1985). Mitochondrial swelling and dilatation of RER cisternae suggests increased membrane permeability due to carbendazim toxicity.

The aggregation of degenerating mitochondria and lysosomes could be attributed to the effect of carbendazim on the functioning of cytoskeletal components, such as, microtubules, microfilaments and intermediate filaments. The cytoskeleton plays a major role in the dynamic movements of organelles within the cell (Olmsted and Borisy, 1973). The administration of the microtubule disrupter, nocodazole, and the actin filament depolarizing agent, cytochalasin D, reduced the movement of cytoplasmic organelles in respiratory epithelial cells (Grosse, Aron, Thevenot, Monsigny & Fajac, 2007). Russell, Malone & Maccurdy (1981) reported an aggregation of mitochondria in cells and tissues treated with the microtubule disrupting agents; colchicines and vinblastine. In the male rat carbendazim caused mitochondria aggregation in the testis (Nakai, Hess, Moore, Gutroff, Strader & Linder, 1992). The reports further explained that the mitochondrial aggregation correlated with microtubule disruption. Although the effect of carbendazim on microfilaments is not clearly stated, it is assumed that the disruption of one cytoskeletal component, such as, microtubules would have a profound effect on the functioning of the other cytoskeletal components.

In the current study, cellular protrusions were a frequent SEM and TEM observation. Similar findings have been reported in the regressing oviduct of birds (Eroschenko & Wilson, 1974) and mammals (Sawyer *et al.* 1984; Steffl, Schweiger, Siguyama & Amselgruber, 2008). In these studies, the protrusion of the apical regions of non-ciliated cells was interpreted as an indicator of oviduct regression. This was probably also the case in the present study.

The presence of Type A and Type B granules in the magnum of the control birds was similar to the observation made in the domestic fowl (Wyburn *et al.*, 1971, Sandoz *et al.* 1971). Type A cells are known to produce ovalbumin, while Type B secretes lysozyme (Wyburn *et al.*, 1970). Following carbendazim exposure, degenerating Type A & B granules were observed in degenerating non-ciliated cells. The degeneration of secretory granules suggests functional impairment of the non-ciliated cells during egg formation. In molting hen, degeneration of secretory granules coupled with glandular cells involution were reported (Yu and Marquardt, 1973).

In the present study, degenerative changes in the basal lamina underlying both the luminal and glandular epithelia were observed from 5 days post-exposure to carbendazim. The observed changes were duplication of the basal lamina and indistinct lamina densa at 12 days post-exposure. Similar degenerative changes in the basal lamina have been reported in degenerating muscle capillaries (Vracko & Benditt 1972; Tilton, Hoffman, Kilo & Williamson, 1981), injured peripheral nerves (Thomas 1964; O'Daly & Imaeda 1967; Salonen, Peltonen, Roytta & Virtanen, 1987) and renal tubules affected by radiation (Madrazo, Suzuki & Churg, 1970). The duplication of the basal lamina observed could be an initial sign of epithelial recovery. A study by Ghosh, Danielson, Alston & Heyner (1991) showed the role of the basal lamina in the differentiation of epithelial cells. According to this report, the basal lamina controls development and stability of the epithelium. It is likely that changes in the morphology of the basal lamina observed in the current study at 32 days post-exposure indicate regeneration of the epithelial cells. This is supported by reduced number of inflammatory cells observed at 32 days post-exposure.

Conclusion

Survival of the poultry industry depends on the quantity and quality of eggs produced. As mentioned earlier, most of the egg white proteins are added to the forming egg in the magal region of the oviduct (Edwards, Luttrell & Nir, 1976). Morphological changes in this region cause a deterioration of egg quality. Degeneration of epithelial, as well as glandular cells, pose a potential threat to the productivity of carbendazim-exposed birds.

3.5 References

- AHDAYA, S.M., MONROE, R.J. & GUTHRIE, F.E. 1981. Absorption and distribution of intubated insecticides in fasted mice. *Pesticide Biochemistry and Physiology*, 16:38-46.
- AILSBY, R.L. & GHADIALLY, F.N. 1973. Atypical cilia in human bronchial mucosa. *Journal of Pathology*, 109:75-78.

- BAKST, M.R. 1978. Scanning electron microscopy of the oviductal mucosa apposing the hen ovum. *Poultry Science*, 57:1065-1069.
- BAKST, M. & HOWARTH, B.Jr. 1975. SEM preparation and observations of hen's oviduct. *Anatomical Record*, 181:211-226.
- BALACHANDRAN, A., BHATNAGAR, M.K. & GCISSINGER, H.D. 1985. Scanning and Transmission electron microscopic studies on the oviducts of pekin ducks fed methyl mercury containing diets. *Scanning Electron Microscopy*, 1:311-322.
- BASCHAL, E.E., CHEN, K.J., ELLIOTT, L.G., HERRING, M.J., VERDE, S.C., WOLKOW, T.D. (2006). The fission yeast DNA structure checkpoint protein Rad26ATRIP/LCD1/UVSD accumulates in the cytoplasm following microtubule destabilization. *BMC Cell Biology*, 24:32.
- BLUM, J.J. 1971. Existence of a breaking point in cilia and flagella. *Journal of Theriogenology and Biology*, 33:257-263.
- BOISVIEUX-ULRICH, E., SANDOZ, D. & CHAILLEY, B. 1980. A thin section and freeze-fracture study of deciliation in bird oviduct. *Biology of the Cell*, 37:261-268.
- BURLAND, T.G. & GULL, K. 1984. Molecular and cellular aspects of the interaction of benzimidazole fungicides with tubulin and microtubules, in *Mode of action of antifungal agents*, edited by A.P.J. Trinci & J.F. Riley. Cambridge: University Press, 299 - 320.
- CABELLO, G., GALAZ, S., BOTELLA, L., CALAF, G., PACHECO, M., STOCKERT, J.C., VILLANUEVA, A., CAÑETE, M. & JUARRANZ, A. (2003). The pesticide malathion induces alterations in actin cytoskeleton and in cell adhesion of cultured breast carcinoma cells. *International Journal of Oncology*, 23:697-704
- CHOUSALKAR, K.K. & ROBERTS, J.R. 2007: Ultrastructural study of infectious bronchitis virus infection in infundibulum and magnum of commercial laying hens. *Veterinary Microbiology*, 122:223-236.

- CHOUSALKAR, K.K. & ROBERTS, J.R. 2008. Ultrastructural changes in the oviduct of the laying hen during the laying cycle. *Cell Tissue and Research*, 332:349-358.
- DAVIDSE, L.C. 1973. Antimitotic activity of methyl benzimidazole-2-yl carbamate (MBC) in *Aspergillus nidulans*. *Pest Biochemistry and Physiology*, 3:317-325.
- DAVIDSON, M.F. 1986. Histological studies of changes in the magnum of the domestic hen associated with the production of watery white eggs. *British Poultry Science*, 27:353-354.
- EDWARDS, N.A., LUTTRELL, V. & NIR, I. 1976. The secretion and synthesis of albumen by the magnum of the domestic fowl (*Gallus domesticus*). *Comparative Biochemistry and Physiology*, 53:183-186.
- EROSCHENKO, V.P. & WILSON, W.O. 1974. Histological changes in the regressing reproductive organs of sexually mature male and female Japanese quail. *Biology of Reproduction*, 11:168-179.
- ESCALIER, D., JOUANNET, P. & DAVID, G. 1982. Abnormalities of the ciliary axonemmal complex in children: An ultrastructural and kinetic study in a series of 34 cases. *Biology of the Cell*, 44:271-282.
- FITZGERALD, T.C. (Ed) 1969. The coturnix quail: *Anatomy and histology*. Ames: Iowa State University Press.
- GARDINER, J.A., KIRKLAND, J.J., KLOPPING, H.L. & SHERMAN, H. 1974. Fate of benomyl in animals. *Journal of Agriculture and Food Chemistry*, 22:419-427.
- GILBERT, A.B. 1979. Female genital organs, in *Form and function in birds*, edited by A.S. King & J. McLelland. London: Academic Press, 1:237-338.
- GHOSH, D., DANIELSON, K.G., ALSTON, J.T. & HEYNER, S. 1991. Functional differentiation of mouse uterine epithelial cells grown on collagen gels or

- reconstituted basement membranes. *In Vitro Cellular and Developmental Biology*, 27:713-719.
- GOLDMAN, J. M., REHINBERG, G. L., COOPER, R. L., GRAY, L. E., HEIN, J. F., & MCERLOY, W. K. 1989. Effects of the benomyl metabolite carbendazim on the hypothalamic-pituitary reproductive axis in the male rat. *Toxicology*, 57:173-182.
- GROSSE, S., ARON, Y., THEVENOT, G., MONSIGNY, M. & FAJAC, I. 2007. Cytoskeletal involvement in the cellular trafficking of plasmid/PEI derivative complexes. *Journal of Controlled Release*, 122:111-117.
- KOHLER, P.O., GRIMLEY, P.M. & O'MALLEY, B.W. 1968. Protein synthesis: differential stimulation of cell specific proteins in the epithelial cells of the chick oviduct. *Science*, 160:86-87.
- LAUSCHOVA, I. 1999. Influence of estrogen and progesterone on ultrastructural indices of oviductal epithelium in sexually immature mice. *Acta Veterinaria Brno*, 68:13-21.
- LU, S.-Y., LIAO, J.-W., KUO, M.-L., WANG, S.-C., HWANG, J.-S. & UENG, T.-H. 2004. Endocrine disrupting activity in carbendazim-induced reproductive and developmental toxicity in rats. *Journal of Toxicology and Environmental Health*, 67:1501-1515.
- MADRAZO, A., SUZUKI, Y. & CHURG, J. 1970. Radiation nephritis. II. Radiation changes after high doses of radiation. *American Journal of Pathology*, 61:37-56.
- MADEKUROZWA, M.-C. 2005. Morphological features of the luminal surface of the magnum in the sexually immature ostrich (*Struthio camelus*). *Anatomia Histologia Embryologia*, 34:350-353.

- MEHASSEB, M.K., BELL, S.C. & HABIBA, M.A. (2009). The effects of tamoxifen and estradiol on myometrial differentiation and organization during early uterine development in the CD1 mouse. *Reproduction*, 138:341-50
- MAO, K.M., SULTANA, F., HOWLIDER, M.A., IWASAWA, A. & YOSHIZAKI, N. 2006. The magnum-isthmus junction of the fowl oviduct participate in the formation of the avian-type shell membrane. *Zoological Science*, 23:41-47.
- MOHAMMADPOUR, A.A. & KESTMANDI, M. 2008. Histomorphometrical study of infundibulum and magnum in turkey and pigeon. *World Journal of Zoology*, 3:47-50.
- NAKAI, M., HESS, R.A., MOORE, B.J., GUTROFF, R.F., STRADER, L.F. & LINDER, R.E. 1992. Acute and long-term effects of a single dose of the fungicide carbendazim (methyl-2-benzimidazole carbamate) on the male reproductive system in the rat. *Journal of Andrology*, 13:507-518.
- O'DALY, J.A. & IMAEDA, T. 1967. Electron microscopic study of Wallerian degeneration in cutaneous nerves caused by mechanical injury. *Laboratory Investigation*, 17:744-766.
- OKA, T. & SCHIMKE, R. 1969. Interaction of oestrogen and progesterone in chick oviduct development II: effects of oestrogen and progesterone on tubular gland cell function. *Journal of Cell Biology*, 43:123-137.
- OLMSTED, J. B. & BORISY, G. G. 1973. Microtubules. *Annual Review of Biochemistry*, 42:507-540.
- O'MALLEY, B.W. 1967. In vitro hormonal induction of specific protein (avidin) in chick oviduct. *Biochemistry*, 6:2546.
- PALMITER, R.D. & GUTMAN, G.A. 1972. Fluorescent antibody localization of ovalbumin, conalbumin, ovomucoid and lysozyme in chick oviduct magnum. *The Journal of Biological Chemistry*, 6459-6461.

- PARIZZI, R.C., SANTOS, J.M., OLIVEIRA, M.F., MAIA, M.O. SOUSA, J.A., MIGLINO, M.A. & Santos, T.C. 2008. Macroscopic and microscopic anatomy of the oviduct in the sexually mature rhea (*Rhea americana*). *Anatomia Histologia Embryologia*, 37:169-176.
- PERCHE, O. & SANDOZ, D. (1988). Immunolocalization of laminin during estrogen-induced differentiation of quail oviduct epithelial cells. *Biology of the Cell*, 64:353-62
- PURCELL, D.A. 1971. The ultrastructural changes produced by infectious laryngotracheitis virus in the tracheal epithelium of the fowl. *Research in Veterinary Science*. 2:455-458.
- REISINGER, K., SZIGETI, J. & VARNAGY, L. 2006. Determination of carbendazim residues in the eggs, liver and pectoral muscle of Japanese quail (*Coturnix coturnix japonica*). *Acta Veterinaria Hungarica*, 54:127-133.
- ROBINSON, D.S. 1972. Egg white glycoproteins and the physical properties of egg white, in *Egg formation and production*, edited by B.M. Freeman & P.E. Lake. Edingburg: British Poultry Science LTD.
- RUEDA-CEDIEL, P., KATTAN, G. & RAMIREZ-PINILLA, M.P. 2008. Ovarian and oviductal morphology of a brood parasitic bird, *Molothrus bonariensis* (Passeriformes, Icteridae). *Acta Zoologica*, 89:261-276.
- RUSSELL, L.D., MALONE, J.P., & MACCURDY, D.S. 1981. Effect of microtubule disrupting agents, colchicines and vinblastine, on seminiferous tubule structure in the rat. *Tissue and cell*, 13:349-367.
- RUTBERG, M. & WALLIN, M. (1993). Estramustine induces disorganization of microtubules, perinuclear retraction of vimentin and endoplasmic reticulum, and inhibits cell migration. *Acta Histochemica*, 95:155-67

- RUZICKA, P., PETER, S., & CZEIZEL, A. 1975. Studies on the chromosomal mutagenic effect of benomyl in rats and humans. *Mutation Research*, 29:201.
- SAGER, P.R. (1988). Selectivity of methyl mercury effects on cytoskeleton and mitotic progression in cultured cells. *Toxicology and Applied Pharmacology*, 94:473-86
- SALONEN, V., PELTONEN, J., ROYTTA, M. & VIRTANEN, I. 1987. Laminin in traumatized peripheral nerv: basal lamina changes during regeneration. *Journal of Neuropathology*, 16:713-720.
- SAWYER, H.R., OLSON, P.N. & GORELL, T.A. 1984. Effects of progesterone on oviductal epithelium in estrogen-primed prepubertal beagles: light and electron microscopic observations. *American Journal of Anatomy*, 169:75-87.
- SEILER, J.P. 1975. Toxicology and genetic effects of benzimidazole compounds. *Mutation Research*, 32:151-168.
- STEFFL, M., SCHWEIGER, M., SIGUYAMA, T. & AMSELGRUBER, W.M. 2008. Review of apoptotic and non-apoptotic events in non-ciliated cells of the mammalian oviduct. *Annals of Anatomy*, 190:46-52.
- TILTON, R.G., HOFFMANN, P.L., KILO, C. & WILLIAMSON, J.R. 1981. Pericytes degeneration and basement membrane thickening in skeletal muscle capillaries of human. *Diabetes*, 16:713-720.
- THOMAS, P.K. 1964. Changes in the endoneurial sheaths of peripheral myelinated nerve fibers during Wallerian degeneration. *Journal of Anatomy*, 98:175-182.
- TUOHIMAA, P. 1975. Immunofluorescence demonstration of avidin in the immature chick oviduct epithelium after progesterone. *Histochemie*, 44:95-101.
- VERHAGE, H.G., MAVROGIANIS, P.A., BOICE, M.L., LI, W. & FAZLEABAS, A.T. 1990. Oviductal epithelium of the baboon: hormonal control and the

- immunogold localization of oviduct specific glycoproteins. *American journal of Anatomy*, 187: 81-90.
- VRACKO, R & BENDITT, EP. 1972. Basal lamina: scaffold for orderly cell replacement. *Journal of Cell Biology*, 55:406-419.
- WASTENEYS, G.O., CADRIN, M., REUHL, K.R., BROWN, D.L. (1988). The effects of methylmercury on the cytoskeleton of murine embryonal carcinoma cells. *Cell Biology and Toxicology*, 4:41-60
- WILLIAMS, T.D. & AMES, C.E. 2004. Top-down regression of the avian oviduct during late oviposition in small passerine birds. *The Journal of Experimental Biology*, 207:263-268.
- WINDER, B.S., STRANDGAARD, C.S. & MILLER, M.G. 2001. The role of GTP Binding and microtubule-associated proteins in the inhibition of microtubule assembly by carbendazim. *Toxicological Science*, 59:138-146.
- WYBURN, G.M., JOHNSTON, H.S., DRAPER, M.H. & DAVIDSON, M.F. 1970. The fine structure of the infundibulum and magnum of the oviduct of *Gallus domesticus*. *Quarterly Journal of Experimental Physiology*, 55:213-232.
- YU, J.Y.-L. & MARQUARDT, R.R. 1973: Development, cellular growth and function of the avian oviduct: studies on the magnum during a reproductive cycle of the domestic fowl (*Gallus domesticus*). *Biology of Reproduction*, 8:283-298.

CHAPTER FOUR

The effect of carbendazim on the structure of the shell gland in the sexually mature Japanese quail: histological, immunohistochemical and ultrastructural study

4.1 Introduction

It is known that the avian egg remains in the shell gland for approximately 20 -22 hours (Wyburn, Johnston, Draper & Davidson, 1973; Richardson 1935 cited by Gilbert, 1979; Fernandez, Moya, Lopez & Arias, 2001). During this period, various organic and inorganic components are added to the eggshell (Arias, Fink, Xiao, Heuer & Caplan, 1993). Several studies have been carried out on the morphology of the shell gland in the domestic fowl (Johnston, Aitken & Wyburn, 1963; Wyburn *et al.*, 1973; Bakst & Howarth, 1974), Japanese quail (Tamura & Fujii, 1966; cited by Gilbert, 1979), mature ostrich (Muwazi, Baranga, Kayanja & Schliemann, 1982), immature ostrich (Madekurozwa, 2007) and rhea (Parizzi, Santos, Oliviera, Maia, Sousa, Miglino & Santos, 2008).

Macroscopically, the shell gland is organized into two parts: a proximal tubular shell gland (*pars cranialis uteri*) and a distal shell gland pouch (*pars major uteri*). Each part performs specific physiological functions. For example, according to a report by Stemberger, Mueller & Leach (1977) the formation of mammillary knobs occurs in the proximal tubular shell gland. In the distal shell gland pouch, the deposition of calcium carbonate, addition of fluid to the albumen (plumping) and pigmentation take place.

Microscopically, the shell gland consists of four distinct layers: *tunica mucosa*, *tela submucosa*, *tunica muscularis* and *tunica serosa*. The mucosal layer, lined by a pseudostratified columnar epithelium, is in contact with the lumen (Wyburn *et al.*, 1973). The epithelium consists of both ciliated and non-ciliated cells. The ciliated cells contain centrally located nuclei, whereas the nuclei of the non-ciliated cells are situated basally (Wyburn *et al.*, 1973). Basal cells and mitochondrial cells are also present in the epithelium (Madekurozwa, 2007).

Underlying the luminal epithelium is the *lamina propria-submucosa*. The layer contains tubular glands (*glandulae uterinus*) and loose connective tissue. Below the *lamina propria-submucosa* is the *tunica muscularis*, which consists of inner circular and outer longitudinal smooth muscle layers. The *tunica serosa* forms the outermost layer of the shell gland. This layer is composed of a simple squamous epithelium and loose connective tissue.

The formation and deposition of organic and inorganic components of the eggshell is a complex process, which involves different cell types. Studies on the domestic fowl have shown that tubular gland cells are involved in calcium transport (Johnston *et al.* 1963; Wyburn *et al.*, 1973). A further study by Hodges (1974) showed that non-ciliated epithelial cells synthesize and release the protein components of the shell matrix. Researchers have shown that the shell gland is particularly sensitive to environmental contaminants, such as 1,1,1-trichloro-2,2-bis(*p*-chlorophenyl)ethane (Friedenbach & Davidson, 1977) and methyl mercury (Balachandran, Batngar & Gcissing, 1985). There is currently a paucity of information on the effect of the environmental contaminant and cytoskeleton disrupting agent carbendazim on the morphology and function of the various cells in the shell gland. Therefore, in this Chapter, morphological changes occurring in the shell gland post-exposure to carbendazim, in the sexually mature Japanese quail, are described.

4.2. Materials and methods

A total of 102 sexually mature female Japanese quails were used in this study. The study was composed of two experiments as described in Chapter One.

4.2.i. Histology

Tissue samples used in this study were collected from the shell gland pouch region. The samples were fixed in 10% buffered formalin for 48 hours. Thereafter, the tissue samples were processed routinely for light microscopy following the standard procedures described in Chapter One.

4.2.ii. Immunohistochemistry

Formalin-fixed and paraffin wax-embedded sections were used in the current study. The tissue sections were processed and immunostained using a LSAB plus kit (Dakocytomation, Denmark) following the standard technique described in Chapter One.

4.2.iii. Transmission and Scanning electron microscopy

Tissue samples from the shell gland were immersion-fixed in 2.5% glutaraldehyde in 0.1M Millonig's buffer (pH 7.3) for 24 hours. Thereafter, the tissue samples were post-fixed in 2% osmium tetroxide. Following post-fixation, samples were processed for transmission electron microscopy (TEM) and scanning electron microscopy (SEM) using standard techniques.

4.3. Results

4.3.1 Tissue morphometry

4.3.1.i Control birds

Morphometrical parameters measured in the control and carbendazim-treated birds are summarized in Table 4.1. The primary folds were between 91.08 μ m and 479.09 μ m in height. The mean height of the luminal epithelium was 26.91 \pm 0.38 μ m. The width of the tubular glands ranged from 10.08 μ m to 26.92 μ m.

4.3.1.ii Carbendazim-treated birds

4.3.1.ii.a. Experiment I (Dose-dependent oviductal degeneration)

The aim of this experiment was to establish the minimum effective dose of carbendazim that would cause pathological changes within 48 hours post-exposure.

There was a general decrease in the height of the primary mucosal folds post-exposure to carbendazim (Table 4.1). When compared to the controls, a significant decrease in the height of the mucosal folds was observed at doses of 400 mg/kg and 800 mg/kg bodyweight carbendazim ($p < 0.05$). Significant changes in mucosal fold height were also observed between the following carbendazim treatment groups: 25mg/kg and 400mg/kg; 25mg/kg and 800mg/kg; 100mg/kg and 400mg/kg; 100mg/kg and 800mg/kg bodyweight carbendazim.

Exposure to doses such as 25mg/kg, 100mg/kg and 400mg/kg bodyweight carbendazim, reduced the height of the luminal epithelium (Table 4.1). A significant decrease in the height of the luminal epithelium was observed at doses of 100mg/kg and 400mg/kg bodyweight carbendazim ($p < 0.05$) when compared to the control. Between the carbendazim-treatment groups, a significant decrease in the height of the luminal epithelium was observed between 25mg/kg and 100mg/kg; 25mg/kg and 400mg/kg; as well as between 100mg/kg and 400mg/kg bodyweight carbendazim. In contrast, a dose of 800mg/kg bodyweight carbendazim caused a significant increase in the height of the luminal epithelium when compared to the controls ($p < 0.05$). A significant increase was also observed between 800mg/kg and the following carbendazim-treatment groups: 25mg/kg, 100mg/kg and 400mg/kg.

A reduction in the width of tubular glands was observed when the birds were exposed to 25mg/kg, 100mg/kg and 400mg/kg bodyweight carbendazim. At a dose of 800mg/kg bodyweight carbendazim, there was an increase in the width of the tubular glands (Table 4.1). When compared to the control group, a significant decrease in the width of tubular glands was observed at doses of 100mg/kg and 400mg/kg bodyweight carbendazim. The decrease was also significant between 25mg/kg and 100mg/kg bodyweight carbendazim. The increase in tubular gland width observed at 800mg/kg bodyweight carbendazim was significant ($p < 0.05$) when compared to the control group. In addition, the observed increase was also significant when compared to the following carbendazim-treatment groups: 25mg/kg, 100mg/kg and 400mg/kg.

Table 4.1: Mean \pm SE of histomorphometrical parameters in control and carbendazim-treated Japanese quails.

Carbendazim dose (mg/kg)	0	25	100	400	800
Primary fold height	320 \pm 18.65	294.84 \pm 19.3 ^b	277.51 \pm 35.09 ^c	96.82 \pm 10.43 ^{abc}	166.23 \pm 27.25 ^{abc}
Epithelium height	26.91 \pm 0.38	25.02 \pm 0.36 ^b	20.82 \pm 0.36 ^{abc}	9.91 \pm 0.11 ^{abcd}	76.12 \pm 0.95 ^{abcd}
Glandular width	17.61 \pm 0.51	16.7 \pm 0.42 ^b	6.07 \pm 0.14 ^{abc}	6.23 \pm 0.12 ^{ad}	51.64 \pm 1.25 ^{abcd}

^a Indicates a significant change from control group

^{bcd} Indicates significant changes between carbendazim-treatment groups

4.3.1.iib. Experiment II (Time-course oviductal degeneration)

Experiment II investigated the short-term (5 hours to 12 days post-exposure) and medium-term (32 days post-exposure) effects of carbendazim on the oviduct of the Japanese quail. A single dose of the minimum effective dose (400 mg/kg bodyweight carbendazim), determined in experiment I, was used.

The measured morphometrical parameters are summarized in Table 4.2 below. Carbendazim exposure caused a general decrease in the height of primary mucosal folds. When compared to the control, a significant decrease in the height of the primary mucosal folds was observed at days 8, 12 and 32 post-exposure ($p < 0.05$). A significant decrease in height was also observed between the 24 hour group and days 8, 12, as well as, day 32 post-exposure. In addition, carbendazim caused a significant decrease in the height of primary mucosal folds between day 5 and days 8, 12 and 32 post-exposure ($p < 0.05$).

The height of the luminal epithelium was also affected by carbendazim exposure. In the initial stages following carbendazim administration, there was an increase in the height of the luminal epithelium (Table 4.2). The epithelial height increase correlated with the increase in oviductal weight shown in Chapter two. This increase in luminal epithelial height was statistically significant ($p < 0.05$) at 5 hours, 24 hours and 5

days, when compared to the control group. At days 8, 12 and 32 post-exposure to carbendazim, a significant decrease in the height of the luminal epithelium was observed when compared to the following groups: control group, 24 hours and 5 days ($p < 0.05$). In addition, a significant decrease in the height of the luminal epithelium was also observed between 8 and 32 days post-exposure to carbendazim.

Similar to the observations made in the luminal epithelium, carbendazim caused an increase in the width of the tubular glands in the initial stages of exposure. An increase in glandular width was observed from 5 hours to 5 days post-exposure. From 8 to 32 days post-exposure to carbendazim, a decrease in the width of the tubular glands was observed (Table 4.2). The initial width increase was statistically significant at 5 hours, 24 hours and 5 days when compared to the control. The subsequent decrease in the width of the tubular glands was statistically significant at days 8, 12 and 32 post-exposure when compared to the control. Between the different sampling periods post-exposure to carbendazim, a significant decrease in tubular gland width was observed between 5 hours and days 8, 12 and 32 post-exposure. In addition, a significant decrease in tubular gland width was observed between 24 hours and days 8, 12 and 32 post-exposure. Between 5 days and days 8, 12 and 32 post-exposure to carbendazim, the decrease in glandular width was statistically significant ($p < 0.05$).

Table 4.2: Mean \pm SE histomorphometrical parameters observed in the control and different periods post-exposure to 400 mg/kg bodyweight carbendazim

Periods	Primary fold height (μm)	Epithelial height (μm)	Glandular width (μm)
Control	320.24 \pm 18.65	26.91 \pm 0.38	17.61 \pm 0.51
5 hrs	260.1 \pm 10.99	105.46 \pm 1.31 ^{ab}	48.01 \pm 2.35 ^{ab}
24 hrs	255.09 \pm 24.86 ^b	100.89 \pm 1.09 ^{abc}	45.74 \pm 1.36 ^{ac}
5 days	264.38 \pm 23.18 ^c	83.57 \pm 1.11 ^{abcd}	45.86 \pm 1.17 ^{ad}
8 days	131.66 \pm 7.7 ^{abc}	18.61 \pm 0.21 ^{abcde}	11.08 \pm 0.23 ^{abcd}
12 days	143.28 \pm 7.62 ^{abc}	15.47 \pm 0.28 ^{abcd}	11.83 \pm 0.27 ^{abcd}
32 days	141.49 \pm 12.14 ^{abc}	10.13 \pm 0.15 ^{abcde}	7.62 \pm 0.19 ^{abcd}

^a Differs significantly from the control ($p < 0.05$)

^{bcde} Indicates significant difference between periods post-exposure ($p < 0.05$)

4.3.2 Histological observations

4.3.2.i. Control birds

The mucosal layer was arranged in primary and secondary folds (Fig. 4.1). Simple to pseudostratified columnar epithelium lined the mucosal layer (Fig. 4.2a). The epithelium was formed by both ciliated and non-ciliated cells.

Tubular glands (*glandulae uterinae*) were observed in the *lamina propria-submucosa* of the shell gland (Fig. 4.2a). The tubular glands were lined by a simple cuboidal epithelium. The gland cells contained round nuclei surrounded by a granular eosinophilic cytoplasm. In some instances, a few vacuoles were identified in the cytoplasm. Interspersed between the tubular glands, was loose connective tissue (Fig. 4.2a).

The *tunica muscularis* was composed of inner circular and outer longitudinal layers (Fig. 4.2b). A few blood vessels were observed in the vascular zone between the two muscle layers. The outer *tunica serosa* was composed of loose connective tissue and a simple squamous epithelium.

4.3.2.ii. Carbendazim treated birds

4.3.2.ii.a. Experiment I (Dose-dependent oviductal degeneration)

No histological degenerative changes were observed in the shell gland 48 hours post-exposure to 25 mg/kg and 100 mg/kg carbendazim. Morphological changes in the tubular gland were seen at doses of 400 mg/kg and 800mg/kg bodyweight carbendazim. At a dose of 400 mg/kg carbendazim, a few pyknotic nuclei were observed in the luminal epithelium. Cells with pyknotic nuclei and cytoplasmic pallor were also observed in the tubular glands (Fig. 4.3a&b).

At a dose of 800 mg/kg bodyweight carbendazim, there was an increase in the height of the luminal epithelial cells. A few cells with pyknotic nuclei were also identified in the luminal epithelium. At this dose, wide interstitial areas containing loose connective tissue separated the tubular glands (Fig. 4.4). No degenerative changes were observed in the *tunica muscularis*.

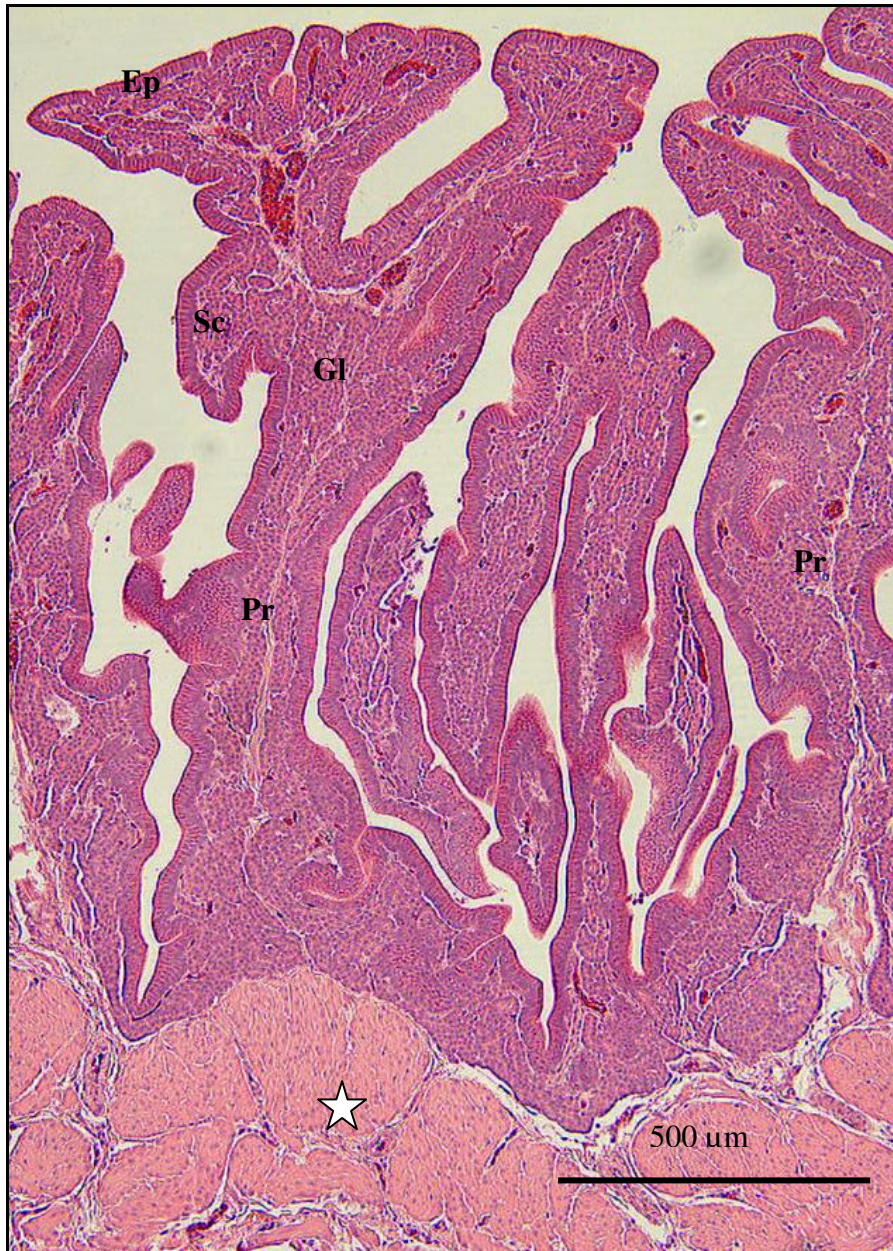


FIG. 4.1: Light photomicrograph of the mucosal layer in the shell gland of a control bird. Primary (Pr) and secondary (Sc) mucosal folds are observed. Tubular glands (GI) are observed in the *lamina propria-submucosa*. Asterisk: *tunica muscularis*. Ep: luminal epithelium. Haematoxylin and Eosin (H&E) stain.

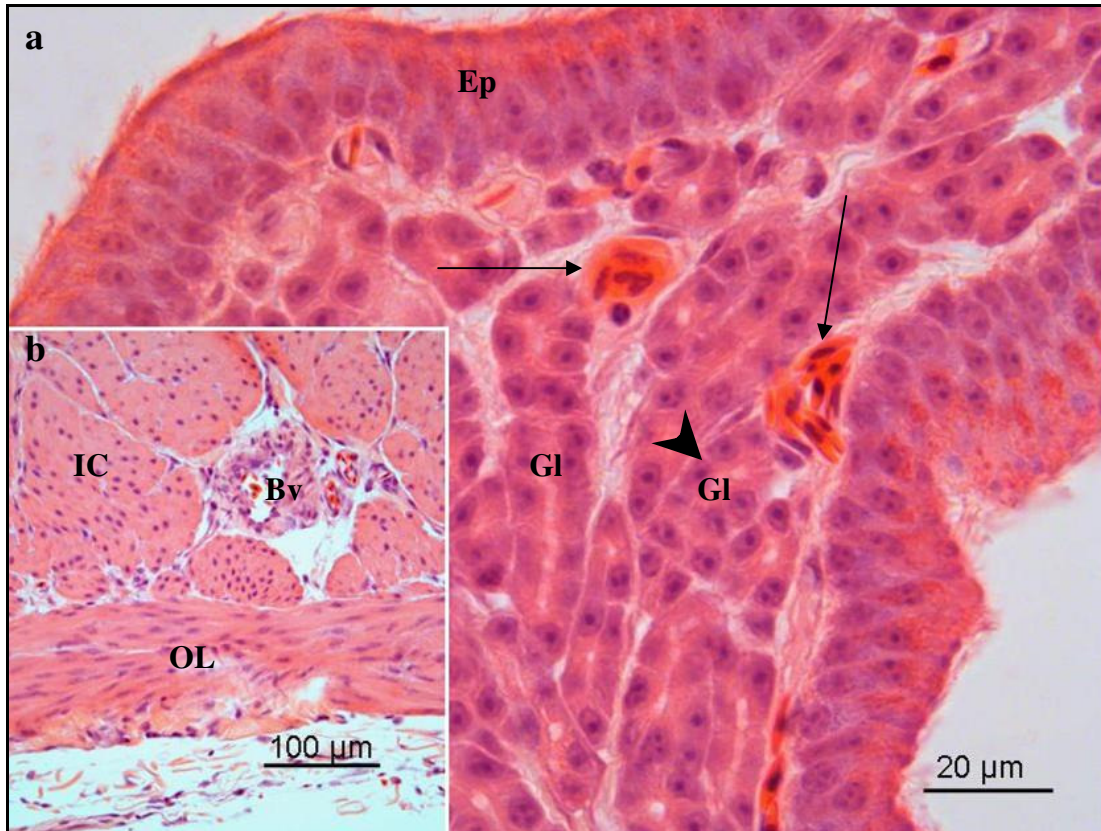


FIG. 4.2: **a.** Light photomicrograph of the mucosal layer in the shell gland of a control bird. Ep: Ciliated pseudostratified columnar epithelium. Gl: tubular glands. Arrows: blood vessels. **b.** Photomicrograph of the *tunica muscularis* containing inner circular (IC) and outer longitudinal (OL) smooth muscle layers. A blood vessel (Bv) is observed in the vascular zone between the two muscle layers. H&E stain.

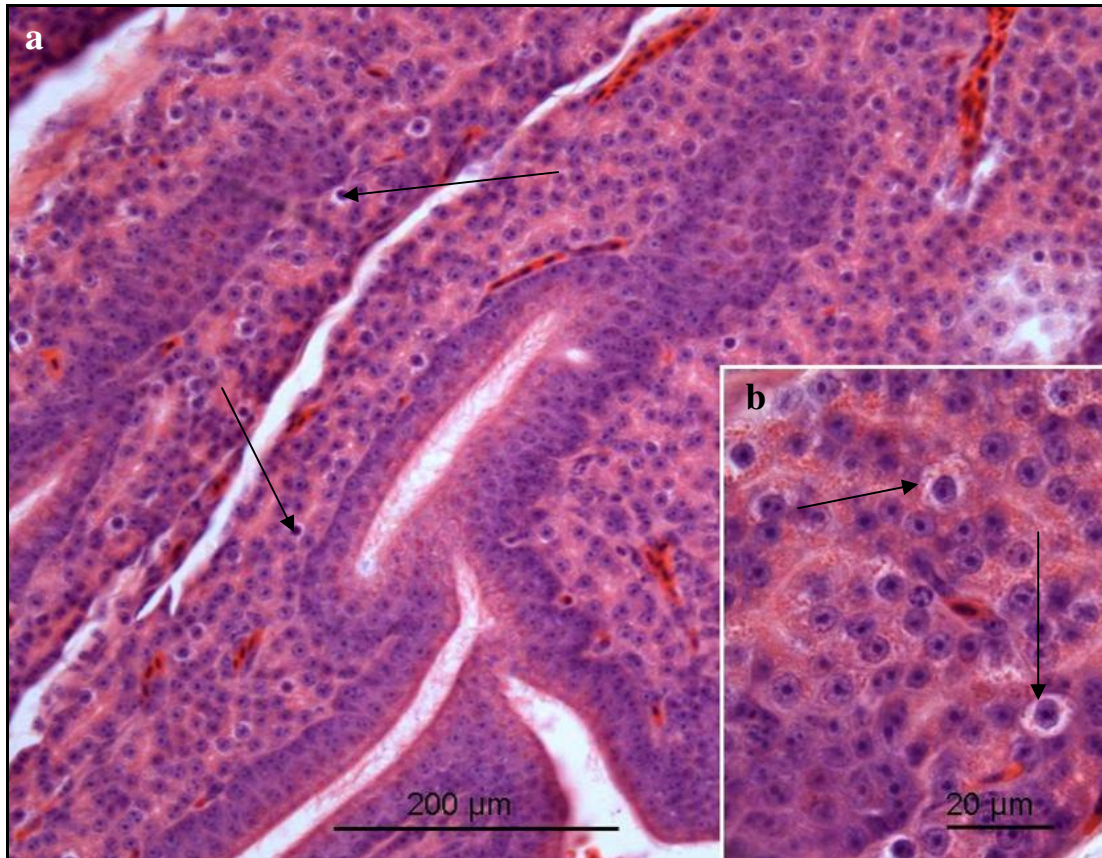


FIG. 4.3: **a.** Light photomicrographs of the mucosal layer in the shell gland of a bird treated with 400 mg/kg bodyweight carbendazim. Cells with pyknotic nuclei (arrows) are seen in degenerating gland cells. **b.** A higher magnification photomicrograph of degenerating tubular glands. A few degenerating gland cells have pale-staining cytoplasm (arrows). H&E stain.



FIG. 4.4: Light photomicrograph of the mucosal layer of the shell gland from a bird treated with 800 mg/kg bodyweight carbendazim. Note the wide interstitial areas (asterisks) between the tubular glands (GI). H&E stain.

4.3.2.iib. Experiment II (Time-course oviductal degeneration)

5 and 24 hours post-exposure

No histological degenerative changes were observed in the shell gland 5 hours post-administration of carbendazim. Twenty-four hours post-exposure to carbendazim, hyperaemia was observed in the *lamina propria-submucosa*. No degenerative changes were observed in the epithelial or glandular cells at this stage.

5 days post-exposure

Five days post-exposure to carbendazim, the mucosal layer was lined by a simple to pseudostratified columnar epithelium (Fig. 4.5a). Degenerating epithelial cells containing pyknotic nuclei and pale-staining cytoplasm were observed (Fig. 4.5a). Cells displaying cytoplasmic pallor were also observed in degenerating tubular gland cells (Fig. 4.5b). In the *lamina propria-submucosa*, hyperaemia and leukocytic infiltrations were encountered (Fig. 4.5c). Aggregations of inflammatory cells were also observed in the vascular zone between the two layers of the *tunica muscularis*.

8 days post-exposure

Eight days post-exposure to carbendazim, the luminal epithelial lining was simple to pseudostratified columnar (Fig. 4.6). In addition, degenerating epithelial cells, which exhibited pale-staining cytoplasm, pyknosis and occasionally karyolysis were observed. At this stage, hyperaemia and leukocytic infiltrations were observed in both the *lamina propria-submucosa* and vascular zone between the two muscle layers of the *tunica muscularis*.

12 days post-exposure

Twelve days post-exposure to carbendazim degenerative changes were observed in both the luminal and glandular epithelia. The luminal epithelium was simple columnar. The degenerating luminal epithelial cells contained pyknotic nuclei surrounded by pale-staining cytoplasm. A few vacuoles were also observed in the degenerating epithelial cells (Fig. 4.7a). Pyknosis and cytoplasmic pallor were also observed in degenerating gland cells (Fig. 4.7b). In some areas, atrophied tubular glands were observed. At this stage, no degenerative changes were observed in the *tunica muscularis*.

32 days post-exposure

Thirty-two days post-exposure to carbendazim, the mucosal surface was lined by simple to pseudostratified columnar epithelium (Fig. 4.8a). The epithelium was lined

by relatively few ciliated cells with intact cilia. Degenerating epithelial cells contained pale-staining cytoplasm (Fig. 4.8b). At this stage, atrophied tubular glands were observed in the *lamina propria-submucosa* (Fig. 4.8a). The atrophied tubular glands were separated by wide interstitial areas, which contained loose connective tissue (Fig. 4.8a). No degenerative changes were observed in the *tunica muscularis*.

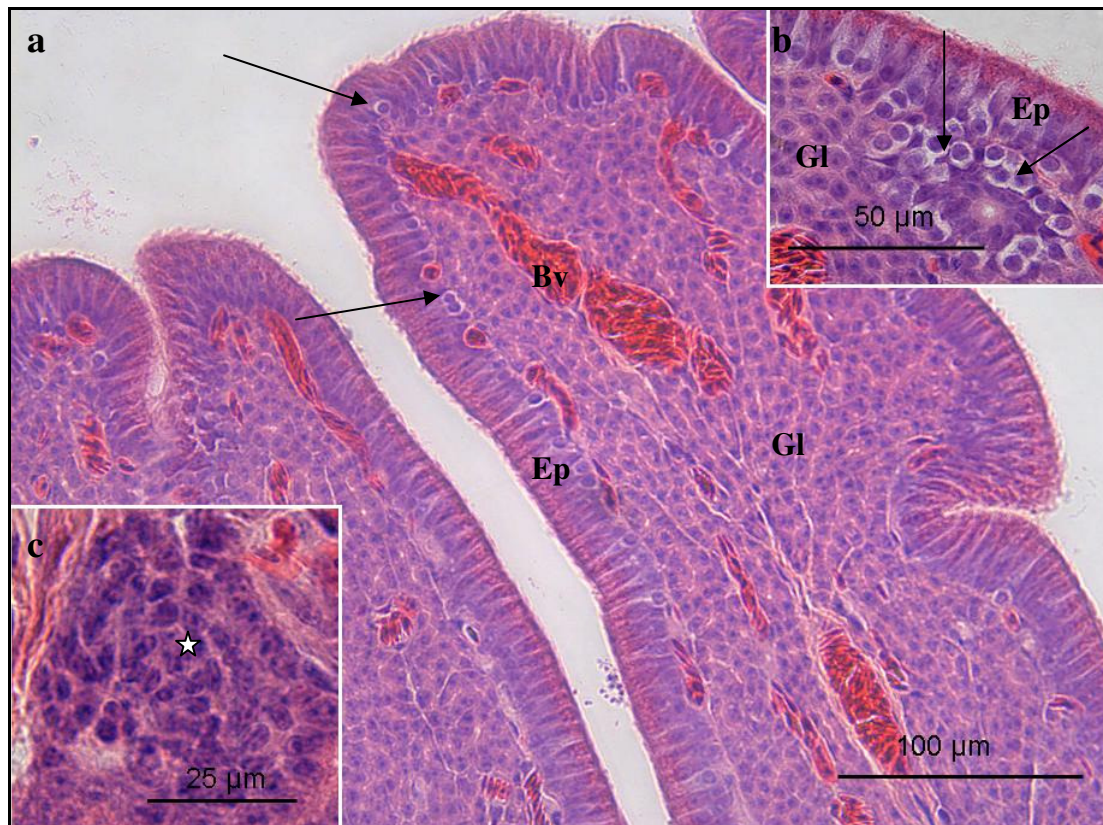


FIG. 4.5: **a.** Light photomicrograph of the mucosal layer of the shell gland, 5 days post-exposure to 400 mg/kg bodyweight carbendazim. A simple columnar epithelium (Ep) lines the mucosa. Arrows: degenerating epithelial cells. Gl: tubular glands; Bv: blood vessels in the *lamina propria-submucosa*. **b.** A higher magnification photomicrograph of the luminal epithelium (Ep) and tubular glands (Gl) in the shell gland. Degenerating gland cells (arrows) contain pale-staining cytoplasm. **c.** Photomicrograph of a leukocytic aggregation (asterisk) in the *lamina propria-submucosa*. H&E stain.

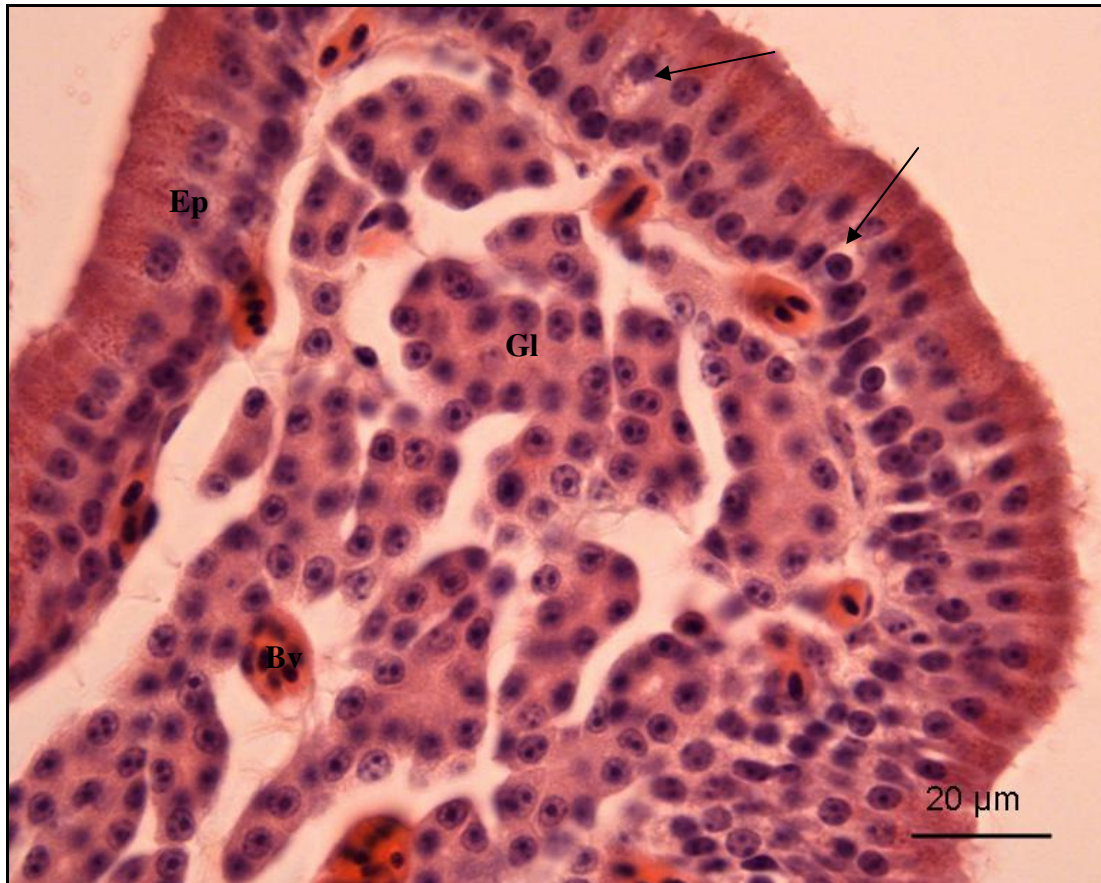


FIG. 4.6: Light photomicrograph of the mucosal layer in the shell gland, 8 days post-exposure to 400 mg/kg bodyweight carbendazim. Mucosal surface is lined by pseudostratified columnar epithelium (Ep). Cells with cytoplasmic pallor (arrows) are observed in the luminal epithelium. Gl: tubular glands; Bv: blood vessels. H&E stain.

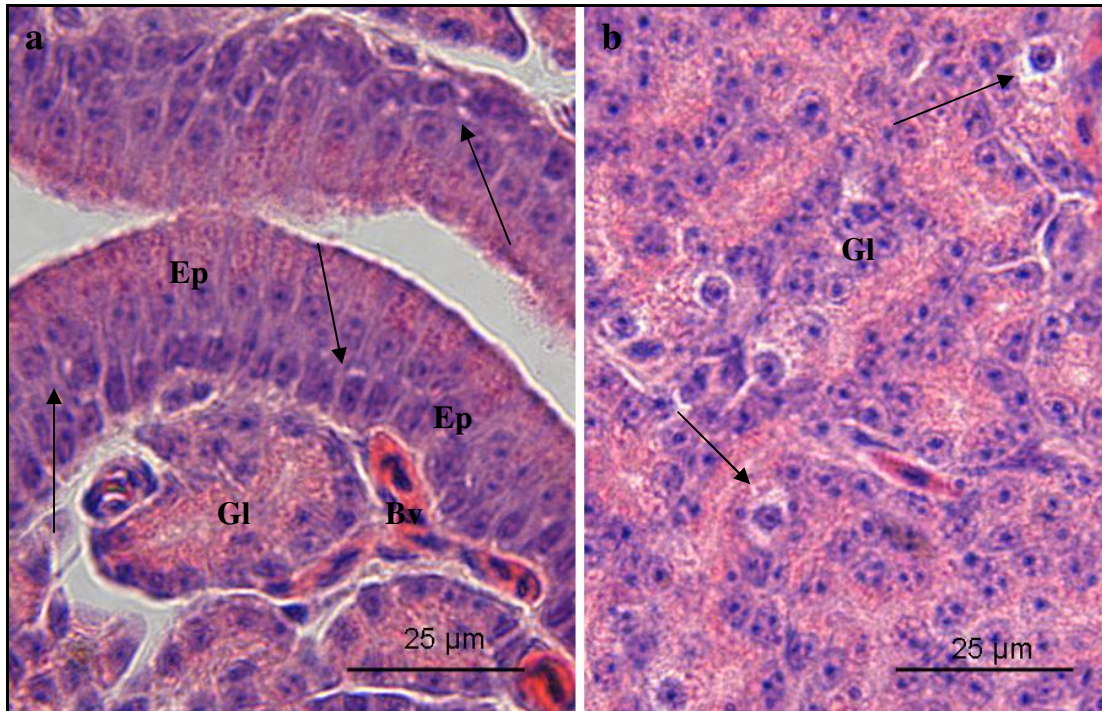


FIG. 4.7: Light photomicrographs of the mucosal layer in the shell gland, 12 days post-exposure to 400 mg/kg bodyweight carbendazim. **a.** Small vacuoles (arrows) are observed in epithelial cells (Ep). Note that at this stage relatively few cilia line the epithelial cells. Gl: tubular gland; Bv: blood vessel. **b.** Degenerating tubular glands (Gl). Cells with pale-staining cytoplasm (arrows) are evident in these glands. H&E stain.

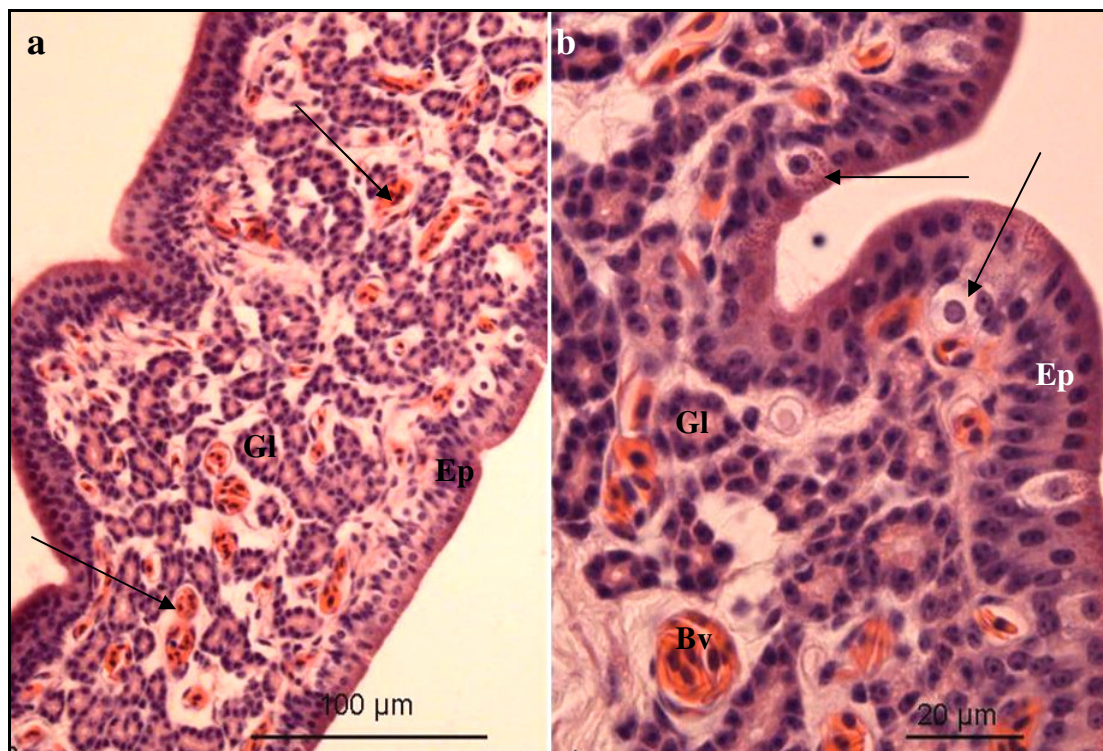


FIG. 4.8: Light photomicrographs of the mucosal layer in the shell gland, 32 days post-exposure to 400 mg/kg bodyweight carbendazim. **a.** Simple to pseudostratified columnar epithelium lined the mucosa. Note relatively few cilia on the epithelium (Ep). Gl: atrophied tubular glands separated by wide interstitial areas. Arrows: blood vessels. **b.** A higher magnification photomicrograph, of the mucosal layer in the shell gland, showing degenerating cells (arrows) in the luminal epithelium (Ep). Gl: tubular glands; Bv: blood vessel. H&E stain.

4.3.3 Histochemistry

The staining intensity for Periodic Acid Schiff (PAS) and Alcian blue recorded in the control and carbendazim-treated birds is summarized in Tables 4.3 a & b. The PAS and Alcian blue staining pattern in the luminal and glandular epithelial cells for each group is detailed below.

4.3.3.i Control birds

A strong reactivity for PAS was observed in the ciliated and non-ciliated cells of the luminal epithelium (Fig. 4.9). Strong PAS staining was limited to the supranuclear regions of the cells (Fig. 4.9). Weak PAS staining was observed in the cytoplasm of

the tubular gland cells. The luminal contents of the majority of tubular glands displayed strong PAS staining. There was no staining for alcian blue in either the luminal or glandular epithelia of the control birds.

4.3.3.ii Carbendazim-treated birds

4.3.3.iii Experiment I

25 mg/kg and 100 mg/kg bodyweight carbendazim

Birds exposed to 25 mg/kg bodyweight carbendazim displayed a PAS/alcian blue staining pattern which was similar to that observed in the control group. At a dose of 100mg/kg bodyweight carbendazim, moderate staining for PAS was exhibited by the non-ciliated luminal epithelial cells (Fig. 4.10a; Table 4.3a). PAS reactive granules were observed in the apical cytoplasmic regions of ciliated cells (Fig. 4.10b). No alcian blue staining was observed in the luminal epithelium. The tubular gland cells showed a weak reaction for PAS and a negative reaction for alcian blue.

400 mg/kg bodyweight carbendazim

At a dose of 400 mg/kg bodyweight carbendazim staining for PAS in the luminal epithelium was weak to moderate (Fig. 4.11a). At this dose, an area of moderate PAS staining was observed directly above the nuclei of ciliated cells. In addition PAS staining was demonstrated directly below the apical plasma membrane. No alcian blue reaction was observed in either the luminal or glandular epithelium at this dose. The tubular gland cells displayed weak PAS staining.

800 mg/kg bodyweight carbendazim

At a dose of 800 mg/kg bodyweight carbendazim, reactivity for PAS in the luminal epithelium varied from moderate to absent (Fig. 4.11b). At this dose, several ciliated cells were negative for PAS. The luminal epithelial cells were negative for alcian blue. No PAS or alcian blue reaction was observed in the tubular gland cells.

Table 4.3a: PAS/Alcian blue staining intensity in the shell gland of control and carbendazim-treated Japanese quails

Carbendazim dose (mg/kg)		0	25	100	400	800
Ciliate cells	PAS	+++	+++	+	+ / +++	-
	Alcian blue	-	-	-	-	-
Non-ciliated cells	PAS	+++	+++	++	+ / +++	++ / -
	Alcian blue	-	-	-	-	-
Gland cells	PAS	+	+	+	+	-
	Alcian blue	-	-	-	-	-

The staining intensities were graded subjectively as follows: - = absent; + = weak; ++ = moderate; +++ = strongly positive

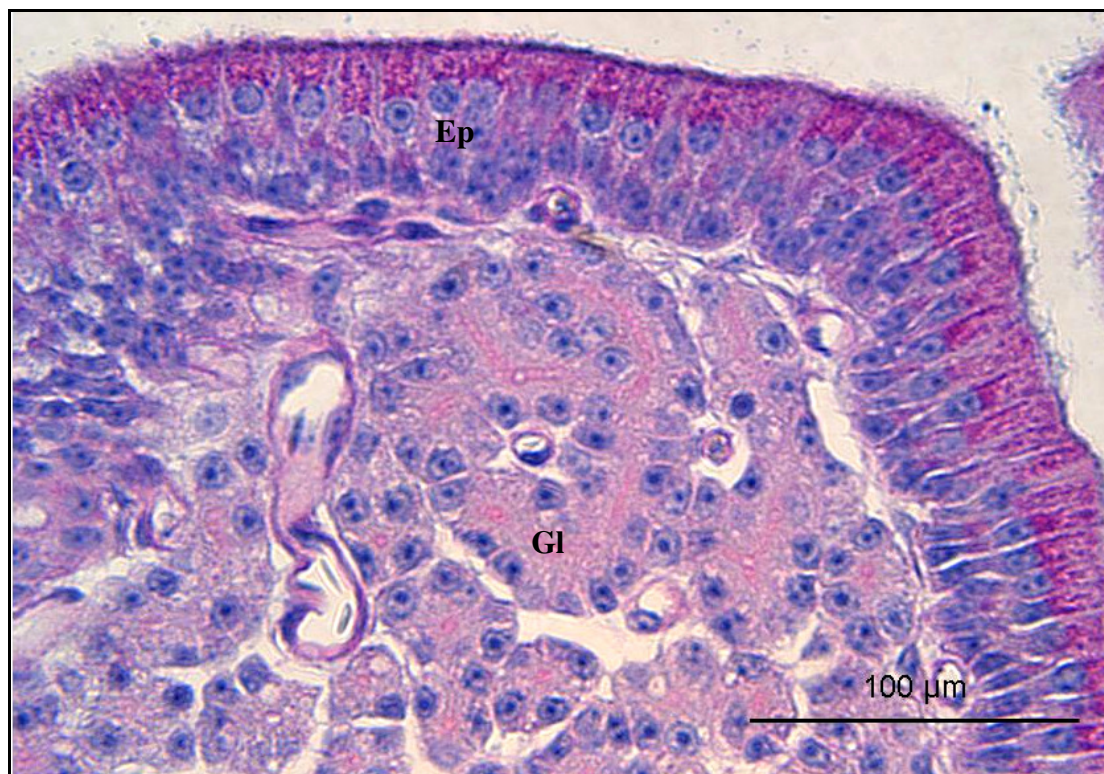


FIG. 4.9: Light photomicrograph of the mucosal layer in the shell gland of a control bird. A strong PAS reaction is observed in the epithelial cells (Ep). Staining for PAS is also observed in the lumina of tubular glands (Gl). Periodic Acid Schiff (PAS) and Alcian blue (Ab) stains.

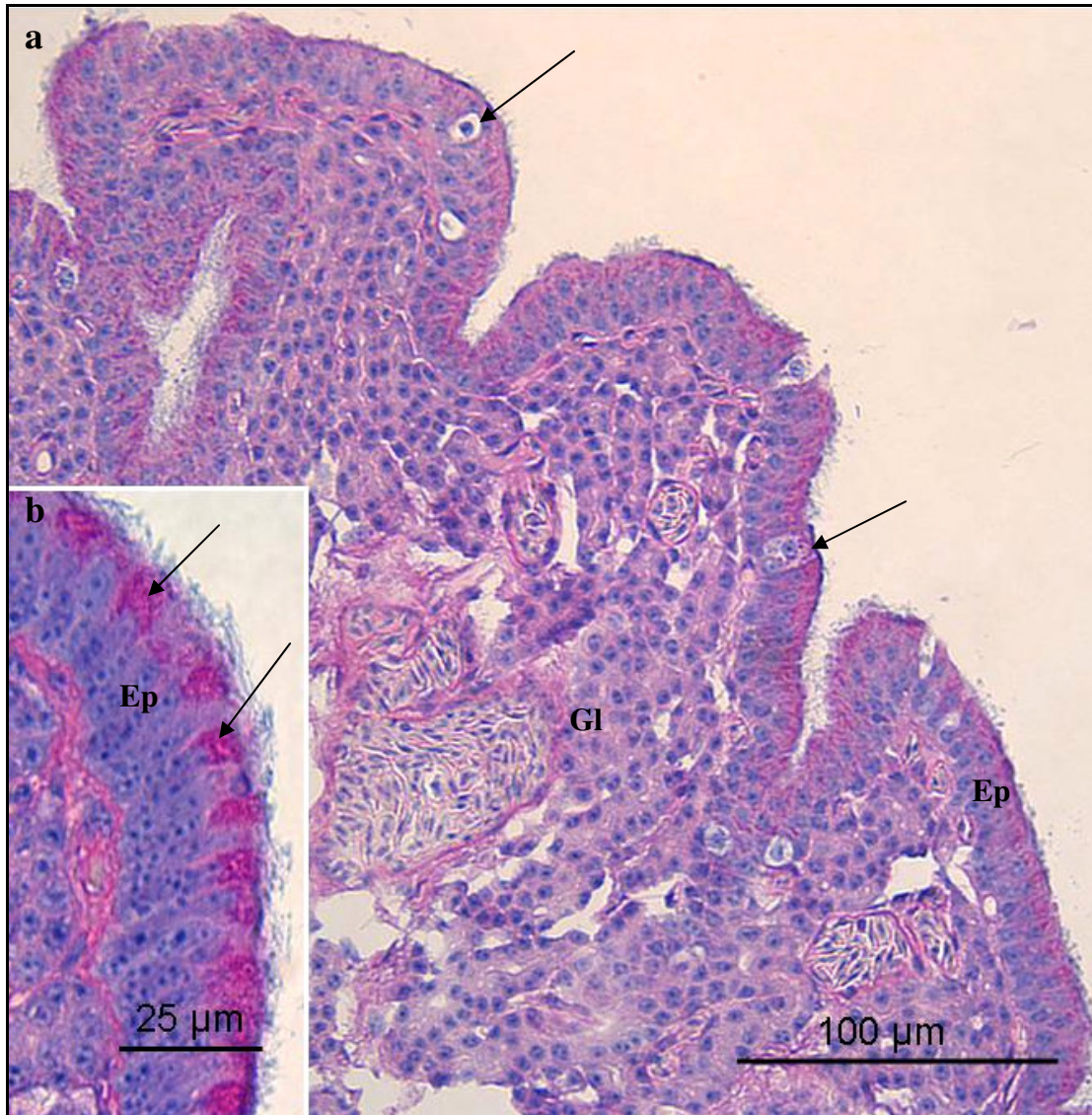


FIG. 4.10: **a.** Light photomicrograph of the mucosal layer in the shell gland of a bird treated with 100 mg/kg bodyweight carbendazim. A moderate PAS reaction is observed in the luminal non-ciliated epithelial cells (Ep). PAS staining tubular gland cells (GI) is weak to absent. Arrows: swollen epithelial cells. **b.** A higher magnification photomicrograph of the luminal epithelium (Ep). PAS positive granules (arrows) are concentrated in the apical cytoplasmic regions. Note that at this dose PAS staining in non-ciliated cells is weak. PAS/Ab stains.

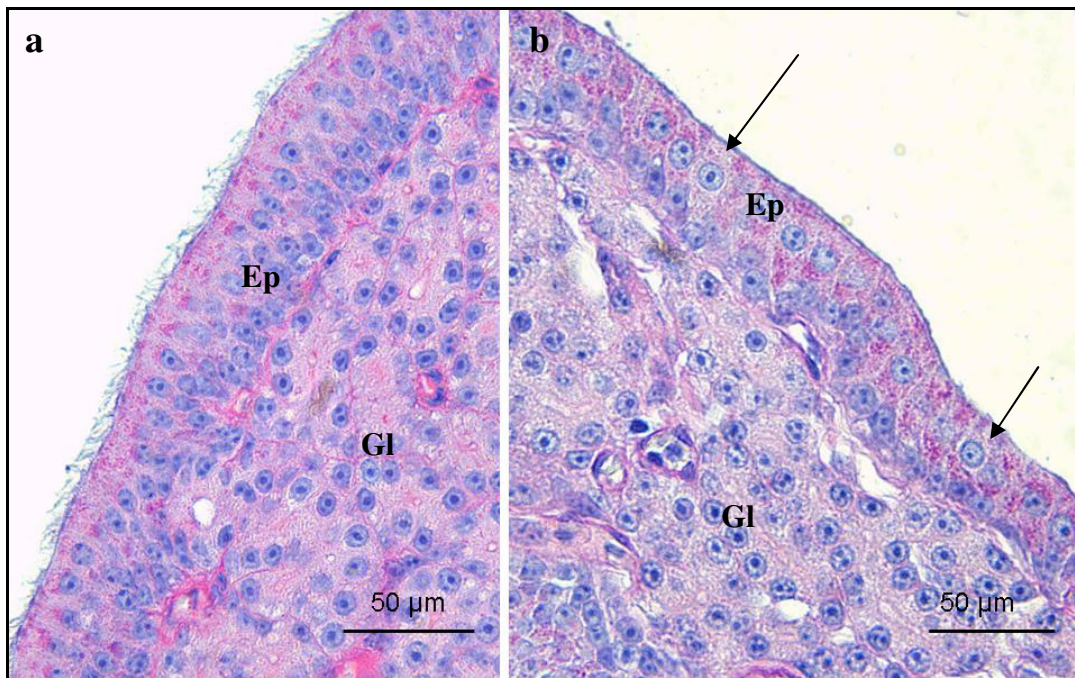


FIG. 4.11: Light photomicrographs of the mucosal layer in the shell gland of a bird treated with (a) 400 mg/kg and (b) 800 mg/kg bodyweight carbendazim. In photomicrograph (a) a weak to moderate PAS staining reaction is observed. Some ciliated cells (arrows) in (b) are negative for PAS. A few basal cells are PAS positive in both a&b photomicrographs. Ep: luminal epithelium; GI: tubular glands. PAS/Ab stain.

2.3.3.iib Experiment II

5 and 24 hours post-exposure

Five and twenty-four hours post-exposure to 400 mg/kg bodyweight carbendazim, a strong reaction for PAS was observed in both the ciliated and non-ciliated cells of the luminal epithelium (Table. 4.3b). Tubular gland cells displayed weak PAS staining. No alcian blue reactive product was observed in either the luminal or glandular epithelial cells.

5 days post-exposure

Five days post-exposure to carbendazim, a strong to moderate PAS reaction was observed in the luminal ciliated epithelial cells (Fig. 4.12). PAS staining in non-ciliated cells was weak to absent. The luminal epithelial cells were negative for alcian

blue. PAS reactivity in the tubular gland cells was weak to absent. No reactivity for alcian blue was observed in tubular gland cells.

8, 12 and 32 days post-exposure

At days 8, 12 and 32 post-exposure to carbendazim, a weak PAS reaction was observed in the luminal ciliated epithelial cells (Table 4.3b). The PAS reactive granules were concentrated in the apical cytoplasmic regions (Fig. 4.13). PAS staining in tubular gland cells was weak or absent. No reactivity for alcian blue was detected in the luminal or glandular epithelial cells.

Table 4.3b: PAS/Alcian blue staining intensity in the shell gland at different periods post-exposure to 400 mg/kg bodyweight carbendazim

Time periods		5 hrs	24 hrs	5 days	8 days	12 days	32 days
Ciliate cells	PAS	+++	+++	+++/**	+	+	+
	Alcian blue	-	-	-	-	-	-
Non-ciliated cells	PAS	+++	+++	+/-	+/-	+/-	+/-
	Alcian blue	-	-	-	-	-	-
Gland cells	PAS	+	+	+/-	+/-	+/-	+/-
	Alcian blue	-	-	-	-	-	-

The staining intensities were graded subjectively as follows: - = absent; + = weak; ++ = moderate; +++ = strongly positive.

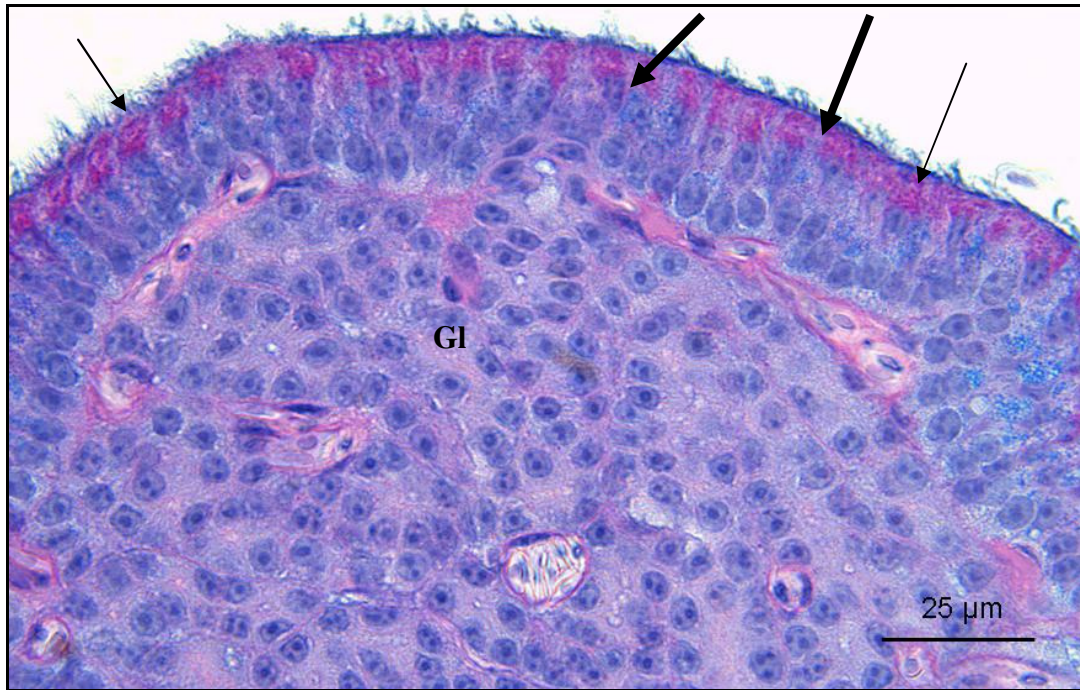


FIG. 4.12: Light photomicrograph of the shell gland mucosal layer, 5 days post-exposure to 400 mg/kg bodyweight carbendazim. Thin arrows: strong to moderate PAS in the apical cytoplasmic regions of the ciliated cells. Thick arrows: weak to negative PAS in non-ciliated cells. GI: gland cells. PAS/Ab stains.

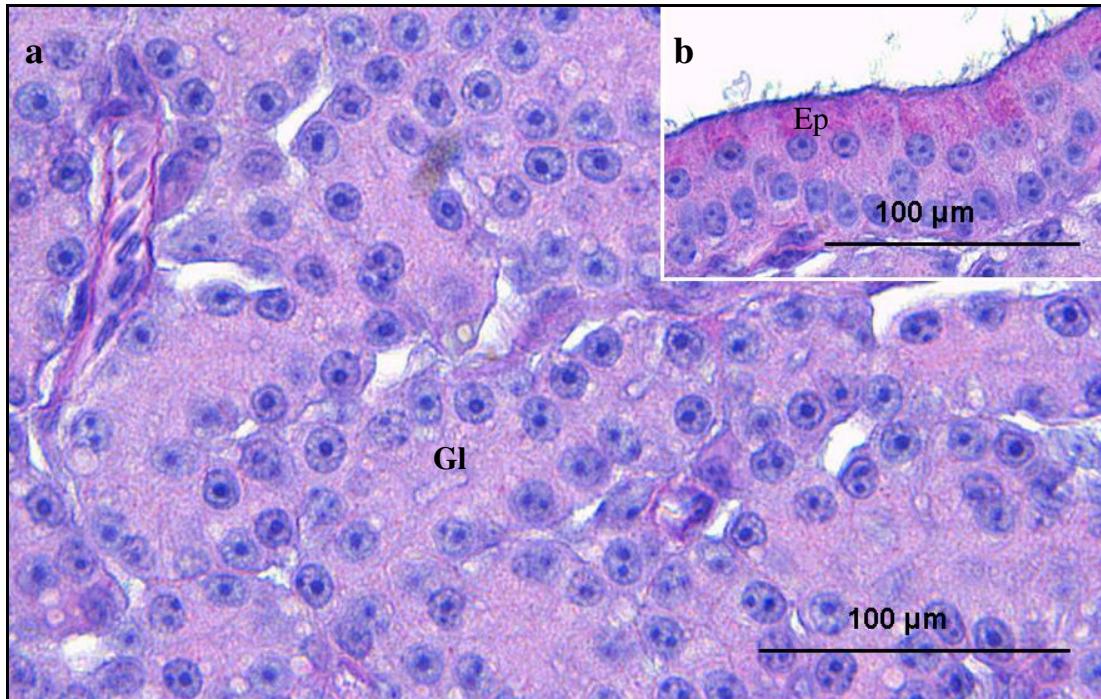


FIG. 4.13: Light photomicrograph of the mucosal layer in the shell gland, 8 days post-exposure to 400 mg/kg bodyweight carbendazim. **a.** PAS staining reaction in the gland cells (Gl) is weak to absent. **b.** The epithelial cells (Ep) contain PAS positive granules in the apical cytoplasmic regions. PAS/Ab stains.

4.3.4 Immunohistochemistry

Immunoreactivity for e-cadherin, laminin and vimentin was assessed in the mucosal layer of the shell gland of both the control and carbendazim-treated Japanese quails. A qualitative assessment of the staining intensity was visually graded as strong (+++), moderate (++) , weak (+) or negative (-). The observed changes in staining intensity are summarized in Tables 4.4 a&b.

4.3.4.1. E-cadherin

4.3.4.1.i. Control group

A strong e-cadherin immunoreaction was observed in the cytoplasm of both ciliated and non-ciliated luminal epithelial cells. The staining were concentrated in the lateral plasma membranes (Fig. 4.14). The tubular gland cells showed moderate to weak immunostaining for e-cadherin (Fig. 4.14).

4.3.4.1.ii. Carbendazim-treated group

4.3.4.1.iii *Experiment I (dose dependent oviductal degeneration)*

25 mg/kg and 100 mg/kg bodyweight carbendazim

There was no immunohistochemical change in the mucosa of the shell gland 48 hours post-exposure to carbendazim at dosages of 25 mg/kg and 100 mg/kg bodyweight.

400 mg/kg and 800 mg/kg bodyweight carbendazim

Forty-eight hours post-exposure to carbendazim, at dosages of 400 mg/kg and 800 mg/kg bodyweight, luminal epithelial cells showed a weak to negative immunoreaction for e-cadherin (Fig. 4.15). A moderate reaction was observed in the glandular cells.

4.3.4.1.iib *Experiment II*

No immunohistochemical changes were observed in the mucosal layer of the shell gland at 5 and 24 hours post-exposure to carbendazim.

5 and 8 days post-exposure

At days 5 and 8, both luminal and glandular epithelial cells showed a weak to negative immunoreaction for e-cadherin (Fig. 4.16).

12 days post-exposure

At day 12 post-exposure to carbendazim, moderate to weak immunoreactivity for e-cadherin was evident in the luminal epithelial cells. At this stage, glandular epithelial cells were e-cadherin negative (Table 4.4b).

32 day post-exposure

At 32 days post-exposure to carbendazim, strong to moderate e-cadherin immunoreactivity was observed in the lateral plasma membrane of the luminal epithelial cells (Fig. 4.17). The glandular epithelial cells showed moderate to weak e-cadherin immunoreaction.

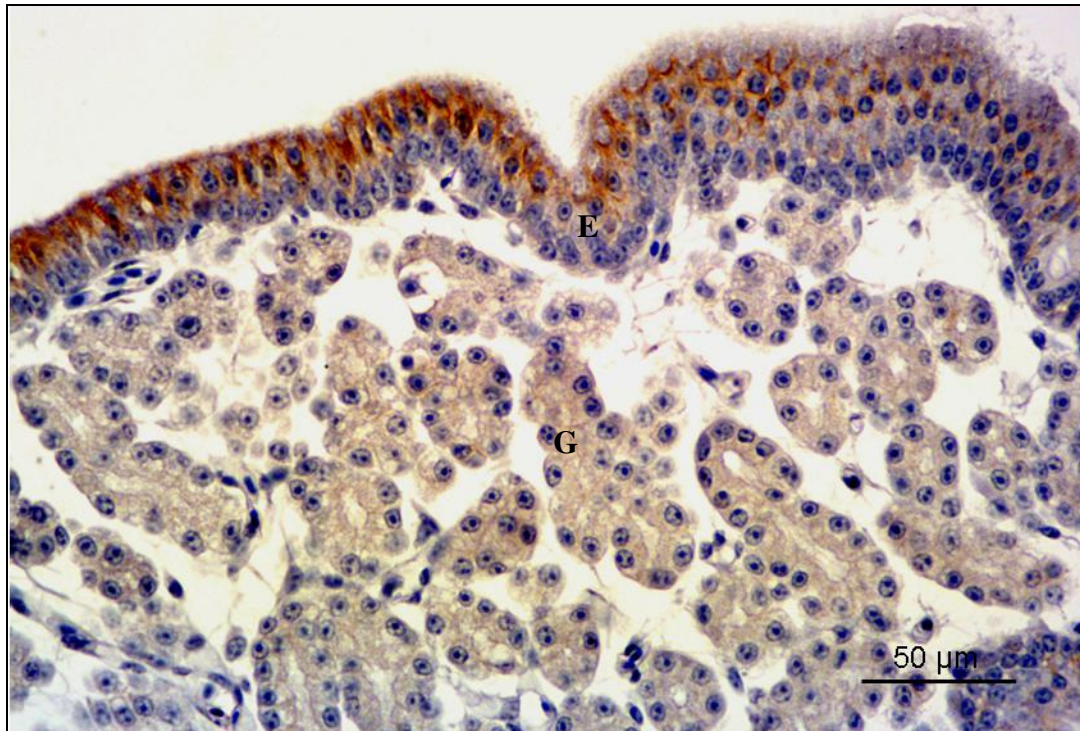


FIG. 4.14: Light photomicrograph of the shell gland from a control bird. Strong e-cadherin immunoreaction is observed in the luminal epithelium (E). Note the concentration of immunoreactive granules in the lateral plasma membrane. Weak e-cadherin immunostaining is evident in the tubular glands (G).

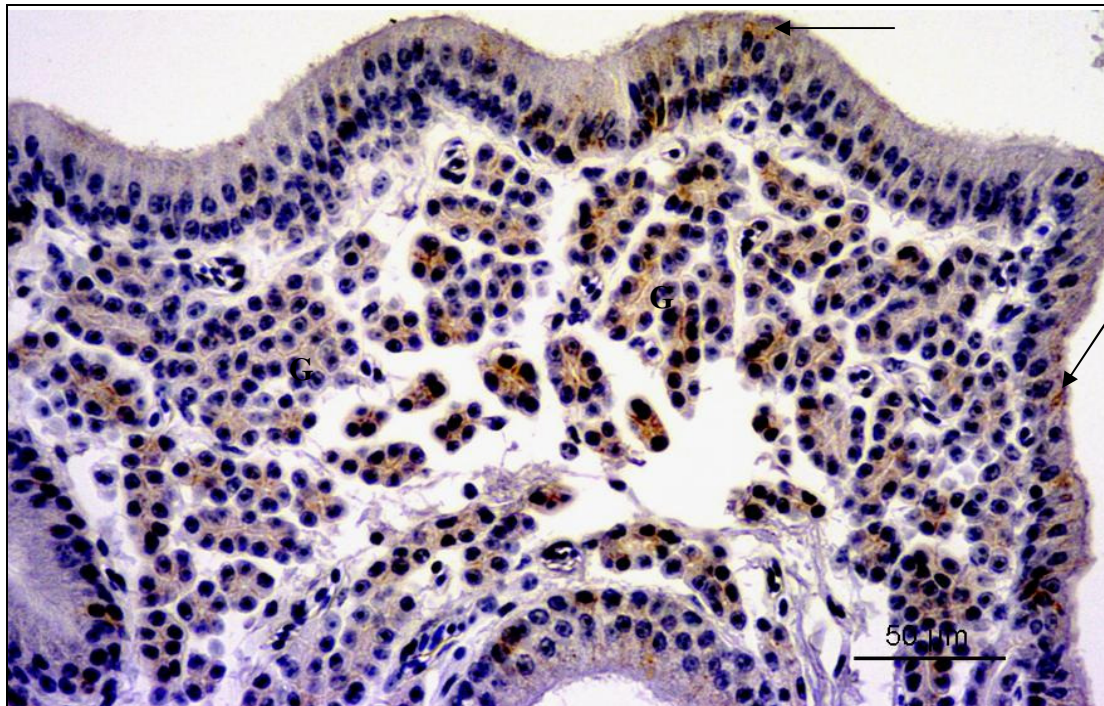


FIG. 4.15: Light photomicrograph of the shell gland from a bird treated with 800 mg/kg bodyweight carbendazim. Only a few luminal epithelial cells (arrows) show positive immunoreaction for e-cadherin. Weak to negative immunoreaction is seen in the tubular glands (G).

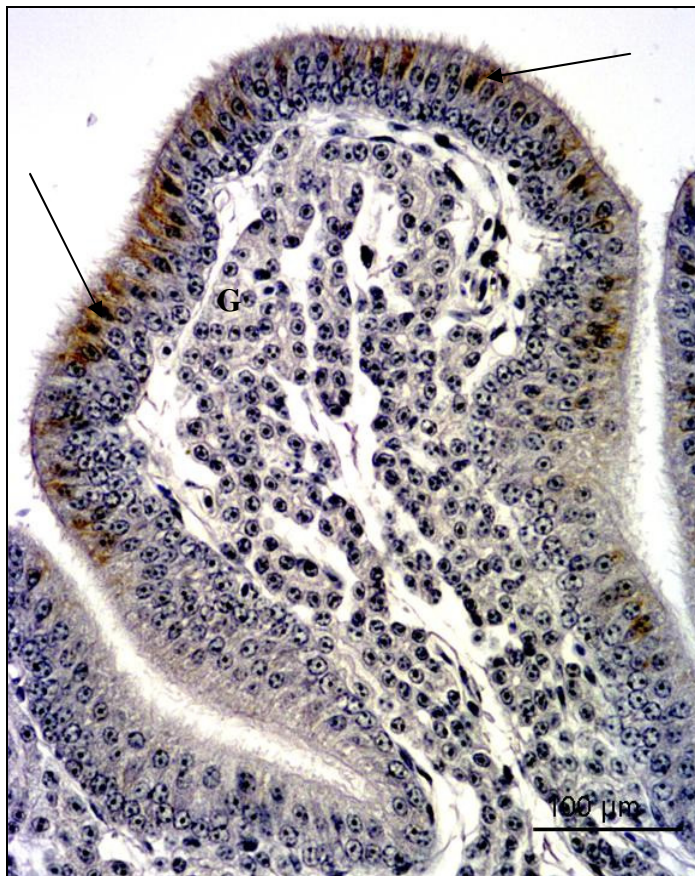


FIG. 4.16: Light photomicrograph of the shell gland 8 days post-exposure to 400 mg/kg bodyweight carbendazim. Weak to negative e-cadherin immunoreaction is observed in the luminal epithelial cells (arrows). Tubular glands (G) are negative

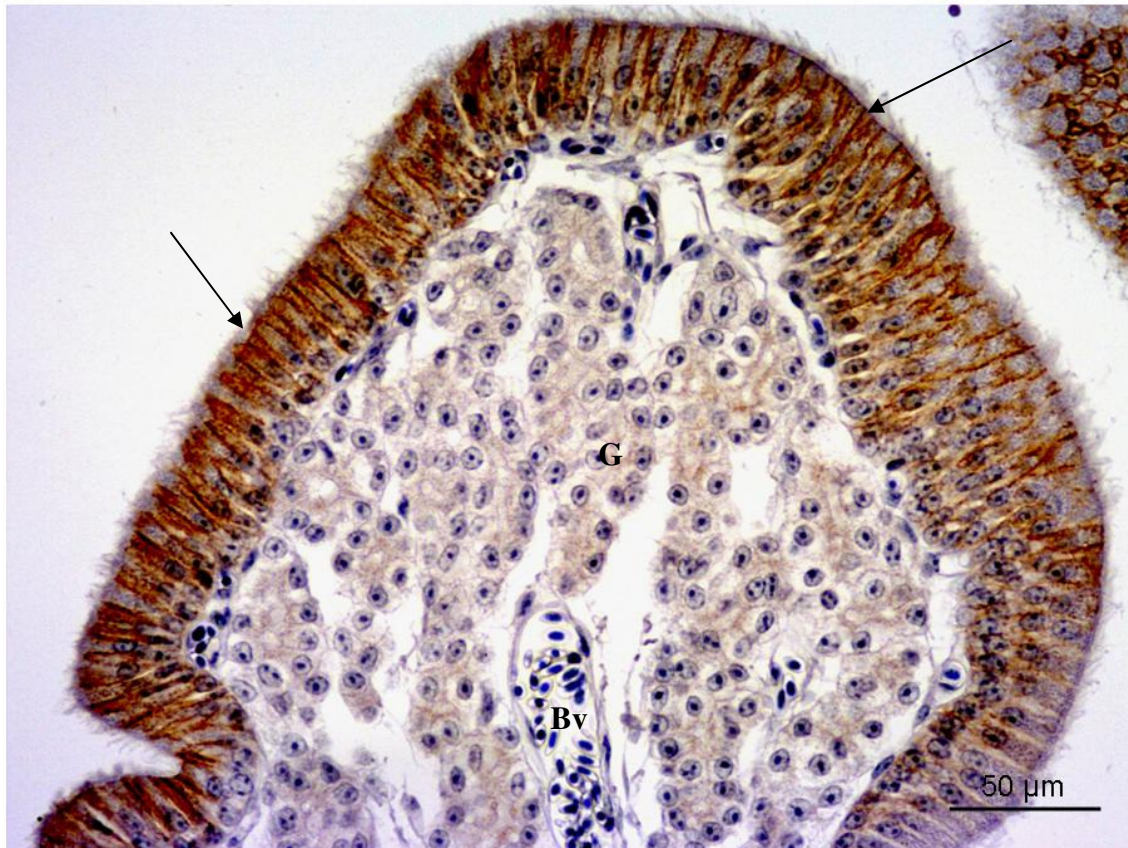


FIG. 4.17: Light photomicrograph of the shell gland 32 days post-exposure to 400 mg/kg bodyweight carbendazim. Strong immunoreaction for e-cadherin is observed in the lateral plasma membrane of the luminal epithelial cells (arrows). Tubular glands (G) show weak e-cadherin immunoreaction. Bv: blood vessel.

4.3.4.2 Laminin

4.3.4.2.i. Control group

Strong laminin immunoreaction was observed in the basement membrane underlying luminal and glandular epithelia. It was also observed in the basement membranes of the endothelium and smooth muscle cells (Fig. 4.18).

4.3.4.2.ii. Carbendazim-treated birds

4.3.4.2.ii.a *Experiment I*

25 mg/kg, 100 mg/kg and 400 mg/kg bodyweight carbendazim-treated groups

No immunohistochemical changes were observed in the mucosal layer of the shell gland 48 hours post-exposure to carbendazim at dosages of 25 mg/kg, 100 mg/kg and 400 mg/kg bodyweight (Table 4.4a).

800 mg/kg bodyweight carbendazim-treated group

Laminin immunoreaction in the basement membrane underlying luminal and glandular epithelia was weak to absent (Table. 4.4a). A moderate to weak laminin immunoreactivity was evident in the basement membrane of the endothelium and smooth muscle cells.

4.3.4.2.ii.b *Experiment II*

5 and 24 hours post-exposure

No immunohistochemical changes were observed in the basement membrane underlying the luminal epithelium, endothelium and tubular glands at 5 and 24 hours post-exposure to carbendazim.

5 and 8 days post-exposure

At t days 5 and 8 post-exposure to carbendazim, the basement membrane underlying these cells stained moderate to weak for laminin antibody (Table 4.4b).

12 days post-exposure

At day 12 post-exposure to carbendazim, a moderate to strong laminin immunoreaction was evident in the basement membrane underlying the luminal

epithelium. The glandular epithelium showed a weak to absent immunoreaction for laminin (Fig. 4.19a). At this stage, the basement membrane surrounding smooth muscle cells in the tunica muscularis stained weak to negative for laminin (4.19b).

32 days post-exposure

At 32 days post-exposure to carbendazim, the basement membrane supporting luminal and glandular epithelia appeared less conspicuous but stained strongly for laminin (Table 4.4b).

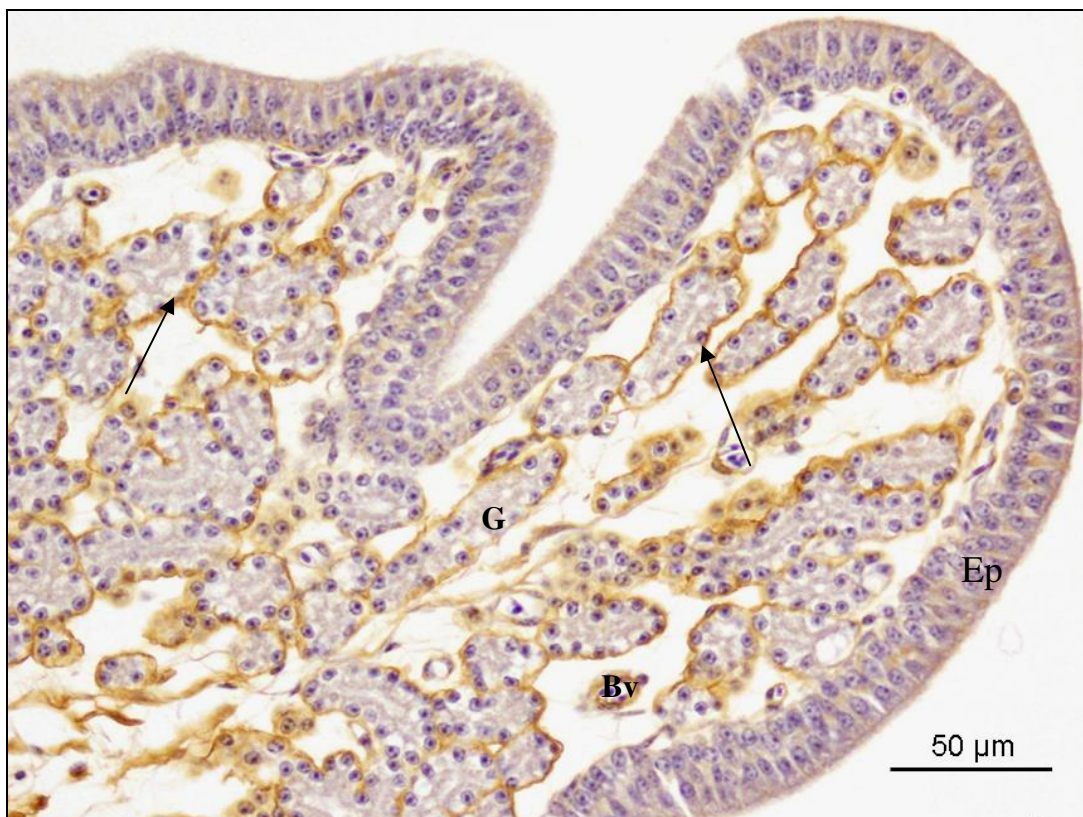


FIG. 4.18: Light photomicrograph of the mucosal layer in the shell gland of a control bird. Strong laminin immunoreactivity is observed in the basement membranes (arrows) underlying luminal epithelium (Ep), tubular glands (G) and endothelium around blood vessels (Bv).

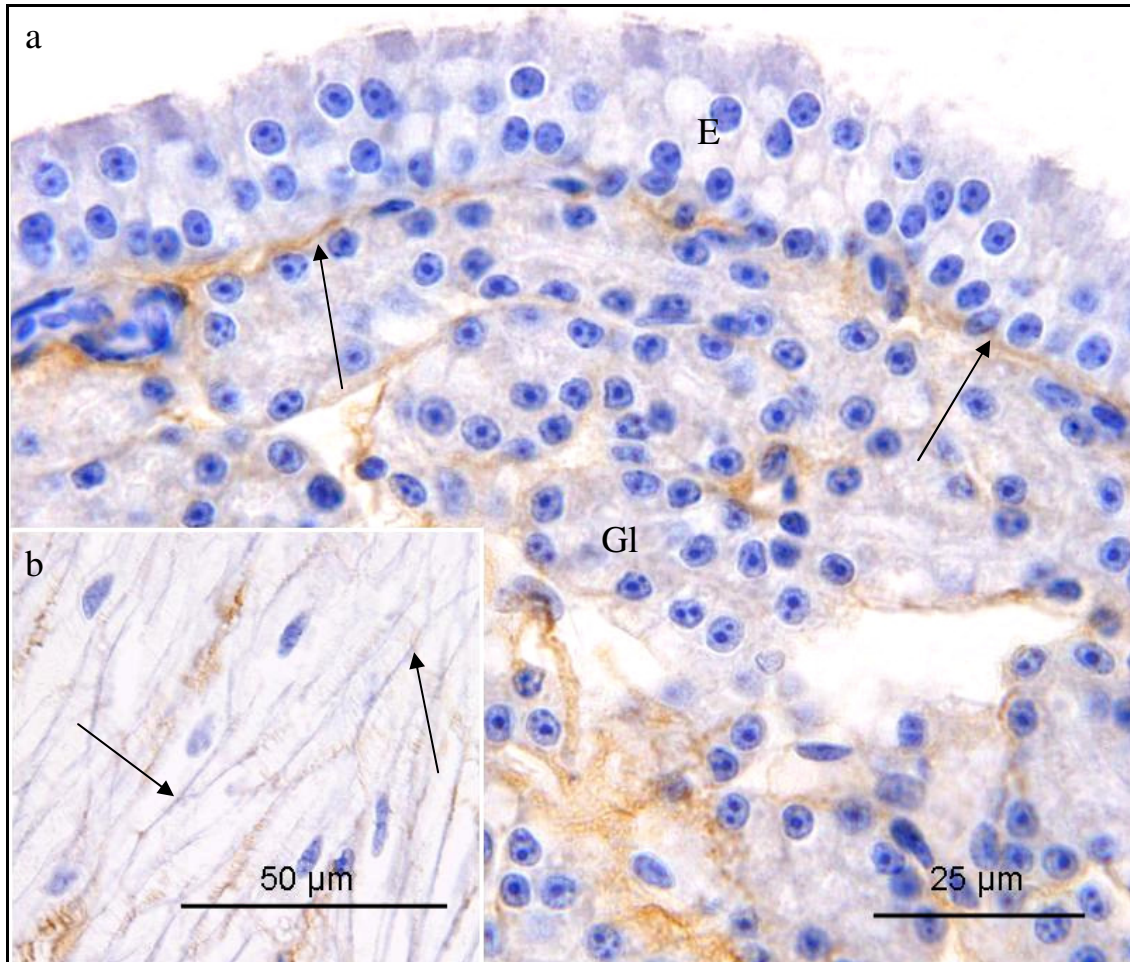


FIG. 4.19: Light photomicrographs of the mucosal layer in the shell gland, 12 days post-exposure to 400 mg/kg bodyweight carbendazim. **a.** A moderate laminin immunoreaction is observed in the basement membrane (arrows) underlying the luminal epithelium (E). The staining intensity in the basement membrane around tubular glands (G) is weak to absent. **b.** Smooth muscle cells of the *tunica muscularis*. Weak to negative laminin immunoreaction is evident in their basement membrane (arrows).

4.3.4.3 Vimentin

4.3.4.3.i Control group

Strong vimentin immunoreactivity was observed in the cytoplasm of endothelial cells lining blood vessels in the lamina propria-submucosa. Luminal epithelial cells showed weak to absent vimentin immunoreaction (Fig. 4.20). Tubular gland cells were vimentin immunonegative.

4.3.4.3.ii Carbendazim-treated birds

4.3.4.3.iii *Experiment I*

No immunoreactivity for vimentin was observed in either epithelial or tubular gland cells 48 hours post-exposure to carbendazim. However, a weak immunoreaction for vimentin was observed in the endothelial cells.

4.3.4.3.iii *Experiment II*

No vimentin immunoreactivity was observed in either epithelial or tubular gland cells following exposure to carbendazim from 5 hours up to 12 days. Vimentin immunoreactivity at these collection periods was observed only in the endothelial cells. The staining intensity decreased from moderate at 5 and 24 hours to weak at 5 and 8 days. It became moderate at day 12 post-exposure.

At day 32 post-exposure to carbendazim, epithelial cells showed weak immunoreactivity for vimentin. Tubular gland cells remained negative for vimentin. At this stage, fibrocytes and endothelial cells stained strongly for vimentin.

Table 4.4a: Immunohistochemical parameters of the control group and birds treated with different doses of carbendazim

Carbendazim dosages	e-cadherin		Laminin		Vimentin	
	Epithelium	Glands	Epithelium	Glands	Epithelium	Glands
0 (control)	+++	++/+	+++	+++	+/-	-
25 mg/kg	+++	++/+	+++	+++	-	-
100 mg/kg	+++	++/+	+++	+++	-	-
400 mg/kg	+/-	+/-	+++	+++	-	-
800 mg/kg	+/-	+/-	+/-	+/-	+	-

+++ : strong; ++ : moderate; + : weak; - : negative

Table 4.4b: Immunohistochemical parameters of the control and carbendazim-treated birds

Periods post-exposure	e-cadherin		Laminin		Vimentin	
	Epithelium	Glands	Epithelium	Glands	Epithelium	Glands
0 hour	++++	++/+	+++	+++	+/-	-
5 hours	+++	++/+	+++	+++	-	-
24 hours	+++	++/+	+++	+++	-	-
5 days	+/-	+/-	++/+	++/+	-	-
8 days	+/-	+/-	++/+	++/+	-	-
12 days	++/+	-	+++	+++	-	-
32 days	+++ / +++	++/+	+++	+++	+	-

+++ : strong; ++ : moderate; + : weak; - : negative

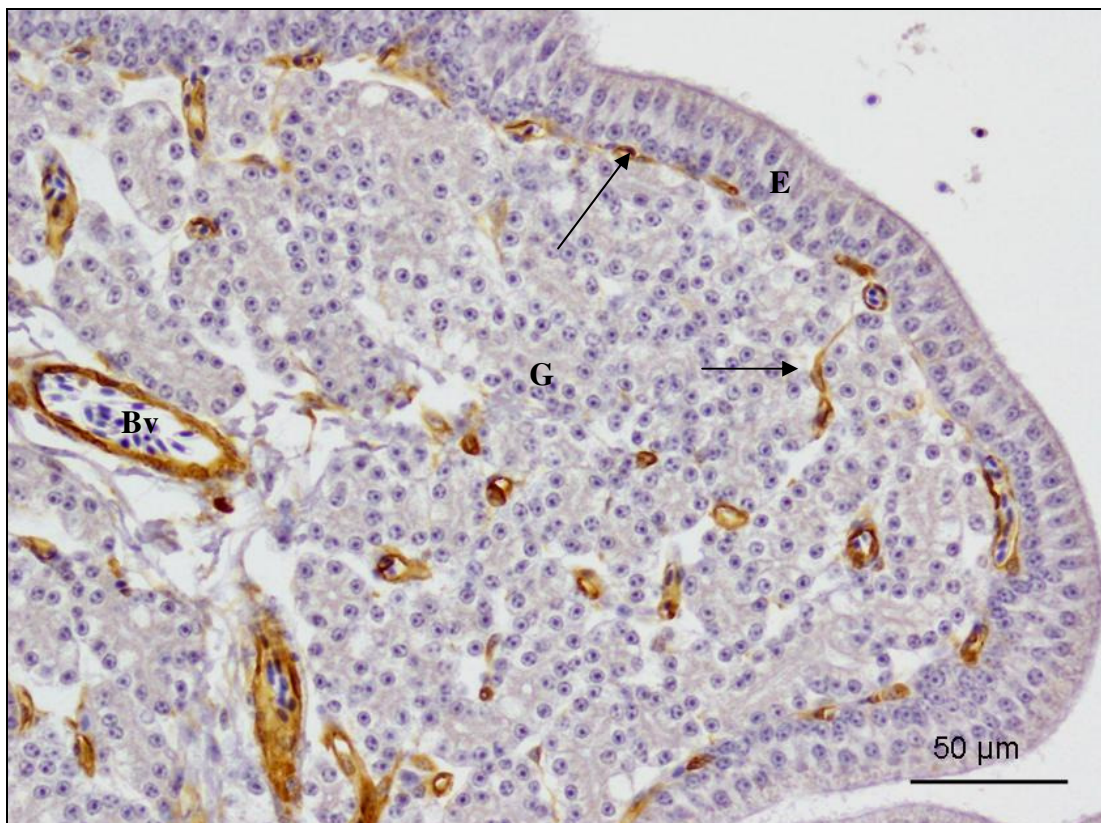


FIG. 4.20: Light photomicrograph of the shell gland from a control bird. Strong vimentin immunoreaction is observed in the endothelial cells (arrows) around blood vessels (Bv) and capillaries in the *lamina propria-submucosa*. Luminal epithelial cells (E) shows weak to negative immunostaining. Note the absence of vimentin immunoreaction in the tubular glands (G).

4.3.5 Ultrastructural observations

4.3.5.1 Scanning electron microscopy

4.3.5.1.i Control birds

The mucosal surface of the shell gland was thrown into longitudinally oriented luminal folds. Both primary and secondary folds were identified (Fig. 4.21a). The epithelium consisted of ciliated and non-ciliated cells (Fig. 4.21b). The ciliated cells, which appeared to be predominant, were lined by long cilia. The non-ciliated cells were dome-shaped and lined by microvilli. Round to oval-shaped glandular openings were identified between the ciliated and non-ciliated cells.

4.3.5.1.ii Carbendazim treated birds

4.3.5.1.ii.a *Experiment I*

25 mg/kg and 100 mg/kg bodyweight carbendazim

There were no degenerative changes observed at a dose of 25 mg/kg bodyweight carbendazim. At a dose of 100 mg/kg bodyweight carbendazim, focal areas of deciliation were observed (Fig. 4.22). A few degenerating ciliated cells were lined with short, damaged cilia. Microvilli lining the surfaces of the non-ciliated cells appeared to be normal.

400 mg/kg bodyweight carbendazim

At a dose of 400 mg/kg bodyweight carbendazim, large areas of cilia loss were observed (Fig. 4.23a). In these areas, isolated, swollen cilia were identified (Fig. 4.23a & b). In some instances, ciliated cells were covered with relatively few cilia (Fig. 4.23c). The surfaces of the non-ciliated cells were covered with short, thick microvilli. A few non-ciliated cells were devoid of microvilli (Fig. 4.23c).

800 mg/kg bodyweight carbendazim

Deciliation was the most notable degenerative change observed at a dose of 800 mg/kg bodyweight carbendazim (Fig. 4.24). In addition, a few inflammatory cells were observed on the mucosal surface.

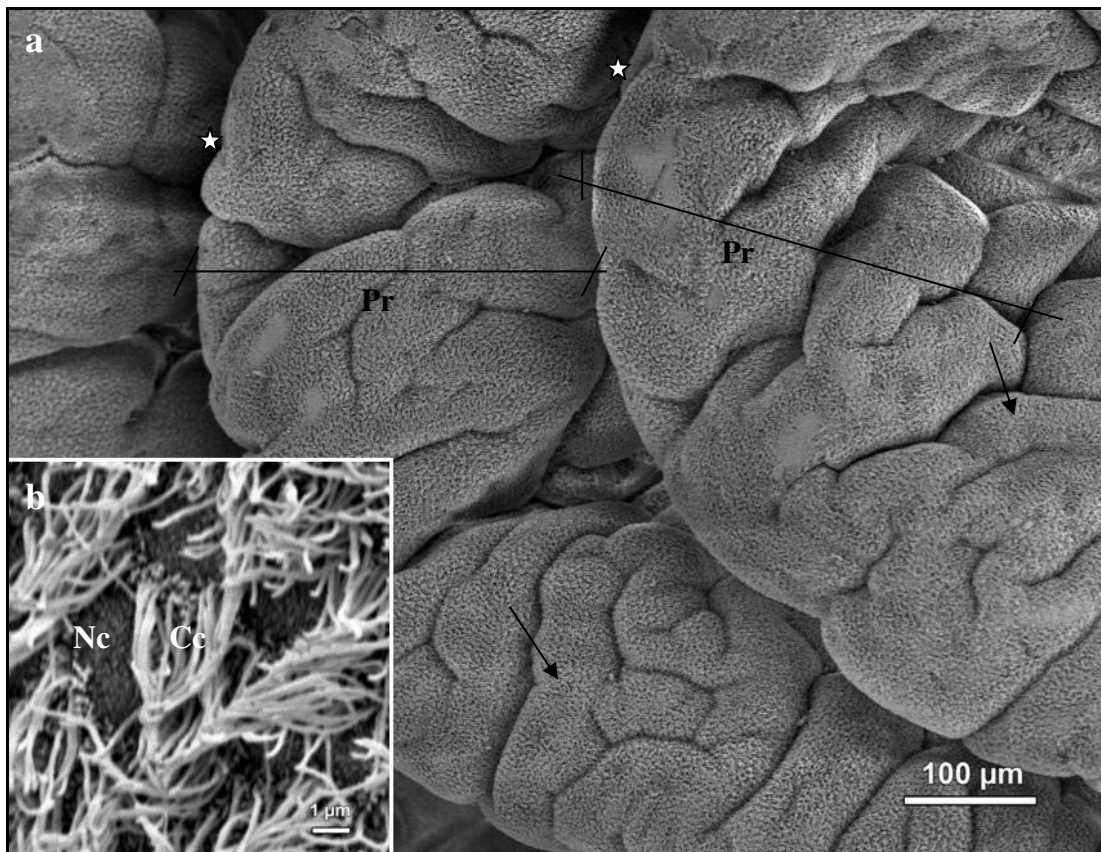


FIG. 4.21: Scanning electron photomicrograph of the mucosal surface of the shell gland in a control bird. **a.** The mucosal surface is thrown into primary (Pr) and secondary (arrows) folds. The primary folds are separated by deep clefts (asterisks). **b.** A higher magnification photomicrograph of the mucosal layer. Ciliated (Cc) and non-ciliated (Nc) cells are observed.

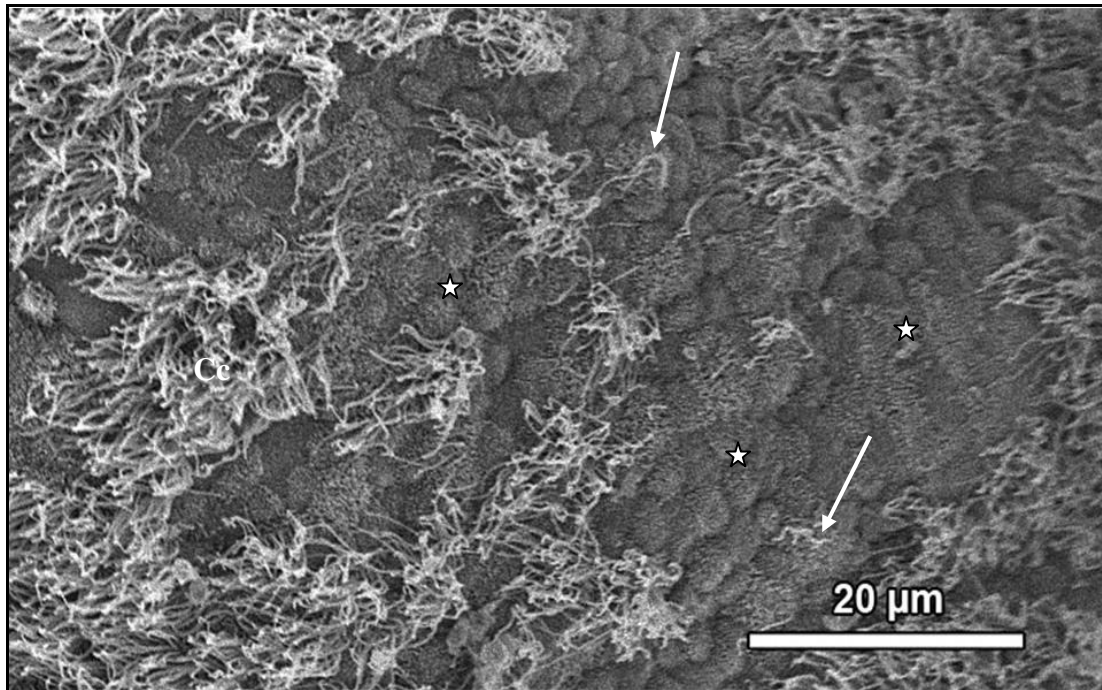


FIG. 4.22: Scanning electron photomicrograph of the mucosal surface of the shell gland in a bird treated with 100 mg/kg bodyweight carbendazim. Areas of deciliation (asterisk) and cells lined with sparse cilia (arrows) are observed. Cc: ciliated cells with tufts of cilia.

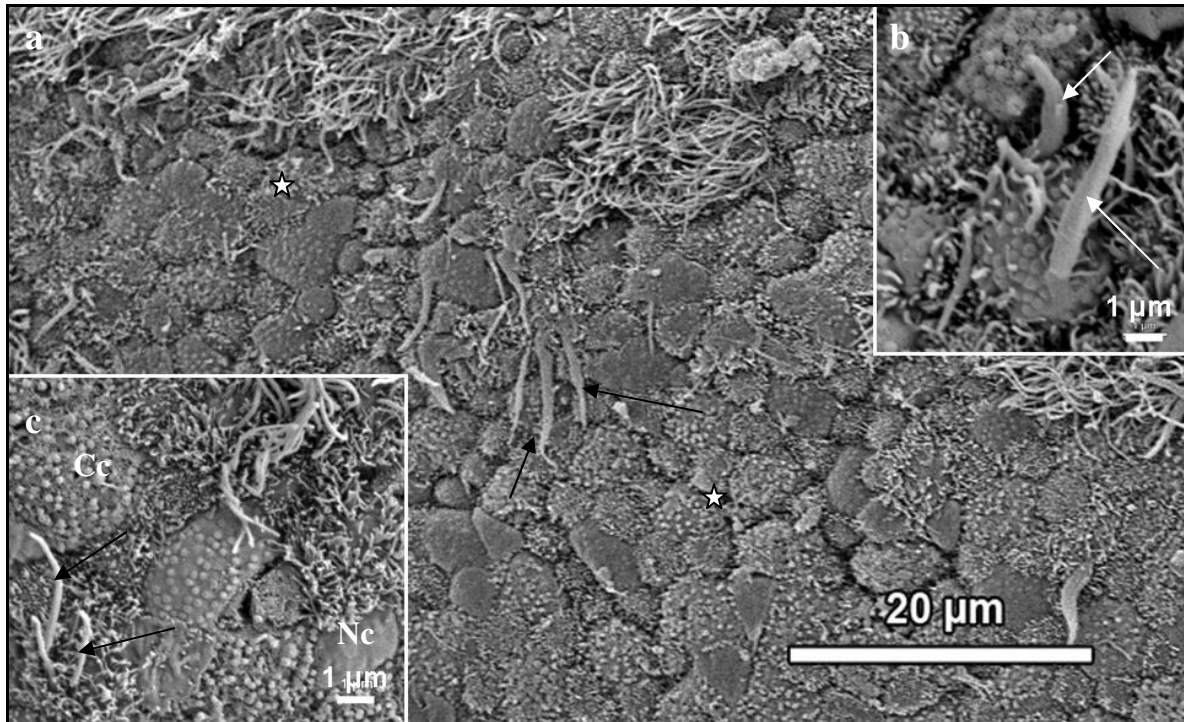


FIG. 4.23: Scanning electron photomicrographs of the mucosal surface of the shell gland in a bird treated with 400 mg/kg bodyweight carbendazim. **a.** Large areas of deciliation (asterisks) are evident. A few degenerating ciliated cells display swollen cilia (arrows). **b.** Higher magnification photomicrograph of degenerating ciliated cells. Swollen cilia (arrows) are observed emerging from the cell surface. **c.** Degenerating epithelial cells in the shell gland. In this figure, ciliated cells with a few cilia (arrows) and short cilia stems (Cc) are observed. The degenerating non-ciliated cell (Nc) shown does not exhibit microvilli.

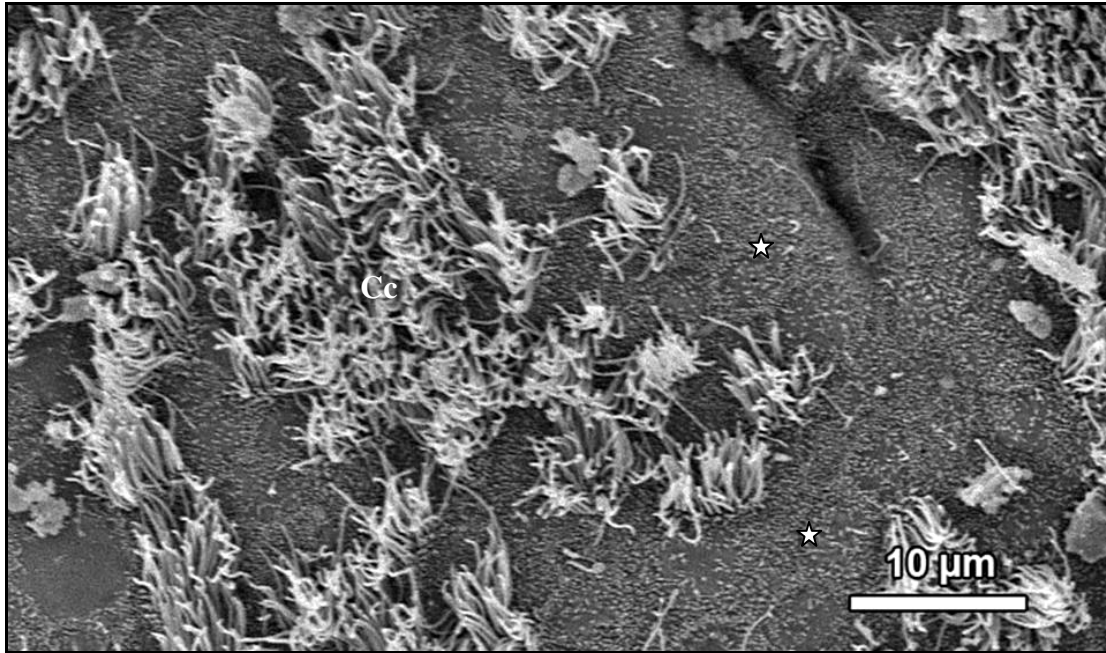


FIG. 4.24: A survey scanning electron photomicrograph of the shell gland mucosal surface of a bird treated with 800 mg/kg bodyweight carbendazim. Asterisks: Ciliary loss. Cc: ciliated cells with intact cilia.

4.3.5.1.iib Experiment II

5 and 24 hours post-exposure

Five hours post-exposure to carbendazim, the mucosal surface did not exhibit any degenerative changes. Both ciliated and non-ciliated cells appeared normal. However, at 24 hours post-exposure to carbendazim, discrete areas of ciliary loss were observed (Fig. 4.25).

5 days post-exposure

Five days post-exposure to carbendazim, deciliation became more extensive (Fig. 4.26a). In some instances, ciliary stems, which were remnants of damaged cilia were observed (Fig. 4.26b). At this stage, the apical parts of the non-ciliated cells were raised above the general surface (Fig. 4.26a). The surfaces of the non-ciliated cells were either devoid of microvilli or lined with a few swollen microvilli (Fig. 4.26c).

8 days post-exposure

Eight days post-exposure to carbendazim, the extent of deciliation was similar to that observed on day 5. Ciliary stems were observed on the apical surfaces of degenerating ciliated cells (Fig. 4.27a). At this stage, the majority of degenerating non-ciliated cells were devoid of microvilli (Fig. 4.27b).

12 days post-exposure

Twelve days post-exposure to carbendazim, sparse, swollen cilia protruded from ciliated cells. In addition, tufts of cilia were occasionally observed on a few degenerating ciliated cells. The degenerating non-ciliated cells displayed short, thick microvilli.

32 days post-exposure

Thirty-two days post-exposure to carbendazim, deciliation continued to be the predominant degenerative feature observed (Fig. 4.28a). A few degenerating ciliated cells were lined by thick cilia. Cilia stems and a disruption of the apical plasma membrane were also observed in degenerating ciliated cells (Fig. 4.28b). The non-ciliated cells were lined by relatively few microvilli (Fig. 4.28b). At this stage, regenerating ciliated cells were lined by intact cilia.

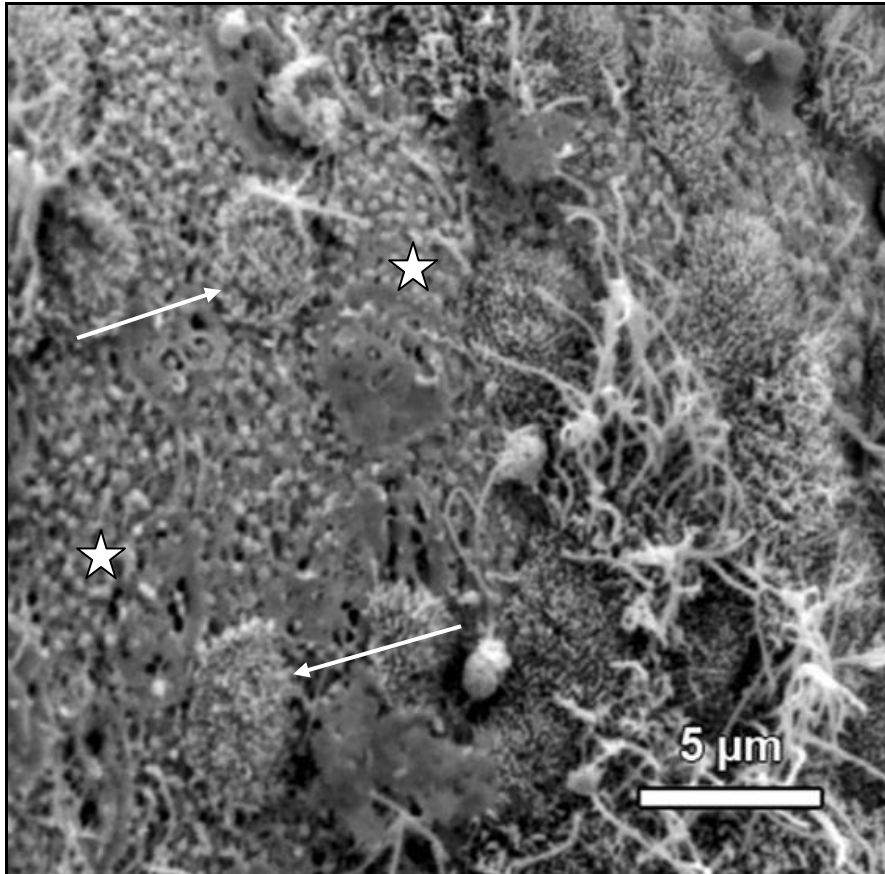


FIG. 4.25: Scanning electron photomicrograph of the shell gland mucosal surface, 24 hours post-exposure to 400 mg/kg bodyweight carbendazim. Areas of cilia loss (asterisks) are observed. Apical protrusions of the non-ciliated cells (arrows) are also observed.

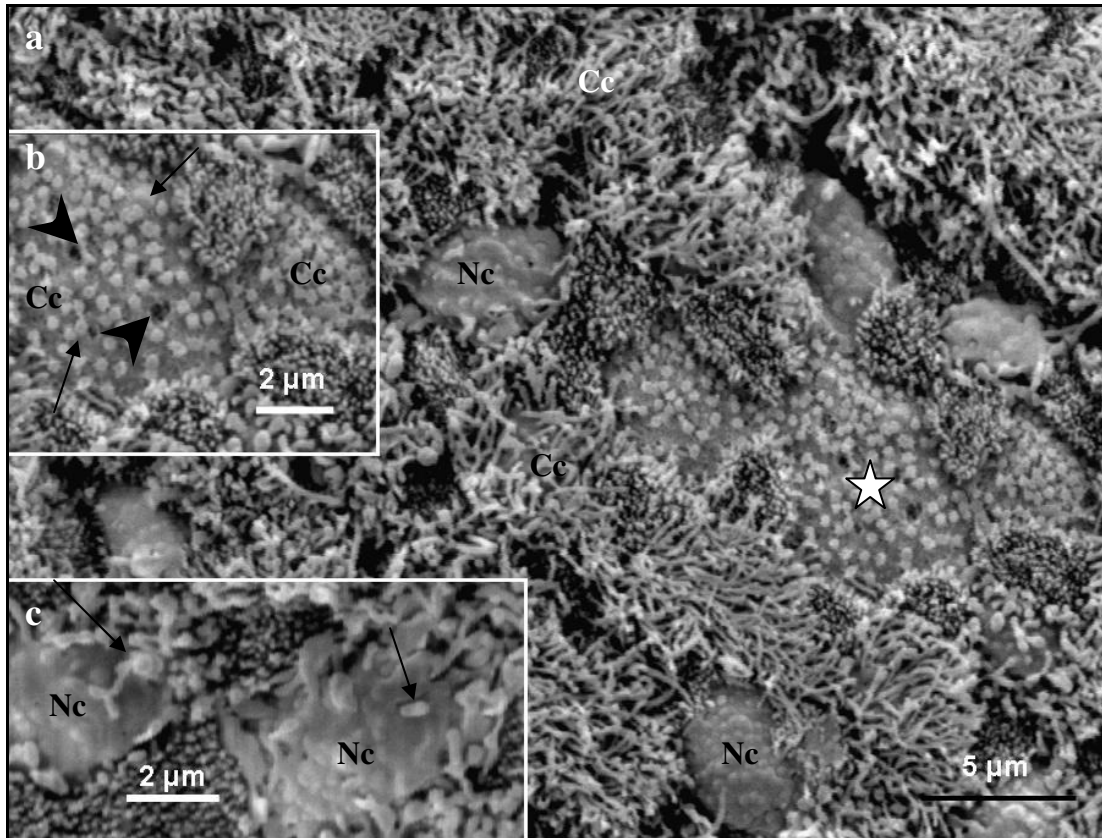


FIG. 4.26: **a.** A survey scanning electron photomicrograph of the shell gland mucosal surface in a Japanese quail, 5 days post-exposure to 400 mg/kg bodyweight carbendazim. Cc: degenerating ciliated cells lined by short cilia. Asterisk: An area of deciliation. Nc: protruded non-ciliated cells. **b.** A higher magnification photomicrograph showing degenerating ciliated cells (Cc). Ciliary stems (arrows) and shallow pits (arrowheads) are observed. **c.** Apical surface of degenerating non-ciliated cells (Nc). The cells are lined by a few swollen microvilli (arrows).

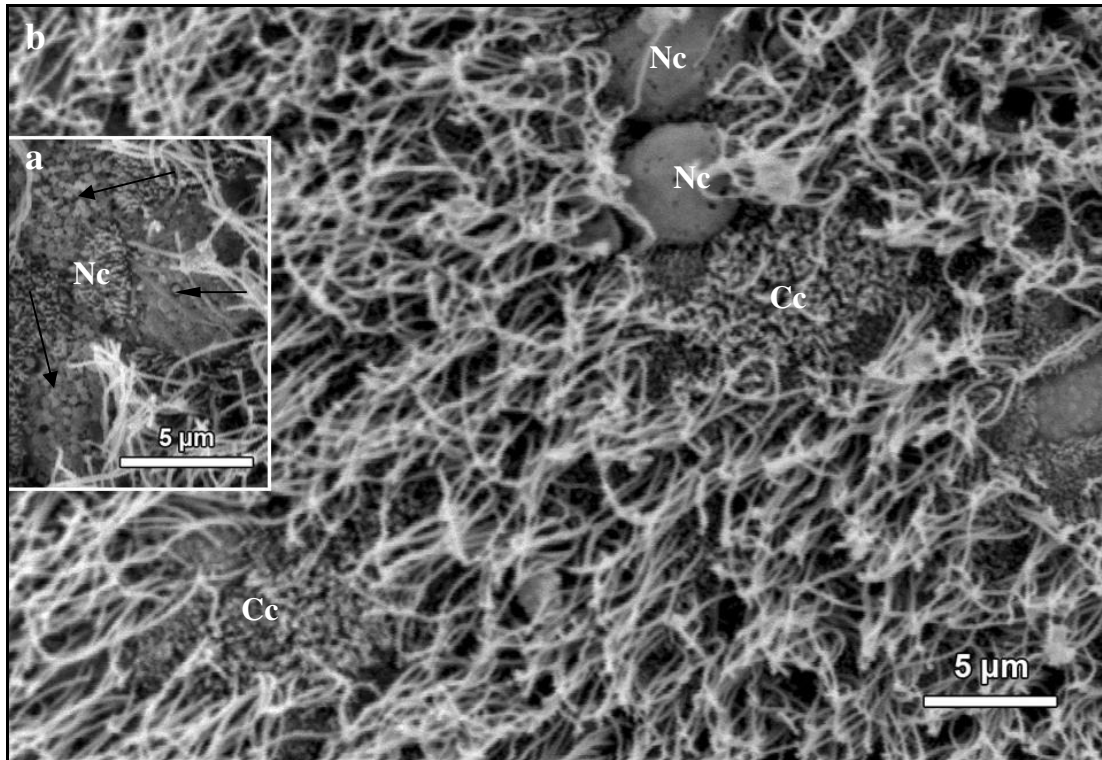


FIG. 4.27: **a.** Scanning electron photomicrograph of the shell gland mucosal surface, 8 days post-exposure to 400 mg/kg bodyweight carbendazim. Arrows: ciliary stems on the surfaces of degenerating ciliated cells. Nc: non-ciliated cell. **b.** A survey scanning electron photomicrograph of the mucosal surface of the shell gland. Note the lack of microvilli on the surfaces of the degenerating non-ciliated cells (Nc) shown. Cc: degenerating ciliated cell.

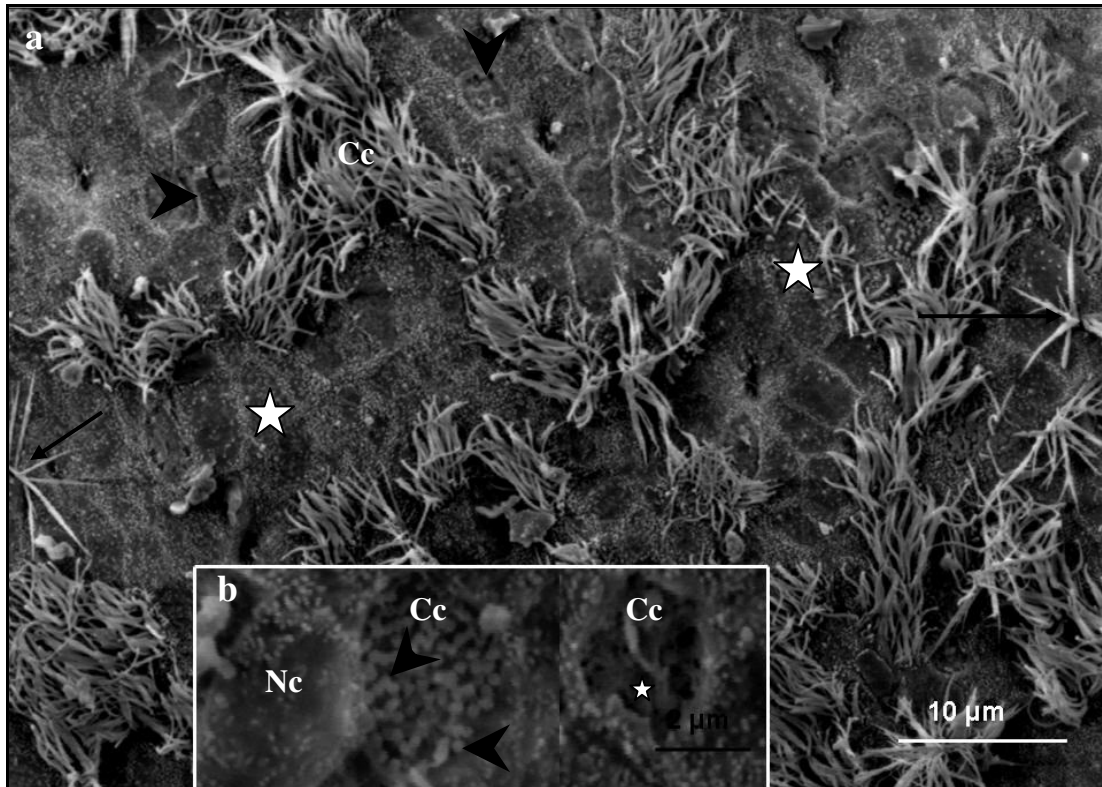


FIG. 4.28: **a.** A survey scanning electron photomicrograph of the shell gland mucosal surface, 32 days post-exposure to 400 mg/kg bodyweight carbendazim. Asterisks: Areas of ciliary loss. Arrowheads: shallow pits. Arrows: thick cilia. Cc: Newly differentiated ciliated cells with intact cilia. **b.** A higher magnification photomicrograph of degenerating ciliated cells (Cc) and a non-ciliated cell (Nc). Note the breakage of apical plasma membrane (asterisk) of a ciliated cell (Cc). Arrowheads: ciliary stems

4.3.5.2 Transmission electron microscopy

4.3.5.2.i Control birds

A pseudostratified columnar epithelium lined the mucosal layer of the shell gland. The epithelium consisted of ciliated and non-ciliated cells, as well as, basal and mitochondrial cells (Fig. 4.29a).

Ciliated cells

The ciliated cells were the predominant cell type. These cells contained centrally-located round to oval-shaped nuclei (Fig. 4.29a). The cytoplasm of the ciliated cells was of an intermediate electron density. Several mitochondria were observed in the

apical and basal cytoplasmic regions. Cisternae of RER and membrane-bound secretory granules were observed in the supranuclear region of the ciliated cells (Fig. 4.29a&b). Secretory granules varied in size and in electron density. In addition, a few lysosomes were observed perinuclearly. The apical plasma membranes of the ciliated cells were lined by cilia, interspersed with microvilli (Fig. 4.29a). The cilia were embedded in the apical cytoplasmic region and supported by corresponding basal bodies. Basal bodies were anchored by basal feet and striated rootlets.

Non-ciliated cells

The non-ciliated cells contained basally-located round nuclei, surrounded by an electron dense cytoplasm (Fig. 4.29a). A few mitochondria and RER profiles were observed in the cytoplasm. In addition, numerous secretory granules, which were generally of a higher electron density than those in ciliated cells, were observed in the apical cytoplasmic regions. The apical plasma membranes of the non-ciliated cells were lined by long, slender microvilli (Fig. 4.30a).

Mitochondrial cells

A few mitochondrial cells were observed in the luminal epithelium. The cells contained oval-shaped nuclei surrounded by cytoplasm of an intermediate electron density (Fig. 4.30b). Numerous mitochondria were observed in these cells. In contrast to ciliated and non-ciliated cells, mitochondrial cells were devoid of secretory granules. A few vacuoles were occasionally observed in the cytoplasm of the mitochondrial cells.

Basal cells

Basal cells with nuclei close to the basal lamina were present. The basal cells contained round nuclei and cytoplasm of an intermediate electron density (Fig. 4.29a). Numerous cisternae of RER were observed throughout the cytoplasm. The cells contained a few mitochondria.

Plasma membranes

Cellular junctions (desmosomes), which linked adjacent epithelial cells, were observed along the lateral plasma membranes (Fig. 4.30a). Interdigitations of the lateral plasma membranes were occasionally observed.

The luminal epithelium rested on a basal lamina of approximately 85 nm in thickness. The basal lamina displayed both a lamina densa and lamina lucida (Fig. 4.30c).

Tubular glands

Tubular glands in the *lamina propria-submucosa* of the shell gland were composed of a single layer of cuboidal or columnar cells. The gland cells contained round to oval-shaped nuclei, which were located basally (Fig. 4.31a). Numerous elongated mitochondria, several Golgi complexes and RER cisternae were observed throughout the cytoplasm (Fig. 4.31a & b). Vacuoles and coated vesicles were also observed. The coated vesicles were round in shape and varied in size (Fig. 4.31b). The coated vesicles occurred singly or in groups in both the apical and basal cytoplasmic regions. The vesicles contained a material of an intermediate electron density.

The apical plasma membranes of the gland cells were lined by long slender microvilli. Cellular junctions (tight junctions) linked adjacent gland cells (Fig. 4.31a). The gland cells rested on a basal lamina of approximately 69 nm in thickness. Both lamina densa and lucida were present (Fig. 4.31c).

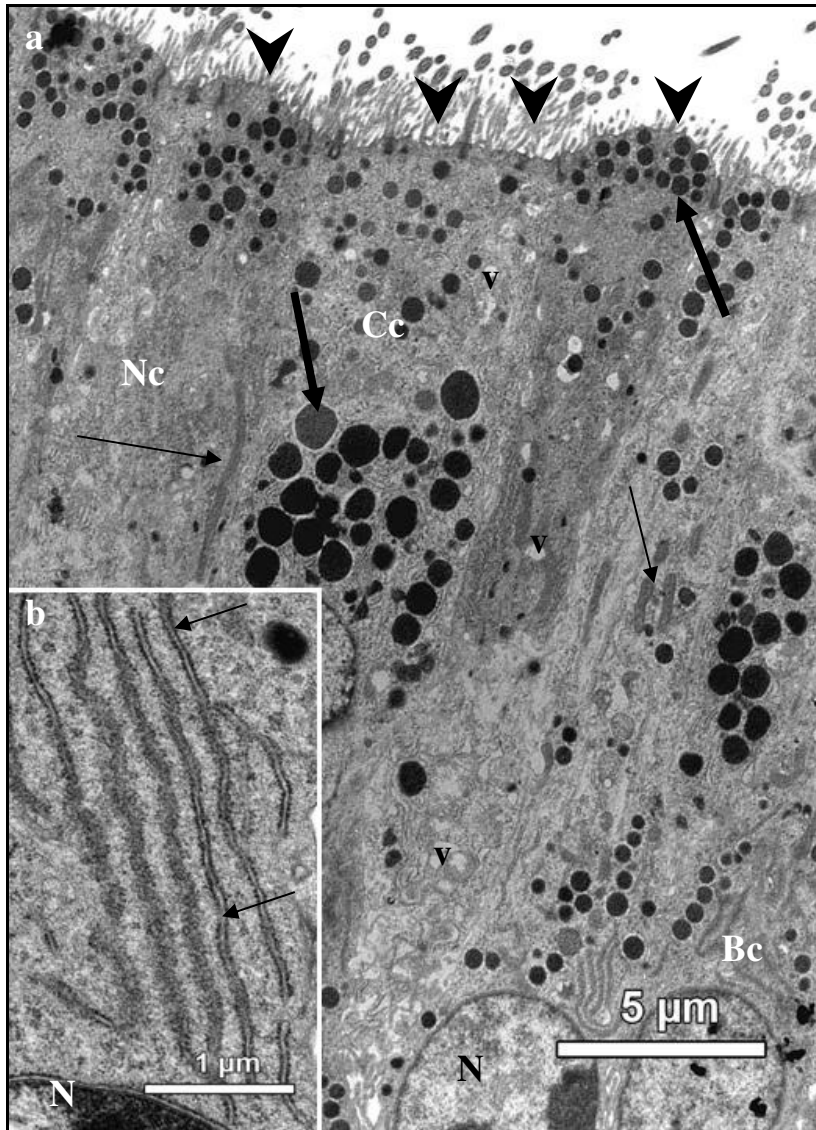


FIG. 4.29: a. A survey transmission electron photomicrograph of the luminal epithelium of the shell gland in a control bird. **a.** Cc: ciliated cells, Nc: non-ciliated and Bc: basal cells in the epithelium. Thick arrows: secretory granules. Thin arrows: mitochondria. Arrowheads: microvilli on the apical plasma membrane of the ciliated and non-ciliated cells. v: vacuoles. N: Nucleus. **b.** A higher magnification electron photomicrograph of the cytoplasm in a ciliated cell. Cisternae of RER (arrows) are observed adjacent to the nucleus (N). *Egg in the shell gland*

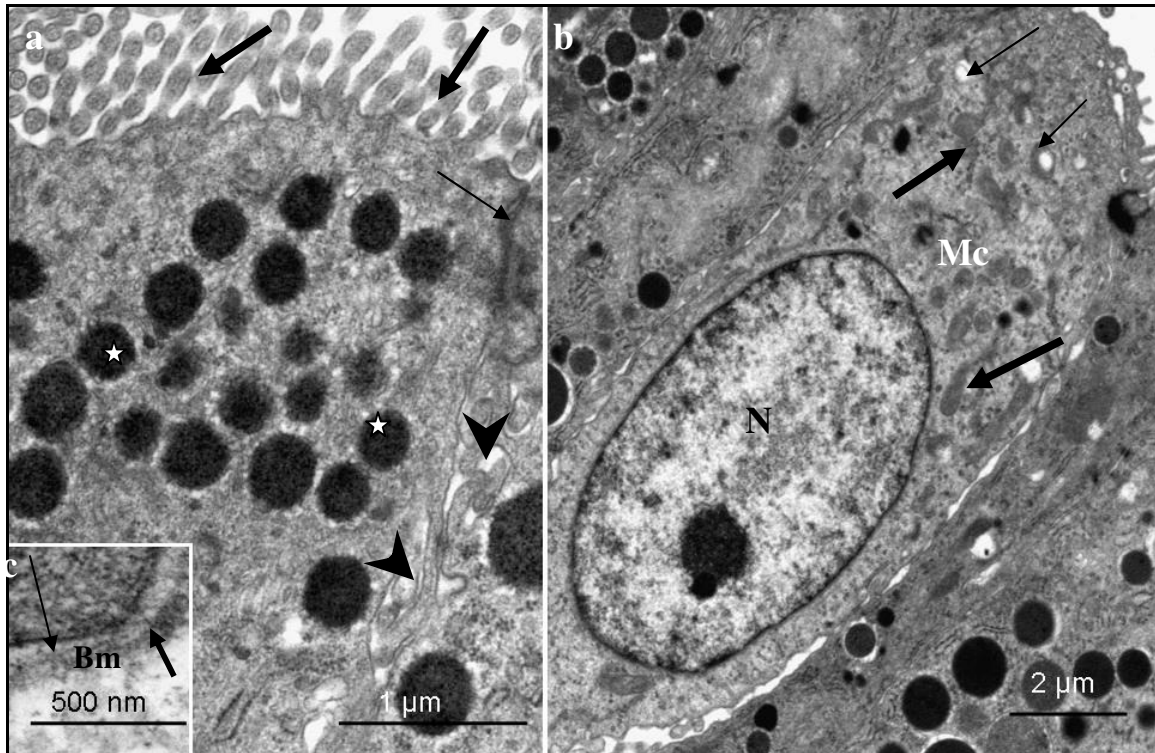


FIG. 4.30: **a.** Transmission electron photomicrograph of a non-ciliated cell in the luminal epithelium of the shell gland in a control bird. Long slender microvilli (thick arrows) line the apical plasma membrane. The cytoplasm contains numerous secretory granules (asterisks). Tight junction (thin arrow) links adjacent cells. Note the interdigitations of the lateral plasma membranes (arrowheads). **b.** Electron photomicrograph of the luminal epithelium showing a mitochondrial cell (Mc). Numerous mitochondria (thick arrows) and vacuoles (thin arrows) are observed in the cytoplasm. N: nucleus. **c.** A higher magnification electron photomicrograph of the basal region of the luminal epithelium. The basal lamina (Bm) displays a lamina lucida (thin arrow) and lamina densa (thick arrow). *Egg in the shell gland*

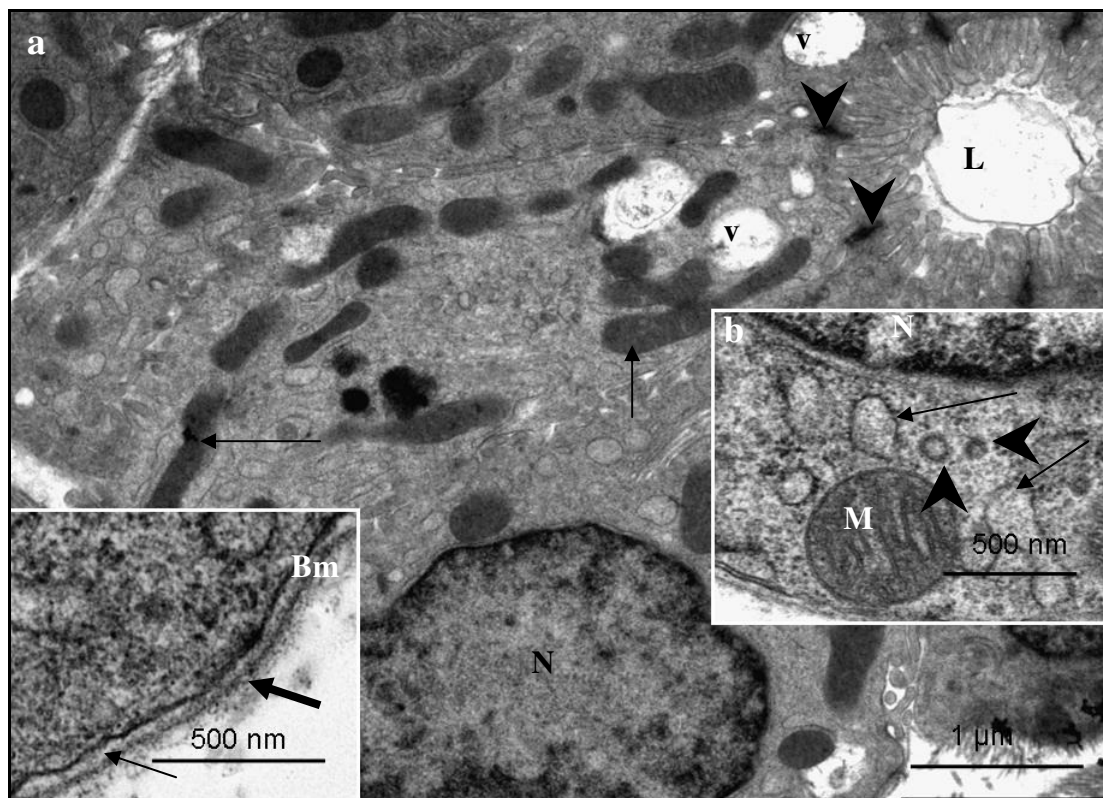


FIG. 4.31: Transmission electron photomicrographs of a tubular gland in the shell gland of a control bird. **a.** N: oval-shaped nucleus. Arrows: elongated mitochondria. v: vacuoles. Arrowheads: tight junctions. L: glandular lumen. **b.** Cisternae of RER (arrows) and coated vesicles (arrowheads) are observed adjacent to the nucleus (N). M: mitochondrion. **c.** Basal lamina (Bm) underlying gland cells. Note the presence of a lamina lucida (thin arrow) and a lamina densa (thick arrow). *Egg in the shell gland.*

4.3.5.2.ii Carbendazim treated birds

4.3.5.2.iii. *Experiment I*

25 mg/kg and 100 mg/kg bodyweight carbendazim

As in the proximal oviductal segments (infundibulum and magnum), no ultrastructural changes were observed at doses of 25 mg/kg and 100 mg/kg bodyweight carbendazim.

400 mg/kg bodyweight carbendazim

At a dose of 400 mg/kg bodyweight carbendazim, degenerative changes were observed in both the luminal and glandular epithelia.

Ciliated cells

In the luminal epithelium, degenerating ciliated cells displayed shortened cilia (Fig. 4.32). The degenerating ciliated cells contained pyknotic nuclei, multi-vesicular bodies and numerous lysosomes. Swollen mitochondria were observed throughout the cytoplasm (Fig. 4.32). In the apical cytoplasmic regions of these cells, coalesced degenerating secretory granules were observed (Fig. 4.33a). The degenerating secretory granules displayed heterogeneous particles of an intermediate electron density. In some instances the contents of the degenerating secretory granules were observed in the lumen of the shell gland (Fig. 4.33b). At this dose, Golgi complexes were structurally normal. Basal bodies supporting the cilia were intact.

Non-ciliated cells

Degenerating non-ciliated cells were characterized by the presence of apical protrusions (Fig. 4.34a). The degenerating non-ciliated cells contained relatively few intact secretory granules. In addition, a few of the degenerating non-ciliated cells contained pyknotic nuclei. Swollen mitochondria and vacuoles were observed in the basal and apical cytoplasmic regions of degenerating non-ciliated cells (Fig. 4.34b).

Mitochondrial and basal cells

No degenerative changes were observed in the mitochondria cells. Swollen mitochondria and vacuoles were the predominant degenerative changes observed in the basal cells.

Plasma membranes

Wide intercellular spaces were observed between the lateral plasma membranes of adjacent cells. In these areas, cellular junctions (desmosomes) displayed relatively few associated filaments (Fig. 4.34c).

At this dose, the basal lamina underlying the luminal epithelium measured approximately 97 nm in thickness. No degenerative changes were evident in the basal lamina.

Tubular glands

Degenerating tubular glands were characterized by the presence of pyknotic nuclei and swollen mitochondria (Fig. 4.35a). Degenerating mitochondria in the gland cells displayed damaged cristae (Fig. 4.35b). Coated vesicles contained electron dense material. In some instances, groups of vesicles were circumscribed by a membrane, forming multi-vesicular bodies. The multi-vesicular bodies were either free in the cytoplasm or associated with Golgi complexes (Fig. 4.35c). Microvilli along the apical plasma membranes and cellular junctions between the lateral plasma membranes were intact (Fig. 4.35d). The basal lamina, which was approximately 60nm thick, displayed both a lamina densa and lucida.

800 mg/kg bodyweight carbendazim

Ciliated cells

Administration of 800 mg/kg bodyweight carbendazim was associated with the deciliation of ciliated cells. Degenerating ciliated cells contained pyknotic nuclei, swollen mitochondria and numerous vacuoles (Fig. 4.36a). Numerous lysosomes and dilated cisternae of RER were observed in the apical cytoplasmic regions of the ciliated cells (Fig. 4.36b). A few degenerating secretory granules were also observed in the apical cytoplasmic regions of the degenerating cells. Although basal bodies were intact, striated rootlets were indistinct. The cytoplasm of the degenerating ciliated cells was electron dense.

Non-ciliated cells

The apical parts of degenerating non-ciliated cells were seen protruding above the general mucosal surface (Fig. 4.36a). The degenerating non-ciliated cells contained irregular-shaped, as well as pyknotic nuclei. In addition, dilated RER cisternae were features of these cells. Swollen mitochondria and vacuoles were distributed in the apical and basal cytoplasmic regions (Fig. 4.37a). In some instances, thick microvilli were seen lining the apical plasma membranes.

Mitochondrial and basal cells

At this dose, degenerating mitochondrial and basal cells contained pyknotic nuclei and swollen mitochondria.

Plasma membranes

Desmosomes along the lateral plasma membranes were intact (Fig. 4.37b). No degenerative changes were observed in the basal lamina underlying the luminal epithelium. The basal lamina was approximately 90 nm thick.

Tubular glands

Degenerating cells in the tubular glands contained pyknotic nuclei and swollen mitochondria (Fig. 4.38a). A few vacuoles were observed in the cytoplasm. Very few coated vesicles were observed in the cytoplasm. The lumina of these glands contained granular electron dense material (Fig. 4.38b). Microvilli along the apical regions and cellular junctions between the lateral plasma membrane were structurally normal. At this dose infolding of the basal plasma membrane and basal lamina was occasionally observed (Fig. 4.38c). The basal lamina contained homogeneous particles of an intermediate electron density (Fig. 4.38c). The lamina lucida was indistinct. The basal lamina measured approximately 70nm in thickness.

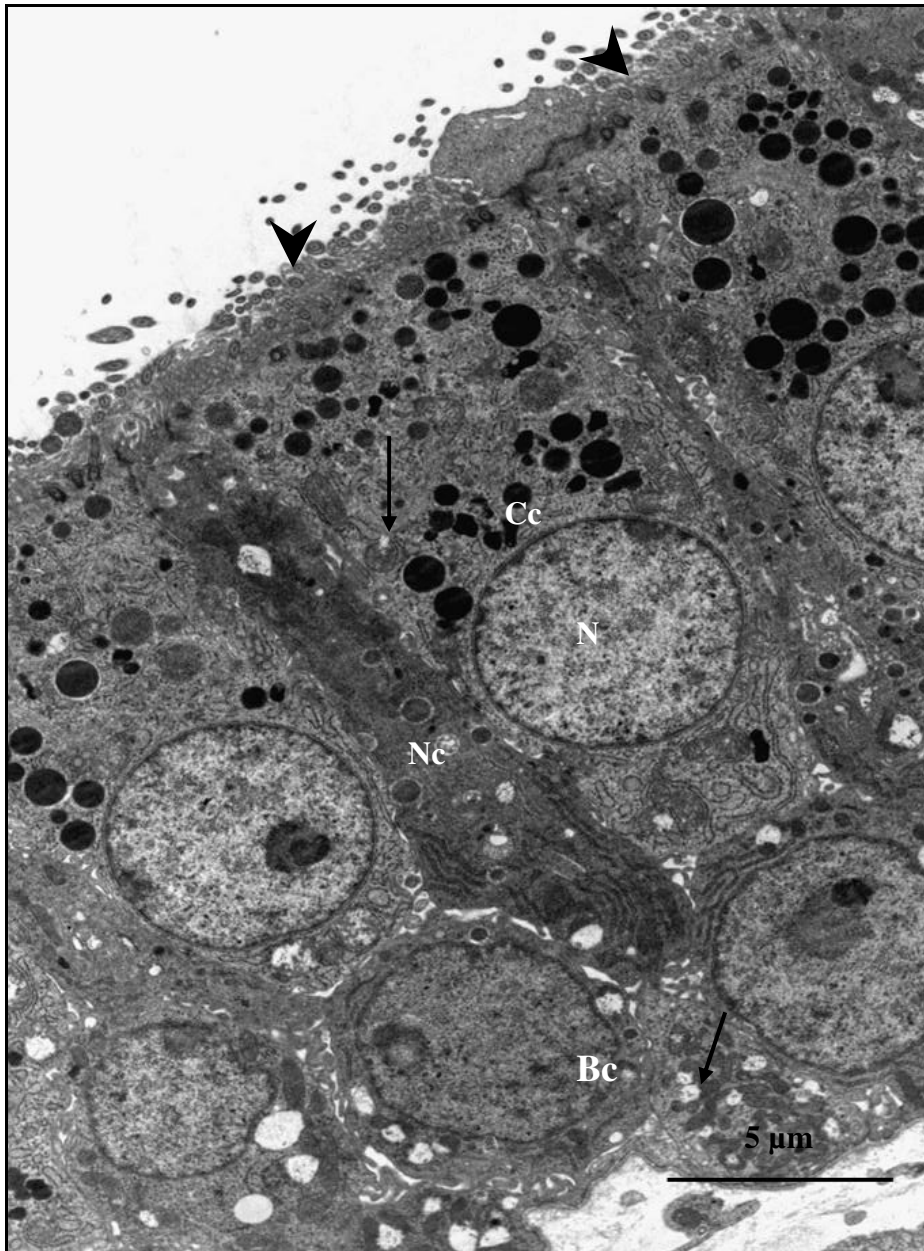


FIG. 4.32: A survey electron transmission photomicrograph of the luminal epithelium in the shell gland of a bird treated with 400 mg/kg bodyweight carbendazim. Ciliated cells (Cc) display short cilia (arrowheads). Swollen mitochondria (arrows) are observed in the cytoplasm of both ciliated and basal cells (Bc). N: nucleus; Nc: non-ciliated cell. *No egg in the reproductive tract.*

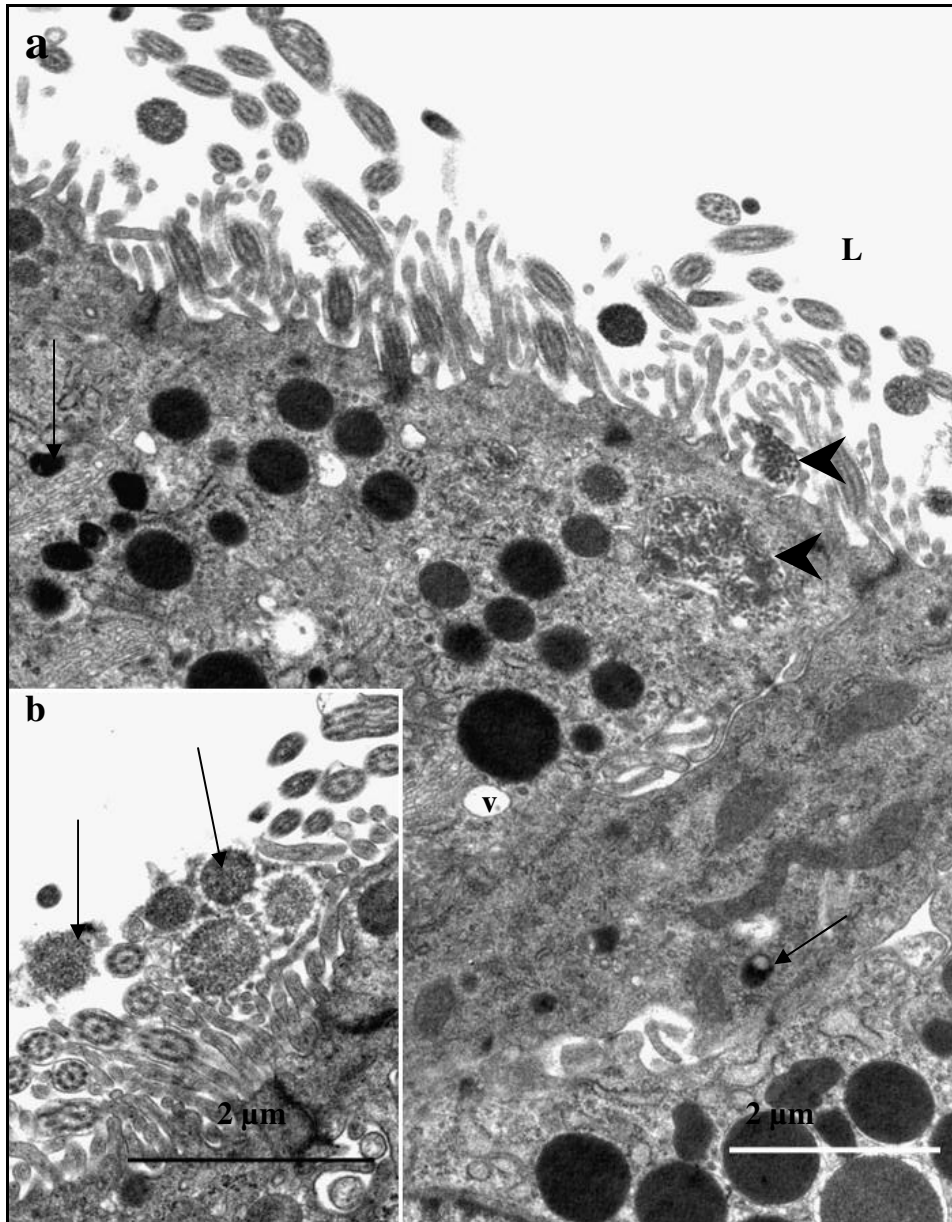


FIG. 4.33: **a.** Transmission electron photomicrograph of the apical region of ciliated cells in the shell gland of a bird treated with 400 mg/kg bodyweight carbendazim. Coalesced degenerating secretory granules (arrowheads) are observed in the apical cytoplasmic region and in the lumen. V: vacuoles; Arrows: lysosomes; L: lumen. **b.** Transmission electron photomicrograph of the apical region of the ciliated cells. Degenerating secretory granules (arrows) are observed in the lumen. *No egg in the reproductive tract.*

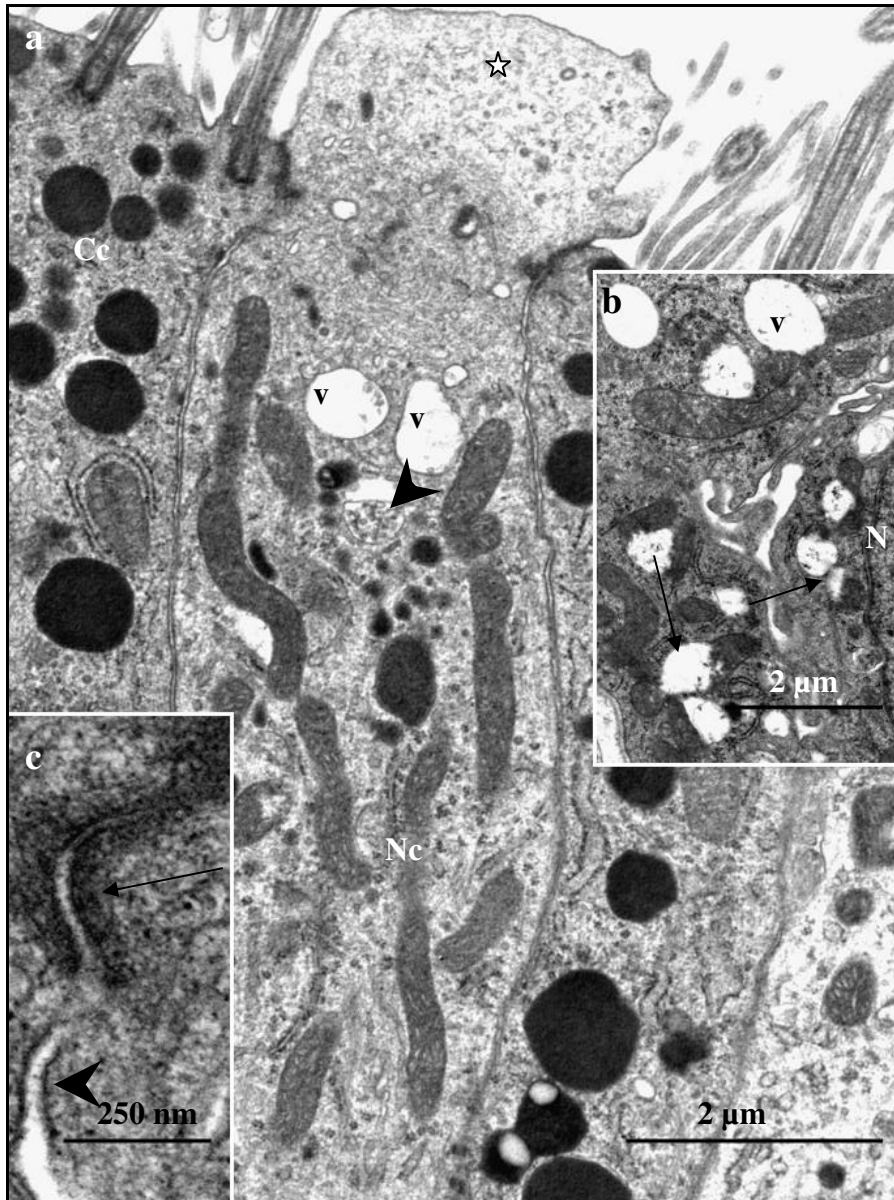


FIG. 4.34: **a.** Transmission electron photomicrographs of ciliated (Cc) and non-ciliated (Nc) cells in the shell gland of a bird treated with 400 mg/kg bodyweight carbendazim. Asterisk: apical protrusion of the non-ciliated cell. Vacuoles (v) and a degenerating secretory granule (arrowhead) in the apical cytoplasmic region. **b.** Basal cytoplasmic region of a non-ciliated cell. Note the aggregations of degenerating swollen mitochondria (arrows) and vacuoles (v). N: nucleus. **c.** Transmission electron photomicrograph showing an intact (arrow) and degenerating (arrowhead) desmosome. The degenerating desmosome is associated with very few filaments. *No egg in the reproductive tract.*

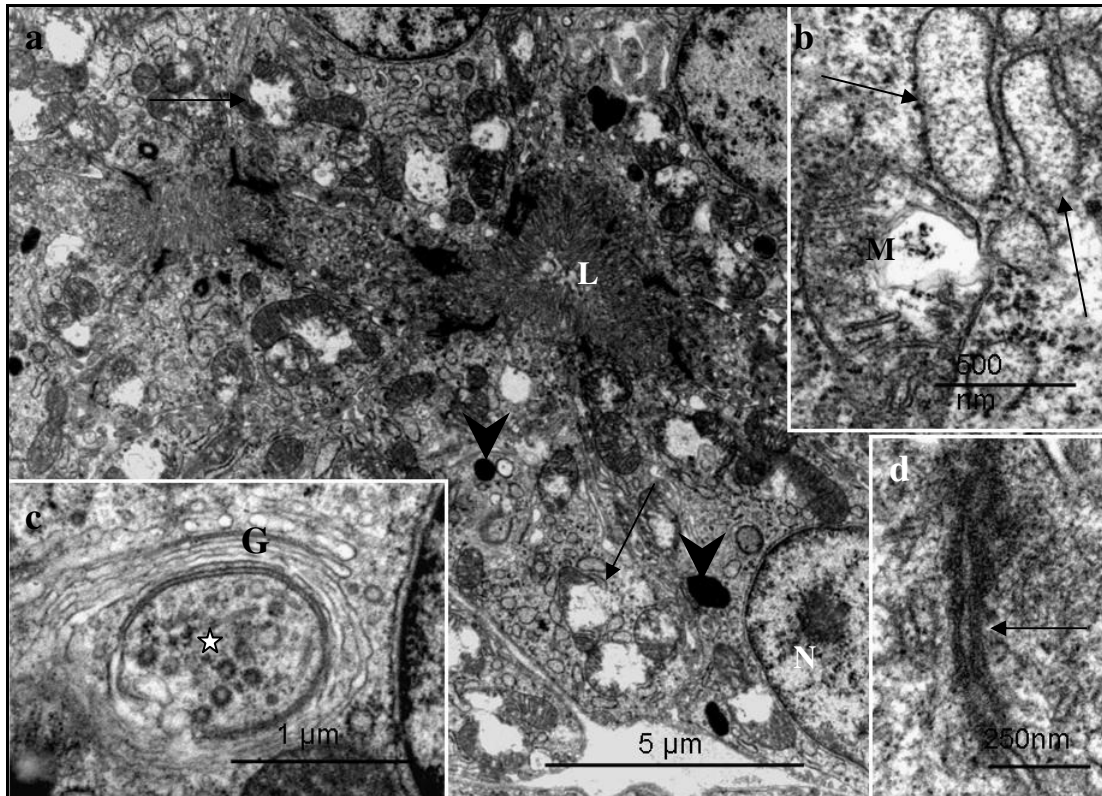


FIG. 4.35: **a.** A survey transmission electron photomicrograph of a tubular gland in the shell gland of a bird treated with 400 mg/kg bodyweight carbendazim. Numerous degenerating mitochondria (arrows) are observed in the cytoplasm. A few lysosomes (arrowheads) are present in the apical and basal cytoplasmic regions. N: nucleus; L: glandular lumen. **b.** A higher magnification transmission electron photomicrograph of the cytoplasm of a degenerating gland cell. Degenerating mitochondrion (M) display a loss of cristae. Arrows: cisternae of RER. **c.** A multi-vesicular body (asterisk) adjacent to a Golgi complex (G). **d.** An intact desmosome (arrow) links lateral plasma membranes of adjacent gland cells. *No egg in the reproductive tract.*

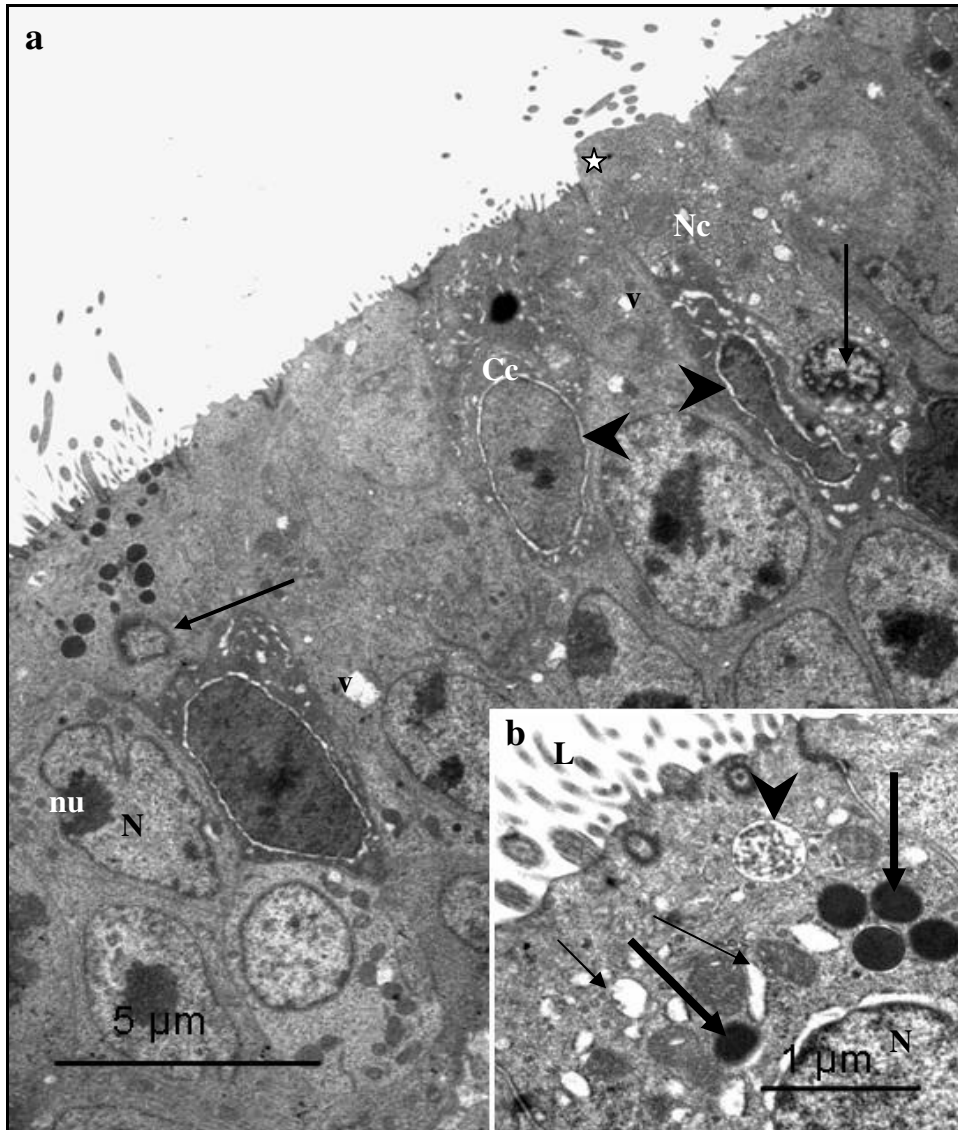


FIG. 4.36: **a.** A survey transmission electron photomicrograph of the luminal epithelium of the shell gland in a bird treated with 800 mg/kg bodyweight carbendazim. Arrows: Nuclei with dilated nuclear pores in both ciliated (Cc) and non-ciliated (Nc) cells. Arrowheads: Condensed nuclei. Asterisk: apical cytoplasmic protrusion arising from a degenerating non-ciliated cell. N: irregular-shaped nucleus with nucleolar margination (nu). V: vacuoles. **b.** Apical region of a degenerating ciliated cell. A vacuole with granular material (arrowhead) and dilated RER cisternae (thin arrows) are observed. N: nucleus. L: epithelial lumen. Thick arrows: secretory granules. *No egg in the reproductive tract.*

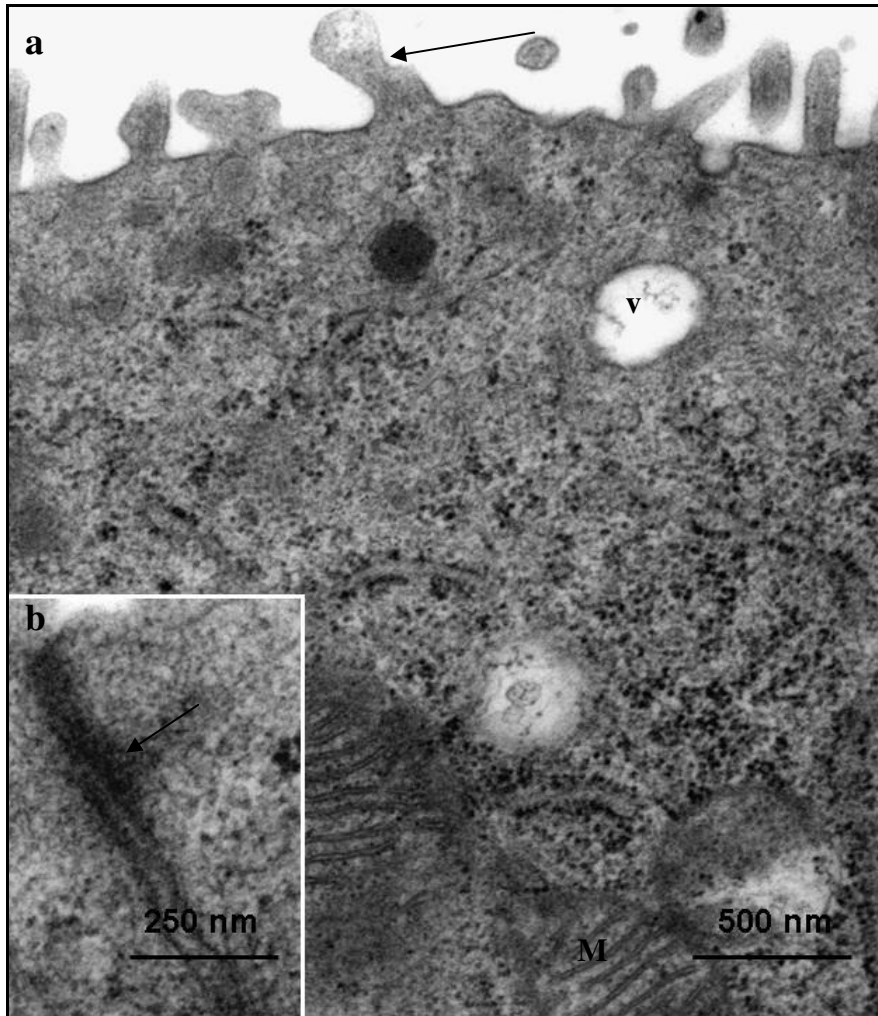


FIG. 4.37: **a.** Transmission electron photomicrograph of the apical region of a degenerating non-ciliated cell in the luminal epithelium of the shell gland from a bird treated with 800 mg/kg bodyweight carbendazim. A few vacuoles (v) are observed in the apical cytoplasmic region. A swollen microvillous (arrow) is observed along the apical plasma membrane. M: mitochondrion. **b.** An intact cellular junction (arrow) linking adjacent epithelial cells. *No egg in the reproductive tract.*

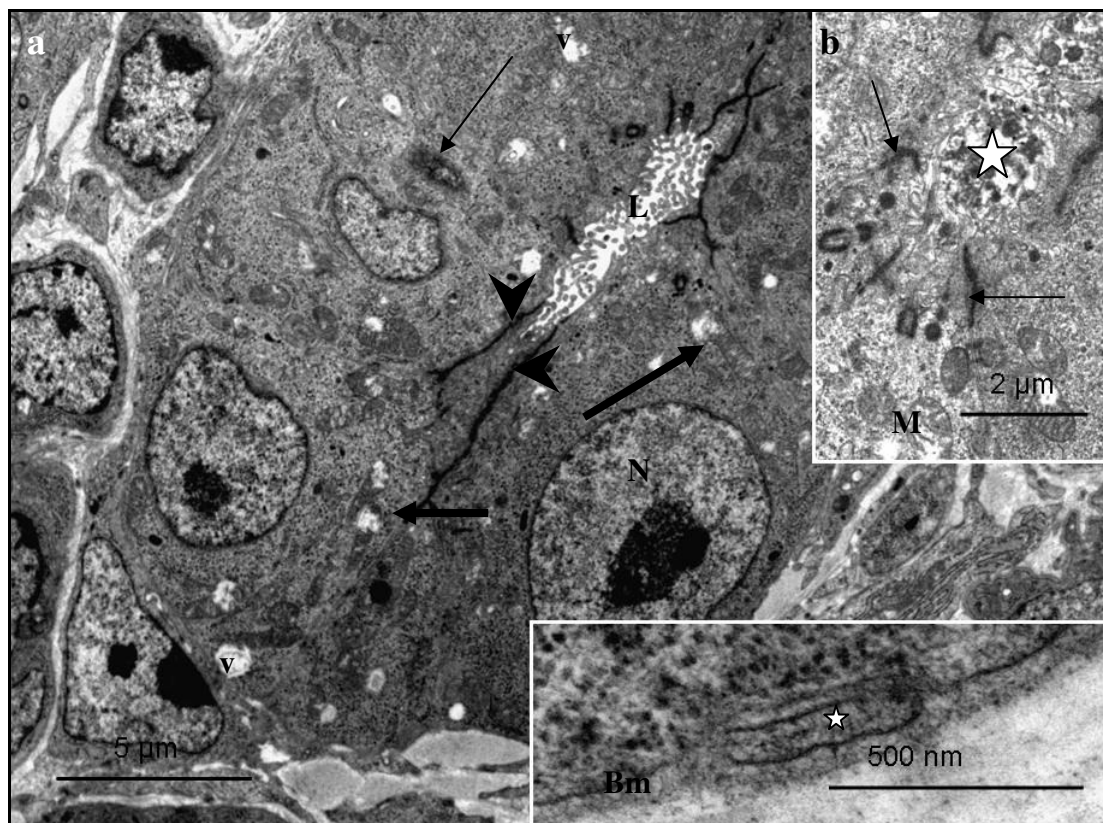


FIG. 4.38: **a.** A survey transmission electron photomicrograph of a tubular gland in the shell gland of a bird treated with 800 mg/kg bodyweight carbendazim. Cells with pyknotic (thin arrow) and normal (N) nuclei are observed. Thick arrows: Swollen mitochondria. v: vacuoles. Note the presence of tight junctions (arrowheads) joining adjacent gland cells. L: glandular lumen. **b.** Apical region of a degenerating tubular gland. The glandular lumen contains a granular electron dense material (asterisk). Arrows: desmosomes; M: swollen mitochondrion. **c.** A higher transmission electron photomicrograph of the basal region of a tubular gland. Folding of the basal lamina (asterisk) is observed. The basal lamina (Bm) lacks a distinctive lamina lucida. *No egg in the reproductive tract.*

4.3.5.2.iib. Experiment II

5 hours post-exposure to carbendazim

Degenerative changes in the luminal epithelium were observed 5 hours post-exposure to carbendazim. At this stage, the epithelium contained a few degenerating ciliated and non-ciliated cells.

Ciliated cells

The degenerating ciliated cells contained irregular-shaped, pyknotic nuclei and electron dense cytoplasm (Fig. 4.39). The apical plasma membranes of a few ciliated cells were lined by cilia with enlarged apical regions (Fig. 4.40a). Several microvilli were observed between the cilia. In some instances, a few vacuoles and degenerating secretory granules were observed in the apical cytoplasmic regions (Fig. 4.40a&b).

Non-ciliated cells

Degenerating non-ciliated cells contained a rarefied cytoplasm with relatively few organelles (Fig. 4.39). Lysosomes and degenerating secretory granules were identified in the apical cytoplasmic regions of these cells (Fig. 4.40a). A few vacuoles and mitochondria with dilated cristae were observed throughout the cytoplasm (Fig. 4.40c).

Mitochondrial and basal cells

No degenerative changes were observed in mitochondrial or basal epithelial cells.

Plasma membranes

Cellular junctions (desmosomes) linking adjacent epithelial cells were intact. No degenerative changes were observed in the basal lamina. The basal lamina measured approximately 91nm in thickness.

Tubular glands

Pyknotic nuclei and dilated cisternae of RER characterized degenerating tubular gland cells (Fig. 4.41). Degenerating nuclei displayed condensed and marginalized chromatin. Cellular junctions along the lateral plasma membranes of the gland cells were intact. Coated vesicles within the cytoplasm of the gland cells appeared

normal. The basal lamina, which measured approximately 68nm in thickness, did not exhibit any degenerative changes.

24 hours post-exposure to carbendazim

Twenty-four hours post-exposure to carbendazim, degeneration of the luminal epithelial cells appeared to be more extensive than in the 5 hours post-exposure group.

Ciliated cells

At this stage, degenerating ciliated cells contained irregular-shaped nuclei with condensed nuclear chromatin. A few vacuoles were observed in the apical cytoplasmic regions of these cells. The apical plasma membranes of the cells were lined by a few cilia and microvilli. Degenerating secretory granules were observed in the apical cytoplasmic regions of the cells (Fig. 4.42). In some instances, degenerating secretory granules were observed in the lumen (Fig. 4.42).

Non-ciliated cells

Secretory granules in the non-ciliated cells contained electron lucent granules. Several lysosomes were observed in the apical cytoplasmic region. A few vacuoles were observed in the middle and basal regions of the cells.

Mitochondrial and basal cells

No marked degenerative changes were observed in the mitochondrial cells. However, at this stage, basal cells contained a few lysosomes.

Plasma membranes

Desmosomes along the lateral plasma membranes were intact. No degenerative changes were observed in the underlying basal lamina. The basal lamina was approximately 73 nm in thickness.

Tubular glands

Degenerating tubular gland cells contained pyknotic nuclei, swollen mitochondria and a few coated vesicles. Cellular junctions along the lateral plasma membranes and the underlying basal lamina were structurally normal.

5 days post-exposure to carbendazim

Degenerative changes were identified in both the luminal and glandular epithelia.

Ciliated cells

Degenerating ciliated cells contained pyknotic nuclei and swollen mitochondria (Fig. 4.43a). Nuclei displaying dilated nuclear pores were observed (Fig. 4.43b). Nuclei displaying condensation and margination of chromatin were also identified (Fig. 4.44a). Numerous vacuoles were seen throughout the cytoplasm. Degenerating secretory granules were observed in the apical cytoplasmic region of ciliated cells (Fig. 4.44b). Intact basal bodies, devoid of anchoring striated rootlets, were observed apically. At this stage, the apical plasma membrane was also lined by short microvilli with swollen tips (Fig. 4.43c). In the basal cytoplasmic region, vacuoles and dilated RER cisternae were identified.

Non-ciliated cells

Pyknotic nuclei were observed in degenerating non-ciliated cells. Numerous degenerating secretory granules, vacuoles and filamentous aggregates were observed in the cytoplasm of these cells (Fig. 4.45a). The degenerating secretory granules contained granular material, which was enclosed by a discontinuous limiting membrane (Fig. 4.45b). Smaller degenerating secretory granules coalesced to form large secretory structures (Fig. 4.45b). The apical plasma membranes of these degenerating non-ciliated cells were lined by short microvilli (Fig. 4.45b).

Mitochondrial and basal cells

At this stage, basal cells contained electron dense cytoplasm. Numerous electron dense bodies were seen in the cytoplasm (Fig. 4.44a). Nuclei of the basal cells displayed nucleolar margination. Mitochondrial cells contained numerous lysosomes and vacuoles.

Plasma membranes

Cellular junctions (desmosomes) along the lateral plasma membranes were intact. The epithelium was supported by a basal lamina of approximately 104 nm in thickness. Although the lamina densa and lamina lucida were distinct, an occasional evagination of the basal lamina was observed. In some instances, the protrusion of the basal regions of epithelial cells through the basal lamina was observed (Fig. 4.45c).

Tubular glands

Degenerating tubular gland cells contained pyknotic nuclei and a few lysosomes (Fig. 4.46a). Mitochondria in the gland cells appeared to be structurally normal. Vacuoles containing electron dense granules were seen in the central and basal cytoplasmic regions of the degenerating gland cells (Fig. 4.46a&b). Coated vesicles, which were sparsely distributed throughout the cytoplasm, contained electron dense material (Fig. 4.46c). Microvilli lining the apical plasma membranes were intact. A few cellular junctions (desmosomes) were intact. However, in some areas increased intercellular spaces between the lateral plasma membranes were observed (Fig. 4.47a). The basal lamina displayed an ill-defined lamina lucida (Fig. 4.47b). Invaginations of the lamina densa were also observed.

8 days post-exposure to carbendazim

Eight days post-exposure to carbendazim, degenerative changes were seen in both luminal and glandular epithelia.

Ciliated cells

Degenerating ciliated cells contained pyknotic nuclei (Fig. 4.48a). Coalescence of degenerating secretory granules was observed in the apical cytoplasmic regions of the ciliated cells (Fig. 4.48b). In some instances, the degenerating secretory granules were seen in the lumen. Basal bodies in the apical cytoplasmic region were intact. However, striated rootlets, which anchor basal bodies, were indistinct. In the apical region, a few vacuoles, swollen mitochondria and dilated cisternae of RER were observed.

Non-ciliated cells

Degenerating non-ciliated cells contained pyknotic nuclei and displayed apical protrusions (Fig. 4.48a & 4.49a). Numerous vesicles were observed throughout the cytoplasm of the degenerating non-ciliated cells. The cytoplasm of degenerating non-ciliated cells varied in electron density (Fig. 4.49a). In addition, large vacuoles containing particles of an intermediate electron density were observed in the apical regions of degenerating non-ciliated cells (Fig. 4.49a). A few lipid droplets, degenerating secretory granules, as well as mitochondria with tubular cristae were observed throughout the cytoplasm (Fig. 4.49b). In some instances a loss of mitochondrial cristae was observed. Microtubular structures were also observed associated with degenerating secretory granules (Fig. 4.49b).

Mitochondrial and basal cells

Pyknotic nuclei and an increased number of lysosomes were the degenerative features observed in the mitochondrial cells. At this stage the basal cells were at different stages of differentiation (Fig. 4.48a). The cytoplasm in the basal cells was electron lucent and contained extensive profiles of RER and differentiating secretory granules. The nuclei in these cells were euchromatic.

Plasma membranes

Desmosomes along the lateral plasma membranes were intact. Underlying the epithelial cells was a basal lamina of approximately 80 nm. Invaginations of the basal lamina were observed frequently (Fig. 4.49c).

Tubular glands

Degenerating tubular glands, 8 days post-exposure to carbendazim contained pyknotic nuclei, as well as, nuclei with nucleoli margination (Fig. 4.50a). Microvilli lining the apical regions of the gland cells were long and uniform (Fig. 4.50b). In a few glands, cellular junctions at the apical borders were intact. However, in majority of gland cells, intercellular spaces between the lateral plasma membranes were increased (Fig. 4.50a).

12 days post-exposure to carbendazim

Ciliated cells

Ciliated cells, with sparse, damaged cilia and ruptured apical plasma membranes were observed 12 days post-exposure to carbendazim (Fig. 4.51a). The degenerating ciliated cells exhibited extensive cytoplasmic vacuolation (Fig. 4.51b). In addition, the cytoplasm contained a few small secretory granules and several lysosomes (Fig. 4.51a). Few intact mitochondria were observed in the degenerating ciliated cells. Nuclei in the degenerating ciliated cells typically displayed chromatin condensation and margination.

Non-ciliated cells

At this stage of degeneration, a few non-ciliated cells were still lined by long, uniform microvilli (Fig. 4.52a). Degenerating non-ciliated cells contained myelin figures, vacuoles and disintegrating secretory granules (Fig. 4. 52b & 4.53a). Degenerating secretory granules contained electron dense particulate material, which became dispersed in the cytoplasm in the later stages of degeneration (Fig. 4.53a). Dilated

RER cisternae and mitochondria with swollen cristae were present in the apical and basal cytoplasmic regions of the degenerating non-ciliated cells (Fig. 4.53b).

Mitochondrial and basal cells

Degenerating mitochondrial cells contained vacuoles of various sizes. In these cells, numerous lysosomes were observed. Basal cells were at advanced stages of differentiation. At this stage, the cytoplasm of the basal cells was electron dense. Extensive profiles of RER were observed in supranuclear region (Fig. 4.52a). A few vacuoles and secretory granules were also observed in the cytoplasm of the basal cells.

Plasma membranes

Cellular junctions (desmosomes) along the lateral plasma membranes were intact. However, wide intercellular spaces occurred between adjacent epithelial cells (Fig. 4.52b). Invaginations of the basal plasma membranes were occasionally observed (Fig. 4.53c). At this stage, the basal lamina underlying the epithelium was approximately 80nm in thickness. The changes in the basal lamina were similar to those observed at day 8 post-exposure.

Tubular glands

Degenerating tubular gland cells were characterized by the presence of nuclei with chromatin margination, as well as cytoplasm with large vacuoles (Fig. 4.54a). The large vacuoles contained electron dense filamentous material (Fig. 4.54b). A few lysosomes were observed in the apical and basal cytoplasmic regions of the gland cells. At this stage, the basal lamina was approximately 70 nm thick. Infolding of the basal lamina was occasionally observed. In some instances, the basal lamina appeared to be discontinuous.

32 days post-exposure to carbendazim

Ciliated cells

Deciliation was still a predominant feature 32 days post-exposure to carbendazim (Fig. 4.55a). Degenerating ciliated cells contained pyknotic nuclei. Nuclei with condensed nuclear chromatin and nuclear membrane blebbing were also encountered (Fig. 4.55b&c). Degenerating ciliated cells with either electron dense or electron lucent cytoplasm were observed. In cells with electron lucent cytoplasm, aggregations of electron dense bodies and swollen mitochondria were observed below the nuclei (Fig. 4.55a). In addition, the cytoplasm contained dilated cisternae of RER and filamentous bundles (Fig. 4.55d). The apical plasma membrane of electron lucent ciliated cells was typically discontinuous (Fig. 4.55a). Ciliated cells with electron dense cytoplasm contained degenerating mitochondria and electron dense bodies. These cells frequently displayed compound cilia (Fig. 4.56a). Fragmented axial microtubules were observed in some cilia (Fig. 4.56b).

Non-ciliated cells

Degenerating non-ciliated cells displayed apical protrusions and short microvilli (Fig. 4.57a). The cells contained pyknotic nuclei and electron dense cytoplasm (Fig. 4.57a). Secondary lysosomes and dilated cisternae of RER were observed in the apical cytoplasmic regions (Fig. 4.57a & b). Aggregates of swollen mitochondria and a few vacuoles were observed in the basal cytoplasmic regions (Fig. 4.57c).

Mitochondrial and basal cells

Mitochondrial cells displayed apical protrusions which were devoid of microvilli (Fig. 4.58a). Large vacuoles containing granules of intermediate density and a few lysosomes were observed in the apical protrusions of the cells. Mitochondria in these cells were structurally normal.

At this stage basal cells were at advanced stages of differentiation. The cells displayed electron lucent cytoplasm, which contained a few secretory granules. In some areas, newly formed cells approached the luminal end.

Plasma membranes

Cellular junctions along the lateral plasma membranes were intact. The basal lamina underlying the epithelium measured approximately 92nm in thickness. Both lamina densa and lucida were evident. However, the basal lamina was discontinuous in some places (Fig. 4.58b).

Tubular gland cells

In the tubular glands, cells with pyknotic nuclei were frequently observed (Fig. 4.59). In a few gland cells, blebbing of the nuclear membrane was evident (Fig. 4.59). The degenerating tubular gland cells were devoid of coated vesicles. Secondary lysosomes were present in the apical cytoplasmic regions of the degenerating gland cells (Fig. 4.60a). Numerous vacuoles were also observed in the cytoplasm of degenerating gland cells (Fig. 4.60a). In these cells, loss of microvilli was evident along the apical plasma membranes (Fig. 4.60a&b). The lumina of these glands contained electron dense material (Fig. 4.60b). At this stage cellular junctions joining adjacent cells were intact (Fig. 4.60c). The basal lamina underlying the tubular gland was similar to that observed at day 12 post-exposure to carbendazim.

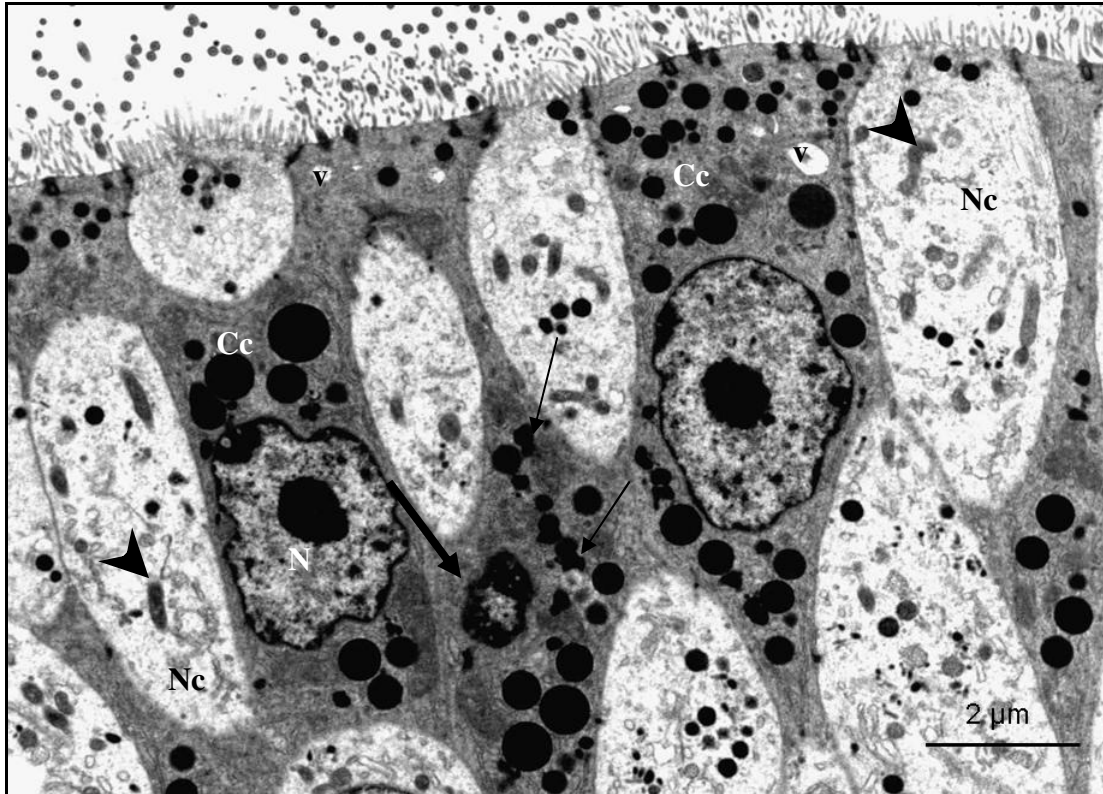


FIG. 4.39. A survey transmission electron photomicrograph of the luminal epithelium in the shell gland, 5 hours post-exposure to 400 mg/kg bodyweight carbendazim. Pyknotic (thick arrow) and irregular-shaped (N) nuclei in degenerating ciliated cells (Cc). v: vacuoles (v). Nc: degenerating non-ciliated cells. Arrowheads: mitochondria. Thin arrows: secretory granules displaying irregular outlines (). *No egg in the reproductive tract.*

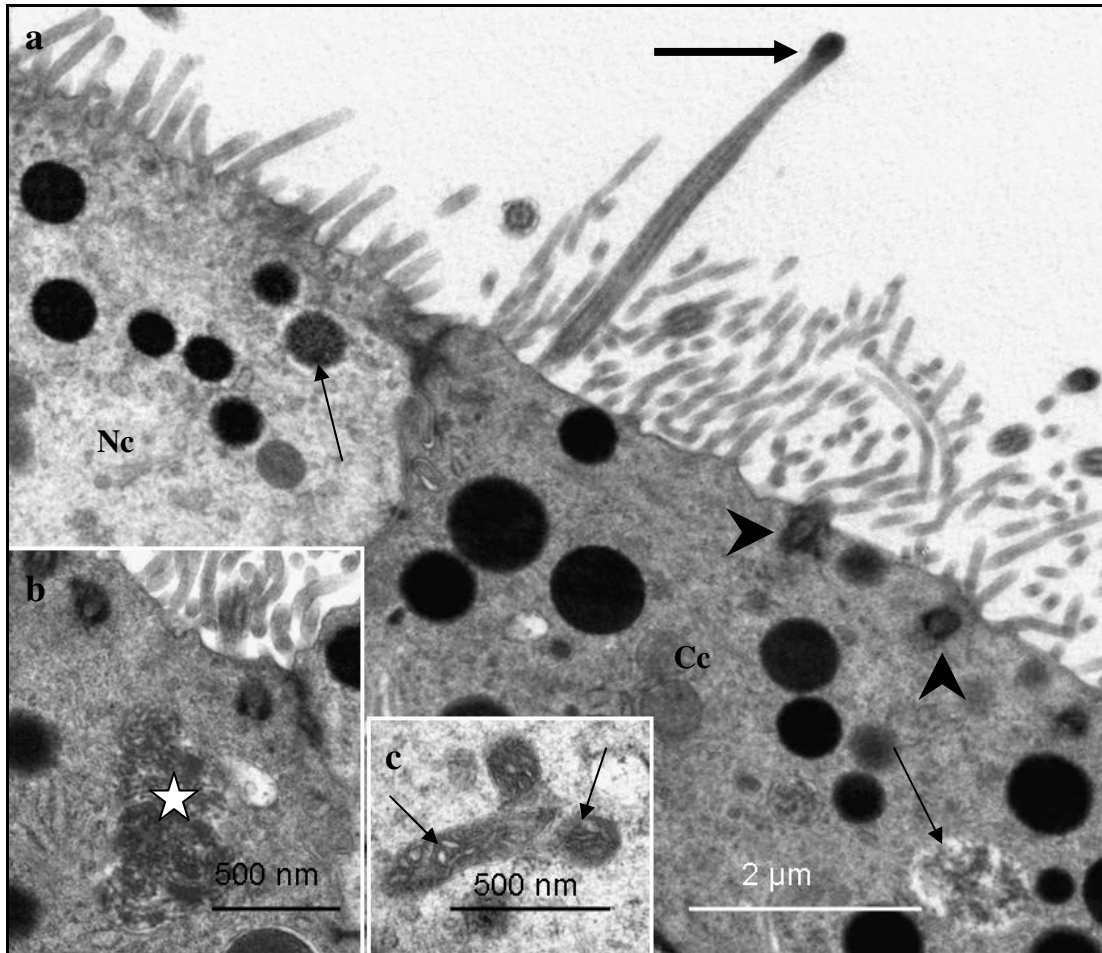


FIG. 4.40: **a.** Transmission electron photomicrograph of the apical region of luminal cells in the shell gland, 5 hours post-exposure to 400 mg/kg bodyweight carbendazim. Thick arrow: a cilium with a swollen tip. Thin arrows: degenerating secretory granules in the apical cytoplasmic regions of ciliated (Cc) and non-ciliated (Nc) cells. Arrowheads: basal bodies. **b.** A higher magnification electron photomicrograph of the apical region of a ciliated cell showing coalesced secretory granules (asterisk). **c.** Mitochondria (arrows) with dilated cristae are observed in the cytoplasm of a degenerating non-ciliated cell. *No egg in the reproductive tract.*

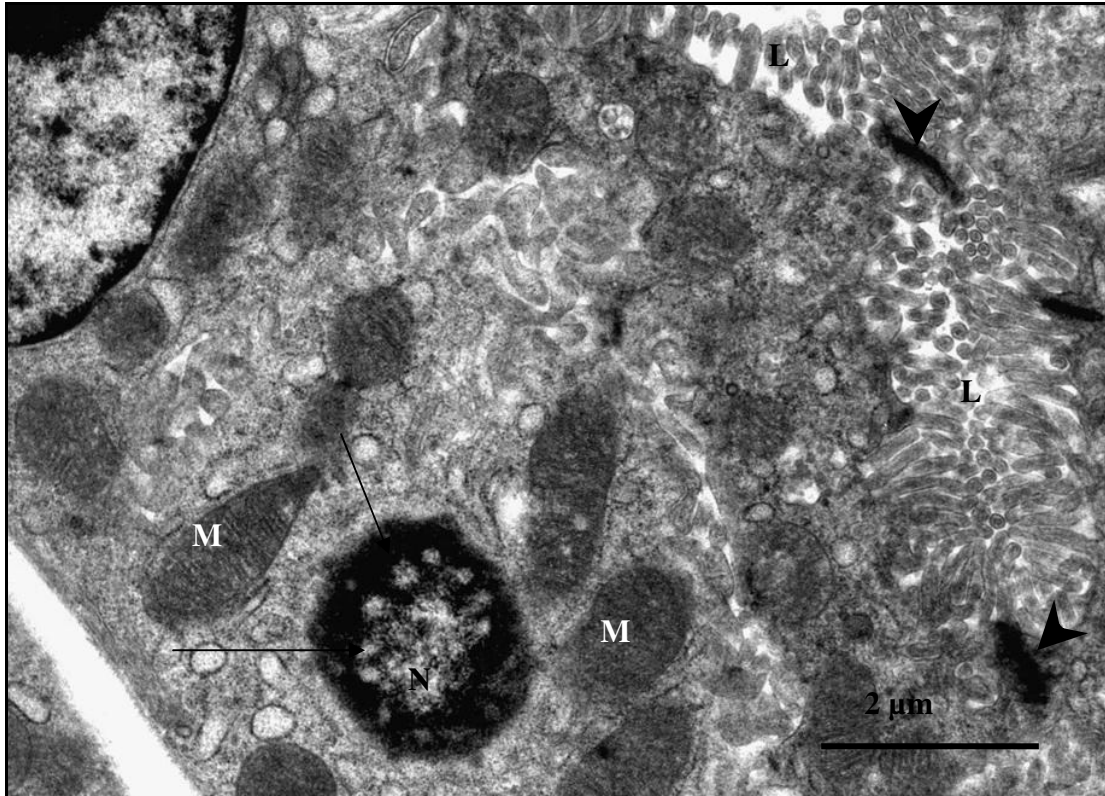


FIG. 4.41: Transmission electron photomicrograph of a gland cell in the shell gland, 5 hours post-exposure to 400 mg/kg bodyweight carbendazim. At this stage dilated nuclear pores (arrows) are evident in the degenerating nucleus (N). Microvilli and cellular junctions (arrowheads) lining the lateral plasma membranes are intact. M: mitochondria; L: glandular lumen. *No egg in the reproductive tract.*

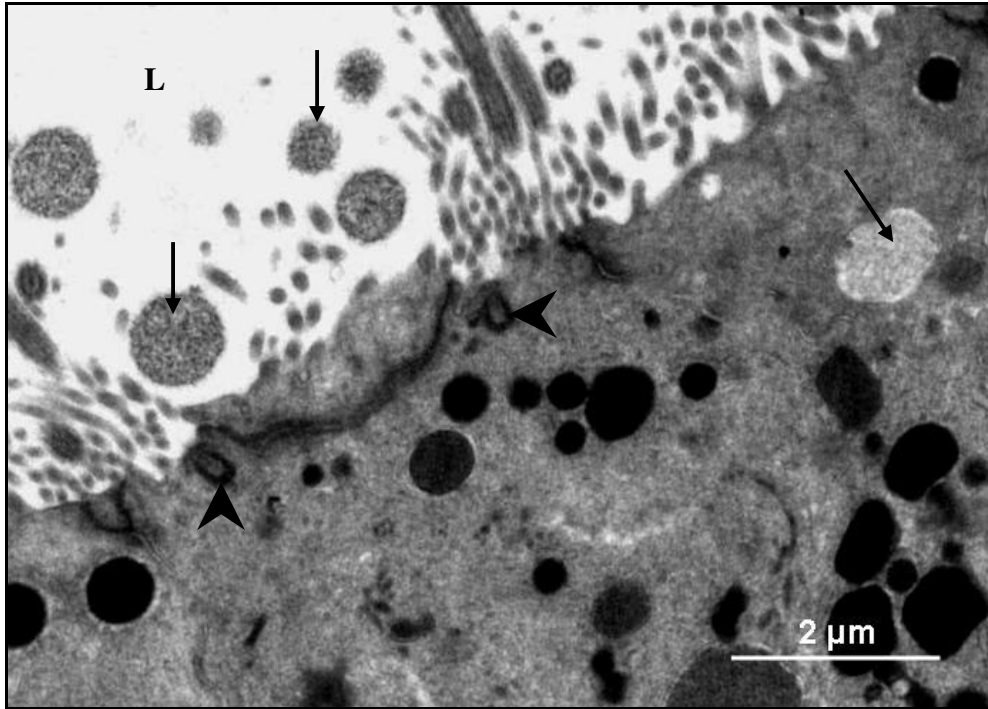


FIG. 4.42: Transmission electron photomicrograph of the apical region of a ciliated cell, 24 hours post-exposure to carbendazim. Secretory granules (arrows) are seen in the lumen (L) and in the apical cytoplasmic region of this cell. Arrowheads: basal bodies. *Egg in the shell gland.*

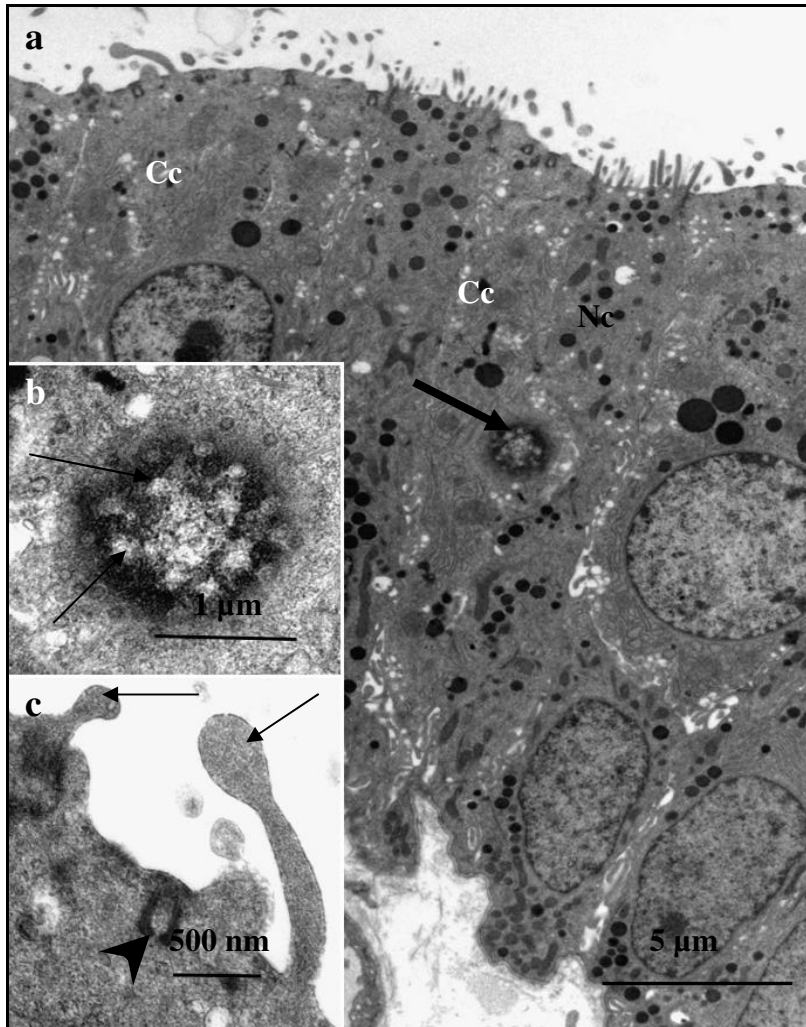


FIG. 4.43: **a.** Transmission electron photomicrograph of the luminal epithelium in the shell gland, 5 days post-exposure to 400 mg/kg bodyweight carbendazim. A nucleus with dilated nuclear pores (thick arrow) is observed in a degenerating ciliated cell (Cc). **b.** A higher magnification photomicrograph of a degenerating nucleus. Dilated nuclear pores (arrows) are evident in this nucleus. **c.** A higher magnification photomicrograph of the apical region of a ciliated cell. Microvilli with swollen tips (arrows) are observed. Arrowhead: basal body. *Yolk in the magnum.*

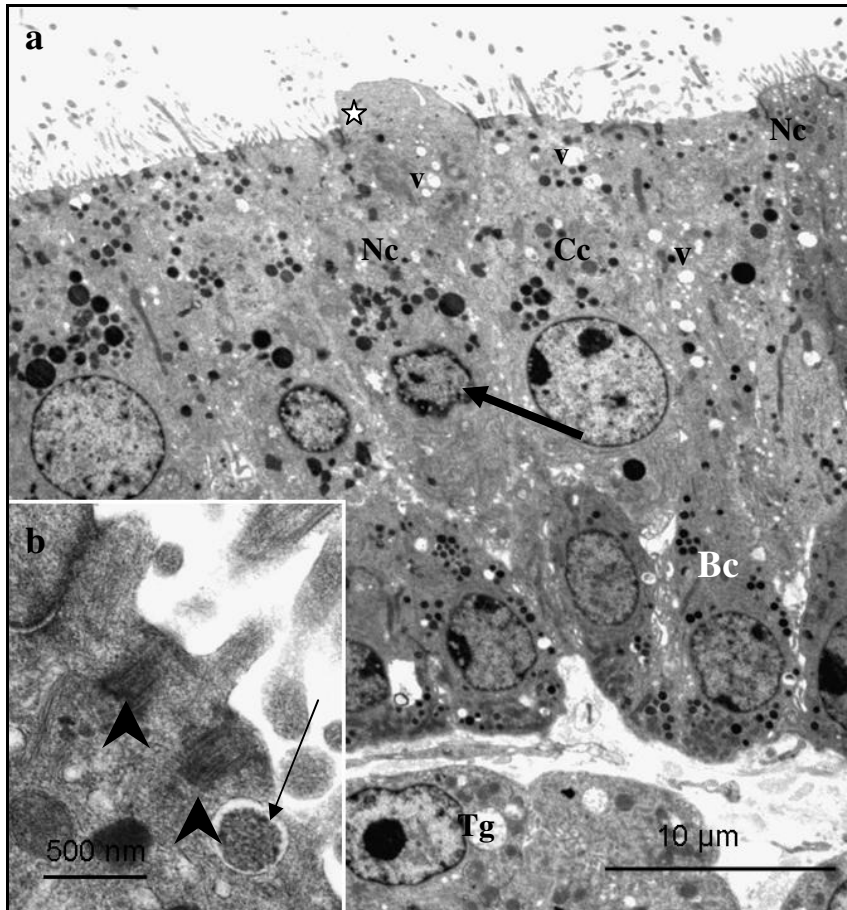


FIG. 4.44: **a.** A survey transmission electron photomicrograph of the luminal epithelium in the shell gland, 5 days post-exposure to 400 mg/kg bodyweight carbendazim. Degenerating ciliated cells (Cc) contain nuclei (arrows) with condensed and marginalized chromatin. Vacuoles (v) are observed in the apical and basal cytoplasmic regions. Degenerating non-ciliated cell (Nc) displaying protruding apical region (asterisk). Bc: degenerating basal cells; Tg: tubular glands. **b.** A higher magnification photomicrograph of the apical cytoplasmic region of a degenerating ciliated cell. A degenerating secretory granule (arrow) is seen close to the apical plasma membrane. Arrowheads: basal bodies. *Yolk in the magnum.*

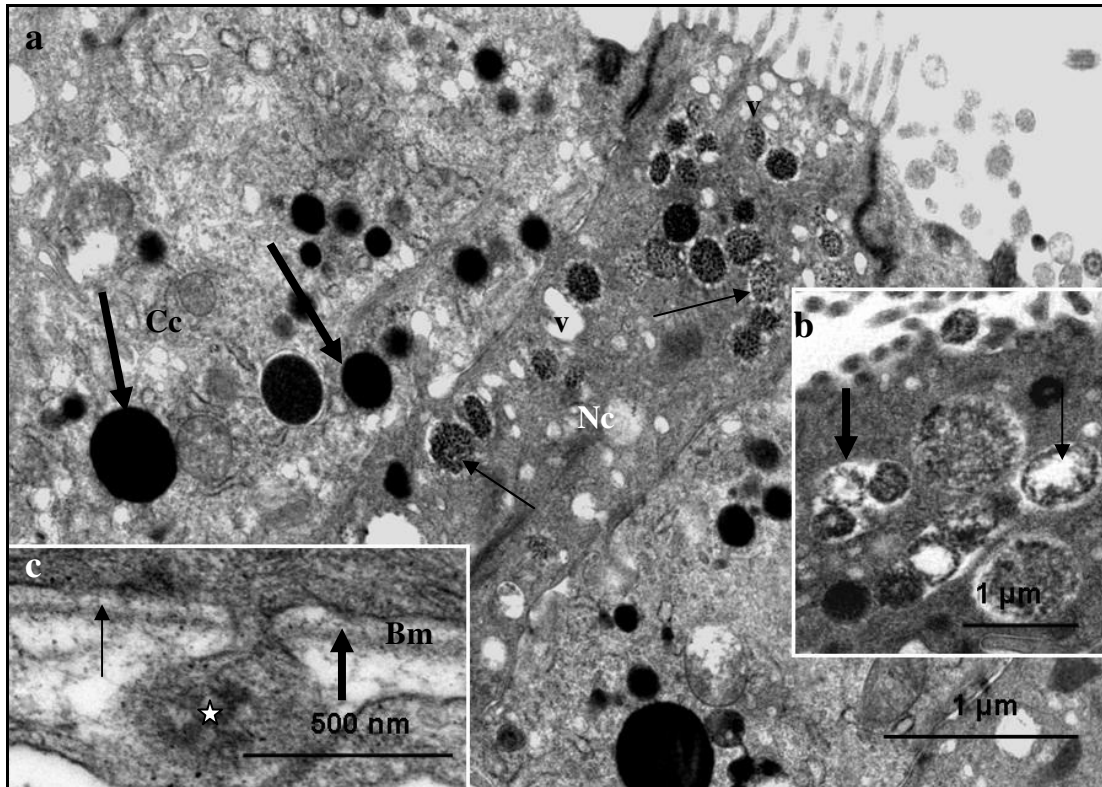


FIG. 4.45: **a.** Transmission electron photomicrograph of the luminal epithelium in the shell gland, 5 days post-exposure to 400 mg/kg bodyweight carbendazim. Thin arrows: degenerating secretory granules in a non-ciliated cell (Nc). v: vacuoles . Thick arrows: normal secretory granules in the ciliated cell (Cc). **b.** A higher magnification photomicrograph of degenerating secretory granules in a non-ciliated cell. Fragmentation of limiting membranes and a granulation of secretory material (thin arrow) are observed. Coalescing of degenerating secretory granules (thick arrow) is also evident. **c.** Electron photomicrograph of the basal region of a degenerating epithelial cell. The basal lamina (Bm) underlying the luminal epithelial cells is discontinuous. An evagination of cytoplasm (asterisk) through the basal lamina is seen. Thin arrow: lamina lucida; Thick arrow: lamina densa. *Yolk in the magnum.*

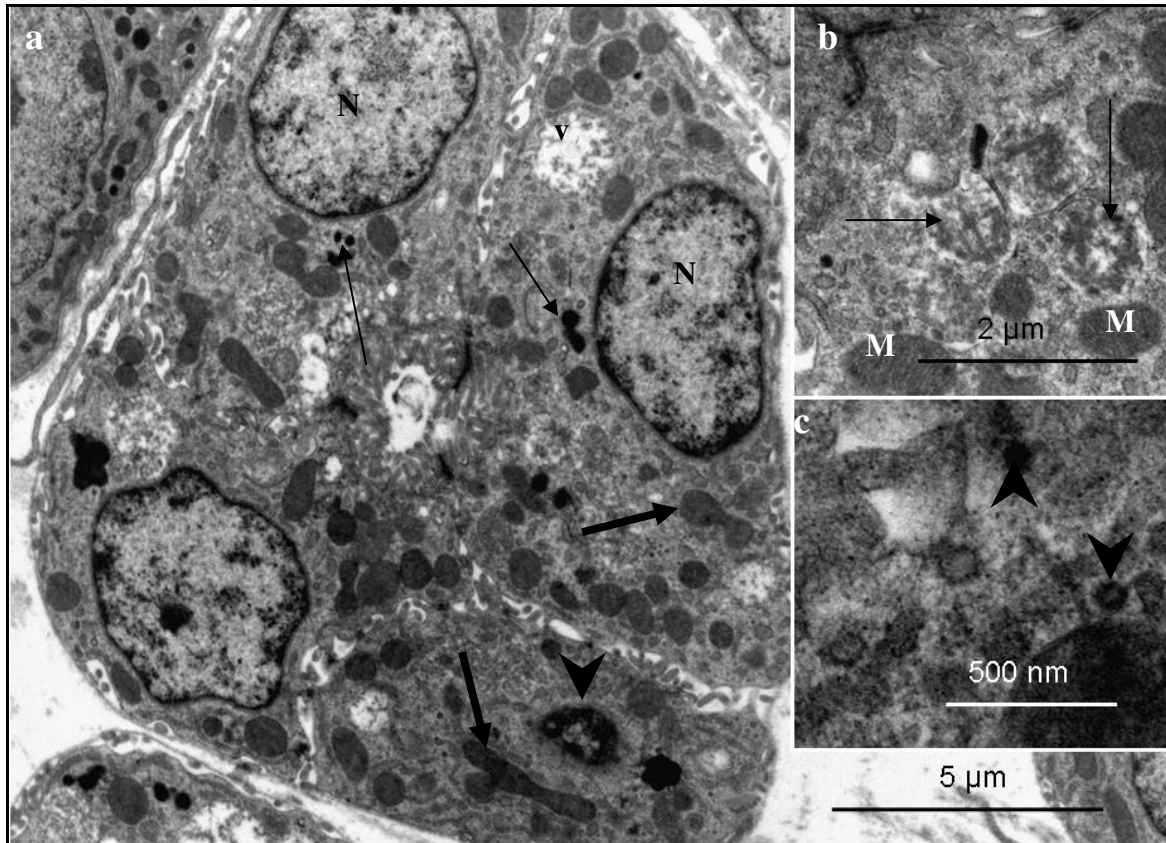


FIG. 4.46: **a.** A survey transmission electron photomicrograph of a tubular gland in the shell gland, 5 days post-exposure to 400 mg/kg bodyweight carbendazim. Arrowhead: pyknotic nucleus in degenerating gland cell. Thin arrows: lysosomes. Thick arrows: normal mitochondria. N: nucleus; v: A vacuole containing electron dense granules. **b.** A higher magnification electron photomicrograph of vacuoles containing electron dense granules (arrows). M: mitochondria. **c.** Electron photomicrograph of the cytoplasm in a degenerating gland cell. Coated vesicles (arrowheads) contain electron dense material. *Yolk in the magnum.*

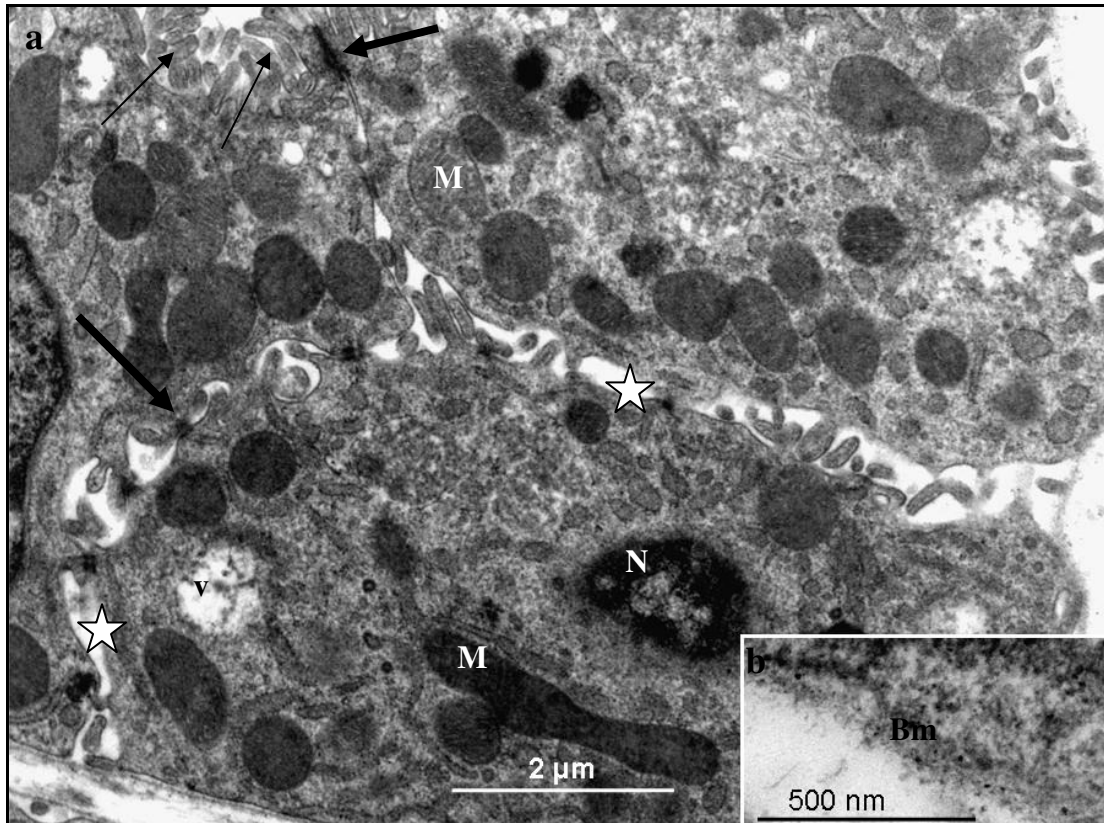


FIG. 4.47: **a.** Transmission electron photomicrograph of degenerating gland cells in the shell gland, 5 days post-exposure to 400 mg/kg carbendazim. Asterisks: wide intercellular spaces between the gland cells. Apical microvilli (thin arrows) appear normal in structure. Thick arrows: desmosomes. N: pyknotic nucleus; M: mitochondria; v: vacuole with a dense, granular material. **b.** Electron photomicrograph of the basal lamina (Bm) surrounding the gland cells. At this stage, the lamina lucida of the basal lamina is indistinct. *Yolk in the magnum.*

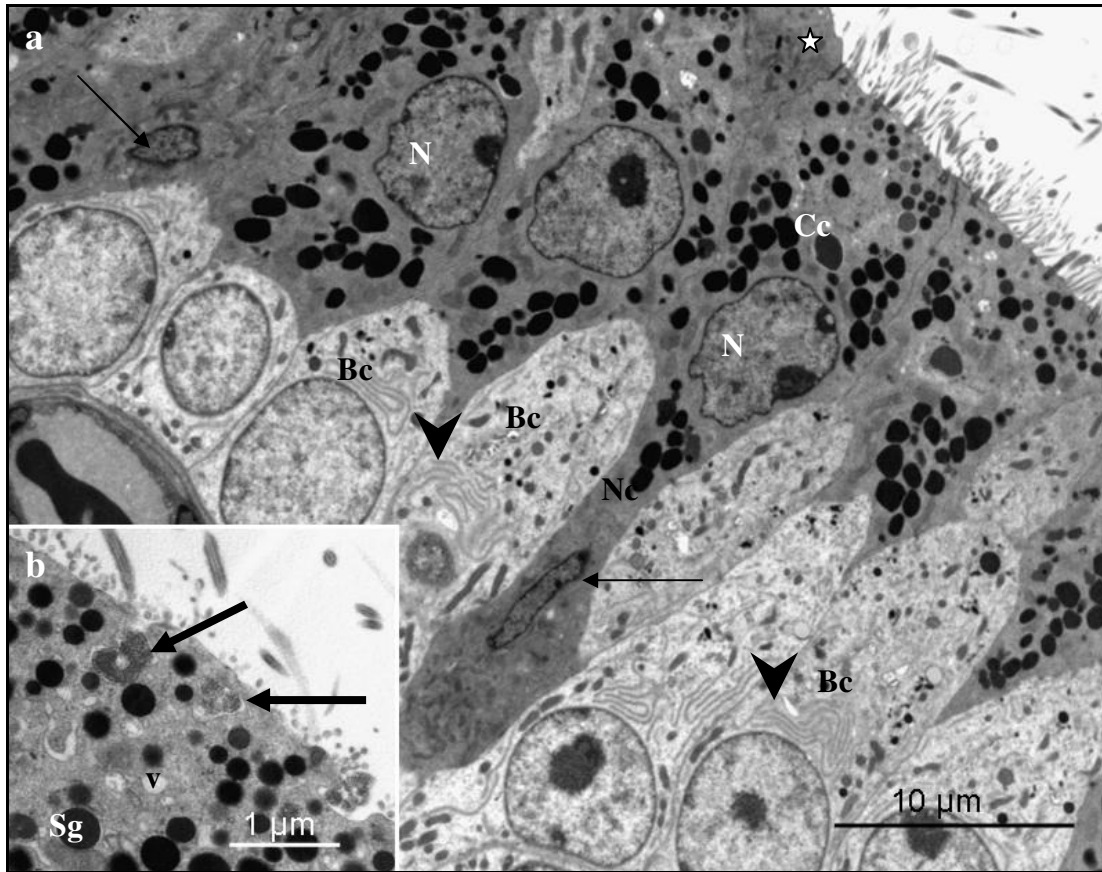


FIG. 4.48: **a.** A survey transmission electron photomicrograph of the luminal epithelium in the shell gland, 8 days post-exposure to 400 mg/kg bodyweight carbendazim. Pyknotic nuclei (arrows) are observed in non-ciliated (Nc) and ciliated (Cc) cells. Note the apical protrusion (asterisk) of a degenerating non-ciliated cell. At this stage, differentiating basal cells (Bc) are observed, containing extensive profiles of RER (arrow heads). **b.** Transmission electron photomicrograph of degenerating secretory granules (arrows) in the apical region of a degenerating ciliated cell. Sg: normal secretory granule; V: vacuole. *No egg in the reproductive tract.*

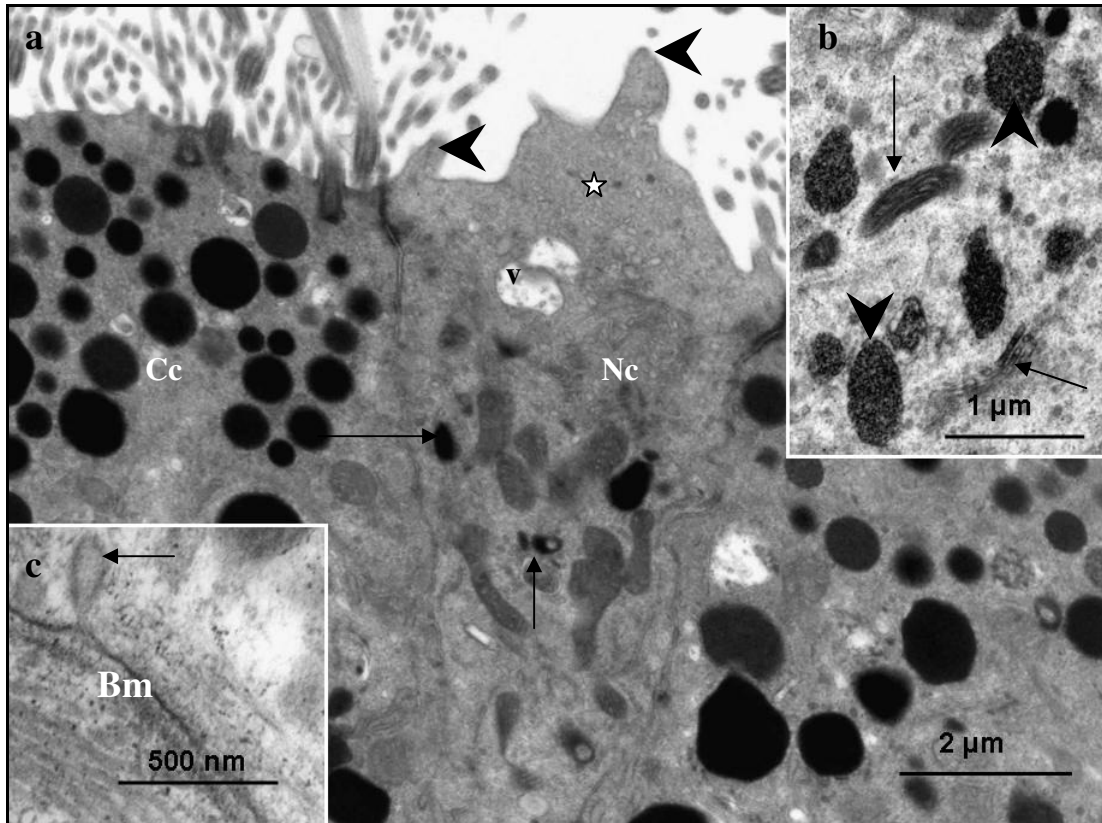


FIG. 4.49: **a.** Transmission electron photomicrograph of the luminal epithelium in the shell gland, 8 days post-exposure to 400 mg/kg bodyweight carbendazim. A degenerating non-ciliated cell (Nc) exhibits an apical protrusion (asterisk), vacuoles (v) and lysosomes (arrows). A few short, thick microvilli (arrowheads) are present. Cc: degenerating ciliated cell. **b.** Transmission electron photomicrograph of microtubular structures (arrows) and degenerating secretory granules (arrowheads) in non-ciliated cells. **c.** Electron photomicrograph of the basal lamina (Bm) underlying the luminal epithelium. An invagination of the basal lamina (arrow) is evident. *No egg in the reproductive tract.*

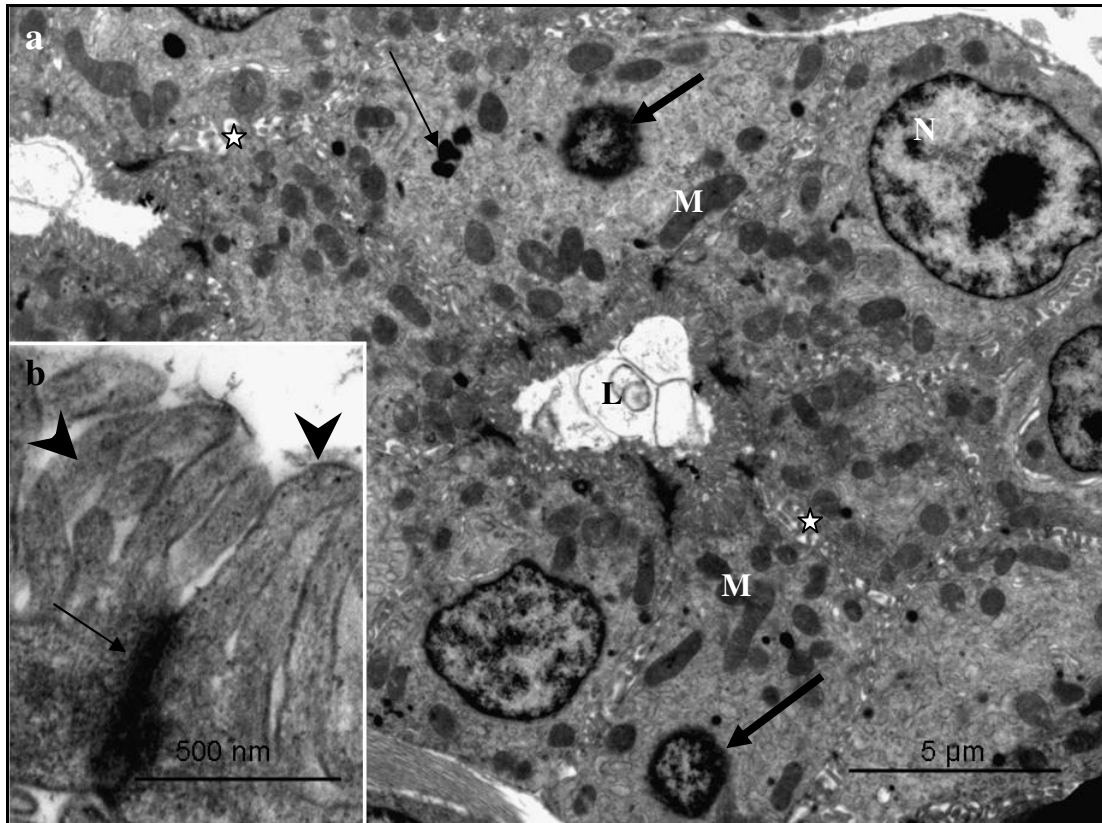


FIG. 4.50: **a.** Transmission electron photomicrograph of a tubular gland in the shell gland, 8 days post-exposure to carbendazim. Nuclei in the early stages of chromatin condensation (thick arrows) are observed. At this stage, wide intercellular spaces are observed between the lateral plasma membranes (asterisks). Thin arrow: lysosomes; M: mitochondria; N: normal nucleus; L: glandular lumen containing secretory debris. **b.** A higher magnification electron photomicrograph of cellular junction (arrow) at the apical border of a tubular gland in the shell gland. At this stage, the microvilli (arrowheads) lining the apical plasma membrane are structurally normal. *No egg in the reproductive tract.*

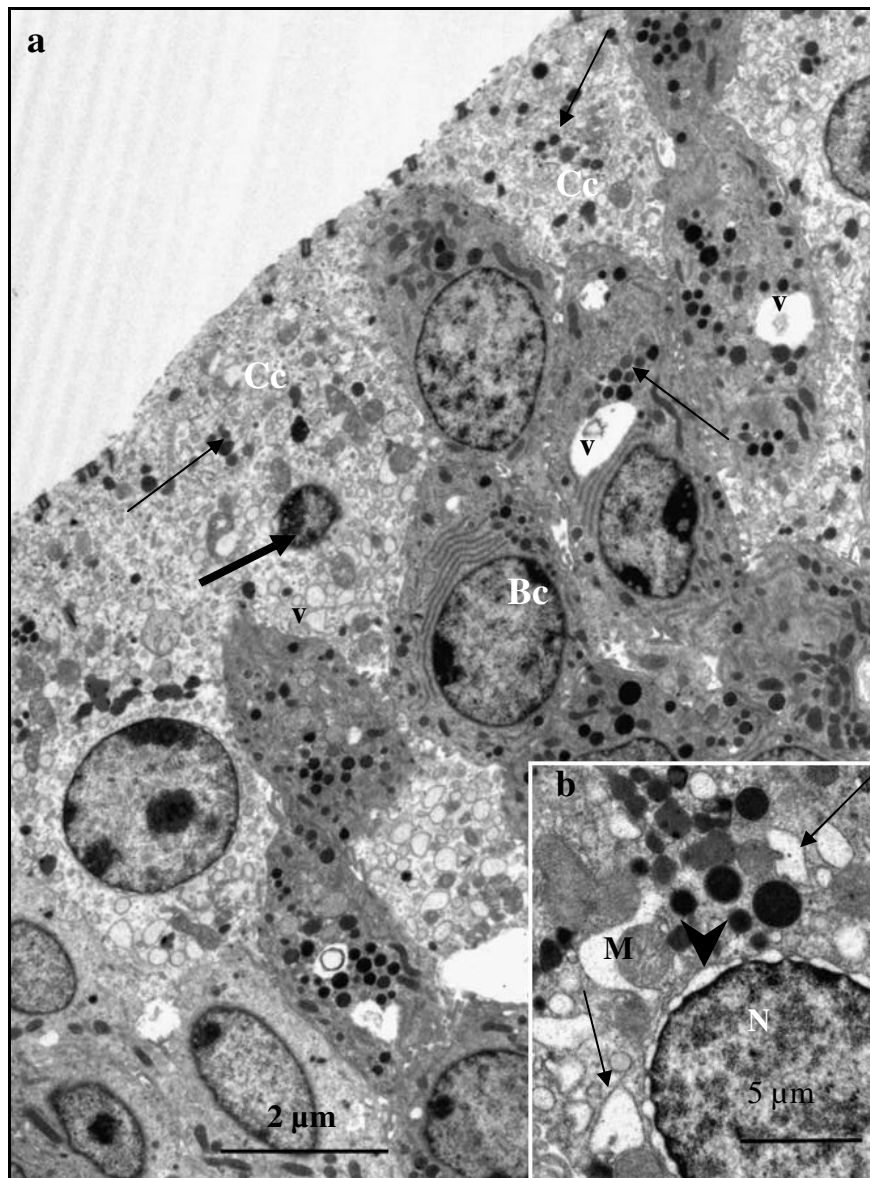


FIG. 4.51: **a.** A survey transmission electron photomicrograph of the luminal epithelium in the shell gland, 12 days post-exposure to 400 mg/kg bodyweight carbendazim. Ciliated cells (Cc) with sparse, damaged cilia and ruptured apical plasma membranes are observed. Thin arrows: lysosomes. Thick arrow: degenerating nucleus. Bc: basal cells at an advanced stage of differentiation, contain extensive profiles of RER and electron dense cytoplasm. v: vacuoles. Arrows: small secretory granules. **b.** A higher magnification transmission electron photomicrograph of a degenerating ciliated cell. Blebbing of the nuclear membrane (arrowhead) and dilated cisternae of RER (arrows) are observed. M: mitochondrion; N: nucleus. *No egg in the reproductive tract.*

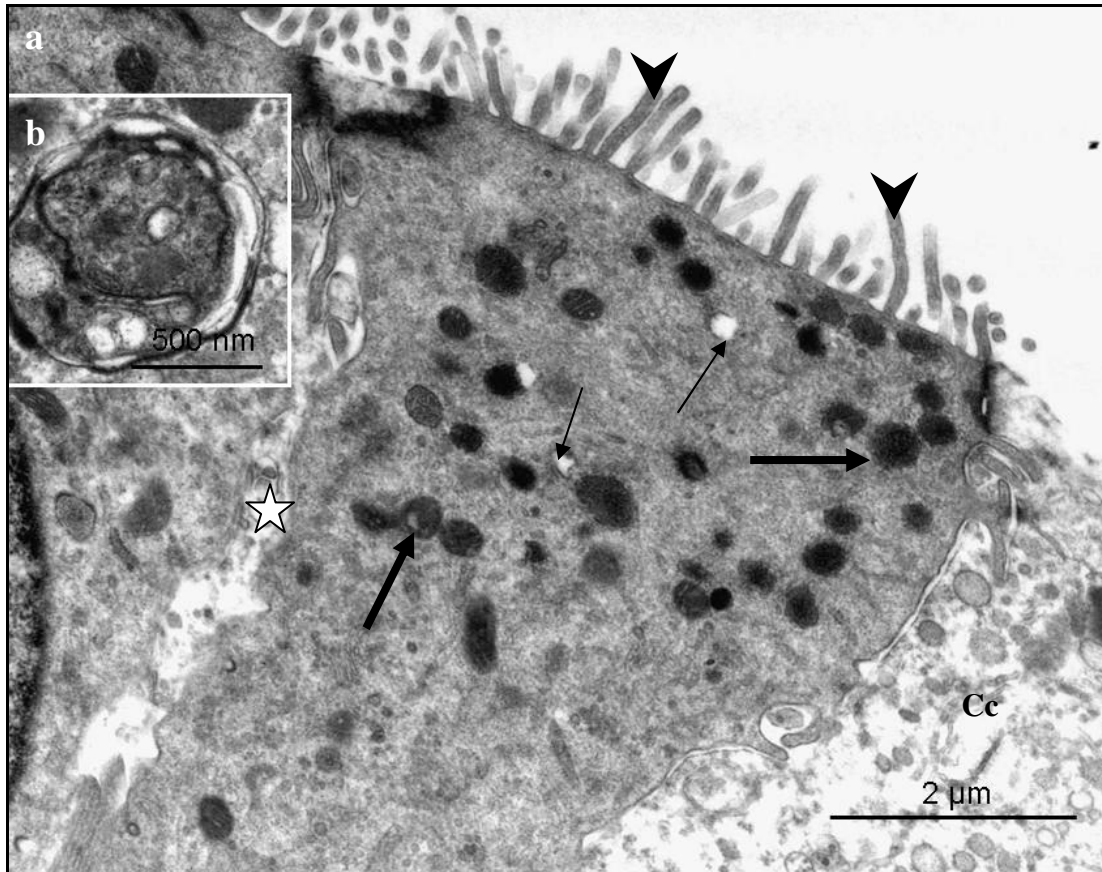


FIG. 4.52: **a.** Transmission electron photomicrograph of the apical region of a non-ciliated cell in the shell gland, 12 days post-exposure to 400 mg/kg bodyweight carbendazim. In the apical cytoplasmic region degenerating secretory granules (thick arrows) and vacuoles (thin arrows) are observed. Note the wide intercellular spaces (asterisk) between adjacent cells. Cc: degenerating ciliated cell. Arrowheads: microvilli. **b.** Electron photomicrograph of a myelin figure observed in the cytoplasm of a degenerating non-ciliated in the shell gland. *No egg in the reproductive tract.*

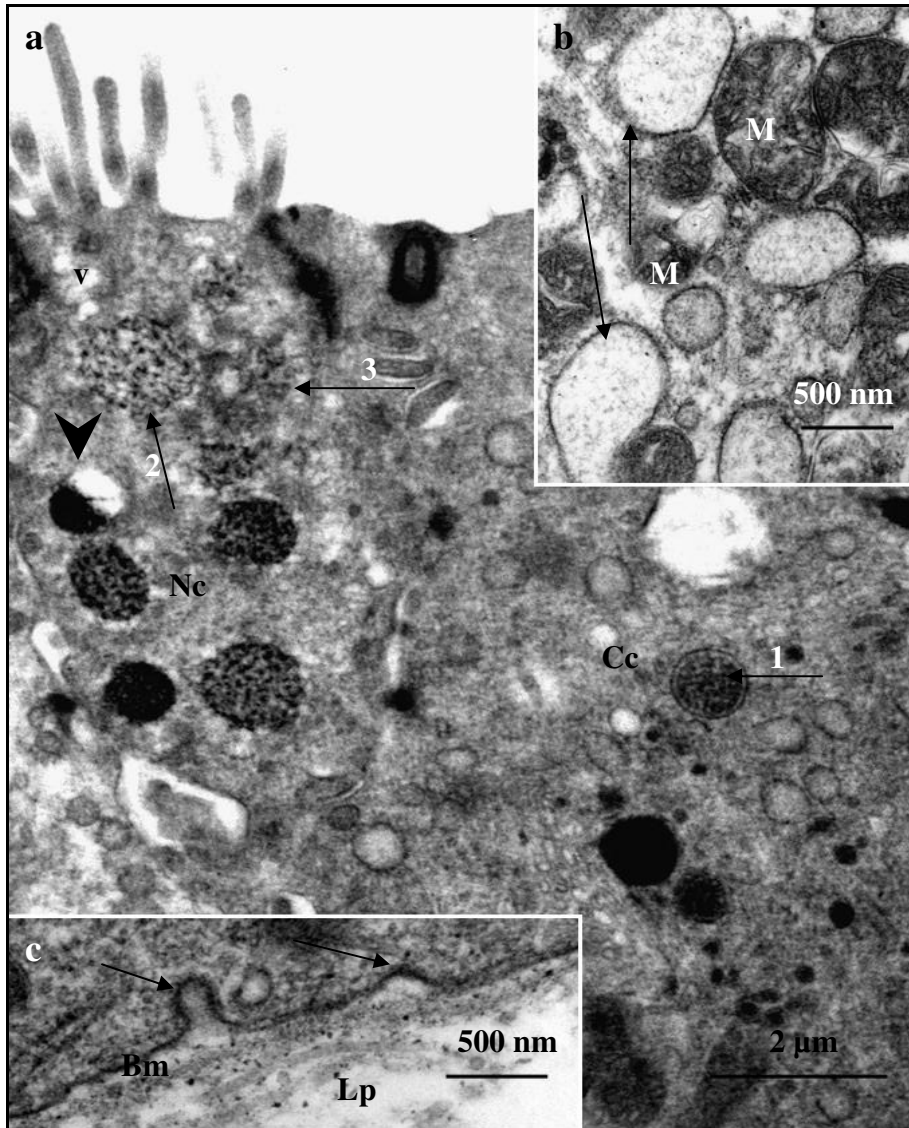


FIG. 4.53: **a.** Transmission electron photomicrograph of the apical region of a degenerating non-ciliated cell (Nc) in the shell gland, 12 days post-exposure to 400 mg/kg bodyweight carbendazim. Secretory granules (arrows) at various stages of disintegration are observed. **Stage 1:** secretory granule has a distinct limiting membrane. **Stage 2:** the limiting membrane is discontinuous. **Stage 3:** secretory materials are dispersed into the cytoplasm. A vacuolated secretory granule (arrowhead) is also observed in this cell. Cc: ciliated cell. **b.** A higher magnification of the basal cytoplasmic region of a degenerating non-ciliated cell. Dilated cisternae of RER (arrows) are observed. M: swollen mitochondria. **c.** Electron photomicrograph of the basal lamina (Bm) underlying the epithelial cells. Invaginations of the basal membrane (arrows) are evident. Lp: *lamina propria-submucosa*. No egg in the reproductive tract.

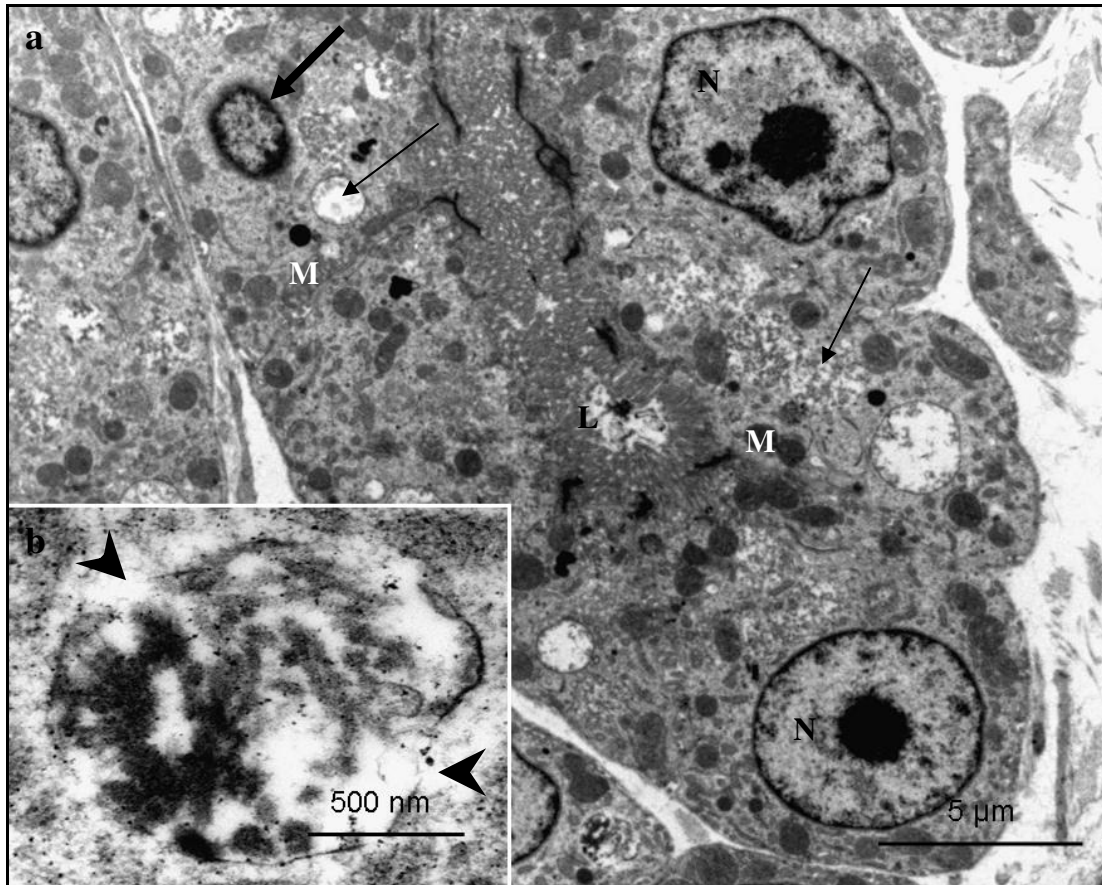


FIG. 4.54: **a.** A survey transmission electron photomicrograph of a tubular gland in the shell gland, 12 days post-exposure to 400 mg/kg bodyweight carbendazim. A nucleus with chromatin margination (thick arrow) is observed. Vacuoles containing electron dense granules (thin arrows) are also observed. N: normal nuclei; M: mitochondria; L: glandular lumen. **b.** A higher magnification electron photomicrograph of a vacuole containing an electron dense filamentous material. Note the fragmentation of the limiting membrane (arrowheads). *No egg in the reproductive tract.*

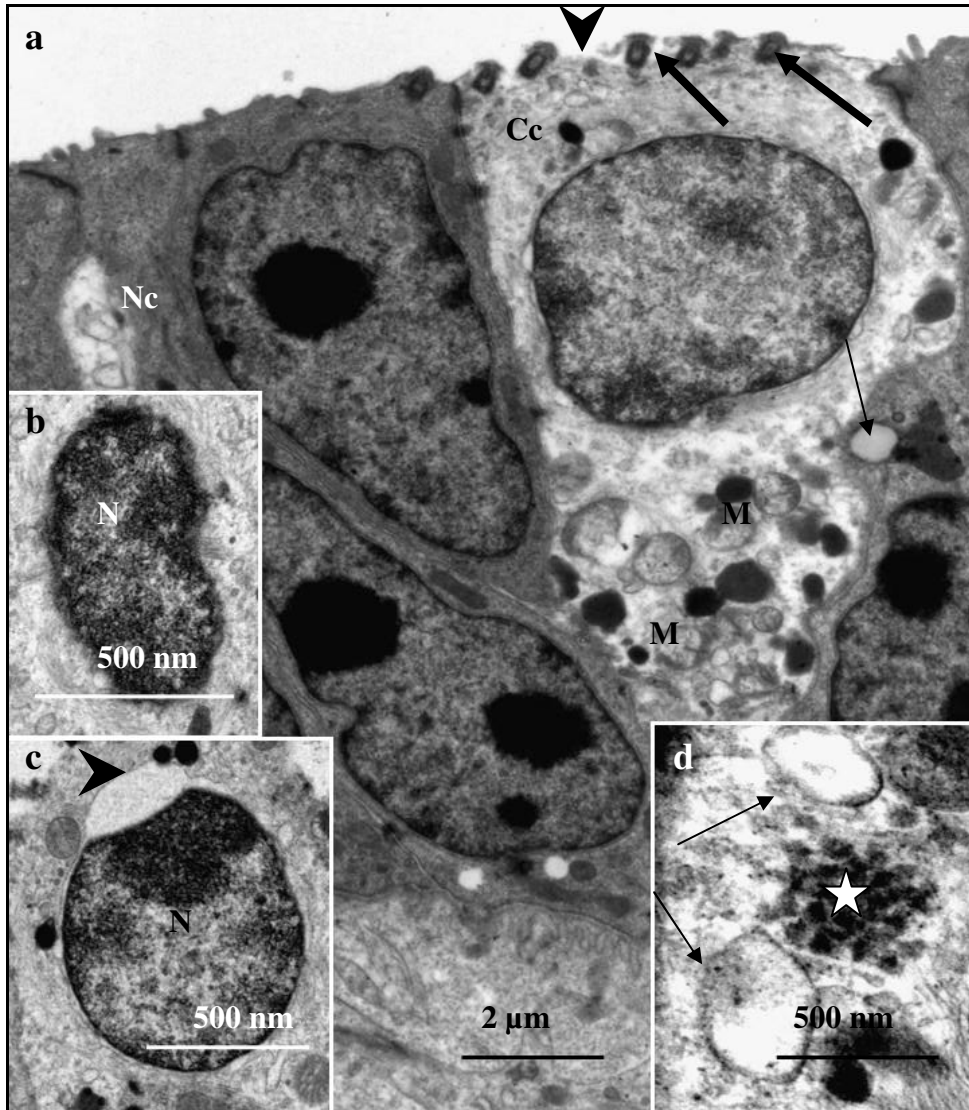


FIG. 4.55: **a.** Transmission electron photomicrograph of the luminal epithelium in the shell gland, 32 days post-exposure to 400 mg/kg bodyweight carbendazim. Cc: ciliated cells displaying loss of cilia and microvilli. Arrowhead: discontinuous apical plasma membranes. Thick arrows: basal bodies without rootlets. Thin arrow: A lipid droplet. M: swollen mitochondria. Nc: non-ciliated cell. **b.** A higher magnification photomicrograph of a nucleus (N) displaying condensed chromatin. **c.** A nucleus (N) showing blebbing of the nuclear membrane (arrowhead). **d.** Apical cytoplasmic region of a degenerating ciliated cell. Filamentous aggregates (asterisk) and dilated cisternae of RER (arrows) are observed. *Egg in the shell gland.*

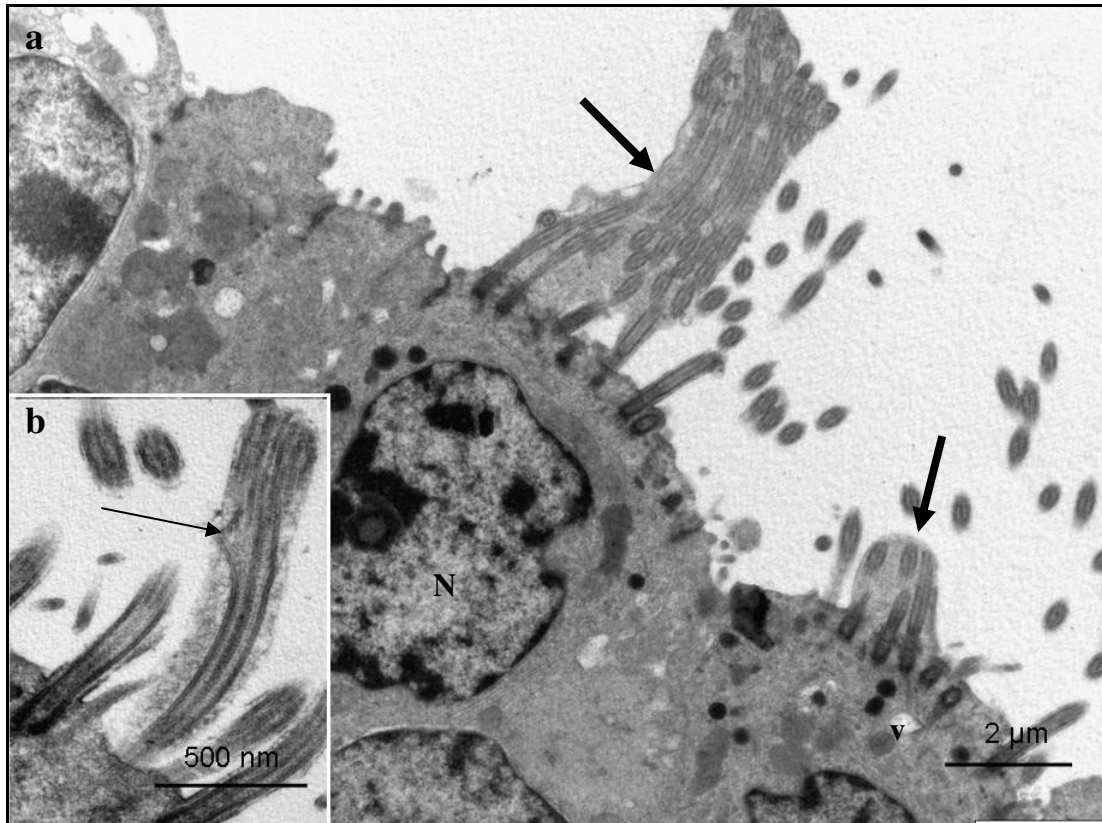


FIG. 4.56: **a.** Transmission electron photomicrograph of the apical region of the epithelial cells in the shell gland, 32 days post-exposure to 400 mg/kg bodyweight carbendazim. Compound cilia (arrows) are observed. N: Nucleus; V: vacuole. **b.** A higher magnification electron photomicrograph of cilia. Note the presence of a fragmented axial microtubule (arrow) in a degenerating cilium. *Egg in the shell gland.*

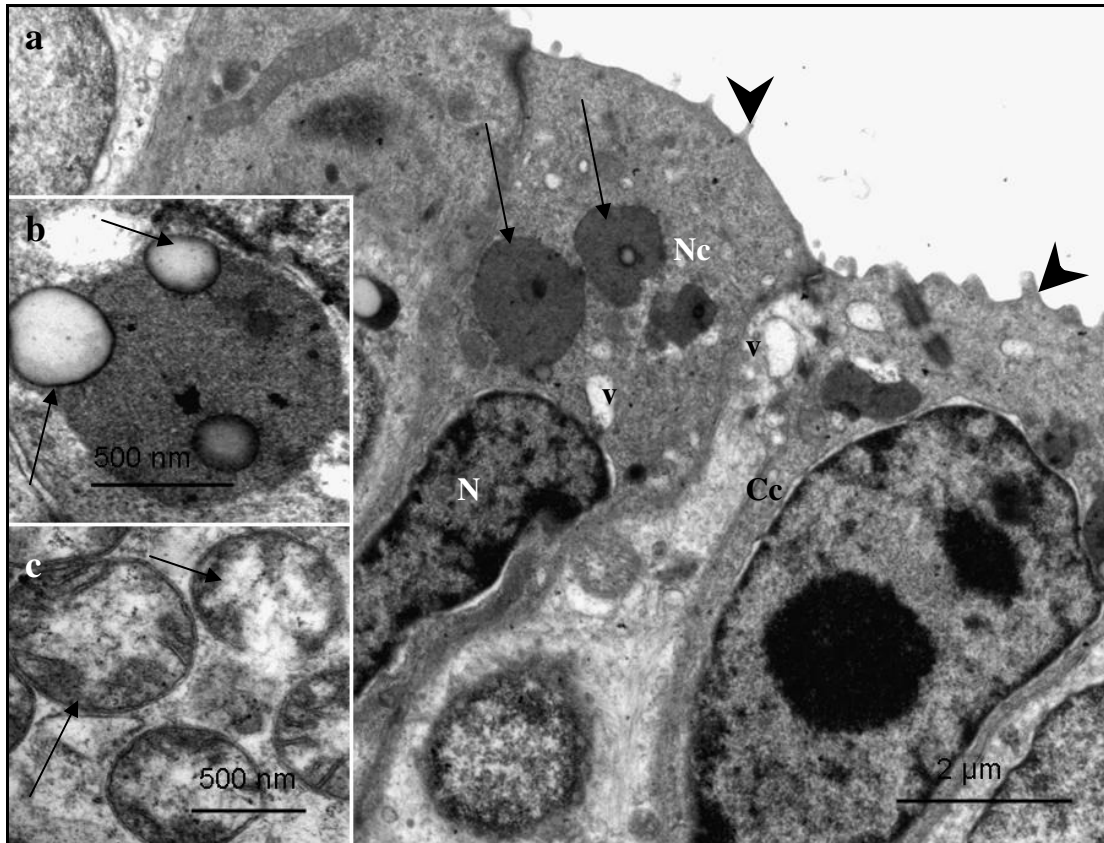


FIG. 4.57: **a.** Electron photomicrograph of the apical region of the epithelial cells in the shell gland, 32 days post-exposure to 400 mg/kg bodyweight carbendazim. A few thick microvilli (arrowheads) line the apical plasma membranes of the ciliated (Cc) and non-ciliated cells (Nc). Secondary lysosomes (arrows) are observed in these cells. N: degenerating nucleus; Cc: ciliated cell; v: vacuoles. **b.** A high magnification transmission electron photomicrograph of a secondary lysosome. The lysosome contains several lipid droplets (arrows) of varying sizes. **c.** Transmission electron photomicrograph of the basal cytoplasmic region of a degenerating non-ciliated cell. Swollen mitochondria (arrows) are observed. *Egg in the shell gland.*

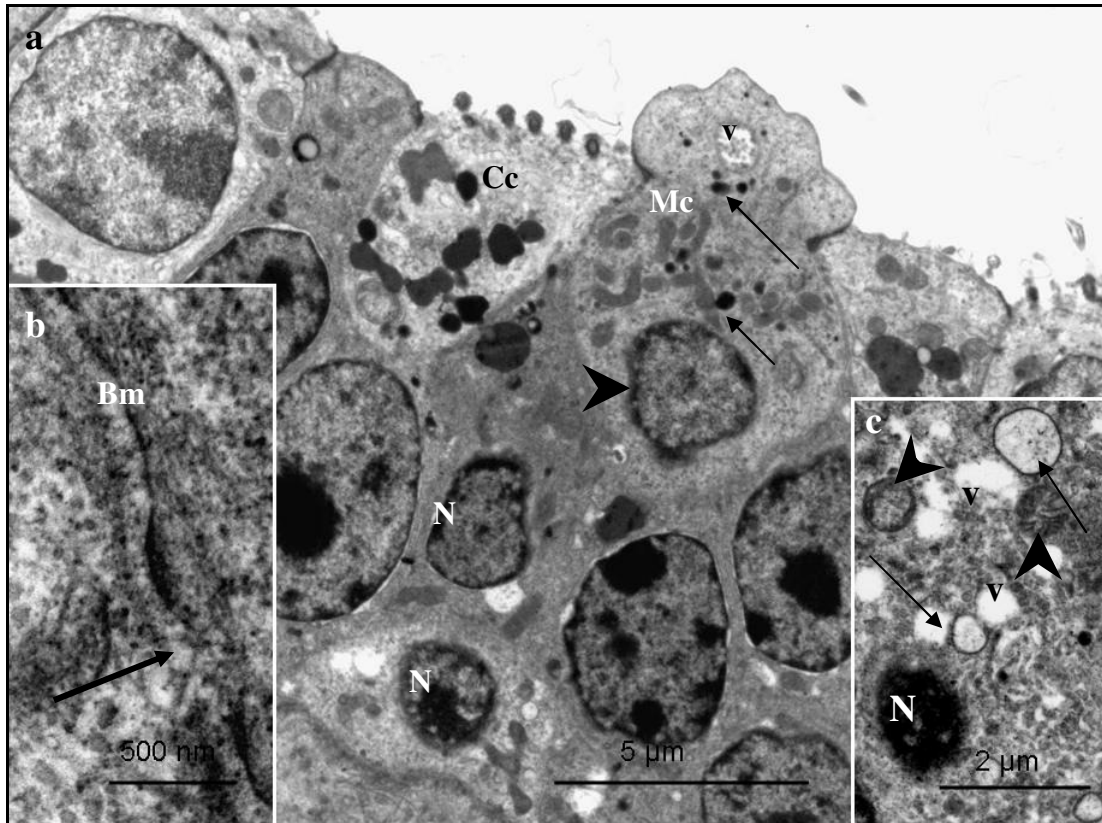


FIG. 4.58: **a.** A survey transmission electron photomicrograph of the luminal epithelium in the shell gland, 32 days post-exposure to 400 mg/kg bodyweight carbendazim. The apical region of degenerating mitochondrial cell (Mc) is observed protruding above the luminal surface. The cell contains a few lysosomes (arrows), a vacuole (v) and a nucleus (arrowhead) displaying chromatin margination. Cc: ciliated cells, N: degenerating nuclei. **b.** Electron photomicrograph of the basal lamina (Bm) underlying the luminal epithelium. A focal discontinuation of the basal lamina (arrow) is observed. **c.** Electron photomicrograph of a degenerating basal cell in the luminal epithelium. A pyknotic nucleus (N), vacuoles (v), swollen mitochondria (arrowheads) and dilated RER cisternae (arrows) are observed in the cytoplasm. *Egg in the shell gland.*

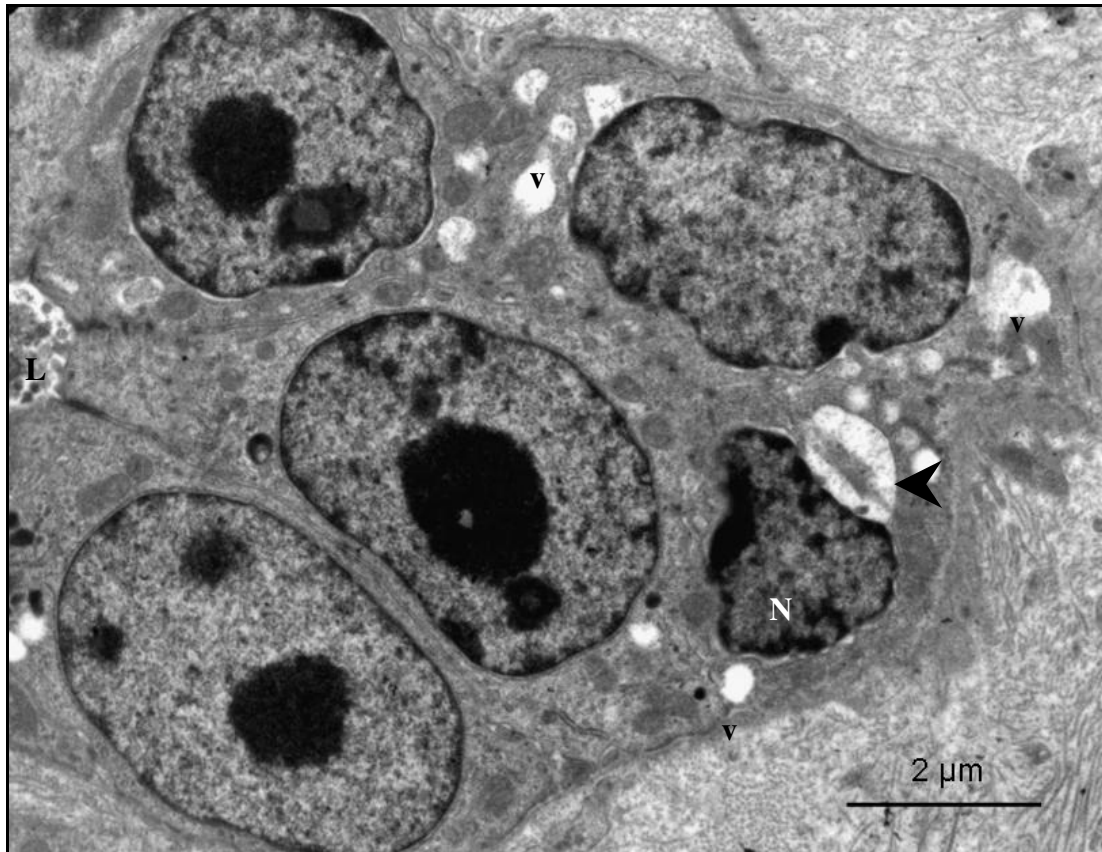


FIG. 4.59: Transmission electron photomicrograph of a tubular gland in the shell gland, 32 days post-exposure to 400 mg/kg bodyweight carbendazim. Nuclear membrane blebbing (arrowhead) and chromatin margination are evident in a degenerating nucleus (N). A few vacuoles (v) are also observed. L: glandular lumen containing cellular and secretory debris. *Egg in the shell gland.*

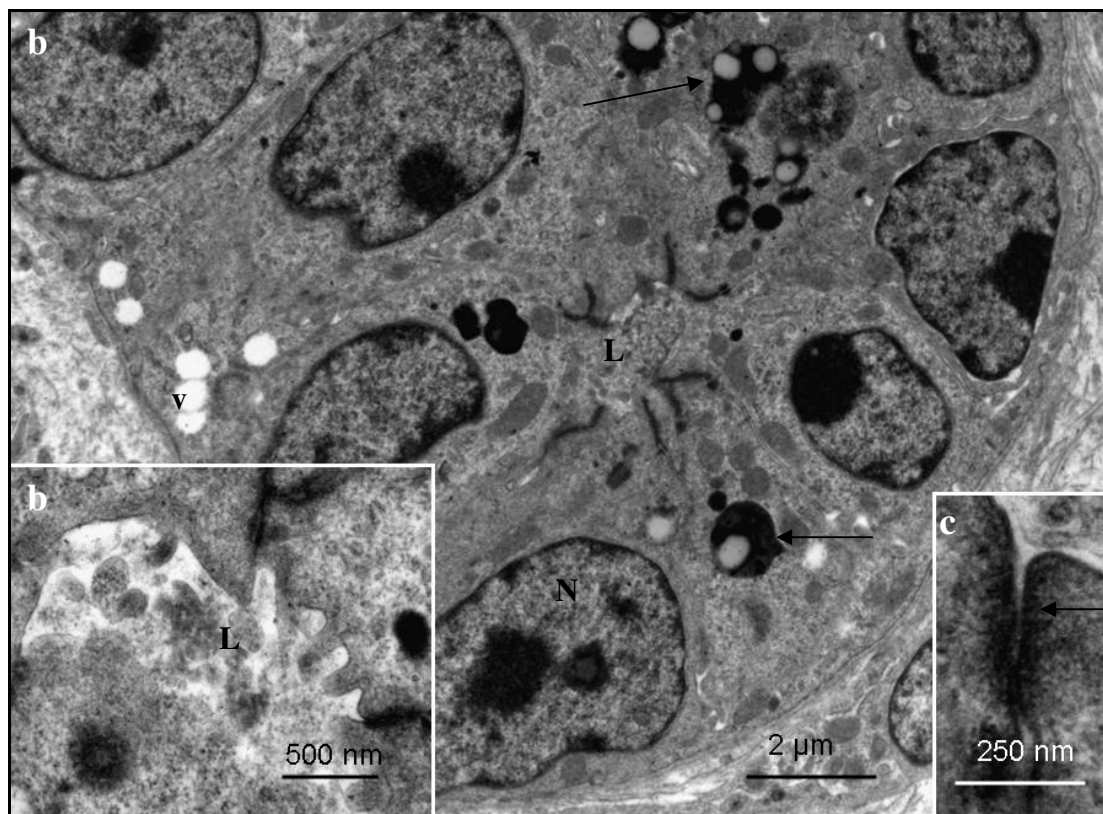


FIG. 4.60: **a.** Transmission electron photomicrograph of a tubular gland in the shell gland, 32 days post-exposure to 400 mg/kg bodyweight carbendazim. Numerous secondary lysosomes (arrows) and vacuoles (v) are observed. The lumen (L) contains secretory debris. N: nucleus. **b.** A higher magnification transmission electron photomicrograph of gland lumen (L). Note the presence of debris and loss of microvilli. **c.** Arrow: A tight junction at the apical border of the plasma membranes. *Egg in the shell gland.*

4.4 Discussion

Histology, histochemistry and statistical analysis

The present study has highlighted the morphological changes that occur in the shell gland following exposure to the cytoskeletal disrupting agent, carbendazim. The results of the morphometric study in experiment I showed that carbendazim reduced the heights of the mucosal folds and luminal epithelium, as well as, glandular width at doses of 25, 100 and 400 mg/kg bodyweight. This decrease could be due to oviductal atrophy caused by carbendazim toxicity. Oviductal atrophy could also be due to an androgenic effect exerted by carbendazim as reported in rats by Lu, Liao, Kuo, Wang, Hwand & Ueng (2004) and Hsu, Chang, Chen, Yuan, Chen, Ueng & Lu

(2011). Hsu *et al.* (2011). The study by Lu *et al.* (2004) showed that carbendazim exposure increased androgen receptor mRNA in a dose-dependent manner. According to Lu *et al.* (2004), carbendazim exposure to pregnant rats increased androgen concentration and consequently induced androgenic effects in male and female offspring. Further investigations are needed to assess the effect of carbendazim on hormones in birds.

Contrary to the observations made at lower doses, at a dose of 800 mg/kg bodyweight, the epithelial height and glandular width increased. A transient increase of these parameters was also observed after the administration of a single dose of 400 mg/kg bodyweight carbendazim. The transient increase in these parameters could be due to the hyperplastic effects of carbendazim linked to its ability to stimulate the synthesis and activity of cytochrome P₄₅₀ aromatase. High levels of cytochrome P450 increase the conversion rate of androgen to oestrogen (Morinaga, Yanase, Nomura, Okabe, Goto, Harada & Nawata, 2004). According to Yu & Marquardt (1973), oestrogen stimulates oviductal development, as well as the formation of tubular glands.

In the current study, the histomorphology of the oviduct in control birds was in agreement with observations made by Breen & De Bruyn (1969) and Wyburn *et al.* (1973) of the oviduct in the domestic fowl. In carbendazim-treated birds degeneration of both luminal and glandular epithelial cells was prominent. Based on the relationship between the morphology and physiological functions of the shell gland cells shown by Breen & De Bruyn (1969), Wyburn *et al.* (1973), Solomon, Fryer & Baird (1975) and Fernandez *et al.* (2001), degeneration of these cells may affect the formation of the eggshell. Further studies on any functional impairment as a consequence of carbendazim administration is proposed.

Histochemical results of the control group showed the presence of PAS reactive granules in both ciliated and non-ciliated luminal epithelial cells. The PAS stain reaction was also observed in the glandular epithelium, as well as in the glandular luminal contents. Similar findings have been reported in the domestic fowl (Robinson, King & Bowen 1968). According to Robinson *et al.* (1968), epithelial cells in the shell gland contain both neutral and acidic mucopolysaccharide granules. The

report further showed that granules in the luminal epithelial cells reactive for PAS contained periodate-reactive and unsubstituted vicinal hydroxyl groups. Following carbendazim treatment, epithelial cells showed a weak to absent reaction to PAS staining. The reduction of PAS reactive granules in the luminal epithelium of carbendazim-treated birds further suggested that carbendazim lowers the secretory function of these cells. In the present study, epithelial cells were negative for Alcian blue. This finding is contrary to the observation made in the domestic fowl, which indicated the presence of strong acidic mucopolysaccharide granules in both the luminal and glandular epithelium (Robinson *et al.*, 1968).

Immunohistochemistry

In the current investigation, immunoreactivity for e-cadherin was observed in the lateral plasma membranes of both epithelial and glandular cells in the control birds. Similar observations have been reported in the uterine epithelial cells in the mouse (Paria, Zhao, Das, Dey & Yoshinaga, 1999). Following carbendazim exposure, there was a decrease in the staining intensity for e-cadherin in these cells. This observation suggested the dismantling of the e-cadherin protein as a result of carbendazim toxicity. As narrated in Chapter Three, cadherin proteins can be dismantled in response to toxicity. This has been observed in cultured cells treated with the pesticide malathion (Cabello, Galaz, Botella, Calaf, Pacheco, Stockert, Villanueva, Canete & Juarranz, 2003). According to the report by Cabello *et al.* (2003), the dismantling of cadherin proteins is correlated with cytoskeletal damage. Similar findings were observed in the current study, in which a reduction in the intensity of e-cadherin immunostaining was correlated with the degeneration of cellular junctions.

In the present study, laminin immunoreactivity was observed in the basement membranes underlying luminal and glandular epithelia, as well as endothelial and smooth muscle cells. No significant changes in staining intensity were observed post-exposure to carbendazim at dosages of 25mg/kg, 100mg/kg and 400mg/kg bodyweight. However, at a dose of 800mg/kg, laminin immunoreactivity in the basement membranes of both luminal and glandular epithelia was weak to absent. The reduction in laminin immunoreaction was consistent with morphological changes

seen at ultrastructural level. These ultrastructural changes included discontinuation, folding and an increased thickness of the basement membrane.

In the current investigation, a weak vimentin immunoreaction was observed in the luminal epithelial cells of the control birds. Glandular cells stained negative for vimentin. A weak or absent vimentin immunoreaction in the shell gland epithelium appears to be normal. Similar findings have been reported in the shell gland of the domestic fowl (Madekurozwa, 2012), as well as the uterus of the mouse (Mehasseb, Bell & Habiba, 2009). Korgun, Cayli, Asar & Demir (2007) reported vimentin immunostaining only in endometrial stromal cells in the uterus of the rat during implantation. The absence of vimentin immunostaining in the luminal epithelium following carbendazim administration suggests cytoskeletal damage, which correlated with morphological changes observed at the ultrastructural level. The re-emergence of vimentin immunoreactivity at day 32 post-exposure to carbendazim suggested epithelial recovery.

Scanning and transmission electron microscopy

The morphology of the mucosal surface revealed by scanning electron microscopy conforms to the observations made in the domestic fowl by Bakst (1978) and in the sexually immature ostriches by Madekurozwa (2007). The administration of high doses of carbendazim caused swelling of cilia and deciliation. Deciliation and the presence of swollen cilia in carbendazim-treated birds are not surprising. These ciliary changes were most likely elicited by the disruption of the microtubular complex forming the cilia, as explained in Chapter three. In addition, deciliation is a normal reaction observed in the mucosal surface when the reproductive tract is exposed to toxins. For example, deciliation was observed in the shell gland mucosal surface of pekin ducks fed diets containing high doses of methyl mercury (Balachandran *et al.* 1985). In the current study, deciliation appeared to be more severe with time lapse post-exposure to carbendazim. At day 12 post-exposure to carbendazim, in addition to deciliation, the mucosal surface was lined by numerous swollen cilia. The presence of swollen cilia could be an indication of the deciliation process. Although the exact cause of ciliary swelling was not apparent, an increased membrane permeability due to carbendazim toxicity is probable.

The ultrastructural morphology of the shell gland mucosa in the control birds was similar to an earlier report by Yamamoto, Ozawa & Nagai (1985). It is also in agreement with findings observed in the domestic fowl (Johnston *et al* 1963; Wyburn *et al.* 1973), immature ostrich (Madekurozwa, 2007) and mature ostrich (Muwazi *et al.* 1982). The mucosal layer was lined by ciliated and non-ciliated cells. Secretory granules of variable sizes were seen in both ciliated and non-ciliated cells. Similar secretory granules have also been observed in the epithelial cells of the domestic fowl (Johnson *et al.*, 1963). According to Johnson *et al.* (1963), secretory granules were the constant feature observed in epithelial cells during the resting phase of laying. Secretory granules varied in size based on the position of the egg in the reproductive tract of the domestic fowl (Johnson *et al.*, 1963). Histochemical studies show that these secretory granules contain dermatan sulphate proteoglycan (ovoglycan) and glycosaminoglycan (Fernandez *et al.*, 2001), which are PAS positive. Following carbendazim exposure, secretory granules exhibited electron dense particles, which diffused into the cytoplasm in the later stages of degeneration. The degeneration of secretory granules observed at the ultrastructural level correlates with the reduced PAS staining shown earlier in the Chapter.

In addition to deciliation and swollen cilia observed at the SEM level, TEM results showed a formation of compound cilia similar to those observed in the magnum of carbendazim-treated birds (Chapter 3). Compound cilia have also been observed in the shell gland of pekin ducks fed diets containing high doses of methyl mercury (Balachandran *et al.* 1985). As discussed in Chapter 3, the formation of compound cilia indicated the progression of a deciliation process in which degenerating cilia were shed in groups. In the current study, degenerating cilia formed ciliary packets, which were seen in the mucosal lumen, as well as in the cytoplasm of luminal epithelial cells. Similar observations have been reported in the regressing oviduct of the marsupial *Monodelphis domestica* (Wick & Kress, 2002). According to Wick & Kress (2002), degenerating cilia were removed in the form of ciliary packets.

As shown in the results, carbendazim caused nuclear degenerative changes, which included pyknosis, karyorrhexis, condensation and nuclear chromatin margination. These observations represented chromosomal damage due to carbendazim toxicity. Reports by Styles & Garner (1974), Piati, Mirabini & Chiesara (1994) and Lebailly,

Vigreux, Godard, Sichel, Bar, Letalaer, Henry-Amar & Gauduchon (1997) support this observation. Styles & Garner (1974) showed chromosomal damage in rats exposed to carbendazim and the carbendazim parent compound, benomyl. Piati *et al.* (1994) reported nuclear degeneration in rat hepatocytes exposed to benomyl. In the study by Piati *et al.* (1994), nuclear degeneration was evidenced by an increased micronuclei frequency and chromosomal damage. According to Lebailly *et al.* (1997) carbendazim caused chromosomal damage in human lymphocytes.

In addition to nuclear degeneration, degenerative changes were also observed in the cytoplasm of carbendazim-treated quails. These degenerative changes were evidenced by the presence of: swollen mitochondria; dilated cisternae of RER and an increased number of lysosomes and vacuoles. In addition, cells with condensed cytoplasm were also encountered. Similar degenerative changes have been observed in the shell gland of pekin ducks post-exposure to methyl mercury (Balachandran *et al.*, 1985). As mentioned in Chapter Three, the degeneration of mitochondria indicates the initiation of an apoptotic process through the activation of the caspase chain (Schultz & Harrington, 2003). The increased number of lysosomes and vacuoles observed, are indicative of the intracellular clearance of the degenerative material within the cell. This hypothesis is supported by a research report by Chousalkar & Roberts (2008), which stated that vacuoles serve as a reservoir for unutilized secretory material during egg formation. In addition, Breen & De Bruyn (1969) showed the removal of secretory material in epithelial cells via the formation of vacuoles.

Ultrastructural observations also revealed morphological changes in the lateral and basal plasma membranes. Along the lateral plasma membranes, cellular junctions were dilated and devoid of filaments. A similar pattern of desmosomal degeneration has been shown in response to toxins, such as kepone (Starcevic, Bortolin, Woodcroft, & Novak, 2001), diclofenac (Triebkorn, Casper, Heyd, Eikemper, Köhler, & Schwaiger, 2004) and formaldehyde (Arican, Sahin, Ustunel, Sarikcioglu, Ozdem & Oguz, 2009). It has also been shown in skin and mucosal diseases (Amagai, Klaus-Kovtun & Stanley, 1991; Amagai, Matsuyoshi, Wang, Andl & Stanley, 2002; Hanakawa, Schechter, Lin, Garza, Yamaguchi, Fudaba, Nishifuji, Sugai & Amagai, 2002). According to these reports, degeneration of desmosomes occurs due to the

disruption of desmosomal proteins, which include cadherins (desmogleins and desmocollins), armadillo (plakoglobin) and plakin (desmoplakin). A lack of filaments in degenerating desmosomes suggests a disruption of the cytoskeleton.

In the present study the degenerating basal plasma membrane was discontinuous and detached from the basal lamina. Infolding of the basal lamina could be attributed to detachment of the basal plasma membrane. Infolding of the basal lamina has been shown in degenerating muscle fibres (Vracko 1974). An increased thickness of the *lamina densa* suggests degeneration of the basal lamina due to carbendazim toxicity. Reports by Starcevic *et al.* (2001) and Arican *et al.* (2009) support this argument. According to these reports, a thickened *lamina densa* was observed in rats treated with the insecticide kepon (Starcevic *et al.*, 2001), as well as, the disinfectant formaldehyde (Arican *et al.*, 2009).

The results of the present study showed the degeneration of tubular gland cells post-exposure to carbendazim. Gland cells are known to release calcium (Ca^{2+}) during the formation of the eggshell (Yamamoto *et al.*, 1985). Tubular glands contain a calcium pump and binding protein (Calbindin-D28k), which facilitate the transportation of calcium for eggshell calcification (Wasserman, Smith, Smith, Brindak, Fullmer, Krook, Penniston & Kumar, 1991). Changes in the morphology of the gland cells interferes with the availability of calcium and its deposition in the forming eggshell. This has been reported in the duck and domestic fowl post-exposure to organochlorides (Friedenbach & Davidson, 1977), as well as in the Japanese quail following the administration of the insecticide Kepone (Eroschenko & Place, 1977). According to these reports, morphological changes in the shell gland resulted in the production of eggs with thin shells, reduced size and weight. In addition, morphological changes in the shell gland mucosa caused eggshell thinning in birds exposed to diethyl-diamino tetrachloride (Hickey & Anderson, 1968; Cooke, 1973; Blus, Wiemeyer & Bunck, 1997).

Epithelial cells in the present study appeared to vary in their sensitivity to carbendazim. Non-ciliated cells appeared to be more affected than ciliated epithelial cells. This was most evident at day 12 post-exposure to carbendazim where most of the non-ciliated cells in the luminal epithelium had degenerated. The reason for the

selective degeneration or sensitivity was not clear. However, the rate of cellular turnover could be a factor. According to Hellman & Laryea (1990), the effect of benomyl (carbendazim parent compound) was more evident in organs, such as the thymus, testis and spleen due to their continuous cellular renewal.

Conclusion

In conclusion, luminal and glandular epithelial cells in the shell gland play a major role in the process of egg and eggshell formation. Degeneration of these cells, as a consequence of carbendazim treatment, poses a potential threat to the productivity of exposed birds.

4.5 References

- AMAGAI, M., KLAUS-KOVTUN, V. & STANLEY, J. R. 1991. Autoantibodies against a novel epithelial cadherin in *pemphigus vulgaris*, a disease of cell adhesion. *Cell*, 67:869-877.
- AMAGAI, M., MATSUYOSHI, N., WANG, Z. H., ANDL, C. & STANLEY, J. R. 2000. Toxin in bullous impetigo and staphylococcal scalded-skin syndrome targets desmoglein 1. *Nat. Medicine*. 6:1275-1277.
- ARIAS, J.L., FINK, D.J., XIAO, S.-Q., HEUER, A.H. & CAPLAN, A.I. 1993. Biomineralization and eggshells: cell-mediated acellular compartments of mineralized extracellular matrix. *International Review of Cytology*, 145:217-250.
- ARICAN, R.Y., SAHIN, Z., USTUNEL, I., SARIKCIOGLU, L., OZDEM, S. & OGUZ, N. 2009. Effects of formaldehyde inhalation on the junctional proteins of nasal respiratory mucosa of rats. *Experimental Toxicology and Pathology*, 61:297-305.
- BAKST, M. & HOWARTH, B. 1974. SEM preparation and observations of the hen's oviduct. *Anatomical Record*, 181:211-226.
- BAKST, M. 1978. Scanning electron microscopy of the oviducal mucosa apposing the ovum. *Poultry Science*, 57:1065-1069.
- BALACHANDRAN, A., BATNGAR, M.K. & GCISSINGER, H.D. 1985. Scanning and transmission electron microscopic studies on the oviducts of pekin ducks fed methyl mercury containing diets. *Scanning Electron Microscopy*, 1:311-322.

- BLUS, L.J., WIEMEYER, S.N. & BUNK, C.M. 1997. Clarification of effects of DDE on shell thickness, size, mass and shape of avian eggs. *Environmental Pollution*, 95:67-74.
- BREEN, P.C. & DE BRUYN, P.P.H. 1969. The fine structure of the secretory cells of the uterus (shell gland) of the chicken. *Journal of Morphology*, 128:35-66.
- CABELLO, G., GALAZ, S., BOTELLA, L., CALAF, G., PACHECO, M., STOCKERT, J.C., VILLANUEVA, A., CAÑETE, M. & JUARRANZ, A. (2003). The pesticide malathion induces alterations in actin cytoskeleton and in cell adhesion of cultured breast carcinoma cells. *International Journal of Oncology*, 23:697-704
- CHOUSALKAR, K.K. & ROBERTS, J.R. 2008. Ultrastructural changes in the oviduct of the laying hen during the laying cycle. *Cell and Tissue Research*, 332:349-358.
- COOKE, A.S. 1973. Shell thinning in avian eggs by environmental pollutants. *Environmental pollution*, 4:85-152.
- EROSCHENKO, V.P. & PLACE, T.A. 1977. Prolonged effects of kepone on strength and thickness of eggshells from Japanese quail fed different calcium level diets. *Environmental Pollution*, 13:255-264.
- FERNANDEZ, M.S., MOYA, A., LOPEZ, L. & ARIAS, J.L. 2001. Secretion pattern, ultrastructural localization and function of extracellular matrix molecules involved in eggshell formation. *Matrix Biology*, 19:793-803.
- FRIEDENBACH, D.J. & DAVIDSON, K.L. 1977. Scanning and transmission electron microscopic changes associated with duck and chicken shell gland cilia after p',p'-DDT administration. *Toxicology and Applied Pharmacology*, 40:291-297.
- GILBERT, A.B. 1979. Female genital organs, in *Form and function in birds*, edited by A.S. King & J. McLelland. London: Academic Press, 1:237-338.
- Hellman, B. & Laryea, D. 1990. Inhibitory effects of benomyl and carbendazim on the [3H] thymidine incorporation in various organs of the mouse- evidence for a more pronounced action of benomyl. *Toxicology*, 61:161-169.
- HICKEY, J.J. & ANDERSON, D.W. 1968. Chlorinated hydrocarbons and eggshell changes in raptorial and fish-eating birds. *Science*, 162:271-273.
- HANAKAWA, Y., SCHECHTER, N. M., LIN, C., GARZA, L., LI, H., YAMAGUCHI, T., FUDABA, Y., NISHIFUJI, K., SUGAI, M. & AMAGAI, M. 2002. Molecular mechanisms of blister formation in bullous impetigo and staphylococcal scalded skin syndrome. *Journal of Clinical Investigations*, 110:53-60.

- HODGES, R.D. 1974 (ed). The Histology of the Fowl. London, Academic Press: 374-384.
- HSU, Y., CHANG, C., CHEN, M., YUAN, C., CHEN, J., MA, J., UENG, T. & LU, S. (2011). Carbendazim-induced androgen receptor expression antagonized by flutamide in male rats. *Journal of Food and Drug Analysis*, 19:418-428
- JOHNSTON, H.S., AITKEN, R.N.C. & WYBURN, G.M. 1963. The fine structure of the uterus of the domestic fowl. *Journal of Anatomy*, 97:333-344.
- KORGUN, E. T., CAYLI, E.S., ASAR, E.M. & DEMIR, E.R. (2007). Distribution of laminin, vimentin and desmin in the rat uterus during initial stages of implantation. *Journal of Molecular Histology*, 38:253–260.
- LEBAILLY, P., VIGREUX, C., GODARD, T., SICHEL, F., BAR, E., LETALAER, J.Y., HENRY-AMAR, M. & GAUDUCHON, P. 1997. Assessment of DNA damage induced *in vitro* by etoposide and two fungicides (carbendazim and chlorothalonil) in human lymphocytes with the comet assay. *Mutation Research*, 375:2005-217.
- Lu, S.Y., Liao, J.W., Kuo, M.L., Wang, S.C., Hwang, J.S. & Ueng, T.H. 2004. Endocrine-disrupting activity in carbendazim-induced reproductive and developmental toxicity in rats. *Journal of Toxicology and Environmental Health. Part A*, 67:1501-1505.
- MADEKUROZWA, M.-C. 2007. Ultrastructural features of the uterus in the sexually immature ostrich (*Struthio camelus*) during periods of ovarian activity and inactivity. *Onderstepoort Journal of Veterinary Research*, 74:209-216.
- MADEKUROZWA, M.-C. 2012. An immunohistochemical study of the oviduct in the domestic fowl (*Gallus domesticus*). *Anatomia Histologia Embryologia*, *In press*. DOI: 10.1111/j.1439-0264.2012.01164.x
- MEHASSEB, M.K., BELL, S.C. & HABIBA, M.A. 2009. The effects of tamoxifen and estradiol on myometrial differentiation and organization during early uterine development in the CD1 mouse. *Reproduction*, 138:341–350.
- MORINAGA, H., YANASE, T., NOMURA, M., OKABE, T., GOTO, K., HARADA, N. & NAWATA, H. 2004. A benzimidazole fungicide, benomyl and its metabolite, carbendazim, induce aromatase activity in a human ovarian granulosa-like tumor cell line (KGN). *Endocrinology*, 145:1860-1869.

- MUWAZI, R.T., BARANGA, J., KAYANJA, F.I.B. & SCHLIEMANN, H. 1982. The oviduct of the ostrich *Struthio camelus massaicus*. *Journal of Ornithology*, 123:425-433.
- PARIA, B.C., ZHAO, X., DAS, S.K., DEY, S.K. & YOSHINAGA, K. (1999). Zonular occludens-1 and e-cadherin are coordinately expressed in the mouse uterus with the initiation of implantation and decidualization. *Developmental Biology*, 208:488-501.
- PARIZZI, R.C., SANTOS, J.M., OLIVIERA, M.F., MAIA, M.O., SOUSA, J.A., MIGLINO, M.A. & SANTOS, T.C. 2008. Macroscopic and microscopic anatomy of the oviduct in the sexually mature Rhea (*Rhea Americana*). *Anatomia Histologia Embryologia*, 37:169-176.
- PIATI, E., MIRABINI, L. & CHIESARA, E. 1994. Increase of micronucleus frequency in cultured rat hepatocytes treated *in vitro* with benomyl and pirimiphos-methyl separately and in mixture. *Mutation Research*, 324:59-64.
- ROBINSON, D.S., KING, N.R. & BOWEN, D.J. 1968. The occurrence of neutral and acidic mucins in the reproductive tract of the laying hen. *Histochemie*, 13:97-104.
- SCHULTZ, D. R. & HARRINGTON, W.J. (2003). Apoptosis: programmed cell death at a molecular level. *Seminars in Arthritis and Rheumatism*, 32:345 - 69.
- SOLOMON, S.E., FRYER, J.R. & BAIRD, T. 1975. The ultrastructural localization of Ca^{2+} in the avian shell gland. *Journal of Microscopy*, 105:215-222.
- STARCEVIC, S.L., BORTOLIN, S., WOODCROFT, K.J., & NOVAK, R.F. 2001. Kepone (chlordecone) disrupts adherens junctions in human breast epithelial cells cultured on matrigel. *In Vivo*, 15:289-294.
- STEMBERGER, B.H., MUELLER, W.J. & LEACH, JR.R.M. 1977. Microscopic study of the initial stages of shell calcification. *Poultry Science*, 56:537-543.
- STYLES, J.A. & GARNER, R. 1974. Benzimidazole carbamate methyl ester- evaluation of its effects *in vivo* and *in vitro*. *Mutation Research*, 26:177-187.
- TRIEBSKORN, R., CASPER, H., HEYD, A., EIKEMPER, R., KÖHLER, H.R. & SCHWAIGER, J. 2004. Toxic effects of the non-steroidal anti-inflammatory drug diclofenac. Part II: cytological effects in liver, kidney, gills and intestine of rainbow trout (*Oncorhynchus mykiss*). *Aquatic Toxicology*, 10:151-66.
- VRACKO, R. 1974. Basal lamina scaffold-anatomy and significance for maintenance of orderly tissue structure. *American Journal of Pathology*, 77:313-346.

- WASSERMAN, R.H., SMITH, C.A., SMITH, C.M., BRINDAK, M.E., FULLMER, C.S., KROOK, L., PENNISTON, J.T. & KUMAR, R. 1991. Immunohistochemical localization of a calcium pump and calbindin-D28k in the oviduct of the laying hen. *Histochemistry*, 96:413-418.
- WICK, R. & KRESS, A. 2002. Ultrastructural changes in the uterine luminal and glandular epithelium during oestrous cycle of the *Marsupial Monodelphis domestica* (Grey short-tailed opossum). *Cell Tissue Organs*, 170:111-131.
- WYBURN, G.M., JOHNSTON, H.S., DRAPER, M.H. & DAVIDSON, M.F. 1973. The ultrastructure of the shell forming region of the oviduct and the development of *Gallus domesticus*. *Quarterly Journal of Experimental Physiology*, 58:143-151.
- YAMAMOTO, T., OZAWA, H. & NAGAI, H. 1985. Histochemical studies of Ca-ATP-ase, succinate and NAD⁺-dependent isocitrate dehydrogenases in the shell gland of laying Japanese quails: with special reference to calcium-transporting cells. *Histochemistry*, 83:221-226.
- Yu, J.Y. & Marquardt, R.R. 1973. Development, cellular growth, and function of the avian oviduct. Studies on the magnum during a reproductive cycle of the domestic fowl (*Gallus domesticus*). *Biology of Reproduction*, 8:283-298.

CHAPTER FIVE

The effect of carbendazim on the structure of sperm storage tubules in the sexually mature Japanese quail: histological, immunohistochemical and ultrastructural study.

5.1 Introduction

It is an established fact that fertilization in avian species continues several days after cessation of copulation (Burke & Ogasawara, 1969; Van Krey, Blander & Compton, 1981). This is possible due to the ability of birds to store spermatozoa for days or weeks after copulation. In the Japanese quail, spermatozoa are stored for up to 10 days following copulation (Birkhead & Fletcher, 1994). The mechanism by which sperm are stored has been established in a number of domesticated and wild avian species (Bilgili & Renden, 1986; Birkhead & Fletcher, 1974; Bakst, 1981; van Krey *et al.*, 1981). The studies show that following copulation or artificial insemination, spermatozoa are stored in specialized tubular glands known as sperm storage tubules (SST), which are located in the utero-vaginal junctions of most avian species (Frieß, Sinowatz & Wrobel, 1978; Schupping, van Krey, Denbow, Bakst & Meyer, 1984; Birkhead, 1992). In addition to the presence of SST in the utero-vaginal junction, a study by Tingari & Lake (1973) in the domestic fowl reported the occurrence of glandular grooves in the caudal extremity of the infundibulum, which are believed to store sperm.

The structure of SST has been extensively studied in the domestic fowl (Fujii 1963; Burke & Ogasawara, 1969; Tingari & Lake, 1973; Das 2003), turkey (Ogasawara & Fuqua, 1972; Bakst, 1981; Schupping *et al.*, 1984), Japanese quail (Frieß *et al.*, 1978; Birkhead & Fletcher, 1994) and Bengalese finch (Birkhead, 1992). The SST are tubular invaginations of the luminal epithelium, which are lined by simple columnar epithelium. The number of SST varies between species (Birkhead & Møller, 1992). Up to 3467 SST have been recorded in the Japanese quail (Birkhead & Fletcher, 1994).

The release of spermatozoa from SST occurs intermittently during fertilization (Birkhead & Fletcher, 1994). However, the mechanism governing this release is still controversial. According to Tingari & Lake (1973) the presence of myoepithelial cells facilitates the release of sperm from SST. This idea was supported by Das (2003) who demonstrated the presence of smooth muscle cells around sperm tubules. In contrast, a report by Frieß *et al.* (1978) in the Japanese quail showed no myoepithelial cells present around SST. Similar observations were also made in the turkey (Schupping *et al.*, 1984) and Bengalese finches (Birkhead 1992). The reports (Schupping *et al.*, 1984 and Birkhead, 1992) suggested that the release of spermatozoa from the storage glands could be controlled by ciliary movements of SST epithelial cells or the flushing action of gland secretions.

Studies of ciliary movement have shown the involvement of cytoskeletal elements such as, microtubules, intermediate filaments and microfilaments (Sandoz, Gounon, Karsenti, Boisvieux-ulrich, Laine & Paulin, 1983; Chailley, Nicolas & Laine, 1989). In the quail oviduct, microfilaments are localized in ciliated cells (Chailley *et al.*, 1989). It was shown that microfilaments in association with other cytoskeletal elements strengthened cilia anchorage and improved ciliary movement (Chailley *et al.*, 1989). Based on the fact that fertilization in avian species depends on the release of spermatozoa from SST, active ciliary movement, as well as structural integrity of glandular cells are important.

Carbendazim disrupts microtubules by binding to the β tubulin subunit of the microtubule (Burland & Gull 1984; Cruz & Edlind, 1997). The disruption of microtubules affects ciliary movements and the cellular skeleton. The effect on ciliary movement and cellular integrity may lead to impaired fertility in exposed birds. To-date, no information appears to be available on the possible morphological changes in the SST following carbendazim exposure. Therefore, in this Chapter, the effects of carbendazim on structural and immunohistochemical changes in the SST of Japanese quail are reported.

5.2 Materials and methods

A total of 102 sexually mature female Japanese quails were used in this study. The study was divided into two experiments as described in Chapter one.

5.2.i. Histology

Tissue samples from the utero-vaginal junction were fixed in 10% buffered formalin for 48 hours. Thereafter, the tissue samples were processed routinely for light microscopy following standard procedures described in Chapter one.

5.2.ii. Immunohistochemistry

Paraffin embedded sections of the utero-vaginal junction were used in the present study. The tissue sections were processed and immuno-stained using a LSAB plus kit (Dakocytomation, Denmark) following a standard technique described in Chapter one. Antibodies against e-cadherin, laminin and vimentin were used at dilutions of 1:100, 1:50 and 1:50 respectively.

5.2.iii. Transmission electron microscopy

Tissue samples from the utero-vaginal junction were immersion fixed in 2.5% glutaraldehyde in 0.1M Millonig's buffer (pH 7.3) for 48 hours. Thereafter, the tissue samples were post-fixed in 2% osmium tetroxide. Following post-fixation, samples were processed for transmission electron microscopy (TEM) using standard techniques.

5.3 Results

5.3.1 Histomorphometrical observations

5.3.1.i Control birds

Sperm storage tubules were observed in the *lamina propria-submucosa*. The glands measured between 22.3 and 35.45 μm (27.22 ± 0.98) in width. The glandular lumena were on average 5.26 μm in diameter. Table 5.1 summarises the measured morphometrical parameters of the SST in the control and carbendazim-treated birds.

5.3.1.ii. Carbendazim-treated birds

5.3.1.ii.a *Experiment I (dose dependent oviductal degeneration)*

There was a general decrease in the width of the SST following administration of carbendazim. When compared to the control, a significant decrease in the width of SST was observed at 100 mg/kg and 400 mg/kg bodyweight carbendazim. A significant decrease was also observed between 25 mg/kg and 100 mg/kg, as well as, between 100 mg/kg and 800 mg/kg bodyweight carbendazim ($p < 0.05$). At a high dose (800 mg/kg bodyweight), carbendazim increased the width of the SST. However, this increase was not statistically significant when compared to the control ($p < 0.05$). The increase was statistically significant between 400 mg/kg and 800 mg/kg bodyweight carbendazim ($p < 0.05$). Consistent with glandular width, the glandular lumena diameters decreased by carbendazim treatment. A significant decrease in the glandular lumena diameters was recorded at 100 mg/kg when compared to the control and 25 mg/kg bodyweight carbendazim groups ($p < 0.05$).

Table 5.1: Mean \pm SE histomorphometrical parameters of the SST in the control and carbendazim treatment groups

Carbendazim dose (mg/kg)	Glandular width (μm)	Glandular lumena diameters (μm)
0	27.22 \pm 0.98	5.26 \pm 0.31
25	24.48 \pm 0.45 ^b	4.61 \pm 0.21 ^b
100	11.77 \pm 3.36 ^{abc}	2.13 \pm 0.21 ^{ab}
400	17.87 \pm 3.36 ^{ad}	3.97 \pm 0.92
800	30.41 \pm 1.3 ^{cd}	3.99 \pm 0.33

^a Differs significantly from the control

^{bcd} Significant difference between treatment groups

5.3.1.iib Experiment II (time-course oviductal degeneration)

The observed changes in morphometrical parameters are shown in Table 5.2 below. Administration of 400 mg/kg bodyweight carbendazim caused a general decrease in the width of the SST. The lowest level of width decrease was observed 8 days post-exposure. When compared to the control, the decrease in the glandular width was observed at 24 hours, as well as, at days 5, 8, 12 and 32 post-exposure to carbendazim ($p < 0.05$). A significant decrease in the glandular width was observed between 5 hours and days 5, 8 and 32 ($P < 0.05$). In addition, the significant decrease was also seen between 24 hours and days 8 and 32 post-exposure. Between days 5 and 8; as well as, 12 and 32, the glandular width decrease was statistically significant ($p < 0.05$).

Table 5.2: Mean \pm SE morphometric parameters in the control and different periods post-exposure to 400 mg/kg bodyweight carbendazim

Periods post-exposure to carbendazim	Glandular width (μm)	Glandular lumena diameters (μm)
0 hour	27.22 \pm 0.98	5.26 \pm 0.31
5 hours	25.05 \pm 0.75 ^b	4.66 \pm 0.28 ^{bc}
24 hours	22.28 \pm 0.63 ^{ac}	4.07 \pm 0.26 ^c
5 days	20.35 \pm 1.59 ^{abd}	3.91 \pm 0.48 ^d
8 days	6.07 \pm 0.31 ^{abcde}	1.14 \pm 0.13 ^{abcde}
12 days	23.39 \pm 0.84 ^{aef}	4.45 \pm 0.41 ^{ef}
32 days	16.76 \pm 23.7 ^{abef}	3.25 \pm 0.35 ^{aef}

^a Significant difference when compared to the control

^{bcdef} Significant difference between periods post-exposure to carbendazim

5.3.2 Histological observation

5.3.2.i. Control birds

The morphology of the mucosal layer in the utero-vaginal junction was similar to that of the shell gland. In the *lamina propria-submucosa*, SST were observed (Fig. 5.1a). The SST were tubular glands formed by luminal epithelial invagination (Fig. 5.1b). A simple columnar epithelium lined the SST (Fig. 5.1c). At the proximal extremity (neck) of the gland, the lining epithelium was simple ciliated columnar (Fig. 5.1b). Spermatozoa were observed in these glands (Fig. 5.1a&c).

5.3.2.ii Carbendazim-treated birds

5.3.2.ii.a *Experiment I (dose dependent oviductal degeneration)*

25 and 100 mg/kg bodyweight carbendazim

No histological degenerative changes were observed in the SST at doses of 25 mg/kg and 100 mg/kg bodyweight, 48 hours post-exposure to carbendazim.

400 mg/kg bodyweight carbendazim

At a dose of 400 mg/kg bodyweight carbendazim, a few spermatozoa were observed in the lumina of the SST (Fig. 5.2a). In some instances the gland lumina were empty. The SST contained a few cells with pale cytoplasm and pyknotic nuclei (Fig. 5.2b).

800 mg/kg bodyweight carbendazim

At a dose of 800 mg/kg, hyperaemia was observed in the *lamina propria-submucosa* (Fig. 5.3a). Perivascular cuffing was also a frequent observation in the *lamina propria-submucosa* (Fig. 5.3b). At this dose, cells with pyknotic nuclei were observed in the SST (Fig. 5.3c). The lumina of SSTs contained no spermatozoa.

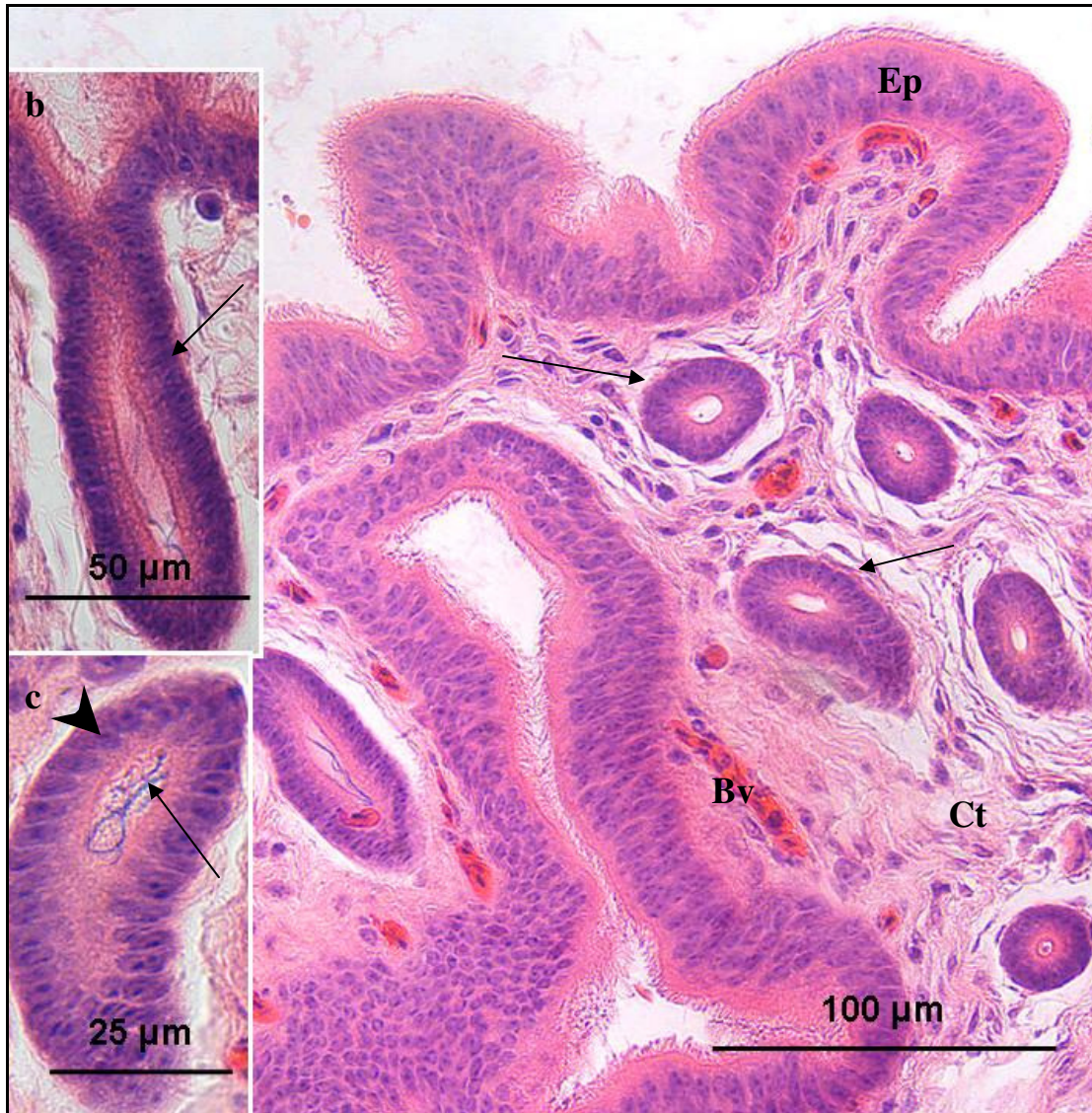


Fig. 5.1: **a.** Photomicrograph of the *mucosa* in the UVJ region of a control bird. SST (arrows) are observed in the *lamina propria-submucosa*. Loose connective tissue (Ct) is seen interposed between the SST. Ep: luminal epithelium; Bv: blood vessels. **b.** A SST (arrow) is seen formed by epithelial invagination. **c.** A simple columnar epithelium (arrow) lines the SST. Note the presence of spermatozoa (arrow) in this tubule.

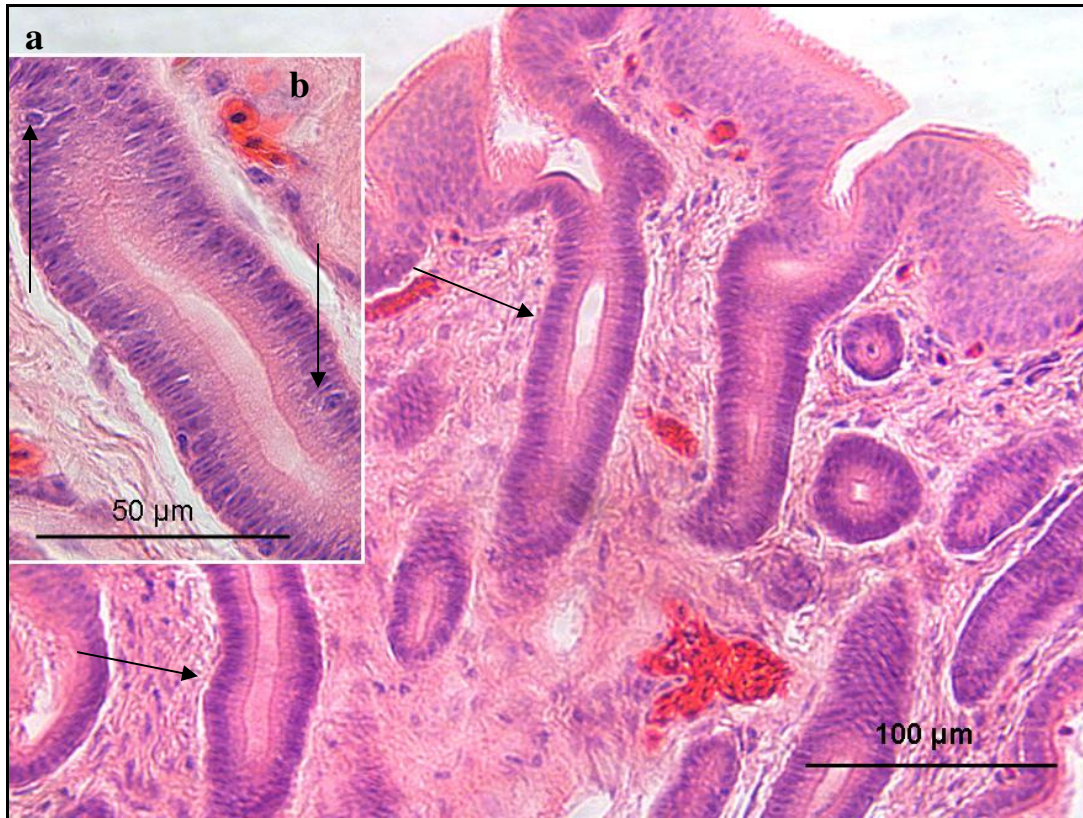


Fig. 5.2: **a.** A low magnification photomicrograph of the *mucosa* in the UVJ region of a bird treated with 400 mg/kg bodyweight carbendazim. Note that at this dose the lumina of SST tubules (arrows) are devoid of spermatozoa. Bv: blood vessels. **b.** A higher magnification photomicrograph of a SST. The gland contains a few cells with pyknotic nuclei (arrows).

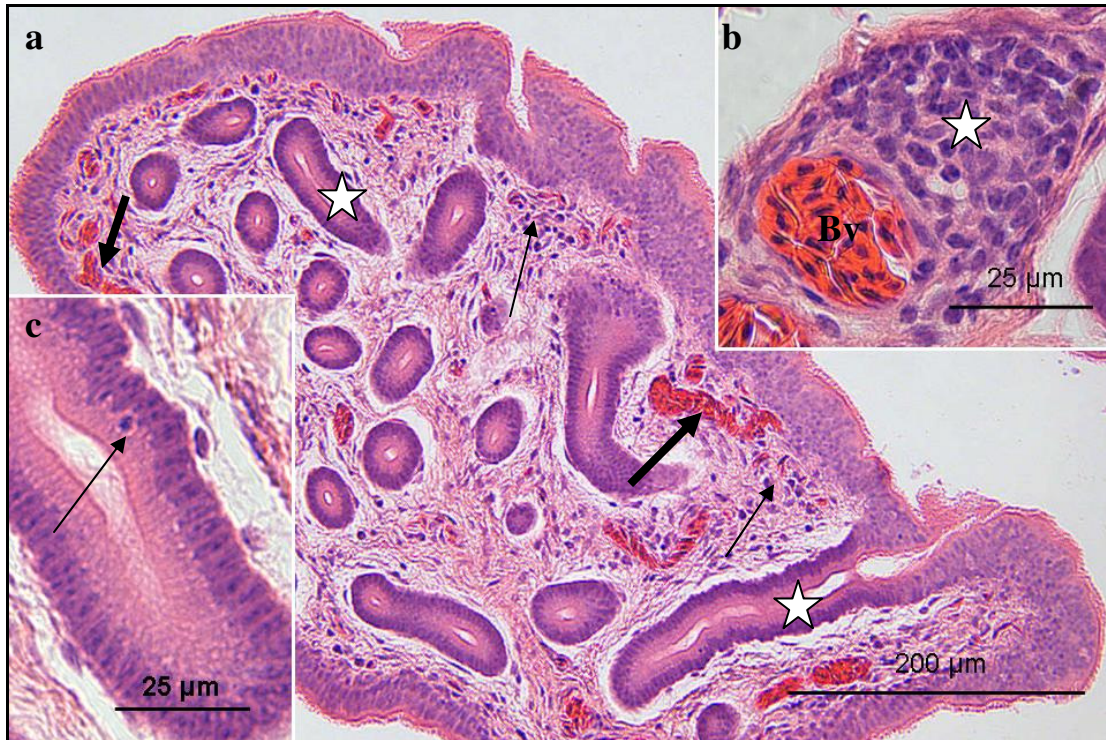


Fig. 5.3: **a.** A low magnification photomicrograph of the *mucosa* in the UVJ region of a bird treated with 800 mg/kg bodyweight carbendazim. Hyperaemic blood vessels (thick arrows) and lymphocytes (arrows) are observed in the *lamina propria-submucosa*. Note absence of spermatozoa in the lumena of SST (asterisks). **b.** A higher magnification photomicrograph showing an aggregation of inflammatory cells (asterisk) around a blood vessel (Bv). **c.** Degenerating SST in the UVJ region. A pyknotic nucleus (arrow) is observed in a degenerating gland cell.

5.3.2.iib Experiment II (time-course oviductal degeneration)

No histological degenerative changes were observed in SST 5 to 24 hours post-exposure to 400 mg/kg carbendazim.

5 days post-exposure

Five days post-exposure to carbendazim, hyperaemia and scattered inflammatory cells were observed in the *lamina propria-submucosa* (Fig. 5.4). At this stage the SST were lined by simple cuboidal epithelium. Glandular lumena contained

degenerating spermatozoa, as well as cellular debris (Fig. 5.4). Fluid accumulation (oedema) was observed in the interstitium and around the degenerating SST (Fig. 5.4).

8 days post-exposure

Eight days post-exposure to carbendazim, the majority of the SST observed were devoid of spermatozoa. A few gland cells contained pyknotic nuclei and pale cytoplasm. In the *lamina propria-submucosa*, inflammatory cell infiltrations were observed.

12 days post-exposure

Twelve days post-exposure to carbendazim, shrinkage (atrophy) of the SST was observed (Fig. 5.5a). At this stage, a few spermatozoa were identified in the glandular lumen. Hyperaemia and aggregates of inflammatory cells were evident in the *lamina propria-submucosa* (Fig. 5.5a). Aggregates of inflammatory cells were also observed adjacent to blood vessels (Fig. 5.5b). Although lymphocytes appeared to be the predominant inflammatory cells observed, a few heterophils were identified (Fig. 5.5b)

32 days post-exposure

Thirty-two days post-exposure to carbendazim, atrophy of the SST was still a notable feature. In addition, a zone of fluid accumulation (oedema) was observed around the SST (Fig. 5.6a). Aggregates of inflammatory cells were observed enclosing the oedematous zone. Scattered leukocytic infiltrations were also evident in the *lamina propria-submucosa*. At this stage, a few SST cells contained pyknotic nuclei. No spermatozoa were observed in the SST lumina.

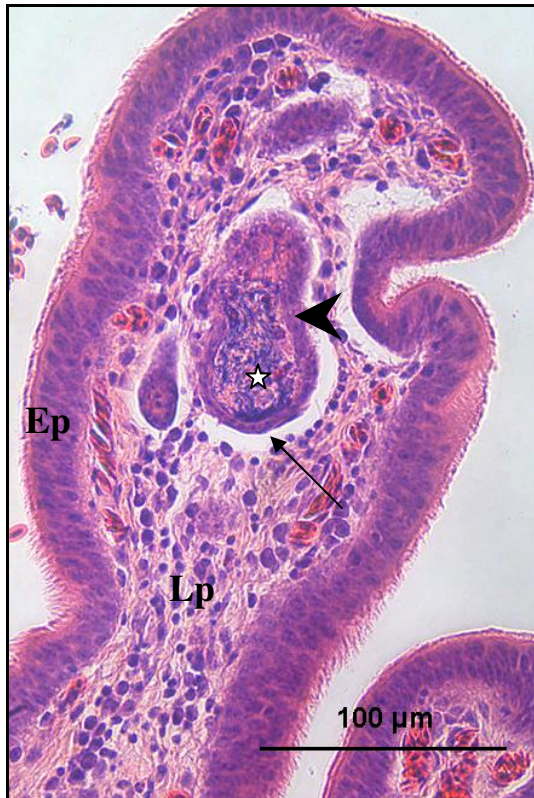


Fig. 5.4: Photomicrograph of the *mucosa* in the UVJ region 5 days post-exposure to 400 mg/kg bodyweight carbendazim. A SST (arrowhead) is lined by a simple cuboidal epithelium. Note the dilatation of the glandular lumen (asterisk) containing debris and spermatozoa. Fluid accumulation (arrow) is observed around the SST. A diffuse leukocytic infiltration is observed in the *lamina propria-submucosa* (Lp). Ep: luminal epithelium.

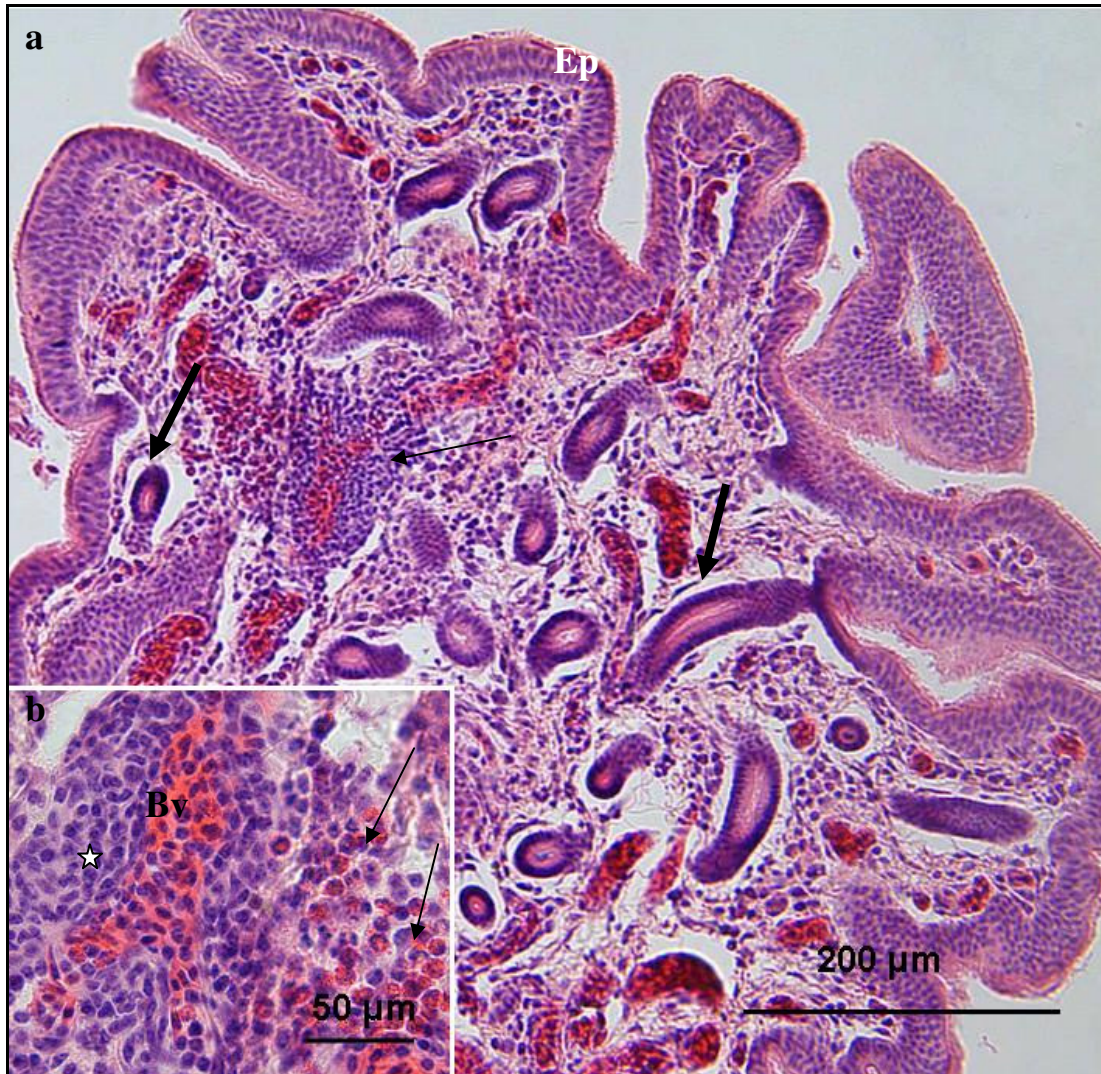


Fig. 5.5: **a.** A low magnification photomicrograph of the *mucosa* in the UVJ region 12 days post-exposure to 400 mg/kg bodyweight carbendazim. Atrophy of the SST (thick arrows) is observed. Leukocytic aggregation (thin arrow) and hyperaemia are observed in the *lamina propria-submucosa*. Ep: luminal epithelium. **b.** Aggregation of inflammatory cells (asterisk) around blood vessel (Bv). Although lymphocytes appear to be the predominant cells, heterophils (arrows) are also observed.

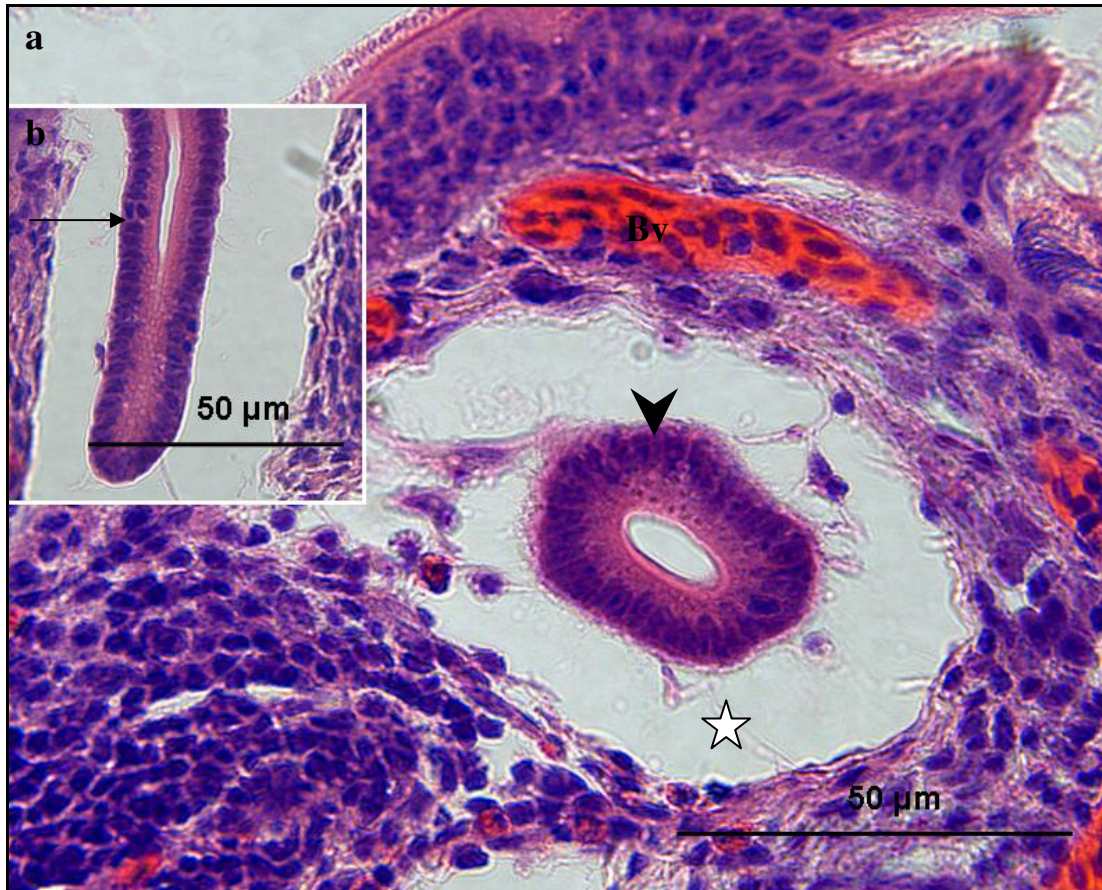


Fig. 5.6. Light photomicrographs of the SST in the UVJ region 32 days post-exposure to 400 mg/kg bodyweight carbendazim. **a.** A zone of fluid accumulation (asterisk) is observed around degenerating SST (arrowhead). Aggregations of inflammatory cells are seen enclosing the fluid zone. Bv: blood vessel. **b.** A cell with mitotic figure (arrow) is observed in a degenerating SST.

5.3.3. Immunohistochemical observations

Immunoreactivity for e-cadherin, laminin and vimentin was assessed in the uterovaginal junction (UVJ) mucosa. The aim was to investigate the immunohistochemical characteristics of sperm storage tubule (SST) cells located in this oviductal region. The assessment was carried out in both the control and carbendazim-treated birds. A qualitative assessment of the staining intensity was visually graded as strong (+++), moderate (++) , weak (+) or negative (-).

5.3.3.1. E-cadherin

5.3.3.1.i. Control group

Moderate immunoreactivity for e-cadherin was observed in the lateral plasma membrane of sperm storage tubule cells (SST). The staining granules were observed in the apical cytoplasmic regions (Fig. 5.7).

5.3.3.1.ii. Carbendazim-treated birds

5.3.3.1.ii.a Experiment I

No immunohistochemical changes were observed in the SST cells 48 hours post-exposure to different dosages of carbendazim.

5.3.3.1.ii.b Experiment II

From 5 hours to 12 days post-exposure to carbendazim, SST cells showed negative immunoreactivity for e-cadherin (Fig. 5.8a). However, at 32 days post-exposure to carbendazim, moderate immunoreactivity for e-cadherin was evident in the lateral plasma membrane of SST cells (Fig. 5.8b).



Fig. 5.7: Light photomicrograph of mucosal layer at UVJ region of the oviduct from a control bird. Sperm Storage Tubule cells (SST) are moderately stained with e-cadherin. E: epithelial cells. L: lumen.

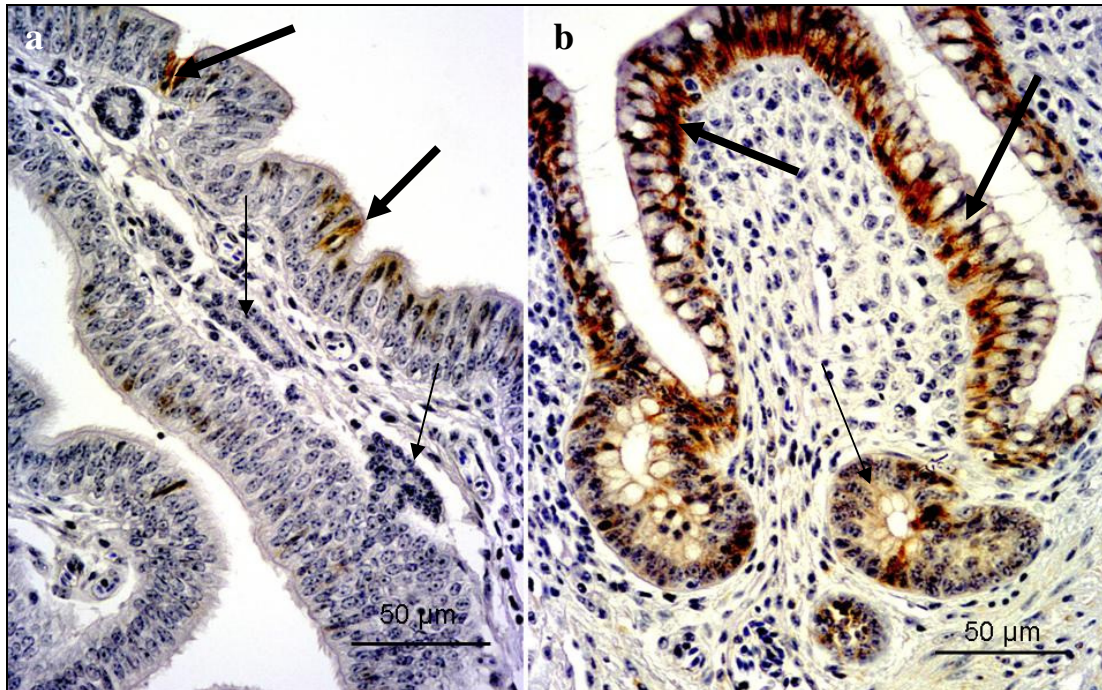


Fig. 5.8: Light photomicrographs of the UVJ mucosa. **a.** Five days post-exposure to carbendazim. SST cells (thin arrows) are negative for e-cadherin. Note the presence of e-cadherin immunoreaction in a few epithelial cells (thick arrows). **b.** Thirty-two days post-exposure to carbendazim. Moderate e-cadherin immunoreaction is observed in the SST cells (arrow). At this stage, strong e-cadherin immunoreaction is evident in the epithelial cells (thick arrows).

5.3.3.2. Laminin

5.3.3.2.i. Control group

Strong immunoreactivity for laminin was observed in the basement membranes lining the SST (Fig. 5.9). Laminin immunoreactivity was also evident in the basement membrane underlying endothelium and smooth muscle cells in the *tunica muscularis*.

5.3.3.2.ii. Carbendazim-treated group

5.3.3.2.iia *Experiment I*

No immunohistochemical changes were observed in the basement membrane 48 hours post-exposure to carbendazim.

5.3.3.2.iib *Experiment II*

At 5 to 24 hours post-exposure to carbendazim, immunoreactivity for laminin in the basement membrane underlying the SST was comparable to the control group.

At 5, 8 and 12 days post-exposure to carbendazim, moderate to weak laminin immunoreaction was observed in the basal lamina underlying the SST (Fig. 5.10 a, b c). At these stages, discontinuation of the basement membrane was evident in some areas of the SST.

At 32 days post-exposure to carbendazim, the staining intensity for laminin was moderate to strong (Fig. 5.11).

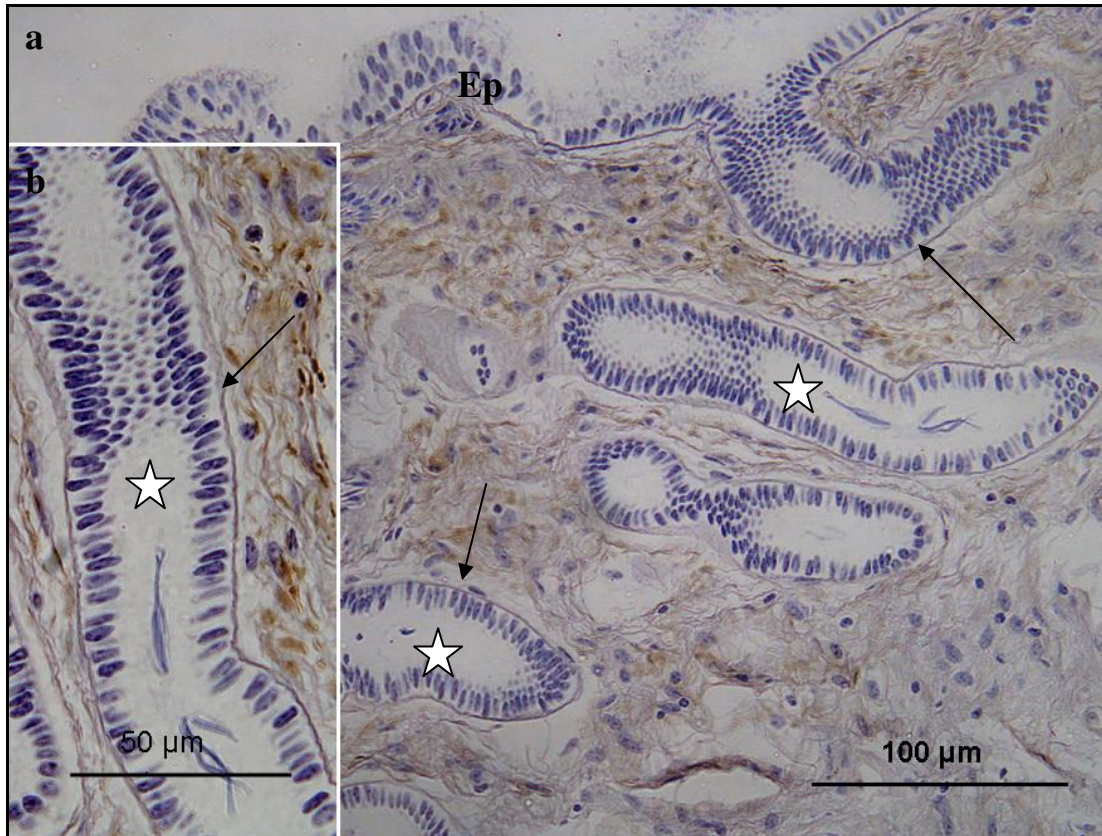


Fig. 5.9: **a.** Light photomicrograph of the UVJ mucosa from a control bird. A strong immunoreaction for laminin is observed in the basement membrane (arrows) of the luminal epithelium (Ep) and SST (asterisks). **b.** A higher magnification photomicrograph showing continuous basement membrane (arrow) that underlines the SST (asterisk).

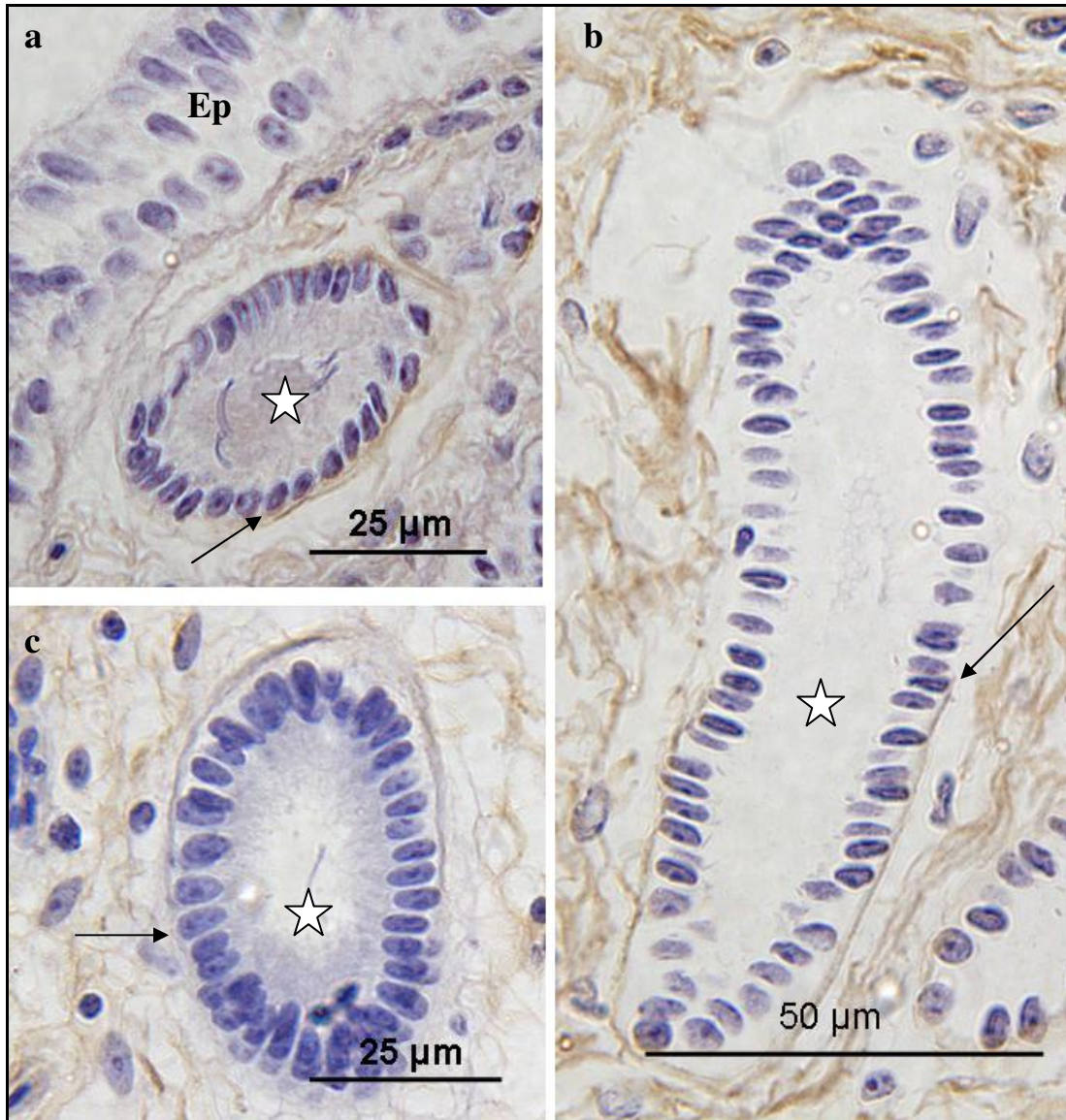


Fig. 5.10: Light photomicrographs of the SST in the UVJ at days (a) 5 (b) 8 and (c) 12 post-exposure to 400 mg/kg bodyweight carbendazim. Note the discontinuation of the basement membrane (arrows) underlining the SST (asterisks). At these stages, the basement membrane has stained weakly for laminin antibody.

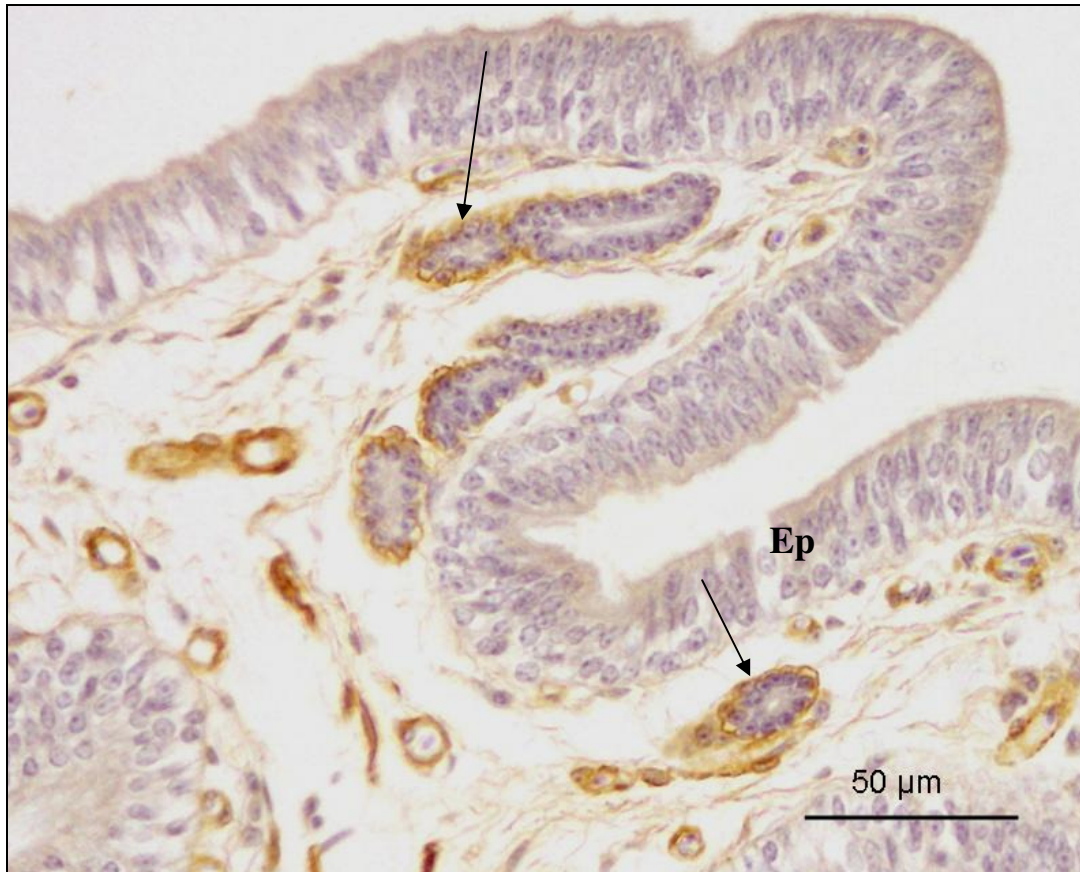


Fig. 5.11: Light photomicrograph of the UVJ mucosa, 32 days post-exposure to 400 mg/kg bodyweight carbendazim. A moderate to weak laminin immunoreaction is observed in the basement membrane underlying the SST (arrows). Note that the basement membrane lining the luminal epithelium (Ep) is indistinct in some areas.

5.3.3.3. Vimentin

5.3.3.3.i. Control group

The SST cells were weakly stained with vimentin (Fig. 5.12). Vimentin immunoreaction was observed in the basal cytoplasmic regions. Vimentin immunoreaction was also observed in the endothelium and fibroblasts in the *lamina propria-submucosa* (Fig. 5.12). Squamous cells lining the *tunica serosa* were also positive for vimentin.

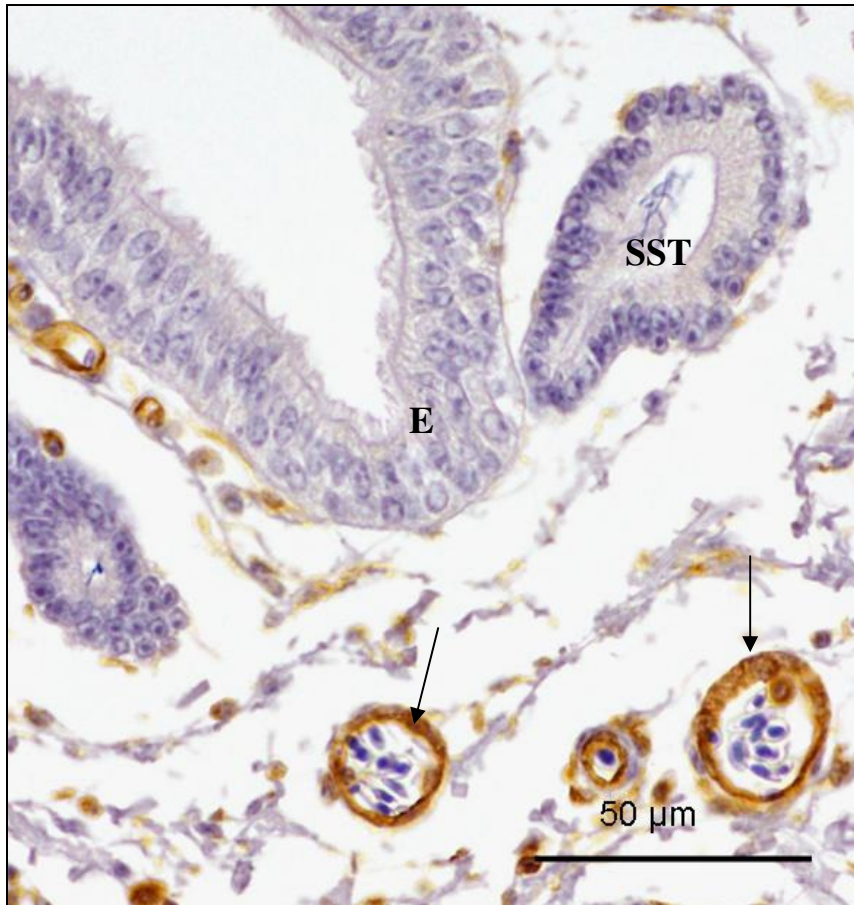


Fig. 5.12: Light photomicrograph of the UVJ mucosa from a control bird. Strong vimentin immunoreactivity is observed in the endothelial cells (arrows) lining the blood vessels. SST cells (SST) are weakly stained with vimentin. Luminal epithelium (E) is negative for vimentin.

5.3.3.3.ii Carbendazim-treated group

5.3.3.3.ii.a *Experiment I*

Following carbendazim treatment, there was no immunoreaction for vimentin observed in the SST cells.

5.3.3.3.ii.b *Experiment II*

At 5 and 24 hours post-exposure to carbendazim, vimentin immunoreactivity in the cytoplasm of SST cells was comparable to that observed in the control group.

From 5 to 32 days post-exposure, SST cells were negative for vimentin. Vimentin immunoreaction was observed in the endothelium, fibroblasts, as well as, in the squamous cells lining the *tunica serosa*. No changes of staining intensity were observed in these cells post-exposure to carbendazim.

5.3.4 Ultrastructural observations

5.3.4.1 Scanning electron microscopy

5.3.4.1.i Control birds

The mucosal surface of the utero-vaginal junction (UVJ) was lined by ciliated and non-ciliated cells. The ciliated cells, which were the predominant cells, contained relatively short cilia compared to those observed in the tubular shell gland (Chapter four) region (Fig. 5.13). The non-ciliated cells were lined by long microvilli. Between the ciliated and non-ciliated cells, openings of sperm storage tubules (SST) were observed (Fig. 5.13).

5.3.4.1.ii Carbendazim-treated birds

5.3.4.1.ii.a *Experiment I*

25 and 100 mg/kg bodyweight carbendazim

There was no degenerative change observed on the mucosal surface at doses of 25 and 100 mg/kg bodyweight carbendazim 48 hours post-exposure.

400 and 800 mg/kg bodyweight carbendazim

Degenerative changes of the UVJ were seen following administration of carbendazim at doses of 400 and 800 mg/kg bodyweight. The observed degenerative changes were: loss of cilia and microvilli; swelling of the microvilli, as well as swollen cilia (Fig. 5.14a&b). Protrusions of the apical regions of the non-ciliated cells were also observed (Fig. 5.14c).

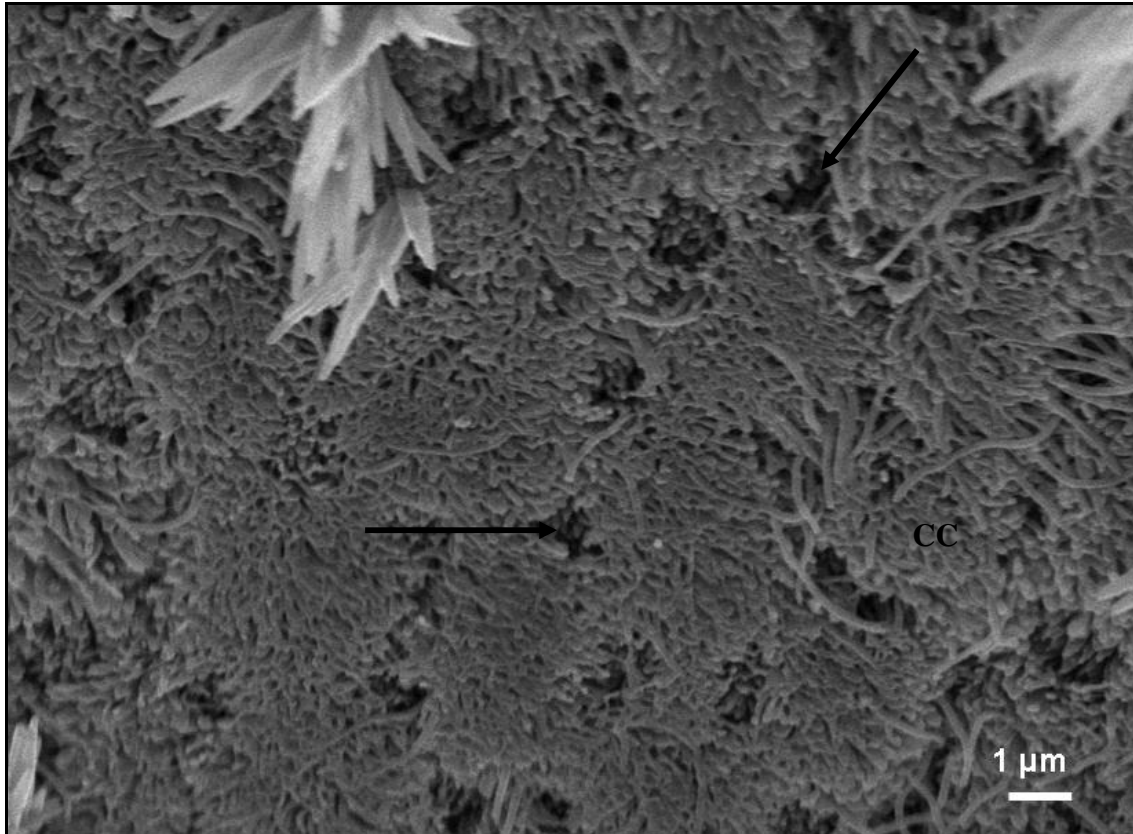


Fig. 5.13: Scanning electron photomicrograph of the mucosal surface in the UVJ region of the oviduct from a control bird. Ciliated cells (CC) are lined by short cilia. Note the presence of SST openings (arrows) between the cells.

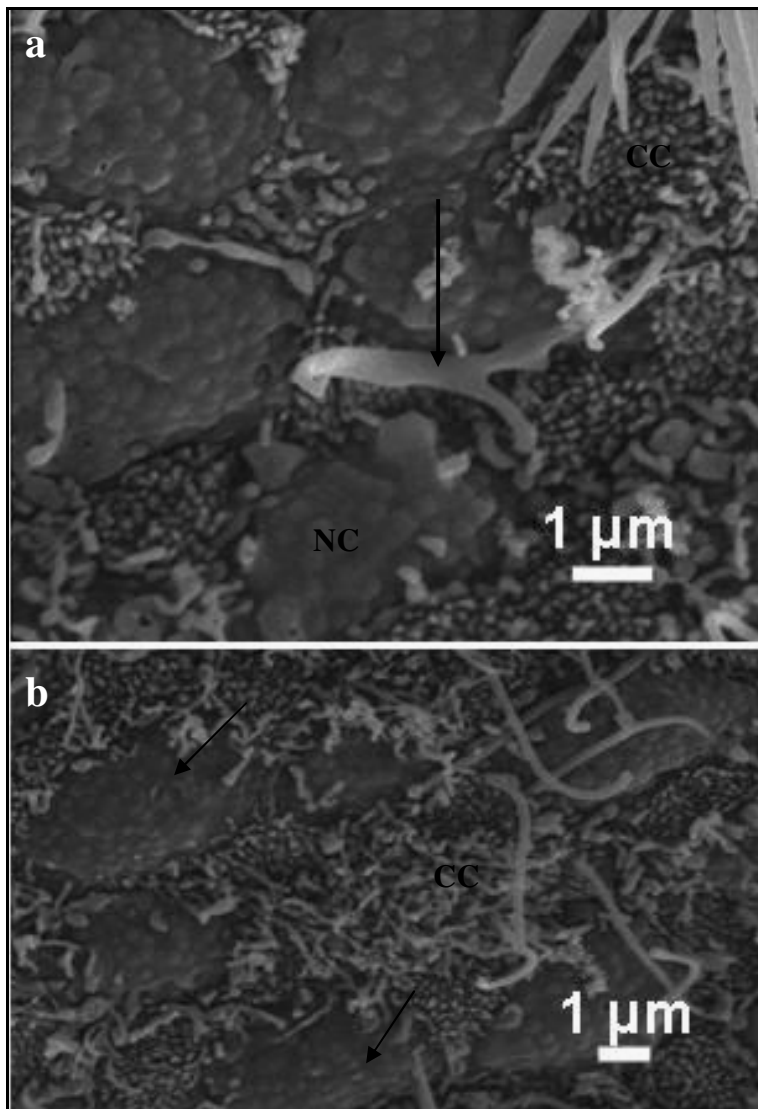


Fig. 5.14: Scanning electron photomicrographs of mucosal surface at UVJ from 400mg/kg bodyweight carbendazim-treated bird. **a.** Ciliary and microvillous loss are observed on the ciliated (CC) and non-ciliated (NC) cells respectively. Arrow: swollen cilia. **b.** Non-ciliated cells (arrows) are seen protruding above the surface. CC: ciliated cells.

5.3.4.1.iib Experiment II

No degenerative changes were observed 5 and 24 hours post-exposure to 400 mg/kg bodyweight carbendazim.

5 days post-exposure

At 5 days post-exposure to carbendazim, a loss of cilia was observed (Fig. 5.15a). In these areas short ciliary stems, which were remnants of lost cilia were identified (Fig. 5.15b). On a few degenerating cells, swollen cilia were encountered (Fig. 5.15b). At this stage, non-ciliated cells were seen protruding above the luminal surface (Fig. 5.15b). The cells were lined by a few microvilli. In some areas, the cells contained no microvilli.

8, 12 and 32 days post-exposure

Deciliation and loss of microvilli, similar to that observed on day 5, were still the predominant degenerative changes seen at days 8, 12 and 32 post-exposure to carbendazim.

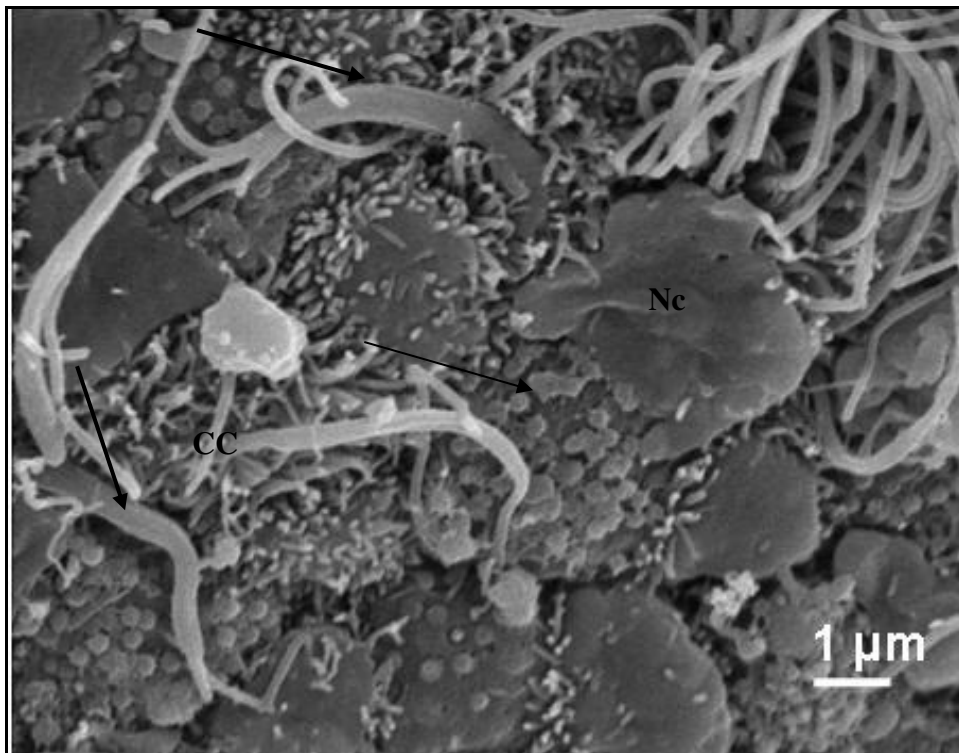


Fig. 5.15: Scanning electron photomicrograph of the mucosal surface at UVJ of Japanese quail 5 days post-exposure to 400 mg/kg bodyweight carbendazim. Note the presence of swollen cilia (thick arrows), cilia stems (thin arrows) and protruding non-ciliated cells (NC).

5.3.4.2 Transmission electron microscopy

5.3.4.2.i Control birds

The sperm storage tubules (SST) were lined by simple columnar epithelium (Fig. 5.16a). The SST cells contained basally located oval nuclei with prominent nucleoli (Fig. 5.16a). On the luminal aspect, the cells were covered by long microvilli (Fig. 5.17a). A few spermatozoa were observed in the lumen (Fig. 5.17b). Desmosomes and occasional tight junctions were observed linking the adjacent cells apically (Fig. 5.17a). Along the lateral plasma membranes, desmosomes and infoldings of the plasma membranes were observed (Fig. 5.17a). In the apical cytoplasmic region, mitochondria, cisternae of rough (RER) and smooth (SER) endoplasmic reticulum, stacks of Golgi complexes and a few vacuoles were observed (Fig. 5.16b&c). In the basal cytoplasmic regions, only a few mitochondria and cisterns of RER were identified (Fig. 5.18a). The cells rested on a basal lamina of approximately 90 nm in thickness. Both the lamina densa and lamina lucida of the basal lamina were clearly identified (Fig. 5.18b).

5.3.4.2.ii Carbendazim-treated birds

5.3.4.2.iii Experiment I

25 and 100 mg/kg bodyweight carbendazim

There were no ultrastructural changes observed in the SST cells at doses of 25 mg/kg and 100 mg/kg bodyweight carbendazim.

400 mg/kg bodyweight carbendazim

At a dose of 400 mg/kg bodyweight carbendazim, the SST contained a few cells with pyknotic nuclei, numerous vacuoles, lipid droplets and a few swollen mitochondria (Fig. 5.19a). Vacuoles were concentrated in the basal cytoplasmic regions. In some cells, lipofuscin granules were observed in the apical regions of the cytoplasm (Fig. 5.19b). Desmosomes and microvilli along the lateral plasma membranes were

structurally normal (Fig. 5.20a). Spermatozoa were still seen in the lumen. Infolding of the basal lamina was also observed (Fig. 5.20b). At this dose, the basal lamina measured approximately 85 nm in thickness. Although both lamina densa and lamina lucida were clearly differentiated, the discontinuation of the basal lamina was observed in some areas (Fig. 5.20b).

800 mg/kg bodyweight carbendazim

At a dose of 800 mg/kg bodyweight carbendazim, degenerating SST cells were lined by relatively short microvilli. The cells contained numerous vacuoles and lipid droplets in both apical and basal cytoplasmic regions (Fig. 5.21a). Swollen mitochondria and numerous lysosomes were observed (Fig. 5.21a). A few degenerating SST cells also contained pyknotic nuclei and those displaying nucleolar margination and condensation of nuclear chromatin. At this dose, desmosomes linking the adjacent cells were intact (Fig. 5.21b). The basal lamina underlying the SST cells was 68 nm in thickness. No degenerative changes were observed in the basal lamina.

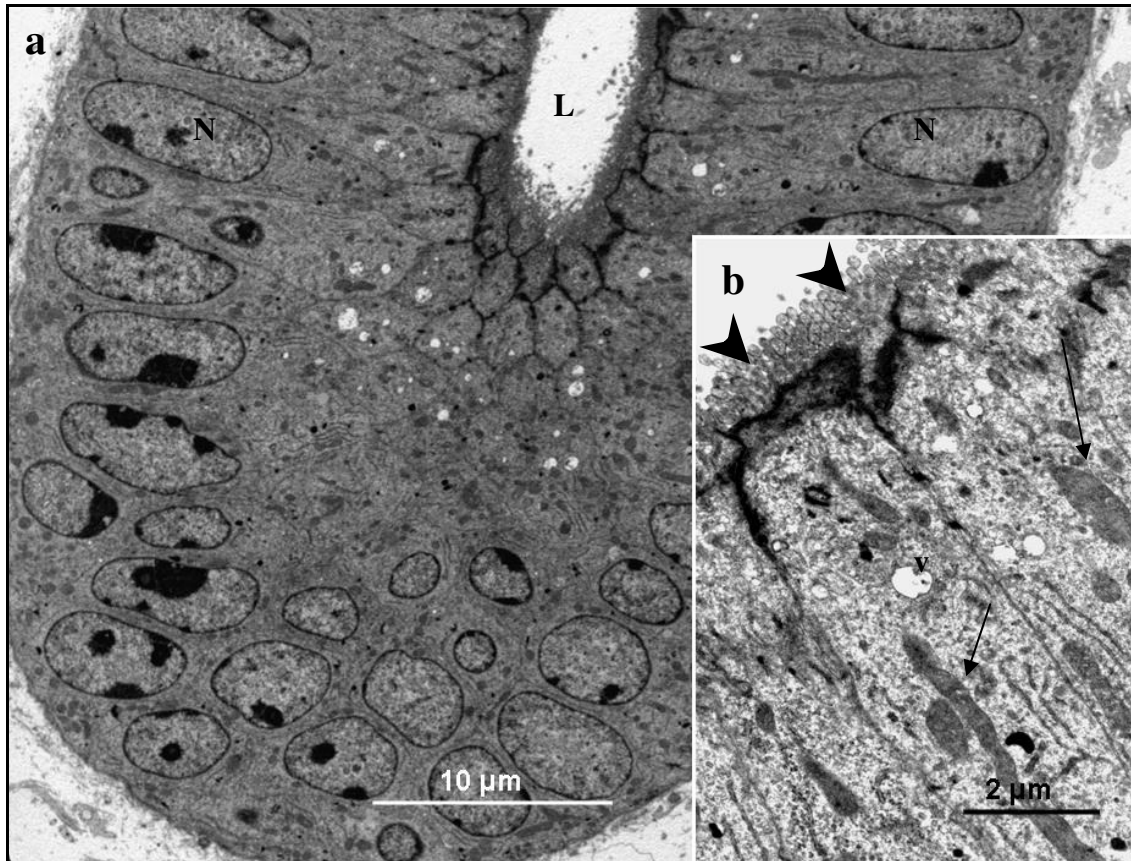


Fig. 5.16: **a.** A survey transmission electron photomicrograph of SST from a control bird. SST are lined by simple columnar epithelium. N: nucleus. L: lumen. **b.** Apical region of the SST cells. The cells are lined by long microvilli (arrow heads). Arrows: mitochondria. v: vacuoles.

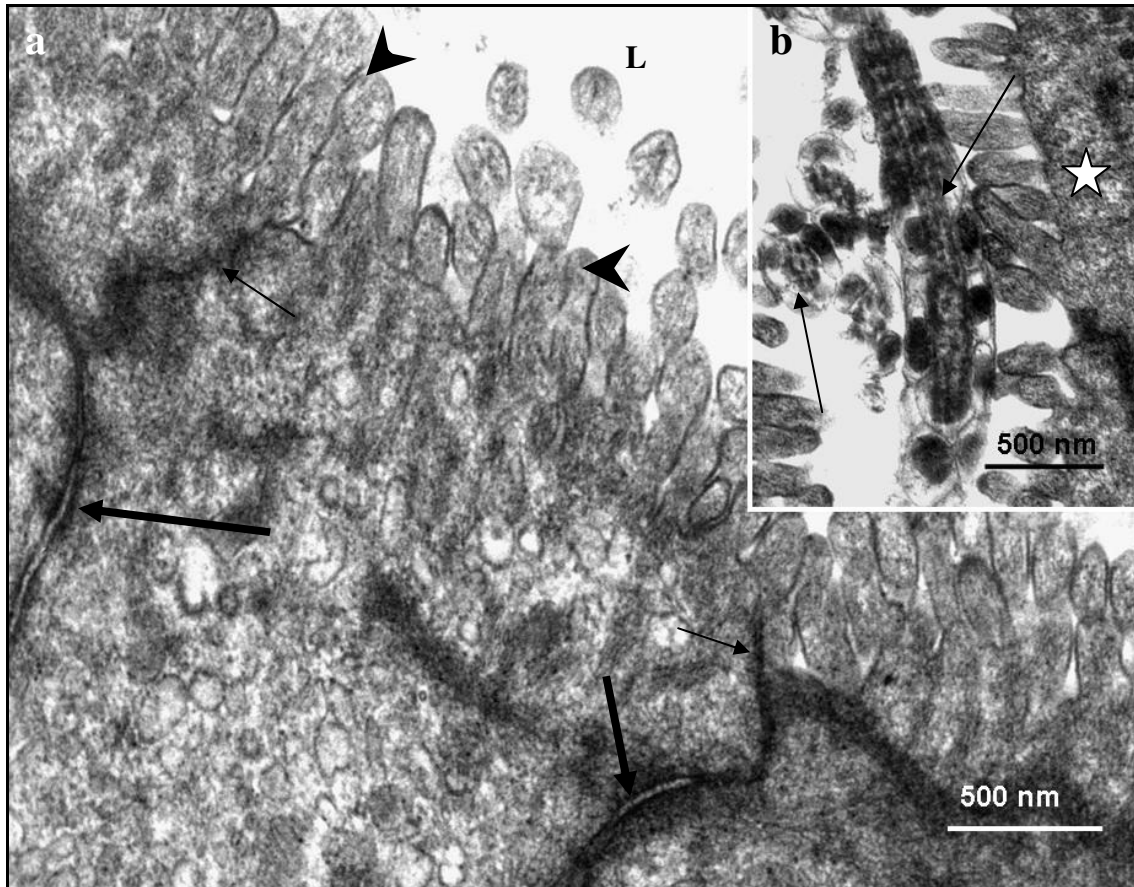


Fig. 5.17: **a.** Apical regions of the SST cells from a control bird. The cells are lined by long microvilli (arrow heads). Desmosomes (thick arrows) and tight junctions (thin arrows) are observed linking the cells. L: lumen. **b.** Electron photomicrograph of the SST lumen showing the presence spermatozoon (arrows). Asterisk: SST cell.

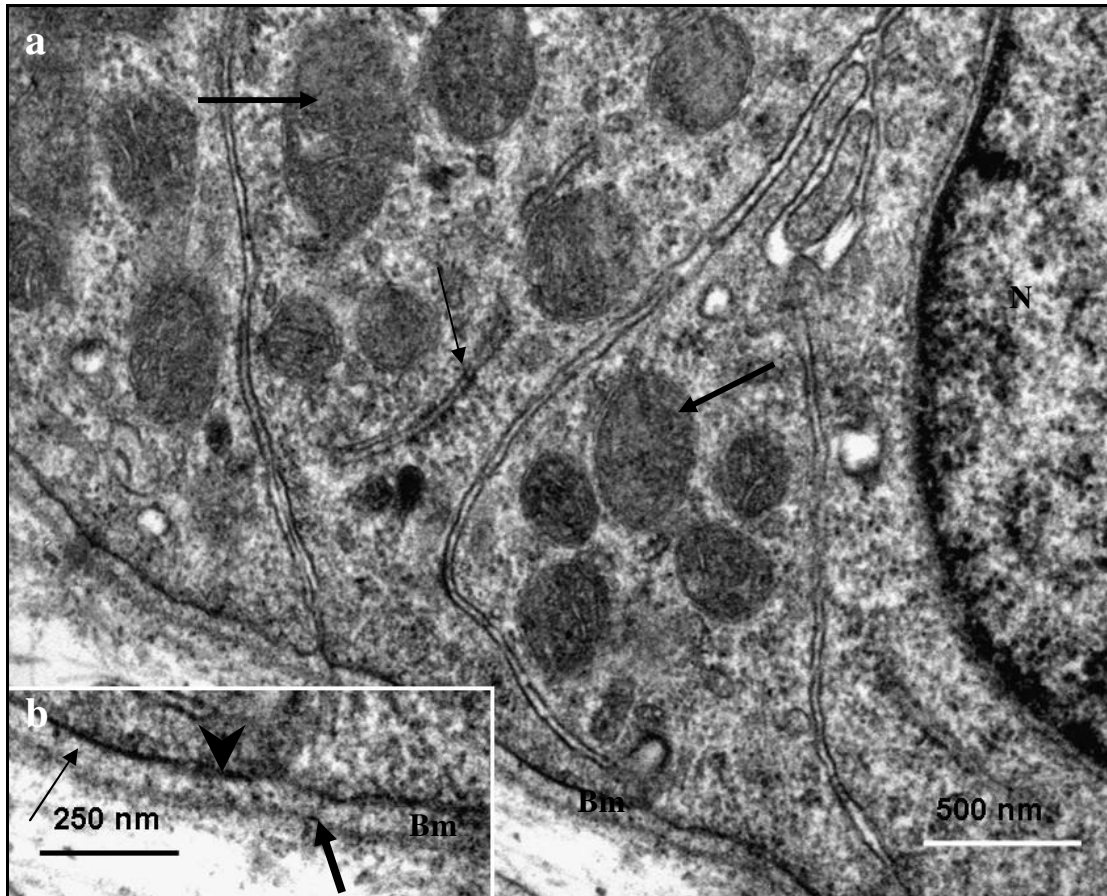


Fig. 5.18: **a.** Electron photomicrograph of the basal regions of SST cells from a control bird. In this region, only mitochondria (thick arrows) and cisternae of RER (thin arrow) are observed. N: Nucleus; Bm: Basal lamina. **b.** A higher electron photomicrograph of the basal lamina (Bm) underlying SST cells. Both lamina densa (thick arrow) and lamina lucida (thin arrow) are clearly observed. Arrow head: basal plasma membrane.

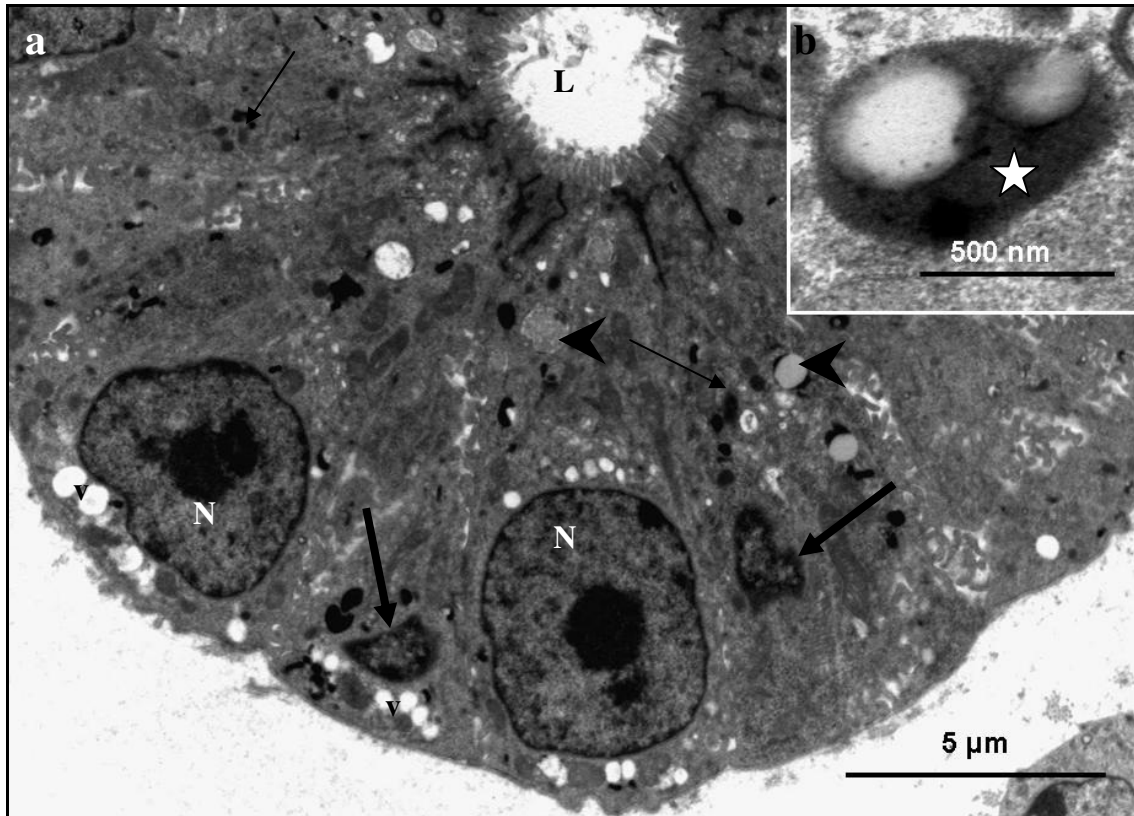


Fig. 5.19: **a.** A survey electron photomicrograph of a SST from a Japanese quail treated with 400 mg/kg bodyweight carbendazim. Arrows: pyknotic nuclei. N: normal nuclei. v: vacuoles. Thin arrows: lysosomes. Arrow heads: lipid droplets. L: lumen. **b.** A higher magnification of lipofuscin granule (asterisk) in degenerating SST cells.

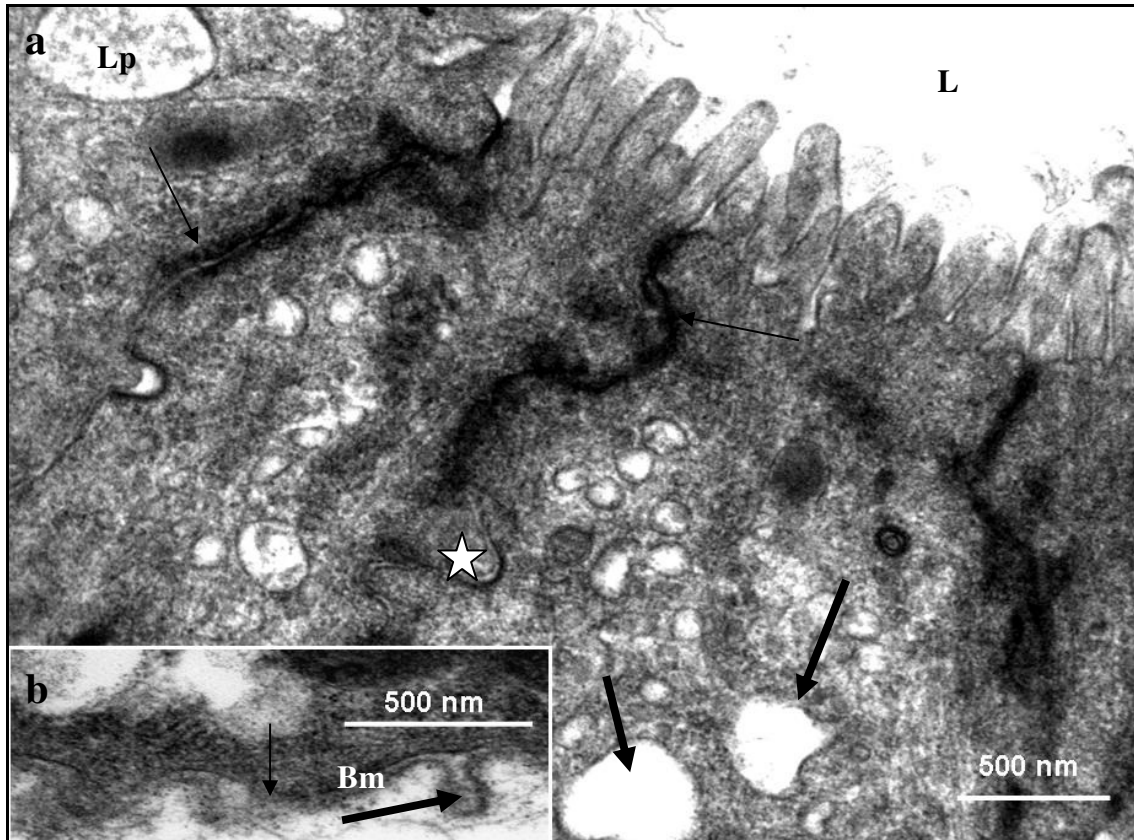


Fig. 5.20: **a.** Electron photomicrograph of the apical regions of degenerating SST cells from a bird treated with 400 mg/kg bodyweight carbendazim. The degenerating SST cells contain dilated RER (thick arrows) and degenerating lipid body (Lp). Thin arrows: intact desmosomes. Asterisk: Infolding of the lateral plasma membranes. L: glandular lumen. **b.** High magnification photomicrograph of a basal lamina (Bm) underlying the SST. Evagination (thick arrow) and discontinuation (thin arrow) are observed.

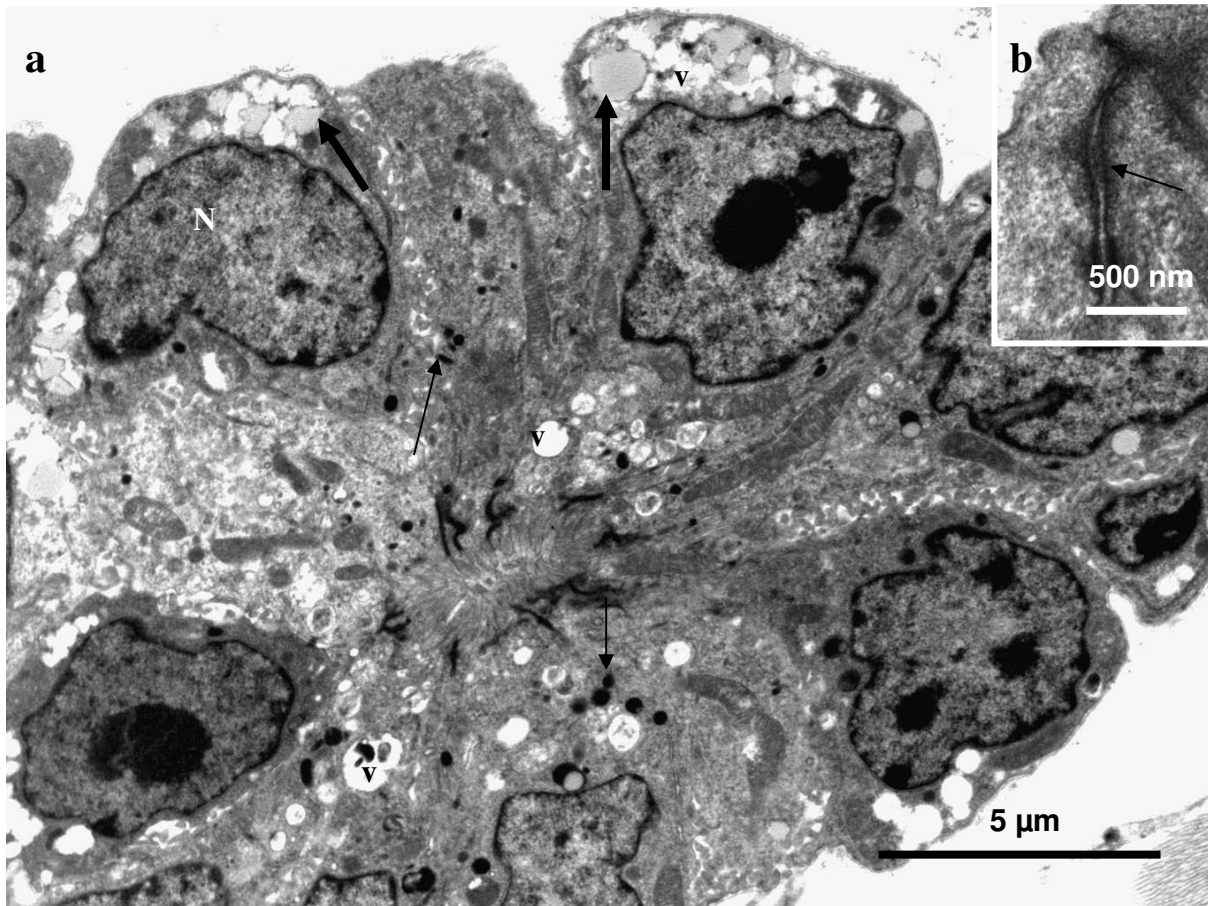


Fig. 5.21: Electron photomicrographs of a SST from a bird treated with 800 mg/kg bodyweight carbendazim. **a.** Degenerating SST cells contain numerous vacuoles (v), lipid droplets (thick arrows) and lysosomes (thin arrows). N: Nucleus with marginalized nucleoli. **b.** Arrow: desmosome.

5.3.4.2.iib Experiment II

5 and 24 hours post-exposure

No degenerative changes were observed in the SST at 5 and 24 hours post-exposure to 400 mg/kg bodyweight carbendazim. The SST were lined by simple columnar epithelium displaying normal morphology.

5 days post-exposure

At 5 days post-exposure to carbendazim, the SST cells were lined by relatively short microvilli. The degenerating cells contained pyknotic nuclei as well as nuclei with condensed chromatin and nucleolar margination (Fig. 5.22 a&b). Swollen mitochondria, numerous vacuoles, lysosomes and lipid droplets were observed in the apical cytoplasmic regions. In addition, myelin figure formation was also a notable degenerative feature in this region (Fig. 5.23a). A few multivesicular and lipofuscin bodies were also seen (Fig. 5.23b). At this stage, the lumina of degenerating SST were either empty or contained degenerating spermatozoa (Fig. 5.22a). Desmosomes along the lateral plasma membranes were structurally normal (Fig. 5.23a). The SST cells were supported by a basal lamina of approximately 80 nm in thickness. No degenerative changes were observed in this lamina.

8 days post-exposure

Eight days post-exposure to carbendazim, degenerating SST cells contained numerous vacuoles in the basal cytoplasmic regions and degenerating lipid droplets in the apical regions of the cytoplasm (Fig. 5.24). Numerous lysosomes were observed throughout the cytoplasm (Fig. 5.25). At this stage, desmosomes along the lateral plasma membranes were intact (Fig. 5.25). Crenated and pyknotic nuclei were also a common feature in degenerating SST cells. No degenerative changes were observed in the underlying basal lamina. Both lamina densa and lucida were clearly observed. The basal lamina measured approximately 80 nm in thickness.

12 days post-exposure

Twelve days post-exposure to carbendazim, degenerating cells in the SST contained nuclei displaying condensation and nuclear chromatin margination (Fig. 5.26a). Numerous swollen mitochondria and a few degenerating lipid droplets were observed perinuclearly (Fig. 5.26b). Lysosomes were observed throughout the cytoplasm. At this stage, coalescing vacuoles were observed in the basal cytoplasmic region (Fig. 5.26a). No spermatozoa were observed in the lumen. The basal lamina, which measured approximately 80 nm in thickness was structurally

normal. Similarly, desmosomes along the lateral plasma membranes were intact (Fig. 5.26c).

32 days post-exposure

Thirty-two days post-exposure to carbendazim, degenerating SST cells contained pyknotic nuclei (Fig. 5.27a&b). A few degenerating SST cells contained irregular-shaped nuclei which displayed nucleolar and chromatin margination (Fig. 5.27b). At this stage, relatively short microvilli lined the apical plasma membranes (Fig. 5.28). However, desmosomes along the lateral plasma membranes were intact (Fig. 5.28). In the apical cytoplasmic regions numerous lysosomes and degenerating lipid droplets were observed (Fig. 5.29a,b&c). A few dilated cisternae of RER were also observed in this region (Fig. 5.29b&c). Myelin figures were seen on the supranuclear regions (Fig. 5.29c). In the basal cytoplasmic regions, numerous vacuoles and swollen mitochondria were identified (Fig. 5.30). A few lipofuscin granules were also seen in this region. A basal lamina which measures approximately 90 nm in thickness underlined the SST cells. Both lamina densa and lucida were observed. In a few degenerating SST the basal lamina was indistinct.

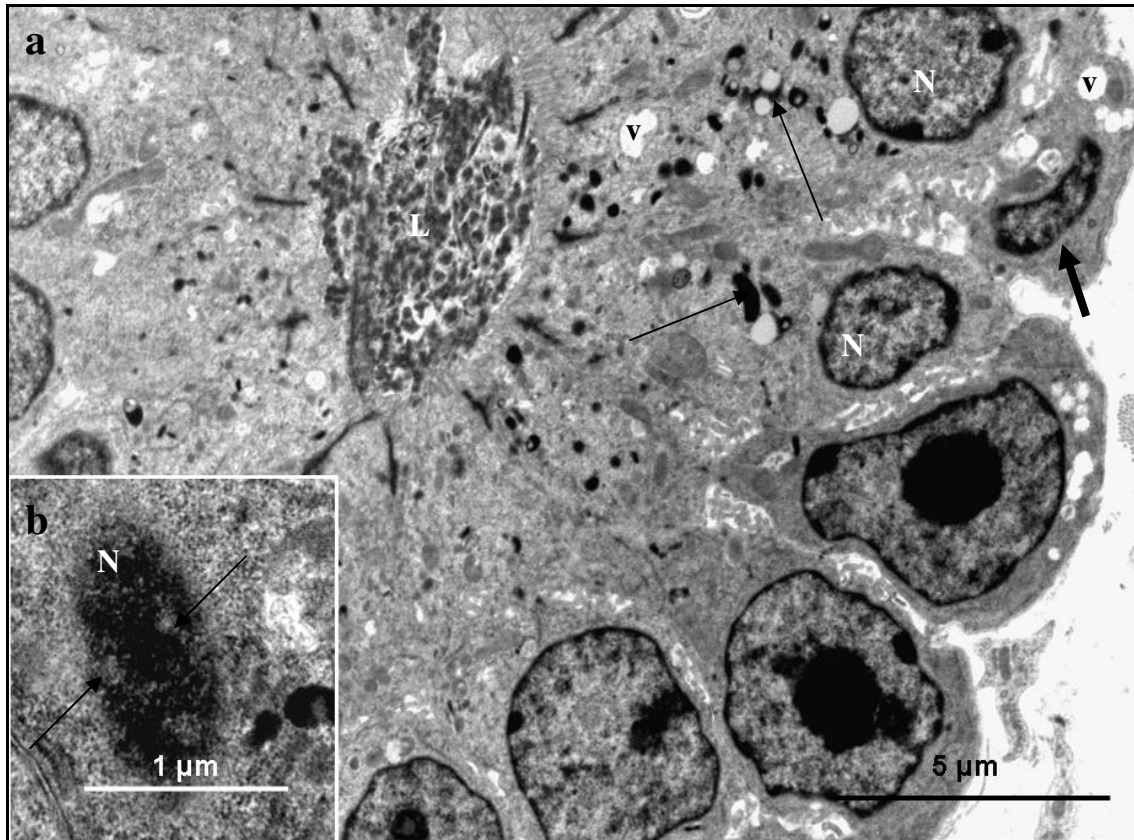


Fig. 5.22: **a.** Survey electron photomicrograph of SST 5 days post-exposure to 400 mg/kg bodyweight carbendazim. Thick arrow: pyknotic nuclei. N: nuclei with condensed chromatin. Thin arrows: lysosomes. Arrow heads: lipid droplets. v: vacuoles. L: lumen containing degenerating spermatozoa and cellular debris. **b.** Pyknotic nucleus (N) in degenerating SST. Note dilatation of nuclear pores (arrows)

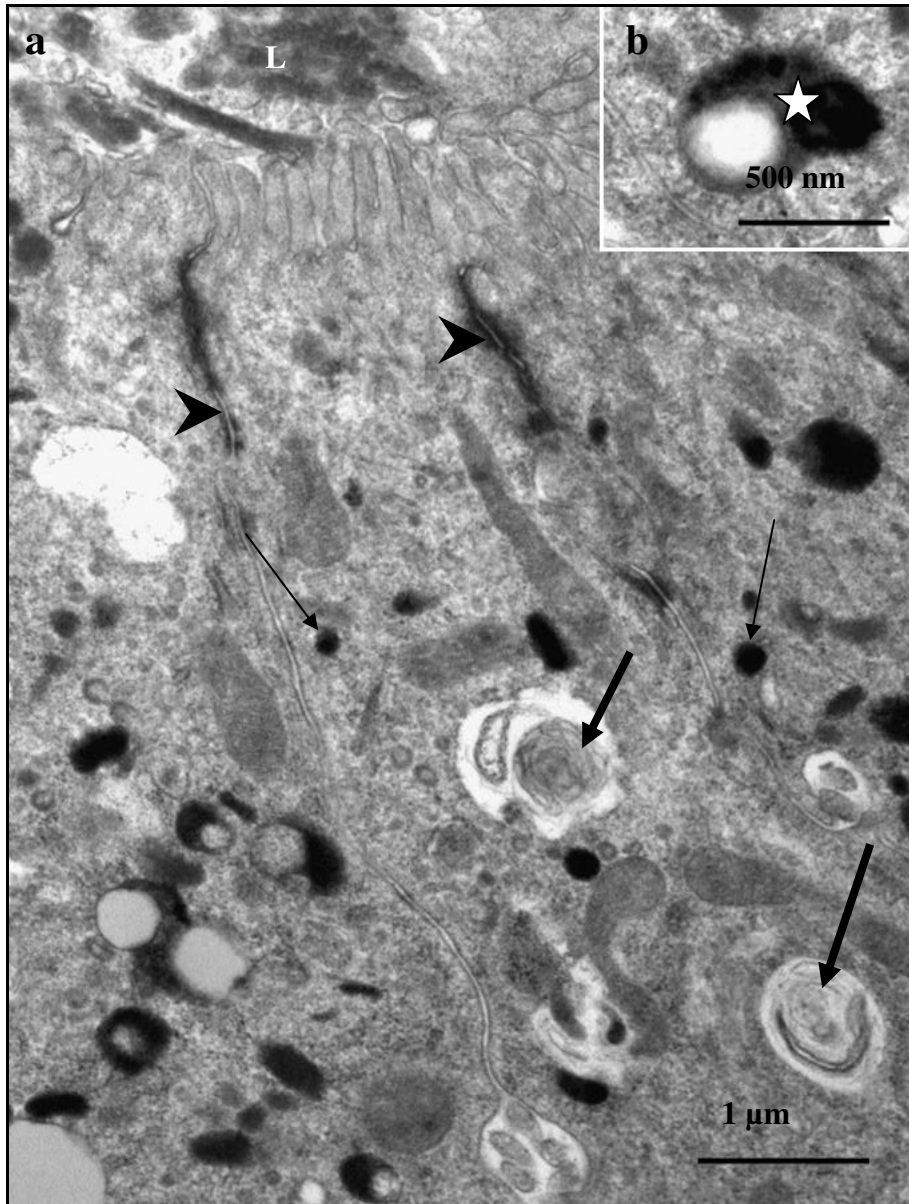


Fig. 5.23: **a.** Electron photomicrograph of apical regions of SST cells 5 days post-exposure to 400 mg/kg bodyweight carbendazim. Note the presence of numerous lysosomes (arrows), myelin figures (thick arrows) and sperm debris in the lumen (L). Arrow heads: Desmosomes. **b.** Lipofuscin granule (asterisk) observed in a degenerating SST cell.

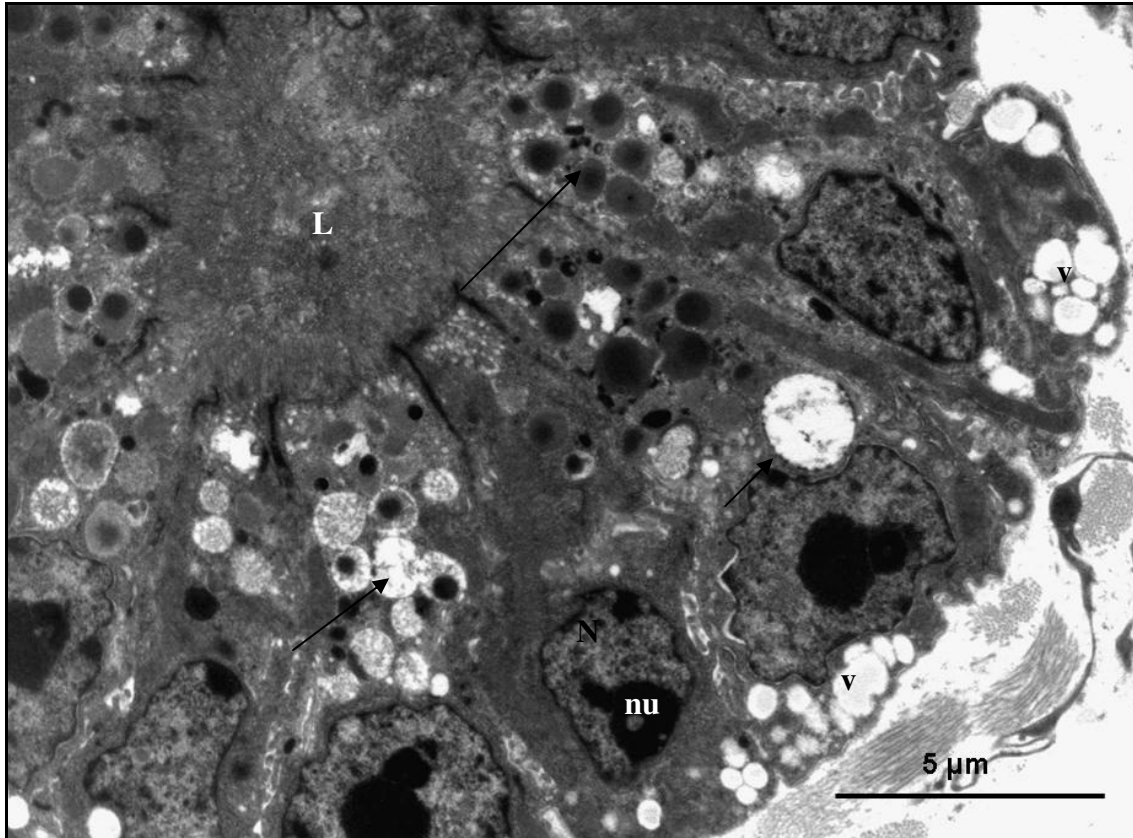


Fig. 5.24: Survey electron photomicrograph of SST 8 days post-exposure to 400 mg/kg bodyweight carbendazim. At this stage the cells contain degenerating lipid granules (arrows) and numerous vacuoles (v). L: lumen. N: Nucleus with marginalized nucleoli (nu).

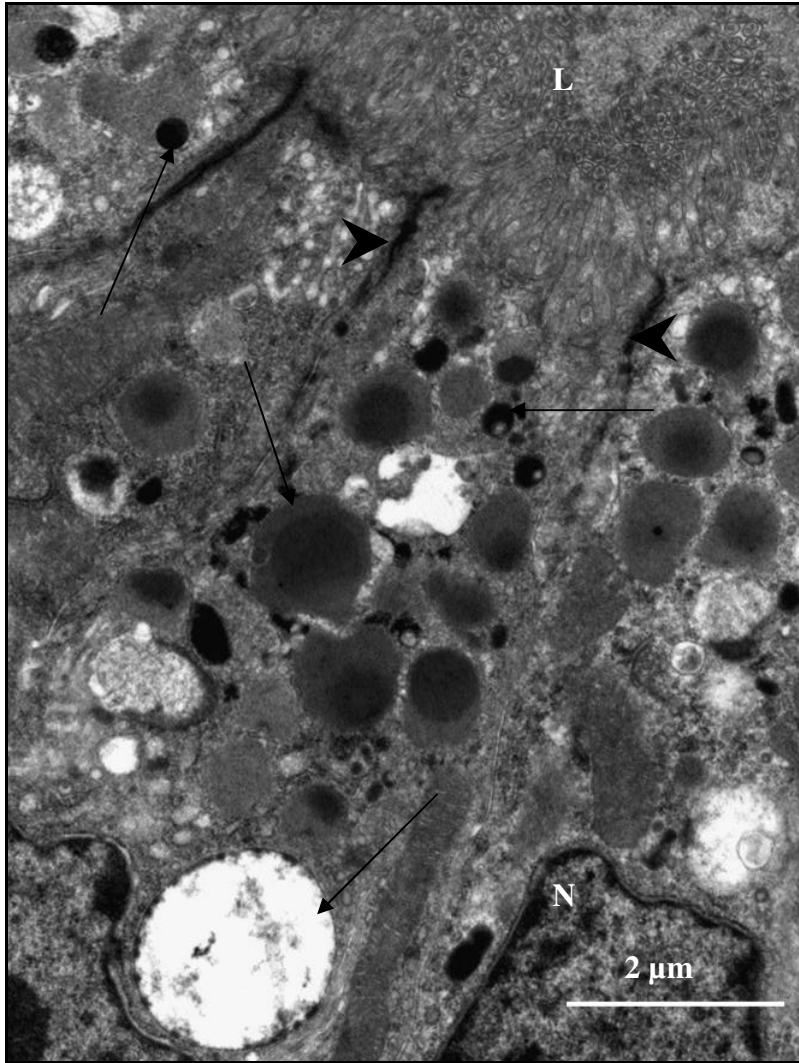


Fig. 5.25: A higher magnification electron photomicrograph of the apical regions of SST cells 8 days post-exposure to 400 mg/kg bodyweight carbendazim. Thick arrows: lipid droplets. Thin arrows: lysosomes. Arrow heads: desmosomes. L: lumen; N: Nucleus.

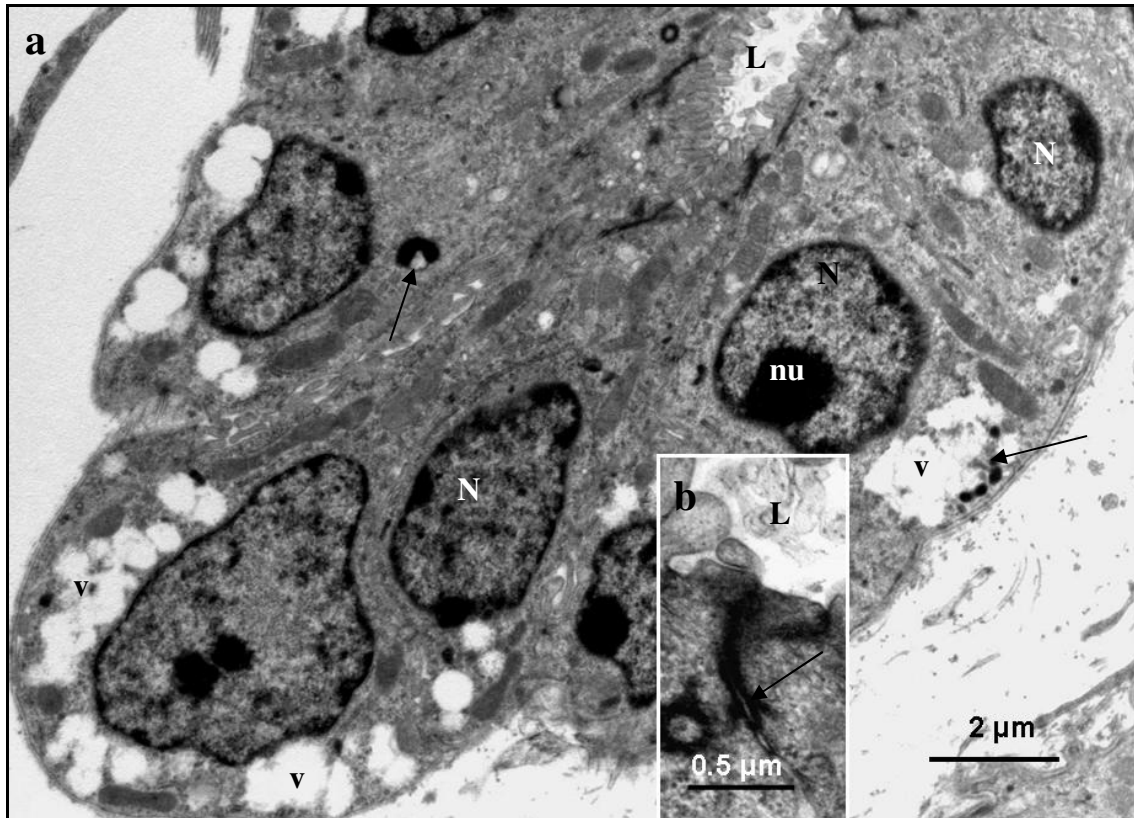


Fig. 5.26: **a.** Electron photomicrograph of SST 12 days post-exposure to 400 mg/kg bodyweight carbendazim. v: coalescing vacuoles. Nuclei (N) displaying chromatin condensation and nucleoli (nu) margination are observed. The lumen (L) contains no spermatozoa. Arrows: lysosomes. **b.** A higher magnification photomicrograph of a desmosome (arrow) along the lateral plasma membrane. L: lumen.

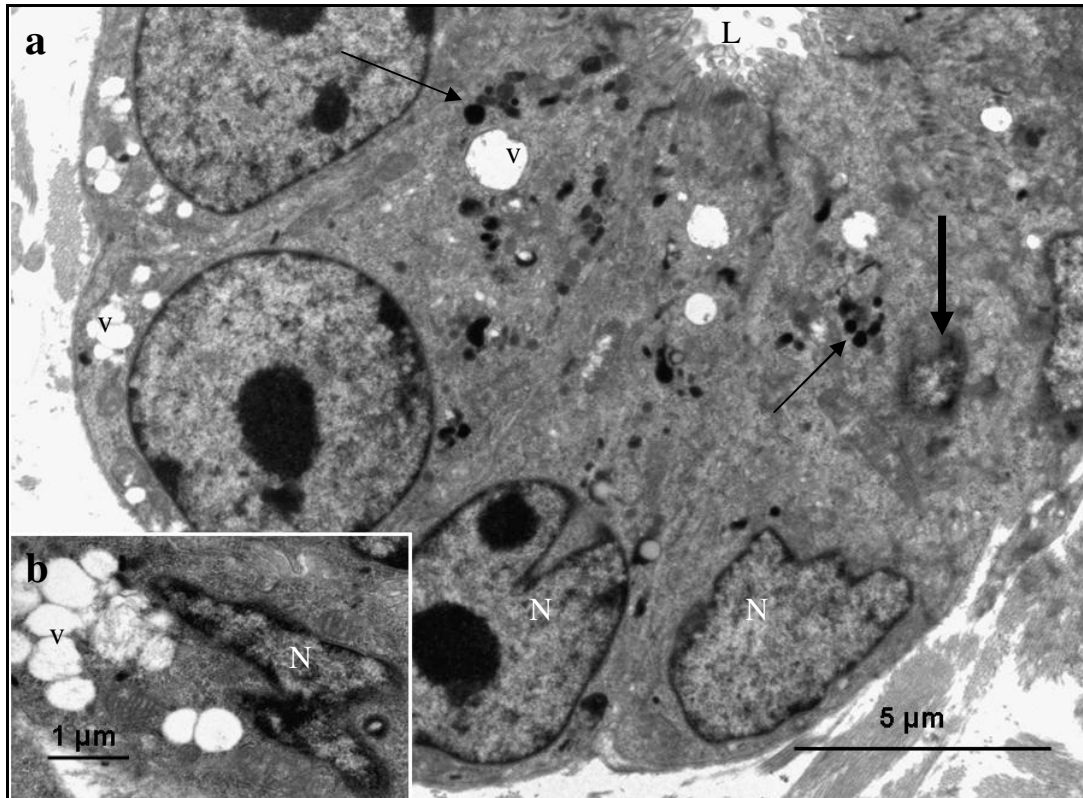


Fig. 5.27: **a.** A survey electron photomicrograph of SST 32 days post-exposure to 400 mg/kg bodyweight carbendazim. Pyknotic (thick arrow) and irregular-shaped (N) nuclei are observed. Thin arrows: lysosomes. v: vacuoles. L: gland lumen. **b.** Electron photomicrograph of degenerating SST cell. Nuclei with condensed chromatin are evident. v: vacuoles.

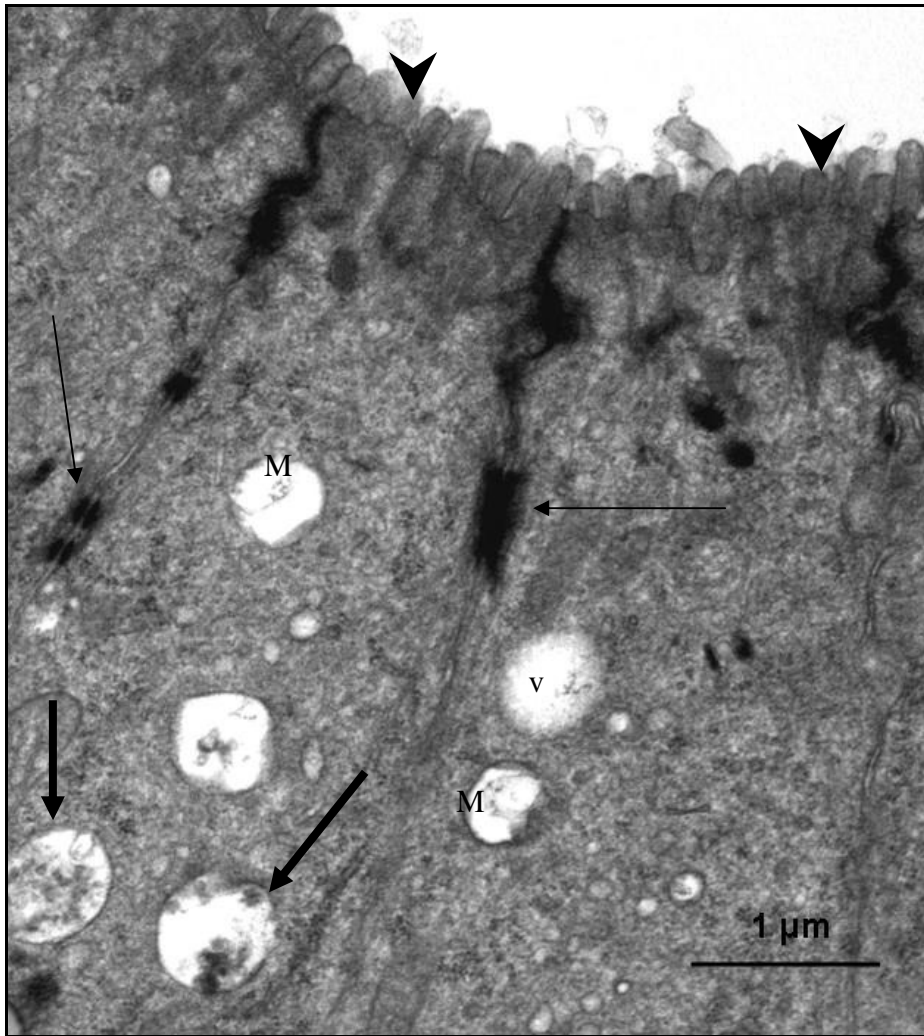


Fig. 5.28: Electron photomicrograph of apical regions of SST cells 32 days post-exposure to 400 mg/kg bodyweight carbendazim. The cells are lined by short microvilli (arrow heads). Desmosomes (thin arrows) linking the lateral plasma membranes are intact. v: vacuole; M: swollen mitochondria; Thick arrows: degenerating lipid droplets.

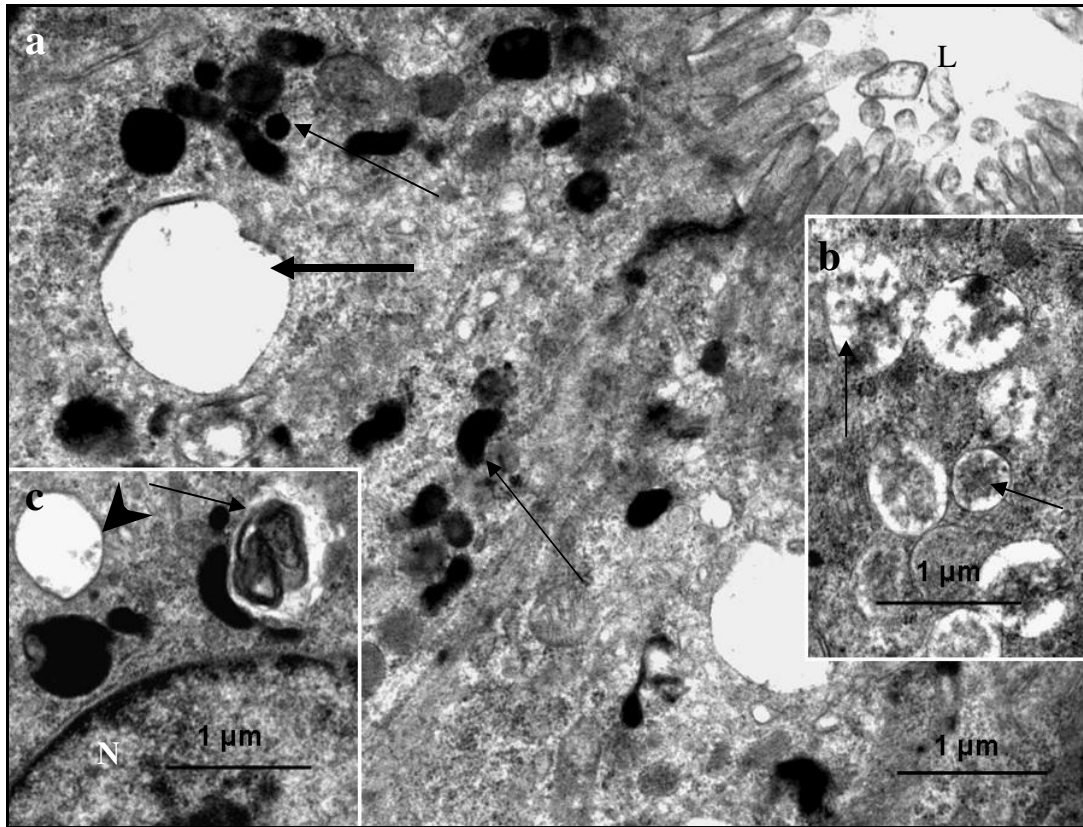


Fig. 5.29: Electron photomicrograph of degenerating SST cells 32 days post-exposure to 400 mg/kg bodyweight carbendazim. **a**. Thin arrows: lysosomes. Thick arrow: dilated cistern of RER. L: gland lumen. **b**: Degenerating lipid droplet (arrows) observed in the apical cytoplasmic region. **c**. A myelin figure (arrow) is seen adjacent nucleus (N). Arrow head: dilated cistern of RER.

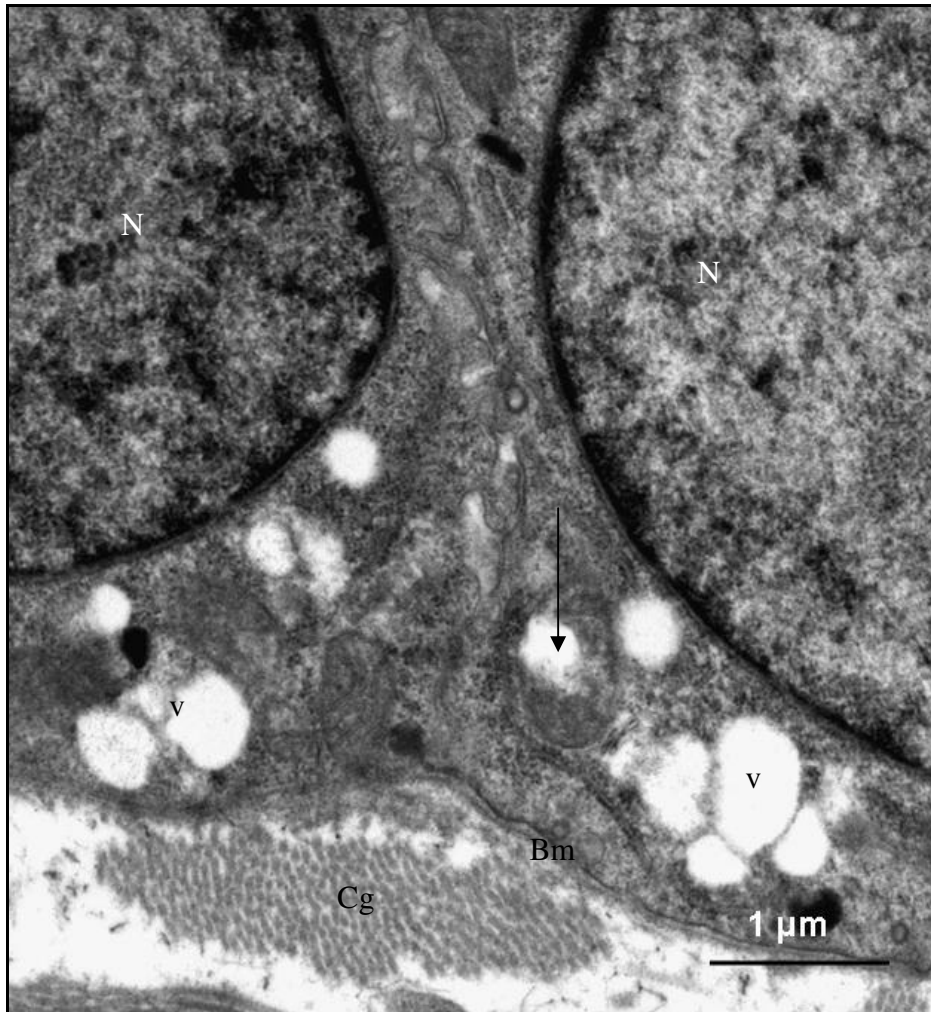


Fig. 5.30: Electron photomicrograph of basal regions of SST cells 32 days post-exposure to 400 mg/kg bodyweight carbendazim. A swollen mitochondrion (arrow) and numerous vacuoles (v) are observed in this region. N: nucleus; Bm: underlying basal lamina; Cg: collagen fibres.

5.4. Discussion

The present investigation has highlighted the morphological changes that occur in the SST of the Japanese quail following exposure to carbendazim. This appears to be the first report to show the possible effects of fungicides on the SST of birds. Several reports are available on the normal structure of the SST in avian species, including the Japanese quail (Frieß *et al.*, 1978; Holm & Ridderstrale, 2002), domestic fowl (Tingari & Lake, 1973) and Turkey (Schupping *et al.*, 1984; Bakst, 1987).

Histology and statistical analysis

In this investigation, the results of the morphometrical study showed that carbendazim exposure caused shrinkage (atrophy) of SST. The shrinkage of the SST observed, might cause a reduction in the amount and storage period of spermatozoa in carbendazim-exposed birds. This idea is supported by research findings in the domestic fowl (Birkhead & Moller, 1992). According to Birkhead & Moller (1992), there is a positive correlation between the volume of SST and number of spermatozoa stored. The report further showed that the size (length) of the SST correlates with the length of spermatozoa, as well as the duration of storage.

Based on histological results, the morphology of SST observed in the control group was generally consistent with published information in the Japanese quail (Frieß *et al.*, 1978; Holm & Ridderstrale 2002), domestic fowl (Tingari & Lake, 1973; Bakst 1998) and turkey (Schuppig *et al.*, 1984; Bakst, 1987). The results showed that SST are tubular invaginations lined by simple columnar epithelium. Contrary to the observation made in the domestic fowl (Tingari & Lake, 1973; Das, 2003), myoepithelial cells were observed around SST in the quail. This observation confirms an earlier finding by Frieß *et al.* (1978) in the Japanese quail. Following carbendazim exposure, degenerative changes such as pyknosis and cuboidal metaplasia were observed. Degeneration of SST cells may lead to an impaired sperm storage capability in carbendazim-exposed birds.

It has been established that SST serve as sperm storage sites for the entire length of the fertile period in birds (Schuppig *et al.*, 1984; Pierson, McDaniel & Krista, 1988; Birkhead, 1992). The reduced number of spermatozoa and the presence of empty SST observed in carbendazim-treated groups might impact negatively on the fertility of exposed birds. This is based on the fact that fertility in birds depends on the proportion of SST containing viable spermatozoa (Bilgili & Renden, 1986; McDaniel, Brake & Eckman, 1981; Brillard & Antoine, 1990). According to these reports, fertility in the domestic fowl was correlated to the number of spermatozoa attached to the perivitelline layer, which was influenced by the proportion of SST containing spermatozoa.

In the current study, the presence of empty SST could have been caused by the degeneration of spermatozoa as a result of carbendazim toxicity. Carbendazim has been shown to cause the degeneration of spermatozoa in mammals (Hess & Nakai, 2000) and birds (Aire, 2005). In the rat and male Japanese quail, carbendazim caused necrosis of spermatozoa and germ cell disruption in the seminiferous tubules.

Immunohistochemistry

In the present study, SST of the control birds showed a moderate e-cadherin immunoreaction. Following exposure to carbendazim, SST became weak to negative for e-cadherin. The absence of e-cadherin immunostaining was consistent with morphological changes observed at the ultrastructural study. As mentioned in Chapter two, e-cadherin is an epithelial cadherin facilitating cell-cell adhesions (Stemmler, 2008). It interacts with microfilaments to form an adherens network (Stemmler, 2008). It is assumed that, the absence of e-cadherin in the present study was caused by the ability of carbendazim to disrupt cytoskeletal elements. The presence of a moderate e-cadherin immunoreaction at day 32 suggests epithelial recovery. This was also seen in the infundibulum, magnum and shell gland.

In the current investigation, laminin immunostaining was demonstrated in the basement membranes of SST in control birds. Following carbendazim exposure, laminin immunoreaction became weak to absent. The disappearance of laminin immunoreaction is not surprising as similar findings have also been reported in degenerating basal lamina underlying muscle cells (Gulati, Reddi & Zalewski, 1983). Laminin is a glycoprotein which forms a larger proportion of the basement membrane. Other elements include fibronectin, chondroitin sulphate, collagen IV and V, as well as, perlecan (Laurie, Leblond & Martin, 1982; Martinez-Hernandez, Gay, & Miller, 1982). According to Ryan, Tizard, Vandevanter & Carter (1994), laminin plays an important role in stabilizing the basement membrane. In addition to stabilizing the basement membrane, laminin also contributes to cytoskeletal reorganization through the surface receptor pathway (Ryan *et al.*, 1994). Considering the ability of carbendazim to disrupt the cellular skeleton, and that laminin is synthesized by epithelial cells (Koch, Olson, Albus, Jin, Hunter, Brunken, Burgeson

& Champliaud, 1999), it is likely that the degeneration of the basement membrane observed was a consequence of epithelial and cytoskeletal damage.

The results of the immunohistochemical study showed vimentin immunostaining in the basal cytoplasmic regions of the SST. The presence of vimentin in the cytoplasm of SST was expected since it is an intermediate filament of mesenchymal cell origin (Steinert & Roop, 1988). Vimentin provides structural integrity to cells and is involved in cellular morphogenesis (Helfand, Chang & Goldman, 2003). However, following carbendazim exposure, no immunoreaction for vimentin was observed. This observation suggests that vimentin filaments were dismantled post-exposure to carbendazim.

Scanning and transmission electron microscopy

At an ultrastructural level, the morphology of the SST in the control birds of the present study was in accordance with the findings of Frieß *et al.* (1978). Following carbendazim exposure, degenerating cells were common in the SST. In these degenerating gland cells, swollen mitochondria were frequently observed. The presence of swollen mitochondria suggests an increased cellular permeability induced by carbendazim through cytoskeletal damage. Heggeness, Simon & Singer (1978) reported an association between the cytoskeleton and mitochondria. The report shows that mitochondria are tightly connected to cytoskeletal elements. The destruction of cytoskeletal elements by colchicine or taxol increased mitochondrial membrane permeability in Ehrlich ascites tumour cells (Evtodienko, Teplova, Sidash, Ichas & Mazat, 1996). In addition, the administration of colchicine induced the release of cytochrome c in cultured cerebellar granule cells (Gorman, Banfoco, Zhivotovsky, Orrenius & Ceccatelli 1999). Cytochrome c is an apoptotic-inducing factor released by damaged mitochondria (Kroemer, Dallaporta & Resche-Regon, 1998).

Pyknosis and nuclear chromatin condensation were also prominent degenerative changes observed at days 12 and 32 post-exposure to carbendazim. Similar observations have also been reported in dentate granule cells exposed to microtubule disrupting agents such as, colchicine, vinblastin, nicodazole and taxol

(Kim, Mitsukawa, Yamada, Nishiyama, Matsuki & Ikegaya, 2002). According to Kim *et al.* (2002), the disruption of cytoskeletal elements induced apoptosis-like degeneration in dentate granule cells. This might also be the case in the present study. However, in this study only chromatin condensation and pyknosis suggested apoptotic cell death. To confirm this, a further investigation using apoptotic makers is proposed.

The basal lamina underlying the SST appeared to undergo degeneration with time lapse post-exposure to carbendazim. This was revealed by the reduced thickness of the basal lamina. At 32 days post-exposure, the basal lamina was indistinct in most of the SST studied.

Conclusion

In conclusion, the present study has shown the effect of carbendazim on the morphology of SST in the Japanese quail. Based on the functional importance of the SST in avian species, the continued use of carbendazim in the field might reduce the reproductive potential of exposed birds.

5.5. References

- AIRE, T. A. 2005. Short-term effects of carbendazim on the gross and microscopic features of the testes of Japanese quails (*Coturnix coturnix japonoca*). *Anatomy and Embryology*, 210:43-49.
- BAKST, M.R. 1981. Sperm recovery from oviducts of turkeys at known intervals after insemination and oviposition. *Journal of Reproduction and Fertility*, 62:159-164.
- BAKST, M.R. 1987. Anatomical basis of sperm storage in the avian oviduct. *Scanning Microscopy International*, 1:1257-1266.
- BAKST, M.R. 1998. Structure of the avian oviduct with emphasis on sperm storage in poultry. *The Journal of Experimental Zoology*, 282:618-626.
- BILGILI, S.F. & RENDEN, J.A. 1986. Sperm release from the uterovaginal storage gland of the chicken: A perfusion study. *Theriogenology*, 26:77-88.
- BIRKHEAD, T.R. 1992. Sperm storage and the fertility period in the Bengalese finch. *The Auk*, 109:620-625.

- BIRKHEAD, T.R. & FLETCHER, F. 1994. Sperm storage and release of sperm from the sperm storage tubules in the Japanese quail *Coturnix japonica*. *Comments*, 136:101-105.
- BIRKHEAD, T.R. & MOLLER, A.P. 1992. Numbers and size of sperm storage tubules and the duration of sperm storage in birds: a comparative study. *Biological Journal of the Linnean Society*, 45:363-372.
- BRILLARD, J.P. & ANTOINE, H. 1990. Storage of sperm in the uterovaginal junction and its incidence on the numbers of spermatozoa present in the perivitelline layer of hen's eggs. *British Poultry Science*, 31:635-644.
- BURKE, W.H. & OGASAWARA, F.X. 1969. Presence of spermatozoa in uterovaginal fluids of the hen at various ovulatory cycle. *Poultry Science*, 48:408-413.
- BURKE, W.H., OGASAWARA, F.X. & FUQUA, C.L. 1972. A study of the ultrastructure of the uterovaginal sperm storage glands of the hen (*Gallus domesticus*), in relation to a mechanism for the release of spermatozoa. *Journal of Reproduction and Fertility*, 29:29-36.
- BURLAND, T.G. & GULL, K. 1984. Molecular and cellular aspects of the interaction of benzimidazole fungicides with tubulin and microtubules, in *Mode of action of antifungal agents*, edited by A.P.J. Trinci & J.F. Riley. Cambridge: University Press, 299 - 320.
- CHAILLEY, B., NICOLAS, G. & LAINE, M.-C. 1989. Organization of actin microfilaments in the apical border of oviduct ciliated cells. *Biology of the Cell*, 67:81-90.
- CRUZ, M.-C. & EDLIND, T. 1997. B-tubulin genes and basis for benzimidazole sensitivity of the opportunistic fungus *Cryptococcus neoformans*. *Microbiology*, 143:2003-2008.
- DAS, S.K. 2003. Evidence for the innervation of sperm host glands (SHG) of native chicken's (*Gallus domesticus*) oviduct. *International journal of poultry science*, 2:259-260.
- EVTODIENKO, Y.V., TEPLOVA, V.V., SIDASH, S.S., ICHAS, F. & MAZAT, J.P. 1996. Microtubule- active drugs suppress the closure of the permeability transition pore in tumour mitochondria. *FEBS Letter*, 393:86-88.

- FRIEB, A.E., SINOWATZ, F., & WROBEL, K.-H. 1978. The uterovaginal sperm host glands of the quail (*Coturnix coturnix japonica*). *Cell Tissue Research*, 191:101-114.
- FUJII, S. 1963. Histological and histochemical studies on the oviduct of the domestic fowl with special reference to the region of the uterovaginal juncture. *Archives of Histology Japan*, 23:447-459.
- GORMAN, A.M., BANFOCO, E., ZHIVOTOVSKY, B., ORRENIUS, S. & CECCATELLI, S. 1999. Cytochrome c release and caspase-3 activation during colchicine-induced apoptosis of cerebellar granule cells. *European Journal of Neuroscience*, 11:1067-1072.
- GULATI, A.K., REDDI, A.H. & ZALEWSKI, A.A. 1983. Changes in the basement membrane zone components during skeletal muscle fibre degeneration and regeneration. *Journal of Cell Biology*, 97:957-962.
- HEGGENESS, M.H., SIMON, M. & SINGER, S.J. 1978. Association of mitochondria with microtubules in cultured cells. *Proceedings of the National Academy of Sciences of the USA*, 75:3863-3866.
- Helfand, B.T., Chang, L. & Goldman, R.D. 2003. The dynamic and motile properties of intermediate filaments. *Annual Review of Cell Developmental Biology*, 19:445-467.
- HESS, R. A. & NAKAI, M. 2000. Histopathology of the male reproductive system induced by the fungicide benomyl. *Histology and Histopathology*, 15:207-224.
- HOLM, L. & RIDDERSTRALE, Y. 2002. Development of sperm storage tubules in the quail during sexual maturation. *Journal of Experimental Zoology*, 292:200-205.
- KIM, J.AH., MITSUKAWA, K., YAMADA, M.K., NISHIYAMA, N., MATSUKI, N. & IKEGAYA, Y. 2002. Cytoskeleton disruption causes degeneration of dentate granule cells in hippocampal slice cultures. *Neuropharmacology*, 42:1109-1118.
- KOCH, M., OLSON, P.F. ALBUS, A., JIN, W., HUNTER, D.D., BRUNKEN, W.J., BURGESSON, R.E. & CHAMPLIAUD, M-F. 1999. Characterization and expression of the laminin γ 3 chain: A novel, non-basement membrane-associated laminin chain. *The Journal of Cell Biology*, 145:605-617.

- KOYONAGI, F. & NISHYAMA, H. 1981. Disintegration of spermatozoa in the infundibular sperm host glands of the fowl. *Cell and Tissue Research*, 214:81-87.
- KROEMER, G., DALLAPORTA, B. & RESCHE-REGON, M. 1998. The mitochondrial death/life regulator in apoptosis and necrosis. *Annual Review of Physiology*, 60:619-642.
- LAURIE, G.W., LEBLOND, C.P. & MATRIN, G.R. 1982. Localization of type IV collagen, laminin, heparin sulphate proteoglycan and fibronectin to the basal lamina of basement membranes. *Journal of Cell Biology*, 95:340-344.
- MARTINEZ-HERMANDEZ, A., GAY, S. & MILLER, E.J. 1982. Ultrastructural localization of type V collagen in rat kidney. *Journal of Cell Biology*, 92:343-349.
- McDANIEL, G.R., BRAKE, J. & ECKMAN, M.K. 1981. Factors affecting broiler breeder performance. 4. The interrelationship of some reproductive traits. *Poultry Science*, 60:1792-1797.
- OGASAWARA, F.X. & FUQUA, C.L. 1972. The vital importance of the uterovaginal sperm host glands for the turkey hen. *Poultry Science*, 51:1035-1039.
- PIERSON, E.E.M., MCDANIEL, G.R. & KRISTA, L.M. 1988. Relation ship between fertility duration and in vivo sperm storage in broiler breeder hens. *British Poultry Science*, 29:199-203.
- RYAN, M.C., TIZARD, R., VANDEVANTER, D.R. & CARTER, W.G. 1994. Cloning of the LamA3 gene encoding the alpha 3 chain of the adhesive ligand epiligrin. Expression in wound repair. *Biological Chememistry*, 269:22779-22787.
- SANDOZ, D., GOUNON, P., KARSENTI, E., BOISVIEUX-ULRICH, E., LAINE, M.-C. & PAULIN, D. 1983. Organization of intermediate filament in ciliated cells from quail oviduct. *Journal of Submicroscopic Cytology*, 15:323-326.
- SCHUPPING, G.T., VAN KREY, H.P., DENBOW, D.M., BAKST, M.R. & MEYER, G.B. 1984. Ultrastructural analyses of uterovaginal sperm storage glands in fertile and infertile turkey breeder hens. *Poultry Science*, 63:1872-1882.
- STEINERT, P. M. & ROOP, D. R. 1988. Molecular and cellular biology of intermediate filaments. *Annual Review of Biochemistry*, 57:593-625.
- STEMMLER, M.P. 2008. Cadherin in development and cancer. *Molecellar Biosystem*, 4:835-50.

- TINGARI, M.D. & LAKE, P.E. 1973. Ultrastructural studies on the uterovaginal sperm host glands of the domestic hen, *Gallus domesticus*. *Journal of Reproduction and Fertility*, 34:423-431.
- VAN KREY, H.P., BLANDER, R.J. & COMPTON, M.M. 1981. Storage and evacuation of spermatozoa from the uterovaginal sperm host glands in domestic fowl. *Poultry science*, 60:871-877.

CHAPTER SIX

General discussion and conclusion

6.1 Overview

In recent years, environmental pollutants have become a major health concern. Both naturally occurring and industrial chemicals are considered to be the cause of reproductive malfunctions in exposed individuals. Industrial chemicals found in the environment include herbicides, pesticides and fungicides. The present study focused on the effects of methyl-2-benzimidazole carbamate (carbendazim) on the morphology of the female reproductive tract in the sexually mature Japanese quail. This study appears to be the first report on the effect of carbendazim on the morphology of the female reproductive system in birds. Earlier toxicological studies measured the endpoint toxicity of carbendazim, using parameters such as bodyweight, eggshell thickness as well as developmental effects (Mineau, 2005). Although interspecies differences in toxicological effects have been reported (Mineau, 2005), the Japanese quail has been shown to be appropriate for toxicological studies in birds (Faqi, Soleki, Pfeil & Hilbig, 1997).

Based on the results of experiment I, a dose of 400 mg/kg bodyweight carbendazim proved to be the minimum effective dose, which caused both gross and histological lesions in the oviduct of the Japanese quail. Similar findings were also observed in male Japanese quail (Aire, 2005), as well as in the rat, rabbit and hamster (Mantovani, Maranghi, Ricciardi, Macri, Stazi, Attias & Zappini, 1998). Comparing the extent of observed pathological changes *visa-vis* the used doses of carbendazim, the effect of carbendazim was dose dependent. This could be due to the elimination time from animal tissues. When administered at high doses, carbendazim residues were found in the liver and muscle tissue of the Japanese quail (Reisinger, Szigeti & Varnagy, 2006). In addition, carbendazim residues have also been reported in the livers of dogs and rats (Gardiner, Kirkland, Klopping & Sherman, 1974). Furthermore, residues have been detected in the milk from cows fed diets containing high levels of the carbendazim parent compound, benomyl

(Ahdaya, Monroe & Guthrie, 1981). At low doses no pathological changes were observed in any section of the oviduct studied.

The results of experiment II showed that the effects of carbendazim in all sections of the oviduct were time-dependent, with pathological changes seen as early as 5 hours post-exposure. Similar observations were also reported in the male Japanese quail (Aire, 2005). The appearance of pathological changes from 5 hours post-exposure is not surprising, as according to reports by Ahdaya *et al.* (1981) and Gardiner *et al.* (1974) the distribution of carbendazim in body tissues is rapid following oral administration. In mice, a half life of distribution ranged from 8 to 17 minutes post-exposure. An interesting finding of the present study was that the degenerative changes were seen until 32 days post-exposure to carbendazim. The presence of degenerative changes up to 32 days post-exposure was not expected, since according to *in vivo* studies, the metabolism and elimination of carbendazim is rapid via urine (Gardener *et al.*, 1974). In the rat only less than 0.01% of the administered dose of carbendazim was found in body tissues 72 hours post-exposure.

In this investigation, carbendazim exposure caused degeneration of both luminal and glandular epithelia in all sections of the oviduct studied. Degeneration of epithelial and glandular cells suggested oviductal regression. As discussed in Chapters 2, 3 and 4, oviductal regression occurs by apoptosis (Steffl, Schweiger, Siguyama & Amselgruber, 2008). However, the techniques used in the present study did not confirm whether the degenerative changes observed were due to apoptosis. Further studies using apoptotic markers will be useful in confirming this assertion.

Considering the physiological function of each oviductal section, the degeneration of epithelial and glandular cells will impact negatively on the fertility and productivity of the exposed birds. For example, the degeneration of the infundibular region will affect fertilization, as well as the formation of chalazae and perivitelline membranes. In addition, infundibular degeneration will increase the number of abdominal yolks due to the failure of the infundibular funnel to properly engulf ovulated oocytes. Studies by Berg, Holm, Brandt & Brunström (2001) and Blomqvist, Berg, Holm, Brandt, Ridderstråle & Brunström (2006) support this theory. According to these

reports, the administration of high levels of DDT and oestrogen, *in ovo*, caused the malfunction of the infundibulum, which consequently increased the incidence of abdominal yolks. In diseases, such as egg drop syndrome, Infectious bronchitis and Newcastle disease, the presence of yolk material in the abdominal cavity is common due to the degeneration of epithelial cells in the infundibulum (Solomon, 2002; Chousalkar & Roberts, 2007). In the magnum, degenerative changes will impair the synthesis and release of albumen. According to a report by Davidson (1986), the degeneration of luminal and glandular epithelia in the magnum resulted in the formation of watery albumen in the domestic fowl. In the shell gland, degeneration of epithelial cells interferes with calcium metabolism and the formation of a calcereous shell.

As shown in Chapter 5, carbendazim exposure caused degeneration of SST cells and increased the number of empty tubules. This observation suggested a decreased fertility in exposed birds. This idea is supported in reports by McDaniel, Brake & Eckman (1981) and Brillard & Antoine (1990), which show a correlation between fertility and the number of SST containing sperm cells.

In the present investigation, the use of TEM proved to be the best technique to study the onset and extent of degenerative changes in all sections of the oviduct. Although laminin immunostaining demonstrated the presence of discontinuous basement membranes, morphological changes of the basal lamina were more apparent at the ultrastructural level.

6.2 Impact on wild birds

The present study has shown the effect of carbendazim on the oviduct of the sexually mature Japanese quail. It is clear that the continuous use of this product in the field contaminates the environment and increases the chance of exposure to the wild birds. As mentioned earlier, carbendazim and benomyl residues are found in the soil, surface and ground water (IPCS, 1986), as well as in plants (Still & Mansager 1975) and fruits (Pico, la Farre, Soler & Barcelo, 2007). Exposure to wild birds could be through the food chain or physical contact in the environment. However, care must be taken when extrapolating the results of this study to the field, simply

because wild birds are exposed to different types of toxicants, which occur in the environment. Exposure to different toxicants can result into either neutralization or synergistic effects. In addition, the level of exposure also determines the extent of pathological changes, as well as, the clinical manifestation of the toxicological effects.

In wild birds, the exposure to pollutant chemicals occurs throughout the reproductive cycle. However, the level of exposure differs depending on the season of the year, as well as the farm activities taking place. It is accepted that birds subjected to a contaminated environment soon after the application a chemical stand a higher risk of severe effects composed to birds exposed a few days later. The frequency of chemical application also contributes to the level of exposure. In addition, the level of exposure also differs depending on the type of food consumed. Thus, the effects of an applied chemical would be expected to appear earlier in herbivorous birds than in insectivorous birds.

Several models have been proposed to extrapolate results from experimental animals to wildlife. The proposed models include: time-weighted average (TWA) which measures the average daily intake over time of exposure; body-burden modeling (BBM) that estimates the rate of intake and elimination; and temporal analysis (TA) which analyzes the changes of exposure levels with time as a result of degradation (Fisher, 2005). Other methods are based on species sensitivity distributions developed by Baril, Jobin, Mineau & Collins (1994), Luttik, Mineau & Roelofs (2005) and Mineau, Baril, Collins, Duffe, Joermann & Luttik (2001).

6.3 Conclusion

In the current study, morphological changes in the oviduct were the main findings observed post-exposure to carbendazim. Other findings of this study are:

1. Carbendazim causes both macroscopic and microscopic morphological changes at high doses.

2. The Lowest Observed Adverse Effect Level (LOAEL) of carbendazim in the female reproductive tract of the Japanese quail is 400 mg/kg bodyweight.
3. The effects of carbendazim in the oviduct are dose dependent.
4. Administration of a single dose of carbendazim caused morphological changes, which persisted as long as 32 days post-exposure, with minor signs of recovery.

This study opens an avenue for further investigations on the effects of carbendazim following embryonic exposure.

This study opens an avenue for further investigation of the effect of this compound following embryonic exposure, as well as, during sexual maturity.

6.4 References

- AHDAYA, S.M., MONROE, R.J. & GUTHRIE, F.E. 1981. Absorption and distribution of intubated insecticides in fasted mice. *Pesticide Biochemistry and Physiology*, 16:38-46.
- AIRE, T. A. 2005. Short-term effects of carbendazim on the gross and microscopic features of the testes of Japanese quails (*Coturnix coturnix japonoca*). *Anatomy and Embryology*, 210:43-49.
- BARIL, A., JOBIN, B., MINEAU, P. & COLLINS, B.T. 1994. A consideration of inter-species variability in the use of the median lethal dose (LD50) in avian risk assessment. Technical report series no. 216, Canadian wildlife service, Canada.
- BERG, C., HOLM, L., BRANDT, I. & BRUNSTROM, B. 2001. Anatomical and histological changes in the oviducts of Japanese quail, *Coturnix coturnix japonica*, after embryonic exposure to ethynloestradiol. *Reproduction*, 121:155-165.
- BLOMQUIST, A., BERG, C., HOLM, L., BRANDT, I., RIDDERSTRÅLE, Y., BRUNSTRÖM, B. 2006. Defective reproductive organ morphology and function in domestic rooster embryonically exposed to o,p'-DDT or ethynylestradiol. *Biology of Reproduction* 74:481-6.

- BRILLARD, J.P. & ANTOINE, H. 1990. Storage of sperm in the uterovaginal junction and its incidence on the numbers of spermatozoa present in the perivitelline layer of hen's eggs. *British Poultry Science*, 31:635-644.
- CHOUSALKAR, K.K. & ROBERTS, J.R. 2007: Ultrastructural study of infectious bronchitis virus infection in infundibulum and magnum of commercial laying hens. *Veterinary Microbiology*, 122:223-236.
- DAVIDSON, M.F. 1986. Histological studies of changes in the magnum of the domestic hen associated with the production of watery white eggs. *British Poultry Science*, 27:353-354.
- FAQI, A.S., SOLECKI, R., PFEIL, R. & HILBIG, V. 1997. Standard values for reproductive and clinical chemistry parameters of Japanese quail. *Deutsche tierärztliche wochenschrift*, 104:167-169.
- FISHER, D.L. 2005. Accounting for differing exposure between laboratory tests and the field in the assessment of long-term risks of pesticides to terrestrial vertebrates. *Ecotoxicology*, 14:853-862.
- GARDINER, J.A., KIRKLAND, J.J., KLOPPING, H.L. & SHERMAN, H. 1974. Fate of benomyl in animals. *Journal of Agriculture and Food Chemistry*, 22:419-427.
- INTERNATIONAL PROGRAM ON CHEMICAL SAFETY, 1986. Environmental health criteria for carbamate pesticides: A general introduction, 64.(www.inchem.org).
- LUTTIK, R., MINEAU, P. & ROELOFS, W. 2005. A review of interspecies toxicity extrapolation in birds and mammals and a proposal for long-term toxicity data. *Ecotoxicology*, 14:817-832.
- MANTOVANI, A., MARANGHI, F., RICCIARDI, C., MACRI, C., STAZI, A.V., ATTIAS, L. & ZAPPINI, G.A. 1998. Developmental toxicity of carbendazim: comparison of No-observed-adverse-effect level and benchmark dose approach. *Food and Chemical Toxicology*, 36:37-45.
- McDANIEL, G.R., BRAKE, J. & ECKMAN, M.K. 1981. Factors affecting broiler breeder performance. 4. The interrelationship of some reproductive traits. *Poultry Science*, 60:1792-1797.
- MINEAU, P. 2005. A review and analysis of study of endpoints relevant to the assessment of long term pesticide toxicity in avian and mammalian wildlife. *Ecotoxicology*, 14:775-7999.

- MINEAU, P., BARIL, A., COLLINS, B.T., DUFFE, J.A., JOERMANN, G. & LUTTIK, R. 2001. Pesticide acute toxicity reference values for birds. *Review of environmental contaminants and toxicology*, 170:13-74.
- PICO, Y., la FARRE, M., SOLER, C. & BARCELO, D. 2007. Identification of unknown pesticides in fruits using ultra-performance liquid chromatography-quadrupole time-of-flight mass spectrometry: Imazilil as a case study of quantification. *Journal of chromatography*, 1176:123-134.
- REISINGER, K., SZIGETI, J. & VARNAGY, L. 2006. Determination of carbendazim residues in the eggs, liver and pectoral muscle of Japanese quail (*Coturnix coturnix japonica*). *Acta Veterinaria Hungarica*, 54:127-133.
- SOLOMON, S.E. 2002. The oviduct in chaos. *World's poultry science journal*, 58:41-48.
- STEFFL, M., SCHWEIGER, M., SIGUYAMA, T. & AMSELGRUBER, W.M. 2008. Review of apoptotic and non-apoptotic events in non-ciliated cells of the mammalian oviduct. *Annals of Anatomy*, 190:46-52.
- STILL, G. G. & MANSAGER, E. R. 1975. Alfalfa metabolism of propham. *Pesticide Biochemical Physiology*, 5:515-522.

Appendix 1: Conference papers

- Kimaro, W.H. and Madekurozwa, M.-C. (2010). Effect of carbendazim (methyl-2-benzimidazole carbamate) on the shell gland of the Japanese quail (*Coturnix coturnix japonica*). Proceedings of the International Anatomical Sciences and Cell Biology Conference. May 2010, Singapore, pp. 147.
- Kimaro, W.H. and Madekurozwa, M.-C. (2009). A morphological study of the effects of carbendazim on the infundibulum of the sexually mature Japanese quail (*Coturnix coturnix japonica*). *Abstract book of the 17th International congress of International Federation of Associations of Anatomists (IFAA)*. August 2009, Cape-town, South Africa.
- Kimaro, W.H. and Madekurozwa, M.-C. (2008). Histological and ultrastructural study of the effect of carbendazim (methyl-2-benzimidazole carbamate) on the magnum and shell gland of the Japanese quail (*Coturnix coturnix japonica*). *Proceedings of the 38th Annual conference of the Anatomical Society of Southern Africa*. April, 2008, p 55.